

AD-A251 010



WRDC-TR-89-3087
Volume I



**DETECTION OF FAILURE PROGRESSION
IN CROSS-PLY GRAPHITE/EPOXY
DURING FATIGUE THROUGH
ACOUSTIC EMISSION**

Jonathan Awerbuch
William F. Eckles
Donald L. Erdman

DTIC
ELECTE
MAY 26 1992
S A D

Drexel University
Department of Mechanical Engineering and Mechanics
Philadelphia PA 19104

November 1989

Final Report for Period June 1984 - April 1989

Approved for public release; distribution is unlimited

92-13544



FLIGHT DYNAMICS LABORATORY
WRIGHT RESEARCH AND DEVELOPMENT CENTER
AIR FORCE SYSTEMS COMMAND
WRIGHT-PATTERSON AIR FORCE BASE, OHIO 45433-6553


92 5 21 014


NOTICE

WHEN GOVERNMENT DRAWINGS, SPECIFICATIONS, OR OTHER DATA ARE USED FOR ANY PURPOSE OTHER THAN IN CONNECTION WITH A DEFINITELY GOVERNMENT-RELATED PROCUREMENT, THE UNITED STATES GOVERNMENT INCURS NO RESPONSIBILITY OR ANY OBLIGATION WHATSOEVER. THE FACT THAT THE GOVERNMENT MAY HAVE FORMULATED OR IN ANY WAY SUPPLIED THE SAID DRAWINGS, SPECIFICATIONS, OR OTHER DATA, IS NOT TO BE REGARDED BY IMPLICATION, OR OTHERWISE IN ANY MANNER CONSTRUED, AS LICENSING THE HOLDER, OR ANY OTHER PERSON OR CORPORATION; OR AS CONVEYING ANY RIGHTS OR PERMISSION TO MANUFACTURE, USE, OR SELL ANY PATENTED INVENTION THAT MAY IN ANY WAY BE RELATED THERETO.


THIS REPORT HAS BEEN REVIEWED BY THE OFFICE OF PUBLIC AFFAIRS (ASD/PA) AND IS RELEASABLE TO THE NATIONAL TECHNICAL INFORMATION SERVICE (NTIS). AT NTIS IT WILL BE AVAILABLE TO THE GENERAL PUBLIC INCLUDING FOREIGN NATIONS.

THIS TECHNICAL REPORT HAS BEEN REVIEWED AND IS APPROVED FOR PUBLICATION.


GEORGE P. SENDECKYJ, Aero Engr
Fatigue, Fracture and Reliability Gp
Structural Integrity Branch


Capt Howard J. Storr, Tech Mgr
Fatigue, Fracture and Reliability Gp
Structural Integrity Branch

FOR THE COMMANDER


JAMES L. RUDD
Chief, Structural Integrity Branch
Structures Division

IF YOUR ADDRESS HAS CHANGED, IF YOU WISH TO BE REMOVED FROM OUR MAILING LIST, OR IF THE ADDRESSEE IS NO LONGER EMPLOYED BY YOUR ORGANIZATION PLEASE NOTIFY WRDC/F1BEC, WRIGHT-PATTERSON AFB, OH 45433-6553 TO HELP MAINTAIN A CURRENT MAILING LIST.

COPIES OF THIS REPORT SHOULD NOT BE RETURNED UNLESS RETURN IS REQUIRED BY SECURITY CONSIDERATIONS, CONTRACTUAL OBLIGATIONS, OR NOTICE ON A SPECIFIC DOCUMENT.

REPORT DOCUMENTATION PAGE			Form Approved OMB No. 0704-0188	
Public reporting burden for this collection of information is estimated to average 1 hour per response, including the time for reviewing instructions, searching existing data sources, gathering and maintaining the data needed, and completing and reviewing the collection of information. Send comments regarding this burden estimate or any other aspect of this collection of information, including suggestions for reducing this burden, to Washington Headquarters Services, Directorate for Information Operations and Reports, 1215 Jefferson Davis Highway, Suite 1204, Arlington, VA 22202-4302, and to the Office of Management and Budget, Paperwork Reduction Project (0704-0188), Washington, DC 20503.				
1. AGENCY USE ONLY (Leave blank)		2. REPORT DATE November 1989		3. REPORT TYPE AND DATES COVERED Final From Jun 84 to Apr 89
4. TITLE AND SUBTITLE Detection of Failure Progression in Cross-Ply Graphite/ Epoxy During Fatigue Loading Through Acoustic Emission Vol. I			5. FUNDING NUMBERS C F33615-84-C-3204 PE 61102F WU 2307N126	
6. AUTHOR(S) J. Awerbuch, W.F. Eckles, and D.L. Erdman				
7. PERFORMING ORGANIZATION NAME(S) AND ADDRESS(ES) Drexel University Philadelphia PA 19104			8. PERFORMING ORGANIZATION REPORT NUMBER N/A	
9. SPONSORING/MONITORING AGENCY NAME(S) AND ADDRESS(ES) Flight Dynamics Laboratory (WRDC/FIBEC) Wright Research & Development Center WPAFB OH 45433-6553			10. SPONSORING/MONITORING AGENCY REPORT NUMBER WRDC-TR-89-3087 Volume I	
11. SUPPLEMENTARY NOTES				
12a. DISTRIBUTION/AVAILABILITY STATEMENT Approved for Public Release; Distribution Unlimited			12b. DISTRIBUTION CODE	
13. ABSTRACT (Maximum 200 words) The applicability of the acoustic emission (AE) technique to detect and locate damage initiation, monitor its progression and accumulation and to identify the major modes of damage associated with the failure process in cross-ply AS4/3502 graphite/epoxy laminates has been investigated. Six pairs of different laminate configurations were studied, having different stacking sequences and containing different ratios of ply thickness. Each pair included one laminate with external 90° plies and one with external 0° plies, e.g. [90 ₂ /0 ₂ /90], and [0 ₂ /90 ₂ /0], respectively. The testing program included determination of mechanical properties and monitoring of failure mechanisms and processes using optical observations, X-radiography, deplying, and scanning electron microscopy. Special efforts were directed toward establishing a correlation between the failure process and the AE results. Acoustic emission was monitored during quasi-static loading to failure in all cross-ply laminates. Results indicate that stacking sequence strongly affects the events intensities, e.g. amplitude, energy, (Continued)				
14. SUBJECT TERMS Composite Materials, Acoustic Emission, Acousto-Ultrasonics, Fatigue, Damage Mechanics, Damage Accumulation			15. NUMBER OF PAGES 340	
			16. PRICE CODE	
17. SECURITY CLASSIFICATION OF REPORT Unclassified	18. SECURITY CLASSIFICATION OF THIS PAGE Unclassified	19. SECURITY CLASSIFICATION OF ABSTRACT Unclassified	20. LIMITATION OF ABSTRACT Unclassified	

(Continued from Block 13)

duration, and counts per event. Also, stacking sequence has a significant effect on damage initiation load and on rate of damage accumulation.

It was determined that a significant amount of emission is generated during fatigue loading not only by damage accumulation and progression but also by the continuous friction that results from the fracture surfaces grating against each other. Consequently, AE caused by grating must be distinguished from that generated by actual damage growth. In this study acoustic emission was monitored during fatigue loading ($R=0.1$). Emphasis was placed on distinguishing AE caused by new damage from friction generated emission. The distinction is based upon the load level and location of the AE events and is made by identifying the characteristic intensities of the events associated with friction. It was determined that the event intensities associated with friction are all below certain threshold values, defined as Friction Emission Threshold (FRET) values. Based on the FRET values the emission caused by actual can be separated from the total emission, damage accumulation curves can be established, and the progression of the matrix dominated failures (i.e. matrix splitting and delamination) can be tracked. Case studies are presented in which the data analysis methodology developed in this research program has been successfully used to monitor damage accumulation and progression during quasi-static and fatigue loading.

It was determined that a significant amount of emission is also generated by the grating among the newly created fracture surfaces during quasi-static loading. Results indicate that matrix dominated failures and fiber breakage result in middle and high range AE source intensities, respectively. Based on these results damage curves were constructed which distinguish among the emission generated by friction, by primarily matrix dominated failures and by fiber breakage. Based on the analysis of the events which are generated primarily by damage formation, the actual extension of the damage was correlated with the AE results.

Acoustic emission was monitored also in specimens subjected to different loading functions including: constant load (hold load); subjecting specimens to spike loads during fatigue loading; quasi-static loading/unloading cycles incrementally increasing the load up to failure; and monotonic quasi-static loading at different loading rates. Results indicate that varying the loading function significantly affects the emission generated. Particular attention was given to the high rate generated during either quasi-static or fatigue loading. Based on the friction generated emission a specific criterion for determining the appropriateness of the loading function was established.

A nondestructive test technique is proposed for detecting existing damage and changes in the state-of-damage in a composite laminate by measuring its frequency response. The Frequency Response (FR) technique is based on introduction of constant amplitude sinusoidal waves of continuously varying frequencies through a wide band piezo-electric transmitter and measuring the frequency response of the composite laminate through an identical receiver located a distance away. The experimental results demonstrate that the FR technique is sensitive to the internal state-of-damage, primarily in terms of amplitude attenuation, downward shift in the dominate (resonance) frequencies, and decrease in the area under the frequency response curve. The FR technique can be applied on line and is simple to use. The acoustoultrasonics technique was also used during quasi-static loading. The preliminary results indicate that this technique is not sufficiently sensitive to the damage which is the dominant failure mode in cross-ply graphite/epoxy laminates.

FOREWORD

This document is a final report on research into the monitoring of acoustic emission in cross-ply graphite/epoxy laminates during quasi-static and fatigue loading. The research program has been conducted in the Composite Mechanics Laboratory, Department of Mechanical Engineering, Drexel University.

The work has been sponsored by the Wright Research and Development Center, Flight Dynamics Laboratory, under contract number F33615-84-3204. Dr. George P. Sendeckyj was the contract monitor.

The Principal Investigator of this program was Dr. Jonathan Awerbuch. The Research Assistant of this program was Mr. William F. Eckles. Mr. Donald L. Erdman performed a significant portion of the data reduction and analysis. Various phases of the research were also performed by Dr. E. Katz (visiting scholar), Mr. Sharhokh Ghaffari, and Mr. B. Gilbert, all of the Department of Mechanical Engineering and Mechanics.

The specimens tested in this program were fabricated and supplied by the Flight Dynamics Laboratory.

Accession For	
NTIS	CRA&I <input checked="" type="checkbox"/>
DTIC	TAB <input type="checkbox"/>
Unannounced	<input type="checkbox"/>
Justification	
By	
Distribution /	
Availability Codes	
Dist	Avail and/or Special
A-1	



TABLE OF CONTENTS

<u>Section</u>	<u>Page</u>
I. SUMMARY	1
II. INTRODUCTION	5
2.1 General	5
2.2 Objectives for Employing Acoustic Emission Technique in Composites	7
2.3 Summary of Representative Research	8
2.4 Failure Processes in Graphite/Epoxy Laminates Under Quasi Static and Fatigue Loading	11
2.5 On the Correspondence Between Event Intensities and Modes of Failure	14
2.6 Friction Emission	16
2.7 Research Objectives	17
2.8 References	17
III. EXPERIMENTAL PROCEDURE	24
3.1 Summary	24
3.2 Material and Specimen Preparation	24
3.3 Mechanical Test Program	26
3.4 Monitoring Acoustic Emission	27
3.5 Failure Modes and Damage Progression	29
3.6 Test Matrix	30
3.7 References	31
IV. MECHANICAL PROPERTIES AND FAILURE MECHANISMS	40
4.1 Summary	40
4.2 Mechanical Properties	40
4.3 Modes of Damage	44

TABLE OF CONTENTS (Continued).

<u>Section</u>	<u>Page</u>
4.4 Conclusions	47
4.5 References	48
 V. MONITORING ACOUSTIC EMISSION DURING QUASI-STATIC LOADING	 51
5.1 Summary	51
5.2 Introduction	51
5.3 Count Rate as a Function of Applied Stress	53
5.4 Cumulative Events	55
5.5 Location Distribution Histograms of Events	58
5.6 Amplitude Distribution Histograms of Events	59
5.7 Other Event Intensities	68
5.8 Effect of Loading Rate	71
5.9 Testing Procedure	74
5.10 Conclusions	76
5.11 References	77
 VI. MONITORING ACOUSTIC EMISSION DURING FATIGUE LOADING	 79
6.1 Summary	79
6.2 Introduction	80
6.3 Experimental Procedure.....	81
6.4 Separation of Acoustic Emission Events by Load Range	82
6.5 Load and Location Distribution Histograms of Acoustic Emission Events	 88
6.6 Acoustic Emission Event Intensities	90
6.7 On the Correspondence Between Event Intensities and Modes of Damage	 94
6.8 Friction Emission Thresholds (FRET) Values.....	96

TABLE OF CONTENTS (Concluded)

<u>Section</u>		<u>Page</u>
6.9	Effect of Loading Rate and Damage Severity on Acoustic Emission Results	101
6.10	Verification of FRET Values	105
6.11	Emission Generated by Actual Damage Progression	107
6.12	Tracking Progression of Damage Growth Through Acoustic Emission	111
6.13	Acoustic Emission During Post-Fatigue Quasi-Static Monotonic Loading	113
6.14	Conclusions	115
6.15	References	116

LIST OF FIGURES

	<u>Page</u>
Figure 4.1. Stress-strain curves of twelve different cross ply laminates, showing the effect of stacking sequence on stiffness and strength: (a) 0° plies external; (b) 90° plies external.	119
Figure 4.2. Effect of number and percent of 0° and 90° plies on axial stiffness of 12 cross-ply laminates. Axial stiffness obeys the rule of mixture, however, it depends on laminate configuration.	120
Figure 4.3. Effect of number and percent of 0° and 90° plies on ultimate of 12 cross-ply laminates. Axial stiffness obeys the rule of mixture, however, it depends on laminate configuration.	122
Figure 4.4. Strength versus axial stiffness for all 12 cross-ply laminates tested showing a linear relation.	124
Figure 4.5. Photomicrographs showing the transverse cracks in three cross-ply laminates: (a) a $[90_2/0_2/90]_S$ laminate after loading to approximately 72 percent of ultimate load; (b) a $[90_2/0/90]_S$ laminate after loading to approximately 81 percent of ultimate load; and (c) a $[90_2/0_2/90]_S$ laminate after loading to approximately 60 percent of ultimate load.	125
Figure 4.6. Deplied cross-ply laminates: (a) general view of the 0° ply in a $[90_2/0_2/90]_S$ laminate, showing the imprints of the tips of the transverse cracks in the neighboring 90° ply; (b) detail view of the 0° ply in a $[90_2/0]_S$ laminate, showing broken fibers; and (c) detail view of the 90° ply in a $[0_2/90]_S$ laminate, showing no broken fibers.	127
Figure 4.7. Scanning electron micrographs showing the fracture surface morphology of a $[90_2/0_2/90]_S$ cross-ply laminate: (a) interfacial failure in the 90° ply; (b) good fiber/matrix bonding in the 0° ply; (c) and (d) matrix serrations and broken fibers in the 90° ply.	130
Figure 4.8. X-Radiograph of a $[90_2/0_2/90]_S$ laminate taken after loading to 59 percent of average ultimate strength showing approximately one transverse crack per mm (20 cracks/inch). Distribution of transverse cracks is quite uniform throughout the length of the specimen.	131
Figure 4.9. Number of transverse cracks as a function of applied load for different laminates. Results indicate that laminate configuration affects damage accumulation.	132

LIST OF FIGURES (Continued)

	<u>Page</u>
Figure 5.1. Count-rate (recorded with the D/E AE system) and strain as a function of far-field applied stress for 12 different cross-ply graphite/epoxy laminates. Arrows indicate emission initiation stress.	139
Figure 5.2. Count-rate (recorded with the D/E AE system) and strain as a function of far-field applied stress for selected pairs of cross-ply graphite/epoxy laminates showing good reproducibility.	145
Figure 5.3. Emission initiation stress (recorded with the D/E AE system) as a function of: (a) number of 0° plies; (b) percent of 0° plies; (c) number of 90° plies; and (d) percent of 90° plies.	148
Figure 5.4. Emission initiation stress (recorded with the D/E AE system) as a function of ultimate stress for all cross-ply laminates: (a) non-dimensional; and (b) dimensional.	150
Figure 5.5. Events accumulated during quasi-static loading to failure (recorded with the D/E AE system) as a function of far-field applied stress for 12 different cross-ply graphite/epoxy laminates: (a) laminates having external 0° plies (Group I); and (b) laminates having external 90° plies (Group II).	151
Figure 5.6. Events accumulated during quasi-static loading to failure (recorded with the D/E AE system) as a function of far-field applied stress for 12 different cross-ply graphite/epoxy laminates assuming that only the 0° carry the load: (a) laminates having external 0° plies (Group I); and (b) laminates having external 90° plies (Group II).	152
Figure 5.7. Events accumulated during quasi-static loading to failure (recorded with the D/E AE system) as a function of far-field applied strain for 12 different cross-ply graphite/epoxy laminates: (a) laminates having external 0° plies (Group I); and (b) laminates having external 90° plies (Group II).	153
Figure 5.8. Location distribution histograms of events (recorded with the D/E AE system) accumulated at different load ranges during quasi-static loading of 12 different cross-ply graphite/epoxy laminates. Each Figure shows two laminates having reversed stacking sequence.	154
Figure 5.9. Location distribution histograms of events (recorded with the D/E AE system) accumulated at different load ranges during quasi-static loading of a double-edge notched [90 ₂ /0 ₂ /90] _s graphite/epoxy laminate.	160

LIST OF FIGURES (Continued)

Page

- Figure 5.10. Amplitude distribution histograms of events (recorded with the D/E AE system) accumulated at different load ranges during quasi-static loading of the same 12 cross-ply graphite/epoxy laminates shown in Figure 5.8. Each Figure shows two laminates having reversed stacking sequence. 161
- Figure 5.11. Amplitude distribution histograms of events (recorded with the D/E AE system) accumulated at different load ranges during quasi-static loading of selected cross-ply graphite/epoxy laminates showing good reproducibility of results. Each Figure shows two laminates having reversed stacking sequence. 167
- Figure 5.12. Amplitude distribution histograms of events (recorded with the D/E AE system) accumulated at different load ranges during quasi-static loading of the same double-edge notched $[90_2/0_2/90]_s$ graphite/epoxy laminate shown in Figure 5.9. 170
- Figure 5.13. Amplitude distribution histograms of events (recorded with the PAC AE system) accumulated at different load ranges during quasi-static loading to failure of 12 different cross-ply graphite/epoxy laminates. Each Figure shows two laminates having reversed stacking sequence. 171
- Figure 5.14. Events of different amplitude ranges accumulated (recorded with the PAC AE system) during quasi-static loading to failure as a function of far-field applied stress for 12 different cross-ply graphite/epoxy laminates. Each Figure shows two laminates having reversed stacking sequence. 177
- Figure 5.15. Events of different amplitude ranges (recorded with the PAC AE system) accumulated during quasi-static loading to failure as a function of far-field applied stress-to-ultimate stress ratio for 12 different cross-ply graphite/epoxy laminates. Each Figure shows two laminates having reversed stacking sequence. 183
- Figure 5.16. Events of 70 dB to 85 dB amplitude range (recorded with the PAC AE system) accumulated during quasi-static loading to failure as a function of far-field applied stress for 12 different cross-ply graphite/epoxy laminates: (a) laminates having external 0° plies (Group I); and (b) laminates having external 90° plies (Group II). 189

LIST OF FIGURES (Continued)

	<u>Page</u>
Figure 5.17. Events of 85 dB to 100 dB amplitude range (recorded with the PAC AE system) accumulated during quasi- static loading to failure as a function of far-field applied stress for 12 different cross-ply graphite/epoxy laminates: (a) laminates having external 0° plies (Group I); and (b) laminates having external 90° plies (Group II).	190
Figure 5.18. Energy-counts, duration, and counts per event distribution histograms of events (recorded with the PAC AE system) accumulated at different load ranges during quasi-static loading to failure for two selected cross-ply graphite/epoxy laminates having reversed stacking sequence.	191
Figure 5.19. Intensity distribution histograms (I.D.H.) of events (recorded with the PAC AE system) accumulated during quasi-static loading to failure in a [0 ₂ /90/0] _s graphite/epoxy laminate: (a) amplitude distribution histogram (A.D.H.) of all the events accumulated; (b) (c) (d) and (e) I.D.H. of events having four different amplitude ranges; (f) A.D.H. events having 55 dB to 70 dB; (g) and (h) I.D.H. of events shown in distribution (f) having below and above 20 energy-counts, respectively.	194
Figure 5.20. Intensity distribution histograms (I.D.H.) of events (recorded with the PAC AE system) accumulated during quasi-static loading to failure in a [90 ₂ /0/90] _s graphite/epoxy laminate: (a) amplitude distribution histogram (A.D.H.) of all the events accumulated; (b) (c) (d) and (e) I.D.H. of events having four different amplitude ranges; (f) A.D.H. events having 55 dB to 70 dB; (g) and (h) I.D.H. of events shown in distribution (f) having below and above 20 energy-counts, respectively.	197
Figure 5.21. Events accumulated during quasi-static loading to failure (recorded with the D/E AE system) as a function of far-field applied stress for: (a) [90 ₂ /0 ₂ /90] _s ; and (b) [90/0 ₂ /90] _s graphite/epoxy laminates subjected to three different stroke rates.	200
Figure 5.22. Events accumulated during quasi-static loading to failure (recorded with the D/E AE system) as a function of far-field applied strain for: (a) [90 ₂ /0 ₂ /90] _s ; and (b) [90/0 ₂ /90] _s graphite/epoxy laminates subjected to three different stroke rates shown for the same specimens of Figure 5.21.	201

LIST OF FIGURES (Continued)

	<u>Page</u>
Figure 5.23. Location and amplitude distribution histograms of events (recorded with the D/E AE system) accumulated during quasi-static loading to failure of a $[90/0_2/90]_s$ graphite/epoxy laminate subjected to three different stroke rates.	202
Figure 5.24. Events accumulated during quasi-static loading to failure (recorded with the D/E AE system) as a function of far-field applied stress for a $[0/90]_{2s}$ graphite/epoxy laminate showing effect of spatial filtering on AE results.	203
Figure 5.25. Events accumulated during quasi-static loading to failure (recorded with the D/E AE system) as a function of far-field applied stress for unidirectional graphite/epoxy laminate showing effect of specimen tabbing material on AE results.	204
Figure 5.26. Events accumulated during quasi-static loading to failure (recorded with the D/E AE system) as a function of far-field applied stress for a $[0/90]_{2s}$ graphite/epoxy laminate showing effect sensor selection on AE results.	205
Figure 6.1 Schematics of loading sequences. Shaded areas indicate fatigue periods analyzed and discussed in this Section. All specimens were subjected to sinusoidal loading function at $R = 0.1$. Dynamic stress amplitude σ_d , loading frequency, f , and fatigue period, N , are indicated in each schematic.	206
Figure 6.2. Accumulative events as a function of number of cycles, distinguishing among emission generated in seven different load ranges during selected periods of the fatigue loading of five representative specimens (results recorded with the D/E AE system). Most of the events occur at the lower load ranges.	209
Figure 6.3. Accumulative events as a function of number of cycles, distinguishing among emission generated in three different load ranges during selected periods of the fatigue loading of four representative specimens (results recorded with the PAC AE system). Most of the events occur at the lower load ranges.	212
Figure 6.4. Three-dimensional plots of load and location distribution histograms of events recorded for two selected specimens.	218

LIST OF FIGURES (Continued)

	<u>Page</u>
Figure 6.5. Three dimensional plots showing events as a function of load, generated during four different periods of the fatigue loading for three selected specimens. Initially, most of the events occur at the upper load range. At later stages events occur repeatedly at specific and low load levels indicating friction emission.	220
Figure 6.6. Three dimensional plots showing location distribution histograms of events generated during the same four periods of the fatigue loading and specimens shown in Figure 6.5. Initially, events occur throughout the specimens' length. At later periods, events occur repeatedly at the same locations indicating friction emission.	226
Figure 6.7. Acoustic emission event intensity and location distribution histograms for all the events accumulated during selected periods of the fatigue loading for four specimens. These distributions depend primarily on laminate configuration, dynamic stress amplitude, and the duration of the fatigue loading.	232
Figure 6.8. Intensities of events as a function of far-field applied stress for all the events accumulated during the same periods of the fatigue loading and specimens shown in Figure 6.7. Events occur throughout the entire load range. High intensity events occur only at the upper load range.	234
Figure 6.9. Intensities of events as a function of number of cycles for all the events accumulated during the same periods of the fatigue loading and specimens shown in Figures 6.7 and 6.8. Rate of events decreases with number of cycles.	236
Figure 6.10. Three-dimensional plots of amplitude distribution histograms of events recorded for the same two specimens shown in Figure 6.4.	238
Figure 6.11. Three dimensional plots showing amplitude distribution histograms for all the events generated during the same periods of the fatigue loading and specimens shown in Figures 6.5 and 6.6. High amplitude events occur primarily during the initial periods of the fatigue loading. During the later periods most of the events are of low amplitude.	239
Figure 6.12. Intensities of events as a function of far-field applied stress for all the events accumulated during the same four periods of the fatigue loading and specimen shown in Figures 6.11a to 6.11d. Events occur throughout the entire load range. High intensity events occur only at the upper load range.	245

LIST OF FIGURES (Continued)

		<u>Page</u>
Figure 6.13.	Intensities of events as a function of far-field applied stress for all the events accumulated during the same four periods of the fatigue loading and specimen shown in Figures 6.11e to 6.11h. Events occur throughout the entire load range. High intensity events occur only at the upper load range.	253
Figure 6.14.	Acoustic emission event intensity and location distribution histograms for all the events accumulated during the same periods of the fatigue loading and specimen shown in Figures 6.11a to 6.11d. All distributions vary with the progression of the fatigue loading.	261
Figure 6.15.	Acoustic emission event intensity and location distribution histograms for those events shown in Figure 6.14d that have four specific amplitude ranges. Events of specific amplitudes correlate with the other three intensities and they occur at specific locations.	263
Figure 6.16.	Accumulative events as a function of number of cycles, distinguishing among emission generated in three different load ranges during three consecutive periods of the fatigue loading of a $[0_2/90_2/0]_s$ laminate.	265
Figure 6.17.	Acoustic emission event intensity and location distribution histograms and intensities of events as a function of far-field applied stress for all the events accumulated during the same periods of the fatigue loading and specimen shown in Figure 6.16. Events occur throughout the entire load range. High intensity events occur only at the upper load range.	267
Figure 6.18.	Acoustic emission event intensity and location distribution histograms for events accumulated during the same periods of the fatigue loading and specimen shown in Figures 6.16 and 6.17: (a) events accumulated at the upper part of the load range; and (b) events accumulated at the lower part of the load range. Friction emission threshold (FRET) values can be assigned to friction generated emission.	270
Figure 6.19.	Acoustic emission event intensity and location distribution histograms and intensities of events as a function of far-field applied stress for all the events accumulated during the two selected periods of the fatigue loading and for the same specimen shown in Figures 6.11g and 6.11h. Events occur throughout the entire load range. High intensity events occur only at the upper load range.	273

LIST OF FIGURES (Continued)

	<u>Page</u>
Figure 6.20. Acoustic emission event intensity and location distribution histograms for events accumulated during the same two periods of the fatigue loading and specimen shown in Figure 6.19. (a) events accumulated at the upper part of the load range; and (b) events accumulated at the lower part of the load range. Friction emission threshold (FRET) values can be assigned to friction generated emission.	275
Figure 6.21. Acoustic emission event intensity and location distribution histograms and intensities of events as a function of far-field applied stress for all the events accumulated during three consecutive periods of the fatigue loading for the same specimen shown in Figure 6.18 at a lower dynamic stress amplitude. Events occur throughout the entire load range. All events are of low intensity indicating emission generated solely by grating.	277
Figure 6.22. Acoustic emission event intensity and location distribution histograms and intensities of events as a function of far-field applied stress for the same specimen and the same four 100-cycle periods of the fatigue loading shown in Figures 6.3e to 6.3h: (a) (c) (e) and (g) for events accumulated at the upper part of the load range; and (b) (d) (f) and (h) for events accumulated at the lower part of the load range. Friction emission threshold (FRET) values can be assigned to friction generated emission.	280
Figure 6.23. Acoustic emission event intensity and location distribution histograms and intensities of events as a function of far-field applied stress for events accumulated during a 50-cycle period of the fatigue loading showing: (a) and (b) all the events accumulated; (c) and (d) events accumulated at the upper and the lower parts of the load range, respectively; (e) and (f) events of amplitude range of 75 dB to 80 dB. Results show effect of loading frequency and state-of-damage on the intensity of friction emission.	284
Figure 6.24. Intensities of events as a function of far-field applied stress for all the events accumulated during four selected periods of the fatigue loading for the same specimen shown in Figures 6.2a and 6.2b. High intensity events occur throughout the lower load range showing the effect of loading frequency and state-of-damage on the intensity of friction emission.	287

LIST OF FIGURES (Continued)

	<u>Page</u>
Figure 6.25. Acoustic emission event intensity histograms and intensities of events as a function of far-field applied stress for all the events accumulated during the first 10,000-cycle period of the fatigue loading of the same specimen shown in Figures 6.4a, 6.4c, and 6.10a. High intensity events occur also at the lowest load range, indicating the occurrence of trains of events.	288
Figure 6.26. Three-dimensional plots of load and location distribution histograms of events recorded for the same specimen and fatigue period shown in Figure 6.3c. Results show that emission is generated repeatedly at specific load levels and at specific sites along the specimen.	289
Figure 6.27. Three-dimensional plots of location and load distribution histograms of events generated within the location range of 30-42 percent of the specimen's gage length shown in Figure 6.26. Events which are generated at a specific location are also generated at specific load levels.	290
Figure 6.28. Three-dimensional plots of location distribution histograms of events generated within the location range of 30-42 percent of the specimen's gage length: (a) detailed plot of the distribution shown in Figure 6.27a; (b), (c), and (d) location distribution histograms of the events generated within three specific different location ranges.	291
Figure 6.29. Three-dimensional plots of load distribution histograms of events generated within the location range of 30-42 percent of the specimen's gage length: (a) load distribution histograms of the events shown in Figure 6.28a; (b), (c), and (d) load distribution histograms of the events generated within the three specific location ranges shown in Figures 6.28b, 6.28c, and 6.28d, respectively. Events which are generated at a specific location are also generated at specific load levels.	293
Figure 6.30. Three-dimensional plots of load and location distribution histograms of events generated within 60-68 percent of the dynamic stress amplitude shown in Figure 6.26b. Events which are generated at a specific load level are also generated at specific sites along the specimen.	295

LIST OF FIGURES (Concluded)

	<u>Page</u>
<p>Figure 6.31. Acoustic emission event intensity and location distribution histograms and intensities of events as a function of far-field applied stress for all the events accumulated within: (a), (b), and (c) the three location ranges shown in Figures 6.28b, 6.28c, and 6.28d, respectively; (d) and (e) the two load ranges shown in Figure 6.30a and 6.30b respectively. Events which are generated repeatedly at the same location and load ranges are all of specific and low intensities.</p>	297
<p>Figure 6.32. Accumulative events as a function of number of cycles, distinguishing among emission generated in three different load ranges (curves No. 1-3) and derived damage (DD) curve for all the events generated (curve No. 4) during selected periods of the fatigue loading of three representative specimens. The amount of emission caused by actual damage accumulation is significantly smaller than the total emission generated during fatigue loading.</p>	302
<p>Figure 6.33. Accumulative events of four different amplitude ranges (curves No. 1-4) and derived damage (DD) curve for all the events generated (curve No. 5) plotted as a function of number of cycles for the same three specimens and fatigue periods shown in Figure 6.32. The number of "damage events" is similar to that of high amplitude events.</p>	308
<p>Figure 6.34. Location distribution histograms of events recorded during the first quasi-static load cycle and during the subsequent first 50 cycles of the fatigue loading for the same specimen shown in Figures 6.3e, 6.5i, and 6.6i. The plots are for: (a) only the events generated by damage; and (b) all the events generated (see curves No. 4 and 1 in Figure 6.32h, respectively).</p>	314
<p>Figure 6.35. Accumulative events as a function of far-field applied stress of events generated during three post-fatigue quasi-static loadings of a [0/90₂/0]_s laminate subjected to the loading sequence shown in Figure 6.1e: (a), (b), and (c) events generated during each of the three loadings; and (d) comparison among the three loadings. Results show that fatigue loading has a delay effect on the emission initiation load and the rate of events accumulation.</p>	316
<p>Figure 6.36. Intensities of events as a function of far-field applied stress for all the events accumulated during the three post-fatigue quasi-static loadings shown in Figure 6.35: (a)-(d) first loading; (e)-(h) second loading; and (i)-(l) third loading. Loading sequence is shown in Figure 6.1e. With increasing damage larger is number of low intensity events.</p>	318

LIST OF TABLES

		<u>Page</u>
TABLE 1.	Laminates Stacking Sequence and Nomenclature	25
TABLE 2.	Test Matrix (Static Loading)	32-34
TABLE 3.	Test Matrix (Fatigue Loading)	35-36
TABLE 4.	Static Tests (Double-Edge Notched Specimens)	37
TABLE 5.	Quasi-Static Loading/Unloading Tests (Transverse Cracks Measurements)	38
TABLE 6.	Constant Load Tests (Hold Load)	39
TABLE 7.	Spike Tests (Fatigue Loading)	39
TABLE 8.	Stiffness and Strength Results	41-42
TABLE 9.	Average Stiffness and Strength Results	43
TABLE 10.	Effect of 0° Ply Volume Fraction on Average Stiffness and Strength Values	43
TABLE 11.	Transverse Cracks Results	49-50
TABLE 12.	Accumulated Number of Events During Monotonic Loading to Failure	57
TABLE 13.	Number of Events Accumulated Within Different Amplitude Ranges	66
TABLE 14.	Effect of Loading Rate	73

I. SUMMARY

The main objective of this research program was to determine the applicability of the acoustic emission (AE) technique to detect and locate damage initiation, monitor its progression and accumulation and to identify the major modes of damage associated with the failure process in graphite/epoxy laminates. For this purpose a comprehensive experimental testing and examination program has been performed. In addition to the acoustic emission, four additional nondestructive examination (NDE) techniques were employed as well, namely, X-radiography, optical observations, acousto-ultrasonics, frequency response, and two destructive techniques, namely, depleting and scanning electron microscopy. Special efforts were directed toward establishing the correlation between the different destructive and non-destructive techniques and the AE results. Emphasis has been placed on establishing the appropriate testing procedure and data analysis methodology for monitoring AE in the subject material. Failure mechanisms and processes have been investigated and micro- and macro-failure modes have been studied.

The material tested in this program was cross-ply graphite/epoxy AS4/3502 laminates. Six pairs of different laminate configurations were studied, having different stacking sequences and containing different ratios of ply thickness. Each pair included one laminate with external 90° plies and one with external 0° plies, e.g. $[90_2/0_2/90]_s$ and $[0_2/90_2/0]_s$, respectively. The features and characteristics of the acoustic emission information and the interpretation of the results depend upon the type of composite system being tested, the laminate configuration, quality of fabrication, mechanical properties, fracture behavior and the dominant failure modes. Therefore, it is imperative that this information be available before acoustic emission data can be properly assessed.

Consequently, the test program included the measurement of axial stiffness, fracture strength, notched strength, and the monitoring of failure mechanisms and processes. For the latter, the number of transverse cracks in unnotched and notched specimens was measured during quasi-static loading and the extent of matrix splitting and delamination in notched specimens were measured during fatigue loading. These measurements were performed optically in real-time via a high magnification (150X) closed circuit television system (CCTV) and from X-radiographs. Selected specimens were depleting and the amount of fiber breaks was determined qualitatively under the scanning electron microscope. The fracture surface morphology of selected specimens

was also examined via the scanning electron microscope.

For baseline data acoustic emission was monitored during quasi-static loading to failure in all cross-ply laminates. The purpose of this phase of the program was to determine the effect of laminate stacking sequence on the emission initiation load, rate of emission accumulated, the correlation between the actual failure processes and AE results, and effect of loading rate. Results indicate that stacking sequence strongly affects the event intensities, e.g. event amplitude, energy, duration, and counts per event. Also, stacking sequence has a significant effect on damage initiation load and on rate of damage accumulation.

Destructive and nondestructive examinations of composite laminates subjected to external loading have indicated that these materials contain a large number of cracks, both on the micro- and macro-scales. Therefore, a significant amount of emission can be generated during fatigue loading not only by damage accumulation and progression but also by the continuous friction that results from the fracture surfaces grating against each other. Consequently, in order to monitor fatigue damage progression in composite laminates by AE, the emission caused by such grating should be distinguished from that generated by actual damage growth. In this study acoustic emission was monitored during fatigue loading ($R=0.1$). Emphasis was placed on distinguishing the emission caused by new damage from friction generated emission. The distinction is based upon the load level and location of the AE events and is made by identifying the characteristic intensities of the events associated with friction. It has been determined that the event intensities associated with friction are all below certain given threshold values, defined as FRIction Emission Threshold (FRET) values. These FRET values were established by analyzing those events known to be generated by friction, (i.e. from the load level and location at which they were generated). Based on the FRET values the emission caused by actual damage could be separated from the total emission and damage accumulation curves could be established and the progression of the matrix dominated failures (i.e. matrix splitting and delamination) could be tracked. Case studies are presented in which the data analysis methodology developed in this research program has been successfully utilized to monitor damage accumulation and progression during quasi-static and fatigue loading.

It has been determined that a significant amount of emission is also generated by the grating among the newly created fracture surfaces during quasi-static loading. In most cases this friction emission exceeds that generated by new damage. The friction

generated emission can also be discriminated using the specific FRET values. Results indicate that the matrix dominated failures and fiber breakage result in middle and high range AE source intensities, respectively. Based on these results damage curves could be constructed which distinguish among the emission generated by friction, by primarily matrix dominated failures and by fiber breakage. Also, a better correspondence could be established between the matrix dominated failures and the amplitude distribution histograms of events considered to be generated primarily by damage. No such correspondence could be established from the distribution histograms of all the events generated. Furthermore, the accumulation of the "damage events" was compared with the actual accumulation of the number of transverse cracks during quasi-static loading and an excellent qualitative correlation has been established.

Based on the analysis of the events which are generated primarily by damage formation, the actual extension of the damage could be correlated with the AE results. For this purpose, measurements of the actual damage progression (made either from X-radiographs or through high magnification (150X) optical observations) were compared with the location distribution histograms (L.D.H.) of the events caused only by damage. From such L.D.H., the extent of the "damaged zone" could be measured. Comparisons between the "damaged zone" based on L.D.H. of "damage events" and the actual extension of the damage (matrix splitting and delamination) during fatigue loading indicate that an excellent correlation can be established between the actual progression of the damage and the L.D.H. of "damage events". Also, the extension of the "damaged zone" which contains primarily matrix transverse cracks could be tracked during quasi-static loading. In other words, the AE data analysis methodology employed in this study can clearly be applied for tracking the progression of damage. No such conclusions could be drawn from the L.D.H. of the total AE events generated.

Acoustic emission was monitored also in specimens subjected to different loading functions including: constant load (hold load); subjecting specimens to spike loads during the fatigue loading; quasi-static loading/unloading cycles incrementally increasing the load up to failure; and monotonic quasi-static loading at different loading rates. Results indicate that varying the loading function significantly affects the emission generated, as expected. Particular attention was given to the high event rate generated during either quasi-static or fatigue loading. Based on the friction generated emission a specific criterion for determining the appropriateness of the loading function could be established.

A nondestructive test technique is proposed for detecting existing damage and changes in the state-of-damage in a composite laminate by measuring its frequency response. The Frequency Response (FR) technique is based upon the introduction of constant amplitude sinusoidal waves of continuously varying frequencies through a wide band piezo-electric transmitter and measuring the frequency response of the composite laminate through an identical receiver located a distance away. The initiation, progression and accumulation of damage in the composite laminate (e.g. matrix cracks, delamination and fiber breakage) will result in changes in the laminate's frequency response. The experimental results demonstrate that the FR technique is sensitive to such internal damage, primarily in terms of amplitude attenuation, downward shift in the dominant (resonance) frequencies, and decrease in the area under the frequency response curve. The FR technique can be applied on line, and it is simple to utilize. The experimental technique and its theoretical foundation are explained and representative results obtained with cross-ply graphite/epoxy laminates subjected to quasi-static uniaxial tensile loading to failure are presented. The experimental results demonstrate that with the FR technique an excellent correlation can be established between the state-of-damage (as represented by the number of transverse cracks) and the frequency response of the subject laminate.

The acousto-ultrasonics technique has also been applied during quasi-static loading/unloading cycles, incrementally increasing the loading up to failure. The variation in the characteristics of the transmitted pulses (i.e. threshold crossings, amplitude, energy, and duration) were correlated with the state-of-damage in terms of the number of transverse cracks. The preliminary results obtained indicate that this technique is not sufficiently sensitive to this damage which is the dominant failure mode in cross-ply graphite/epoxy laminates.

II. INTRODUCTION

2.1 General:

Monitoring of acoustic emission (AE) during fatigue loading of composites has received increasing attention in recent years. Emphasis has been placed on the potential of the AE technique as a nondestructive tool to detect damage initiation and accumulation in real time. This is of particular interest both in small-scale laboratory studies on the fatigue behavior of composite laminates and in structural applications. The most commonly used nondestructive testing (NDT) techniques to date have been the ultrasonic C-scan and X-radiography for detecting primarily internal delamination and free-edge matrix cracking, respectively. Laboratory studies have focused primarily on characterizing matrix dominated failures, e.g. matrix cracking and delamination, and on their rate of accumulation and progression during fatigue loading. In order to monitor such fatigue damage, however, the conventional examination procedure is to interrupt the fatigue loading, remove the specimen from the test fixture and examine the damage using either NDT technique. Such a procedure is highly undesirable for two reasons. First, the frequent interruption and resumption of the fatigue test may affect the actual fatigue results recorded. Second, the procedure is neither cost-effective nor efficient, since in most instances, the decision as to when periodic inspections of the specimen should be performed are made arbitrarily and inspection does not necessarily follow immediately after the actual occurrence of damage initiation and/or progression. In composites, such a decision might be of the utmost importance, since damage progression and accumulation does not increase continuously, but rather intermittently. Matrix dominated damage modes, such as matrix splitting and delamination, can progress abruptly to extended distances. This characteristic of damage progression is primarily due to the brittle nature of the constituents in advanced resin-matrix (e.g. graphite/epoxy) composite systems. In addition it should be noted that while the conventional NDT techniques, such as ultrasonic C-scan and X-radiography, reveal precisely the shape, size, severity, and location of the damage, a comprehensive analysis (primarily numerical) is always required in order to determine damage criticality. This is of particular importance since the criticality of a given damage strongly depends on the specific constituent properties, laminate configuration, loading function, environment, etc.

The acoustic emission technique appears to offer a very practical procedure for detecting fatigue damage and damage growth. This NDT is particularly attractive because

of the simplicity of its application, the acquisition of data in real-time, its potential for monitoring damage initiation, progression and accumulation, for anticipating failure sites, for identifying the different failure mechanisms and determining damage criticality, and its sensitivity to nonvisual damage such as fabrication inhomogeneities, impact damage, etc. This is crucial for composite systems, since the composite material is fabricated during the manufacturing of the composite structure; thus, some means of NDT of the complete component, including data analysis in real-time is required. Also, monitoring AE during fatigue loading may indicate when a fatigue test should be interrupted for detailed inspection of the size and shape of the fatigue damage through other NDT procedures. Thus, it may serve as an early warning device, and can also indicate the location in the composite structure where detailed inspection should be made. In other words, its cost-effectiveness may be realized both in reducing the number of periodic inspections required and in the scope of the inspections themselves.

The potential of AE for providing reliable information and the ease with which it is applied in service depend largely on the AE instrumentation available. Significant improvements and modifications have been made on AE instrumentation, including features for the detection and location of defects, amplitude analysis, frequency analysis, RMS, spatial discrimination, and voltage controlled gating, among others, which are coupled with data acquisition systems to display information in real-time. The more modern systems should enable determination, not only of the existence of damage, but of the type and extent of damage, and from this information attempts could be made to infer the location of specimen failure and the probable mechanisms of failure.

In spite of the promise shown by the AE technique as an NDT procedure, and the recent advances in available instrumentation, the level of effort directed toward AE in composites is comparatively smaller than that devoted to other NDT techniques such as ultrasonic C-scan and X-radiography. Fundamental research is still very much needed to advance this field. Problems remain to be solved, however; such as the proper interpretation of the voluminous data obtained, the appropriate test methodology to be employed, and the correlation between AE results and the actual deformation characteristics and failure processes in the composite systems, among others. Before AE can be reliably applied to composites small scale laboratory testing should be conducted to obtain base-line data and to identify the parameters most relevant for evaluating existing damage, failure mechanisms, and damage criticality. Such small-scale laboratory testing should be conducted on well-defined specimens which include known internal damage and are subjected to a variety of loading functions. The resulting information will

identify the capabilities and limitations of the AE technique and establish the appropriate test methodology to be employed with AE data obtained for composite structural components. If the potential of the AE technique can be realized, it may become an important supplementary tool, both for characterizing new composite systems in laboratory testing and ultimately for assessing the structural integrity of composite structures.

The applicability of the AE technique to composites also requires a thorough understanding of the failure mechanisms in the different composite systems, of the AE instrumentation, testing procedures, and of the different data analysis procedures. This Section briefly reviews some of these aspects, establishing the foundations, rationale, and background from which this research program has been executed.

2.2 Objectives for Employing the Acoustic Emission Technique in Composites:

Among the major objectives of research studies on the acoustic emission in composite materials are the detection of damage initiation, the location of the source of damage and of existing non-visual damage (e.g. impact damage), monitoring damage accumulation, tracking damage progression, determining material quality and damage severity, and identifying the major failure mechanisms and processes. The attractiveness of the AE technique results from these multiple applications and the fact that results can be obtained in real-time. Significant efforts have been spent during the past two decades on the applicability of AE as a nondestructive testing technique for composite materials. Most of the studies are basic research in small scale laboratory testing, with limited efforts being made toward the testing of large aircraft and aerospace structures.

Each of the seven objectives listed above has been extensively addressed with varying success. The detection of damage initiation is relatively the simplest task. It has been repeatedly shown that by recording the number of events, counts or count rate, the level of external stimulation at which damage initiates can be easily and precisely determined in real-time (e.g. applied stress during proof loading, cycle number during fatigue loading, time during creep test, etc.). Attempts to locate a specific source of damage initiation, or existing non-visual damage, have met with mixed success. The difficulties arise primarily from the anisotropic characteristics of the composite, wave dispersion and attenuation, and the multiple and simultaneous sources of emission in composites (local stress raisers such as fiber ends, voids, etc.). The monitoring of damage accumulation has relied primarily upon accumulated AE events. Relatively little has

been done to correlate the accumulated emission with observed accumulation of actual damage. Similarly, relatively few efforts have been directed toward the tracking of damage progression. This latter issue can be addressed only when damage can be confidently located. The quality of the subject material and/or the severity of damage have been addressed primarily with regard to the validity of the Kaiser and Felicity effects, which is discussed in Section 2.3.

A major challenge in the application of the AE technique has been the identification of specific failure mechanisms and the monitoring of failure processes in composites subjected to external stimulation. The approach to date has been to seek a correspondence between the AE event intensities and the different modes of failure which are known to occur in a composite laminate. The event intensities studied are primarily the events amplitude, duration, energy, and counts per event. More sophisticated data analyses of the AE waveforms, frequency spectra, etc., have been performed as well. However, the great majority of studies attempt to correlate modes of failure with the event amplitude and, to a lesser degree, with the event energy and its duration. The event amplitude has received most of the attention for two reasons: (1) it is relatively simple to measure; and (2) it was suggested during the early stages of research into AE in composites that a relatively simple correspondence exists between the three major modes of failure (matrix cracking, delamination and fiber failure) and the low, middle and high AE event amplitude levels, respectively. Consequently, the work of many researchers has addressed the details of this correspondence.

2.3 Summary of Representative Research:

The acoustic emission technique has received attention for a variety of practical and research applications, such as leak monitoring, metal working, geotechnical and petrochemical applications, corrosion cracking and fatigue, offshore applications, etc. Researchers have more recently become interested in the applicability of AE to composite structures, for example, in the vessels and pipes made of fiber-reinforced plastics used by the chemical industry. Although some research has been directed toward the advanced composites used in aerospace applications, this area is still in its infancy. One area in which AE shows promise is in the evaluation of nonvisual damage in composites. Such damage is crucial in composite systems and an NDT technique is needed which can detect, locate and evaluate damage severity and track damage progression and accumulation. Surprisingly few studies have systematically addressed the potential of AE for these applications.

A large amount of research has recently focused on the viability of AE as an NDT technique for composite materials. Because of the variety of issues to be addressed in any characterization of composite materials, i.e. not only the validity of the test technique in question, but also the numerous materials systems and laminate configurations to be examined and the validity of the experimental test procedures and data analysis methodologies for their proper characterization, research into the application of AE to composite material evaluation has encountered difficulties in establishing quantitative conclusions. Generally, however, all the reports to date have reached favorable conclusions as to the potential of AE for detecting damage and monitoring damage growth in various composite systems.

Acoustic emission has been monitored during loading of various fiber-reinforced plastics (FRP) structures, e.g. filament-wound pressure vessels [1-3], bottles [4], and FRP pipes and tanks [5]. The effect of composite manufacturing processes (e.g. curing process) on AE results has been addressed as well [6]. Results indicate that the cool-down rate has an effect on internal damage. Several other investigations into the effect of manufacturing processes on AE results have reached similar conclusions as to the high sensitivity of this technique to the initiation of internal damage.

The AE results for damage around loaded holes in graphite/epoxy composites indicate the potential for using AE to detect damage as it occurs during loading [7]. Results on graphite/epoxy laminates demonstrate that the amplitude distribution technique, using counts as an indicator of signal amplitude, could be used to distinguish fiber fracture from matrix cracking [7]. Deformation and fracture studies in graphite/epoxy composite [8-10], boron/epoxy [11] and glass/epoxy [12-14] have also received wide attention.

Anticipation of failure in graphite/epoxy $[0/\pm 45]_s$ laminate was addressed in [9], showing that a sudden dip in AE count-rate occurs prior to failure. This dip is attributed to the failure process of the laminate, i.e., the in-plane shear failure of the $\pm 45^\circ$ plies. This dip in AE count-rate was then followed by a sudden increase in count-rate as the 0° failed just prior to catastrophic fracture. That study attributed in-plane shear deformation in the 45° plies with being the primary source of emission.

Monitoring of AE during fatigue loading of composites has been investigated in [15-20]. Acoustic emission was monitored during strain and load controlled fatigue tests of angle-ply boron/aluminum and boron/epoxy [16]. AE results were correlated with

dynamic compliance and the study concluded that a good correlation could be established between the amount of AE and amount of damage, as well as between rate of emission and rate of damage development. In order to eliminate emission generated by fretting (friction) when significant delamination has developed, the AE signal can be gated so that emission is recorded "only during the top half of the loading cycles". The use of such a gating technique can result in a better agreement between the amount and rate of emission and the extent and rate of overall damage [16].

Relatively little work has been conducted so far to monitor AE in impact-damaged composites [21] or in the specimens which contain artificially induced delamination [22]. The study in [21] on graphite/epoxy laminate showed that impact damage could be detected and that the impact-damaged region could be located during a proof-test to approximately 20 percent of ultimate strength, although the damage could not be located visually. The work conducted in [22] showed that flawed specimens could be distinguished from unflawed specimens through the amplitude distribution technique. Estimation of residual strength in composites (glass/epoxy and graphite/epoxy) through AE has been attempted in [23]. In this study the effect of defects on AE results and the correlation between AE results and residual strength have been studied. Two types of artificial defects were introduced: (1) breaking a very small number of fibers, which significantly affected strength (by 40 percent); and (2) delamination in the fiber direction, which had little, if any effect on strength. Both types of defects resulted in a significant change in AE counts when compared with non-defective specimens.

The concept of the Kaiser Effect [24]* has been applied to composites to provide a criterion for sorting or grading pressure vessels made of Kevlar-49/epoxy and used as rocket motor chambers [25]. Those chambers which generated high AE activity in the "Kaiser Effect Zone" demonstrated lower performance than those with little or no activity in that zone. The premature failure correlated with a high number of counts, early onset of emission and early high amplitude emissions. A comparison among various chambers indicated that such parameters can provide an acceptance/rejection criterion for this structure for propellant loading [25]. The existence or nonexistence of the Kaiser Effect in composites has been addressed in numerous works, e.g. [5, 25-31]. Although conflicting results have been obtained, most works show a breakdown of the Kaiser Effect. As a result, attempts have been made to use this early initiation of acoustic

* The Kaiser Effect refers to "the immediately irreversible characteristic of acoustic emission phenomenon resulting from an applied stress. If the effect is present, there is little or no acoustic emission until previously applied stress levels are exceeded" [24].

emission in composites (termed the "Felicity Effect" in the literature) to quantify damage severity, and the concept of the Felicity Ratio (i.e. the ratio of the load at onset of emission to the maximum previously applied load) [5, 31] has been introduced as a measure of damage severity. The effect of strain rate on AE results for unidirectional glass/epoxy and graphite/epoxy has been studied in [32]. For glass/epoxy, a slower loading rate resulted in higher AE activity. For graphite/epoxy, no effect of strain rate on AE results was found [32].

Additional research results on AE in a variety of composite systems are reported in the proceedings of two symposia organized by the Committee on Acoustic Emission from Reinforced Plastics (CARP) of the Society of Plastic Industry Inc. [33-34], in the Proceedings of the International Acoustic Emission Symposia organized by the Japanese Society for Non-Destructive Inspection (JNSDI), e.g. [35-37], and in the Proceedings of the Acoustic Emission Working Group (AEWG), e.g. [38]. Review of the numerous works reported in these proceedings and in references therein (which is beyond the scope of this summary) clearly indicate the many advantages in using the AE technique for monitoring damage in composites.

This short review of the recent studies into the applicability of the AE technique to composite materials primarily demonstrates the amount of research that must yet be performed before AE can be confidently used to assess the structural integrity of structures made of a new composite system. Small scale laboratory testing for base-line data should be conducted on well-defined specimens which include known damage.

2.4 Failure Processes in Graphite/Epoxy Laminates Under Quasi-Static and Fatigue Loading:

The acoustic emission technique can be confidently applied to composites provided that a thorough understanding of the failure mechanisms and processes in the different composite systems is established. This is of particular importance when a correspondence between the AE results and a specific mode of damage is sought. Because of the multiplicity of the modes of damage and the complexity of their interaction establishing such a correspondence is particularly difficult. Below are given typical case studies on the failure processes in graphite/epoxy laminates. It should be kept in mind that the different modes of damage are sources of emission.

The failure mechanisms and failure processes in composite laminates have been

studied extensively, both analytically and experimentally, e.g. [39-45]. Numerous results have been reported analyzing damage initiation, propagation and accumulation in a variety of composite systems and laminate configurations both on the micro-scale (e.g., fiber breakage and pull-out, fiber matrix interfacial failure, matrix micro-cracking and laceration, etc.) and macro-scale (e.g., matrix cracking, delamination, etc.). Clearly, many of these failure mechanisms are coupled and or interactive. For example, broken fibers or matrix voids may serve as stress raisers causing local matrix cracking which may coalesce and create longer matrix cracks on the sublaminar scale [41]. Such matrix cracks will propagate toward the ply interface with increasing external stimulation (load, load cycles, etc.) and thus initiate delamination. This type of interaction, among many other possible "scenarios", depends on a variety of variables, intrinsic (e.g., constituents, laminate orientation and stacking sequence, fabrication procedures, etc.) and extrinsic (e.g., loading functions, environmental conditions, etc.), all of which affect the structural performance of the subject laminate [41].

Recently, the issue of sublaminar transverse matrix cracking and delamination and their interaction has also received special attention, e.g. [39-45]. The effects of laminate configuration, stacking sequence, ply thickness and other variables have been investigated experimentally and analytically and the damage sequence has been studied. Generally it was found that in most cases, transverse cracking in the 90°-layers occurs prior to delamination [39-42] and it has been shown [39] that many of these matrix cracks initiate at matrix voids. Photomicrographs and/or replicas of the specimen's free edges reveal that the delamination in a variety of laminates is not necessarily confined to an interface. The interaction of transverse cracking, cracks which initiate randomly at matrix voids, and delamination causes quite an irregular fracture surface (i.e. delamination) and follows a completely random path that is contained by the two interfaces of the 90°-layer [39-45]. The delamination itself progresses abruptly and intermittently [39-40] with increasing load, although it might not extend across the specimen's width [40]. Under fatigue loading delamination may separate the specimens along the delaminated interfaces [39-40].

The thickness of the 90° layer can affect the failure process. When the 90° layer is thin, as it is in $[\pm 25/90_n]_s$ graphite/epoxy laminate, (discussed in [41]), edge delamination can be induced prior to the transverse cracking that occurs only at high load levels (e.g. for $n = 1/2, 1$); while for thicker 90° layers (e.g. $n > 2$) the sequence is reversed [41].

The effect of the 90° ply thickness on the initiation of transverse cracking under

uniaxial tensile quasi-static and fatigue loading has been investigated in detail in [41-43]. In all cases it was determined that under quasi-static loading, the load at which transverse cracking initiates is strongly influenced by the thickness of the 90° layer. The thinner the layer, the higher the initiation load and the higher the crack density. The only exception is in the case of $n = 1$, where "failure of 0° layer at high load interrupted the development of more transverse cracks," Wang [41]. Similar observations were reported in [43], where this relationship is attributed to the constraining effect of the neighboring 0° layers. The transverse ply cracking strain is also affected by the thickness of the $[0_4/90_8/0_4]_T$ and may decrease from 0.0065 to 0.003 for $[0_4/90_n/0_4]_T$ and $[0_4/90_8/0_4]_T$, respectively, graphite/epoxy laminates [42]. It was concluded that "it is the total strain energy trapped in the 90° -layer which determines the onset of cracking, not the in-situ tensile stress" [44].

Under tension-tension fatigue loading the effect of the transverse ply thickness is also significant. Comparison between the rate of accumulation of transverse cracks in $[0_2/90_2]_S$ and in $[0_2/90_3]_S$ graphite/epoxy laminates indicates that the thicker the transverse ply is, the lower the cycle number at which transverse cracking initiates [42]. It should be noted that these cracks occur at fatigue stress levels which are much below the quasi-static threshold levels at which they appear. Similar tests were conducted on $[0_4/90_n/0_4]_T$ ($n = 1, 2, 4, 8$) graphite/epoxy laminates [44] and it was found that transverse matrix cracking occurs during fatigue loading at strain levels much below the threshold static strain levels and, again, the thicker the 90° -layer is, the earlier matrix cracking occurs.

The effect of the 90° ply thickness on the failure process, sequence of damage progression, and on the final failure mechanisms has been studied extensively by Wang [41] for a variety of graphite/epoxy laminates. For laminates with thick 90° layers, e.g., $[0_2/90_8]_S$ and $[\pm 25/90_8]_S$ the final failure is triggered by fiber matrix interfacial failure (splitting) along the 0° and $\pm 25^\circ$ fibers, respectively. No such splitting was observed in the case of thin 90° -layers, e.g. $[0_2/90_2]_S$ and $[\pm 25/90_2]_S$ [41]. Moreover, while the $[0_2/90_2]_S$ laminate exhibits matrix cracking at load levels as high as 80 percent of the ultimate load and with no edge delamination, the $[0_2/90_8]_S$ laminate exhibits transverse cracking and local delamination at 75 percent of the ultimate load and significant splitting that initiates in the vicinity of the transverse cracks already at 85 percent of the the ultimate load. The final failure load of the $[0_2/90_8]_S$ laminate is approximately 82 percent of that recorded for $[0_2/90_2]_S$ laminate [41]. In other words, the thickness of the 90° layer may have a significant effect on the load at which transverse cracking, delamination, and

failure of the load-carrying lamina initiates.

This brief description of the failure mechanisms and processes in graphite/epoxy laminates subjected to uniaxial quasi-static and fatigue loading in tension is obviously not comprehensive. The subject is complex and, as mentioned previously, considerable experimental and analytical work has been published in recent years. Clearly, for a proper interpretation of the acoustic emission caused by the different modes of damage, the failure process in the different laminates should be well understood. Once a correlation between the failure process and the acoustic emission results can be established, the AE technique could be applied as a reliable nondestructive testing technique.

2.5 On The Correspondence Between Event Intensities and Modes of Failure:

As stated above, research into the correspondence between AE event intensities and composite failure mechanisms has focused on event amplitudes and, to a lesser degree, on energy and duration. In reviewing the literature one finds conflicting results reported by different researchers. Most studies have concluded, for example, that matrix cracking, delamination and fiber breakage generate emission of low, medium, and high amplitude ranges, respectively, e.g. [15, 46-51]. However, recent works have shown that fiber breakage generates low amplitude events while matrix cracking and delamination will generate medium and high amplitude events, respectively, e.g. [52-54]; while other works, e.g. [55], report that delamination generates events of amplitudes which cover most of the dynamic range of the AE system. Where event duration is concerned, results show that fiber breakage and the onset of delamination generate emission of short and medium duration while events caused by matrix cracking, splitting and massive delamination are of longer duration [52]. Much longer event durations, by order of magnitude were reported in [56] to be caused by delamination. Relatively few works report on model composites in which a single dominant mode of failure is known to occur.

This brief review presents only a few of the most recent works. The findings listed above are also argued or substantiated in many other works and referenced by the authors reviewed here. There are several reasons for the conflicting results obtained by researchers in this field. The first and most obvious problem is that the various investigations have utilized different AE instrumentations, transducer types, system gains, dead-time, or experimental set-up. Also, most research is concerned with intrinsic

comparisons rather than the absolute values of the material response. The second problem is that different investigations study different material systems, laminate configurations, specimen geometries and specimen tabbing procedures. In addition, AE results obtained by subjecting specimens to different loading functions and loading rates are reported. All these different intrinsic and extrinsic variables can significantly influence the recorded acoustic emission.

The third problem regards the multiplicity and complexity of the failure mechanisms in composites, their interaction, and their simultaneous occurrence. This issue has been studied extensively, both analytically and experimentally, as reviewed briefly in Section 2.2. Due to this complexity in the development of the different failure modes, a direct correspondence with the intensities of the AE events should be difficult to establish conclusively. Moreover, the state-of-damage is continuously changing (in terms of number of matrix cracks and splitting, number of broken fibers, interfacial failures, and delaminated areas). The damage formation that develops during loading will clearly affect the compliance of the subject laminate and thus its frequency response. Consequently, different characteristics of the stress waves will be depicted by the AE transducer in different states-of-damage, even though the modes of damage (i.e. the sources of emission) are identical.

The last important difficulty in establishing a correspondence between the AE event intensities and the failure modes is the fact that a significant amount of emission is also generated by the grating among existing fracture surfaces. When the fiber/matrix interfacial failures, matrix splitting, delaminations, and transverse cracks all occur in increasing number, a nearly infinite number of fracture surfaces are created. The emission created by the continuous grating among these fracture surfaces must first be characterized, analyzed, and properly distinguished from the emission caused by actual damage. It has been shown in [57-67] that such emission actually occurs under both quasi-static and fatigue loading in tension. Moreover, it has also been shown that in graphite/epoxy laminates the amplitude of the events caused by friction can be similar to that caused by matrix dominated failures. Thus, fundamental research is still required before this technique can be confidently used to distinguish specific failure mechanisms.

It is also of importance to realize that the AE technique is highly sensitive to damage initiation and progression. In composites, due to the multiplicity of failure mechanisms and the corresponding complexity of damage progression, a considerable amount of emission is generated. Both the micro- failures (e.g., fiber breakage, interfacial

failure, fiber pull-out, local matrix deformation, micro-cracking, etc.) and macro-failures (e.g., delamination, matrix splitting, ply failure, etc.) generate significant amounts of emission at very high rates. The system records this emission in real-time, which is one of the features which makes the AE technique attractive, but this same sensitivity causes difficulties in distinguishing among the variety of possible failure modes. The very high rate of emission generated during quasi-static loading is especially problematic, and precise acquisition is, in most cases, beyond the capability of the AE instrumentation. During fatigue loading, however, the rate of emission per load cycle is much lower (provided low loading rate is applied and damage severity is not as pronounced), and analyses of the individual AE events are much more reliable. The characteristics of damage progression and accumulation during fatigue loading are a major concern with composite materials, and it seems that the AE technique can provide viable information under such loading conditions.

2.6 Friction Emission:

Surprisingly little work has been directed toward the analysis of emission generated by the grating among existing or newly created fracture surfaces. Since a composite laminate contains a nearly infinite number of fracture surfaces, both on the micro- and macro-scale, and especially when catastrophic fracture is imminent, it should be expected that a significant amount of emission is generated by fretting. This is particularly so since damage generates emission once at the time of its occurrence, while the resulting new fracture surfaces generate emission during long periods of loading due to the continuous and repeated contact (fretting) among them.

The problem of eliminating emissions generated by friction, e.g., crack closure, has been recognized for many years in the AE studies of metals. For this purpose, a voltage controlled gating is incorporated into the AE instrumentation to screen emissions occurring within a predetermined load range of the load cycle. In composites, due to the large amount of interfacial failure, matrix cracking and delamination, the continuous fretting among existing fracture surfaces during fatigue loading may generate substantially more emissions than the newly created damage. However, because of the rapid and intermittent character of fatigue damage progression in composites, emission generated by new damage can fail to be recorded by the AE instrumentation. In such a case, the only indication of damage progression may be the sudden surge in friction-generated emission that corresponds to the sudden increase in fracture surfaces associated with the newly created damage. Consequently, emission generated by friction

can also serve to reveal fatigue damage progression.

2.7 Research Objectives:

In this research program a detailed and comprehensive experimental investigation to evaluate the AE technique as a nondestructive testing procedure for composites has been performed. In particular, emphasis was placed on identifying the major failure mechanisms, i.e. fiber breakage and matrix cracking which occur during quasi-static and fatigue loading of cross-ply graphite/epoxy laminates. The AE results were compared and correlated with other nondestructive (X-radiography and optical observations) and destructive (deplying technique and scanning electron microscopy) examinations of the failure process so that a complete evaluation can be made. In particular, the potential for detecting and locating existing nonvisual damage, as well as the potential for anticipating fracture sites were addressed. Damage accumulation during quasi-static and fatigue loading has been monitored. Efforts were made for developing the proper data analysis procedure for tracking damage progression, in particular matrix splitting and delamination. The effect of loading function on the AE results, i.e. the potential of the AE technique to determine severity of damage in composite structures subjected to simulated service load, have been determined. Particular attention was placed on monitoring the emission generated by the grating among existing fracture surfaces and on distinguishing this emission from that caused by actual damage initiation and progression. The proper testing procedure, e.g. loading function, loading rate, specimen gripping, etc., and the significance of the various AE parameters were studied. Data obtained also include strength, stiffness, and damage accumulation in terms of number of transverse cracks for the various cross-ply laminates studied. Finally, an acoustic emission data analysis methodology has been developed by which the AE data can be more reliably interpreted and correlated with the actual initiation, accumulation, and progression of damage in composite laminates when subjected to quasi-static and fatigue loading.

2.8 References:

1. M.A. Hamstad, "Variabilities Detected by Acoustic Emission from Filament-Wound Aramid Fiber/Epoxy Composite Pressure Vessels," Intl. Instrumentation Symposium, Vol. 24, 1978, pp. 419-431.
2. R.G. Liptai, "Acoustic Emission from Composite Materials," Composite Materials: Testing & Design (2nd Conference), ASTM STP 497, American Society for Testing and Materials, 1972, pp. 285-298.

3. M. Fuwa, A.R. Bunsell and B. Harris, "Acoustic Emission Studies of Filament-Wound Fibre Reinforced Rings and Pressure Vessels," *Journal of Strain Analysis*, 11, 1976, pp. 97-101.
4. M.A. Hamstad and T.T. Chiao, "Acoustic Emission Produced During Burst Tests of Filament-Wound Bottles," *Journal of Composite Materials*, Vol. 7, 1973, pp. 320-332.
5. T.J. Fowler and E. Gray, "Development of an Acoustic Emission Test for FRP Equipment," preprint 3583, ASCE Winter Convention, Boston, MA, April 1979.
6. W.W. Houghton, R.J. Shurford and J.F. Sprouse, "Acoustic Emission as an Aid for Investigating Composite Manufacturing Process," 11th Natl. SAMPE Technical Conference, Nov. 1979, pp. 131-150.
7. S.M. Freeman, C.D. Bailey, R.T. Beall and J.M. Hamilton, "Detection and Verification of Internal Fiber Fracture Around Loaded Holes in Graphite/Epoxy Composites," 11th Natl. SAMPE Conference, Nov. 1979, pp. 944-952.
8. M. Fuwa, A.R. Bunsell and B. Harris, "Tensile Failure Mechanisms in Carbon Fibre Reinforced Plastics," *Journal of Materials Science*, Vol. 10, 1975, pp. 2062-2070.
9. J.M. Carlyle, "Imminent Fracture Detection in Graphite/Epoxy Using Acoustic Emission," *Experimental Mechanics*, 1978, pp. 191-195.
10. C.B. Bailey, S.M. Freeman and J.M. Hamilton, Jr., "Acoustic Emission Monitors Damage Progression in Graphite Epoxy Composite Structure," *Materials Evaluation*, 1980, pp. 21-27.
11. J.M. Fitz-Randolph, D.C. Phillips, P.W.R. Beaumont, and A.S. Tetelman, "The Fracture Energy and Acoustic Emission of a Boron/Epoxy Composite," *Journal of Materials Science*, Vol. 7, 1972, pp. 298-294.
12. J. Brecht, H.J. Swalbe and J. Eisenblaetter, "Acoustic Emission as an Aid for Investigating the Deformation and Fracture of Composite Materials," *Composites*, October 1976, pp. 245-248.
13. J.T. Barnby and T. Parry, "Acoustic Emission from a Notched Glass-Fibre-Reinforced Polymer in Bending," *Journal of Applied Physics* 9D, 1976, pp. 1919-1926.
14. F.J. Guild, M.G. Phillips and B. Harris, "Acoustic Emission Studies of Damage in GRP," *NDT Intl.*, October 1980, pp. 209-218.
15. J.T. Ryder and J.R. Wadin, "Acoustic Emission Monitoring of a Quasi-Isotropic Graphite/Epoxy Laminate Under Fatigue Loadings," Lockheed-California and Dunegan/Endevco Co., Internal Report.
16. R.S. Williams and K.L. Reifsnider, "Investigation of Acoustic Emission During Fatigue Loading of Composite Specimens," *Journal of Composite Materials*, Vol. 8, 1974, pp. 340-355.

17. A.F. Weyhreter and C.R. Horak, "Acoustic Emission System for Estimation of Ultimate Failure Strength and Detection of Fatigue Cracks in Composite Materials," 33rd Annual Technical Conference, Reinforced Plastics/Composite Institute, The Society of Plastic Industry, Inc., Section 24B, pp. 1-5.
18. M.A. Hamstad and T.T. Chiao, "Acoustic Emission from Stress Rupture and Fatigue of an Organic Fiber Composite," Composite Reliability, ASTM STP 580, American Society for Testing and Materials, 1975, pp. 191-201.
19. R.S. Williams and K.L. Reifsnider, "Real-Time Nondestructive Evaluation of Composite Materials during Fatigue Loading," Materials Evaluation, August 1977, pp. 50-54.
20. M. Fuwa, B. Harris and H.R. Bunsell, "Acoustic Emission during Cyclic Loading of Carbons Reinforced Plastics," Journal of Applied Physics, Vol. 8D, 1975, pp. 1460-1471.
21. C.D. Bailey, J.M. Hamilton, Jr., and W.M. Pless, "Acoustic Emission of Impact-Damaged Graphite/Epoxy Composites," Materials Evaluation, May 1979, pp. 43-54.
22. J.H. Williams, Jr., and S.S. Lee, "Acoustic Emission from Graphite/Epoxy Composites Containing Interlaminar Paper Inclusions," NDT Intl., February 1979, pp. 5-7.
33. A. Rotem, "The Estimation of Residual Strength by Composites by Acoustic Emission," 23rd Natl. SAMPE Symposium and Exhibition, pp. 329-353.
24. J. Kaiser, "Untersuchungen Uber das Auftreten von Gerauschen beim Zugversuch," Dr. -Ing. Thesis, Tech. Hochschule, Munich, 1950.
25. E.C. Jessen, H. Spanheimer and A.J. DeHerrera, "Prediction of Composite Pressure Vessels Performance by Application of the Kaiser Effect in Acoustic Emission," 2nd Natl. Conference on Pressure Vessels and Piping Technology, ASME Mtg., San Francisco, 1975.
26. T.J. Fowler and R.S. Scarpellini, "Acoustic Emission Testing of FRP Equipment I," Chemical Engineering, October 1980, pp. 145-148.
27. T.J. Fowler and R.S. Scarpellini, "Acoustic Emission Testing of FRP Equipment II," Chemical Engineering, November 1980, pp. 293-296.
28. T.J. Fowler and R.S. Scarpellini, "Acoustic Emission Testing of FRP Equipment," ASME Design Conference, Chicago, May 1979.
29. F.J. Guild, D. Walton, R.D. Adams and D. Short, "The Application of Acoustic Emission to Fibre-Reinforced Composite Materials," Composites 1976, pp. 173-179.
30. J. Awerbuch, M. R. Gorman and M. Madhukar, "Monitoring Acoustic Emission During Quasi-Static Loading/Unloading Cycles of Filament-Wound Graphite/Epoxy Laminate Coupons," Materials Evaluation, Vol. 43, 1985, pp. 754-765.

31. M. Drog, "Recommended Practice for Acoustic Emission Testing of Fiberglass Reinforced Plastic Resin (FRP) Tanks/Vessels," Committee on Acoustic Emission from Reinforced Plastics (CARP), Society of the Plastic Industry (SPI), Proceedings of the First International Symposium on Acoustic Emission From Reinforced Composites, The Society of the Plastics Industry, Inc., San Francisco, CA, July 19-21, 1983, Session 4, 3:25-4:00 P.M., pp. 1-17.
32. A. Rotem, "Effect of Strain Rate on Acoustic Emission from Fiber Composites," Composites, 1978, pp. 33-36.
33. Proceedings of the First International Symposium on Acoustic Emission From Reinforced Composites, The Society of the Plastics Industry, Inc., San Francisco, CA, July 19-21, 1983.
34. Proceedings of the Second International Symposium on Acoustic Emission From Reinforced Composites, The Society of the Plastics Industry, Inc., Montreal, Canada, July 21-25, 1986.
35. Progress in Acoustic Emission I, Proceedings of the 6th International Acoustic Emission Symposium, M. Onoe, K. Yamaguchi, and T. Kishi, Edts., The Japanese Society for Non-Destructive Inspection, Susono, Japan, October 31-November 3, 1982.
36. Progress in Acoustic Emission II, Proceedings of the 8th International Acoustic Emission Symposium, M. Onoe, K. Yamaguchi, and H. Takahashi, Edts., The Japanese Society for Non-Destructive Inspection, Zao, Japan, October 23-36, 1984.
37. Progress in Acoustic Emission III, Proceedings of the 7th International Acoustic Emission Symposium, M. Onoe, K. Yamaguchi, and H. Takahashi, Edts., The Japanese Society for Non-Destructive Inspection, Zao, Japan, October 23-36, 1986.
38. Proceedings of the Second International Conference on Acoustic Emission, Lake Tahoe, Nevada, October 28-November 1, 1985, appears in the Journal of Acoustic Emission, Vol. 4, No. 2-3, April-September, 1985.
39. J. Awerbuch, "Monitoring Damage Progression through Acoustic Emission in Filament-Wound Graphite/Epoxy Laminate Coupons During Quasi-Static and Fatigue Loading," Internal Tech. Report, Hercules Bacchus, Inc., Magna, UT, Contract No. ARIB-05911, 1982.
40. K.L. Reifsnider, E.G. Hennecke II, and W.W. Stinchomb, "Delamination in Quasi-Isotropic Graphite/Epoxy Laminates," in Composite Materials: Testing and Design (4th Conf.), ASTM STP 617, American Society for Testing and Materials, 1972, pp. 93-105.
41. A.S.D. Wang, "Fracture Mechanics of Sublaminar Cracks in Composite Materials," in Characterization, Analysis and Significance of Defects in Composite Materials, AGARD Conf. Proc. No. 355, April 10-15, 1983, London U.K. pp. 15-1-15-19. Also in Composite Technology Review, Vol. 6, 1984, pp. 45-62.
42. A.S.D. Wang, P.C. Chou and S.C. Lei, "A Stochastic Model for the Growth of Matrix Cracks in Composite Laminates," in Advances in Aerospace Structures, Materials and Dynamics, ASME AD-06, 1983 Winter Annual Mtg. of the American Society of Mechanical Engineers, Boston, MA, November 13-18, 1983. Also, Journal of Composite Materials, Vol. 18, 1984, pp. 239-254.

43. M.G. Bader, J.E. Bailey, P.T. Curtis, and A. Parvizi, "The Mechanics of Initiation and Development of Damage in Multi-Axial Fiber-Reinforced Plastic Laminates," in the Proc. of the 3rd Conference on Mechanical Behavior of Materials (ICM-3), the Japan Society of Material Sciences (JSMS), 1979, pp. 227-239.
44. R.P. Harrison and M.G. Bader, "Damage Development in CFRP Laminates Under Monotonic and Cyclic Stressing," Fiber Science and Technology, Vol. 18, 1983, pp. 163-180.
45. R.Y. Kim, "A Technique for Prevention of Delamination," in Proc. of the 7th Annual Mechanics of Composites Review, AFWAL Report, AFWAL-TR- 82-4007, 1982, pp. 218-230.
46. G. Newaz, "Analysis of Mode I Delamination Damage in Unidirectional Composites Using Acoustic Emission," Proceedings of the Second International Symposium on Acoustic Emission From Reinforced Composites, The Society of the Plastics Industry, Inc., Montreal, Canada, July 21-25, 1986, pp. 12-15.
47. I. Roman and K. Ono, "Acoustic Emission Characterization of Failure Mechanisms in Woven Roving Glass-Epoxy Composites," Progress in Acoustic Emission II, Proceedings of the 7th International Acoustic Emission Symposium, M. Onoe, K. Yamaguchi, and H. Takahashi, Edts., The Japanese Society for Non-Destructive Inspection Zao, Japan, October 23-36, 1984, pp. 496-503.
48. B. Ponsot, D. Valentin, "Acoustic Emission Analysis of the Dependence of Damage Accumulation in Composites on Matrix Properties," Proceedings of the Second International Symposium on Acoustic Emission From Reinforced Composites, The Society of the Plastics Industry, Inc., Montreal, Canada, July 21-25, 1986, pp. 5-11.
49. L. Li, J.H. Zhao, "The monitoring of Damage Growth Processes in Glass Fiber Reinforced Composite by Amplitude Analyses," Proceedings of the Second International Symposium on Acoustic Emission From Reinforced Composites, The Society of the Plastics Industry, Inc., Montreal, Canada, July 21-25, 1986, pp. 90-95.
50. A. Mittelman, I. Roman, and G. Marom, "Acoustic Emission Characterization of Tensile Failure Mechanisms in Kevlar 49-Epoxy Composites," Progress in Acoustic Emission II, Proceedings of the 7th International Acoustic Emission Symposium, M. Onoe, K. Yamaguchi, and H. Takahashi, Edts., The Japanese Society for Non-Destructive Inspection Zao, Japan, October 23-36, 1984, pp. 504-509.
51. N. Sato, T. Kurauchi, and O. Kamigaito, "Fracture Mechanisms of Unidirectional Carbon-Fibre Reinforced Epoxy Resin Composite," Journal of Materials Sciences, Vol. 21, 1986, pp. 1005-1010.
52. K. Ono, "Acoustic Emission Behavior of Flawed Unidirectional Carbon Fiber-Epoxy Composites," Proceedings of the Second International Symposium on Acoustic Emission From Reinforced Composites, The Society of the Plastics Industry, Inc., Montreal, Canada, July 21-25, 1986, pp. 22-28.
53. D. Valentin, P. Bonniau, and A.R. Bunsell, "Failure Mechanism Discrimination in Carbon Fiber Reinforced Epoxy Composites," Composites, October 1983, pp. 345-351.

54. R.D. Jamison, "On the Interrelationship Between Fiber Fracture and Ply Cracking in Graphite/Epoxy Laminates," *Composite Materials: Fatigue and Fracture*, ASTM STP 907, H.T. Hahn Ed., American Society for Testing and Materials, Philadelphia, 1986, pp. 252-273.
55. M.R. Gorman, R.F. Foral, "Acoustic Emission Studies of Fiber/Resin Double Cantilever Beam Specimens," *Proceedings of the Second International Symposium on Acoustic Emission From Reinforced Composites*, The Society of the Plastics Industry, Inc., Montreal, Canada, July 21-25, 1986, pp. 104-109.
56. M.R. Gorman, T.H. Rytting, "Long Duration AE Events in Filament Wound Graphite/Epoxy in the 100-300 KHz Band Pass Region," *Proceedings of the Second International Symposium on Acoustic Emission From Reinforced Composites*, The Society of the Plastics Industry, Inc., San Francisco, CA, July 19-21, 1983, Session 6, 11:05-11:20, pp. 1-5.
57. J. Awerbuch, M. Madhukar, and M. R. Gorman, "Monitoring Damage Accumulation in Filament-Wound Graphite/Epoxy Laminate Coupons During Fatigue Loading Through Acoustic Emission," *Journal of Reinforced Plastics and Composites*, Vol. 3, 1984, pp. 2-39.
58. J. Awerbuch and S. Ghaffari, "Monitoring Progression of Matrix Splitting During Fatigue Loading Through Acoustic Emission in Notched Graphite/Epoxy Composite," in the *Proceedings of the Second International Symposium on Acoustic Emission From Reinforced Composites*, The Society of the Plastics Industry, Inc., Montreal, Canada, July 21-25, 1986, pp. 51-58. Also, *Journal of Reinforced Plastics and Composites*, Vol. 7, May 1988, pp. 245-264.
59. S. Ghaffari and J. Awerbuch, "Monitoring Acoustic Emission in Impact-Damaged Composites," in the *Proceedings of the Second International Symposium on Acoustic Emission From Reinforced Composites*, The Society of the Plastics Industry, Inc., Montreal, Canada, 1986, pp. 120-125.
60. W.F. Eckles and J. Awerbuch, "Monitoring Acoustic Emission in Cross-Ply Graphite/Epoxy Laminates During Fatigue Loading," in the *Proceedings of the Second International Symposium on Acoustic Emission From Reinforced Composites*, The Society of the Plastics Industry, Inc., Montreal, Canada, July 21-25, 1986, pp. 78-84. Also, *Journal of Reinforced Plastics and Composites*, Vol. 7, May 1988, pp. 265-283.
61. J. Awerbuch and W.F. Eckles, "Detection of Failure Progression in Cross-Ply Graphite/Epoxy Through Acoustic Emission," in the *Proceedings of International Symposium on Composite Materials and Structures*, T.T. Loo and C.T. Sun Edts., Beijing, China, June 10-13, 1986, pp. 889-898.
62. J. Awerbuch, and S. Ghaffari, "Effect of Friction emission on Monitoring Damage in Composite Laminates through Acoustic Emission," in *Progress in Acoustic Emission III*, The Japanese Society of NDI, 1986, pp. 638-652.
63. J. Awerbuch, and S. Ghaffari, "Tracking Progression of Matrix Splitting During Static Loading Through Acoustic Emission in Notched Unidirectional Graphite/Epoxy Composites," in *Progress in Acoustic Emission III*, The Japanese Society of NDI, 1986, pp. 575-585.

64. J. Awerbuch, "On Monitoring Damage Progression in Composite Laminates Through Acoustic Emission," Seiken Symposium IIS, University of Tokyo, October 27-28, 1986, pp. SI-(6)-1-SI-(6)-31.
65. J. Awerbuch, "On the Identification of Failure Mechanisms in Composite Laminates Through Acoustic Emission," in the Proceedings of Acoustic Emission Deutsche Gesellschaft fur Metallkunde E.V. (DGM), Bad Nauheim, Federal Republic of Germany, 19-20 March 1987, pp. 47-58.
66. J. Cohen and J. Awerbuch, "Tracking Progression of Delamination in Model Graphite/Epoxy Composites Through Acoustic Emission During Quasi-Static Loading," MEM CML-8702, Drexel University, October 1987 (to be published in the Journal of Composite Materials).
67. J. Awerbuch, B. Gilbert, and J. Cohen, "Experimental Investigation on Delamination Progression and Acoustic Emission in Arall Laminate," Drexel University Technical Report, MEM CML-8701, 1987.

III. EXPERIMENTAL PROCEDURE

3.1 Summary:

The main objective of this research program is to determine the applicability of the acoustic emission technique to detect and locate damage initiation, monitor its progression and accumulation and to identify the major modes of damage associated with the failure process in composites. For this purpose a comprehensive experimental testing and examination program has been performed. In addition to the acoustic emission technique, four additional nondestructive examination (NDE) techniques were employed as well, namely; X-radiography, optical observations, acousto-ultrasonics, frequency response, and two destructive techniques, namely, depleting and scanning electron microscopy. Special efforts were directed toward establishing the correlation between the different destructive and non-destructive techniques and the acoustic emission results. Emphasis has been placed on establishing the appropriate testing procedure and data analysis methodology for monitoring acoustic emission in the subject material. Failure mechanisms and processes have been investigated and micro- and macro-failure modes have been studied.

3.2 Material and Specimen Preparation:

The material tested in this program was cross-ply graphite/epoxy AS4/3502 laminates. Six pairs of different laminate configurations were studied, where each pair included one laminate with external 90° plies and one with external 0° plies, e.g. $[90_2/0_2/90]_s$ and $[0_2/90_2/0]_s$, respectively. Laminate stacking sequences and nomenclatures are listed in Table 1. The lamina properties are [1]: longitudinal stiffness = 133.1 GPa (19.3 MSi); transverse stiffness = 8.96 GPa (1.3 MSi); longitudinal shear modulus = 5.72 GPa (0.83 MSi); and major Poisson's ratio = 0.33. The plates were fabricated at the Wright Research and Development Center (WRDC), Flight Dynamics Laboratory (FDL). Panels were cured using the prepreg supplier recommended cure cycle. The panels were trimmed to a width equal to the specimen length. Aluminum end tabs, 38 mm (1.5 inch) in width, were bonded along the trimmed panels. Specimens were machined and cut with a diamond impregnated wheel into 25 mm (1.0 inch) wide and 200 mm (8.0 inch) long parallel sided tensile coupons. In selected specimens double-edge notches (see schematic on page 38) were introduced using a diamond impregnated wheel. The location of each specimen on each of the plates was recorded so that designation of specimens according to loading function, type of experiment, etc.,

TABLE 1. LAMINATES STACKING SEQUENCE AND NOMENCLATURE

PLATE NO.*	LAY-UP	% 0°	PLATE NO.*	LAY-UP	% 0°
5C 5D	[0 ₂ /90 ₂ /0] _s	60	3A 3B	[90 ₂ /0 ₂ /90] _s	40
3C 3D	[0 ₂ /90 _{1/2}] _s	80	4A 4B	[90 ₂ /0 _{1/2}] _s	20
6C 6D	[0/90/0/90 _{1/2}] _s	57	5A 5B	[90/0/90/0 _{1/2}] _s	43
4C 4D	[0 ₂ /90/0] _s	75	6A 6B	[90 ₂ /0/90] _s	25
8C 8D	[0 ₂ /90] _s	67	7A 7B	[90 ₂ /0] _s	33
7C 7D	[0/90 ₂ /0] _s	50	8A 8B	[90/0 ₂ /90] _s	50

* Number indicates laminate configuration and letter indicates plate number.

could be made randomly to ensure reliable test results.

3.3 Mechanical Test Program:

Five different loading functions were applied in this program, all uniaxial in tension. They are:

1. quasi-static monotonic loading to failure;
2. quasi-static loading/unloading, incrementally increasing the load up to failure;
3. constant amplitude tension-tension fatigue loading ($R = 0.1$) at different maximum dynamic stresses (ranging from 30 percent to 95 percent of static ultimate) and at different load frequencies (ranging from 0.001 Hz to 10.0 Hz).
4. constant stress at different percentage of ultimate (ranging from 30 percent to 95 percent of static ultimate).
5. constant amplitude tension-tension fatigue loading ($R = 0.1$) subjecting the specimens to single cycle spike loads of different magnitudes (ranging from 60 percent to 95 percent of static ultimate) and at different load frequencies (ranging from 0.001 Hz to 10.0 Hz).

Through the first loading function the basic mechanical properties of axial stiffness and strength of the different laminates were determined, acoustic emission was monitored and results were analyzed, all of which served as base line information for the fatigue test studies. The second loading function was applied in order to determine the rate of damage initiation and accumulation (in terms of number of transverse cracks in the 90° plies, matrix splitting and delamination), and its effect on the acoustic emission results. In this loading function the acousto-ultrasonics and the frequency response techniques were applied and results were correlated with the state-of-damage of the subject material. Primary emphasis was placed on monitoring acoustic emission during fatigue loading where special efforts were placed on identifying the characteristics of the emission generated by the grating among existing fracture surfaces. The fourth and fifth loading functions were applied in order to better understand the correlation between the acoustic emission results and the state-of-damage.

All test were performed on a closed loop servo-hydraulic Instron testing machine (Model 1331). The quasi-static tests were carried out under stroke-control mode at a rate of 0.05 mm/min (0.002 in/min). Each specimen was instrumented with an extensometer

to obtain the global stress-strain curves. The extensometer was also used for the notched specimens in order to obtain "global" load-displacement curves and compliances. Steps were taken to ensure loading axiality. For all specimens, initial stiffness, stress-strain curves, load-displacement curves, and strength data were recorded.

All quasi-static test results were recorded on X-Y-Y recorders to monitor the test progression in real-time. The testing system is also interfaced with a data acquisition system (PDP 1103 Model MINC-11 of Digital Equipment Corporation). Post-test analyses provide complete load-displacement and stress-strain curves and mechanical properties such as strength and stiffness. Print-outs of stress-strain data in tabular form are also available.

The fatigue tests were carried out under load control mode at constant amplitude tension-tension ($R = 0.1$) loading. Initial loading (first cycle) was carried out quasi-statically under stroke-control mode to obtain additional acoustic emission results and load-displacement curves. Similarly, the initial loading for the fourth and fifth loading functions listed above, were all carried out quasi-statically under stroke-control mode.

3.4 Monitoring Acoustic Emission:

The acoustic emission (AE) technique has been utilized for detecting and locating existing damage, monitoring damage growth and accumulation during quasi-static and fatigue loading, determining the severity of damage and identifying the major failure mechanisms and processes.

In this program, attention has been placed on monitoring acoustic emission during quasi-static and fatigue loading as an early warning device for damage initiation and progression. The acoustic emission results also indicate the load level or cycle number at which crack growth initiates, its location, and the primary source of emission. From this information, decisions could be made as to the frequency with which other non-destructive techniques must be applied (e.g. X-radiography, and ultrasonics) during the tests to determine the actual state-of-damage.

Special attention was placed on identifying the major failure mechanisms and failure processes in real-time and results were compared with visual observations, and with destructive examinations.

For all specimens tested in this program, acoustic emission was monitored using two AE instrumentation systems. The main system of Physical Acoustic Corporation (PAC-3000/3004) is a microprocessor-controlled instrumentation. It allows for detailed and elaborate post-test analysis of the AE events accumulated during loading (e.g. amplitude, duration, energy, frequency spectrum, rise-time, data filtering, etc.). The pertinent operating parameters were: Resonance (150 KHz) transducers, Type R-15, system threshold level of 0.1 Volt, fixed gain of 40 dB preamplifier (Model 1220A), postamplifier gain control of 20 dB, and dead-time of 1 msec. Post-test spatial filtering to eliminate the unwanted emission was performed. Thus, only the events generated within 20 percent to 80 percent of the gage length were analyzed. The second system of Dunegan/Endevco (D/E 3000) series has been operative in our laboratory for the past eight years and significant experience has been gained in its use. Thus, its simultaneous utilization enables comparisons with previous results obtained for composites. Although this AE system is more limited in its data analysis capabilities, it currently has certain advantages over the PAC system, such as data filtering and ease in monitoring AE in real-time. The operating parameters applied with the D/E system were similar to those used with the PAC system. For most specimens both AE system were applied simultaneously.

It should be noted that a variety of AE variables should be analyzed and the significance of these variables and a correlation among them and with the external stimulation of load and deformation for various levels of applied stress or damage should be established. These variables include, for example:

1. Accumulation of events, counts, and count-rate versus load and deformation level.
2. Location distribution histograms of events.
3. AE events signature histograms (such as amplitude, duration, energy, and counts).
4. Cumulative Events Amplitude Distribution (CEAD), and similar results can be obtained for all other AE event variables at different load and deformation levels.
5. Cross-correlation among the various AE event variables.
6. All the above at various load ranges of the load cycle.
7. Felicity Ratio for determining damage severity.
8. Correlation among the AE variables with type and extent of damage, loading history, degradation of stiffness, compliance and strength, etc.

9. Correlation among the AE event intensities and the different failure mechanisms and processes.
10. Effect of the emission generated by friction among existing and newly created fracture surfaces on the interpretation of the AE results.

In this study emphasis has been placed on the applicability of the AE technique to monitor damage progression. Consequently, there has been a focus on the analysis of those AE events associated with fiber breakage through analyses of the event intensities (i.e. amplitude, energy, duration and counts per event) distribution histograms. During the course of the program it has been determined that a significant amount of emission is generated by the grating among existing fracture surfaces. In most cases this emission exceeds that caused by actual damage. Consequently, a great deal of efforts were directed toward the distinction of this friction emission. For this purpose a data analysis methodology and testing procedure have been developed and successfully employed in this study. The AE results were correlated with the state-of-damage as detected optically (150X) in real-time through the closed circuit television system (CCTV).

3.5 Failure Modes and Damage Progression:

The failure mechanisms and processes and the characteristics of damage progression were investigated by employing three techniques, namely, post-test examinations of the fracture surface morphology via the scanning electron microscope, post-test examinations of the interply modes of failure utilizing the deplying technique, visual observations in real-time through a closed-circuit television system, and X-radiography.

For a selected number of specimens, fracture surfaces were examined through the scanning electron microscope (SEM). In order to obtain a better view of the fracture surface morphology and better understand the different micro-failure mechanisms, stereo or three-dimensional views of the fracture surfaces were also obtained. These examinations indicate the quality of the matrix and fiber-matrix bonding, degree of matrix micro-cracking, crack site initiation and possibly direction of crack propagation. Differences between static and fatigue fracture surfaces were addressed primarily through comparisons of the static and fatigue fracture surface morphologies. The extent of fiber pull-out and pull-out length was also examined.

The deply technique has been applied on a selected number of specimens in order

to determine the extend of fiber breakage in the 0° plies at the tips of the transverse cracks in the 90° plies. The procedure applied for deplying the cross-ply laminates is similar to that described in [2-5].

Damage progression during the quasi-static and fatigue loading was also monitored in real-time using a closed-circuit television system (CCTV). This system enables magnifications of up to 250X and results were recorded on video cassette recorder tapes which can be replayed during presentation of the program results. From these observations, number of transverse cracks as a function of applied load and extent of delamination and matrix splitting were determined. These observations also served to demonstrate the amount of emission that can be generated by fretting. The damage progression was recorded for post-test qualitative correlation with the AE results. The optical observations were made for most specimens tested in this program.

The state-of-damage was also determined through X-radiography. For this purpose, selected specimens were removed from the testing machine at predetermined load levels (during quasi-static test) or number of cycles (during fatigue tests) and X-radiographs were taken. A Hewlett-Packard Faxitron Model 43804N X-ray cabinet with a 3 mA continuous current and Beryllium window (0.63 mm thick), was used with a focal distance of 6.45 mm. The specimens were X-radiographed at 25 KV and exposed for 60 seconds. The penetrant used was 1,4 - Di-iodobutane (D.I.B.) which was applied after specimen removal from the testing machine. All photographs used Polaroid Type 52 film. Primary emphasis here was directed toward determining the number of transverse cracks per unit length and results were compared with those recorded through the CCTV.

3.6 Test Matrix:

The list of specimens tested in this program, the type of data recorded, and the different examinations conducted are shown according to the five loading functions employed (see Section 3.3) in Tables 2 to 7. Based on the data analysis methodology developed during the course of this research program, the data analysis of the acoustic emission results recorded for the last three loading functions is highly time consuming, as discussed in the corresponding Sections of this report. Consequently, only selected portions of the loading sequences were analyzed in detail, as indicated, for example in Table 2. It should also be noted here that voluminous data have been obtained for each specimen tested. Therefore, this report presents a condensed summary of selected cases only. Based on the total data recorded and analyzed, the results reported here should be

considered as representative.

3.7 References:

1. G. P. Sendeckyj, AFWAL, FDL, Private communication.
2. S.M. Freeman, "Characterization of Lamina and Interlaminar Damage in Graphite/Epoxy Composites by the Deply Technique," presented at 6th Conf. on Materials, American Society of Testing and Materials, 1981, pp. 1-19.
3. S.M. Freeman, "Characterization of Lamina and Interlaminar Damage in Graphite/Epoxy Composites by the Deply Technique," in Composite Materials: Testing and Design (Sixth Conference), ASTM STP 787, American Society for Testing and Materials, Philadelphia, 1982, pp. 50-62.
4. S.M. Freeman, "Damage Progression in Graphite/Epoxy by a Deplying Technique," in Proc. of the 7th Annual Mechanics of Composites Review, AFWAL Report, AFWAL-TR-82-4007, 1982, pp. 30-41.
5. C.E. Harris and D.H. Morris, "A Characterization of the Fracture Behavior of Thick, Notched, Laminated Graphite/Epoxy Composites," VPISU Tech. Report No. VPI-E-83-31, VA Polytechnics Inst. and State University, Blacksburg, VA, 1983.

TABLE 2. TEST MATRIX (Static Loading)

LAY-UP	SPEC. NO.	STIFF.	STRENGTH	AE INST. D/E PAC	ADDITIONAL EXAMINATIONS*
[90 ₂ /0 ₂ /90] _s	3A6/1	✓	✓	✓	--
	3A6/2	✓	✓	--	--
	3A8/1**	✓	✓	✓	✓
	3A8/2	✓	--	✓	--
	3A10/1	✓	✓	✓	--
	3A10/2	✓	✓	✓	✓
	3B5/1	✓	✓	✓	✓
	3B5/2	✓	✓	✓	--
	3B6/1	✓	✓	✓	✓
					X, SEM
					DEPLY
[90 ₂ /0 _{1/2}] _s	4A8/1	✓	✓	✓	✓
	4B4/2	✓	✓	✓	✓
[90/0/90/0 _{1/2}] _s	5A4/1	✓	✓	✓	✓
	5B6/1	✓	✓	✓	✓
	5B7/2	✓	✓	✓	✓
					SEM
[90 ₂ /0/90] _s	6B4/2	✓	✓	✓	✓
	6A8/2	✓	✓	✓	✓
	6A10/2	✓	✓	✓	✓
	6A4/2	✓	✓	✓	--
	6A4/1	✓	✓	✓	✓
	6A5/2	✓	--	✓	--
	6A8/1	✓	✓	✓	✓
	6A9/2	✓	✓	✓	--
					X
					X
					AU
					AU, SEM

* AU-ACOUSTO ULTRASONICS
 DEPLY- DEPLYING TECHNIQUE
 FR- FREQUENCY RESPONSE
 PM- PHOTOMICROGRAPHY
 SEM- SCANNING ELECTRON MICROSCOPY
 X- RADIOGRAPHY

** DOUBLE- EDGE NOTCHED SPECIMEN

TABLE 2. (Continued).

LAY-UP	SPEC. NO.	STIFF.	STRENGTH	AE INST. D/E	PAC	ADDITIONAL EXAMINATIONS*
[90 ₂ /0] _s	7A9/2**	✓	--	✓	--	DEPLY
	7A8/2	--	--	--	--	X, PM
	7A5/1	✓	✓	✓	✓	SEM
	7B5/1	✓	✓	✓	✓	
	7B10/1**	✓	✓	✓	✓	
[90/0 ₂ /90] _s	8A5/1	✓	✓	✓	✓	
	8A5/2	✓	✓	✓	✓	
	8B8/1	✓	✓	✓	✓	
	8B9/2	✓	--	✓	--	PM
	8B10/1	✓	✓	✓	✓	
	8B10/2	✓	✓	✓	--	
	8B7/1	✓	✓	✓	--	
[0 ₂ /90 _{1/2}] _s	3C9/2	✓	✓	✓	✓	
	3D3/2	✓	✓	✓	✓	
[0 ₂ /90/0] _s	4C9/1	✓	✓	✓	✓	
	4C2/2	✓	✓	✓	✓	
[0 ₂ /90 ₂ /0] _s	5C1/2	✓	--	--	--	AU
	5D4/2	✓	✓	✓	✓	
	5D7/1	✓	✓	✓	✓	
	5D9/1**	--	✓	--	--	
	5C8/1	--	✓	✓	✓	SEM
[0/90/0/90 _{1/2}] _s	6C4/2	✓	✓	✓	✓	
	6C7/1	✓	✓	✓	✓	

TABLE 2. (Concluded).

LAY-UP	SPEC. NO.	STIFF.	STRENGTH	AE INST. D/E	PAC	ADDITIONAL EXAMINATIONS*
[0/90 ₂ /0] _s	7D3/2	✓	✓	✓	✓	SEM
	7C10/1	✓	✓	✓	✓	
	7D2/1	✓	✓	✓	--	
	7C7/1	✓	✓	✓	✓	
	7D6/2	✓	✓	✓	✓	
	7D4/2**	✓	✓	✓	✓	
[0 ₂ /90] _s	8C3/2	✓	✓	✓	--	
	8C6/2**	✓	--	✓	✓	DEPLY
	8C10/2	✓	✓	✓	✓	
	8D4/2**	--	--	--	--	X, PM
	8C2/1	✓	✓	✓	✓	
	8C2/2**	✓	✓	✓	✓	SEM
	8D9/1**	✓	✓	✓	✓	
	8D9/2**	✓	✓	✓	✓	

TABLE 3. TEST MATRIX (Fatigue Loading)*

LAY - UP	SPEC. NO.	STIFF.	N [1E+03]	f [Hz]	S.R.*	AE INST. D/E PAC	ADDITIONAL EXAMINATION
[90 ₂ /0 ₂ /90] _s	3B6/2	✓	0-1.0	0.1,1.0	0.61	✓ ✓	
	3B7/1	--	0-11.0	1.0	0.35	✓ --	X
	3B7/2	--	0-15.0	1.0	0.35	✓ ✓	X
[0 ₂ /90/0] _s	4D5/2	✓	0-10.0	1.0	0.43	✓ --	
[90/0/90/0 _{1/2}] _s	5A5/2	✓	0-10.0	1.0	0.30	✓ ✓	
			75.0-85.0	1.0	0.30	✓ ✓	
[0 ₂ /90 ₂ /0] _s	5C1/1	✓	0-1.00	0.1,1.0	0.37	✓ ✓	
			0-11.5	1.0	0.27	✓ ✓	X
	5C3/1	✓	15.4-19.5	1.0	0.27	✓ ✓	
			61.3-62.9	1.0	0.27	✓ ✓	
			66.2-68.4	1.0	0.27	✓ ✓	
			0-88.00	0.1, 1.0	0.22	-- --	X
			0.0-0.6	0.1, 1.0	0.70	✓ ✓	
	5C6/1	✓	0.6-1.6	0.1, 1.0	0.54	✓ ✓	
			77.00	0.1	0.86	✓ ✓	
			0-14.50	1.0	0.24	✓ ✓	X
			14.5-66.3	1.0	0.24	-- ✓	
			68.0-79.0	1.0	0.24	-- ✓	
[0 ₂ /90 ₂ /0] _s	5C8/2	--	0-0.30	0.01	0.90	✓ ✓	
			0.30-0.7	0.01	0.90	✓ ✓	
			0.7-1.0	0.01	0.91	✓ ✓	
			0.965-1.14	0.01	0.91	✓ ✓	
			1.14-1.50	0.01	0.92	✓ ✓	
	5D1/2**	✓	1.50-1.51	0.01	0.93	✓ ✓	
			0-0.05	0.01	0.54	✓ ✓	
			0.05-0.10	0.1	0.54	✓ ✓	
			0.10-0.15	1.0	0.54	✓ ✓	
			0.20-0.25	10.0	0.54	✓ ✓	
			0.30-0.35	0.1	0.54	✓ ✓	
			0.35-5.30	1.0	0.54	-- ✓	
			5.30-7.25	1.0	0.74	-- ✓	

* Optical observations performed for most tests.

TABLE 3. (Concluded).

LAY - UP	SPEC. NO.	STIFF.	N [1E+03]	f [Hz]	S.R.*	AE INST. D/E PAC	ADDITIONAL EXAMINATION
[90 ₂ /0] _s	7B7/1	✓	0-60.9	1.0	0.17	✓	✓
	7B8/1**	✓	0-0.050	0.001	0.50	✓	✓
			0.05-2.05	1.0	0.52	✓	✓
			2.05-4.05	1.0	0.53	✓	✓
			4.05-6.675	1.0	0.57	--	--
			6.675-6.75	1.0	0.61	✓	✓
[0/90 ₂ /0] _s	7D10/2	✓	0-1.0	1.0	0.32	✓	✓
	7D3/1	✓	10-11.5	1.0	0.32	✓	✓
			20-22.5	1.0	0.32	✓	--
			36-36.5	1.0	0.32	--	✓
			40-41	1.0	0.32	✓	✓
			80-81	1.0	0.32	✓	✓
			90-91	1.0	0.32	✓	✓
			0-1000	1.0	0.26	✓	✓
			2.5-2.75	0.1	0.26	✓	✓
			10-11	1.0	0.26	✓	✓
			12.5-12.75	0.1	0.26	✓	✓
			20-35	1.0	0.26	✓	✓
			STATIC	--	0.51	✓	✓
			35-36	1.0	0.51	✓	✓
			36.5-36.75	0.1	0.51	✓	✓
			37-43	0.1	0.51	--	✓
			45-46	1.0	0.51	✓	✓
			44.25-44.5	0.1	0.51	✓	✓
			STATIC	--	0.60	✓	✓
			[0 ₂ /90] _s	8C3/1**	--	0-0.06	0.005
		0.06-0.12		0.01	0.75	✓	✓
		0.12-0.18		0.01	0.75	✓	✓
		0.18-0.24		0.01	0.75	✓	✓
		0.24-0.30		0.01	0.77	✓	✓
		0-0.30		0.01	0.7	✓	✓

* Stress ratio

** Double-edge notched specimens (see schematic on page 38).

TABLE 4. STATIC TESTS (Double-Edge Notched Specimens*)

LAY-UP	SPEC. NO.	a/W	AE INST. D/E	PAC	REMARKS
[90 ₂ /0 ₂ /90] _s	3A8/1	0.11	✓	✓	
[90 ₂ /0] _s	7A8/2	0.11	—	—	CCTV
	7A9/2	0.11	✓	✓	DEPLY
	7B10/1	0.11	✓	✓	
[0 ₂ /90 ₂ /0] _s	5D9/1	0.11	—	—	Strength Only
[0/90 ₂ /0] _s	7D4/2	0.11	✓	✓	
[0 ₂ /90] _s	8C2/2	0.11	✓	✓	
	8C6/2	0.11	✓	✓	DEPLY
	8D9/1	0.11	✓	—	
	8D9/2	0.11	✓	✓	

* see schematic below.

$L = 305 \text{ mm}$

$W = 25 \text{ mm}$

$a / W = 0.11$

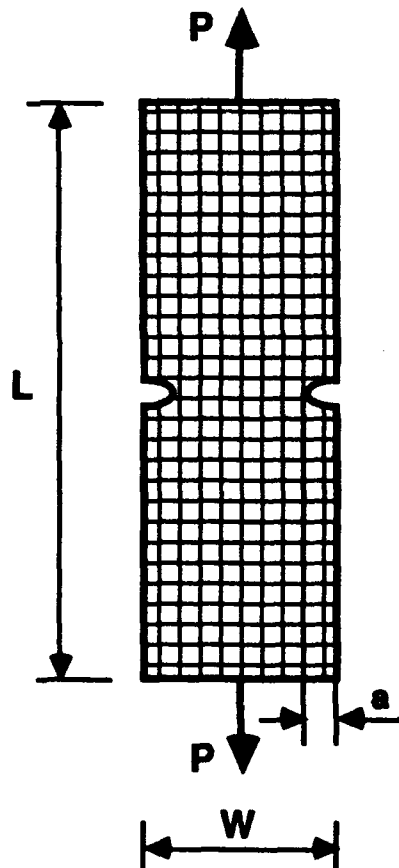


TABLE 5. QUASI-STATIC LOADING/UNLOADING TESTS
(Transverse Cracks Measurements)

LAY-UP	SPEC. NO.	NO OF LOAD CYCLES	STRENGTH	AE INST.		REMARKS *
				D/E	PAC	
[90 ₂ /0 ₂ /90] _s	3B9/1	7	✓	--	--	TC
[0 ₂ /90 ₂ /0] _s	5C1/2	11	✓	--	--	TC
	5C2/2	7	✓	--	--	TC, FR, AU
	5C4/1	9	✓	--	--	TC, FR, AU
	5D1/1	10	✓	--	--	TC
[90 ₂ /0] _s	7A9/1	7	✓	--	--	TC
[0/90 ₂ /0] _s	7C10/2	9	✓	--	--	TC
	7D9/1	23	✓	--	--	X
[90/0 ₂ /90] _s	8A10/1	13	✓	--	--	TC
[0 ₂ /90] _s	8C6/1	9	✓	--	--	TC
	8D7/2	10	✓	--	--	TC
	8D10/1	28	✓	--	--	X
[0 ₂ /90 ₄] _s	9E6/14	16	✓	--	--	TC, FR
[0 ₂ /90 ₄] _s	10F7/11	15	✓	--	--	TC, FR
[0 ₂ /90 ₈] _s	11G8/14	14	✓	--	--	TC, FR

X - X-Radiography

TC - Transverse cracks measurements

FR - Frequency response tests

AU- Acousto-ultrasonics tests

TABLE 6. CONSTANT LOAD TESTS (Hold Load)

LAY-UP	SPEC. NO.	2a/W*	AE INST. D/E	PAC	REMARKS
[0 ₂ /90] _s	8D8/2	0.17	✓	✓	9 Hold Periods
	8D10/2	0.17	✓	--	Bad test
	8D8/1	0.17	--	✓	4 Hold Periods

* see schematic on page 38.

TABLE 7. SPIKE TESTS (Fatigue Loading)

LAY - UP	SPEC. NO.	STIFF.	N [1E+03]	f [Hz]	S.R.	AE INST. D/E	PAC	REMARKS
[90 ₂ /0 ₂ /90] _s	3B6/1	✓	0.613	0.1	0.35	✓	✓	Six spikes
[0 ₂ /90 ₂ /0] _s	5D9/2	--	0.300	0.1	0.30	--	--	Single spike
		--	.30-1.0	0.01	0.30	✓	✓	

IV. MECHANICAL PROPERTIES AND FAILURE MECHANISMS

4.1 Summary:

The features and characteristics of the acoustic emission information and the interpretation of the results depend upon the type of composite system being tested, the laminate configuration, quality of fabrication, mechanical properties, fracture behavior and the dominant failure modes. Therefore, it is imperative that this information be available before acoustic emission data can be properly assessed.

The test program included the measurement of axial stiffness, fracture strength, notched strength, and the monitoring of failure mechanisms and processes. For the latter, the number of transverse cracks in unnotched and notched specimens and extent of matrix splitting and delamination in notched specimens (the latter two modes of damage will be discussed in the following Sections) as a function of far-field applied load were measured optically in real-time via a high magnification (150X) closed circuit television system (CCTV) and from X-radiographs. Selected specimens were depled and the amount of fiber breaks was determined qualitatively under the scanning electron microscope. The fracture surface morphology of selected specimens was also examined via the scanning electron microscope.

4.2 Mechanical Properties:

Representative stress-strain curves for all laminate configurations tested are shown in Figure 4.1*. As expected, all stress-strain curves are linear up to failure for both groups of laminates, i.e. those containing 0° and 90° on the outer plies. These stress-strain curves were recorded using an extensometer. The jumps in displacements seen in several curves should be attributed primarily to vibrations of the extensometer when sudden massive failure occurred in the subject laminate. It will be shown in Section V that these jumps are associated with sudden surges in emission that correspond to rapid damage growth.

Table 8 lists the stiffness and strength results measured for all specimens tested. The average values of the stiffness and strength are listed in Tables 9 and 10. The stiffness values were determined from the initial part of the load-displacement curves

* Figures are listed at the end of this report.

TABLE 8. STIFFNESS AND STRENGTH RESULTS

a. 0° PLIES OUTSIDE

LAY - UP : [0₂/90_{1/2}]_s

SPEC. NO.	E _x [GPa]	σ _x [MPa]
3C9/2	108.70	1,822.00
3D3/2	89.30	1,248.10
Avg.	99.00	1,535.05

LAY - UP : [0₂/90/0]_s

SPEC. NO.	E _x [GPa]	σ _x [MPa]
4C9/1	100.00	1,695.90
4C2/2	104.20	1,664.00
Avg.	102.1	1,679.95

LAY - UP : [0/90₂/0]_s

SPEC. NO.	E _x [GPa]	σ _x [MPa]
7D3/2	85.30	1,158.20
7C10/1	85.30	1,199.60
7D2/1	84.00	1,372.25
7C7/1	74.60	1,096.10
7D6/2	76.50	1,110.00
Avg.	81.14	1,187.23

LAY - UP : [0/90/0/90_{1/2}]_s

SPEC. NO.	E _x [GPa]	σ _x [MPa]
6C4/2	83.78	1,200.00
6C7/1	80.77	1,327.23
Avg.	82.28	1,263.61

LAY - UP : [0₂/90₂/0]_s

SPEC. NO.	E _x [GPa]	σ _x [MPa]
5C1/2	88.00	—
5D4/2	77.86	1,424.85
5D7/1	97.06	1,537.36
5C8/1	—	1,407.80
Avg.	87.64	1,456.67

LAY - UP : [0₂/90]_s

SPEC. NO.	E _x [GPa]	σ _x [MPa]
8C3/2	102.60	1,633.50
8C6/2	96.40	*
8C10/2	96.40	1,537.30
8C2/1	93.60	1,444.90
Avg.	97.25	1,538.57

* Not to failure

TABLE 8. (Concluded).

b. 90° PLIES OUTSIDELAY - UP: [90₂/0₂/90]_s

SPEC. NO.	E _x [GPa]	σ _x [MPa]
3A6/1	60.00	889.00
3A6/2	63.54	919.70
3A8/2	64.76	*
3A10/1	58.47	898.82
3A10/2	66.72	988.50
3B5/1	77.12	930.70
3B5/2	58.92	941.96
3B6/1	53.47	915.93
Avg.	62.87	926.40

LAY - UP: [90₂/0_{1/2}]_s

SPEC. NO.	E _x [GPa]	σ _x [MPa]
4A8/1	33.30	399.58
4B4/2	34.72	458.14
Avg.	34.01	428.86

LAY - UP: [90₂/0]_s

SPEC. NO.	E _x [GPa]	σ _x [MPa]
7A5/1	53.04	730.69
7B5/1	55.20	731.59
Avg.	54.12	731.14

LAY - UP: [90₂/0/90]_s

SPEC. NO.	E _x [GPa]	σ _x [MPa]
6A8/2	38.60	536.80
6B4/2	41.60	452.20
6A10/2	—	467.40
6A4/2	39.80	515.95
6A4/1	47.00	579.00
6A8/1	41.63	489.13
6A5/2	46.80	*
6A9/2	38.40	495.40
Avg.	41.98	505.13

LAY - UP: [90/0/90/0_{1/2}]_s

SPEC. NO.	E _x [GPa]	σ _x [MPa]
5A4/1	62.51	1,010.72
5B6/1	55.16	796.50
5B7/2	65.65	912.20
Avg.	61.12	906.47

LAY - UP: [90/0₂/90]_s

SPEC. NO.	E _x [GPa]	σ _x [MPa]
8A5/1	78.03	1,115.10
8A5/2	72.56	1,048.00
8B8/1	79.84	1,180.04
8B10/1	83.60	1,167.60
8B10/2	80.20	1,079.80
8B7/1	83.40	1,144.40
8B9/2	86.00	*
Avg.	80.52	1122.49

TABLE 9. AVERAGE STIFFNESS AND STRENGTH RESULTS

LAY - UP	E_x [GPa]	σ_x [MPa]	LAY - UP	E_x [GPa]	σ_x [MPa]
$[0_2/90_{1/2}]_s$	99.00	1,535.05	$[90_2/0_{1/2}]_s$	34.01	428.86
$[0_2/90]_s$	97.25	1,538.57	$[90_2/0]_s$	51.12	731.14
$[0_2/90/0]_s$	102.10	1,679.95	$[90_2/0/90]_s$	41.98	505.13
$[0_2/90_2/0]_s$	87.64	1,456.67	$[90_2/0_2/90]_s$	62.87	926.40
$[0/90_2/0]_s$	81.40	1,187.23	$[90/0_2/90]_s$	80.52	1,122.49
$[0/90/0/90_{1/2}]_s$	82.28	1,263.61	$[90/0/90/0_{1/2}]_s$	61.12	906.47

TABLE 10. EFFECT OF 0° PLY VOLUME FRACTION ON AVERAGE STIFFNESS AND STRENGTH VALUES

LAY-UP	NO. OF TESTS E_x/σ_x	PERCENT OF 0° PLIES	E_x^* [GPa]	σ_x^* [MPa]
$[90_2/0_{1/2}]_s$	2/2	20	34.01	428.86
$[90_2/0]_s$	4/2	33	51.12	731.14
$[90_2/0/90]_s$	7/7	25	41.98	505.13
$[90_2/0_2/90]_s$	8/6	40	62.87	924.10
$[90/0_2/90]_s$	7/6	50	80.52	1,122.49
$[90/0/90/0_{1/2}]_s$	3/3	43	61.12	906.47
$[0_2/90_{1/2}]_s$	2/2	80	99.00	1,535.05
$[0_2/90]_s$	4/3	67	97.25	1,538.57
$[0_2/90/0]_s$	2/2	75	102.10	1,679.95
$[0_2/90_2/0]_s$	3/3	60	87.64	1,456.67
$[0/90_2/0]_s$	5/5	50	81.40	1,187.23
$[0/90/0/90_{1/2}]_s$	2/2	57	82.28	1,263.61

* Average values

(using an extensometer of 25 mm gage length), e.g. Figure 4.1. The experimental stiffness values are well within those predicted from laminate plate theory. The strength data are based on the maximum load to failure. With a few exceptions the scatter in the stiffness and strength data is as expected for the subject material. Since the mechanical characterization of cross-ply graphite/epoxy laminates are well established, no efforts were made to identify the reasons for the extreme values as this subject is beyond the scope of this investigation.

The results of stiffness and strength listed in Table 9 are plotted in Figures 4.2 and 4.3, respectively. From these Figures the effects of the number and percent of the 0° and 90° plies, and of the laminate configuration on these two mechanical properties can be clearly determined. From the nondimensional plots it could be concluded that both stiffness (Figures 4.2b and 4.2d) and strength (Figures 4.3b and 4.3d) vary linearly with the percentage of 0° and 90° plies, as expected. This linear relationship agrees quite closely with predictions based on the rule of mixture (not shown here), using the basic laminae properties given in Section III.

It should be noted, however, that the thickness and sequences of the 0° and 90° plies affects both stiffness and ultimate strength. It would be shown later that the laminate configuration also affects the rate of damage accumulation (e.g. number of transverse cracks). These issues have been investigated in detail both experimentally and analytically by Wang et. al. [1-2]. The experimental results shown in Figures 4.2a and 4.2c and in Figure 4.3a and 4.3c basically confirm their result, that the thicker the 90° plies the lower the stiffness and strength values are. However, in the present study the variation in the 90° plies is not sufficiently large to demonstrate the thickness effect very dramatically. Since the present experimental results indicate that both stiffness and strength vary linearly with the volume fraction of either the 0° or 90° plies, both properties can be predicted independent of laminate configuration. Moreover, it is interesting to note that the strength and stiffness of the different cross-ply laminates are also related linearly, Figure 4.4. This is a direct result from the linear relation of both properties with volume fraction.

4.3 Modes of Damage:

Damage initiation and progression was monitored applying five techniques: (1) X-radiography; (2) real-time optical observations through a closed-circuit television system using a high magnification (150X) microscope; (3) photomicrography; (4) the

deplying technique; and (5) examining the fracture surface morphology via the scanning electron microscope. The first two techniques were applied primarily in order to monitor the initiation and accumulation of the number of transverse cracks with load for the purpose of comparison with the acoustic emission results. Also, matrix splitting and delamination growth in the double-edge notched specimens were monitored and results compared with the associated acoustic emission. The third technique was applied in order to determine the details of the transverse cracks and the fourth technique was applied in order to determined the extent of fiber breaks in the different cross-ply laminates. From the fifth examination procedure the details of the micro-failures could also be identified.

Typical cross-sections of specimens loaded quasi-statically to approximately 60-80 percent of ultimate load are shown in the photomicrographs of Figure 4.5. All transverse cracks extend throughout the entire thickness of the 90° plies. When such a laminate is deplied, the imprints of the tips of the transverse cracks in the 90° plies can be easily seen in the 0° plies, Figure 4.6a. Detailed examination of the deplied 0° ply through the scanning electron microscope clearly reveal a relatively large number of broken fibers, Figure 4.6b, while no broken fibers were found in the 90° plies, Figure 4.6c, as expected. These observations are essentially similar to the results reported by Jamison [3], where a detailed study on application of the deplying technique was conducted for determining the distribution of fiber breaks in cross-ply graphite/epoxy laminates.

Examinations of the fracture surface morphology of a cross-ply graphite/epoxy laminate via the scanning electron microscope, Figure 4.7, revealed several typical micro-failures.

1. Fiber/matrix interfacial failures were observed throughout the entire fracture surfaces of the 90° plies, Figure 4.7a. The fiber imprints seen in the 90° plies indicate that many were removed or pulled out. In the 0° plies a good fiber/matrix bonding and a limited amount of fiber pull-out were observed, Figure 4.7b. Relatively few fibers are covered with matrix residue.
2. Detailed examinations of the matrix fracture surfaces reveal that failure occurs in the form of matrix serrations, Figure 4.7b. Viewing these serrations via a stereo viewer reveals that most of them are located on planes oriented at approximately 45° to the loading direction.

3. These serrations appeared in clusters throughout the fracture surface and they are more pronounced in the resin-rich areas. In the interface-dominated fracture surfaces, that is, in the matrix between adjacent fibers, Figure 4.7c, they appear to be smaller in size and of higher density. The appearance of resin-rich areas probably results from a lack of uniformity in fiber distribution.
4. The fracture surfaces of the 90° plies contain a small number of broken fibers, randomly distributed, Figures 4.7a, 4.7c, and 4.7d. It is not clear whether these fibers were broken during prepreg fabrication or as a result of the catastrophic fracture.
5. Finally, examinations of the fracture surfaces via a stereo viewer reveal quite an irregular fracture surface. The irregularity is along its length and its width, resulting primarily from the broken fibers. The extent of the irregularity is approximately one to two fiber diameters.

The observations of the fracture surface morphology discussed above for the $[90_2/0_2/90]_s$ laminate are typical and they were also observed in other cross-ply laminates, as expected.

On the macro scale, the dominant mode of damage is the transverse matrix cracks in the 90° plies. A significant amount of research has been conducted on monitoring the initiation of these matrix cracks and the characteristics of their accumulation during quasi-static and fatigue loading, e.g. [4-6], and these characteristics are well established. In this research an attempt was made to establish a correlation between the acoustic emission results and the accumulation of the transverse cracks. For this purpose the number of transverse cracks as a function of applied load has been determined for selected cross-ply laminates applying both X-radiography and optical observations. The X-radiograph shown in Figure 4.8 clearly indicate that indeed a large number of transverse cracks occur during quasi-static loading. In the particular radiograph of Figure 4.8 the number of transverse cracks is approximately 0.6/mm (15/inch). Practically all the transverse cracks extend throughout the entire width of the specimen, which could also be verified through optical observations.

Applying X-radiography for monitoring the accumulation of transverse cracks during loading requires the interruption of the loading sequence and the removal of the specimen from the testing fixture for radiography, a procedure which can adversely affect

the reliability of the acoustic emission results. Furthermore, the radiographs are taken after the specimen has been unloaded and many of the cracks closed. This makes it difficult for the penetrant (see Section III) to penetrate into all the existing cracks in the laminate and/or penetrate to their entire length. Therefore, in this program the accumulation of transverse cracks was monitored optically in real-time using a high magnification (150X) closed-circuit television system (CCTV, as explained in Section III). It has been verified that the results measured from the radiographs are identical to those measured optically. Moreover, since the optical measurements are taken during loading, all cracks are open and can be more easily and precisely counted.

Consequently, in this research all the results were obtained via the CCTV. The results on the number of transverse cracks as a function of applied load are listed in Table 11 and plotted in Figure 4.9 for selected specimens. The results indicate that the characteristics of damage accumulation depends on laminate configuration. However, the precise correlation is difficult to establish due to the large scatter in the results among identical laminates. Generally it could be stated that when the 90° plies are external, the initiation load is lower and the rate of accumulation is higher than when the 0° plies are external.

4.4 Conclusions:

In this Section the results on the mechanical properties and modes of damage in the different cross-ply laminates tested in this program have been presented. For the proper interpretation of the acoustic emission results to be presented in the following Sections, this background information is imperative. First, it has been demonstrated that the mechanical response of cross-ply laminates is strongly affected by laminate configuration. Second, the failure process of the subject material includes a variety of modes of damage, on both the micro- and the macro-scales, all of which are sources of emission generated during loading. Thirdly, the rate of progression of damage and its accumulation is also affected by laminate configuration.

4.5 References:

1. A.S.D. Wang, "Fracture Mechanics of Sublaminar Cracks in Composite Materials," in Characterization, Analysis and Significance of Defects in Composite Materials, AGARD Conf. Proc. No. 355, April 10-15, 1983, London U.K. pp. 15-1-15-19. Also, Composite Technology Review, Vol. 6, 1984, pp. 45-62.
2. A.S.D. Wang, P.C. Chou and S.C. Lei, "A Stochastic Model for the Growth of Matrix Cracks in Composite Laminates," in Advances in Aerospace Structures, Materials and Dynamics, ASME AD-06, 1983 Winter Annual Mtg. of the American Society of Mechanical Engineers, Boston, MA, November 13-18, 1983. Also, Journal of Composite Materials, Vol. 18, 1984, pp. 239-254.
3. R.D. Jamison, "Advanced Fatigue Damage Development in Graphite/Epoxy Laminates," Ph.D. Dissertation, Virginia Polytechnic Institute and State University, Blacksburg, VA, 1982.
4. M.G. Bader, J.E. Bailey, P.T. Curtis, and A. Parvizi, "The Mechanics of Initiation of Development of Damage in Multi-Axial Fiber-Reinforced Plastic Laminates," in the Proc. of the 3rd Conference on Mechanical Behavior of Materials (ICM-3), the Japan Society of Material Sciences (JSMS), 1979, pp. 227-239.
5. R.P. Harrison and M.G. Bader, "Damage Development in CFRP Laminates Under Monotonic and Cyclic Stressing," Fiber Science and Technology, 18, 1983, pp. 163-180.
6. A. Charewicz and I.M. Daniel, "Damage Mechanisms and Accumulation in Graphite/Epoxy Laminates," Composite Materials: Fatigue and Fracture, ASTM STP 907, H.T. Hahn Ed., American Society of Testing and Materials, Philadelphia, PA, 1986, pp. 274-297.

TABLE 11. TRANSVERSE CRACKS RESULTS

LAY - UP :	[90 ₂ /0 ₂ /90] _s	[0 ₂ /90 ₂ /0] _s	[90 ₂ /0] _s	[0/90 ₂ /0] _s
SPEC. NO. :	3B9/1	5C1/2	7A9/1	7C10/2
STRENGTH :	1,055.40	1,427.07	318.51	1,160.84
	[MPa]			

%ULT. T.C./mm		%ULT. T.C./mm		%ULT. T.C./mm		%ULT. T.C./mm	
38.5	0.157	44.4	1.220	39.1	0.512	34.4	0.079
46.5	0.433	50.0	2.520	47.8	0.787	39.3	1.457
57.8	1.929	55.6	3.031	52.2	0.906	44.3	1.968
67.4	2.716	61.1	3.543	56.5	1.063	49.2	2.638
75.4	3.150	66.7	4.173	65.2	1.339	54.1	2.835
83.5	3.661	72.2	—	73.9	1.653	59.0	3.189
91.4	4.094	77.8	5.040	91.3	1.693	63.9	3.661
		83.3	5.236			83.6	4.685
		88.9	5.354			90.2	5.236
		94.4	5.630				
		100.0	5.866				

LAY - UP :	[0 ₂ /90 ₂ /0] _s	[0 ₂ /90] _s	[0 ₂ /90] _s	[90/0 ₂ /90] _s
SPEC. NO. :	5D1/1	8C6/1	8D7/2	8A10/1
STRENGTH :	1,498.00	1,578.70	1,216.10	1,065.63
	[MPa]			

%ULT. T.C./mm		%ULT. T.C./mm		%ULT. T.C./mm		%ULT. T.C./mm	
48.0	0.157	52.7	0.118	42.4	0.039	39.0	0.236
53.3	0.315	58.2	0.354	48.7	0.118	44.1	0.551
58.6	0.512	69.1	0.945	55.1	0.157	49.2	0.866
64.0	0.748	74.5	1.063	61.4	0.196	54.2	1.300
69.3	1.062	78.2	1.574	67.8	0.236	59.3	2.283
74.6	1.062	81.8	2.520	74.2	0.551	64.4	2.835
80.0	1.417	87.3	2.638	80.5	0.709	69.5	3.622
85.3	1.693	92.7	2.667	86.9	1.260	74.6	4.449
90.6	2.638	100.0	2.716	95.3	1.460	79.7	5.197
95.9	3.818			100.0	2.640	84.7	5.394
						89.8	6.181
						94.9	6.147
						100.0	6.457

TABLE 11. (Concluded).

LAY - UP :	[0 ₂ /90 ₂ /0] _s	[0 ₂ /90 ₂ /0] _s	[0 ₂ /90 ₈] _s	[0 ₂ /90 ₄] _s
SPEC. NO. :	5C2/2	5C4/1	11G8/14	10F7/11
STRENGTH :	1375.72	1351.45	448.88	663.33
[MPa]				

%ULT. T.C./mm		%ULT. T.C./mm		%ULT. T.C./mm		%ULT. T.C./mm	
0.59	0.10	0.36	0.21	0.41	0.03	0.14	0.04
0.65	0.26	0.48	0.84	0.44	0.08	0.22	0.08
0.71	2.52	0.54	1.15	0.46	0.16	0.29	0.28
0.76	2.62	0.60	2.41	0.48	0.26	0.32	0.31
0.82	2.83	0.66	3.15	0.52	0.31	0.36	0.43
0.88	3.10	0.72	3.83	0.55	0.39	0.39	0.47
0.94	3.62	0.78	4.25	0.58	0.52	0.43	0.59
		0.84	4.72	0.61	0.52	0.47	0.63
		0.96	5.30	0.66	0.55	0.50	0.67
				0.71	0.55	0.54	0.79
				0.76	0.60	0.61	0.91
				0.80	0.60	0.68	0.98
				0.88	0.63	0.75	1.10
				0.96	0.68	0.82	1.18
						0.90	1.34

LAY - UP :	[0 ₂ /90 ₂] _s
SPEC. NO. :	9E6/14
STRENGTH :	1024.58
[MPa]	

%ULT. T.C./mm		%ULT. T.C./mm	
0.50	0.08	0.77	1.06
0.54	0.16	0.81	1.10
0.57	0.39	0.84	1.26
0.61	0.55	0.87	1.30
0.64	0.71	0.90	1.30
0.67	0.87	0.93	1.34
0.71	0.98	0.97	1.34
0.74	1.02	1.00	1.38

V. ACOUSTIC EMISSION DURING QUASI-STATIC LOADING

5.1 Summary:

In this Section, results of acoustic emission monitoring during monotonic quasi-static loading to failure are presented. Results include count-rate and accumulation of events as a function of far-field applied stress and strain. The location distribution histograms of events at different load levels for unnotched and notched specimens are shown. The distribution histograms of the major event intensities, namely, amplitude, energy, duration, and counts per event at different load levels are also presented. The effect of laminate configuration is discussed. Finally, the effect of loading rate and testing procedure is also addressed. Results recorded using both D/E-3000 and PAC-3000/3004 are compared. Voluminous data have been recorded and for the sake of conciseness only selected results are discussed, representing the different laminates studied.

5.2 Introduction:

An important subject in assessing the potential of acoustic emission (AE) as a nondestructive examination technique for composites is its ability to detect damage initiation and accumulation, locate the damage, and identify the major modes of damage. The features and characteristics of the AE information depend upon the type of composite system being examined, laminate configuration, mechanical properties, fracture behavior, failure mechanisms, specimen geometry, loading conditions, and testing procedure. Since the laminates tested in this program are all of the same material system, were all fabricated following identical fabrication procedures, and were all tested under the same conditions, the AE results should indicate primarily the effect of laminate configuration on the emission associated with the formation of new damage.

The simplest way to detect damage initiation is by recording the load (or strain) level at which emission initiates. This emission is usually monitored in terms of count-rate (i.e. counts per unit time, load, strain, etc.), and cumulative counts and cumulative events as a function of the external stimulation. Similarly, the conventional procedure for determining the rate of damage accumulation is to monitor the rate of the emission accumulated. This procedure depends strongly on the rate at which the AE instrumentation can acquire data. Since the rate of damage accumulation depends largely on the loading rate, the effect of rate of loading on the AE results deserves special attention. Testing conditions and procedure can also affect the AE results.

Under certain testing conditions the site of the source of internal damage can be located. In laboratory testing of coupons this is achieved by placing two AE sensors some known distance apart (e.g. at both ends of the specimen). From the time difference between stimulation of each transducer by an AE event (namely, occurrence of damage) and a priori knowledge of the wave speed in the subject material (usually obtained by proper calibration of the AE instrumentation), the location at which the AE event occurs can be determined in real-time. With increasing load, AE events will emanate from throughout the specimen length, resulting in location distribution histograms of events at various load levels. It is expected that the AE activity will be more pronounced at the location of stress raisers (e.g. notches), and thus existing damage could be detected and located and its progression could be tracked. Similarly, increased AE activity is expected to occur at weak sites along the specimen, and thus the fracture site could be anticipated in real-time. However, fracture load and site can not always be clearly anticipated, primarily due to the extremely high event rate that occurs when the load approaches ultimate.

Determination of the major failure mechanisms using AE can be based upon a variety of AE source intensity analyses, such as event amplitude, duration, energy, counts per event, frequency spectrum, rise-time, etc. The goal here is to seek and establish a direct correspondence between a specific mode of damage and a specific range of selected event intensities. The great majority of studies attempt to correlate the modes of failure with the event amplitude and, to a lesser degree, with the event energy and its duration. The event amplitude has received most of the attention for two reasons: (1) it is relatively simple to measure; (2) it was suggested during early stages of research into AE in composites that a relatively simple correspondence exists between the three major modes of failure (matrix cracking, delamination, and fiber breakage) and low, middle, and high AE event amplitude ranges, respectively. Consequently, the work of many researchers has addressed this correspondence.

This Section presents selected results discussing all the above mentioned issues, with primary emphasis on the effect of laminate configuration on AE results. The results presented include: count-rate as a function of applied stress and the corresponding far-field stress-displacement curves; events as a function of applied stress and strain; location distribution histograms at different load ranges; and distribution histograms of selected event intensities at different load ranges. A detailed data analysis of the events amplitude is also given. Finally, a brief discussion on the effect of testing conditions and procedure is presented.

5.3 Count-Rate as a Function of Applied Stress:

Representative acoustic emission results in term of count-rate (per 0.2 second) as a function of applied stress are shown in Figure 5.1 for all twelve laminate configurations. The corresponding far-field stress-displacement curves are shown as well. These are linear to fracture as discussed in Section 4.2. In other words, from these stress-displacement curves neither damage initiation nor damage accumulation could be detected.

The count-rate results, however, indicate precisely the load at which damage initiation occurred. In the laminates which contain external 0° plies (which are defined here as Group I), Figures 5.1a to 5.1f, the emission initiation load is much higher than it is in the laminates which contain external 90° plies (defined here as Group II), Figures 5.1g to 5.1l. These results correspond with the optical observations (Figure 4.9) which showed that in the latter laminates transverse cracking initiated at relatively lower load levels than it did in the former laminate configuration.

Beyond the emission initiation load a rapid increase in the count-rate is noticed within a limited load range in all six laminates which contain external 0° plies (Group I). With further increase of the load a decrease in the count-rate occurs. The relatively low count-rate continues for a significant portion of loading with random surges in emission. These AE results suggest that the rate of damage accumulation is higher during initial loading as compared with that occurring at elevated loads. This rise and fall in the count-rate occurs within the load range of approximately 30 - 50 percent of ultimate. However, from optical observations it could be concluded that the actual increase in the matrix transverse cracking continues much beyond this load range, Figure 4.9. In other words, the source of emission during the initial phase of loading should be attributed to other failure mechanisms as well.

It seems that matrix microcracking, which occurs internally as well as externally (at weak sites along the specimen's edges) throughout the specimen length, is the major source for this emission. These microcracks are the precursors of transverse matrix macro-cracks, observed optically and from radiographs. The fall in the count-rate can be attributed to two phenomena: either the formation rate of void nucleation, crazing, and microcracking decreases rapidly beyond a certain load level, or a high event rate occurs which locks-up the AE instrumentation (which is discussed below), or a combination of both. These assumptions should be considered as preliminary. Significantly more work

is required to fully understand this issue.

The low and nearly constant count-rate recorded in the middle range of loading indicates a constant rate of damage accumulation. This conclusion can be partially supported by the nearly constant rate at which matrix transverse cracks accumulate, Figure 4.9. The few random surges in emission can be attributed primarily to a sudden, rapid and simultaneous occurrence of several matrix cracks.

In the laminates which contain external 90° plies (Group II) a somewhat different behavior is seen. Here the rise and fall in the count-rate is hardly noticeable. In this group of laminates matrix transverse cracking occurs at load levels as low as 35 percent of ultimate. The microvoid nucleation, matrix crazing, and microcracking all cause early and rapid initiation and propagation of matrix transverse cracking in the external 90° plies. With increasing load a significant amount of delamination occurs at the $90^\circ/0^\circ$ interface, causing an extremely high rate of emission. Emission is also caused by grating among the delaminated fracture surfaces. This important source of emission will be explained in greater detail in Section 6.7. Such high rates of damage accumulation and continuous grating can also affect the AE results, as explained in Section 6.9.

Based on results such as those shown in Figure 5.1, it is not yet possible to anticipate fracture. The commonly used criterion for anticipating specimen fracture through AE is based, for example, on a sudden surge in the count-rate or a rapid increase in AE activity as the load approaches ultimate. Only in a few cases was such AE activity noticed prior to catastrophic fracture. In all such cases, surges in emission also occurred at lower load levels. Thus, applying such a criterion would have indicated imminent fracture prematurely. In all other cases, specimen fracture occurred without prior warning, i.e. the count-rate activity did not indicate imminent fracture.

The reproducibility of the count-rate plots is shown in Figure 5.2 for three selected laminates of Group II. For each laminate the results recorded for two specimens are shown. The comparison within each pair indicates that the results are generally quite reproducible. The differences within each pair (i.e. in emission initiation load, load at which surges in emission occur, number of counts, etc.) should be attributed to the scatter in rate of damage accumulation among the different specimens. In other words, the count-rate plots can give a general indication of the characteristics of damage accumulation in any specific specimen examined.

The effect of the number and percent of the 0° and 90° plies on the emission initiation stress is shown in Figure 5.3 in non-dimensional format for both groups of laminates. The ordinate indicates the far-field emission initiation stress-to-ultimate stress ratio. The emission initiation stress, depicted from the count-rate plots, is defined here as the far-field stress level at which emission is generated continuously. In other words, single events generated randomly at the low load ranges were ignored. The results shown in Figure 5.3 indicate that initiation of emission occurs within 10 to 40 percent of ultimate load. The higher the percentage of 0° plies the higher is the emission initiation stress ratio, Figures 5.3b and 5.3d. In other words, specimen fracture can be approximately anticipated at an early stage of loading and in real-time, however, with a relatively low level of accuracy, ± 20 percent.

The emission initiation load as a function of ultimate stress is shown in Figure 5.4, in both non-dimensional and dimensional formats. The emission initiation stress ratio is practically independent of ultimate stress, Figure 5.4a. However, the results clearly indicate that the emission initiation stress increases, nearly proportionally, with ultimate stress, Figure 5.4b. This is a direct consequence of the results shown in Figure 5.3.

5.4 Cumulative Events:

The rate at which damage accumulates can be based on monitoring the rate at which events (and counts) accumulate with increasing external stimulation (e.g. far-field stress and strain).

The cumulative events as a function of applied stress are shown in Figures 5.5 for the six pairs of laminates. The emission initiation load can be determined from these plots as well. Similar to the results shown in Figure 5.1, the emission initiation stress in the laminates of Group I is higher than it is in the laminates of Group II. For both Groups the emission initiates within 10 to 40 percent of ultimate stress.

In all twelve laminates, there is a distinct 'knee' in the events versus stress curves. This was expected because as the load approaches ultimate, the rate of emission can be very high, depending upon laminate configuration. Based on the events versus applied stress curves, Figure 5.5, a qualitative correlation can be established between laminate configuration (e.g. strength, percent of 90° plies, etc.) and the rate or amount of emission. This is particularly so for the events versus stress plot for Group II, Figure 5.5b. Here the results indicate that the larger the percentage of the 90° plies, or the lower the ultimate

stress, the higher is the event rate. This higher event rate is clearly associated with a high rate of damage accumulation.

The AE results recorded for Group I laminates do not reveal any such correlation, Figure 5.5a. Note, that here the difference in ultimate strength among the different laminates is not as large as it is for Group II laminates. Thus, the correlation with the AE results is not as distinct. When the data shown in Figure 5.5a are replotted according to the format shown in Figure 5.6a, the data of Group I can be clearly separated into two subgroups of laminates which contain single and double layers of 90° plies. In the laminates which contain double layers of 90° plies the initial rate of emission and the total number of events accumulated is significantly lower than in the three laminates which contain only a single layer of 90° plies. The data for Group II, replotted in Figure 5.5b, are now spread within a much more limited range. The significance of these results is not clear and additional investigation should be conducted with cross-ply laminates made of varying ply thicknesses.

The plots of events versus applied strain, Figure 5.7, include only the first 1,000 events. Because of the large amount of transverse cracks and local delamination, primarily for Group II laminates, the extensometer readings are not reliable beyond a certain global strain level. These plots show only the emission accumulated during the initial phase of loading. Consequently, no specific correlation could be established between the rate of emission with increasing applied strain and laminate configuration. Such is also the case during initial loading in the events versus applied stress plots, Figure 5.5.

Finally, the total number of events accumulated in the different specimens does not reveal any specific trend, Table 12. Here the problem is even more complex. This number depends not only on laminate configuration but also on ultimate stress, loading rate, and rate of damage accumulation. The higher the ultimate stress, the higher is the number of events. Scatter in strength within the same laminate will result in an even larger scatter in the total number of events accumulated. On the other hand, the higher the loading rate, the lower is the number of events recorded due to instrumentation lock-up. When specimens are of different quality the rate of damage accumulation will also be different, resulting in varying amounts of emission. In other words, the total number of events accumulated can not be an indicator for material performance unless an extensive data base is available.

TABLE 12. ACCUMULATED NUMBER OF EVENTS DURING
MONOTONIC LOADING TO FAILURE

LAY-UP	SPEC. NO.	EVENTS (D/E)	EVENTS (PAC)
[0 ₂ /90 _{1/2}] _s	3C9/2	22,028	16,561
	3D3/2	6,996	6,286
[0 ₂ /90/0] _s	4C2/2	28,133	15,566
[0 ₂ /90 ₂ /0] _s	5D4/2	15,831	8,728
	5D7/1	15,686	14,997
[0/90/0/90 _{1/2}] _s	6C4/2	33,435	21,424
	6C7/1	24,406	14,847
[0/90 ₂ /0] _s	7C10/1	10,369	3,062
	7D3/2	8,927	8,442
	7D2/1	30,780	—
	7D6/2	6,980	9,972
[0 ₂ /90] _s	8C3/2	23,195	—
	8C2/1	10,492	11,763
[90 ₂ /0 ₂ /90] _s	3A6/1	22,346	—
	3A10/1 **	1,450	—
	3A10/2 *	7,839	12,078
	3B5/1 **	574	1,407
	3B5/2 **	904	—
[90 ₂ /0 _{1/2}] _s	4A8/1	5,921	4,381
	4B4/2	18,213	14,501
[90/0/90/0 _{1/2}] _s	5A4/1	37,281	17,380
	6A4/2	16,200	—
	6A8/1	7,565	4,957
	6A8/2	8,871	9,369
	6A10/2	6,852	2,228
	5B6/1	20,894	12,871
	6B4/2	5,202	6,343
	5B7/2	11,495	8,907
[90 ₂ /0] _s	7A5/1	20,196	10,323
	7B5/1	12,703	19,721
[90/0 ₂ /90] _s	8A5/1 **	1,624	4,447
	8A5/2 *	6,016	—
	8B7/1	9,191	7,583
	8B8/1	11,750	7,182
	8B9/2	4,650	—
	8B10/1	14,500	—
	8B10/2 **	1,966	—

LOAD RATE = 0.04 mm/min. except as noted otherwise:
(*) 0.40 mm/min; (**) 1.3 mm/min

5.5 Location Distribution Histograms of Events:

As mentioned previously, the AE technique can locate the site of internal damage. By placing two AE sensors some known distance apart (e.g. at both ends of the specimen) the source location can be determined by measuring the time at which the two sensors were hit by an AE event. From the measured time interval and using a proper calibration of the AE instrumentation the source location can be determined in real-time. By recording the source location of all AE events a location distribution histogram (L.D.H.) of events at the desired load level can be plotted. The purpose of obtaining such L.D.H. is three-fold: (1) anticipating the site of catastrophic fracture; (2) locating existing damage, e.g. notches; and (3) determining material quality. The basic concept is that increased AE activity will occur at regions of increased internal damage, stress raisers (e.g. notches), etc., and thus existing damage could be detected and located. Fracture sites could be anticipated in real-time based on increased AE activity at weak sites along the specimen.

Location distribution histograms of events, recorded at selected stress levels, are shown in Figure 5.8* for all twelve laminates. These plots were recorded in real-time during monotonic loading to failure. The stress level and the number of events contained in each L.D.H. are indicated in each distribution. Note that the L.D.H. are for the events generated from the entire gage length, however, the number of events listed in the distributions includes only those which were generated from within the window of 10 to 90 percent of the gage length (see Section 3.4).

Without exception, all L.D.H. show that events were generated from throughout the specimens' gage length. This is expected since matrix transverse cracks, micro-failures at weak sites along the specimen's edges, grating among fracture surfaces, etc., all occur throughout the entire length of the specimen. No distinction between the two groups of laminates can be made, except in the stress level at which emission is first detected, as previously discussed. In most cases shown here a significant amount of emission is generated at both ends of the specimens (i.e. locations 0-10 percent and 90-100 percent). This emission is generated near the stress concentration regions of the end tabs.

* The original plots of all distribution histograms recorded with the D/E-3000 AE system were optically scanned and digitized into a Macintosh computer file and printed on a laser writer by MACreations and Associates, Media, Pennsylvania.

Based on L.D.H. such as those shown in Figure 5.8 the fracture site of the specimen could not be anticipated. In no case is there a distinct region within which AE activity occurred, and all specimens fractured in several locations, due either to tensile fracture or to local buckling which occurred subsequent to the tensile fracture. It should be noted that as the applied stress approaches ultimate the rate of emission becomes very high. When this occurs, a distorted L.D.H. will be recorded. For example, when two events occur at two different locations within a very short time interval (shorter than the travel time between the two AE sensors) they may be recorded as a single event, generated from a single location.

When the specimens contain stress raisers, e.g. notches, the sites of these notches can easily be located. An example is shown in Figure 5.9. This L.D.H. is for a double-edge notched specimen. The notches were machined with a diamond impregnated wheel at the center of the specimen's gage length at location "50" in Figure 5.9. Similar L.D.H. were recorded for other laminates, Table 4. In all cases the notches could be located at a relatively early stage of loading, at approximately 30 percent of ultimate load. In the case of Group I laminates, a significant amount of emission is generated also from throughout the specimen's length at elevated loads. This emission is attributed primarily to the accumulation of matrix transverse cracks throughout the specimen's length, progression of matrix splitting in the 0° plies, delamination, and the associated grating. During initial loading most of the emission is generated from the notch site. In Group II laminates, most of the emission is generated at the vicinity of the artificially induced notch, at location "50". The amount of matrix splitting in this laminate configuration is limited to the notch region only. Most of the emission is due to transverse cracks in the 90° plies. During initial loading these cracks are formed primarily at the notch site. With increasing load they spread away from the notch toward the end tabs. These observations as well as more detailed AE data analysis on these issues will be discussed in Section VII.

5.6 Amplitude Distribution Histograms of Events:

One of the major goals in applying AE to composite laminates is the ability to identify the dominant modes of damage and the failure process. If this goal can be realized several objectives in the research studies of advanced composites could be met, primarily a better understanding of the complex process of failure and of sequence of the formation of the different modes of damage, and for determining damage criticality.

The determination of the failure mechanisms in composites is based upon the analysis of the AE event intensities (e.g. amplitude, energy, RMS, duration, and counts per events, etc.) and upon establishing a correspondence between a specific range of a selected event intensity and a particular mode of damage. The approach is to record the selected intensity of all the events generated during loading, plot the results in an intensity distribution histogram (I.D.H.) format, and assign a specific intensity range to a particular failure mechanism. The interpretation of the AE results is based on the apriori knowledge of the failure process in a given composite laminate and on assuming a relative level of energy released when a particular type of damage occurs. For example, most researchers have assumed that in resin-matrix composites fiber breakage generates high amplitude events while delamination and matrix cracking (or crazing) generate middle and low amplitude ranges, respectively. Another similar approach, is to conduct experiments on a set of different laminate configurations, all of the same material system. If the dominant modes of failure in the different laminates are different and known apriori, the correspondence between the event intensities and the mode of damage can be established through a comparison among the different I.D.H. [1].

Attempts to establish a direct correspondence between I.D.H. and the failure process have met with mixed success. Because the various failure mechanisms occur simultaneously (and at elevated load they occur at high rates), it is difficult to capture a single AE event and associate it directly with a particular mode of damage. In fact, only when model composites are studied can such a direct correspondence between the I.D.H. and the dominant mode of damage be established, e.g. [2-4]. Also, the amount of emission generated is very large and the recorded results only have meaning probabilistically. A significant amount of emission is also generated by the grating among the fracture surfaces. Any interpretation of the results requires the separation of this emission from that generated by the formation of new damage. Finally, different researchers have studied different material systems and laminate configurations, applying different loading functions, utilizing different AE instrumentations and instrumentation set-ups (e.g., using different sensors). Therefore, the research literature contains some contradictory results.

As explained previously, most of the attention in the research studies on AE in composites has been given to the analysis of the AE events amplitude. In the subsequent discussion primary emphasis will be given to comparison between the amplitude distribution histograms (A.D.H.) of the different laminates investigated in this program. Issues such as the effect of the friction emission, loading rate, etc. will be discussed in

later Sections.

Amplitude distribution histograms of all the events generated at different load ranges are shown in Figure 5.10. The A.D.H. shown here are representative for all twelve laminates studied and they are for the same specimens for which the L.D.H. are shown in Figure 5.8. For the purpose of comparing the results recorded for Group I and II, the A.D.H. of two identical cross-ply laminates having reversed stacking sequences are shown next to each other. In order to present clear plots (in terms of scale and resolution), only the A.D.H. recorded during the first 40 to 50 percent of loading are shown for most specimens. Also note that in several cases the A.D.H. are plotted to different scales.

The A.D.H. plotted in Figure 5.10 clearly show that events are generated at three distinct amplitude ranges. The number of events in the different amplitude ranges and the rate of their increase strongly depends on the stacking sequence, and this may indicate different failure processes. The results also show that different A.D.H. are recorded for the two groups of laminates, containing 0° and 90° external plies (Groups I and II, respectively). The A.D.H. of Group I laminates contain events that fall predominantly into two amplitude ranges of 40 dB to 45 dB and 50 dB to 75 dB. On the other hand, most of the events of Group II laminates are in the 45 dB to 60 dB amplitude range and there is a relatively large number of events in the 90 dB to 100 dB amplitude range. For example, the A.D.H. for the $[0_2/90_{1/2}]_s$ laminate, Figure 5.10a, contain events primarily in the 50 dB to 75 dB range, and only at the higher load levels are low amplitude events (40 dB to 45 dB) being generated. On the other hand, in the $[90_2/0_{1/2}]_s$ laminate, Figure 5.10b, most of the events are in the 45 dB to 60 dB range throughout loading, with a relatively large number of high amplitude events (approximately 95 dB). The only exceptions are in the $[0/90/0/90_{1/2}]_s$ and $[90/0/90/0_{1/2}]_s$ laminates, Figures 5.10g and 5.10h, respectively. The similarity between these two A.D.H. is expected due to the similarity in the configuration of these two laminates.

For the reasons explained above, it is difficult to establish a direct correspondence between the low (40 dB to 45 dB) and middle (50 dB to 75 dB) amplitude ranges and the modes of damage. Generally, it seems that most of the low amplitude events are generated by the grating among the fracture surfaces, and this type of emission will increase with the increasing amount of damage. Also, subcritical failures such as matrix crazing, fiber/matrix interface debonding, and fiber pull-out could be sources for low energy emission. The AE instrumentation is sufficiently sensitive to record emission

from these relatively low energy release sources. The middle range amplitude events can be associated with several mechanisms such as matrix cracking, delamination, and matrix splitting. However, emission of the middle amplitude range could also be caused by grating and by the variety of subcritical micro-failures mentioned above. Consequently, at this stage it would be presumptuous to attempt specific designations because no direct correlation is yet available between the actual failure mechanisms and the A.D.H. of events in the 40 dB to 80 dB range. The results are also susceptible to AE system lock-up at high load levels. In addition, the effect of the grating among existing fracture surfaces complicates the analysis because the range of event amplitudes associated with friction overlaps the amplitude range associated with actual matrix dominated damage.

The A.D.H. recorded for the different cross-ply laminates generally show that for laminates containing external 90° plies (Group II) a significantly larger number of high amplitude events are generated than for laminates containing external 0° plies (Group I). In Group I laminates only the laminates which contain double 90° plies generated high amplitude events, Figures 5.10e and 5.10i, while practically no high amplitude events were generated in those laminates which contain single 90° plies. Note that laminates of similar configuration resulted in similar A.D.H., e.g. $[0_2/90_2/0]_s$ and $[0/90_2/0]_s$ (Figures 5.10e and 5.10i, respectively). The A.D.H. of Group II laminates, however, contain a relatively large number of events of high amplitude. The laminates of this group which have double 90° plies generate events of a distinct amplitude range of approximately 95 dB. Those laminates which contain single 90° plies generate also events in the 75 dB to 90 dB range, e.g. Figures 5.10h and 5.10j.

Since high amplitude events are primarily associated with fiber fracture, it is expected that a larger number of fiber breaks are generated in the 0° plies of the laminates containing external 90° plies. For the purpose of substantiating these AE results, identical laminates with reversed stacking sequences were loaded to a predetermined load level (approximately 50 percent of ultimate), unloaded and depled. Subsequent examination of the individual plies under the scanning electron microscope (see Section 4.3) clearly revealed the number of broken fibers in the laminates containing external 90° plies to be significantly larger than in the laminate containing external 0° plies. All the broken fibers were found in the vicinity of the tips of the transverse cracks. It should be noted that in the laminates having external 90° plies the crack opening displacements of the transverse cracks, as observed through the CCTV, were much larger than in the other laminates having external 0° plies, where the 90° plies are constrained

by the neighboring 0° plies. The effect of stress concentrations at the tip of the transverse cracks in the former laminates is expected to be more significant, resulting in an earlier initiation of fiber breakage. This is also indicated by the A.D.H. shown in Figure 5.10. Also, optical observations revealed that the number of transverse cracks and the crack opening displacements of these cracks were much larger in laminates containing double 90° plies as compared with those which contain only a single 90° ply. A larger number of broken fibers is therefore expected in the former case.

The degree of reproducibility of the A.D.H. is shown in Figure 5.11 for three different laminate configurations of Group II. The comparison between the two specimens of each of the three laminate configurations reveal that the A.D.H. are qualitatively very similar. Note that the A.D.H. of the two different specimens of each laminate are for events accumulated during different load ranges. The number of events accumulated in two so-called identical specimens during similar load ranges can be significantly different. In other words, for identical conditions (of laminate configuration, fabrication procedure, specimen geometry, machining procedure, loading function, testing procedure, etc.) the number of events accumulated within similar load ranges can be quite different. This is true whether the specimens were of different plates, Figures 5.11a to 5.11d, or of the same plate, Figures 5.11e and 5.11f. It could be concluded therefore, that the rate of damage accumulation is different among identical cases, however the qualitative similarity in the A.D.H. indicates that the failure process is quite the same.

The A.D.H. of a double-edge notched specimen are quite similar to those recorded for an unnotched specimens. Figure 5.12 shows the A.D.H. for a notched specimen having the same lay-up as those shown for the unnotched specimen in Figure 5.10f. The major difference is that in the unnotched specimen the number of high amplitude events associated with fiber breakage is much smaller. This is expected since the ultimate load is much lower for the notched specimen, thus, the total number of events generated is smaller. Also, in the unnotched specimen fiber breakage can occur at the tips of each transverse crack. The number of transverse cracks in the notched specimen is more limited, and most of them occur in the vicinity of the artificially induced notch. Thus, in the notched case fiber breakage occurs primarily at the vicinity of the notch-tip rather than randomly throughout the entire specimen's gage length. The second difference is that in the notched specimen the relative number of low amplitude (40 dB to 45 dB) events is quite high compared with the unnotched specimen. The reason is that in the notched specimen delamination and matrix splitting emanate from the

notch-tip (to be shown in Section VII), generating large fracture surface areas. With increasing load these fracture surfaces grate against each other, generating low amplitude emission.

All the results shown in Figures 5.1 to 5.12 were recorded with the Dunegan/Endevco (D/E-3000) AE instrumentation. It is capable of rapid real-time data display, however, it is quite limited in its capabilities for post-test data analysis. Since the emphasis in this research was on the appropriate interpretation of the AE results, a significant amount of post-test data analysis was required. Thus, all testing in this research was conducted by using both the D/E-3000 and the Physical Acoustics Corporation (PAC-3000/3004) AE instrumentations simultaneously, as explained in Section 3.4. It should be emphasized here that the AE results recorded depend to a significant extent on the AE instrumentation used and on the instrumentation setup. Thus, it is of interest to compare, for example, the A.D.H. recorded by the two AE instrumentations. Note, that similar instrumentation set-ups were used in both AE systems (see Section 3.4).

The A.D.H. recorded with the PAC system at specific stress ranges (of $R = 40, 60, 70, 80$, and 100 percent of ultimate stress) are shown in Figure 5.13 for the same specimens shown in Figure 5.10 (which were recorded with the D/E AE system). The comparison between the A.D.H. obtained with the two AE systems indicates that the distributions are generally quite similar. Thus, both sets of Figures (5.10 and 5.13) yield similar conclusions. However, the relative number of events within the different amplitude ranges discussed previously and the rate of their accumulation can be quite different. Also, the total number of events accumulated up to failure is different, being lower with the PAC system, Table 12.

The A.D.H. shown in Figures 5.10 to 5.13 can give a qualitative picture of the rate of emission generated within the various amplitude ranges in real-time. More precise quantitative values can be obtained through a post-test analysis of the emission by separating the events generated within selected amplitude (and other intensity) ranges. Representative results of such post-test analyses (based on amplitude) are shown in Figures 5.14 and 5.15 in both dimensional and non-dimensional formats, respectively. The results shown here are in terms of accumulated number of events in five different amplitude ranges as a function of the far-field applied stress. The total number of events generated, Curve No. 1 (40 dB to 100 dB), was separated into four subsets of events having amplitude ranges of 40 dB to 55 dB, 55 dB to 70 dB, 70 dB to 85 dB, and 85 dB to 100

dB, Curves Nos. 2, 3, 4, and 5, respectively. The results shown in Figures 5.14 and 5.15 are for the same specimens shown in the A.D.H. of Figure 5.13. The actual number of events generated within the different amplitude ranges is listed in each Figure and in Table 13.

The results show that in each laminate the accumulated rate of events generated within the different amplitude ranges can be quite different. The cumulative total events (Curve No. 1) follows a nearly exponential curve. In other words, the accumulation rate increases with applied far-field stress up to fracture. This characteristic has been reported in the literature for practically all composites. In four cases, all of Group I laminates, the curves of total events accumulated versus load indicate initially a high event rate, followed by a slower rate, and finally an increasing rate (nearly exponential) as the load approaches ultimate, Figures 5.14a,c,g,i and Figures 5.15a,c,g,i. In all these cases only the curves of the amplitude range of 55 dB to 70 dB follow this trend. It seems therefore that this amplitude range might indicate a specific characteristic of the failure sequence. Efforts were made to identify the cause for this behavior, however, no conclusions could be reached. The events versus applied load curves of the events accumulated within 40 dB to 55 dB and 55 dB to 70 dB amplitude ranges (Curves Nos. 2 and 3) are quite similar to those of the total events, although at lower rates of accumulation.

On the other hand, the characteristic rate and accumulation of events within 70 dB to 85 dB and 85 dB to 100 dB amplitude ranges (Curves Nos. 4 and 5) are quite different. These characteristics can be better seen in Figures 5.16 and 5.17 for the same 12 laminates of Figures 5.14 and 5.15, showing (in dimensional and non-dimensional formats) the event versus applied stress curves for events generated within these two amplitude ranges, respectively. Following initial loading, a relatively high rate of emission occurs in most laminates. However, with further increase in the far-field stress the rate of accumulation decreases. In most laminates the events versus stress curve nearly reaches a plateau as the applied stress approaches ultimate. In the laminates of Group II, the rate of accumulation of the high amplitude events is generally constant up to fracture, Figure 5.17b.

A general qualitative trend in the effect of laminate configuration on the number and rate of events accumulated within the two higher amplitude ranges can now be established. When the laminates of both Groups are made of single 90° plies, the number of events in the 70 dB to 85 dB amplitude range (which are associated with matrix cracks) is much higher than it is in the laminates which contain double 90° plies, and the events initiate at higher loads, Figure 5.16a. This agrees with experimental

TABLE 13. NUMBER OF EVENTS ACCUMULATED WITHIN DIFFERENT AMPLITUDE RANGES

SPEC. NO/ LAY - UP	STRENGTH [MPa]	AMPLITUDE RANGE [dB]				
		40-100	40-55	55-70	70-85	85-100
3 - C9/2 [0 ₂ /90 _{1/2}] _s	1,822	16,560	7,232	7,634	1,550	144
4 - A8/1 [90 ₂ /0 _{1/2}] _s	400	4,381	2,811	1,054	159	357
4 - C2/2 [0 ₂ /90/0] _s	1,664	15,560	6,234	7,521	1,757	48
6 - A8/1 [90 ₂ /0/90] _s	489	4,957	2,947	1,421	150	439
5 - D4/2 [0 ₂ /90 ₂ /0] _s	1,425	8,728	4,897	2,710	692	429
3 - A10/2* [90 ₂ /0 ₂ /90] _s	989	12,070	6,530	4,332	580	628
6 - C7/1 [0/90/0/ 90 _{1/2}] _s	1,327	14,841	6,461	5,828	2,444	108
5 - B6/1 [90/0/90/ 0 _{1/2}] _s	797	12,871	3,805	5,586	2,928	552
7 - C7/1 [0/90 ₂ /0] _s	1,096	10,921	6,806	3,326	324	465
8 - B8/1 [90/0 ₂ /90] _s	1,180	7,182	4,049	1,702	749	682
8 - C10/2 [0 ₂ /90] _s	1,537	13,035	8,756	3,566	539	174
7 - B5/1 [90 ₂ /0] _s	732	19,721	10,210	8,059	971	481

observations and predictions that the thinner the 90° layers are the larger the number of transverse cracks per unit length and the higher the load at which they initiate, e.g. [5-7]. It should be noted here that in all laminates of Group II the events of the 70 dB to 85 dB amplitude range initiate at approximately 25 percent of ultimate stress. This corresponds with optical observations that in this Group of laminates transverse cracks occurred at approximately 35 percent of ultimate stress, Figure 4.9. In most laminates of Group I the events of the 70 dB to 85 dB amplitude range initiate at approximately 35 percent of ultimate stress. This corresponds with optical observations that in this Group of laminates transverse cracks occurred at approximately between 35 to 50 percent of ultimate stress, Figure 4.9.

The effect of laminate configuration on the accumulation of events in the 85 dB to 100 dB amplitude range associated with fiber breakage is shown in Figure 5.17. The results for Group II laminates show that the higher the percentage of the 0° plies, the higher is the number of high amplitude events, as expected. On the other hand, in Group I laminates no correlation can be established between the laminate configuration and the number of high amplitude events. It should be noted here that these specimens fracture at much higher loads than do the Group II laminates. At these high load levels the rate of emission is extremely high, causing inaccurate measurement of the event intensities.

These characteristics of the rate of accumulation of events in the two higher amplitude ranges agree quite well with the damage accumulation curves (in terms of number of matrix transverse cracks) shown in Figure 4.9. It has also been shown in many other studies, e.g. [5-7], that the number of transverse cracks per unit length reaches a plateau as the applied stress approaches ultimate. Thus, it seems that only the higher range amplitude events (i.e. approximately 70 dB to 100 dB) should be associated with the accumulation of critical damage. The nearly exponential curves of events versus stress, reported frequently in the literature on AE in composites, are not necessarily the correct indication of the characteristics of damage accumulation. The reason for the exponential behavior could be, for example, the emission caused by the grating among the fracture surfaces. It should be recalled here that damage generates emission once, when it actually occurs. However, the resulting fracture surfaces can grate against each other for long periods of the loading, resulting in ever increasing emission. The low amplitude range events (i.e. approximately 40 dB to 70 dB) could be associated with such grating. Another source of the low amplitude events can also be the subcritical micro-failures such as matrix crazing, free edge damage and fiber/matrix interface debonding all of

which may generate low amplitude events.

As discussed previously, a comparison of the results between Groups I and II laminates indicates that the emission in Group I initiates at much higher load levels. It is of interest to note that this is the case irrespective of the events amplitude range. However, the high range amplitude events occur at slightly higher load levels. It seems that the micro-failures generating low amplitude events are precursors to the events caused by the more critical damage such as matrix transverse cracking and fiber breakage.

Finally, the curves shown in Figures 5.14 to 5.17 indicate that no sudden surge of emission occurred prior to catastrophic fracture of the specimens irrespective of the amplitude range. In other words, imminent fracture could not be determined even when detailed examination of the rate of accumulation of events of the different amplitude ranges was performed.

5.7 Other Event Intensities:

Acoustic emission events can be analyzed in terms of other intensities as well, e.g. event duration, energy, counts, rise-time etc. As mentioned in Section 5.6, in the research studies of the failure process in composites, the events amplitude is the most commonly used event intensity. Its measurement is relatively simpler, and when the testing procedure is performed properly it is also the most accurate. Second, the state-of-damage in a composite laminate is continuously changing as the number of internal cracks increases during loading. In fact, a nearly infinite number of cracks (including, for example, fiber/matrix debonding) occur at elevated loads. Thus, two identical modes of damage, generating two identical bursts of emission (i.e. releasing the same level of strain energy) in the same specimen, but one in an undamaged state and the other in an already damaged state, will be depicted by the AE sensors as two events of different intensities. The intensities most likely to be affected by the 'current' state-of-damage are, for example, the event duration, energy, and rise-time. The event amplitude will also be affected, but to a significantly lesser degree. Therefore, establishing a correspondence between specific ranges of these different intensities and a particular mode of damage is very difficult. Consequently, only selected results on other event intensities are discussed below, and are shown here only for the sake of completeness. Nevertheless, on a qualitative basis, analyses of these intensities can help in the interpretation of the AE results, primarily in terms of identifying and separating the emission caused by grating.

Figure 5.18 shows the energy counts, duration, and count per event distribution histograms of events generated in two cross-ply laminates of a reversed stacking sequence, during monotonic loading to failure. The corresponding A.D.H. are shown in Figures 5.13c and 5.13d. The distributions shown are for events accumulated during specific load ranges of $R = 40, 60, 70, 80$, and 100 percent of ultimate stress. The plots clearly show that the rate of emission accumulated within the different ranges of intensities varies with increasing load. This is particularly pronounced when the far-field stress approaches ultimate. Also, the characteristics of the distribution histograms are strongly affected by laminate configuration. Note that for the sake of clarity the histograms shown in the Figure are plotted for the full scale of the intensity range of 100 in energy counts, 500 μsec in duration, and 100 in counts per event. In fact, these intensities can be much higher, as will be shown later.

During initial loading most of the events are of approximately 5 to 15 and 1 to 10 in energy counts in the two lay-ups shown, Figures 5.18a and 5.18b, respectively, with only a relatively small number of events outside these ranges. With increasing load, many additional events having intensities outside the above ranges are generated. As the load approaches ultimate (i.e. $R = 80$ to 100 percent), most of the events generated in both laminates are of low energy, below 10 energy counts. These events should be attributed primarily to the grating among existing fracture surfaces. Note, that at elevated loads a nearly infinite number of fracture surfaces exist.

Similar results were recorded for the duration and counts per events, Figures 5.18c to 5.18f. In the laminate which contains external 0° plies most of the events during initial loading are of 50 to 250 μsec in duration and of 10 to 40 counts per events. In the laminate which contains external 90° plies most of the events are of 20 to 150 μsec in duration and below 25 counts per events. When the load approaches ultimate many events generated are also of low intensities, below 50 μsec in duration and below 10 counts per event. Generally, the events generated in the laminate which contains external 0° plies are of higher intensities than those generated in the laminate which contains external 90° plies.

From the histograms such as those shown in Figure 5.18 no direct correspondence can be established between the intensity ranges and a particular mode of damage. However, the rapid accumulation of low intensity events at the upper load levels indicates that a different source of emission is active at this load range. The source of this emission could be the grating among the many fracture surfaces generated during

loading. It will be shown in Section 6.7 that the emission caused by grating is all of low intensities. Such grating will generate a much larger number of AE events, by several orders of magnitude compared with that caused by new damage. Thus, in order to be able to apply the AE technique for monitoring damage progression and the failure process in composites, the emission caused by the grating must first be separated from the data file. This can be achieved if a specific range of intensities can be assigned to the emission caused by grating. A detailed discussion on this issue and the data analysis procedure required are discussed in detail in Section VI.

Before the emission caused by grating can be separated, the correlation between the different ranges of the different intensities should be identified. Obviously, such a correlation depends strongly on the AE instrumentation used, AE parameters selected, type of sensors, etc. An example is shown in Figures 5.19 and 5.20 for the two specimens shown in Figure 5.18. The A.D.H. of all the events generated, Figures 5.19a and 5.20a (taken from Figures 5.13c and 5.13d, respectively) have been separated according to four amplitude ranges of 40 dB to 55 dB, 55 dB to 70 dB, 70 dB to 85 dB and 85 dB to 100 dB, and the corresponding intensity distribution histograms are shown in Figures 5.19b to 5.19e and 5.20b to 5.20e.

As expected, for most events, the higher the amplitude range is, the higher is the intensity range. For the event amplitude range of 40 dB to 55 dB, Figures 5.19b and 5.20b, most of the events are of energy counts, duration, and counts per events below 10, 100 μ sec, and 20, respectively, with many events of extremely low intensities. However, there are also several events of higher intensities. Note that the ordinates of the different distributions are plotted on different scales. Fewer low intensity events occur when amplitude range is of 55 dB to 70 dB. Here, most of the events are within the ranges of 5 to 20 in energy counts, 50 to 200 μ sec in duration, and 10 to 40 in counts per events, Figures 5.19c and 5.20c. The relative number of the higher intensity events is now much larger. For the higher amplitude ranges (i.e. 70 dB to 85 dB and 85 dB to 100 dB) the distribution histograms still contain events of intensities below the above stated values, however, the great majority of the events are of much higher intensities.

A similar separation of events can be performed on the subsets of events in each of the four amplitude ranges in terms of different ranges of the other event intensities. For example, the events contained in the amplitude range of 55 dB to 70 dB, Figures 5.19f and 5.20f, were separated in terms of the energy counts ranges. The resulting amplitude, duration and counts per event distribution histograms are shown in Figures 5.19g,h and

5.20g,h for those events having energy counts above and below 20 energy counts. For both laminates, the majority of the events (6,157 out of 7,521 events (82 percent) and 1,242 out of a total of 1,421 events (87 percent) in the two laminates, respectively) are of energy counts below 20, of duration below 250 μ sec, and below 40 counts per events. When the energy counts of the events contained in the 55 dB to 70 dB amplitude range is above 20, practically all the events are of duration longer than 250 μ sec and counts per event larger than 40. A similar data analysis can be performed for the other amplitude ranges.

It should be noted here that these values strongly depend on the AE instrumentation used, instrumentation set-up, AE sensors, and specimen geometry. Moreover, these intensities are related to each other. For example, for a particular set of AE test variables a 250 μ sec event duration should contain approximately 40 counts when a 150 KHz sensor is used. Since all testing was performed using identical AE variables, these intensity ranges could be used for the AE data analysis.

In conclusions, most of the events contained within the amplitude range of 40 dB to 70 dB are of very low intensities, below 20 in energy counts, 250 μ sec in duration, and 40 in counts per events. Most of these events are caused by the grating among the fracture surfaces (see Section 6.7). However, it has been argued in many of the research studies on AE in composites during the past two decade, that events generated within this amplitude range are associated with matrix dominated failures. This conclusion seems to be premature as long as the events generated by the grating are not first separated from the events caused by damage. In fact, it will be shown later (Section VII) that matrix cracking generates events of amplitudes higher than 70 dB.

5.8 Effect of Loading Rate:

Any AE data analysis can encounter significant difficulties in obtaining reliable information. These difficulties arise from the inherent limitation of all AE instrumentations in acquiring high rates of emission. This is of particular importance at elevated loads at which damage accumulation can occur at extremely rapid rates. In fact, a high rate of emission is expected in most brittle resin-matrix composites (such as graphite/epoxy). In addition, at high load levels a nearly infinite number of fracture surfaces are created, some simultaneously, on the micro-scale (e.g. fiber/matrix debonding) and on the macro-scale (e.g. matrix cracking and splitting). The grating among these fracture surfaces will generate additional emission. Consequently, at elevated loads a high rate of emission will occur, locking-up (disabling) the AE

instrumentation. In other words, multiple events, i.e. trains of events, will be recorded by the AE instrumentation as single events. Thus, the number of events acquired will be always smaller than the actual number of events hitting the sensor. The higher the emission rate is, the larger the difference will be. Only at low load levels, at which the rate of damage accumulation is relatively low and the number of fracture surfaces is relatively small, can the AE data acquired be considered meaningful.

The problem is compounded when the loading rate is too high. In fact, at high loading rate the AE instrumentation will become completely disabled, not acquiring any events. When the number of fracture surfaces is too large and contact among the different fracture surfaces occurs simultaneously at several locations, a high event rate will occur at the lowest possible loading rate. The lower the loading rate the higher will be the loading level at which reliable AE data can be recorded.

High event rates will also cause distorted location distribution histograms of events. For example, when several bursts of emission are generated simultaneously, or within a time interval shorter than the traveling time of the stress waves between the two transducers, the pair of transducers (used for linear location) will 'report' the information as a single event generated from a single site located randomly within the specimen's gage length. The precise location will depend on the time interval between the original emission bursts. The distribution histograms of event intensities will also be distorted, generally indicating higher intensities than actually occurred.

In summary, the AE data recorded at elevated load, during high loading rate, or when a severe state-of-damage exists will cause unreliable results in terms of: number of events, events as a function of applied load (or time), location, amplitude, and other event intensities histograms. In order to illustrate these difficulties, several tests were conducted in which specimens were subjected to monotonic loading to failure at three different stroke rates of 0.04 mm/min (the standard quasi-static test), 0.4 mm/min, and 1.3 mm/min.

The data listed in Table 14 show the effect of loading rate on the total number of events recorded with the D/E-3000 system in two laminates. Clearly, the higher the event rate the smaller is the number of events recorded. The many trains of events generated were recorded by the AE system as single events. The results also show that the loading rate has a significant effect on the load level at which emission initiated. However, this phenomenon should be attributed primarily to the time - dependent

TABLE 14. EFFECT OF LOADING RATE

SPEC. NO.	3-A6/1	3-A10/2	3-B5/1	8B10/1	8-A5/2	8-A5/1
LAY - UP	[90 ₂ /0 ₂ /90] _s			[90/0 ₂ /90] _s		
Stroke Rate [mm/min]	0.04	0.4	1.3	0.04	0.4	1.3
Stiffness [GPa]	60	67	77	84	73	78
Strength [MPa]	873	989	930	1,168	1,048	1,115
AE Init. Stress [MPa]	75	234	308	209	267	311
Init. Stress/Strength [%]	8.6	23.7	33.1	17.9	23.1	27.9
No. of Events (D/E)	22,346	7,839	574	14,500	6,016	1,624
No. of Counts (D/E)	381,742	389,648	99,201	>400,000	269,023	193,426

characteristics of damage initiation and formation.

The total number of events accumulated during the monotonic loading at the three loading rates as a function of applied stress and strain is shown in Figures 5.21 and 5.22, respectively. The results clearly show that loading rate has a significant effect on the rate at which AE events are accumulated. For most laminates an increasing rate of accumulated events (i.e. a nearly exponential behavior) has been recorded under the quasi-static loading of 0.04 mm/min. This is quite typical in Graphite/Epoxy laminates and has been extensively reported in the literature. At the higher loading rate, the emission rate recorded decreases drastically rather than increasing. Note that, as with the data presented in Figure 5.7, only the emission generated during the initial loading (i.e. the first 1,000 events) has been plotted in Figure 5.22 for the reasons explained previously. During this initial loading, varying the loading rate has only a marginal effect on the event rate. This is expected since at this loading range the rate of damage (and thus of emission) generated is relatively low.

The location and amplitude distribution histograms of events recorded in the three different loading rates are shown in Figure 5.23, respectively. Clearly, both distributions are strongly affected by the rate of loading. It is interesting to note, however, that the different distributions are qualitatively quite similar. In any event, the results shown in Figures 5.21 through 5.23 clearly demonstrate that when AE is monitored, the loading rate can have a significant effect on the AE results.

5.9 Testing Procedure:

Finally, many other issues have to be addressed when AE is monitored in coupon specimens made of composites. These include, for example, utilizing spatial filtering (i.e. using a single sensor versus a pair of AE sensors), type of sensor, specimen gripping procedure, tabbing material, dead-time, system gain, etc. Selection of any combination of testing procedures will significantly affect the AE results, and a proper selection of different procedures is crucial for obtaining meaningful AE data. Several examples are shown below.

a. Spatial Filtering - When a pair of sensors is applied some known distance apart, spatial filtering can be applied either in real-time (in the D/E-3000 system) or during post-test data filtering (PAC-3000/3004 system). In either method, events generated outside a preselected "window" along the specimen's length can be eliminated.

For example, by applying spatial filtering, events generated from the grip regions (i.e. unwanted noise) can be filtered from the data file. Similarly, events generated due to friction at the sensor/specimen contact area (which can occur primarily during cyclic loading) can be eliminated. Obviously, such data filtering can not be achieved when only a single sensor is used. In that case, all the events generated from throughout the specimen's length will be included in the data recorded. This issue is mentioned here since a relatively large number of research studies are conducted using a single AE sensor. Figure 5.24 shows, for example, the events as a function of load plots recorded without (Curve No. 1) and with (Curve No. 2) spatial filtering [8]. Clearly, in the former case emission is initiated at a much lower load level. The early initiation of emission resulted from grip slippage causing friction emission. Without spatial filtering, the rate of emission and the total number of events accumulated are significantly higher and not reliable.

In many studies guard transducers are used by which the emission generated from the grip regions are rejected by the AE system. Although this method is quite popular it still raises serious questions regarding the validity of the data recorded. When the guard transducers are activated (by the unwanted emission from the grips) the AE system is disabled, and valid emission generated from within the specimen's gage section can not be acquired by the AE system. The AE system can be disabled for a relatively long period, depending upon the duration of the rejected events, the preselected dead time, and the data processing time. Moreover, when unwanted emission is generated at high rates, the AE system can be deactivated for long periods.

b. Tabbing Material - Special care should be taken in selecting and applying the tabbing material. Reinforced plastics (e.g. Glass/Epoxy) had been, for many years, the most commonly used tabbing material. Emery paper has also been used for specimen gripping, in order to avoid slippage. However, both gripping methods generate a very large amount of emission. In this research program an aluminum alloy (6061F) was selected as the tabbing material and it has been applied as explained in Section 3.4. A comparison of events as a function of load plots recorded with the three tabbing materials applied to unidirectional graphite/epoxy (without spatial filtering) is shown in Figure 5.25 [8]. Clearly, using either emery paper or Glass/Epoxy as the tabbing material generates emission immediately upon loading. In these two cases the rate of emission and the total events accumulated are significantly higher compared with the cases where aluminum tabs are used. In the former two cases, the rate of the emission recorded decreases with increasing load. This decrease resulted from the extremely high rate of

emission. The trains of events generated from the grip regions caused lock-up of the AE system. With the emery paper AE system saturation occurs already at very low load levels, while with the aluminum tabs it occurs only when the load approaches ultimate.

c. Acoustic Emission Sensors - The issue of selecting the appropriate AE sensor is a subject of continuous debate. Emphasis is directed primarily toward the proper balance between sensor frequency response vis-a-vis sensor sensitivity. Most investigators working with composites use sensors of resonance frequency between 140 to 180 KHz, while others are using broad band sensors. A detailed discussion on this issue is beyond the scope of this section. Here only a simple example is shown on the effect of sensor selection on the events versus load curves, Figure 5.26 [8]. As expected, the 175 KHz sensor is more sensitive than the broader band sensor.

In summary, the few examples shown above clearly indicate that for a reliable acquisition of acoustic emission data special care must be taken when selecting a specific testing procedure. Issues such as selection of dead-time, system gain, etc. also deserve special attention. A detailed preliminary investigation on these and other aspects of the testing procedure led to the specific testing variables applied in this study as outlined in Section 3.4. The testing variables applied were identical throughout this investigation.

5.10 Conclusions:

Acoustic emission has been monitored during monotonic loading in twelve different cross-ply graphite/epoxy laminates. Results presented include count-rate and accumulation of events as a function of far-field applied stress and strain, location amplitude, energy counts, duration, and counts per event distribution histograms of events at different load levels, analyses of events in different amplitude ranges, and effect of loading rate and testing procedure on AE results. The correspondence between the different AE results and damage initiation and accumulation and the modes of damage has been discussed, as well as the effect of laminate configuration on AE results. Results presented here were obtained by using both D/E-3000 and PAC-3000/3004 AE systems. Based on the voluminous data that have been recorded and analyzed the following major conclusions could be drawn:

1. The far-field stress and strain at which damage initiates can be precisely determined in real-time from either the count-rate, cumulative counts, or cumulative events curves. No such determination can be achieved from the

stress-strain curves.

2. Significant differences in AE results between laminates having external 0° and 90° plies exist. The major differences between these two groups of laminates are in terms of damage initiation load, cumulative events as a function of stress and strain curves, amplitude, energy counts, duration, and counts per event distribution histograms of events, and rate of events accumulated within different amplitude ranges. However, within each of these two Groups little correlation could be established between the laminate stacking sequence and the AE results.
3. Based on the AE results presented here fracture load and site could not be anticipated. No indication of imminent fracture could be obtained from either the count-rate or events versus applied stress curve, or from the results of the detailed analyses of the event intensities. Similarly, the fracture site could not be anticipated from the location distribution histograms of events.
4. It has been demonstrated that loading rate, testing procedure and AE instrumentation set-up can all have a significant effect on the recorded emission. Primary emphasis should be given to applying the slowest possible loading rate, and eliminating unwanted emission.

5.11 References:

1. M.S. Madhukar and J. Awerbuch, "Monitoring Damage Progression in Center-Notched Boron Aluminum Laminates Through Acoustic Emission", in Composite Materials: Testing and Design (Seventh Conference), ASTM STP 893, J.M. Whitney, Ed., American Society for Testing and Materials, 1986, pp. 337-367.
2. J. Awerbuch and S. Ghaffari,, "Tracking Progression of Matrix Splitting During Static Loading Through Acoustic Emission in Notched Unidirectional Graphite/Epoxy Composites", in Progress in Acoustic Emission III, The Japanese Society of NDI, 1986, pp. 575-585.
3. J. Cohen and J. Awerbuch, "Monitoring Delamination Progression in Graphite/Epoxy Composite Through Acoustic Emission During Fatigue Loading", in the Proceedings of the Fourth Japan-US Conference on Composite Materials, Washington, D.C. June 27-29, 1988, pp. 1035-1046.
4. J. Cohen and J. Awerbuch, "Tracking Progression of Delamination in Model Graphite/Epoxy Composites Through Acoustic Emission During Quasi-Static Loading", MEM CML-8602, Drexel University, October 1987 (to be published in the Journal of Composite Materials).

5. F.W. Crossman and A. S. D. Wang, "The Dependence of Transverse Cracking and Delamination on Ply Thickness in Graphite-Epoxy Laminates," in *Damage in Composite Materials*, Ed. K. L. Reifsnider, ASTM STP 775, 1982. pp. 118-139.
6. M.G. Bader, J.E. Bailey, P.T. Curtis, and A. Parvizi, "The Mechanics of Initiation and Development of Damage in Multi-Axial Fiber-Reinforced Plastic Laminates", in the Proc. of the 3rd Conference on Mechanical Behavior of Materials (ICM-3), the Japan Society of Material Sciences (JSMS), 1979, pp. 227-239.
7. A.S.D. Wang, "Fracture Mechanics of Sublaminar Cracks in Composite Laminates," in Proc. AGARD Specialists Meeting on Defects in Composite Materials, London, 1983. Also, *Composite Technology Review*. Vol. 6, 1984. pp. 45-62.
8. J. Awerbuch, "Effect of Test Conditions on Monitoring Acoustic Emission in Graphite/Epoxy Laminates", Technical Report No. IB 131-81/27, Institut für Strukturmechanik, DFVLR, Braunschweig, Federal Republic of Germany, 1981.

VI. MONITORING ACOUSTIC EMISSION DURING FATIGUE LOADING

6.1 Summary:

Destructive and nondestructive examinations of composite laminates subjected to external loading have indicated that these materials contain a large number of cracks, both on the micro- and macro-scales. Consequently, a significant amount of emission can be generated during fatigue loading not only by damage accumulation and progression but also by the continuous grating among the existing fracture surfaces. Therefore, in order to monitor fatigue damage progression in composite laminates by acoustic emission (AE), the emission caused by this grating should be distinguished from that generated by actual damage growth.

In this study, AE was monitored during fatigue loading in a variety of cross-ply graphite/epoxy laminates. The specimens were subjected to tension-tension ($R = 0.1$) cyclic loading under different dynamic stress amplitudes and loading frequencies. Emphasis was placed on distinguishing the AE events caused by new damage, defined here as "damage events", from the emission generated by grating, defined here as "friction emission". This was done by identifying the emission generated at different load ranges of the load cycle, by the location at which the emission occurs, and by the characteristic intensities of the AE events associated with grating. It has been determined that the great majority of the events should be attributed to grating, and that such emission can occur repeatedly at the same load levels and locations. Furthermore, the event intensities (i.e. energy counts, duration, and counts per event) associated with friction emission are all below given threshold values. Based on these results, the friction emission could be identified and the emission attributed primarily to actual damage accumulation could be separated from the total emission.

A voluminous amount of AE data has been generated and analyzed, Table 3. For the sake of conciseness, only selected case studies are reported here. These are essentially representative of all the tests and data analyses performed in this program.

6.2 Introduction:

Significant research has been conducted during the past decade to characterize the modes of damage and failure processes in composite laminates during fatigue loading. In a cross-ply graphite/epoxy laminate, transverse cracks are first observed in the 90° plies. The number of these transverse cracks per unit length increases with the number of load cycles until reaching saturation, after which there is no further increase in the number of transverse cracks. At the tip of these transverse cracks, which lie at the $90^\circ/0^\circ$ interface, fiber breaks in the adjacent 0° layer occur. Depending upon the loading condition, laminate configuration, and material system, additional local failures such as matrix splitting and delaminations may also form. Detailed discussions of the failure processes in composite laminates during fatigue loading are given for example in [1], and in the references contained therein.

It is of interest to determine the sequence of the failure process in composite laminates and to identify in real-time the development of the various damage modes during fatigue loading. The acoustic emission (AE) technique can offer such a nondestructive testing technique, provided that the characteristics of the AE events can be associated with a particular mode of damage. The complex damage formation that develops during loading, the sensitivity of the AE technique in depicting the occurrence of local deformations and damages (e.g. fiber/matrix interfacial failure), the need for establishing appropriate AE instrumentation parameters, testing procedures, and data analysis methodologies, all make the research into the applicability of this technique highly challenging.

An important issue which has been given relatively little attention in the AE studies performed with composites is the preponderance of emission generated by grating. Due to the complex state-of-damage in composite laminates, it should be expected that a near-infinite number of fracture surfaces are created during the life of the structure. This situation is particularly dominant in advanced resin-matrix composites, such as graphite/epoxy, which are used in today's aircraft and aerospace structures. During fatigue loading, the multiple fracture surfaces (e.g. transverse cracks and local delaminations) repeatedly grate against each other and generate emission continuously. This phenomenon has been frequently observed optically through a high magnification (150X) closed circuit television (CCTV) system. It is essential that this friction generated emission be distinguished from emission generated by new damage before conclusions regarding the failure process and damage accumulation and progression can be

confidently made based on AE analysis.

In a related study [2] it has been demonstrated that the characteristics of the majority of the AE events generated by friction can be identified for the simple case of a notched unidirectional graphite/epoxy composite which contains basically four macro-cracks in the form of matrix splits. In this Section some of the concepts introduced in [2] are further developed and applied to a multidirectional (cross-ply) graphite/epoxy laminate. Emphasis is placed on identifying the emission generated by friction. The effect of loading frequency and rate of emission on AE results, and the correlation between these results and the actual failure process are also discussed. By excluding those events that are attributed to grating, damage accumulation curves have been developed, showing events versus number of cycles curves of those events attributed primarily to the actual damage accumulation. This Section also presents the application of this data analysis methodology to a selected case study in which damage progression is assessed during quasi-static and fatigue loading in cross-ply graphite/epoxy laminate.

A very large number of events is generated during each fatigue test. The rate of emission generated and the characteristics of the event intensities can vary significantly during the progression of the fatigue loading. Thus, for each fatigue test, AE data have been analyzed separately for selected phases of the fatigue loading. For the sake of conciseness only selected case studies from the entire test matrix shown in Table 3 are reported here.

6.3 Experimental Procedure:

Cross-ply graphite/epoxy AS4/3502 laminates of different stacking sequences and ply thicknesses were subjected to uniaxial tension-tension fatigue loading ($R = 0.1$) under load control mode at different frequencies, ranging from 0.01 Hz to 10 Hz, and at different dynamic stress amplitudes. All tests were performed on a closed-loop servo-hydraulic testing machine (Instron Model 1331).

Acoustic emission (AE) was monitored using Physical Acoustics Corporation (PAC) 3000/3004 and Dunegan/Endevco (D/E) 3000 AE instrumentation on the same specimens simultaneously, described in detail in Section III. Post-test spatial filtering to eliminate the unwanted emission was performed. Thus, only the events generated within 20 to 80 percent of the gage length were analyzed. Prior to the fatigue loading,

each specimen was loaded quasi-statically to the preselected dynamic stress level and then unloaded. The discussion of the AE results obtained during the fatigue loading does not include the events generated during the first quasi-static load cycle.

In order to identify the effects of load frequency, damage severity, amount of friction generated emission, etc., the different specimens were subjected to different loading sequences. In each period of the loading sequence the specimen was subjected to a different loading function (i.e. dynamic stress level σ_d , load frequency, f , and number of cycles, N). Only results of selected specimens and loading periods are presented in this Section. Schematics of the loading sequence applied for the different specimens discussed in this Section are shown in Figure 6.1.

All fatigue tests were terminated prior to catastrophic fracture of the specimen. The voluminous number of AE events generated during a complete fatigue test exceeds the available computer disk storage in the AE system. Also, the data analysis of a complete test would be highly time consuming and impractical.

6.4 Separation of Acoustic Emission Events by Load Range:

The simplest and most straightforward way to separate the emission caused by damage accumulation from that generated by friction is by recording only the events generated at the upper load range of the load cycle and concentrating on the data analyses of those events alone. This procedure is frequently applied in the monitoring of AE in metals. A voltage controlled gating is used by which the emission generated in preselected lower load ranges of the load cycle is eliminated from the recording system.

In composites, however, due to the multiple fracture surfaces and the interaction between different damage modes throughout the entire load cycle, there is a high probability that emission is being generated by grating at loads which approach and even equal the maximum dynamic stress level. Furthermore, in many instances the damage (particularly the matrix dominated failures in resin-matrix composites such as graphite/epoxy) propagates so rapidly that the AE instrumentation may fail to record all the emission associated with that particular failure. However, the subsequent grating among these newly created fracture surfaces can continue for extended periods of the loading. Consequently, a significant amount of friction emission can be generated. This friction generated emission can indicate the precise cycle number at which damage occurs and the intermittent nature of its accumulation and progression [2].

Several examples of this phenomenon are shown in the events versus number of cycle plots (E-N curves), recorded with the D/E AE system, Figure 6.2*. Events were recorded in seven different load ranges of the load cycle, accumulated during different periods of the fatigue loading**. A detailed explanation of the data reduction procedure employed for extracting the events recorded in the different load ranges is given in [3]. Briefly, the D/E AE system has been interfaced with a data acquisition system (DEC-MINC-11). Using a specially developed computer program, plots of the events accumulated within predetermined load ranges of each load cycle as a function of number of cycles have been obtained.

For example, Figures 6.2a and 6.2b show the E-N curves for events accumulated during two 1,000-cycle periods of the fatigue loading of a $[0/90_2/0]_s$ laminate. From such E-N curves it could be concluded that during the initial loading (i.e. 100 cycles) most of the emission occurs at the upper load ranges while a relatively small amount of emission is generated at the lower load ranges. In other words, it seems that most of the damage occurs during the initial part of the fatigue loading, whereas a relatively small amount of emission is due to friction during that period of loading. With increasing number of cycles, however, the amount of emission generated at the lower load range (i.e. caused by grating) increases continuously, Figures 6.2a, and 6.2b, while that generated at the upper load range (i.e. caused by damage) rapidly reaches a plateau for relatively long periods of the fatigue loading. This is expected since damage progression generates emission only once, when it actually occurs, while the emission due to the grating among the new fracture surfaces will continue as long as they come in contact with each other. Moreover, as mentioned previously, matrix dominated damage such as transverse cracks in the 90° plies and matrix splitting in the 0° plies progress very rapidly, generating relatively few events. However, the grating among the resulting large fracture surfaces will cause sudden surges of emission. Therefore, the sudden surge of the friction emission can be a better indicator of the cycle number at which damage occurred than does the upper load range emission. This point is clearly illustrated in Figures 6.2b, and 6.2c.

* The specific test conditions, specimen number, laminate configuration, etc. were not incorporated into the text. This information is indicated in all subsequent Figures.

** The results of the AE data analysis shown in all subsequent Figures do not include the events which were generated during the first loading cycle, which was conducted quasi-statically.

There are many exceptions to the general behavior described above. Three examples are discussed below:

1. When additional fracture surfaces are formed (i.e. when new damage occurs), the existing fracture surfaces may now grate at load levels which are different from those at which grating took place previously. Alternatively, the grating among the existing fracture surfaces will cease. Thus, during the fatigue loading surges of emission may occur randomly within different load ranges, e.g. Figure 6.2d. Furthermore, in some instances a significant amount of damage can progress so rapidly that only a few events may be recorded by the AE instrumentation. However, the new fracture surfaces will generate a substantial amount of friction emission, Figure 6.2c.
2. During the initial phase of the fatigue loading most of the emission may be accumulated at the upper load ranges while the rate of emission accumulated at the lower load range is quite low, as mentioned previously. However, high rates of emission can occur at the low load ranges precisely when the rate of emission at the upper load range dramatically decreases, Figure 6.2e. Under load controlled loading any new damage will cause further opening of all existing cracks, reducing the preponderance of the fracture surfaces to grate against each other, which is usually the case during the initial phase of the fatigue loading. Once no additional damage occurs, grating among the newly created fracture surfaces can occur, causing friction emission.
3. The observation that most of the emission is generated at the upper load range during initial fatigue loading requires some qualifications. For example, when the dynamic stress is very high a significant amount of damage is caused during the first load cycle. The grating of this existing damage will generate a significant amount of friction emission immediately during the initial phase of the fatigue loading, Figure 6.2f. A similar situation can arise when a specimen is subjected to a large number of fatigue cycles during which a significant amount of damage occurred. When emission is monitored during randomly selected periods of an extended fatigue loading, emission will be recorded immediately at the lower load ranges, Figure 6.2b. Therefore, it is important that the loading history and/or the state-of-damage are known.

In other words, the existing state-of-damage in the laminate can have a significant

influence on the rate of emission accumulated at the different load ranges. Clearly, loading history also affects the characteristics of the emission accumulation. Thus, any interpretation of AE results requires apriori knowledge of the initial state-of-damage, loading levels, loading history, etc.

Events versus number of cycle curves were also generated using a second AE system, i.e. of PAC 3000/3004 (see Section 6.3). The analysis of the event intensities of events generated throughout the load range of each load cycle, and throughout the entire fatigue loading, can be more readily made with a microprocessor controlled AE system (such as the PAC 3000/3004). Therefore, the latter AE system has been extensively employed in this program*. Consequently, the discussion in the remainder of this Section will be concerned only with the AE data recorded and analyzed with this AE system.

Typical E-N curves for events generated within three different load ranges are shown in Figure 6.3 **. The results shown in Figures 6.3a to 6.3d are for events generated during four arbitrarily selected 1,000-cycle periods of the fatigue loading of a $[0_2/90_2/0]_s$ laminate. The actual load sequence applied is shown in Figure 6.1a. The E-N curves clearly indicate that the rate of accumulation and the number of events accumulated within the different load ranges can vary significantly during fatigue loading. For example, while initially most of the events occurred at the upper load range, Figures 6.3a and 6.3b, with increasing number of cycles no emission was generated at that load range, Figures 6.3c and 6.3d. Also, the total number of events accumulated during each of these periods can vary significantly. The E-N curves recorded with the PAC AE system are generally similar to those recorded with the D/E AE system, shown in Figure 6.2.

Similar results are shown for the second specimen, Figures 6.3e to 6.3h, showing E-N curves of events generated during four 50-cycle periods (see Figure 6.1b) of the fatigue loading of a double-edge notched $[0_2/90_2/0]_s$ laminate. The specimen was subjected to a maximum dynamic stress, σ_d , of 55 percent of the ultimate static strength of the unnotched specimen, or, 77 percent of the ultimate static strength of the notched specimen. Notch length-to-width ratio (a/W) was 0.11. A schematic of the specimen

* The specific fatigue periods selected for the data analysis are indicated in all subsequent Figures. Reference should be made to the schematics shown in Figure 6.1.

** All E-N curves shown in the Figure and in all subsequent Figures are for events accumulated within (10-100 percent) σ_d , (10-60 percent) σ_d , and (95-100 percent) σ_d . Note that plots are in different scales.

geometry is shown in Figure 6.1c. It should be noted that at this stress level, transverse matrix cracks occur during the first load cycle, which was conducted under quasi-static condition. During fatigue loading matrix splitting and delamination emanate from the tips of the notches. As a result of this type of damage repeated grating among these fracture surfaces will occur.

During the first period of the fatigue loading, the E-N curves indicate that most of emission has been generated in the upper load range of the load cycle. In fact, also in this case the relative number of events generated at the upper load range decreases rapidly during the fatigue loading, i.e. from 83 percent during the first 50-cycle period down to 58 percent, and 26 percent, during the second and third 50-cycle period, respectively. However, the relative number of events generated at the upper and lower load ranges changes as the fatigue loading progresses. For example, during the fourth 50-cycle period, Figure 6.3h, the relative number of events generated at the upper load range increased to 45 percent of the total number of events.

When the dynamic stress level is relatively low most of the emission occurs at the upper load range of the load cycle. The events accumulated during the entire fatigue loading (65,000 cycles), for a specimen loaded as shown in Figure 6.1d, are shown in Figure 6.3i. The detail of the E-N curves (for the first 20,000 cycles) is shown in Figure 6.3j from which the intermittent nature of the damage progression can be identified. The intermittency of the damage progression can be seen more clearly in the event-rate plots shown for the two different fatigue periods in Figures 6.3k and 6.3l.

The different cases discussed above clearly indicate that no general rule should be formulated since no two specimens will generate similar characteristics of rate and accumulation of emission. The variability in the state-of-damage among different specimens, loading history applied in different tests, etc., will affect the AE results. The monitoring of AE during fatigue loading will indicate, however, the characteristics of emission caused by damage and grating in each individual specimen tested under the specific loading conditions applied.

From the results such as those shown in Figures 6.2 to 6.3 the following conclusions could be made:

1. Most of the emission is generated at the lower load range, e.g. (10 to 95 percent) σ_d , and it should be attributed primarily to friction;
2. Initially, a larger amount of emission is generated at the upper load range. However, with increasing number of cycles the associated E-N curve rapidly reaches a plateau;
3. The rate of emission at the lower load range, attributable to friction, continues to increase. With increasing number of cycles, the amount of friction generated emission becomes much larger than that generated at the upper load range;
4. The intermittent increases in the rate of the friction-generated emission that result from the creation of new fracture surfaces can quite accurately indicate the intermittent nature of damage progression;
5. Due to the rapidity of damage progression in resin-matrix composite laminates, the AE instrumentation may fail to record all the associated events. However, based on changes in the rate of increase of the AE events associated with friction, the occurrence of new damage can be easily determined in real-time. Therefore, the emission attributable to friction should not be eliminated from the recording system as it is frequently done in the study of metals.
6. The lower rate of increase in the number of events due to friction during different phases of loading can be due to either: a. extension of the damage so that surfaces formerly in contact are spread apart; or b. the presence of a significant damage which generates simultaneous trains of events from fretting between large contact areas. In the latter case the AE instrumentation may become partially locked-out, failing to record individually all the AE events generated. This issue will be discussed in detail in Section 6.9.

In summary, the amount of friction generated emission becomes much larger than that generated by damage. This is expected since damage produces emission only once, at the time of its occurrence, while the subsequent friction among damage surfaces can occur repeatedly whenever the existing fracture surfaces come in contact. When the delamination progresses too rapidly for the AE system to record, the occurrence of damage can be inferred from the subsequent increase in the friction-generated emission.

Moreover, the cycle number at which a sudden damage growth occurs can be easily and precisely determined based upon the sudden surge in the friction generated emission.

6.5 Load and Location Distribution Histograms of Acoustic Emission Events:

The results shown in Figures 6.2 to 6.3 are confirmed by the three dimensional plots of Figure 6.4. The Figure shows the load distribution histograms of events generated during the first 10,000 cycles for two different specimens. The results show that during the initial part of the fatigue loading, most of the emission occurred at the upper load range, with scattered events at the low load range at various load levels. With increasing number of cycles, the number of events which occur at the higher load range diminishes. This emission is then followed by emission generated consistently at specific low load levels, e.g. Figure 6.4a. This highly regular emission could only be attributed to the repeated fretting among the fracture surfaces during crack closure. Note that only the transverse cracks could be seen through optical observations. The other modes of damage such as matrix splitting in the 0° plies and local delaminations at the tips of the transverse cracks could not be detected through the CCTV. However, the local matrix splitting and/or internal delamination (which can not be detected optically due to the smallness of the damage) were most probably the source of this low load emission. Such non-visual damage is easily detected by the highly sensitive AE system. When the dynamic stress amplitude is relatively low, the pattern of emission occurring repeatedly at the same load level may not appear, e.g. Figure 6.4b, indicating a limited degree of damage. The location distribution histograms of events shown in Figures 6.4c and 6.4d, for the same two specimens, indicated that emission occurred randomly throughout the specimens' gage length.

With an increasing number of cycles emission is generated at additional load levels with the pattern of consistency continuing, which indicates friction resulting from an increasing number of fracture surfaces. This phenomenon can be clearly seen in Figure 6.5 showing the load distribution histograms of events generated during four different periods (arbitrarily selected) of three specimens. When the dynamic stress level is raised during the fatigue loading, e.g. Figure 6.1e, the sequence in which AE events are generated will repeat itself. That is, immediately upon raising the load most of the emission will occur again at the upper load range, Figure 6.5g, which is associated with the formation of new damage. As the fatigue loading progresses, however, this emission will diminish and most of the events will occur again repeatedly at the same low load levels, Figure 6.5h. It should be noted that the general appearance of the

three-dimensional plots, such as those shown in Figures 6.4 and 6.5, does depend on the selected time scale, which can be seen by comparing Figure 6.4a with Figure 6.5a showing the load distribution histograms during the first 10,000 and 1,000 fatigue cycles of the same specimen.

These results agree well with the location distribution histograms of events shown in Figure 6.6 for the same specimens and cycle periods shown in Figure 6.5. Initially, most of the events occurred throughout the specimen gage length. With an increasing number of cycles, as the amount of damage increases, emission was recorded at specific locations throughout the rest of the fatigue cycle. Since most of this emission was generated at the lower load ranges, (to be demonstrated later) it could be concluded that this emission was caused primarily by friction. When the dynamic stress level is raised during the fatigue loading the new damage will generate again emission throughout the specimen's gage length, Figure 6.6g. However, soon after the pattern of consistency will continue, and emission will occur again repeatedly at the same locations, Figure 6.6h. The emission generated by actual damage at these locations is not necessarily detected by the AE instrumentation (due to its rapidity), however the subsequent friction generated emission identifies these new damage sites. Similarly, when such emission occurs at several locations, a qualitative indication of damage severity can also be established.

The basic assumption made so far was that the emission generated at the upper load ranges, e.g. (95 - 100 percent) σ_d , is associated only with newly created damage. This is the assumption made in monitoring AE during fatigue loading in metals. However, in composite laminates grating can occur also at the upper load range. The reason is that material inhomogeneities, variations in material properties within the same specimen, and lack of perfect symmetry in the far-field load may cause local failures (e.g. a matrix transverse crack, local delamination at the tips of the transverse cracks, and matrix splits) at specific sites within the specimen. These different modes of damage will initiate and progress asymmetrically. Thus, at relatively early stages of loading a locally asymmetrical state-of-stress exists even when care is taken to apply a symmetric (uniaxial) far-field load. This type of damage progression causes extensive fretting among the fracture surfaces throughout the load range and also when the load approaches the maximum dynamic stress. This phenomenon has been clearly identified through optical observations via the CCTV.

Consequently, a sole reliance on the load range for identifying and separating the damage emission is not sufficient. Moreover, the load range at which emission is caused by fretting can not be predetermined before the testing begins, as is done when a voltage controlled gating is applied. The emission generated at different load ranges must be continuously analyzed during the entire fatigue loading. This is necessary since the characteristics of the rate and accumulation of the emission (and its intensities, to be shown latter) also change throughout the fatigue loading as discussed previously.

In summary, the results demonstrate that as the fatigue loading progresses, most of the emission is accumulated during the lower load ranges, i.e. a significantly greater amount of emission is generated by friction than by new damage. This emission occurs repeatedly at specific load levels and at specific sites along the specimen. This phenomenon confirms that this emission should be attributed to the repeated grating among existing fracture surfaces.

6.6 Acoustic Emission Event Intensities:

The conventional procedure for determining the failure modes in composites through AE is to analyze the distribution histograms of event intensities such as events amplitude, duration, energy, counts per event, etc. Four examples of the distribution histograms of these major event intensities of all the events accumulated during selected periods of the fatigue loading are shown in Figure 6.7*. These intensity distributions histograms (I.D.H.), as well as all subsequent Figures, are for the events accumulated within 20 to 80 percent of the specimens' gage length as indicated by the location distribution histograms of the events shown in the Figure. The comparison among the I.D.H. clearly indicates that different laminate configurations generate AE events of different intensity distributions. For example, while for a $[90_2/0_2/90]_s$ laminate most of the events are of the low intensity range, Figure 6.7a, for the laminate of the reverse stacking sequence, i.e. $[0_2/90_2/0]_s$, a relatively large number of middle and high intensity events were generated, Figure 6.7b. The loading sequences of these two specimens are shown in Figures 6.1f and 6.1g, respectively.

When a $[90_2/0]_s$ laminate is subjected to fatigue loading most of the events are of the low and middle intensity range, Figure 6.7c. The presence of artificially induced damage can also affect the I.D.H. For example, comparing the I.D.H. of an unnotched

* Note that in the subsequent Figures the different distributions shown are plotted in different scales.

specimen, Figure 6.7b, with that of a double-edged notched specimen (both of a $[0_2/90_2/0]_s$ laminate), Figure 6.7d, shows that in the latter the events intensities are of significantly lower ranges. The large number events of low and middle amplitude ranges in the notched laminate is due primarily to the grating resulting from the extensive matrix splitting and delamination which emanate from the notch-tips during fatigue loading.

Based on the results such as those shown in Figure 6.7 it is difficult to establish any correspondence between the dominant modes of damage and the different ranges of the event intensities. The relationships are particularly questionable since the grating among the fracture surfaces generate emission of intensity similar to that caused by matrix dominated failures. This issue is discussed in great detail in the following Sections.

The load levels at which the events are generated and their intensities can be seen in the point-plots shown in Figure 6.8. These point-plots are for the same specimens shown in Figure 6.7. The distributions of the event intensities indicate that emission can occur throughout the entire load range. The amount of emission generated at the lower load ranges will depend on the current state-of-damage in the subject laminate. The more severe the damage the more emission will be generated by grating at the lower load ranges. In other words, the amount of this emission will depend upon the material system under study, laminate configuration, dynamic stress level, and the number of cycles.

It is of interest to note that most of the emission generated at the lower load ranges is of low intensities. High intensity events occurred only at the upper load range, i.e. at approximately (95 to 100 percent) σ_d . However, at this load range a significant number of low intensity events occurred as well. Note that the precise number of events of a particular intensity generated at a particular load level can not be seen from the point plots such as those shown in Figure 6.8.

The sequence at which each of the different intensity ranges occurred is shown in the point-plots of Figure 6.9 (for the same specimens shown in Figures 6.7 and 6.8). These plots show that events of all intensity ranges are generated throughout the fatigue loading. However, the number of high intensity events per cycle decreases as the fatigue loading progresses. The intermittent nature of damage accumulation can also be determined from these point-plots from the cycle number at which high intensity events occur.

The results shown in Figures 6.7 to 6.9 are illustrated more clearly in the three-dimensional plots of Figure 6.10 showing amplitude distribution histograms (A.D.H.) of events for the same two specimens shown in Figure 6.4. At the lower load ranges only low amplitude events occurred while at the upper load range events of the entire dynamic range were generated. Similar results were recorded for all other event intensities. The sequence at which the events of the different amplitudes occurred can be seen in Figure 6.11 for three specimens during four different periods of the fatigue loading. The results clearly show that with increasing number of cycles the number of high amplitude events decreases. This decrease corresponds to the decrease in event rate at the upper load range, Figure 6.3, since high amplitude events occur only at that load range, Figures 6.8 and 6.10. When the fatigue loading extended to a relatively large number of cycles, events of specific low amplitudes were repeatedly generated, e.g. Figures 6.11c and 6.11d.

The results discussed previously clearly demonstrate that during fatigue loading AE events occur throughout the entire load range. From the point-plots such as shown in Figure 6.8 the load levels at which AE events occur and their intensities can be accurately determined. However, it is important to note that both the load levels at which events occur and the event intensities vary throughout the fatigue loading. Two examples are shown in Figures 6.12 and 6.13 for two different specimens. The Figures show the four major event intensities as a function of applied stress during the same four selected periods of the fatigue loading shown in Figure 6.5.

During the initial phase of the fatigue loading, Figure 6.12a, a significant number of high intensity events are generated. Practically all the events are generated in the upper load range, at approximately 95 to 100 percent of σ_d , with a few in the middle and low load ranges of the load cycle. As the fatigue loading progresses, a different distribution of event intensities is recorded, such as that shown in Figure 6.12b. Here, only a few events occurred in the upper load range while events also occurred at the lowest load level. With an additional increase in the number of cycles completely different distribution of event intensities were recorded, such as those shown in Figures 6.12c to 6.12d. In these two 1,000-cycle periods practically no events occurred in the upper load range; rather they occurred primarily in the low and middle ranges of the load cycle. All these events occurred within narrow ranges of the load cycle. In two periods of the fatigue loading, Figures 6.12b and 6.12c, many events occurred even at the lowest load level. These plots indicate that these events were all caused by the repeated grating among the fracture surfaces when the load reaches specific levels. The intensities of

these friction generated events are all low, which may support the argument that the friction generated events could be identified by their low intensities.

The comparison between the point-plots recorded during the different loading periods also indicates the intermittent nature of damage progression, Figure 6.12. During the first 1,000-cycle period most of the events were generated in the upper load range, where the high intensity events are most probably due to damage accumulation, whereas during the later periods events were generated in the middle and lower ranges of the load cycle where no additional damage is expected to occur. It should be noted here that Figure 6.12 shows only four representative 1,000-cycle periods of the entire fatigue loading. The characteristics of the events intensities as shown in Figure 6.12 can repeat themselves randomly as the fatigue loading progresses. Thus, from these AE results, the intermittent nature of damage growth is indicated by the characteristics of both the E-N curves and the point-plots shown in Figures 6.3 and 6.12, respectively.

Depending upon laminate configuration, dynamic stress level, and loading history, the characteristics of the AE results can vary. For example, the results shown in Figure 6.12 for the first two 1,000-cycles periods are different than those shown for a different laminate and dynamic stress amplitude in Figure 6.13. In the latter Figure only a few low intensity events are seen at the low and middle load ranges. When the dynamic stress level is raised during the fatigue loading, Figure 6.1e, many events will again occur near or at the maximum load level. This can be seen in the point-plots of events generated during the third 1,000-cycle period shown in Figure 6.13. At that load level many high intensity events will be generated. As the fatigue loading progresses further (see fourth 1,000-cycle period in Figure 6.13) the number of events at the high load range will again decrease dramatically, while a significant number of events will be generated at the low and middle load ranges and all these events are of low intensities. In other words, by monitoring AE during fatigue loading a sudden change in the rate of damage accumulated due, for example, to a sudden surge in external load, can be easily identified.

The results such as those shown in Figures 6.11 to 6.13 demonstrate that no two cases are similar and no generalization can be made on the pattern in which AE events are accumulated during fatigue loading. Loading function and loading history play an important role in the way acoustic emission is generated. In addition, the type of material studied, laminate configuration, differences in the mode of damage and in the nature of damage accumulation, the inherent scatter among different specimens,

specimen geometry, and AE instrumentation parameters, etc., all affect the AE results. However, the monitoring of AE during fatigue loading can provide a qualitative evaluation of the characteristics of damage accumulation and damage severity in each individual specimen tested.

With a few exceptions, all the events accumulated during the latter periods of the fatigue loading, Figures 6.12 and 6.13, are of low intensities. Since these events are expected to be caused by friction it is not surprising that most of them occurred at practically the same load level. The repeated grating among the fracture surfaces is, in fact, expected to occur at the same load level. Thus, as a preliminary conclusion it could be stated at this stage that the friction generated emission is characterized by a short event duration, low energy counts, and a relatively small number of counts per event.

6.7 On the Correspondence Between Event Intensities and Modes of Damage:

Clearly, establishing a direct correspondence between a particular mode of damage and a specific range of event intensity is difficult. The repeated grating generates emission of intensities similar to those caused by matrix dominated failures. In order to illustrate this issue, the I.D.H. of all the events accumulated during four 1,000-cycle periods of one specimen are shown in Figure 6.14 together with the corresponding L.D.H. The corresponding E-N curves are shown in Figure 6.3. For example, the A.D.H. of all the events recorded during the first 1,000 load cycles shows that events were generated in the entire low and middle amplitude ranges (i.e. 40 dB to 60 dB and 60 dB to 80 dB, respectively), with a few events of higher amplitudes, Figure 6.14a. Based on such results it is difficult to determine any precise correlation between any of the dominant modes of damage governing the failure process of this laminate and any specific range of events amplitude. The lack of any particular correspondence is seen also in the other three I.D.H. (of energy counts, duration, and counts per events) which are all of a wide range, Figure 6.14a.

The relationships are particularly questionable since the I.D.H. recorded during the other three 1,000-cycle periods (Figure 6.14b to 6.14d) display completely different characteristics. Here, the A.D.H. shows primarily low amplitude events during the second 1,000-cycle period, Figure 6.14b. During the third 1,000-cycle period, Figure 6.14c, a large number of events of specific amplitudes of approximately 44 dB and 53 dB is noticeable. A different distribution has been recorded during the fourth 1,000-cycle period, Figure 6.14d. Here, most of the events are of specific amplitudes of approximately

41 dB, 48 dB, 52 dB, and 56 dB. Although most of the events generated during the latter two fatigue periods are of specific amplitude ranges, they do not necessarily correspond to any particular mode of damage. In fact, practically all the events contained in the I.D.H. of these two 1,000-cycle periods, Figures 6.14c and 6.14d, are caused by repeated grating. This can be concluded from the fact that most of the events occurred at specific and low load levels, Figures 6.5c and 6.5d (and Figure 6.12), respectively, and they were generated at specific locations, Figures 6.6c and 6.6d, respectively. It should be noted here that in the literature on AE in composites, the lower amplitude ranges are correlated with matrix dominated modes of damage. The results shown in Figure 6.14 clearly illustrate that friction emission can also be of a similar amplitude range. Although the high amplitude events, Figure 6.14a, could be attributed primarily to fiber breakage [4] no definite conclusions can be made regarding the source (i.e. damage mode) of the low and middle range amplitude events.

Similar distribution histograms were obtained for the other event intensities, that is, as the fatigue loading progresses the event intensities are lower and occur within a narrower range. For example, all the events generated during the fourth 1,000-cycle periods, Figure 6.14d, were separated into four subsets of events based on the following four amplitude ranges: (1) 43 dB to 44 dB; (2) 46 dB to 48 dB; (3) 51 dB to 53 dB; and (4) 56 dB to 58 dB. These ranges were selected based on the specific amplitude ranges seen in the A.D.H. of all the events generated, Figure 6.14d. The I.D.H. of these four subsets of events are shown in Figure 6.15 together with their L.D.H. and they can be compared with those shown in Figure 6.14d for all the events generated. As expected, the events of a specific amplitude range are also of specific duration, energy counts, and number of counts per events. The higher the amplitude range the higher the other intensities are. This is particularly noticeable in Figures 6.15c and 6.15d showing the I.D.H. of the subsets of events of the two higher amplitude ranges. The correlation between the A.D.H. of the events of the two lower amplitude ranges with the corresponding I.D.H., Figures 6.15a and 6.15b, is more difficult because these events are all of extremely low intensities. Finally, all the events of a specific amplitude range are generated at specific locations. This is expected since most of the events generated during this fatigue period are due to grating, as explained previously.

It should be mentioned here that a few high intensity events may occur during the latter periods of the fatigue loading. These events occur randomly, primarily when actual damage occurs. These events can be identified and the cycle number at which they occur can be determined only when the data reduction scheme performed here is

conducted for the entire loading sequence. However, due to the repeated grating among the fracture surfaces at many different sites along the specimen, during each load cycle, a very large number of events is generated. The number of events may exceed the memory size of the AE data acquisition system and will make the data reduction and analysis extremely time consuming and impractical.

6.8 Friction Emission Thresholds (FRET) Values:

The point-plots of Figures 6.8, 6.12, and 6.13 clearly show that all high intensity events occurred at the upper load range, suggesting that these are associated with actual damage accumulation, primarily transverse cracks in the 90° plies, matrix splitting in the 0° plies, local delaminations at the tips of the transverse cracks, and some limited amount of fiber breakage.

On the other hand, it has been shown previously, Figures 6.8, 6.12, and 6.13, that in the lower load range, e.g. below 60 percent of σ_d , only low intensity events were generated. Since in this load range no new damage is expected to occur, it seems that such low intensity events are associated with emission caused by friction. Such low intensity events also occurred throughout the entire load range and many were generated at the upper load range as well. Thus, if the low intensity events are in fact due primarily to grating, a significant amount of friction emission is generated at both the upper and lower load ranges. As a preliminary conclusion it could be stated at this stage that the friction generated emission is characterized by a relatively low energy level, short event duration, and a small number of counts per event.

In order to determine more accurately the characteristics of the friction generated events as recorded by the AE instrumentation, and to investigate the effects of load frequency, state-of-damage, and event rate on the event intensities, a comprehensive experimental program has been conducted with a variety of cross-ply laminates and detailed data analysis and reduction schemes have been developed. Representative results of two such experiments are discussed below.

The first example is for a specimen loaded as shown in Figure 6.1h. The E-N curves for the events accumulated within three different load ranges during the three periods of the first section of the fatigue loading are shown in Figure 6.16. The intensity distribution histograms of these events and the corresponding point plots of event intensity as a function of applied load are shown in Figure 6.17. In order to distinguish

the intensities of the events generated by friction, the events generated at two load ranges of the load cycle were separated through post-test filtering and their intensities were analyzed. The event intensities distribution histograms of the events generated at the upper, (95-100 percent) σ_d , and the lower, (10-60 percent) σ_d , load ranges, Figure 6.16, are plotted in Figure 6.18 for the three periods of the first section of the fatigue loading.

Clearly, the events generated at the lower load range, i.e. (10-60 percent) σ_d , are due to friction only, while those accumulated at the upper load range, i.e. (95-100 percent) σ_d , are caused by a combination of damage progression and friction. It is of interest to note that with an increasing number of cycles the number of events generated at the upper load range decreases, Figure 6.16, similarly to the results shown in Figure 6.3. In the specific example shown in the Figure, during the first fatigue period 72 percent of the events were generated at the upper load range, while only 29 and 27 percent of the events were generated at that load range during the two subsequent periods.

From the amplitude distribution histograms of events, it could be concluded that at the upper load range only a few events are of high amplitude, i.e. above 75 dB, while most of the events are in the low and middle amplitude ranges, between approximately 40 and 70 dB, Figure 6.18. The amplitude of most of the AE events due solely to friction, i.e. those generated within (10 - 60 percent) σ_d , are also within that same range (of 40 to 60 dB). In other words, the A.D.H. alone do not distinguish between friction generated emission and emission generated by matrix dominated failure, in this case primarily by transverse cracks, matrix splitting, and delamination.

A comparison of the other event intensities (i.e. energy counts, duration, and counts per event) generated at the upper and lower load ranges, indicates some interesting differences between the two subsets of events. While at the upper load range high event intensities were generated, at the lower load range all the event intensities are of relatively low values. In fact, from the results shown in Figure 6.18 there appear to be specific threshold values associated with the events generated by friction, i.e. they are nearly all less than approximately 20 in energy counts, less than 250 μ sec in duration, and less than 40 counts per event. In other words, specific Friction Emission Threshold (FRET) values can be assigned to all the event intensities generated by friction. Recalling that a 150 KHz resonance transducer is being used, the FRET values of duration and counts per event are related, as expected. The results such as those shown in Figure 6.18 were obtained repeatedly in this study for the different laminates. In other words, a detailed analysis of the events recorded at the lower load range in a variety of specimens,

having different stacking sequences and ply thicknesses, yielded the same conclusion repeatedly, namely, that at the lower load range only low intensity events were generated. Moreover, all the recorded event intensities were below given threshold values. Similar results were recorded for several different graphite/epoxy laminates which exhibit different modes of damage [13-15]. Also from the distribution histograms of event intensities, studied for various laminate configurations, it could also be concluded that many high intensity events were generated at the upper load range, while no such events were recorded at the lower load range.

It should be noted that the specific FRET values stated above are only approximate values and they may vary slightly among the different specimens. They may also vary during the fatigue loading of a specific specimen, as can be seen in the I.D.H. of Figure 6.18. In many cases the event intensities can be lower than approximately 10 in energy counts, less than 120 μ sec in duration, and less than 20 counts per event, e.g. Figure 6.18f. The FRET values also depend on the morphology of the fracture surfaces which grate against each other. When rugged fracture surfaces with a large amount of matrix serrations come in contact, the friction emission might be of higher intensities than it is when grating occurs among smooth fracture surfaces. Branching of matrix splitting and delamination, fiber bridging, etc. will all affect the intensity of the friction emission. However, in repeated testing, over 90 percent of the events recorded were below the FRET values mentioned above, of approximately 20 in energy counts, less than 250 μ sec in duration, and less than 40 counts per event.

The loading rate can also affect the results. For example, in the specific case shown in Figure 6.18 the specimen was subjected to two different loading frequencies of $f = 0.1$ Hz and $f=1.0$ Hz. While approximately 3-4 events per cycle were recorded at a load frequency of 1.0 Hz, 7-8 events per cycle were recorded at a load frequency of 0.1 Hz. The issue of the effect of loading rate and damage severity on the AE results will be discussed in more detail in Section 6.9.

A second example is shown in Figures 6.19 and 6.20 for a specimen in which the dynamic stress level, σ_d , was increased during the fatigue loading. The Figures show the I.D.H. and the point-plots of event intensities as a function of applied stress for all the events generated during the sixth and eighth periods of the fatigue loading, Figure 6.1e. The corresponding load and location distribution histograms are shown in Figures 6.5g and 6.5h and in Figures 6.6g and 6.6h, respectively. Note that σ_d was increased prior to the beginning of the sixth and eighth fatigue periods and that the Figures do not include

the events generated during the first load cycle (performed quasi-statically) of each fatigue period. Figure 6.19 shows the distribution histograms of all the events generated during these two fatigue periods while Figure 6.20 shows the I.D.H. of the two subsets of events generated at the upper and lower load ranges.

Generally, the results recorded for this specimen, Figure 6.19 and 6.20, are very similar to those shown in Figures 6.17 and 6.18. That is, when the dynamic stress level is increased mid-loading the AE results are very similar to those generated during the initial phase of the fatigue loading. The results shown in Figure 6.19 demonstrate that when the dynamic stress is increased mid-loading the AE will indicate an increased rate of damage accumulation. This can be concluded from the relatively large number of high intensity events, which are associated with new damage, and which were generated at the upper load range, Figure 6.19b. Furthermore, a large number of low intensity events were generated at the lower load ranges. These events, which are due to the grating, indicate the extensive amount of existing damage which has been created during the previous phases of the fatigue loading. When the fatigue loading further progresses, most of the emission is primarily of low intensity, Figures 6.20c and 6.20d, and it should be attributed primarily to grating. Practically all the emission generated at the lower load range is of intensity below the FRET values, Figures 6.20b and 6.20d. With increasing number of cycles events of specific intensity ranges are generated, similar to the case shown in 6.14d. Finally, it should be noted that the relative amount of emission generated at the upper load range decreases as the fatigue loading progresses. While during the sixth fatigue period approximately 45 percent of the events were generated at the upper load range, Figure 6.20a, during the eighth period only 3 percent of the events were generated at that load range, Figure 6.20c. This trend has been discussed previously, Figures 6.3 and 6.16.

The amplitude distribution histograms of events generated at the lower load range, Figures 6.18 and 6.20 include events both in the low (40 dB to 50 dB) and middle (50 dB to 70 dB) amplitude ranges. These event amplitude ranges are commonly associated in the AE literature with matrix dominated failures, e.g. matrix cracking and delamination. It seems that such a conclusive correlation can not be made without knowing apriori that these events are actually caused by damage accumulation. For example, from the results of the event amplitudes shown in Figures 6.18 and 6.20 at the lower load range, one may conclude that accumulation of matrix dominated failures has occurred, while in fact all of the events occurring at the middle and lower load ranges of the load cycle are undoubtedly generated by friction alone. Thus, a sole reliance on the

amplitude distribution histograms of events, or any event intensity distribution histogram by itself, may lead to erroneous conclusions regarding the state-of-damage in composite laminates. It seems that a combination of criteria is necessary in order to detect and identify the failure process more confidently in such material systems.

The fact that friction emission is all of low intensity and below certain FRET values can also be proven by applying a reduced dynamic stress amplitude to a specimen which has already been subjected to a given loading history and thus already contains internal damage. The specific example discussed below is for the specimen subjected to the loading sequence shown in Figure 6.1h. The AE results recorded during the first section of loading were discussed previously, Figures 6.16 to 6.18. After 600 load cycles the maximum dynamic stress level has been reduced to 77 percent of the previous level for an additional 1,000 cycles at loading frequencies of 0.1 Hz and 1.0 Hz, Figure 6.1h. At that reduced load level very little if any additional damage is expected to occur. The I.D.H. of events generated during the first 50-cycle period (at 0.1 Hz.) of this second section of loading, Figures 6.21a and 6.21b, clearly show that all the events are of intensities below the FRET values, verifying again that friction emission is all of low intensity. On the other hand, during the second period of this section of loading, when the load frequency was increased to 1.0 Hz for 900 cycles, several events were of intensities above the FRET values, Figures 6.21c and 6.21d. Most of these events occurred at approximately 30 percent of the current σ_d , thus, they should also be attributed to friction. It will be shown in Section 6.9 that when the loading rate is too high, events overlap and friction emission could be recorded by the AE instrumentation as a single event of increased intensities. In the third period of this section of loading, the loading frequency was reduced back to 0.1 Hz for 50 load cycles. Here again, all the emission is of intensity below the FRET values, Figures 6.21e and 6.21f. Note, that a similar number of events was recorded during the first and third periods, i.e. 58 events and 69 events, respectively.

Similar results were recorded also for the double-edge notched specimen, Figure 6.22. The E-N curves of events accumulated during the four 50-cycle periods are shown in Figures 6.3e to 6.3h. The corresponding load and location distribution histograms are shown in Figures 6.5i to 6.5l and 6.6i to 6.6l, respectively. The results of a detailed analysis of the events recorded in the lower load range show again that only low intensity events are generated, Figure 6.22. During the fatigue loading, the FRET values varied here between 12-20 in energy counts, 180-220 μ sec in duration, and 35-40 in counts per event. It should be noted that the FRET values obtained for the cross-ply laminates

are very similar to those obtained for double-edge notched unidirectional specimens [2]. In the latter case the friction generated emission is caused by fretting along the length of the split fracture surfaces, while in the case of the double-edge notched cross-ply laminates this emission is caused by transverse crack closure in the 90° plies, fretting due to local delaminations in the $0^\circ/90^\circ$ interface, delamination and matrix splitting at the tips of the notches, and fiber/matrix interfacial failure in the 0° plies. As mentioned previously, similar FRET values were recorded for different laminate configurations [2, 5-9]. It seems, therefore, that in graphite/epoxy laminates the mode of fracture surface does not significantly affect the FRET values.

It is of interest to note that the amplitude distribution histograms of events generated in the lower load range include events in the low (40 dB to 65 dB) amplitude range. However, with an increasing number of cycles the event amplitudes are higher, approaching 70 dB, Figure 6.22h. It is possible that these high amplitude events resulted from superposition of overlapping events. Such overlapping events can occur also during low frequency fatigue loading particularly when a severe state-of-damage exists, as explained in Section 6.9. In that case, grating among the fracture surfaces at different sites along the specimen will generate simultaneous events, recorded by the AE system as a single event of increased intensity. Thus, although the 50 dB to 70 dB amplitude range is commonly associated in the AE literature with matrix dominated failures, e.g. matrix cracking and delamination, it seems that such a conclusive correlation can not be made without knowing apriori that these events are actually caused by damage accumulation. For example, from the results of the event amplitudes shown in Figure 6.22h, one may conclude that accumulation of matrix dominated failures has occurred, while in fact all of the events occurring in the middle and lower load ranges of the load cycle are undoubtedly generated by friction alone.

6.9 Effect of Loading Rate and Damage Severity on Acoustic Emission Results:

Before any criteria for distinguishing friction emission from that generated by new damage can be formulated, and before any attempt is made to establish a correspondence between event intensities and a particular mode of damage, it is important to determine the effect of test conditions and state-of-damage on the recorded AE results. The primary source of difficulty is the situation in which trains of events are recorded by the AE instrumentation as a single event with increased intensities. This situation may arise when the loading frequency is too high or when a severe state-of-damage already exists in the material. The latter situation will cause several events to be generated

simultaneously by grating at different fracture surfaces along the specimen, and these events are recognized by the AE instrumentation as single events with high intensities even though the load frequency is sufficiently slow. In both situations events may be generated individually or simultaneously. When such events are generated individually, they may occur within a time interval shorter than the preselected dead-time. Such a train of events will be recorded as a single event of increased duration, energy, and counts per event. Alternately, when the events are generated simultaneously they may overlap, causing the AE instrumentation to record a single event of increased duration, energy counts, and counts per event and, in this case, increased amplitude as well.

The effects of load frequency and state-of-damage on the recorded event intensities are shown in Figure 6.23. The Figure shows the distributions of the event intensities generated during the last 50-cycle period, which followed 350 load cycles at various frequencies (see Figure 6.1b), for the same specimen shown in Figure 6.22. During this period the specimen was subjected to a loading frequency of 1.0 Hz. The I.D.H. show that high intensity events were generated, Figure 6.23a, with several events as high as 80 dB in amplitude, 35 in energy counts, 325 μ sec in duration, and 50 in counts per events. It could be assumed, therefore, that additional damage was generated during that period of loading. The point-plots shown in Figure 6.23b indicate, however, that practically all the high intensity events occurred at the lower load ranges, i.e. at approximately 20 percent of σ_d . In other words, these high intensity events could not be attributed to new damage, but rather to grating.

In order to illustrate this point more clearly, the events shown in the I.D.H. of Figure 6.23a were separated into two subsets of events, for the events generated at the upper and at the lower load ranges. The I.D.H. of these events show that only a few high intensity events were generated at the upper load range, Figure 6.23c. In fact, most of the high intensity events occurred at the lower load range, Figure 6.23d. The comparison of the I.D.H. of the events generated at the lower load range during the previous 50-cycle fatigue period, Figure 6.22h, with those shown in Figure 6.23d, clearly illustrates that increasing the loading frequency (from 0.01 Hz to 1.0 Hz) can significantly affect the recorded event intensities. Although no new damage is expected at that load range and none appeared to occur (through the optical observations) during the latter two periods of the fatigue loading, an increase in event intensities has been recorded for the higher loading frequency. One possible reason is that the grating generated AE events simultaneously at various locations along the specimen. These trains of events were

depicted by the AE instrumentation as single events with increased intensities.

A detailed data analysis of the high amplitude events, in terms of the load level at which they were generated and their location, conclusively revealed them to be caused by grating. For example, the events of amplitude range of 75 dB to 80 dB, depicted in Figure 6.23d, were separated and their intensities were analyzed. The corresponding I.D.H., L.D.H., and point-plots of these events are shown in Figures 6.23e and 6.23f. The Figure shows that all these high amplitude events (i.e. 75 dB to 80 dB) are also of specific high energy counts, long duration, and large number of counts per events (of approximately 35, 330 μ sec, and 50, respectively), as expected. Moreover, all these events occurred at a very low load level, i.e. 20 percent of σ_d , at which no new damage is expected to occur, and they were generated repeatedly at the same location. If the occurrence of trains of events (or overlapping events) had not been identified, these events would have been prematurely attributed to the failure process of the graphite/epoxy laminate.

The fact that high intensity events can also occur when a high rate of friction emission is generated is illustrated in Figure 6.24. The Figure shows the point-plots of amplitude and energy counts of events generated during four different periods of the fatigue loading. During the initial 1,000-cycle period all the events occurred at the upper load range. These events are of both low and high intensities, with the latter being attributed primarily to new damage accumulation. A similar distribution was recorded during the second fatigue period, however, a much smaller number of events were generated during this period and a few high intensity events occurred also at the lower load range, Figure 6.24b. As the fatigue loading progresses, practically all the emission occurred within 20 - 90 percent of σ_d , as seen in the point-plots of the events generated during the third and fourth 1,000-cycle periods, Figures 6.24c and 6.24d, respectively. Many of these events are of high intensities although they should all be attributed to grating. For example, Figure 6.24c shows that events of amplitude as high as 70 dB were generated at 20 percent of σ_d . Recalling that the specimen was subjected to a sinusoidal loading function, the loading rate at that load range is quite slow.

Thus, the only explanation for the high intensity friction emission can be that a severe state-of-damage exists in the subject specimen. During fatigue loading, contact among the existing fracture surfaces occurs along the specimen at many sites simultaneously, generating overlapping events which are recorded by the AE instrumentation as single events of increased intensities. A similar situation is shown for a different specimen in Figure 6.25. Here, high intensity events (of 80 in energy

counts, 800 μsec in duration and 130 counts per events) were generated at approximately 15 percent of σ_d . These high intensity events can be attributed only to overlapping friction events. Thus, although friction emission is all of low intensity, in these specific examples the grating resulted in the recording of high intensity events as well.

The effect of loading rate on the recorded event intensities can also be seen in the point-plots such as those shown in Figure 6.24d. Note, that most high intensity events occurred within the middle load range where (under a sinusoidal loading function) the loading rate is the highest. Therefore, the propensity for the occurrence of trains of events is the highest in this load range. The point-plots of Figure 6.24c show high intensity events which are due to the combined effect of both the extensive grating at the lower load range and the high loading rate at the middle load range. Another case showing the occurrence of trains of events due to high loading rate was shown in Figure 6.21d. The point-plots of friction events (recorded during 900-cycle periods at 1.0 Hz) clearly show high intensity events at approximately 30 percent of σ_d . On the other hand, no high intensity events occurred during the preceding 50-cycle period or during the subsequent 50-cycle period, Figures 6.21b and 6.21f, respectively.

It should be noted here that when grating generates trains of events the distinction between friction emission and damage emission based on the FRET values is not possible. Since these trains of events are recorded by the AE instrumentation as single events of increased intensities, the data filtering based on the FRET values will count the trains of friction events as "damage events". However, the data analysis procedure described above can give a good indication on the appropriateness of the testing procedure employed. When events known to be generated by grating are of high intensities the conclusion is that either the loading rate is too high or a severe state-of-damage already exists in the subject material. When the latter condition occurs, it is possible that trains of friction events will occur also under the slowest possible loading rate. For example, it was shown in [10] that in unidirectional silicon-carbide/titanium-6Al-4V such trains of events can occur also when the loading frequency is as low as 0.001 Hz. If this is the case, the monitoring of AE can be advantageous only in terms of qualitatively determining that a severe state-of-damage actually exists in the subject specimen, while no conclusions regarding damage accumulation or the modes of damage should be drawn. Finally, the data analysis methodology proposed here can not identify the occurrence of trains of "damage events".

6.10 Verification of FRET Values:

The three-dimensional plots of Figures 6.5 and 6.6, plotted for four selected periods of the loading sequence (for three different specimens), show events that were generated repeatedly at the same location and at the same load levels. Therefore, these events could be attributed only to the repeated grating among existing fracture surfaces which occurs during cyclic loading. In order to demonstrate that: (1) the events generated at a specific low load level also have to be generated repeatedly at the same location; (2) the events generated repeatedly at a specific location also have to be generated repeatedly at the same low load level; and (3) the intensities of these events are all below the FRET values, a detailed data analysis of these events has been conducted.

One such example is discussed below for the events generated during the 1,000-cycle period shown in Figures 6.5c and 6.6c. These two Figures are replotted at a higher resolution in Figure 6.26. The three-dimensional plots shown in the Figure indicate that practically all the events occurred repeatedly at three location ranges of approximately 30-42 percent, 50-62 percent, and 68-80 percent of the specimen's gage length. These events also occurred repeatedly within three load ranges of 48, 240, and 272 MPa (12, 60, and 68 percent of σ_d). The events which occurred at a specific location also occurred at a specific load level. For example, the events which were generated within the location range of 30-42 percent of the specimen's gage length (depicted from Figure 6.26a), are replotted in Figure 6.27a. The majority of these events occurred at the specific stress level of 272 MPa (68 percent of σ_d), Figure 6.27b. In other words, when grating occurs at a specific location it also occurs at a specific (and low) load ranges. Furthermore, several events also occurred at the lowest load level, i.e. at approximately 12 percent of σ_d . Thus, under certain conditions, friction emission which occurs at a specific location can occur in several specific load ranges of the load cycle.

In order to determine more precisely the location and load ranges at which friction emission occurred, the L.D.H. shown in Figure 6.26a is replotted in Figure 6.28a, on an expanded scale, showing only the events generated within 35-45 percent of the specimen's gage length. This Figure shows more precisely that these events did not occur in a single location but rather at three different locations. These events were separated by location (of 38.5-39 percent, 39-39.6 percent, and 39.6-40.5 percent) and their L.D.H. are plotted in Figures 6.28b, 6.28c, and 6.28d, respectively. The load ranges at which the four subsets of events (shown in Figure 6.28) occurred can be seen in the three-dimensional plots of Figure 6.29. Clearly, most of the events occurred at the same

two stress levels, of 48 and 272 MPa. Thus, different fracture surfaces which are located at different sites along the specimen may come in contact at the same load range of the load cycle.

Similarly, when the events that are generated repeatedly at the same load range are analyzed, it is found that they also all occur at specific locations. For example, the events which occurred at the two higher load ranges (of 240 and 272 MPa), Figure 6.26b, were separated by load into two subsets of events as shown in Figures 6.30a and 6.30b. The L.D.H. of these events are shown in Figures 6.30c and 6.30d, respectively. Clearly, most of the events occurred repeatedly at specific locations. Moreover, events which occurred at a specific load range, Figure 6.30a, could occur at two different locations, Figure 6.30c. In other words, contact among different fracture surfaces can occur within the same load range of the load cycle.

As mentioned previously, emission which occurs repeatedly at specific locations and at specific low load ranges could be attributed only to the repeated grating among existing fracture surfaces which occur during cyclic loading. Thus it should be expected that the intensity of this emission should all be below the FRET values. In order to prove this point the event intensities of the five subsets of events discussed above (shown in Figures 6.28b,c,d and 6.30a,b) were analyzed. The corresponding I.D.H. and point-plots (together with the corresponding L.D.H.) are shown in Figure 6.31. The I.D.H. show that the events which occurred at specific (but different) locations are all of the same specific intensities (44 dB in amplitude, 2 in energy counts, less than 40 μ sec in duration and less than 6 counts per events), independent of the location at which they occurred, Figures 6.31a to 6.31f. Similarly, events which occurred at specific load levels are also of specific intensities, Figures 6.31g to 6.31j. However, comparison between the I.D.H. shown in Figures 6.31g and 6.31i indicates that the intensity of the events which occurred at different load levels might be different. In all cases, however, all the intensities of the events caused by grating (i.e. they were generated at low load level and at the same location) are below the FRET values.

The data analysis procedure proposed here outlines a methodology for determining the viability of the data interpretation and for distinguishing the majority of the trains of events recorded by the AE system as single events of high intensities. Such a procedure is of importance when reliable information regarding the monitoring of damage progression is sought. It has been demonstrated here that merely relating event intensities to the different modes of damage progression in composites can lead to

erroneous conclusions. However, if the friction generated emission can be identified and extracted and the occurrence of trains of events can be prevented, then damage curves can be derived which appear to be reliable, as discussed in the next Section.

6.11 Emission Generated by Actual Damage Progression:

A simple and straightforward data analysis procedure was employed in this study by which the majority of the events caused by friction during fatigue loading can be distinguished from those generated by actual damage progression. The first stage was to determine the FRET values of the event intensities for the particular material system. This was done by analyzing the intensities of the events known to be generated by friction, that is, those generated during the lower load ranges of the load cycle. The second stage was to identify the occurrence of trains of events due to either a relatively high load frequency or to a relatively large fracture surface area, or to a combination thereof. It is essential that these recorded trains of events be identified before any conclusions regarding damage progression are made. These events can be identified by the load and location at which they occur. If they occur repeatedly at the same (low) load level and at specific locations along the specimen, and in particular if they all have similar intensities that are above the FRET values, it could be concluded that these recorded single events are in fact trains of events and should be excluded from the data file. Obviously, many of the difficulties that arise from the recording of trains of events are eliminated when the load frequency is sufficiently low. Therefore, specimens were excluded from analysis if the AE data were suspected of containing trains of events. The subsequent discussion concerns only those results deemed reliable according to these criteria.

All the events with intensities above the FRET values could be considered to be caused by actual damage progression, and they are referred to here as "damage events". Thus, when AE is applied for monitoring damage accumulation and progression, the entire set of the events generated should be separated into two sub-sets; those having intensities above the FRET, caused by damage; and those having intensities below the FRET, due to friction. The intensity distribution histograms of these two subsets of events were shown in previous Figures.

Two points should be emphasized regarding the determination of damage generated emission:

1. Damage events are defined here as events for which all three intensities (energy counts, duration, and counts per events) exceed the FRET values. If any of the three intensities is below the FRET values, the source of the subject event is considered to be friction. Therefore, the distributions of the friction events shown in previous Figures also include events for which one or two intensities are above the FRET values.
2. It has been demonstrated that all the events caused by friction are of intensities below the FRET values. However, this does not mean that all the events below the FRET values are due solely to friction. It is plausible that some events caused by damage are included in the subset of events having intensities below the FRET. However, such events of low intensities could be considered to be caused by micro-failures, e.g. sub-critical matrix crazing, fiber/interface failure, matrix micro-cracking, etc.

The criteria for damage emission used in this analysis are highly conservative, ensuring that only the events generated by macro-damage progression are counted as new damage. The employment of this data analysis methodology resulted in a much clearer picture of damage accumulation and progression as depicted by the acoustic emission. In the following discussion the rate of accumulation of "damage events" is compared with the rate of events accumulated within different load ranges and with the rate of accumulation of events of different amplitude ranges. From the analysis of the event intensities obtained (shown in previous Figures), it could be concluded that practically no trains of events were recorded as single events during the relevant periods of the fatigue loading.

Figure 6.32 shows the accumulative events as a function of number of cycles for the events generated during different periods of the fatigue loading of three different specimens. The total number of events (curve No. 1) was separated into three subsets of events: those accumulated within the upper load range (curve No. 2); those accumulated within the lower load range (curve No. 3); and the accumulation of those events having intensities above the FRET values (curve No. 4). Since these events are attributed here primarily to actual damage accumulation, the corresponding curve is defined here as "Derived Damage" Curve (DD-curve). The first three curves are the same E-N curves as shown in Figures 6.3 and 6.16.

The results shown in Figure 6.32 clearly indicate that the number of events

attributed to actual damage is significantly smaller than the number of events accumulated at the upper load range (95 -100 percent of σ_d). During the initial phase of the fatigue loading the DD-curves indicate a relatively larger number of "damage events". This number will depend on the dynamic stress amplitude, among other test and material variables. It should be recalled here that the plots shown in Figure 6.32 (as in all previous E-N curves) do not include the events generated during the first loading cycle performed quasi-statically. As the fatigue loading progresses, the number of the accumulated "damage events" decreases. During certain periods of the fatigue loading only a few if any "damage events" were generated, e.g. Figures 6.32c, 6.32d, 6.32i, 6.32j, and 6.32k. This situation occurs primarily in the latter phases of the fatigue loading.

It is not surprising that the number of events attributed to damage is much smaller than those accumulated at the upper load range. Based on the different point-plots shown in the previous Figures it has been concluded that a relatively large number of low intensity events (below the FRET values) also occur at the upper load range. In fact, because of the multiplicity of fracture surfaces, which are oriented in different directions throughout the specimen's length, grating could occur during fatigue loading also when the load approach the maximum dynamic stress level, σ_d . Optical observations revealed that such grating actually takes place. Consequently, attributing the emission generated in the upper load range of the load cycle solely to damage accumulation, as shown in Figure 6.2, may not be sufficiently resolute.

However, it has been demonstrated that by separating the events that occur in the low load ranges, the intensities of events attributable solely to friction can be identified. In this way it is possible to establish the FRET values characteristic of a particular laminate configuration and material system. Based on the FRET values, the emission generated primarily by damage accumulation in the upper load range can then be distinguished from that generated by friction.

As discussed in Section II, the most conventional way of establishing a correspondence between the different modes of damage and AE is by comparing the events amplitude. Thus, a comparison between the accumulation of "damage events" and the accumulation of events of different amplitude ranges was performed as well. Figure 6.33 shows the results analyzed for the same three specimens and the same fatigue periods shown in Figure 6.32. The total number of events (curve No. 1) was first separated into four sub-sets of four amplitude ranges, i.e. for the events within the 40 dB to 55 dB (curve No. 2), 55 dB to 70 dB (curve No. 3), and 70 dB to 100 dB (curve No. 4).

Finally, all the events accumulated throughout the entire load range (10 to 100% of σ_d) were analyzed and only those events having intensities above the FRET values were plotted as a function of number of cycles (curve No. 5).

The resulting curves show a continuous increase in the number of events accumulated within the two lower amplitude ranges. The events of the low amplitude range (i.e. 40 dB to 55 dB) are primarily due to grating, while those of the middle amplitude range (i.e. 55 dB to 70 dB) can be due to a combination of both grating and matrix dominated failures. The rate of accumulation of events of these two amplitude ranges can be different, depending upon the state-of-damage. For example, Figure 6.33a shows that during the initial phase of the fatigue loading the rate of accumulation of the events of the two amplitude ranges is very similar. However, as the fatigue loading progresses, Figure 6.33c, practically all the events are of the low amplitude range. It has been shown previously (e.g. Figures 6.26 and 6.32c) that during this fatigue period only a few events were generated in the upper load range. Moreover, a detailed analysis of the events of the low amplitude range indicated that most of them have intensities below the FRET values. Thus, most of the events are caused by grating and therefore a fewer number of middle range amplitude events are expected to occur. However, during a different period of the fatigue loading the accumulation of the middle range amplitude events may resume, indicating the occurrence of additional matrix dominated failures, Figure 6.33d. The continuous increase in the number of low amplitude events is primarily due to the continuous grating within the laminate.

A different situation is shown in Figures 6.33e to 6.33g. Here, the specimen was subjected to a much higher dynamic stress amplitude. Thus, a significant amount of damage was created already during the first quasi-static load cycle. Consequently, the grating among these fracture surfaces will generate a relatively large number of low amplitude events already within the first few hundred cycles. In the case of the notched specimen, Figures 6.33h to 6.33k, the rate of events accumulation is nearly the same for both sub-sets. Here, the significant amount of matrix splitting and delamination at the tips of the notches will generate middle range amplitude events, while the resulting grating among these fracture surfaces will generate friction emission. The accumulated number of events of the middle amplitude range includes events which are caused by grating as well as by the matrix dominated failures. Therefore, no distinction between these two sources of emission can be made based on the event amplitudes alone, as previously discussed. Only when the friction emission is eliminated (based on the FRET values), the events amplitude associated with the matrix dominated failures can be

identified.

The accumulated number of events generated within the higher amplitude range increases at a much lower rate. Most of these events have intensities higher than the FRET values. This is concluded by comparing curve No. 4 with curve No. 5, showing that the number of events accumulated within the higher amplitude range is very similar to the total number of events having intensities above the FRET values, Figure 6.33. It should be noted here that most of the events having intensities above the FRET values were generated in the upper load range of the load cycle (i.e. 95 to 100 percent of σ_d), as expected. For example, only six out of a total of 483 events which were generated in the lower load range (see Figures 6.5i and 6.32h) are included in the DD-curve of Figure 6.33h. These high intensity events could result either from the occurrence of trains of events, or from contact between two rugged fracture surfaces, or due to actual damage which may have occurred at the lower load range.

The number of events generated by the actual damage progression is much smaller than that generated by friction. The comparison between the curves representing the total events with those having intensities above the FRET values indicates that the great majority of the events are due to friction. The continuous increase in emission is primarily due to continuous fretting within the laminate. Thus, a more precise picture of the damage accumulation and progression can be obtained from the Derived Damage-curves, such as shown in Figures 6.32 and 6.33. The damage accumulation in a composite laminate, as represented by the DD-curve, shows very clearly the intermittent nature of damage growth. For several cases in this study it was determined that there are periods during the fatigue loading where little if any new damage has occurred, while the emission generated by friction will keep accumulating. This behavior was clearly seen through real-time optical observations. The DD-curves of those tests (not shown here) clearly depicted the pattern of damage growth for those cases.

6.12 Tracking Progression of Damage Growth Through Acoustic Emission:

The data analysis procedure proposed here has been applied to a case study to determine its viability for monitoring damage initiation and progression during quasi-static and fatigue loading. The double-edge notched $[0_2/90_2/0]_s$ laminate whose AE results during the first 50-cycle period of the fatigue loading were shown in Figures 6.32h and 6.33h was initially subjected to quasi-static loading to the maximum dynamic stress, σ_d , followed by fatigue loading as described in Figure 6.1b. The events recorded during

the quasi-static loading and the first 50-cycle period were analyzed. Those events having intensities below the FRET values were eliminated, resulting in a subset of events presumably generated primarily by damage progression. No trains of events were generated during the fatigue phase of loading ($f = 0.01$ Hz) and special care was taken to minimize the rate of events during the quasi-static phase of the loading, i.e. by applying a loading rate of 2.2 KN/sec (0.5 Lb/sec).

The resulting location distribution histograms of the events retained as being attributable to damage are shown in Figure 6.34a. Note that the events shown in the fatigue section of the Figure are those that were included in the DD-curve of Figure 6.33h. From these L.D.H. of events the pattern of damage progression can be clearly seen. During the initial part of the quasi-static loading, damage occurred only at the notched region (location "50"), as expected. With increasing load, damage accumulation in the notched region becomes more pronounced, and damage begins to accumulate throughout the specimen length. This occurs at approximately 30 percent of the ultimate unnotched strength of the subject laminate. This is the stress at which emission initiates in the unnotched specimens, caused primarily by the initiation of transverse cracks throughout the specimen length, as discussed in Section IV. As the load is further increased, a relatively fewer number of events are generated by damage at the notched region, possibly indicating that no additional matrix dominated failures occur. Instead, damage progresses slowly away from the notched region, although it is still contained within the stress concentration regions of the growing damage. During the fatigue loading, very little additional emission is caused by damage. Emission occurred primarily in the same locations where the damage progressed during the quasi-static loading phase. No new damage occurred at the center of the specimen, which is expected since most of the damage has already occurred. These AE results were conclusively verified through optical observations via the CCTV.

When all the events generated were included in the location distribution histograms, no specific trends could be identified. The results shown in Figure 6.34b, indicate that events were distributed throughout the specimen length without any specific pattern. This is expected since emission can be generated by friction also during quasi-static loading, as previously discussed. Similar results were reported when matrix splitting [11-12] and delamination [9,13] were the dominant modes of damage. It could be concluded therefore that the data analysis methodology proposed here does result in a more accurate picture of the damage progression as monitored by acoustic emission.

6.13 Acoustic Emission During Post-Fatigue Quasi-Static Monotonic Loading

The effect of loading history on emission initiation load and the rate of events accumulation during post-fatigue quasi-static loading has been investigated. For this purpose, specimens were subjected to monotonic quasi-static loading following a predetermined number of fatigue cycles. The results of one such test, performed with a $[0/90_2/0]_S$ laminate, are discussed below. The loading sequence for this specimen was as follows (Figure 6.1e): (1) quasi-static loading to $\sigma_d = 304$ MPa; (2) fatigue loading for 35,000 cycles at $\sigma_d = 304$ MPa; (3) quasi-static loading to 608 MPa; (4) fatigue loading for 9,500 cycles at $\sigma_d = 608$ MPa; (5) quasi-static loading to 710 MPa. The location and load distribution histograms for selected periods of the fatigue loading are shown in Figures 6.5 and 6.6, respectively, and the corresponding point-plots of the event intensities are shown in Figure 6.13.

The events versus far-field applied stress curves for the three quasi-static loadings are shown in Figures 6.35a, 6.35b, and 6.35c, respectively. The curve corresponding to the first loading, Figure 6.35a, is quite similar to the initial curve shown in Figure 5.14i (which has been recorded during quasi-static loading to failure) in terms of emission initiation load and rate of accumulation. Following the fatigue cycles, however, quite different events versus stress curves have been recorded, Figures 6.35b and 6.35c. Several observations can be made from the comparison between the pre-fatigue and post-fatigue events-versus-stress curves, Figure 6.35d:

1. Post-fatigue emission initiation load, σ_{in} , is higher than the maximum dynamic stress, σ_d . This increase could result from the fact that the damage created once during the fatigue loading cannot occur again during the subsequent static loading. The degree of increase in the initiation load will depend on the number of fatigue cycles, dynamic stress level, and on the existing state-of-damage. For example, the ratio of σ_{in}/σ_d for the second quasi-static loading is approximately 1.20, while for the third quasi-static loading it is approximately 1.02.

The lower ratio in the latter case could result from the fact that a severe state-of-damage already existed in the laminate and generated friction emission at earlier stages of the quasi-static loading. Such a conclusion could be based on the point-plots of event intensities such as those shown in Figure 6.36. During the first and second quasi-static loading, Figures 6.36a to 6.36d and Figures 6.36e

to 6.36h, respectively, many high intensity events were generated. However, the intensities of most of the events generated during the third quasi-static loadings, Figures 6.36i to 6.36l, are below the FRET values, i.e. a significant amount of friction emission was generated.

2. The ratio of post-fatigue initiation stress to pre-fatigue initiation stress, σ_{in}/σ_{io} , can be very large. In the example shown in Figure 6.35d this ratio is approximately 1.3 and 2.4 for the second and third quasi-static loadings, respectively. The importance of this lies in the fact that AE results for a specimen subjected to an unknown load history, e.g. fatigue loading, may lead to erroneous conclusions regarding the material quality or the actual state-of-damage. The high emission initiation load may wrongly indicate a good quality material. Therefore, without a precise knowledge of load history, typical AE information such as emission initiation load and rate of accumulation is not only valueless but may lead to completely wrong conclusions. It is imperative that when AE is monitored for structures subjected to an unknown load history, preliminary testing to obtain base-line data should be conducted on virgin specimens.
3. There can be a large scatter among seemingly identical specimens in the number of events generated during the pre-fatigue quasi-static loading, during the fatigue loading, and during the post-fatigue quasi-static loading. Moreover, the number of events accumulated during the post-fatigue loading is independent of the number of fatigue cycles, and no correlation between them could be established. Therefore, the actual number of events generated in each of the loading phases does not provide much valuable information regarding the state-of-damage. However, the fatigue loading has the effect of shifting the event-versus load curve to the right, leading to a significantly lower number of events at a given load level. Therefore, if AE results for virgin specimens are available, a qualitative indication as to the degree of damage severity could be made. It is unclear whether such a shift can indicate life spent, and studies including fatigue testing with much larger number of cycles are warranted.
4. The combined number of events accumulated during the pre-fatigue and post-fatigue quasi-static loading to failure (not shown here) is much lower than the number of events accumulated during quasi-static loading to failure. The large difference is a direct consequence of the so-called shift in the

events-versus-load curves discussed previously. Several explanations can be given to this phenomenon, the most probable being that a significant amount of internal damage has already been accumulated during fatigue loading and this damage does not generate new emission during the post-fatigue loading. Most of the fatigue damage accumulation is non-critical damage, however, since no significant effect on either ultimate strength or stiffness has been detected (note that in this study specimens were subjected to a relatively low number of fatigue cycles).

6.14 Conclusions:

Acoustic emission results in cross-ply graphite/epoxy laminates during fatigue loading indicate that a significant amount of emission is generated at loads significantly below the maximum dynamic stress level, and this emission can be attributed to the grating among newly created fracture surfaces.

It has been demonstrated that: (1) in most cases, the amount of emission generated by such friction exceeds that generated by actual new damage; (2) the friction emission is expected to occur repeatedly at the same location for an extended period of the fatigue loading; (3) the emissions which occur repeatedly at the same location also occur repeatedly within a limited load range; (4) the amount of emission generated at the low load ranges and the number of locations where repeated emission occurs may potentially indicate the severity of damage; (5) friction emission can occur also at the maximum dynamic stress level; and (6) the load at which friction emission occurs could vary as the fatigue loading progresses, due primarily to the extension of the damage.

The friction generated emission can be discriminated through a proper correlation using the AE event intensities (except event amplitude) and the load range in which these events occur. The amplitude distribution histograms of friction generated events are very similar to those generated by matrix controlled failures, e.g. matrix cracks, raising serious questions as to the validity of the correlations between the event amplitude ranges and the matrix controlled failure mechanisms in composites.

It has been shown, however, that the other event intensities (i.e. energy counts, duration and counts per events) of most friction generated events have intensities which are below a given value, defined in this Report as the friction emission threshold (FRET) values. Specifically, the intensities of the events known to be generated by friction are all

below the FRET values of 20 in energy counts, 250 μ sec in duration and 40 in counts per event.

Consequently, the emission generated by fretting among the fracture surfaces in composite laminates can be identified by the intensities of the AE events and by the load levels and locations at which it occurs. It should be emphasized that the specific FRET values discussed here depend on the AE instrumentation, laminate configuration, material system, type of fracture surface, etc. However, for each specific case these values are highly reproducible and can be easily determined by following the data analysis proposed here.

Special care should be given to limit the occurrence of trains of events which are recorded by the AE instrumentation as single events of increased intensities. A data analysis procedure proposed here outlines a methodology for determining the viability of the data interpretation and the appropriateness of the testing procedure and for distinguishing the majority of the trains of events. Such a procedure is of importance when reliable information regarding the monitoring of damage progression is sought. It has been demonstrated here that merely relating event intensities to the different modes of damage progression in composites can lead to erroneous conclusions.

Thus, based on the FRET values, the emission generated by friction could be distinguished from that caused by actual damage growth. By excluding those events whose intensities are below the FRET values, only the events generated primarily by damage are accounted for, yielding the derived damage (DD) curves. Based on these DD-curves, damage accumulation could be more accurately determined. A case study has been presented in which the data analysis methodology developed in this study has been successfully applied to a notched cross-ply graphite/epoxy laminate. By utilizing the events which are included in the DD-curves, damage initiation and progression during quasi-static and fatigue loading could be clearly established.

6.15 References:

1. K.L. Reifsnider, W.W. Stinchomb, E.G. Henneke, and J.C. Duke, "Fatigue Damage-Strength Relationships in Composite Laminates," Air Force Wright Aeronautical Laboratories, Technical Report No. AFWAL -TR-83-3084, Vol. I, 1983.
2. J. Awerbuch and S. Ghaffari, "Monitoring Progression of Matrix Splitting During Fatigue Loading Through Acoustic Emission in Notched Graphite/Epoxy Composite," in the Proceedings of the Second International Symposium on

- Acoustic Emission From Reinforced Composites, The Society of the Plastics Industry, Inc., Montreal, Canada, July 21-25, 1986, pp. 51-58. Also, Journal of Reinforced Plastics and Composites, Vol. 7, May 1988, pp. 245-264.
3. J. Awerbuch, M. Madhukar, and M.R. Gorman, M. R., "Monitoring Damage Accumulation in Filament-Wound Graphite/Epoxy Laminate Coupons During Fatigue Loading Through Acoustic Emission," Journal of Reinforced Plastics and Composites, Vol. 3, No. 1, 1984, pp. 2-39.
 4. J. Awerbuch and W. F. Eckles, "Detection of Failure Progression in Cross-Ply Graphite/Epoxy Through Acoustic Emission," in the Proceedings of the International Symposium on Composite Materials and Structures, Beijing, China, June 10-13, 1986, pp. 889-898.
 5. W.F. Eckles and J. Awerbuch, "Monitoring Acoustic Emission in Cross-Ply Graphite/Epoxy Laminates During Fatigue Loading," in the Proceedings of the Second International Symposium on Acoustic Emission From Reinforced Composites, The Society of the Plastics Industry, Inc., Montreal, Canada, July 21-25, 1986, pp. 78-84. Also, Journal of Reinforced Plastics and Composites, Vol. 7, May 1988, pp. 265-283.
 6. S. Ghaffari and J. Awerbuch, "Monitoring Acoustic Emission in Impact-Damaged Composites," in the Proceedings of the Second International Symposium on Acoustic Emission From Reinforced Composites, The Society of the Plastics Industry, Inc., Montreal, Canada, 1986, pp. 120-125.
 7. J. Awerbuch, and S. Ghaffari, "Effect of Friction Emission on Monitoring Damage in Composite Laminates through Acoustic Emission," in Progress in Acoustic Emission III, The Japanese Society of NDI, 1986, pp. 638-652.
 8. J. Awerbuch, "On the Identification of Failure Mechanisms in Composite Laminates Through Acoustic Emission," in the Proceedings of Acoustic Emission Deutsche Gesellschaft fur Metallkunde E.V. (DGM), Bad Nauheim, Federal Republic of Germany, 19-20 March 1987, pp. 47-58.
 9. J. Cohen and J. Awerbuch, "Monitoring Delamination Progression in Graphite/Epoxy Composite Through Acoustic Emission During Fatigue Loading," in the Proceedings of the Fourth Japan-US Conference on Composite Materials, Washington, D.C. June 27-29, 1988, pp. 1035-1046.
 10. J.G. Bakuckas and J. Awerbuch, "Crack-Tip Damage Progression and Acoustic Emission in Unidirectional Silicon-Carbide/Titanium 6Al-4V Composite," in the Proceedings of the 13th International Symposium for Testing and Failure Analysis, ISTFA/87, ASM, Los Angeles, California, 9-13 November, 1987, pp. 33- 42.
 11. J. Awerbuch and S. Ghaffari, "Tracking Progression of Matrix Splitting During Static Loading Through Acoustic Emission in Notched Unidirectional Graphite/Epoxy Composites," in Progress in Acoustic Emission III, The Japanese Society of NDI, 1986, pp. 575-585.
 12. S. Ghaffari and J. Awerbuch, "Monitoring Initiation and Growth of matrix Splitting in a Unidirectional Graphite/Epoxy Composite," in the Proceedings of the World Meeting on Acoustic Emission, March 20-23, 1989, Charlotte, North Carolina, Journal of Acoustic Emission, Vol. 8, No. 1-2, Jan.-June 1989, pp. 301-305.

13. J. Cohen and J. Awerbuch, "Tracking Progression of Delamination in Model Graphite/Epoxy Composites Through Acoustic Emission During Quasi-Static Loading," MEM CML-8702, Drexel University, October 1987 (to be published in the Journal of Composite Materials).

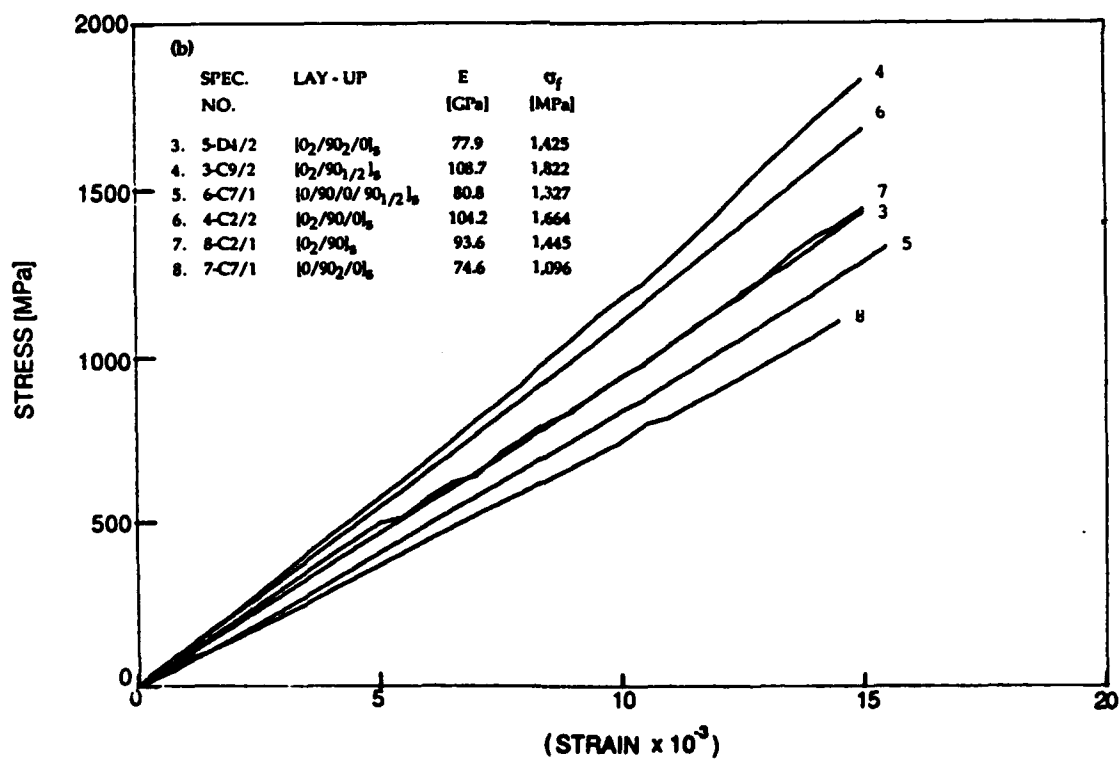
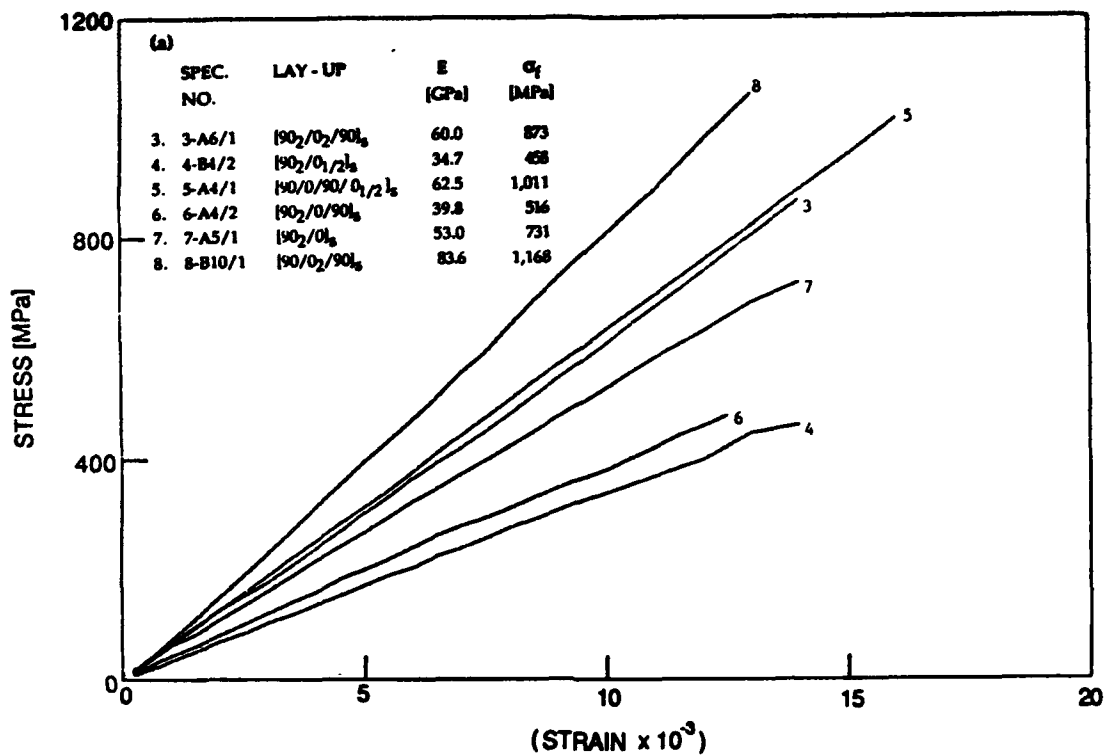


Figure 4.1. Stress-strain curves of twelve different cross ply laminates, showing the effect of stacking sequence on stiffness and strength: (a) 0° plies external; (b) 90° plies external.

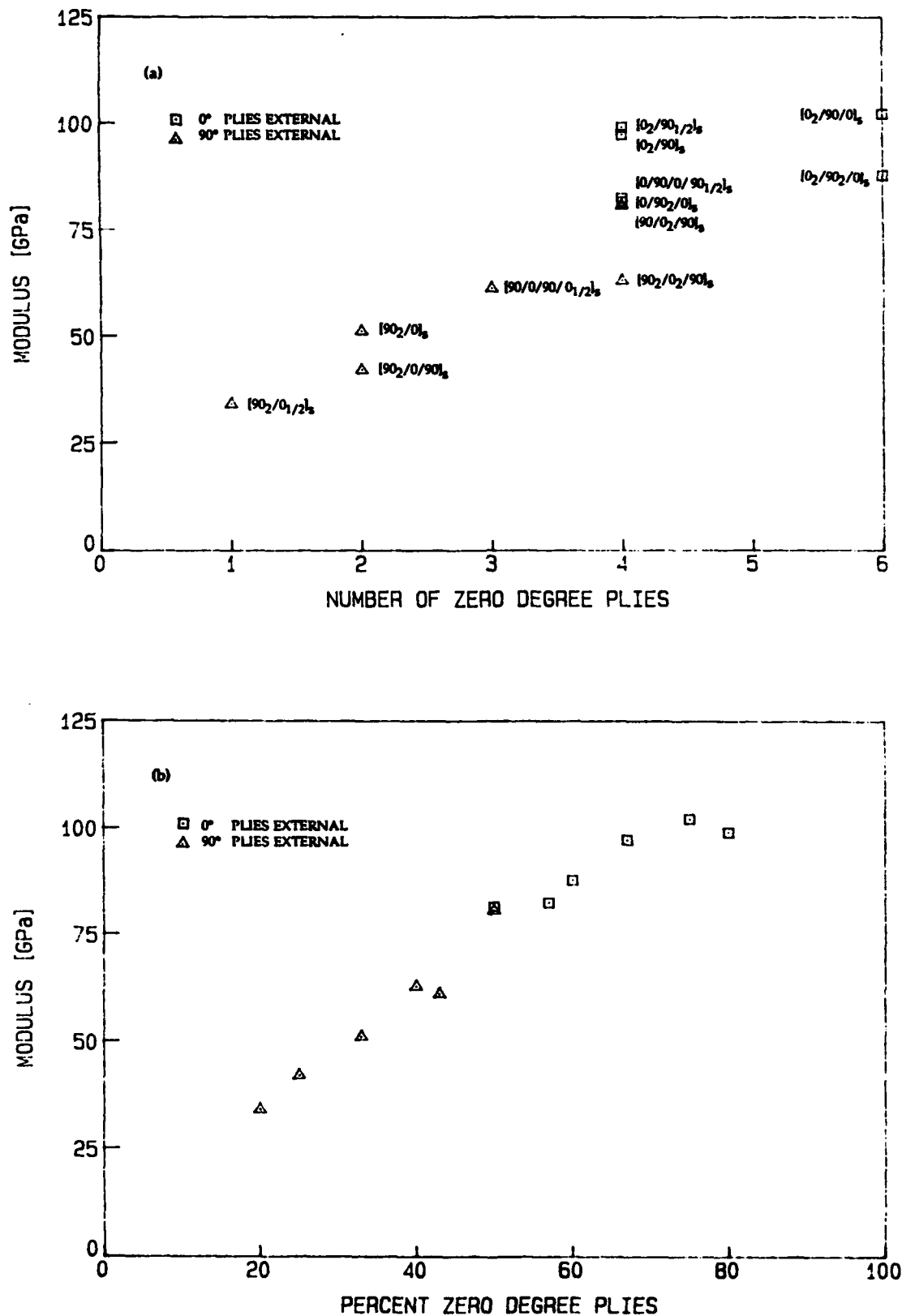


Figure 4.2. Effect of number and percent of 0° and 90° plies on axial stiffness of 12 cross-ply laminates. Axial stiffness obeys the rule of mixture, however, it depends on laminate configuration.

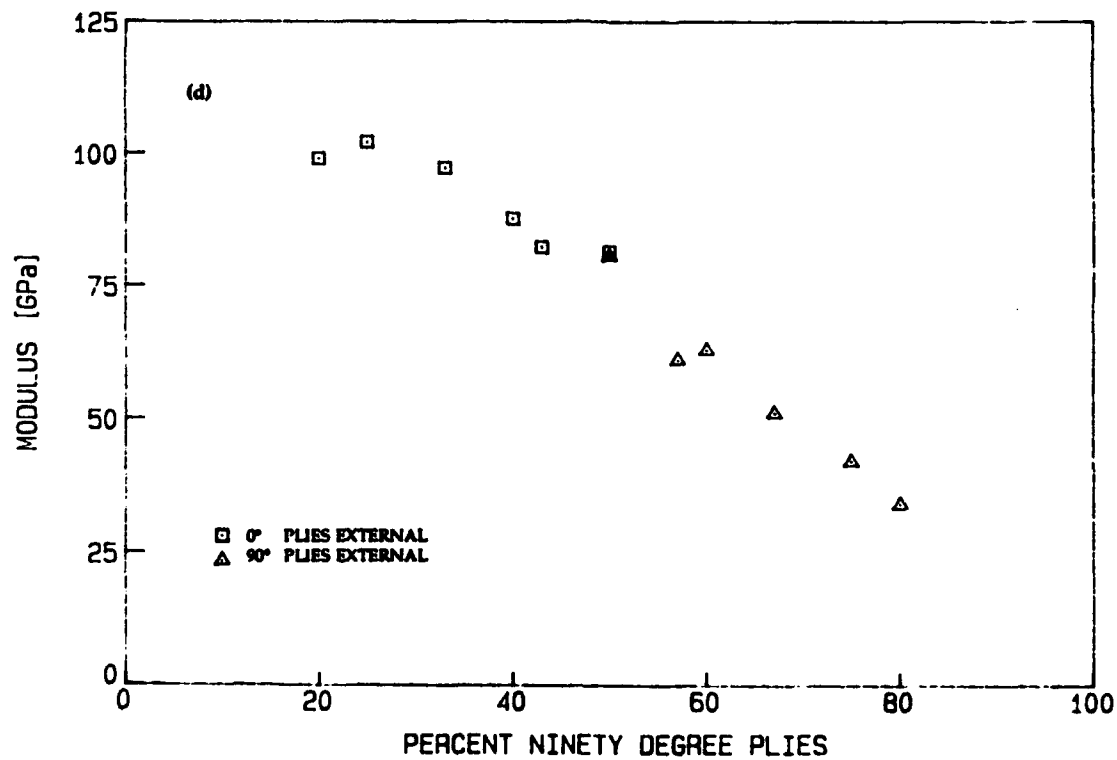
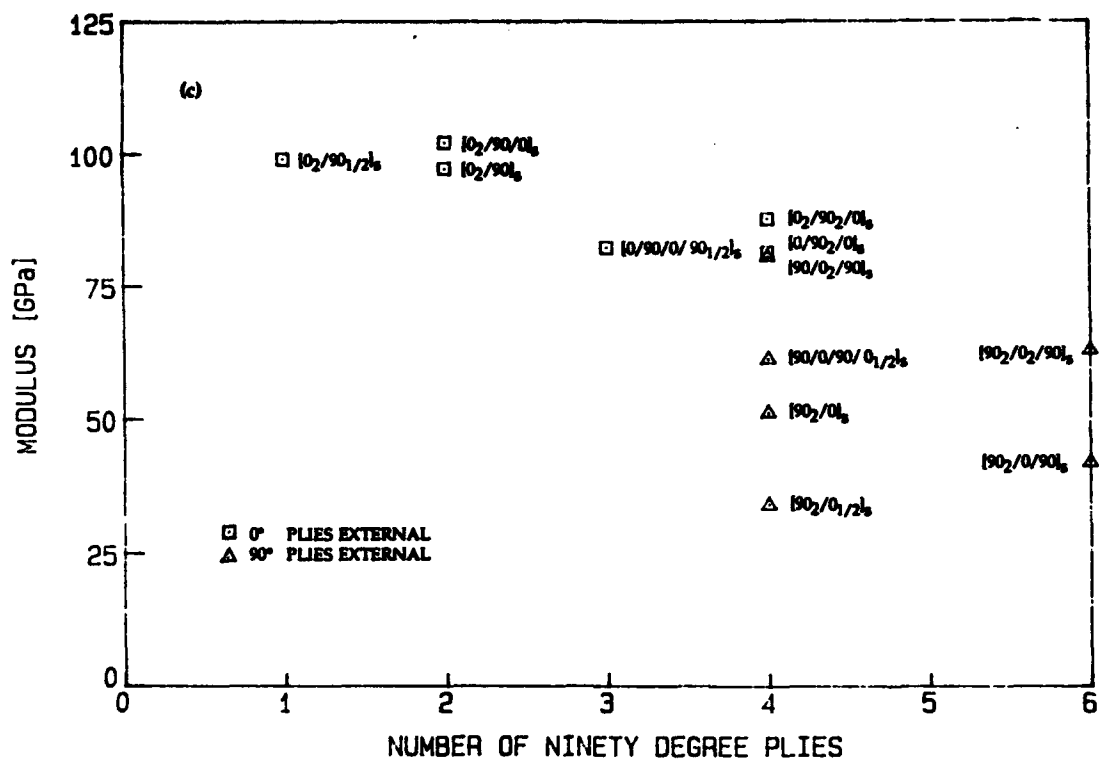


Figure 4.2. Concluded.

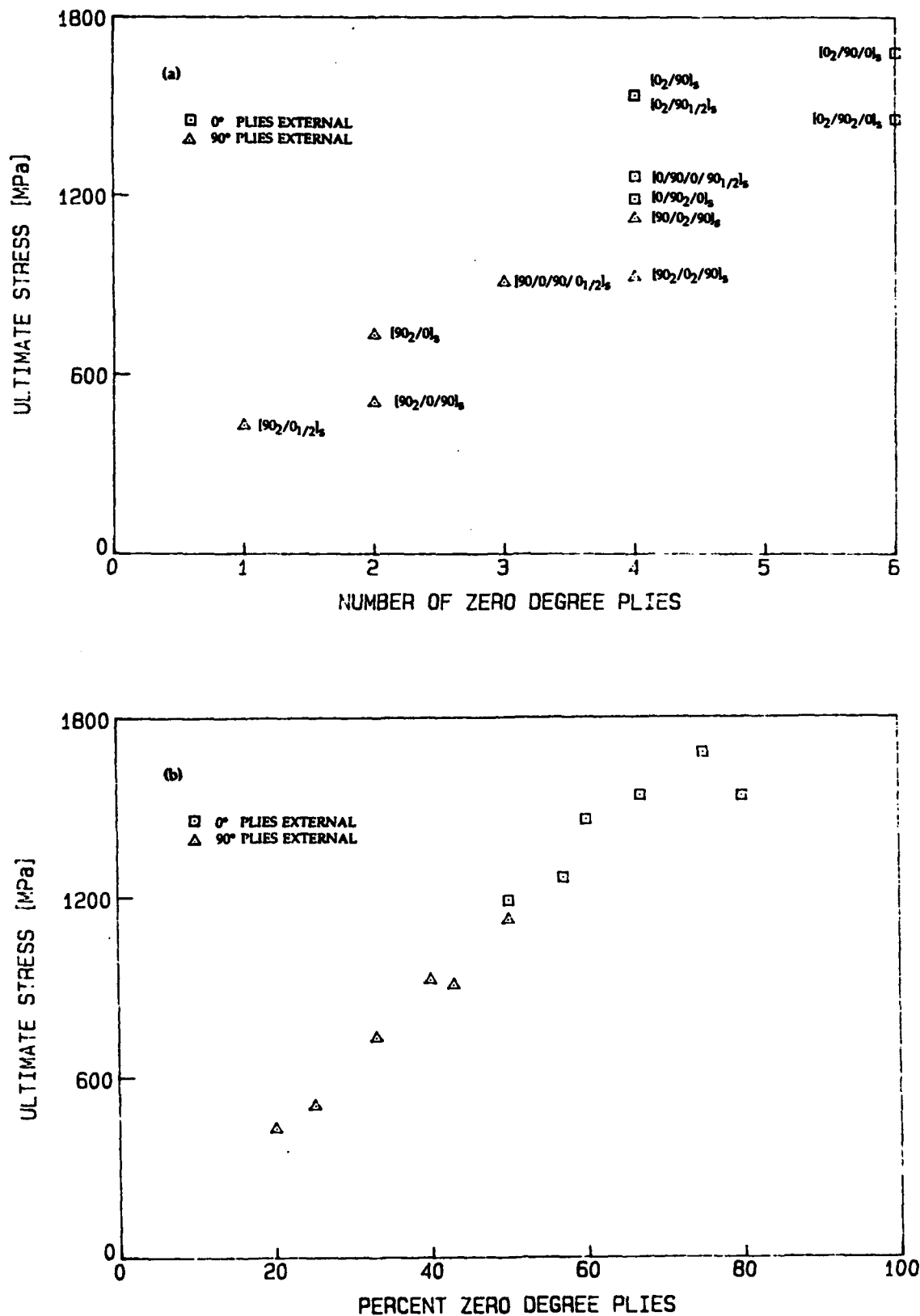


Figure 4.3. Effect of number and percent of 0° and 90° plies on ultimate of 12 cross-ply laminates. Axial stiffness obeys the rule of mixture, however, it depends on laminate configuration.

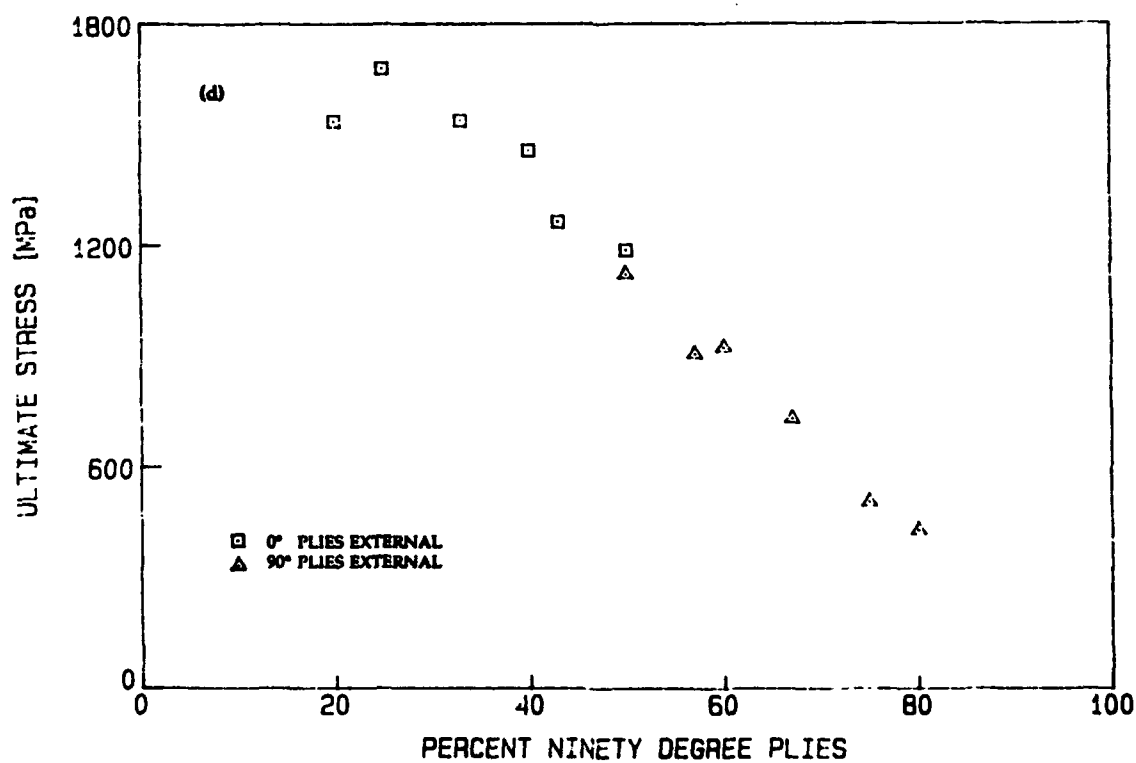
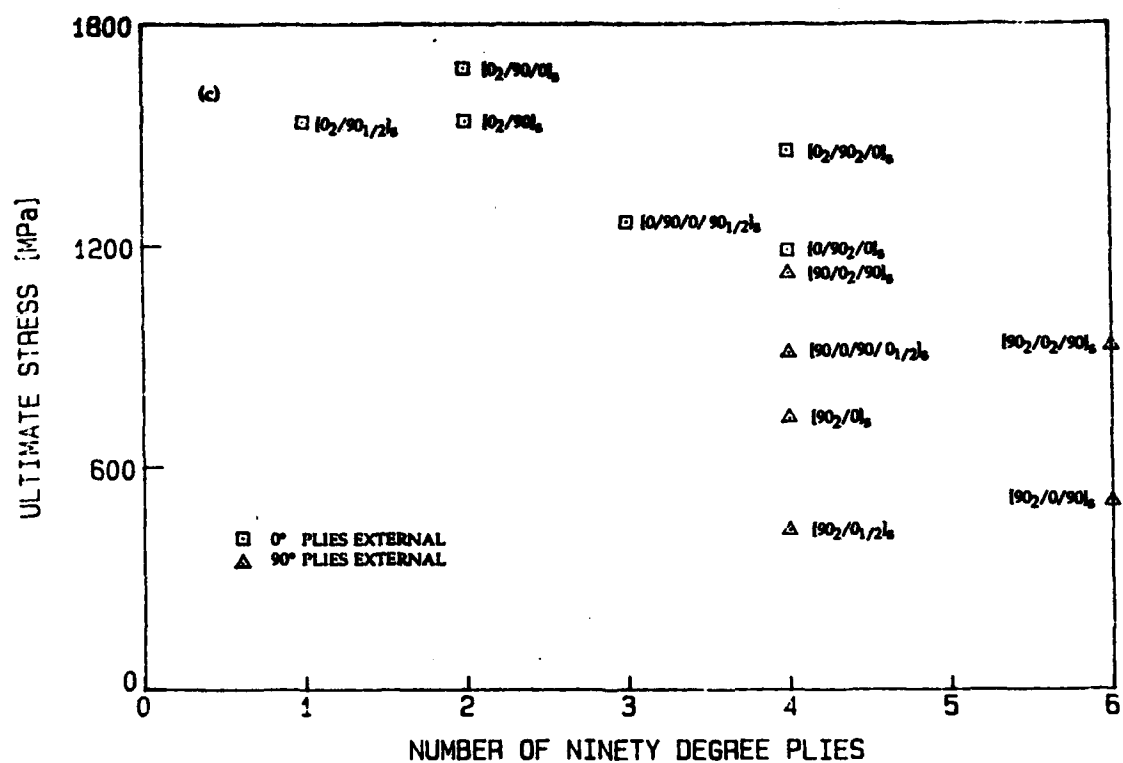


Figure 4.3. Concluded.

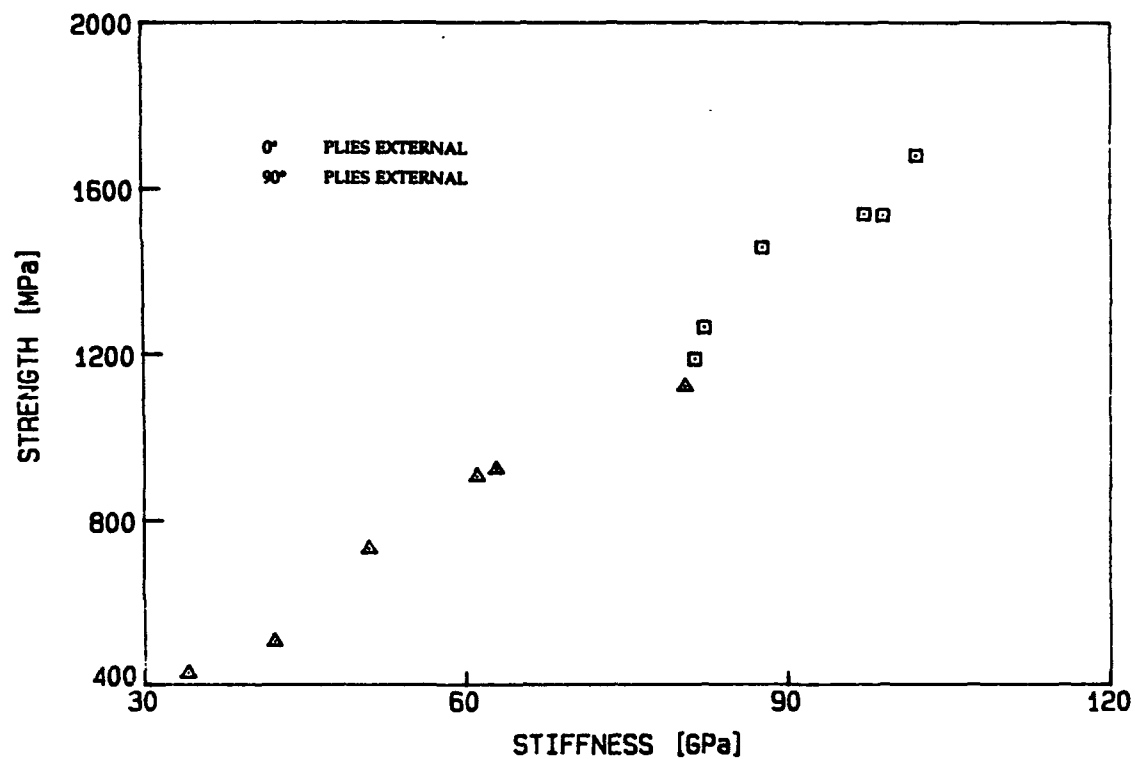


Figure 4.4. Strength versus axial stiffness for all 12 cross-ply laminates tested showing a linear relation.

(a) SPEC. NO. 8-B9/2
LAY-UP: $[90/0_2/90]_s$

$\sigma/\sigma_f = 0.72$



(b) SPEC. NO. 6-A5/2
LAY-UP: $[90_2/0/90]_s$

$\sigma/\sigma_f = 0.81$

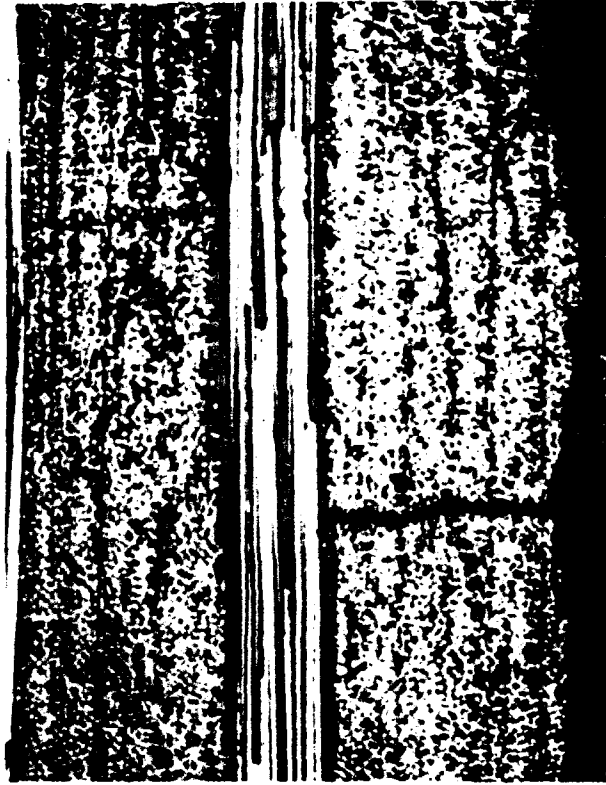


Figure 4.5. Photomicrographs showing the transverse cracks in three cross-ply laminates: (a) a $[90/0_2/90]_s$ laminate after loading to approximately 72 percent of ultimate load; (b) a $[90_2/0/90]_s$ laminate after loading to approximately 81 percent of ultimate load; and (c) a $[90_2/0_2/90]_s$ laminate after loading to approximately 60 percent of ultimate load.

(c) SPEC. NO. 3-A8/2
 LAY-UP: $[90_2/0_2/90]_s$
 $\sigma/\sigma_f = 0.60$

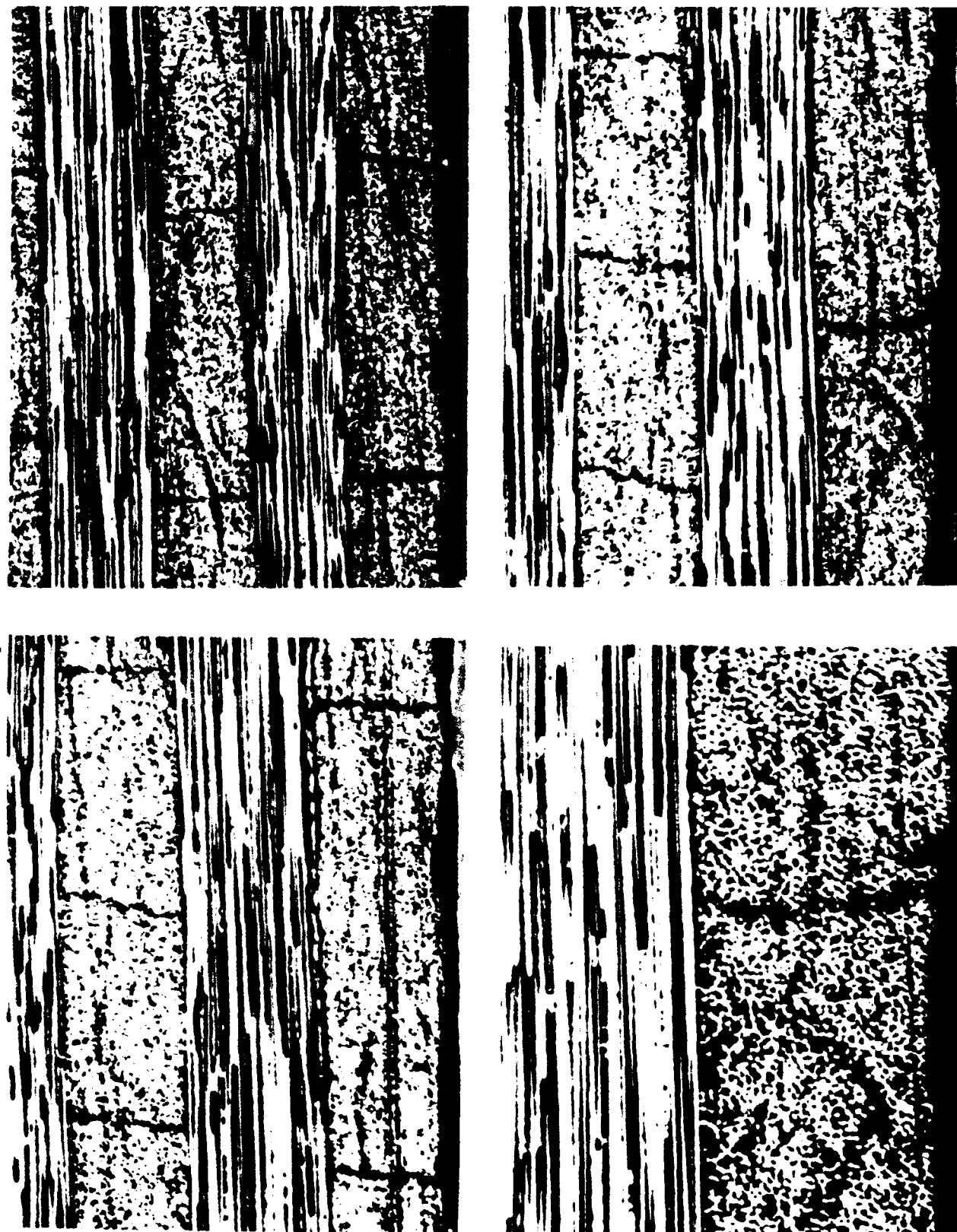


Figure 4.5. Concluded.

(a) SPEC. NO. 3-B6/1
LAY-UP: $[90_2/0_2/90]_s$
 $\sigma_f = 914.4 \text{ MPa}$

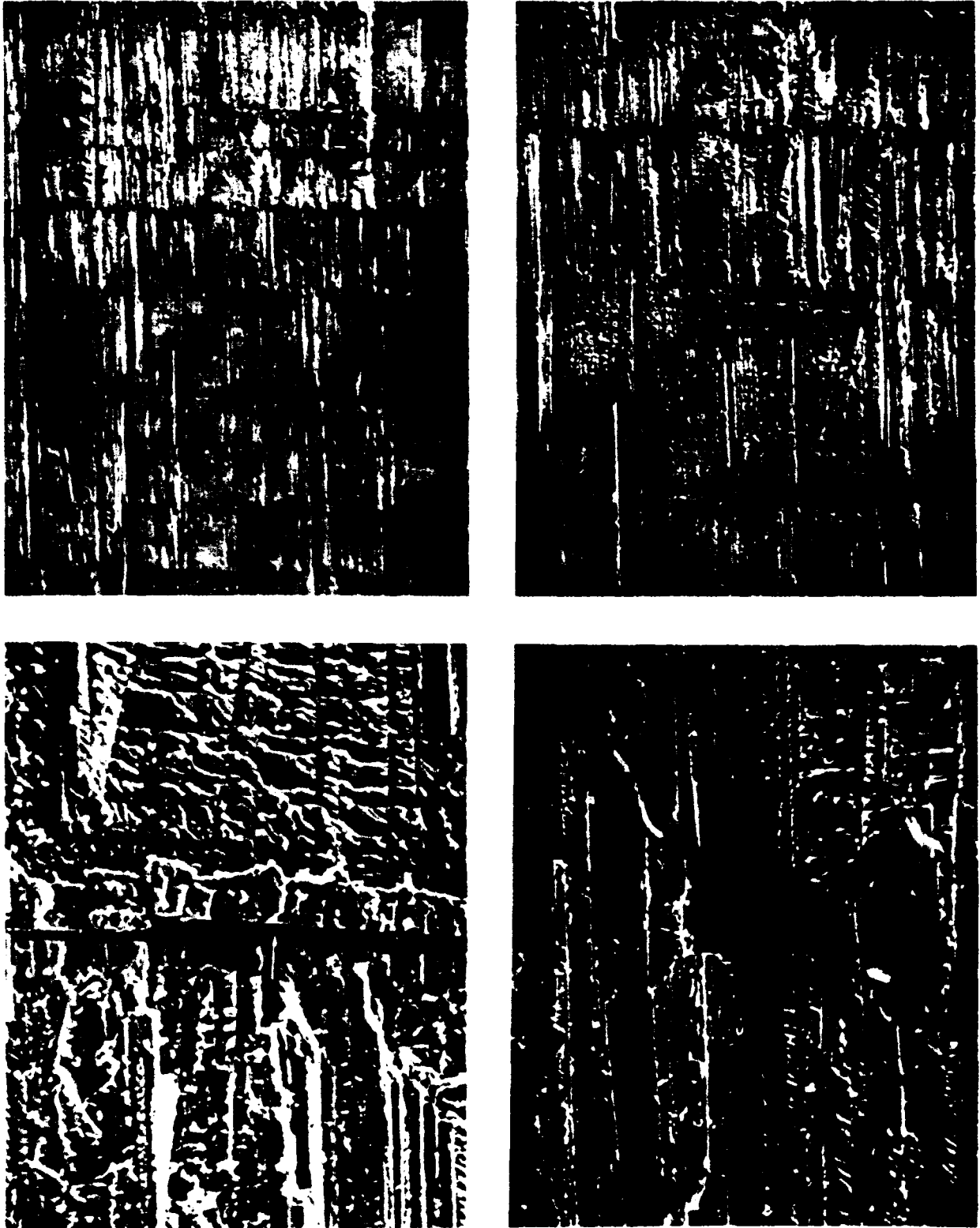


Figure 4.6. Deplied cross-ply laminates: (a) general view of the 0° ply in a $[90_2/0_2/90]_s$ laminate, showing the imprints of the tips of the transverse cracks in the neighboring 90° ply; (b) detail view of the 0° ply in a $[90_2/0]_s$ laminate, showing broken fibers; and (c) detail view of the 90° ply in a $[0_2/90]_s$ laminate, showing no broken fibers.

(b) SPEC. NO. 7-A9/2
LAY-UP: $[90_2/0]_8$
 $\sigma_f = 335.7 \text{ MPa}$
 $a/W = 0.11$

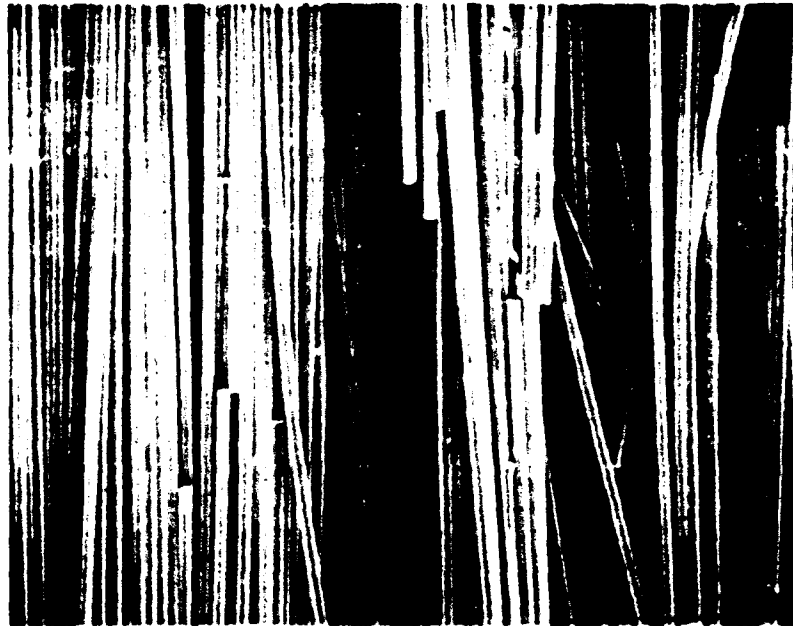


Figure 4.6. Continued.

(c) SPEC. NO. 8C6/2
LAY-UP: $[0_2/90]_8$
 $\sigma_f = 640.7 \text{ MPa}$
 $a/W = 0.11$

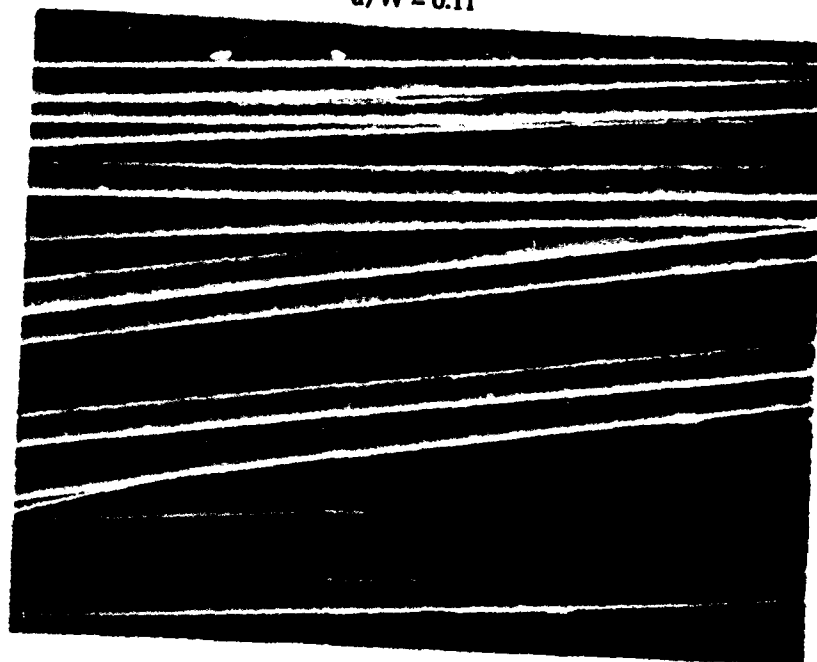
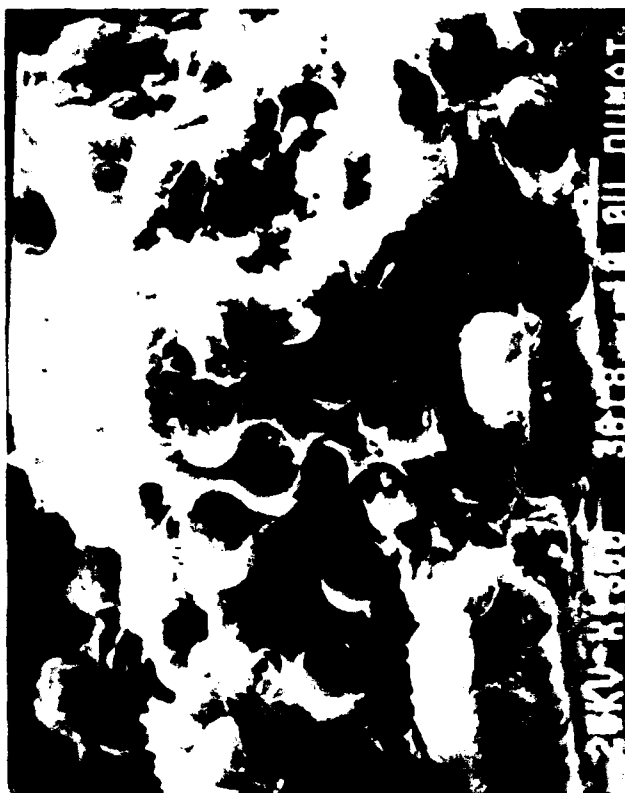


Figure 4.6. Concluded.

SPEC. NO. 3 - A8/1
 LAY - UP: $[90_2/0_2/90]_s$
 $\sigma_f = 538 \text{ MPa}$
 $a/W = 0.11$



(a)



(b)



(c)



(d)

SPEC. NO. 3-A8/2
LAY-UP: $[90_2/0_2/90]_5$
 $\sigma = 549 \text{ MPa}$

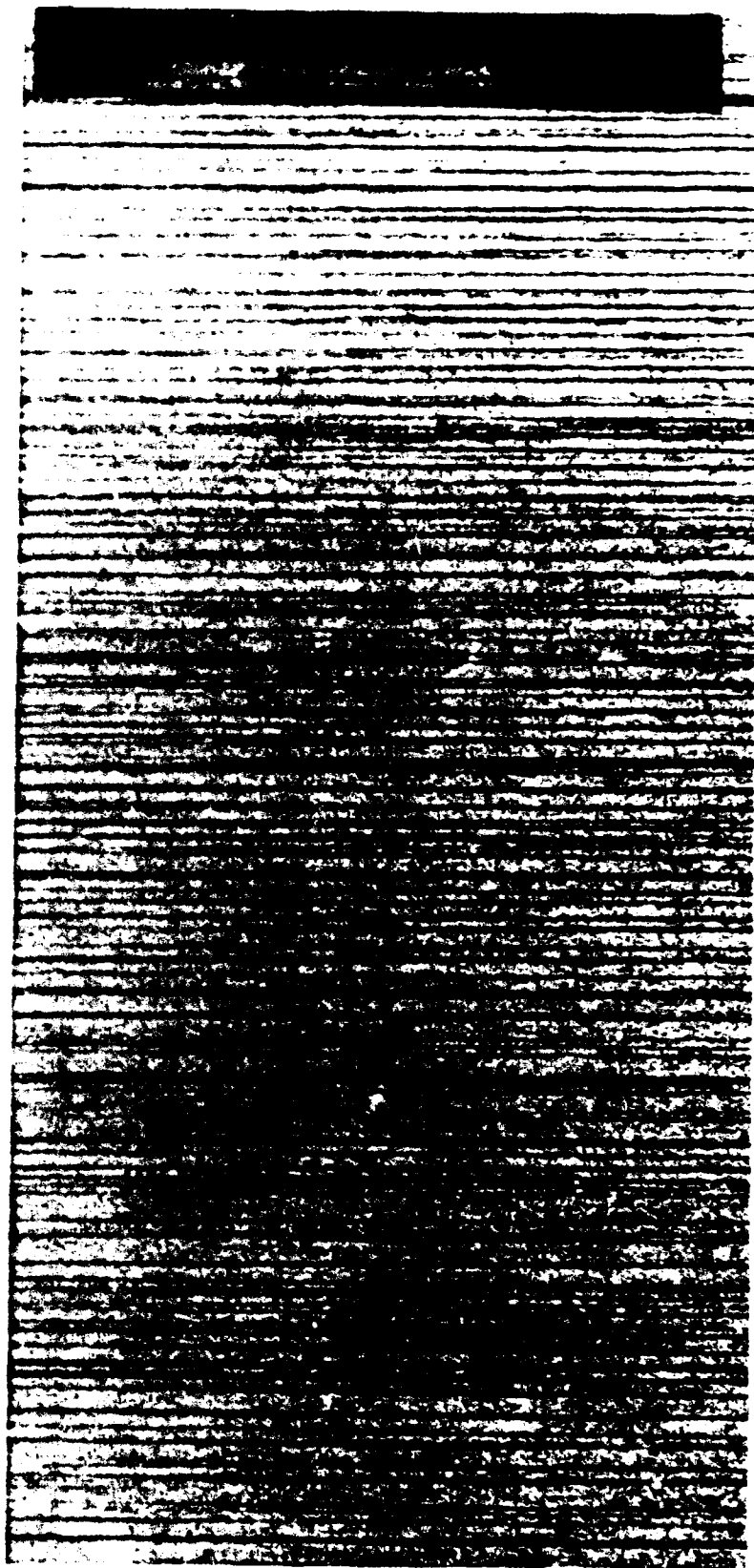


Figure 4.8. X-Radiograph of a $[90_2/0_2/90]_5$ laminate taken after loading to 59 percent of average ultimate strength showing approximately one transverse crack per mm (20 cracks/inch). Distribution of transverse cracks is quite uniform throughout the length of the specimen.

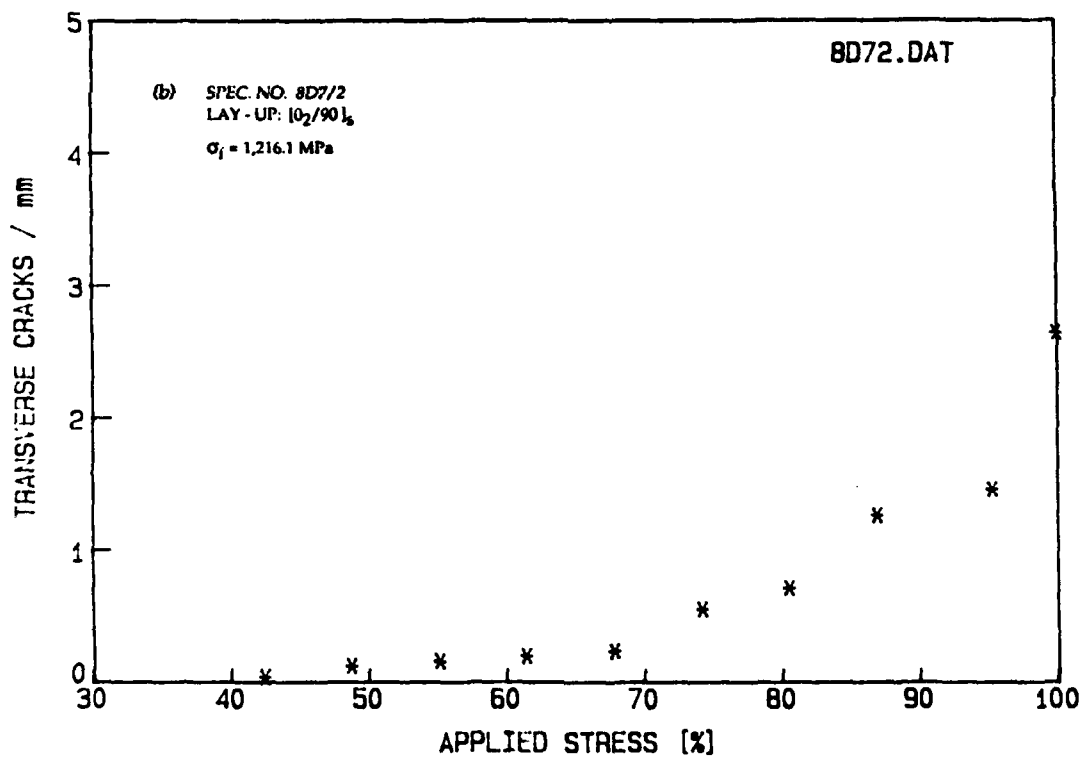
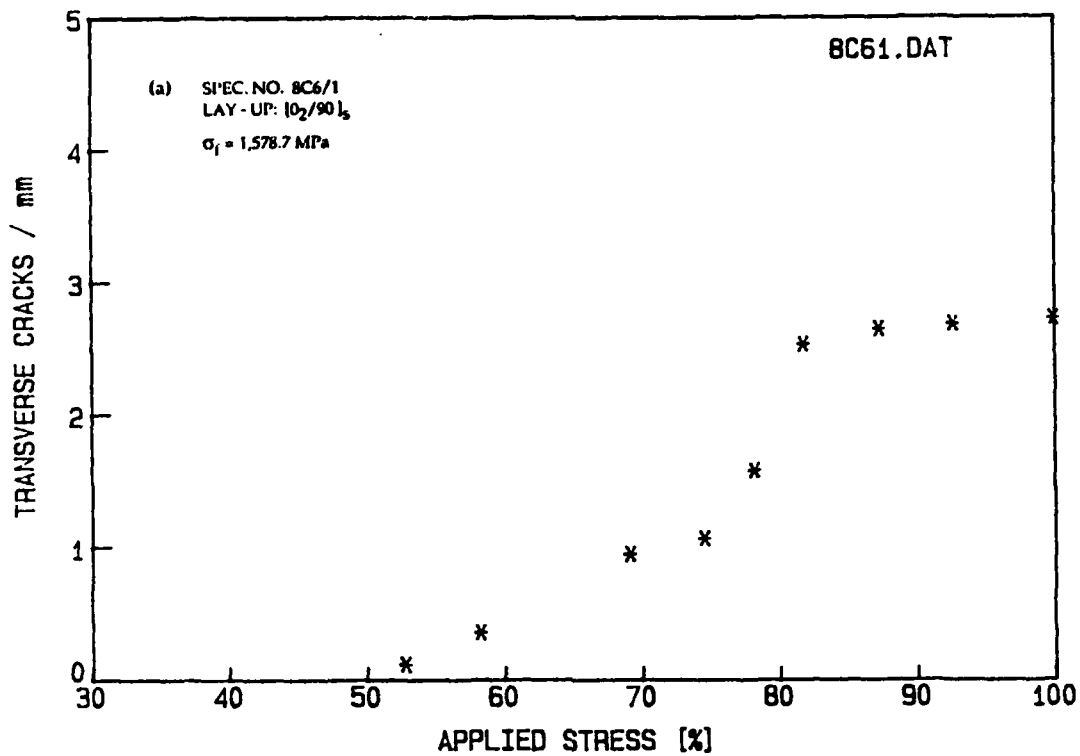


Figure 4.9. Number of transverse cracks as a function of applied load for different laminates. Results indicate that laminate configuration affects damage accumulation.

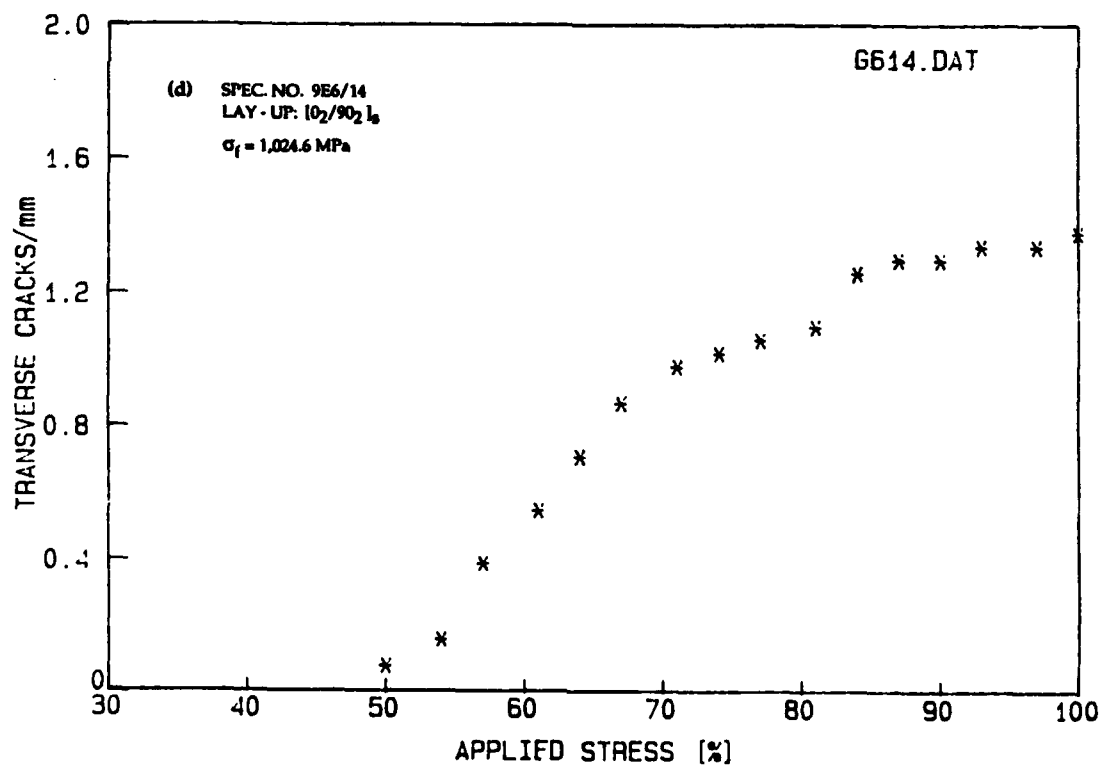
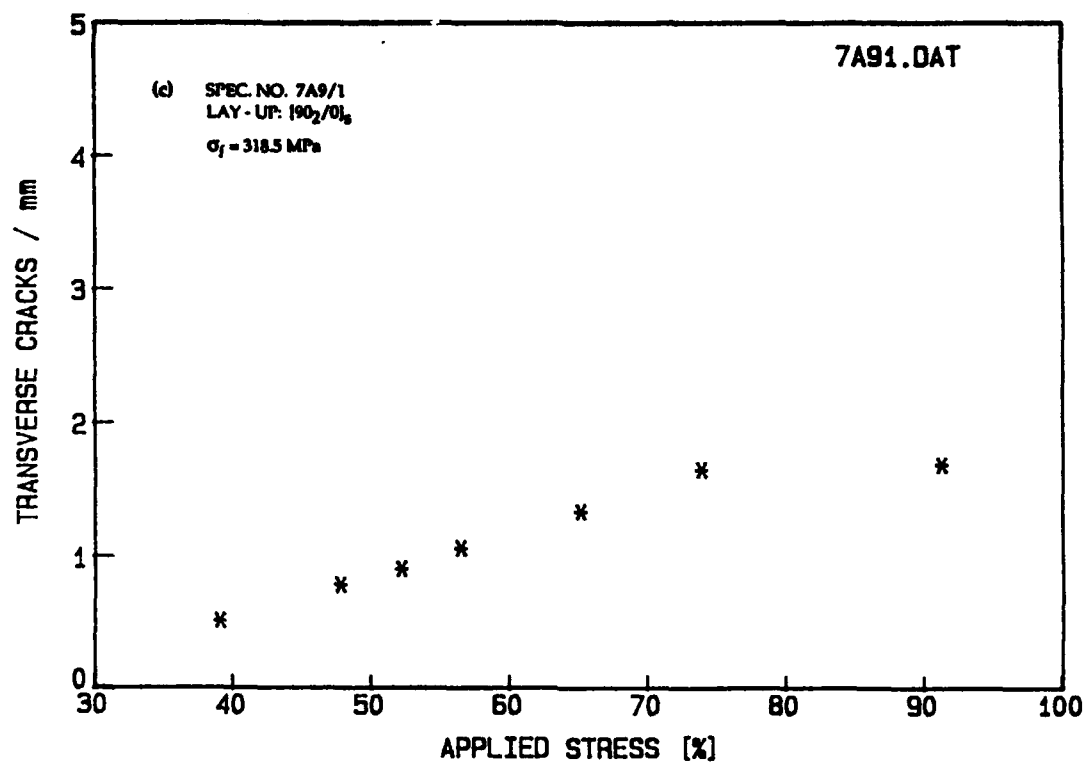


Figure 4.9. Continued.

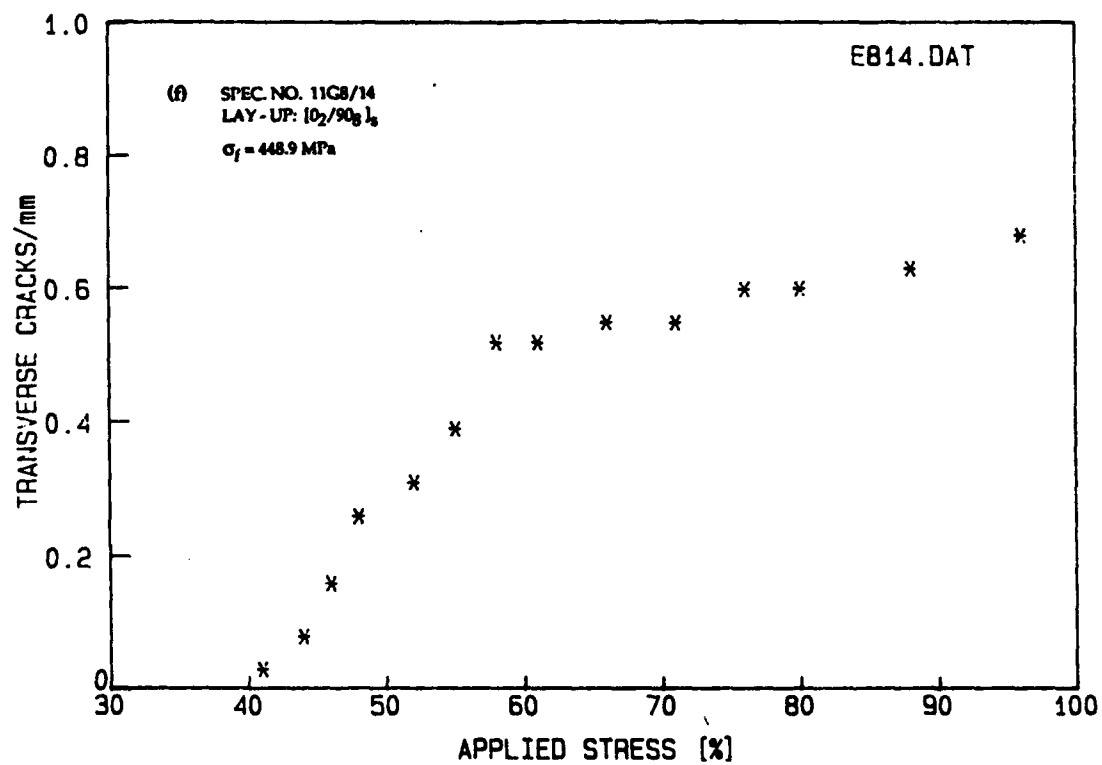
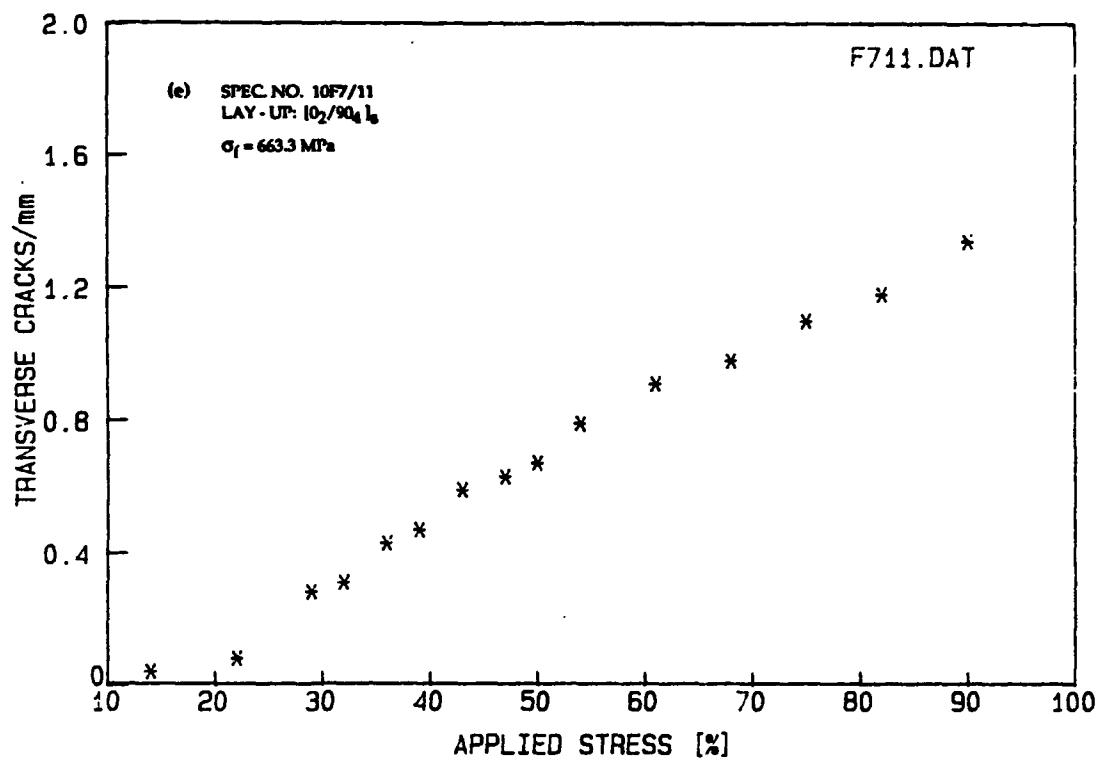


Figure 4.9. Continued.

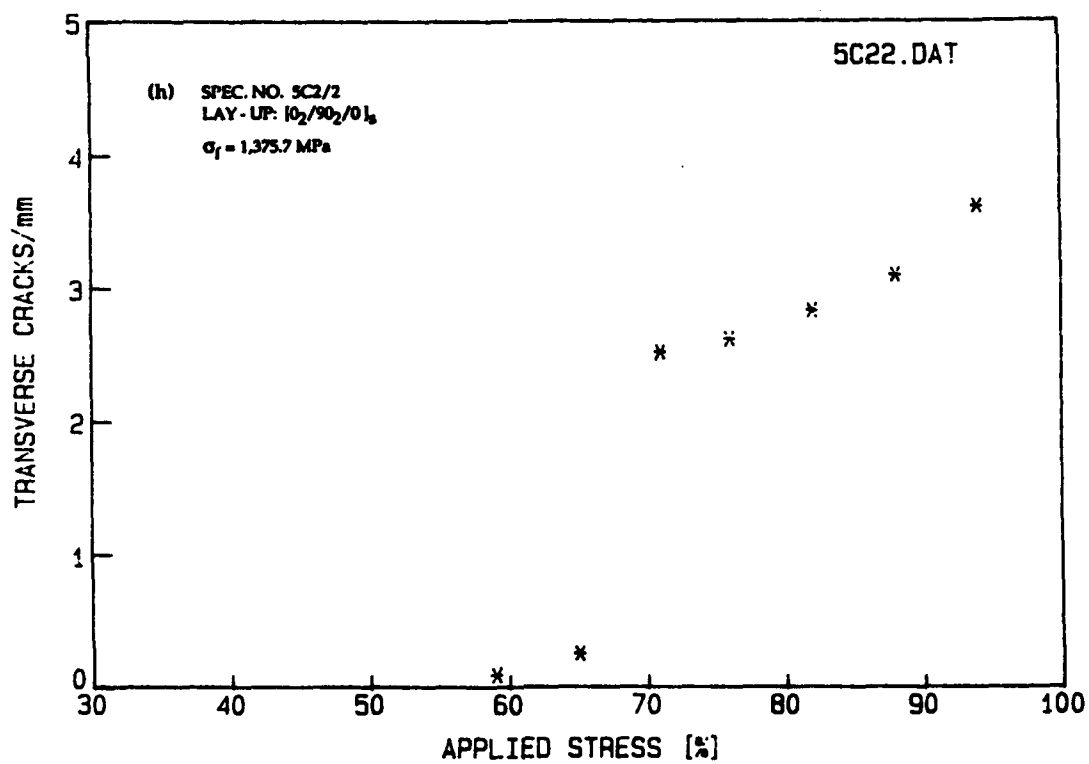
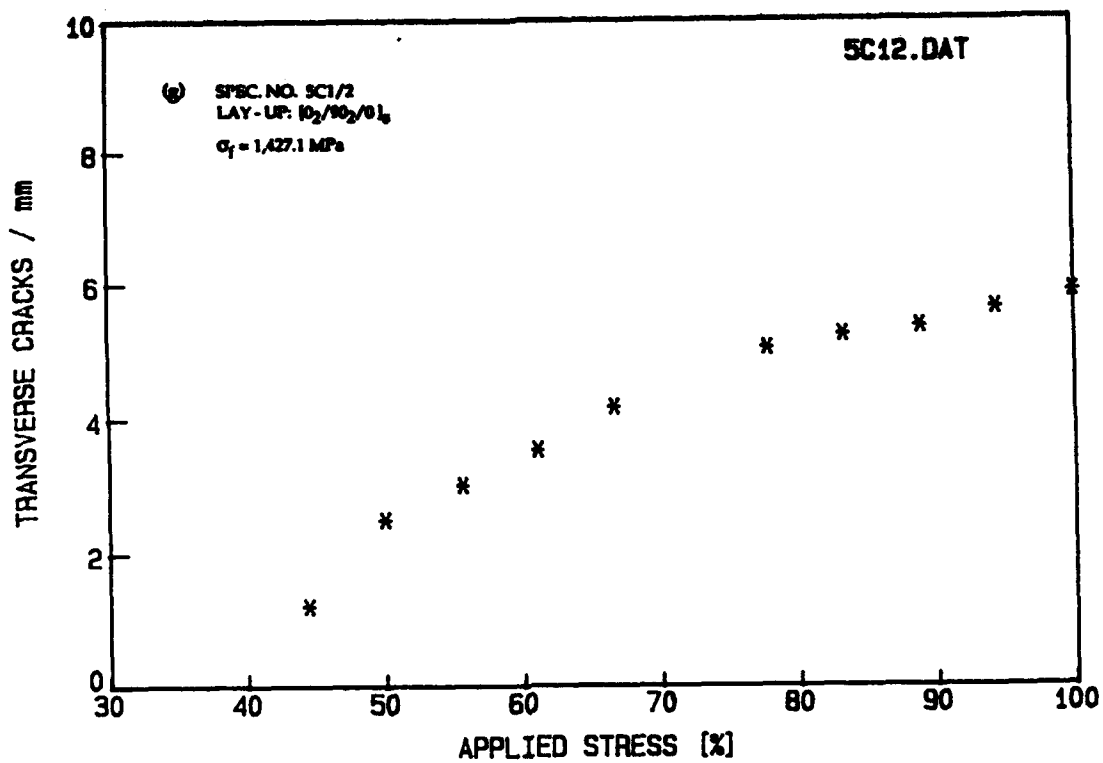


Figure 4.9. Continued.

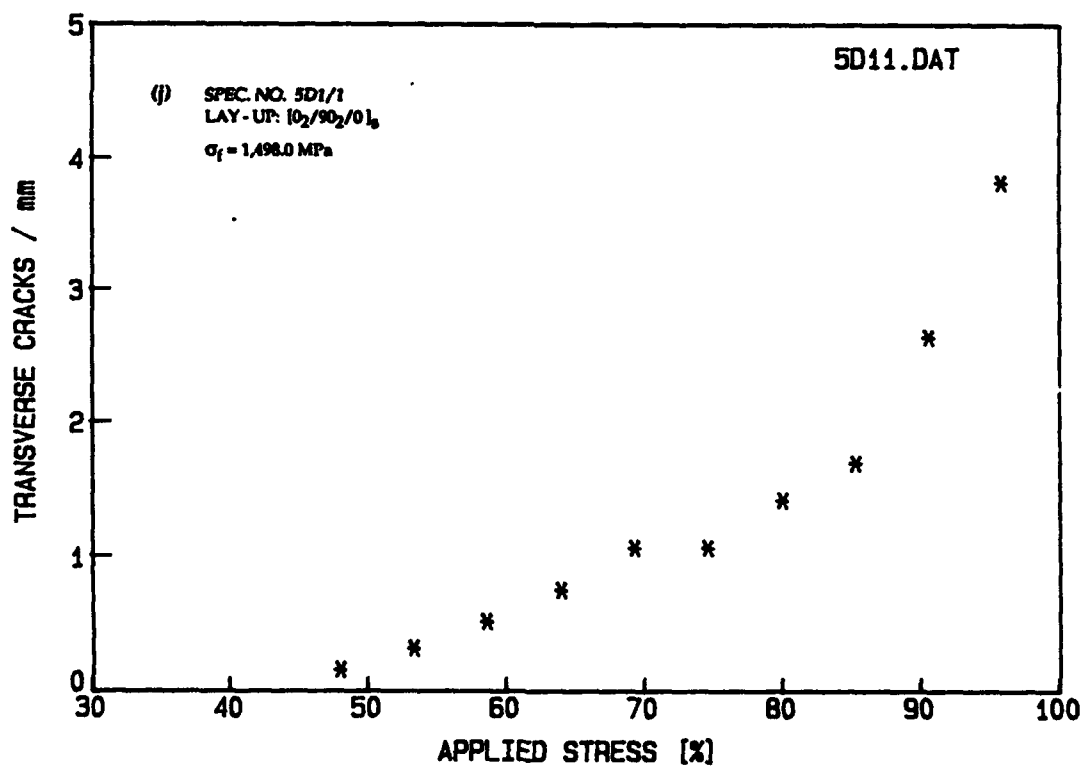
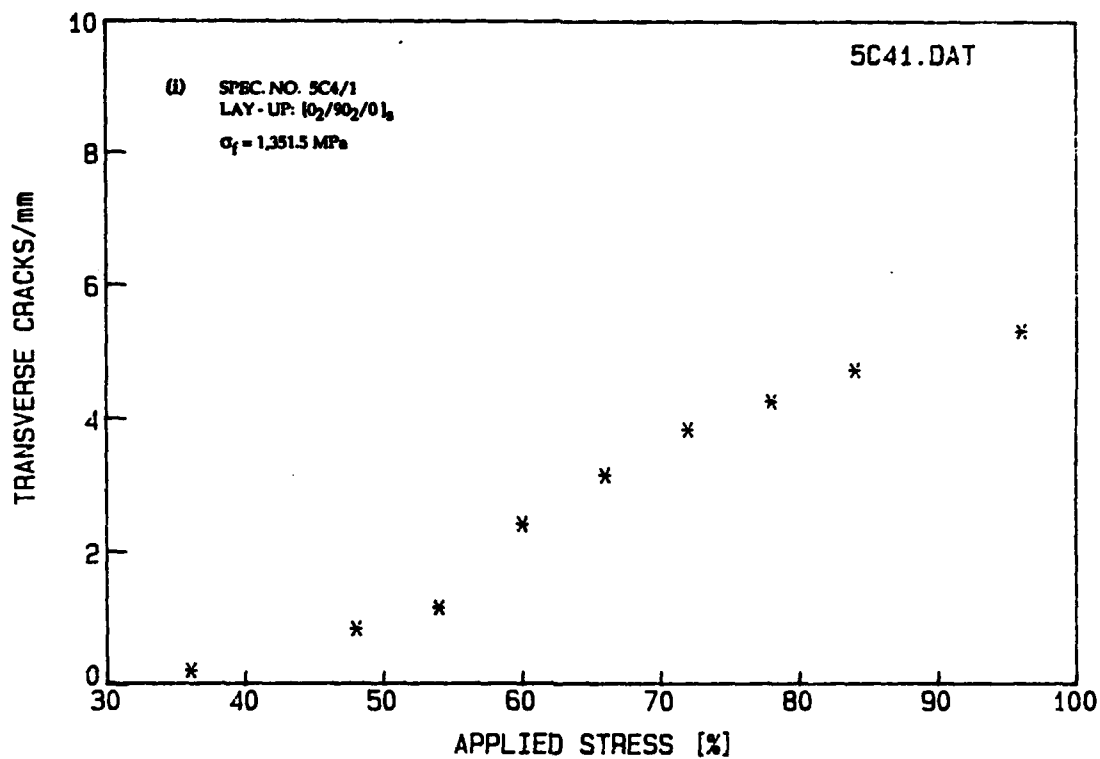


Figure 4.9. Continued.

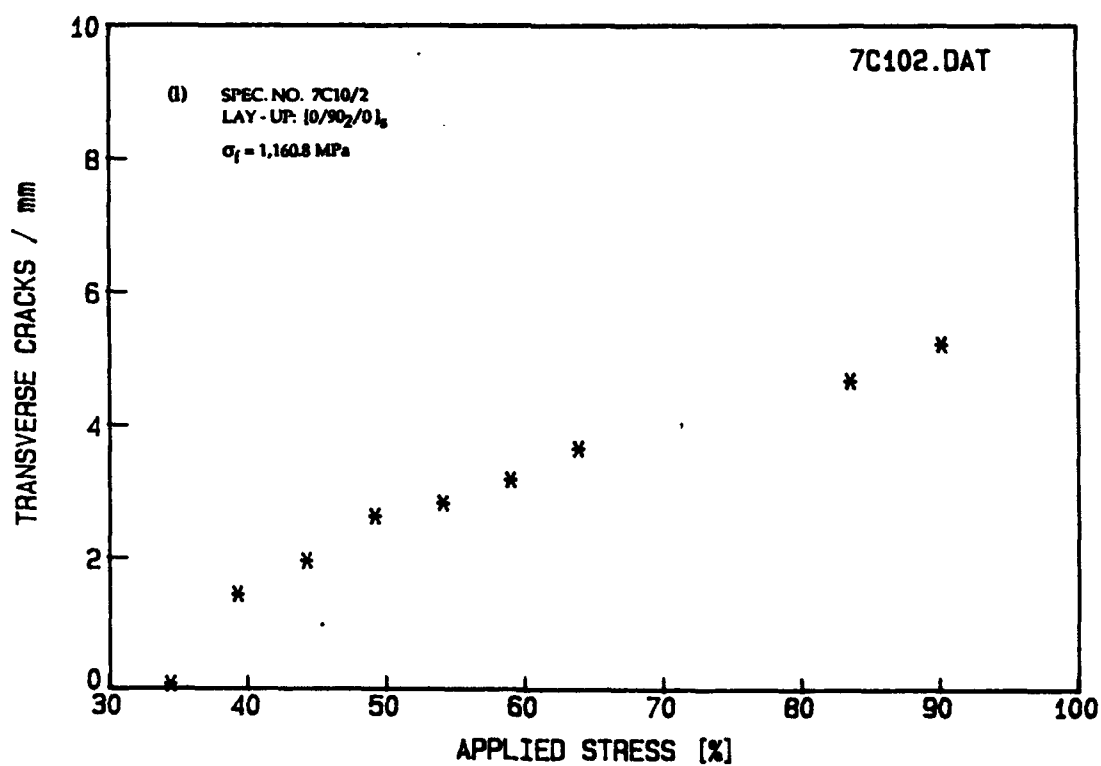
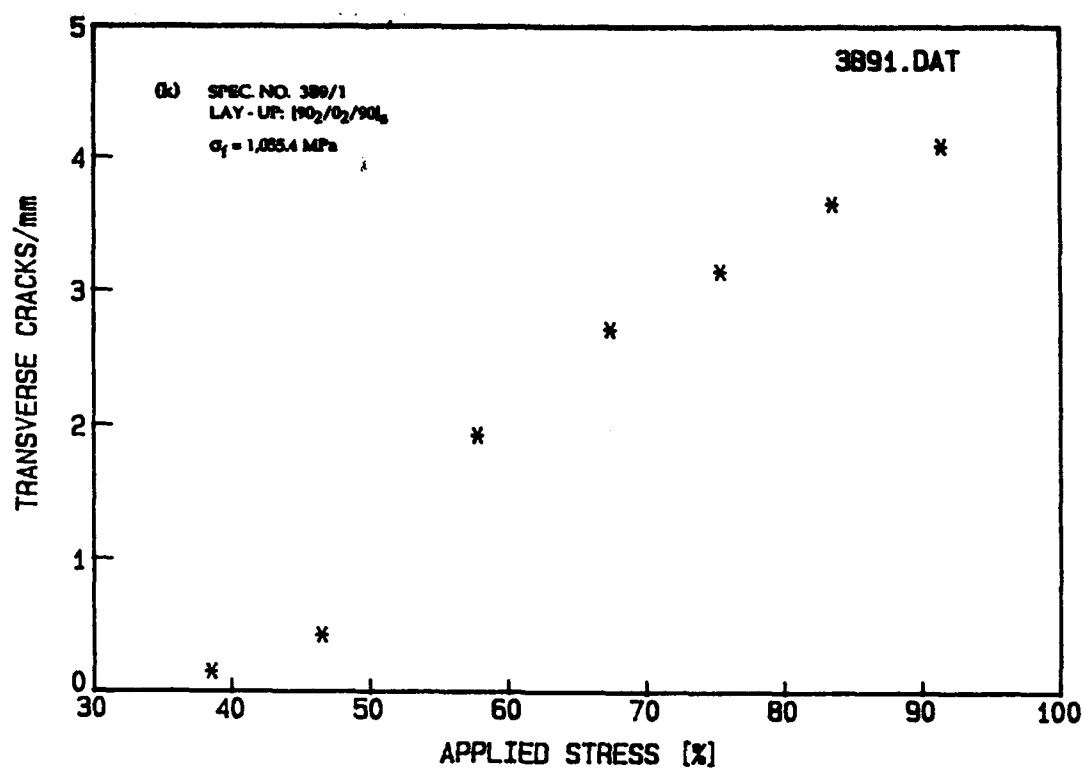


Figure 4.9. Continued.

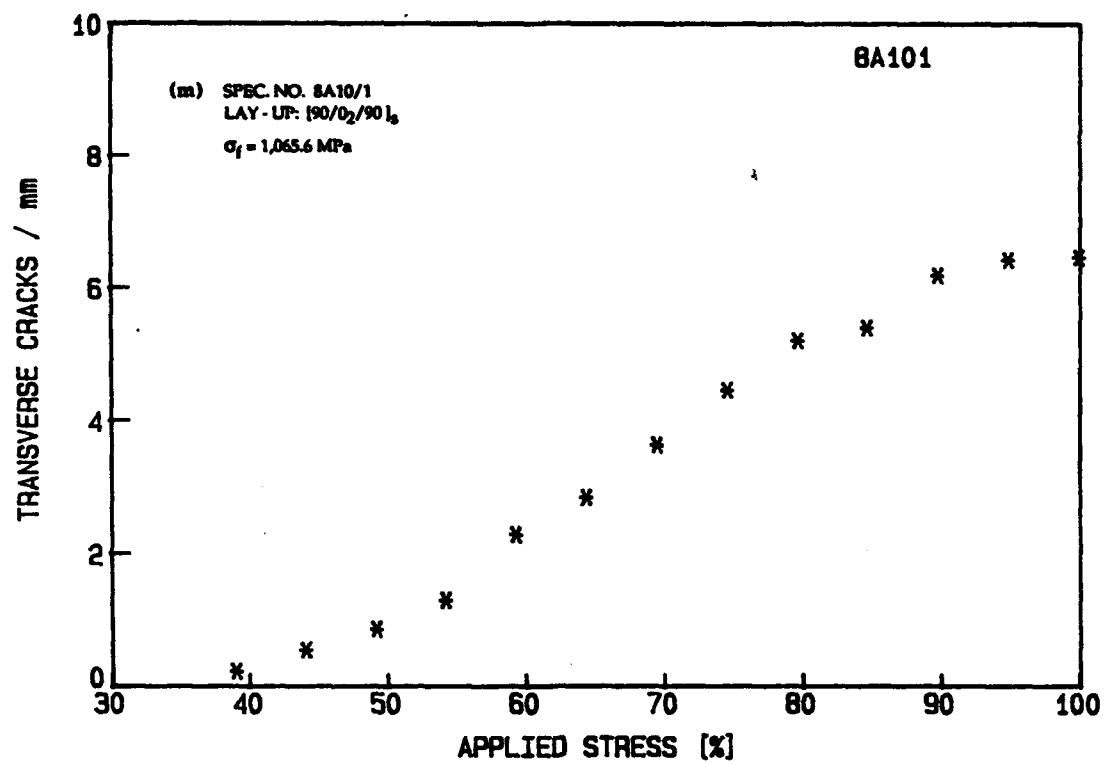


Figure 4.9. Concluded.

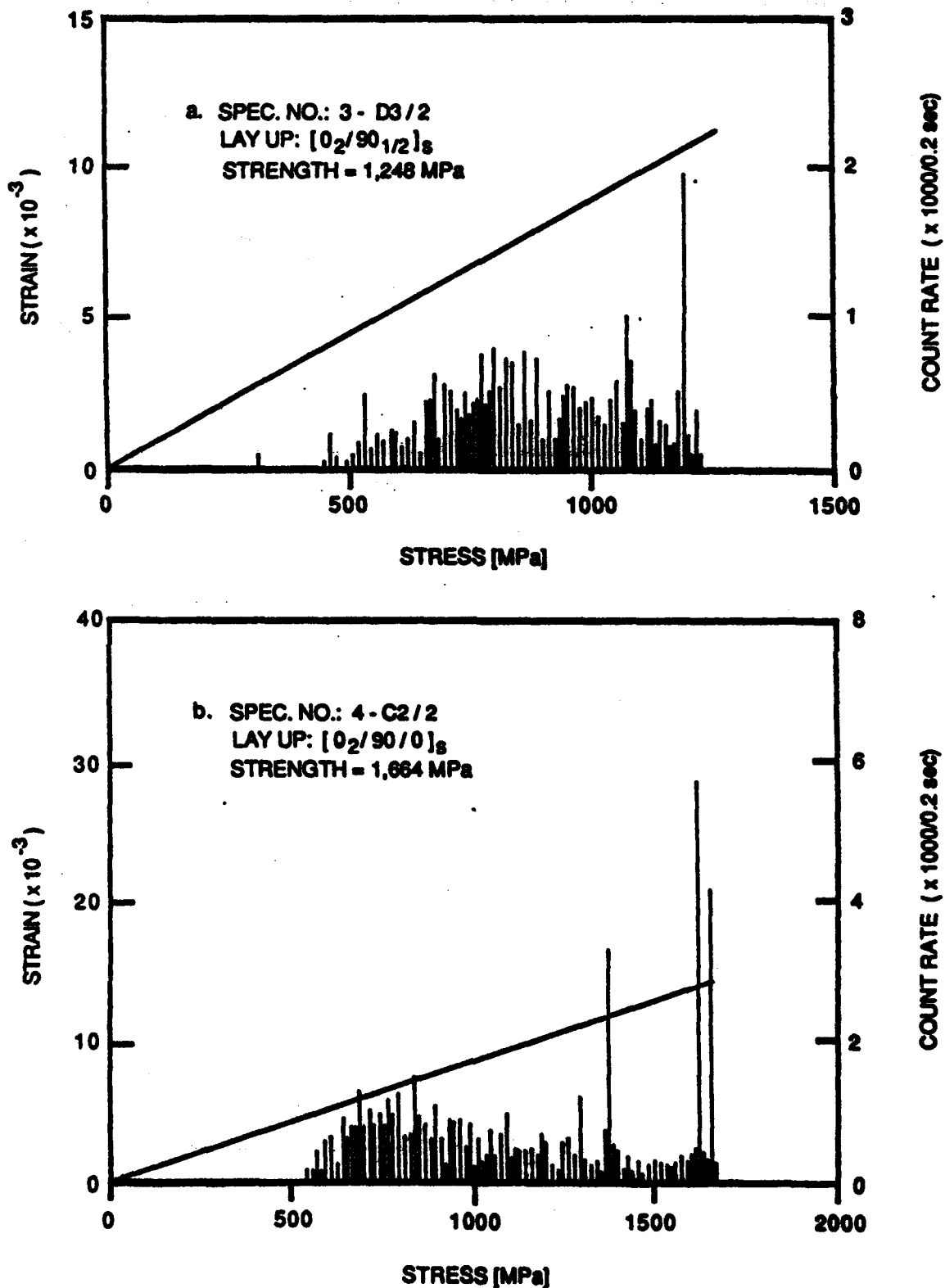


Figure 5.1. Count-rate (recorded with the D/E AE system) and strain as a function of far-field applied stress for 12 different cross-ply graphite/epoxy laminates. Arrows indicate emission initiation stress.

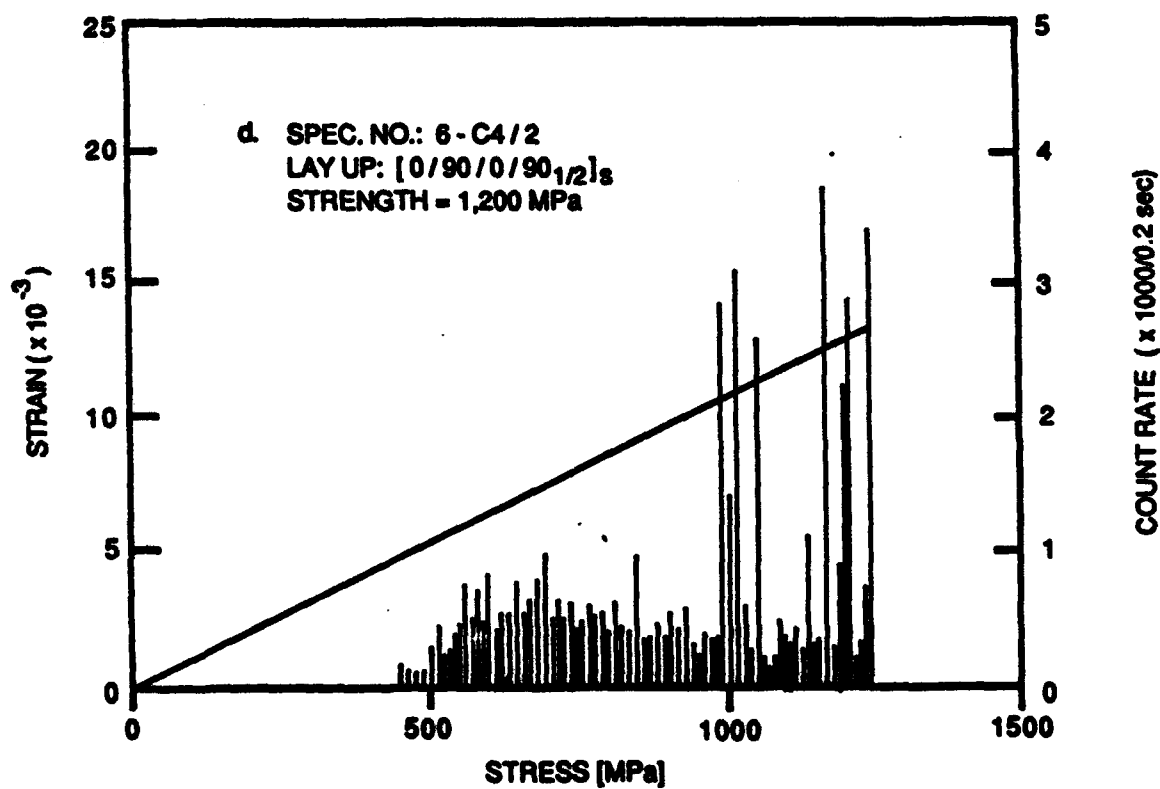
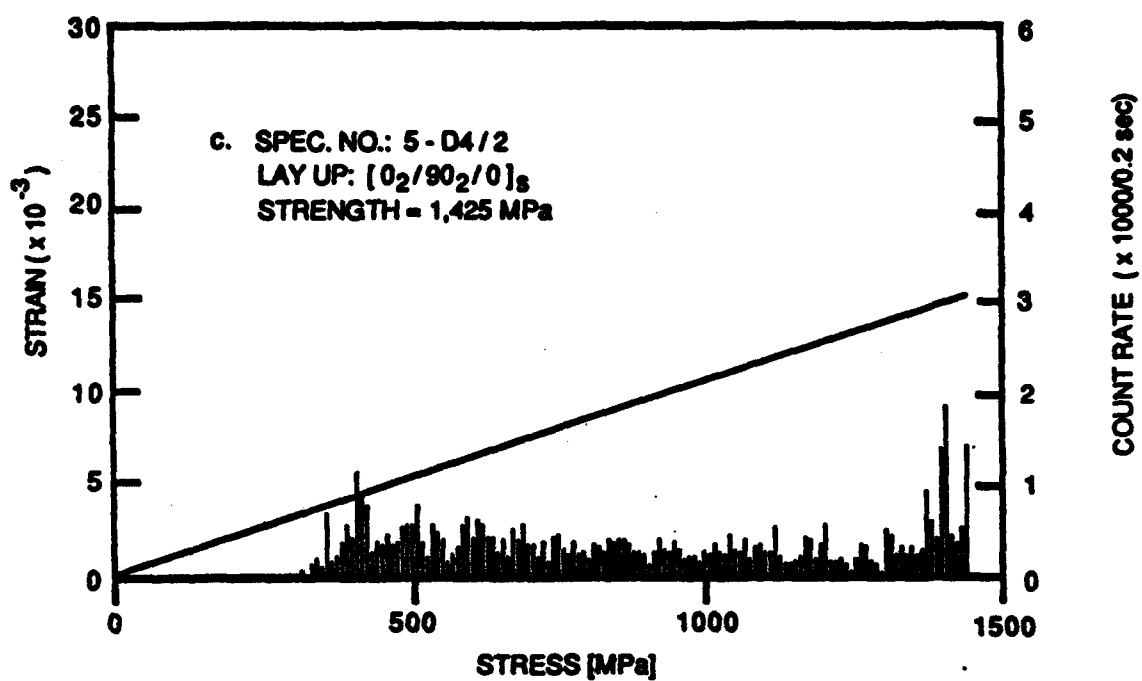


Figure 5.1. Continued.

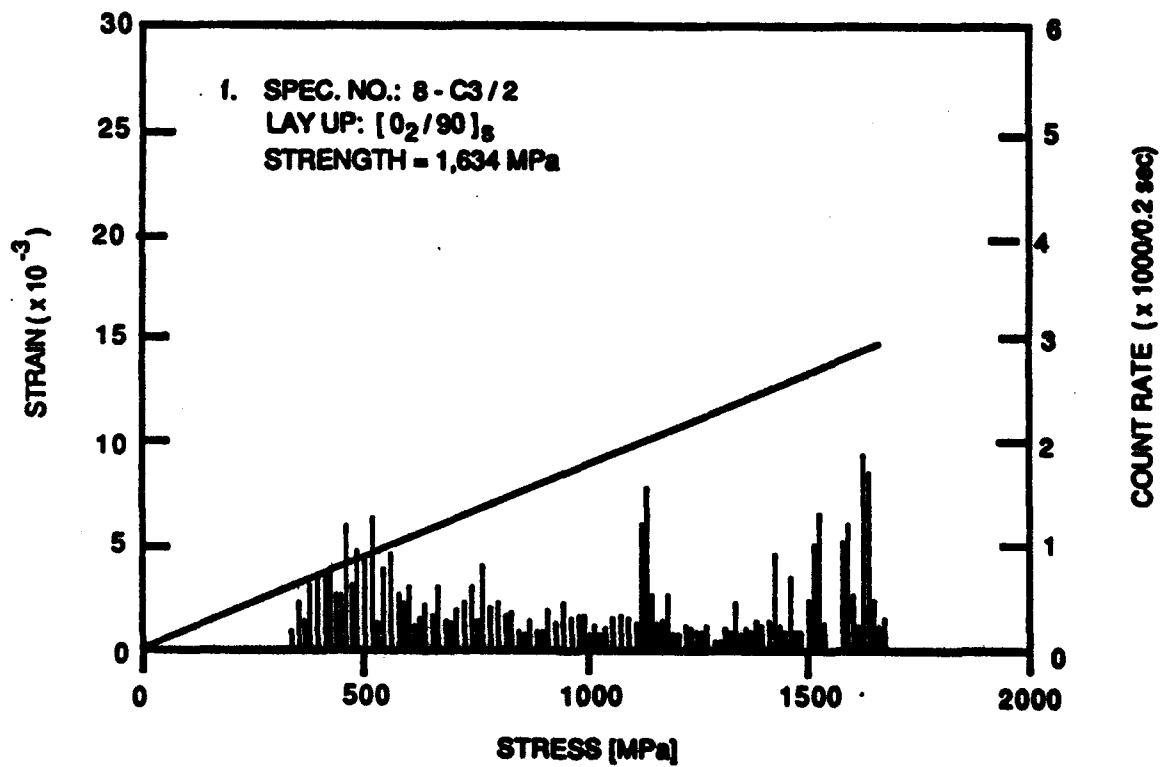
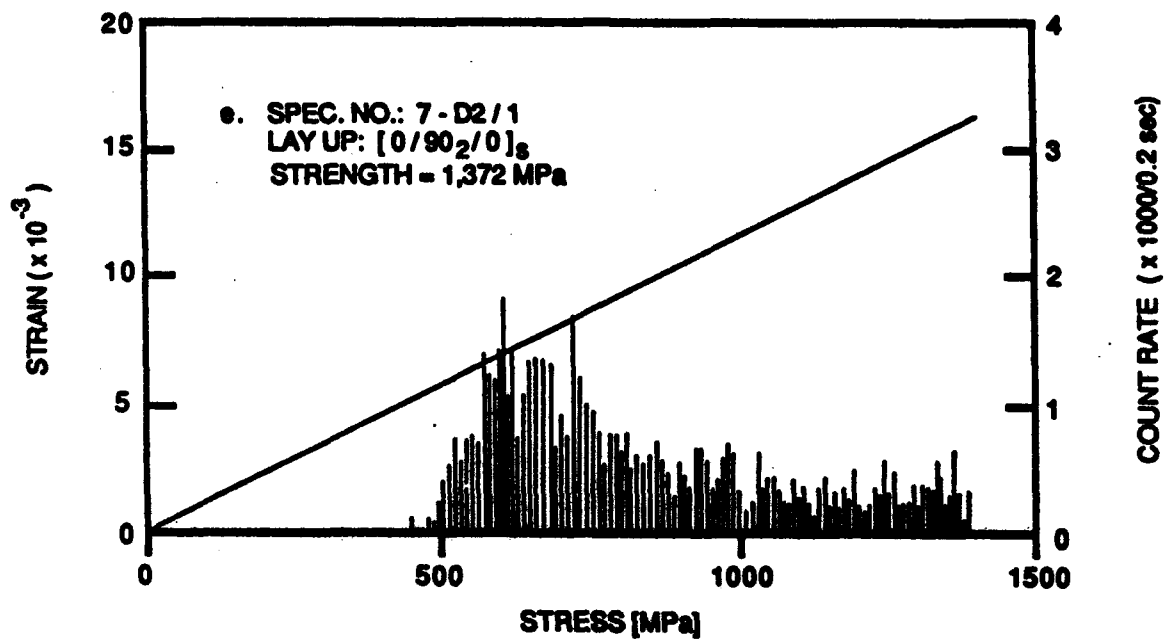


Figure 5.1. Continued.

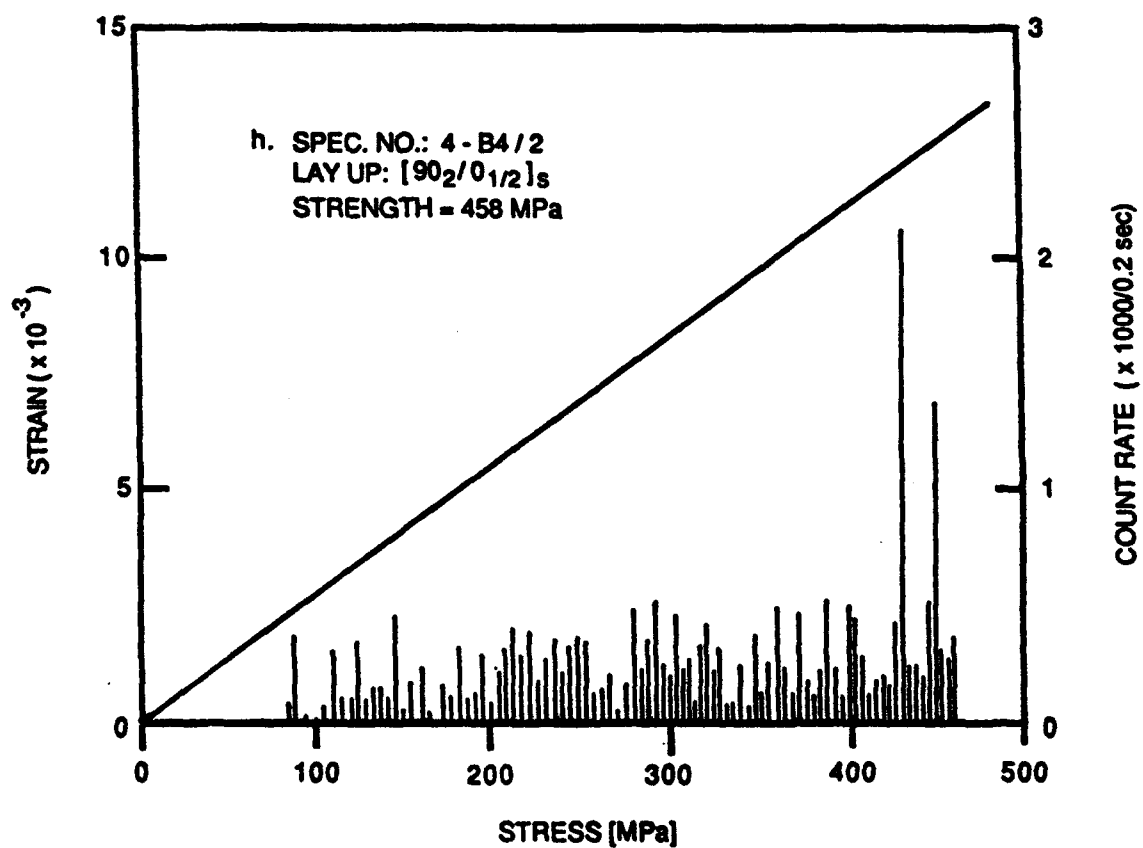
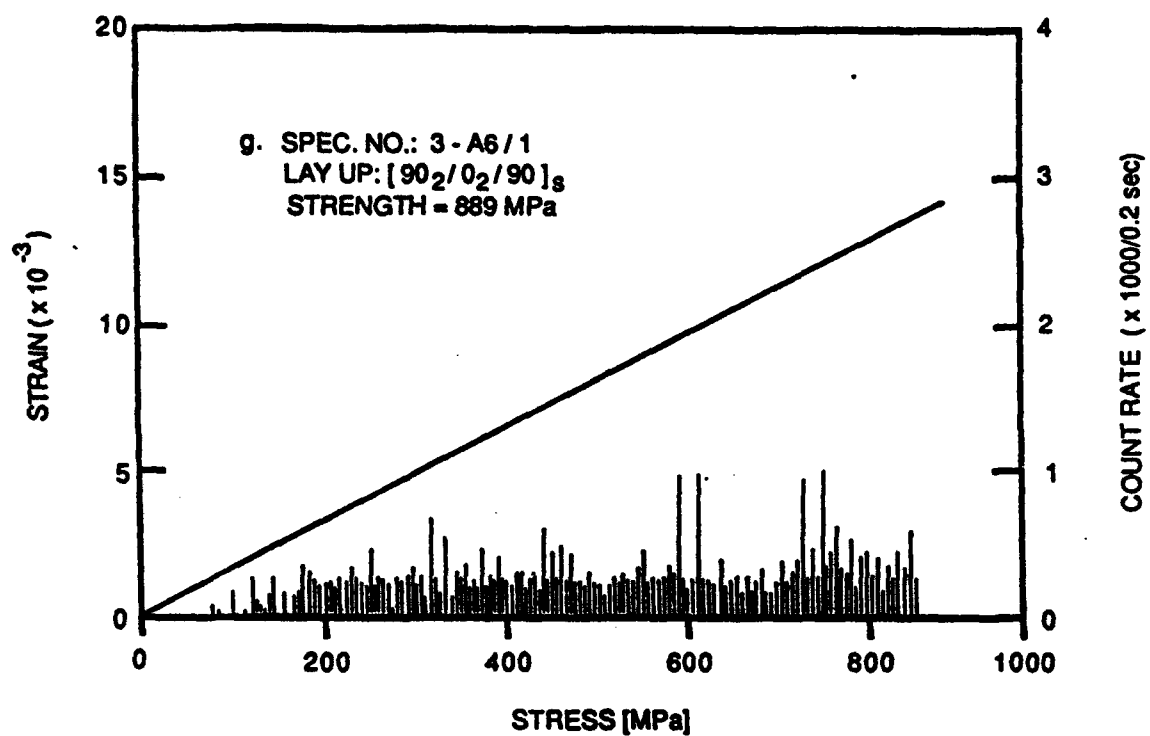


Figure 5.1. Continued.

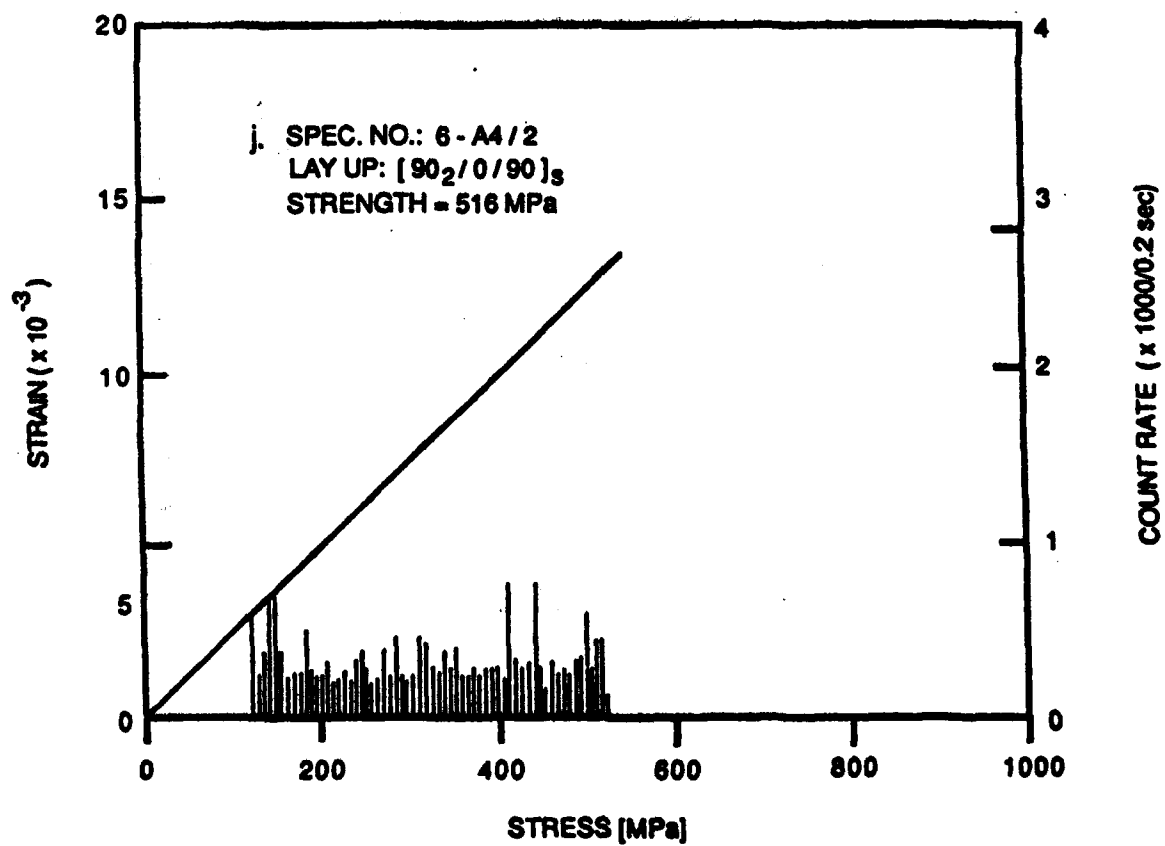
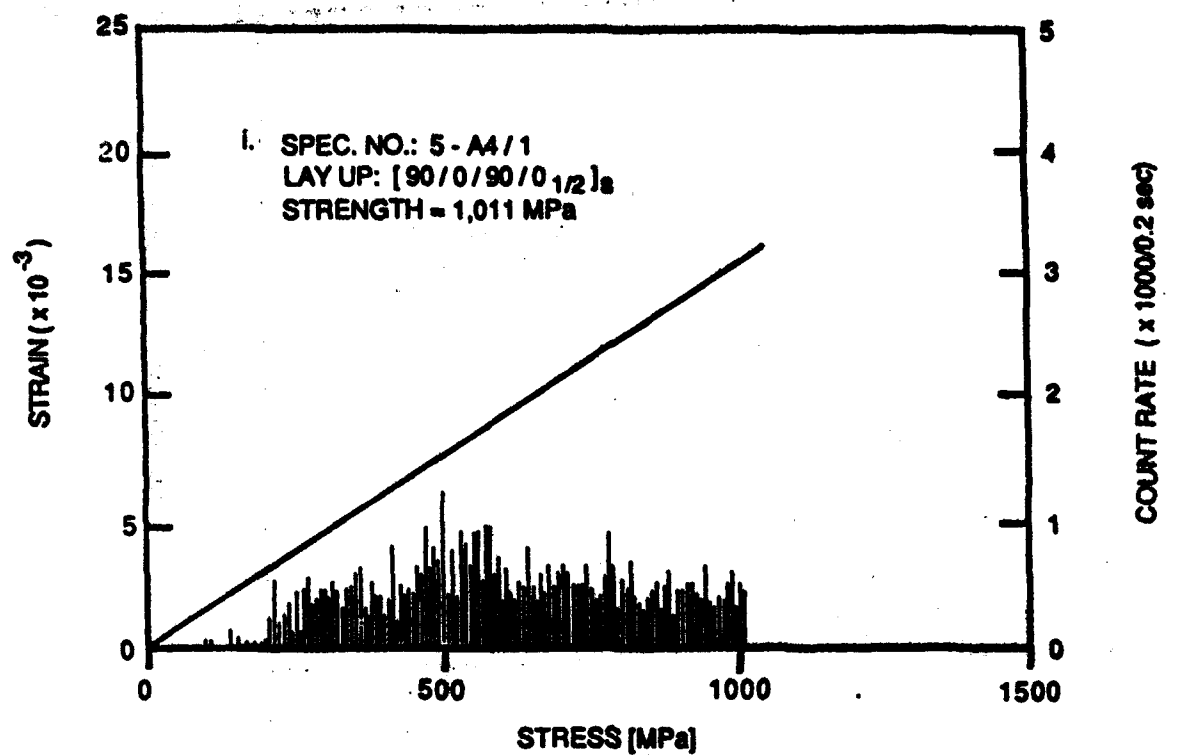


Figure 5.1. Continued.

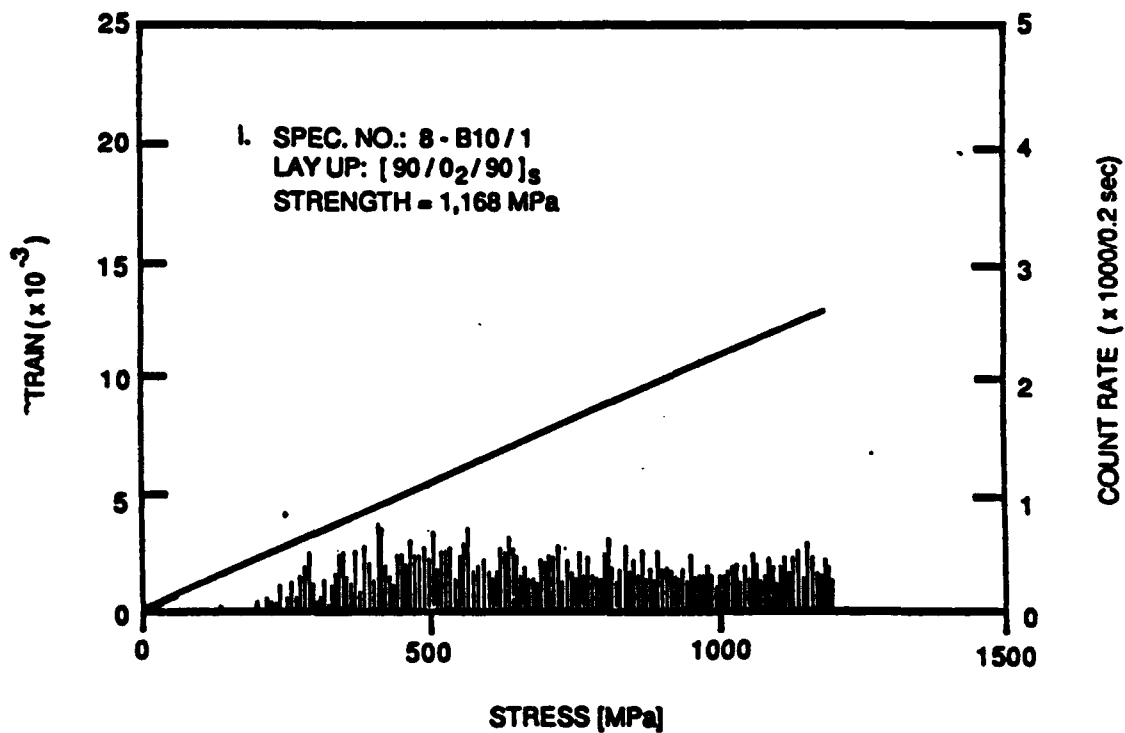
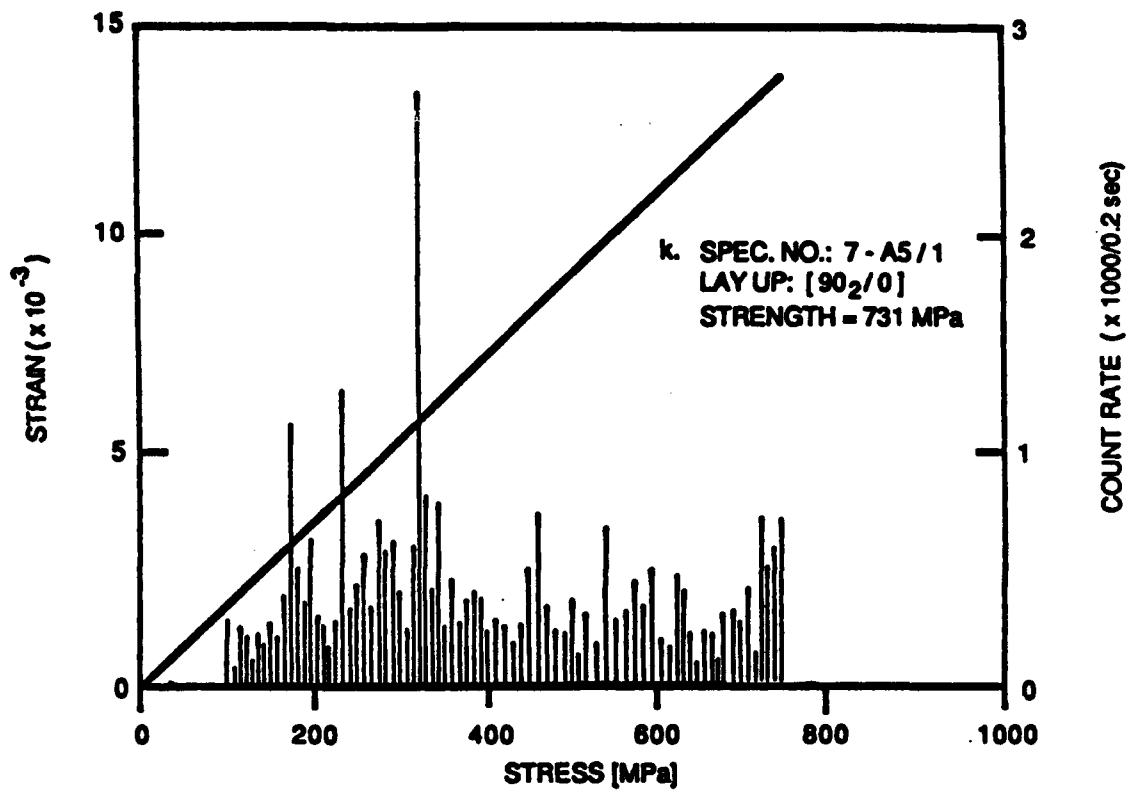


Figure 5.1. Concluded.

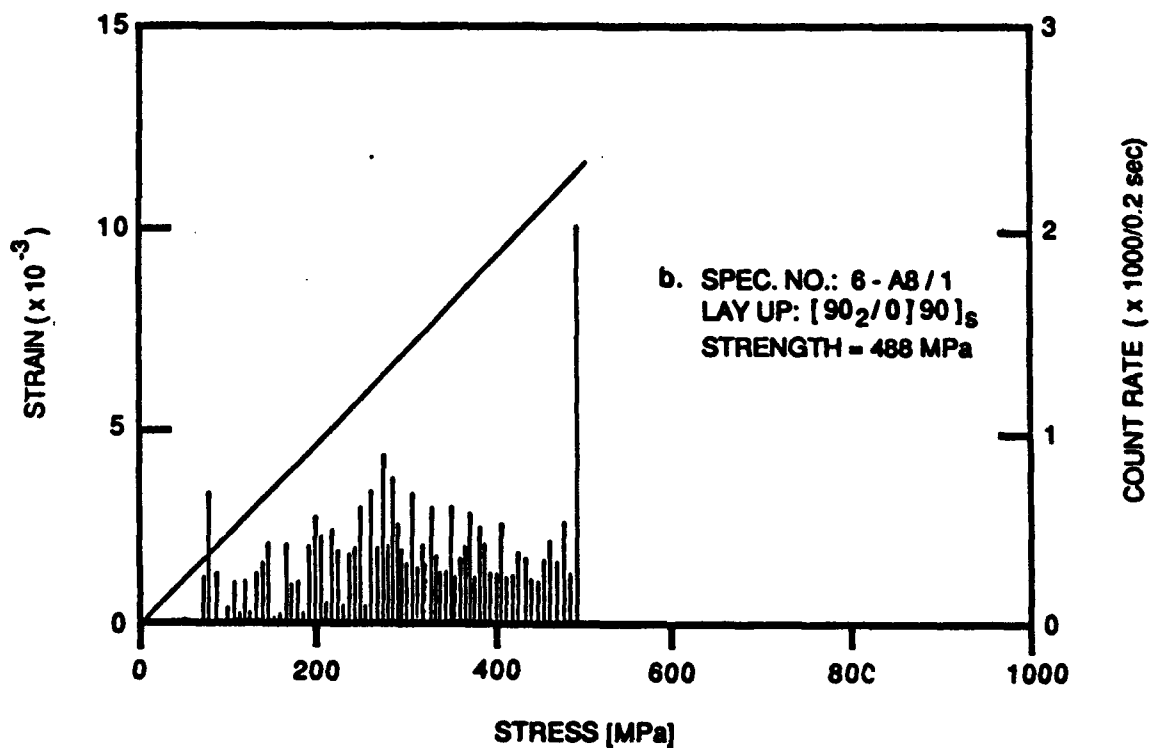
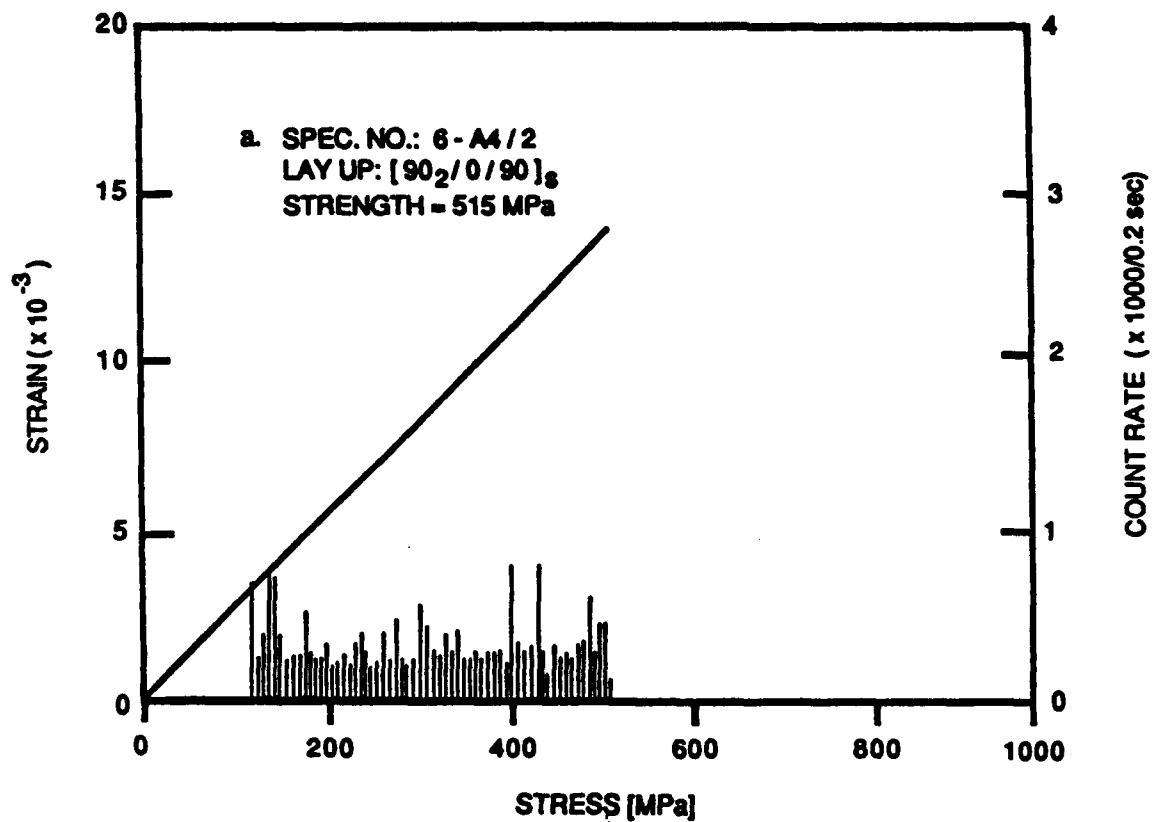


Figure 5.2. Count-rate (recorded with the D/E AE system) and strain as a function of far-field applied stress for selected pairs of cross-ply graphite/epoxy laminates showing good reproducibility.

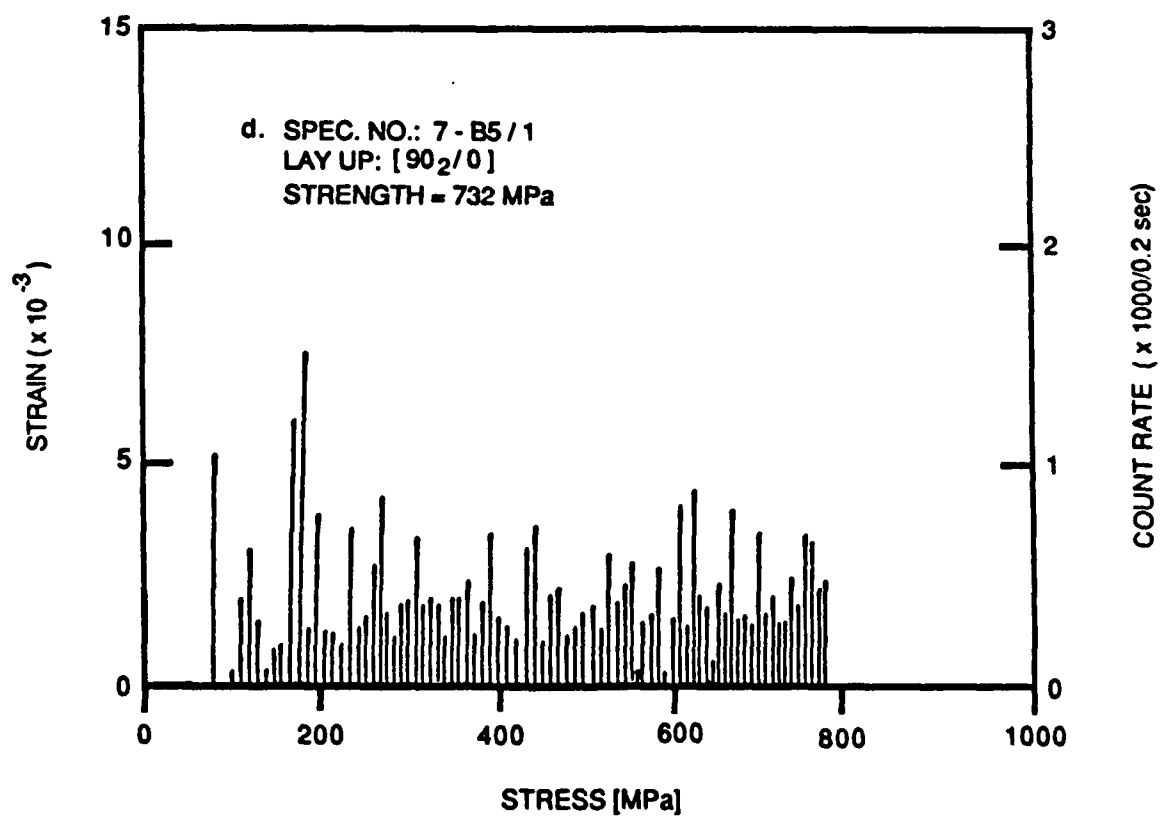
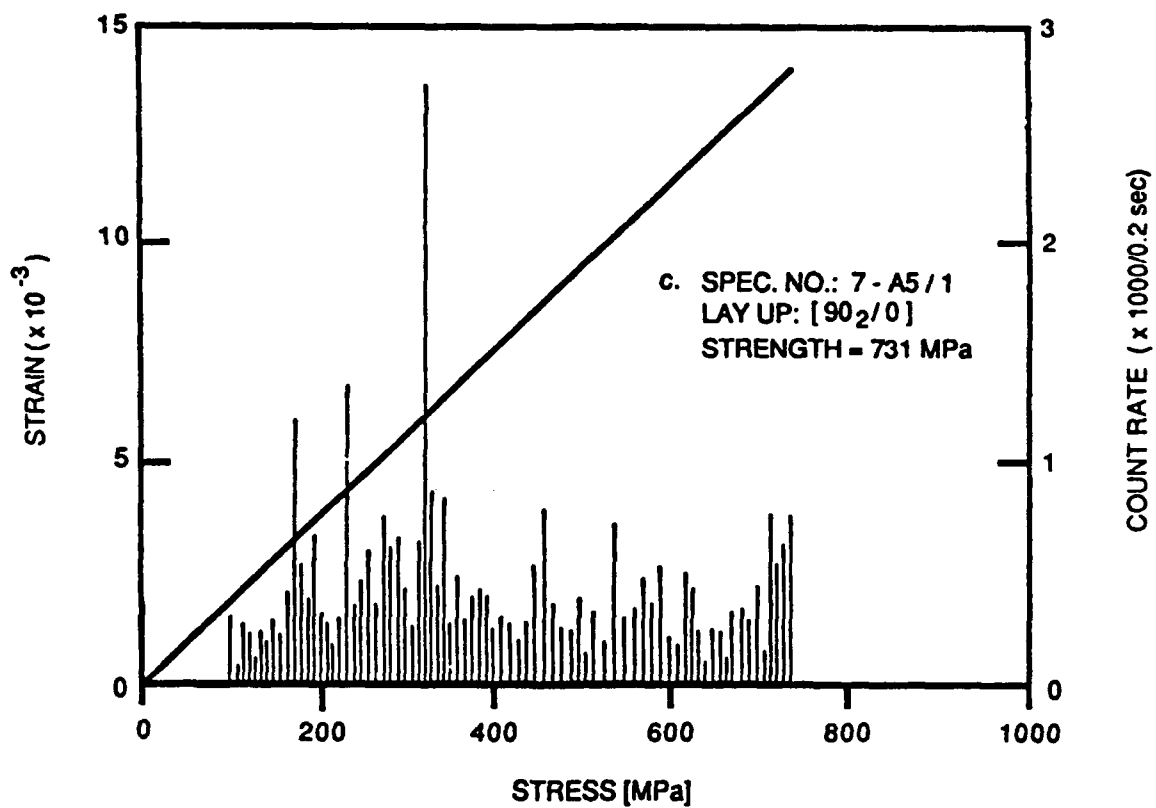


Figure 5.2. Continued.

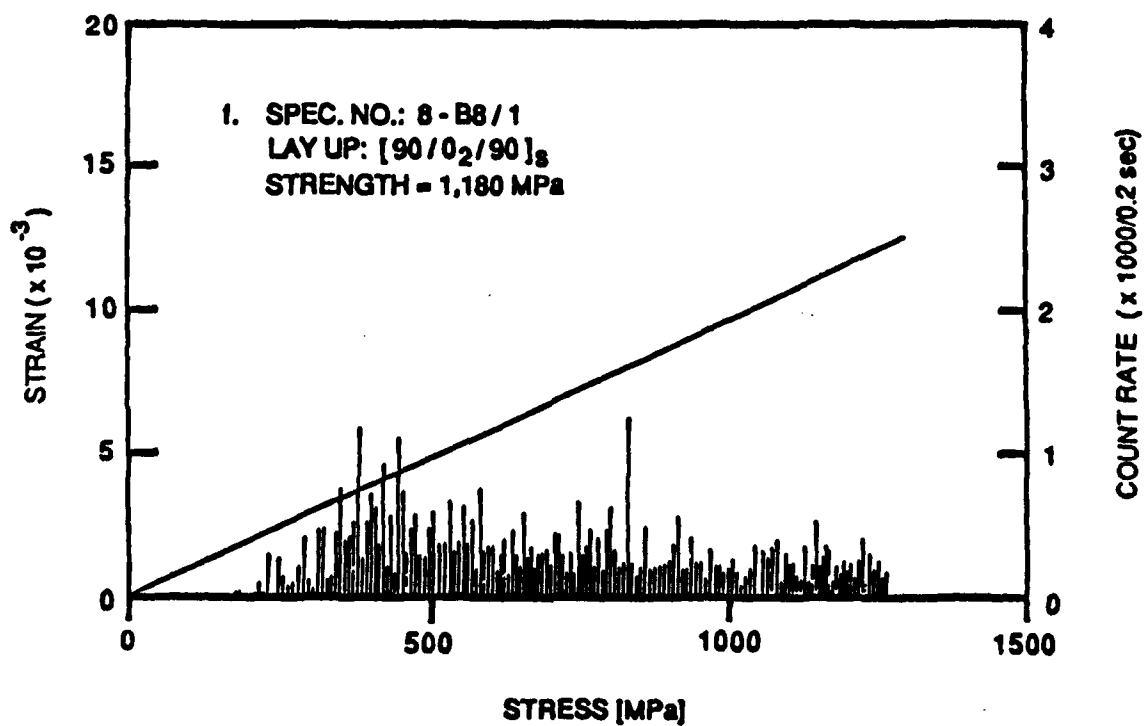
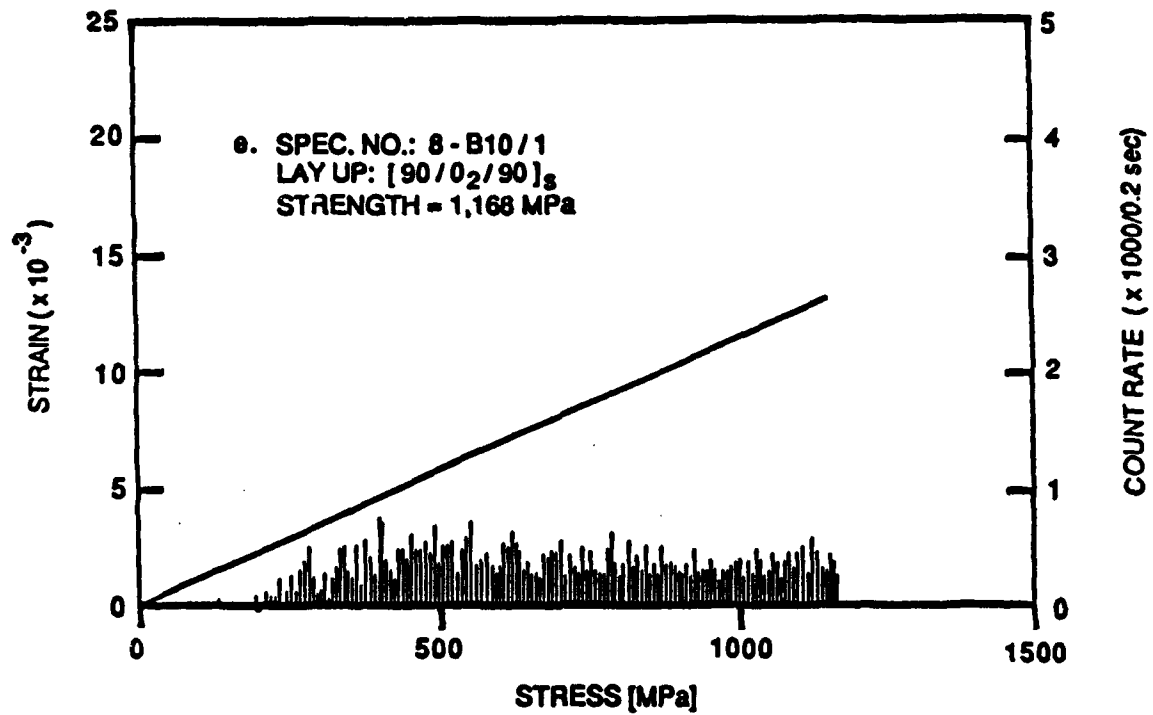


Figure 5.2. Concluded.

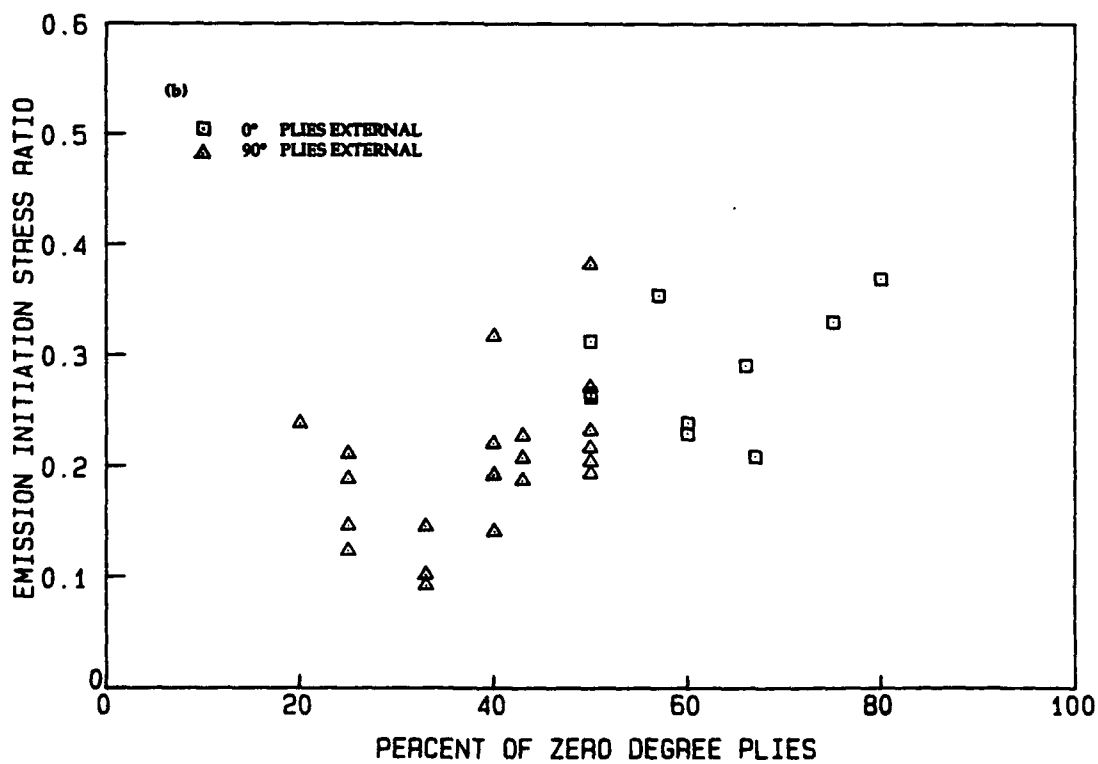
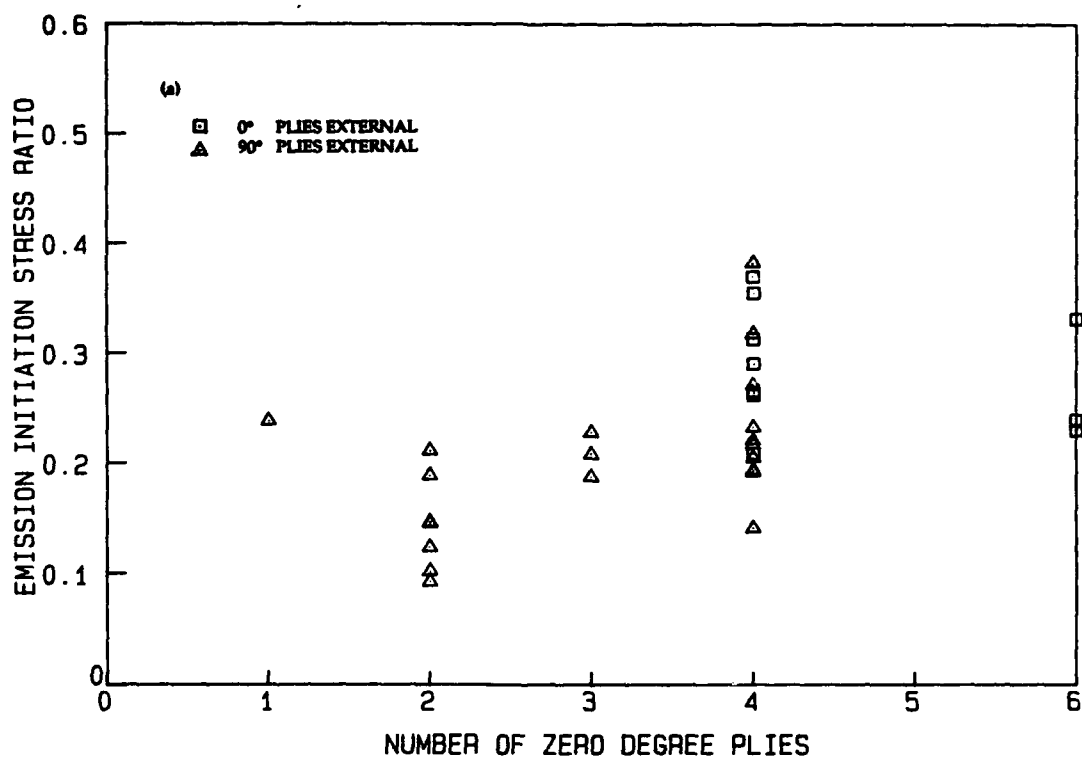


Figure 5.3. Emission initiation stress (recorded with the D/E AE system) as a function of: (a) number of 0° plies; (b) percent of 0° plies; (c) number of 90° plies; and (d) percent of 90° plies.

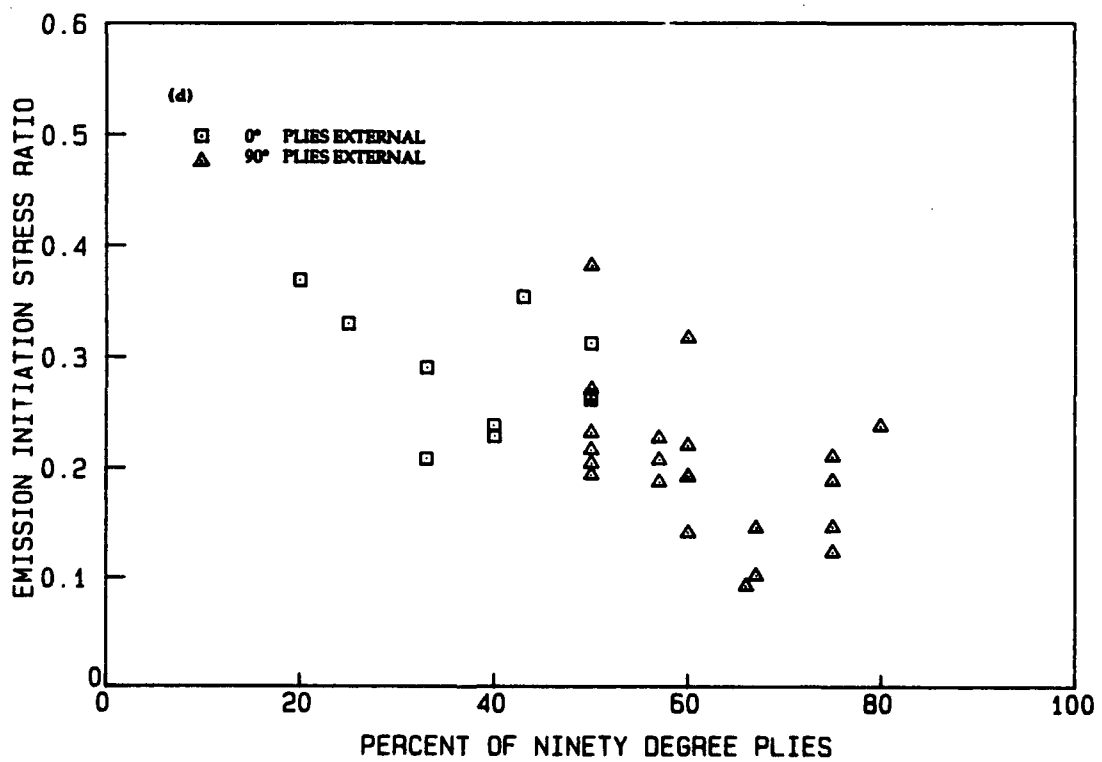
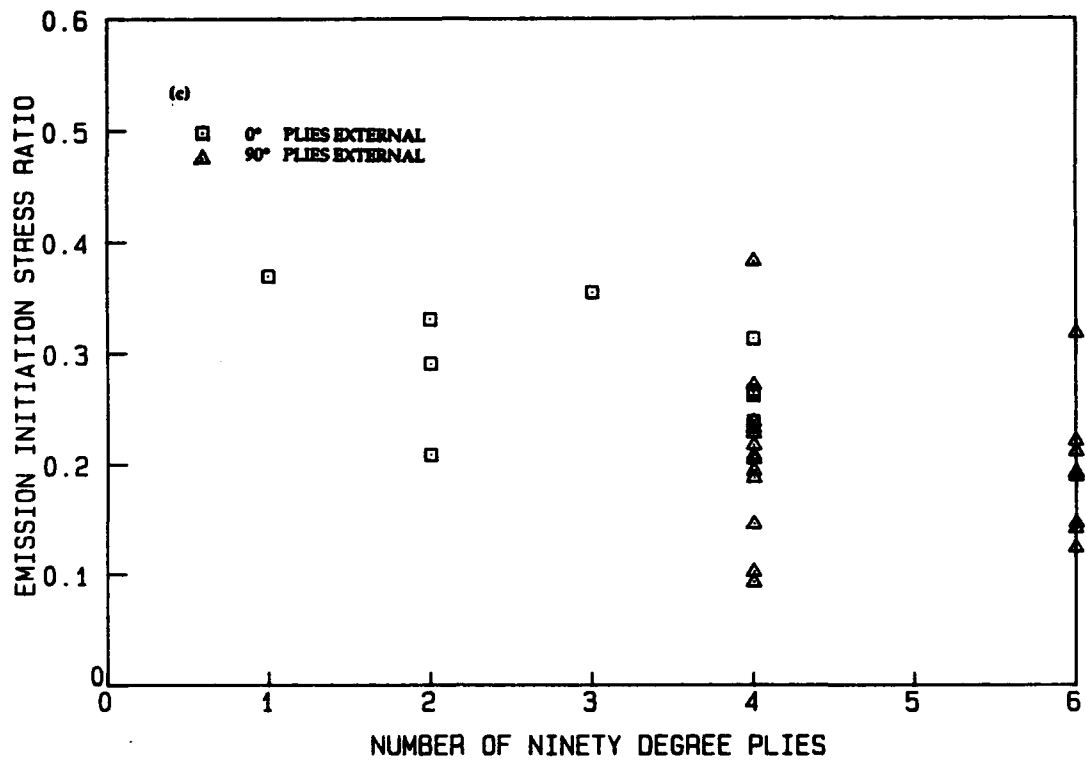


Figure 5.3. Concluded.

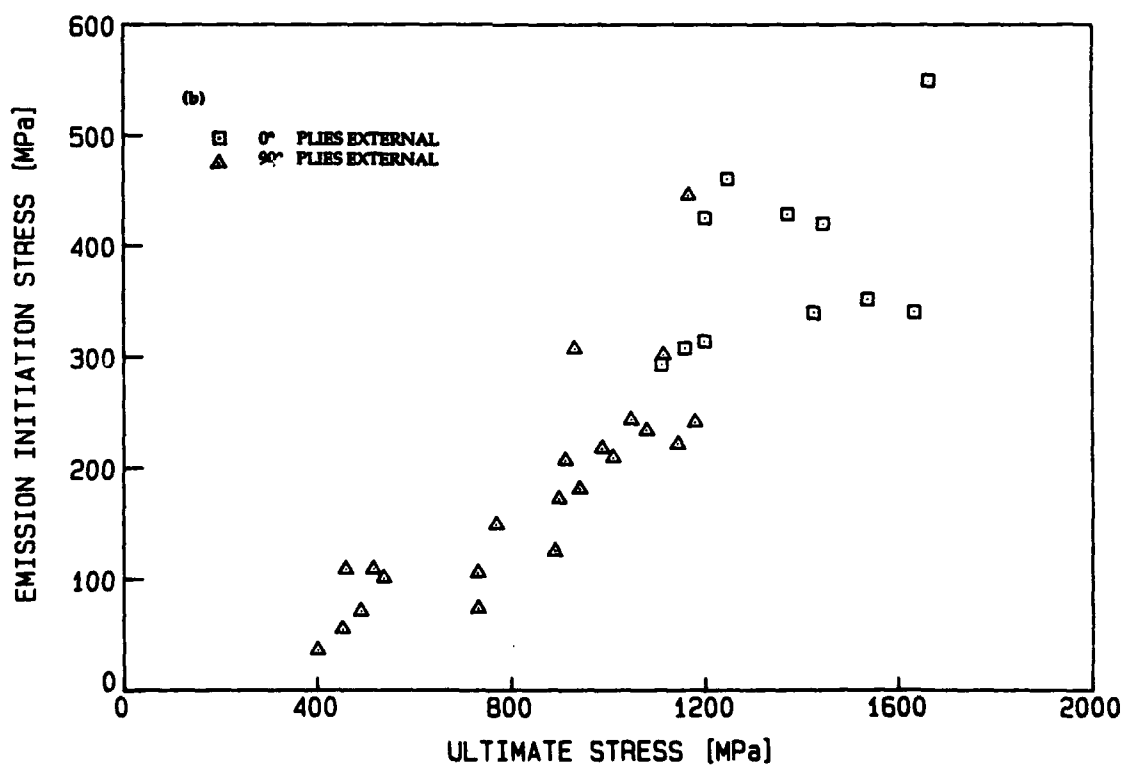
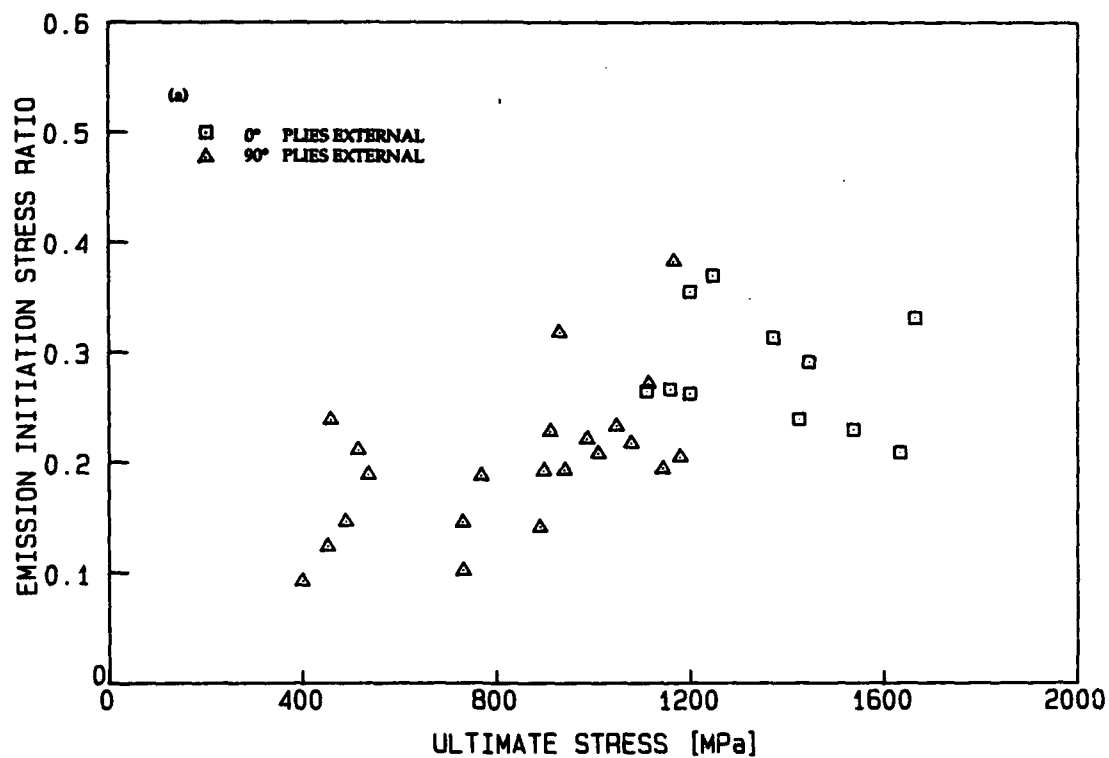


Figure 5.4. Emission initiation stress (recorded with the D/E AE system) as a function of ultimate stress for all cross-ply laminates: (a) non-dimensional; and (b) dimensional.

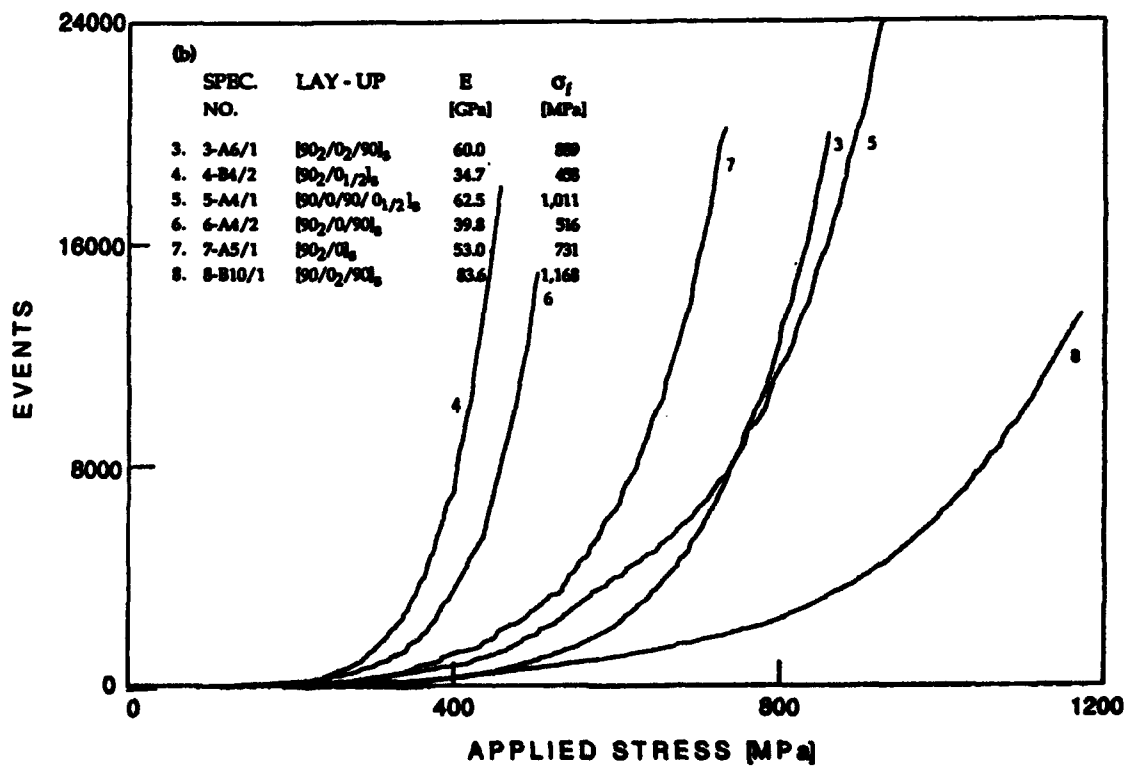
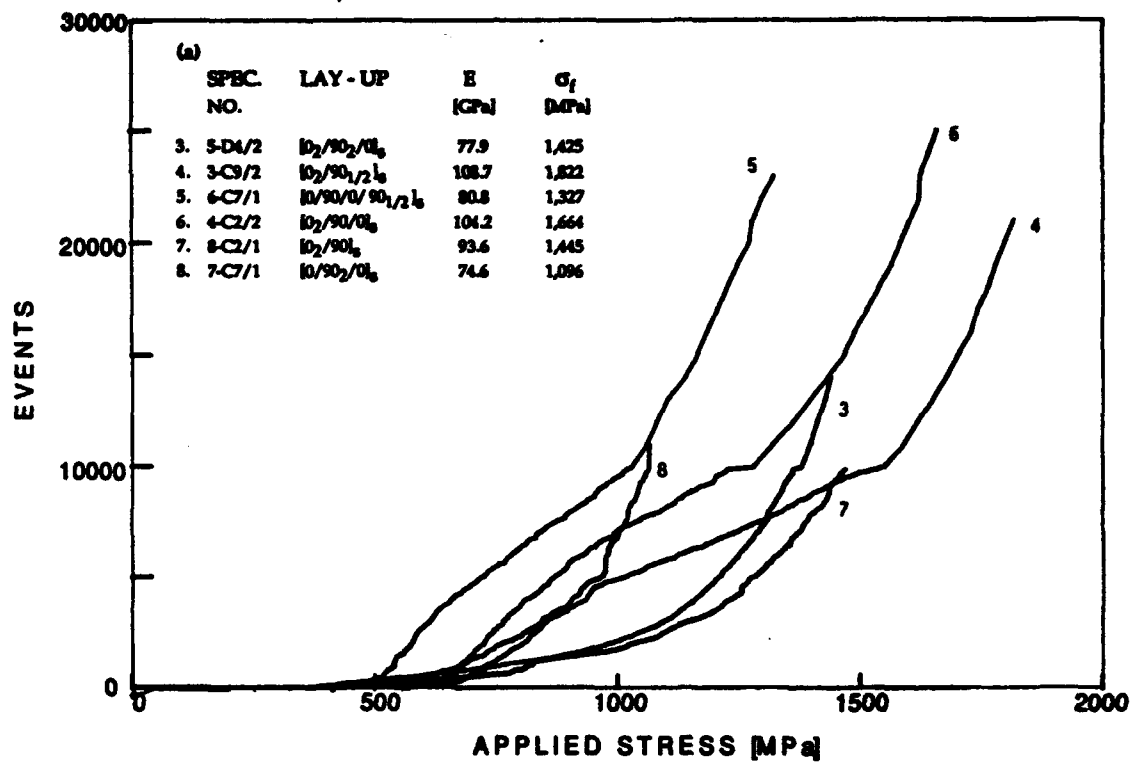


Figure 5.5. Events accumulated during quasi-static loading to failure (recorded with the D/E AE system) as a function of far-field applied stress for 12 different cross-ply graphite/epoxy laminates: (a) laminates having external 0° plies (Group I); and (b) laminates having external 90° plies (Group II).

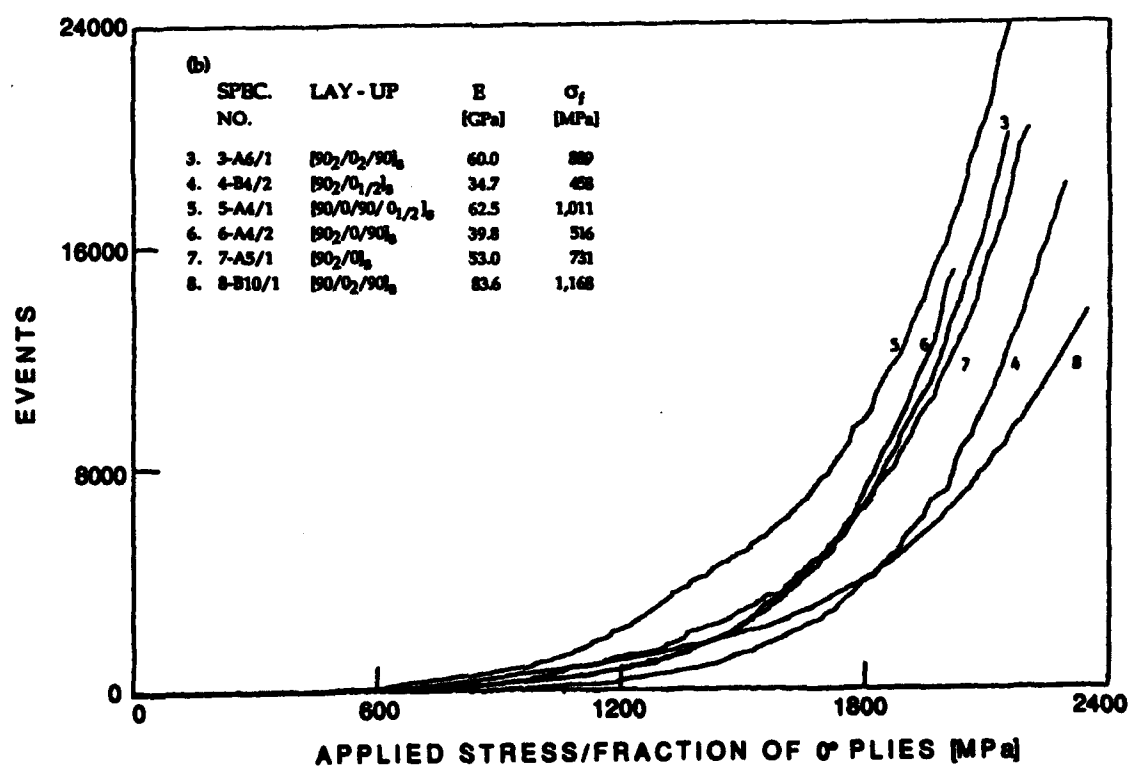
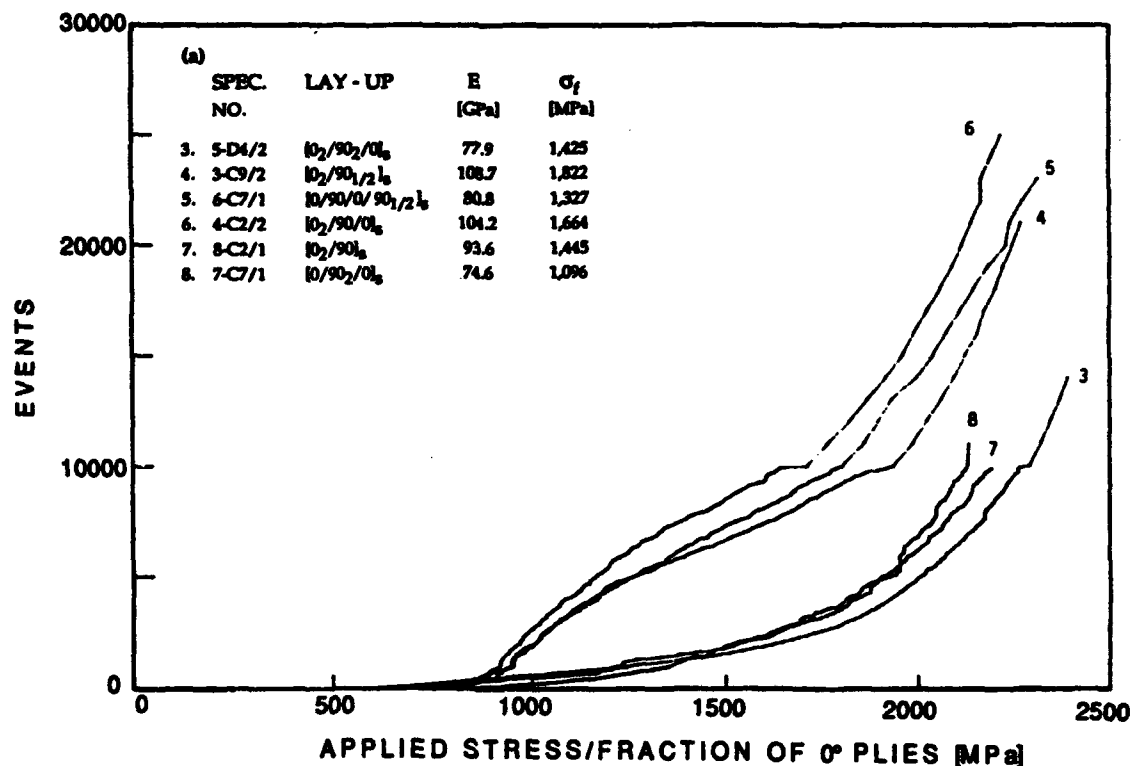


Figure 5.6. Events accumulated during quasi-static loading to failure (recorded with the D/E AE system) as a function of far-field applied stress for 12 different cross-ply graphite/epoxy laminates assuming that only the 0° carry the load: (a) laminates having external 0° plies (Group I); and (b) laminates having external 90° plies (Group II).

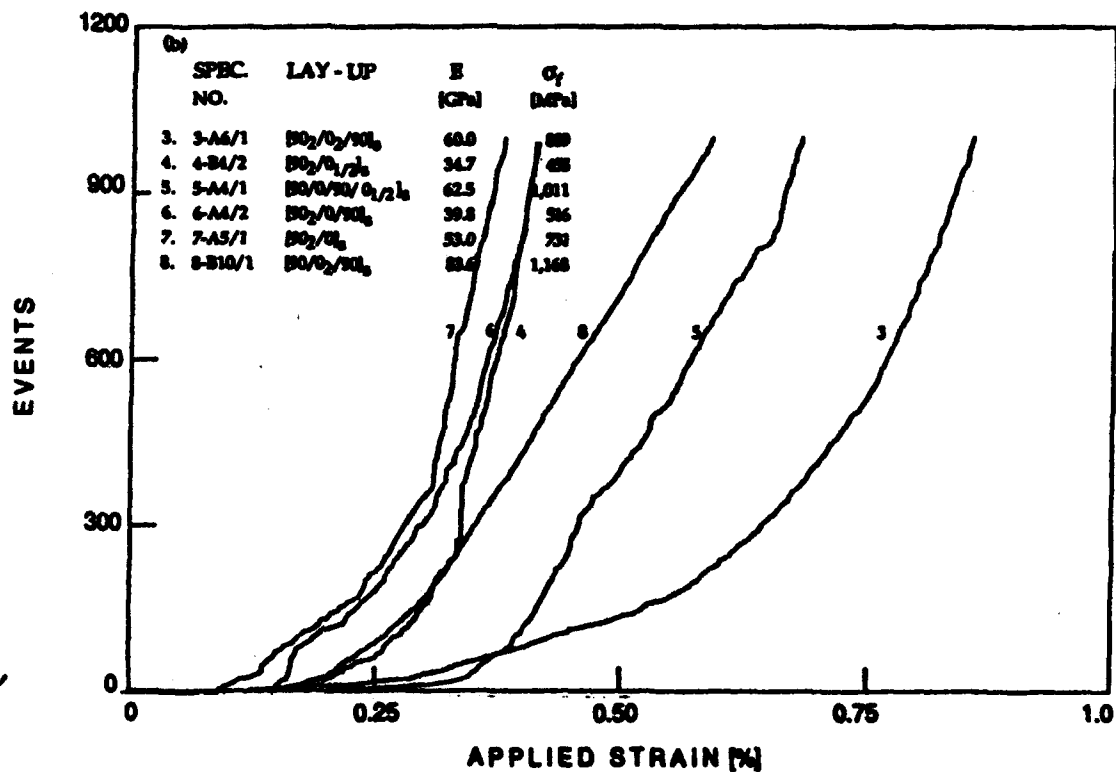
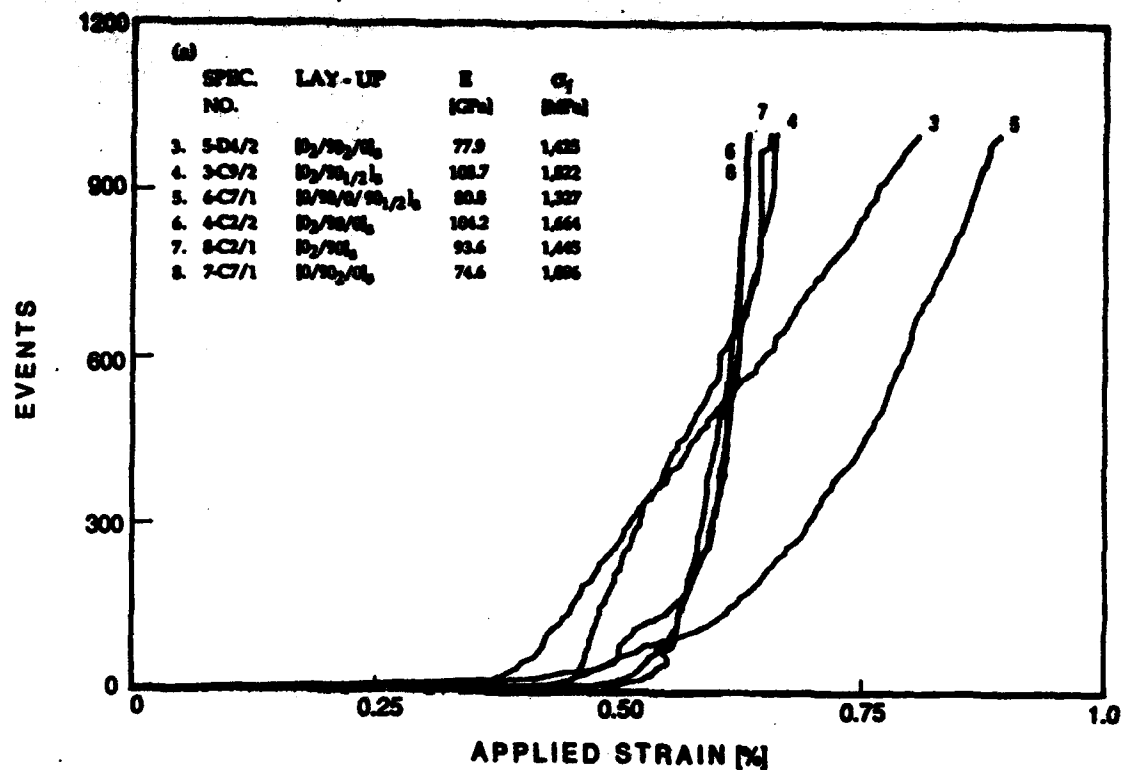


Figure 5.7. Events accumulated during quasi-static loading to failure (recorded with the D/E AE system) as a function of far-field applied strain for 12 different cross-ply graphite/epoxy laminates: (a) laminates having external 0° plies (Group I); and (b) laminates having external 90° plies (Group II).

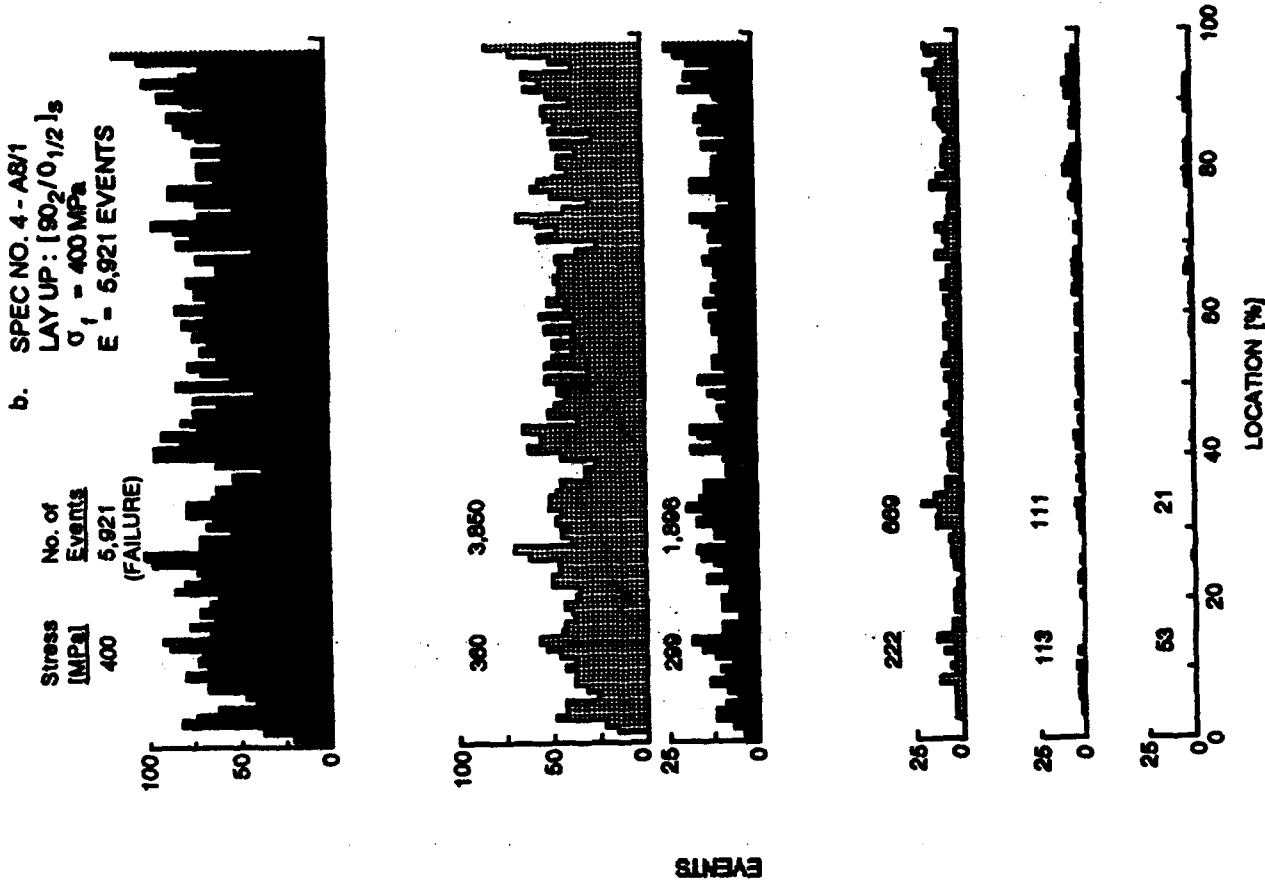
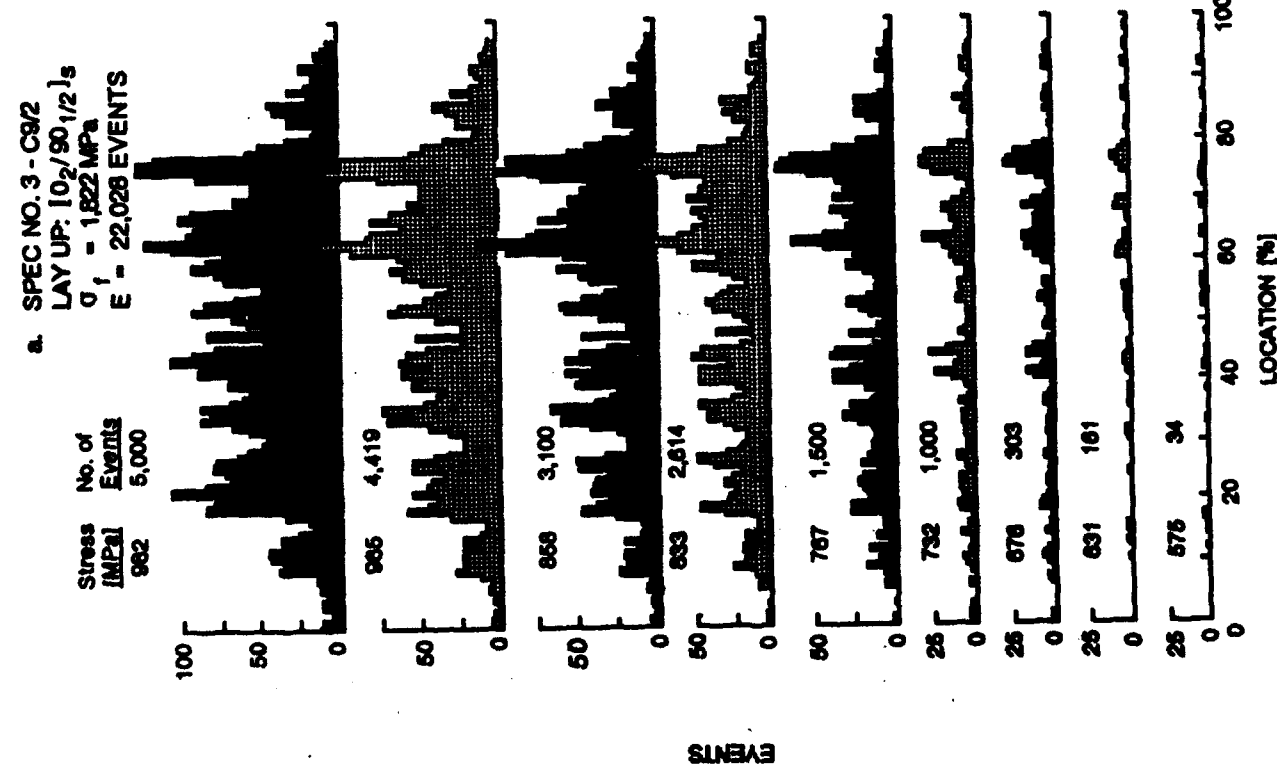


Figure 5.8. Location distribution histograms of events (recorded with the D/E AE system) accumulated at different load ranges during quasi-static loading of 12 different cross-ply graphite/epoxy laminates. Each Figure shows two laminates having reversed stacking sequence.

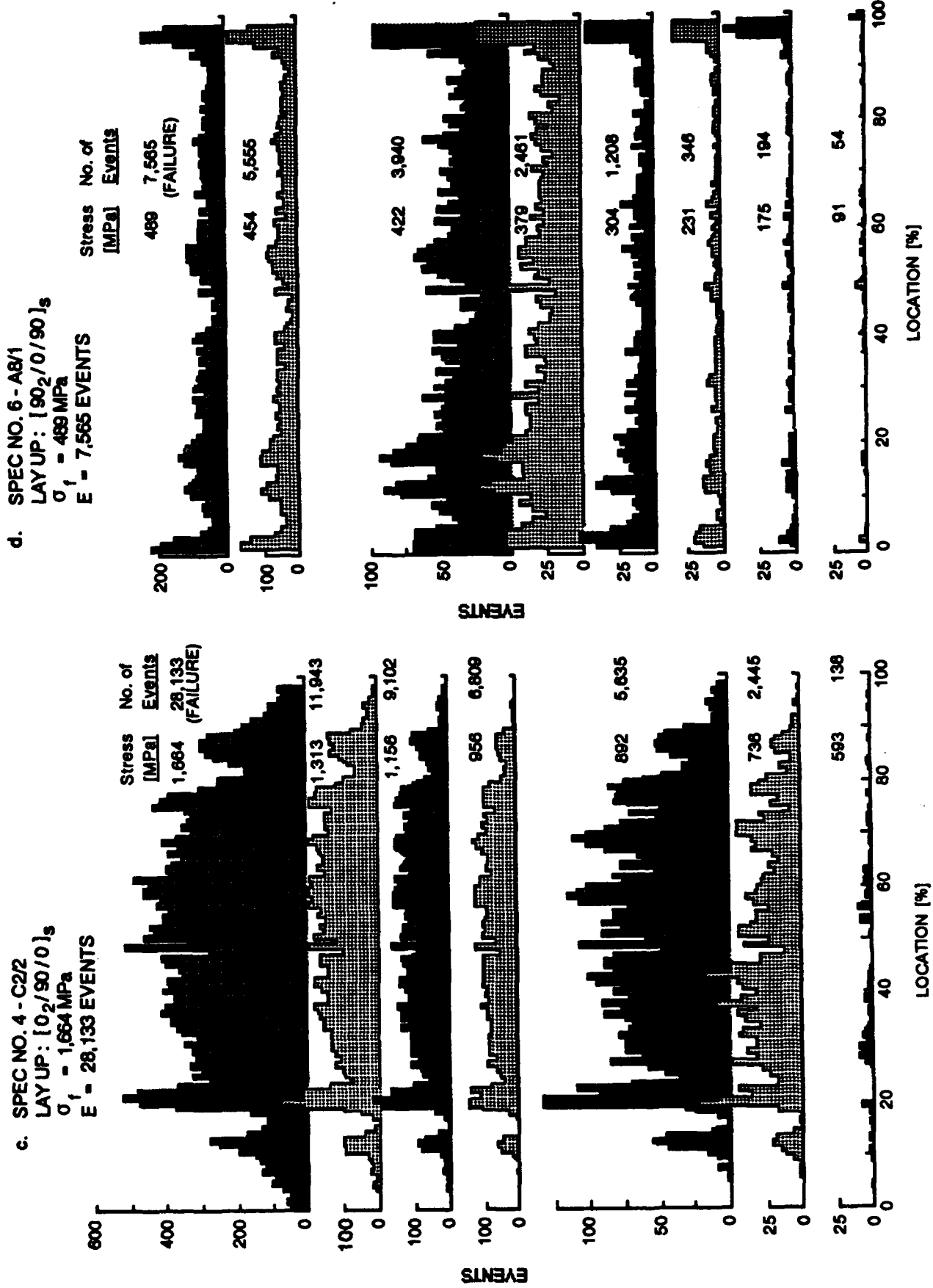


Figure 5.8. Continued.

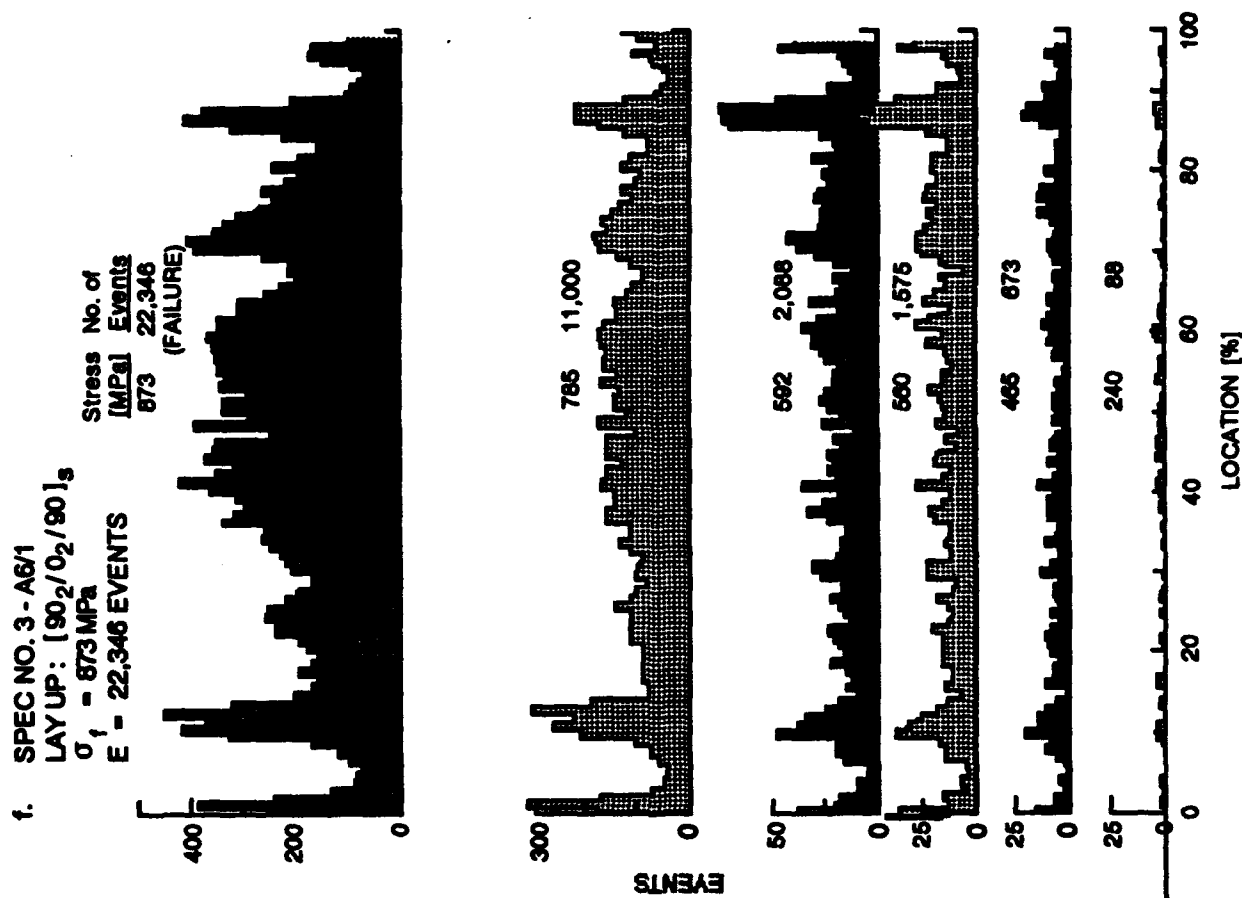
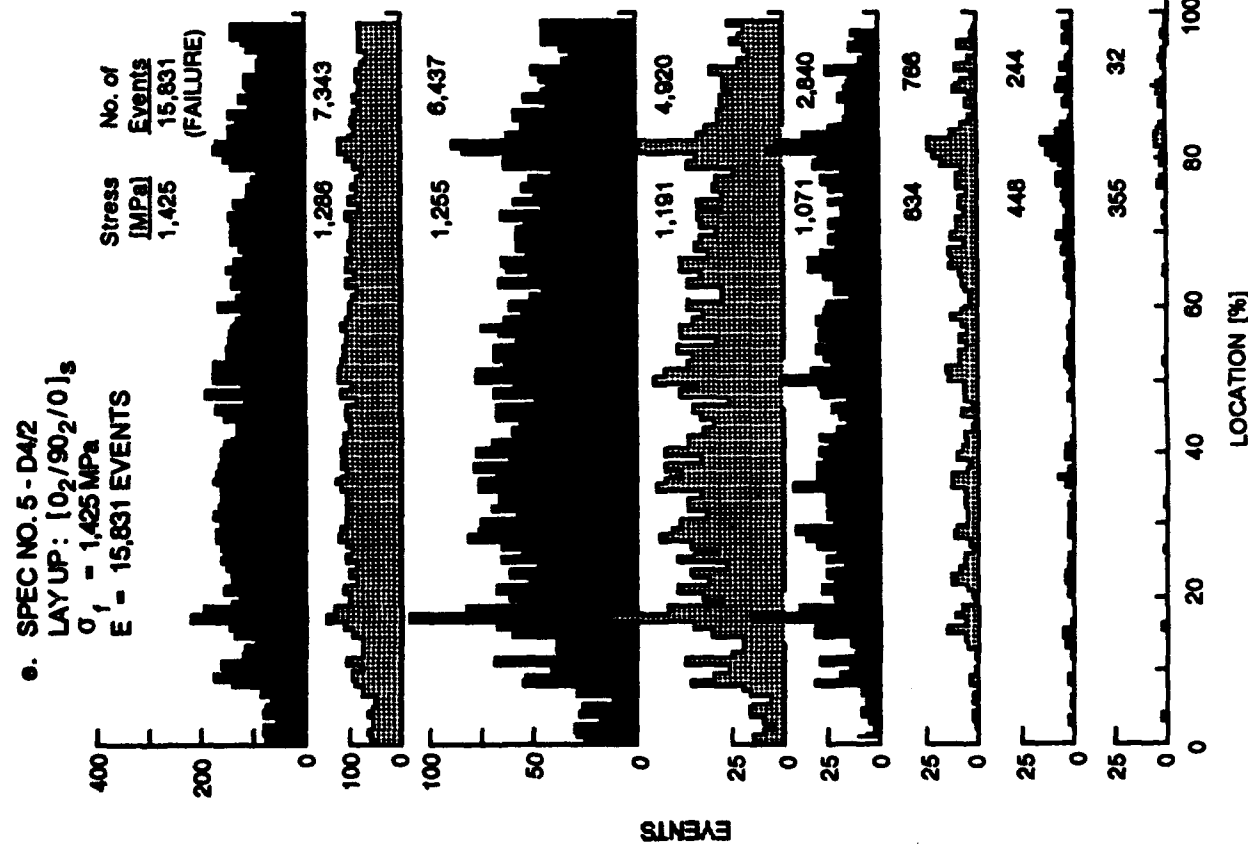
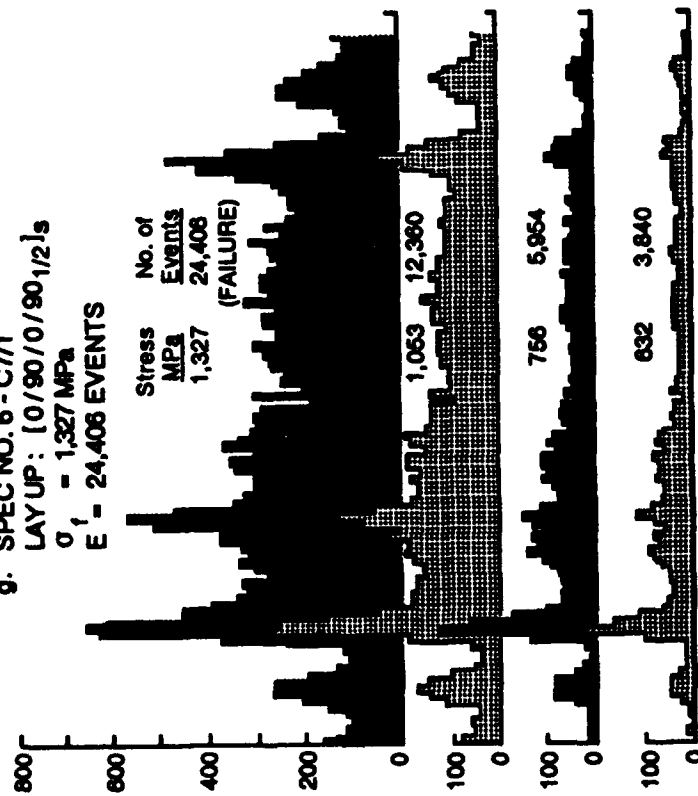


Figure 5.8. Continued.

9. SPEC NO. 6 - C7/1
LAY UP: [0/90/0/90]_{1/2}s
 $\sigma_1 = 1,327 \text{ MPa}$
E = 24,406 EVENTS



EVENTS

157

h. SPEC NO. 5 - B6/1
LAY UP: [90/0/90/0]_{1/2}s
 $\sigma_1 = 797 \text{ MPa}$
E = 20,894 EVENTS

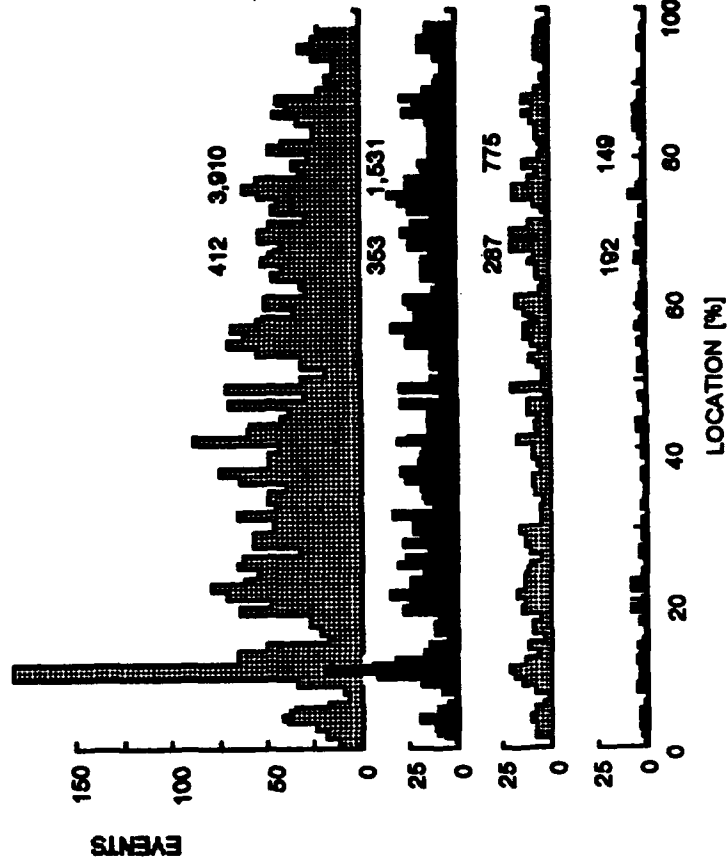
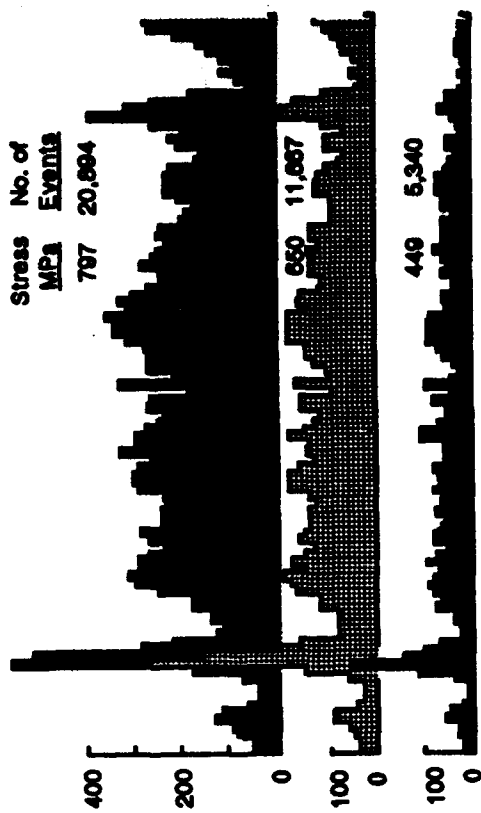
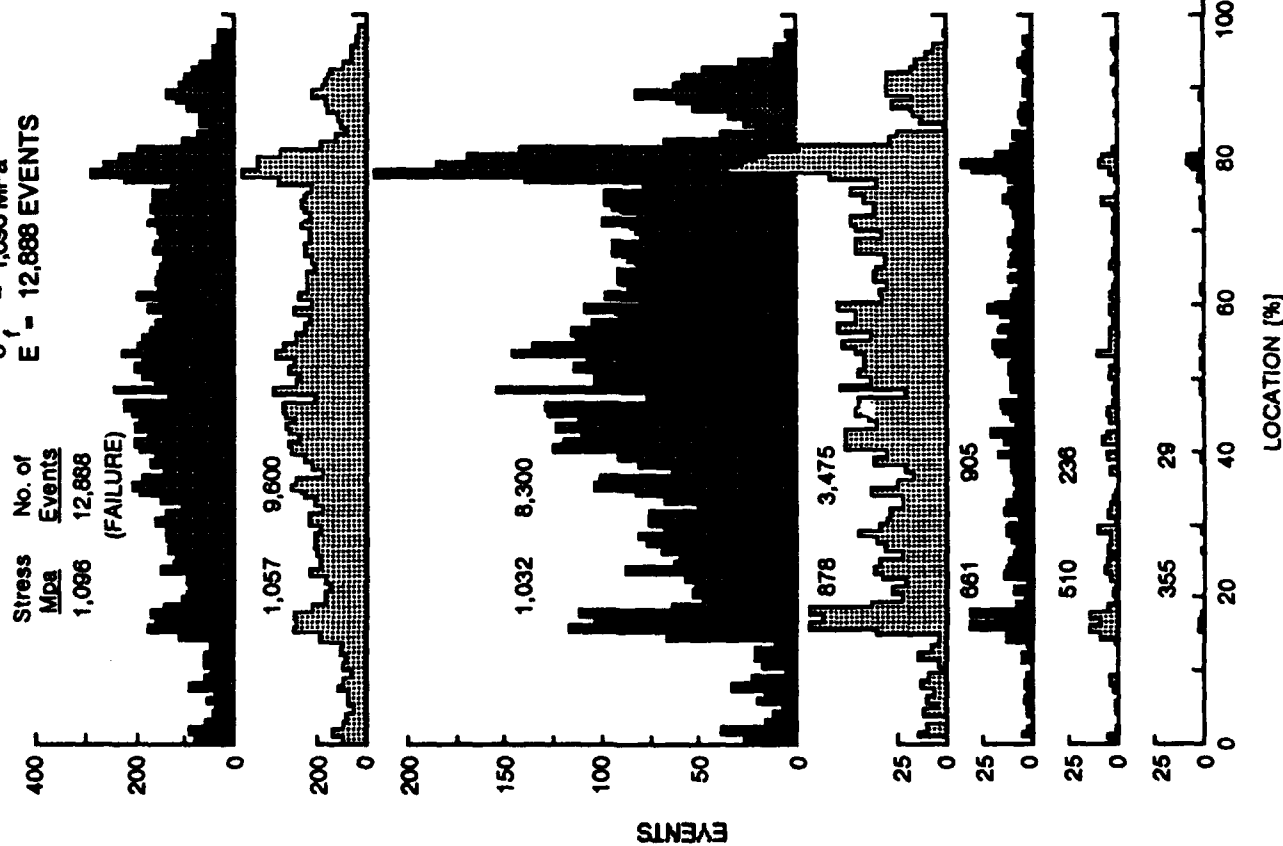


Figure 5.8. Continued.

I. SPEC NO. 7 - C7/1
LAYUP: [0/90₂/0]_s
 $\sigma_f = 1,096 \text{ MPa}$
E = 12,888 EVENTS



J. SPEC NO. 8 - B8/1
LAYUP: [90/0₂/90]_s
 $\sigma_f = 1,180 \text{ MPa}$
E = 11,750 EVENTS

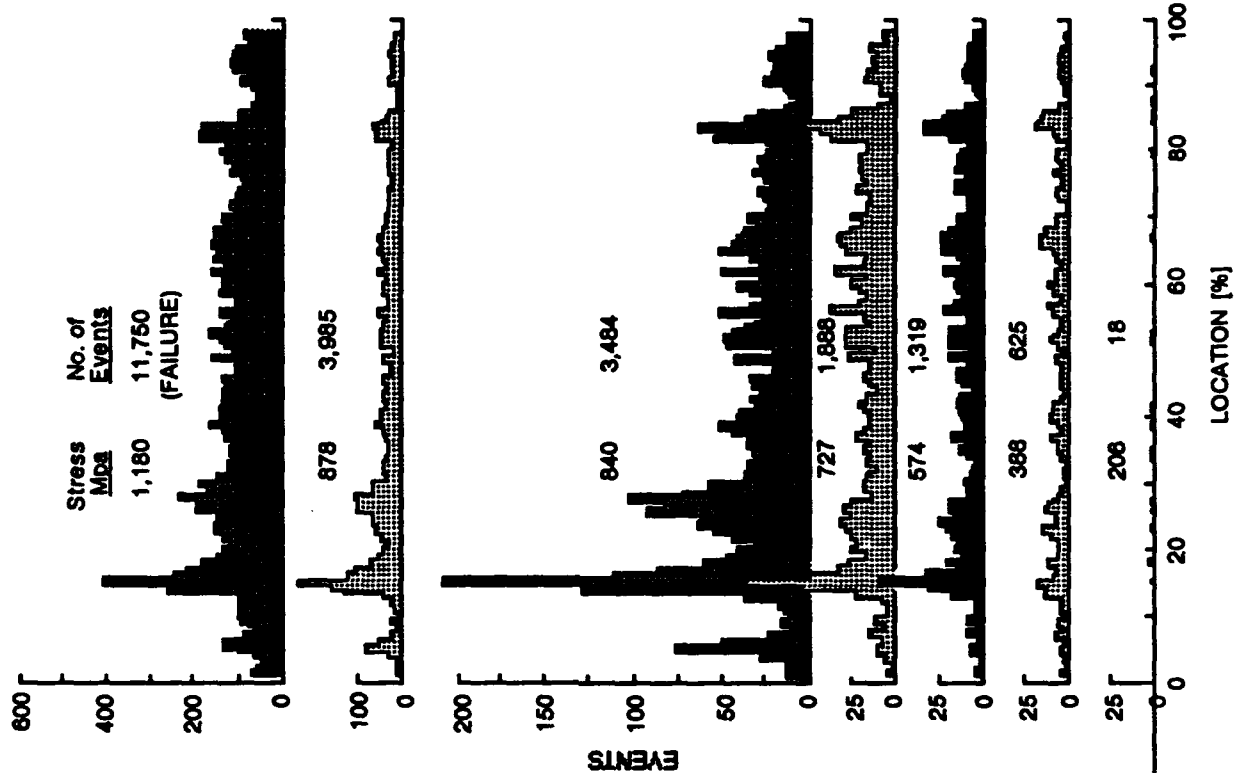


Figure 5.8. Continued.

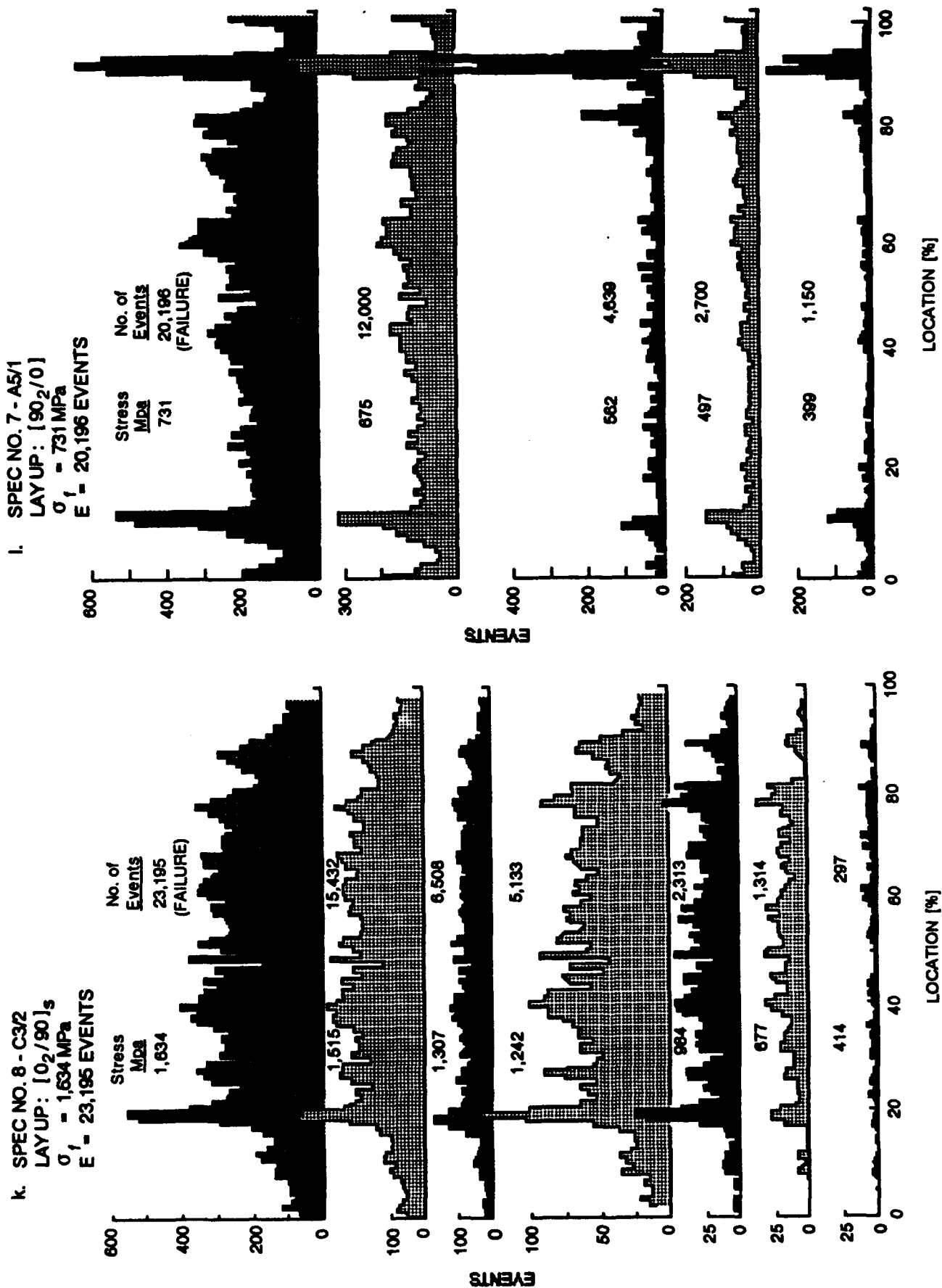


Figure 5.8. Concluded.

SPEC. NO. 3-A8/1
 LAY UP: $[90_2/0_2/90]_s$
 $\sigma_1 = 558 \text{ MPa}$
 $E = 8,720 \text{ EVENTS}$
 $a/W = 0.11$

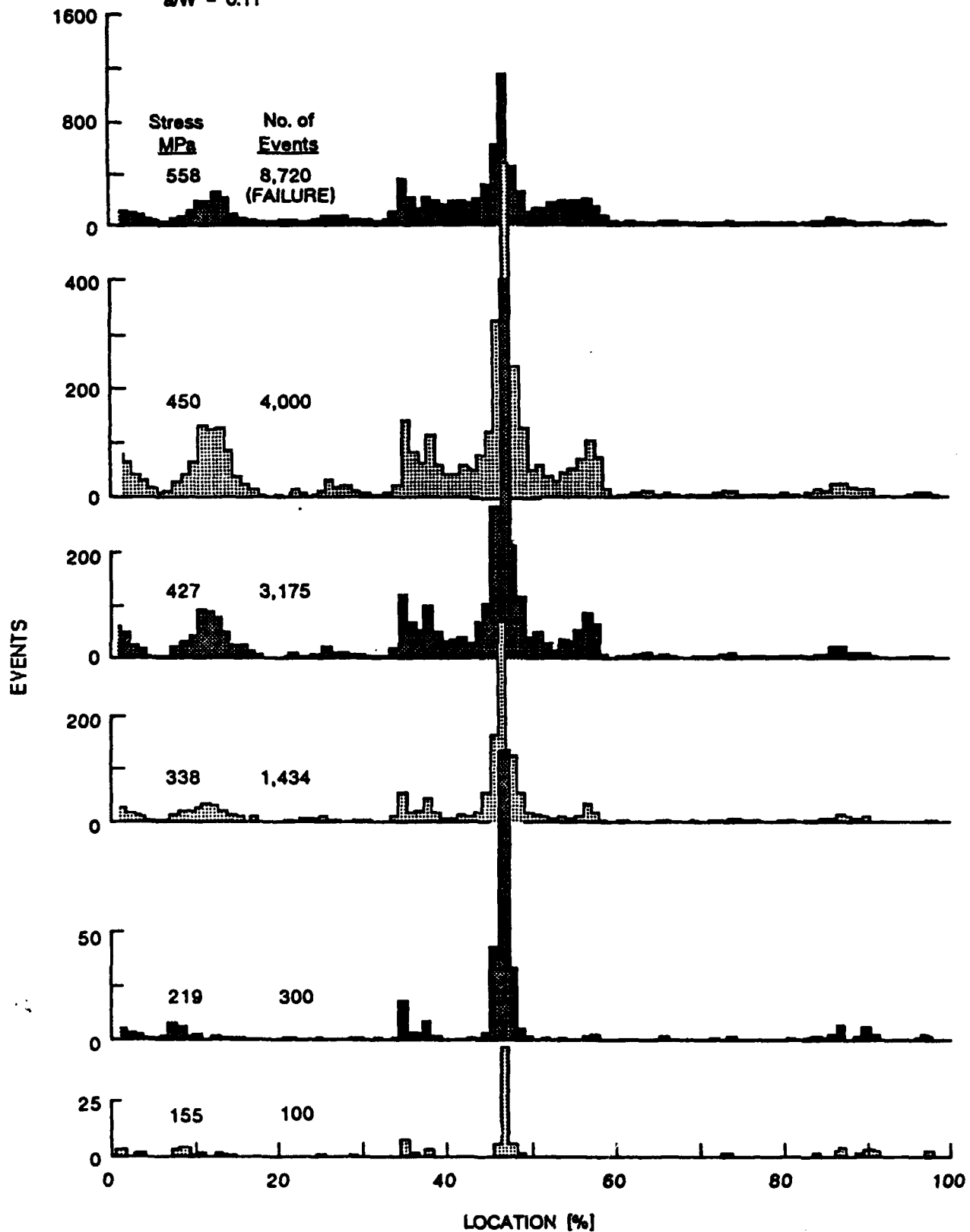
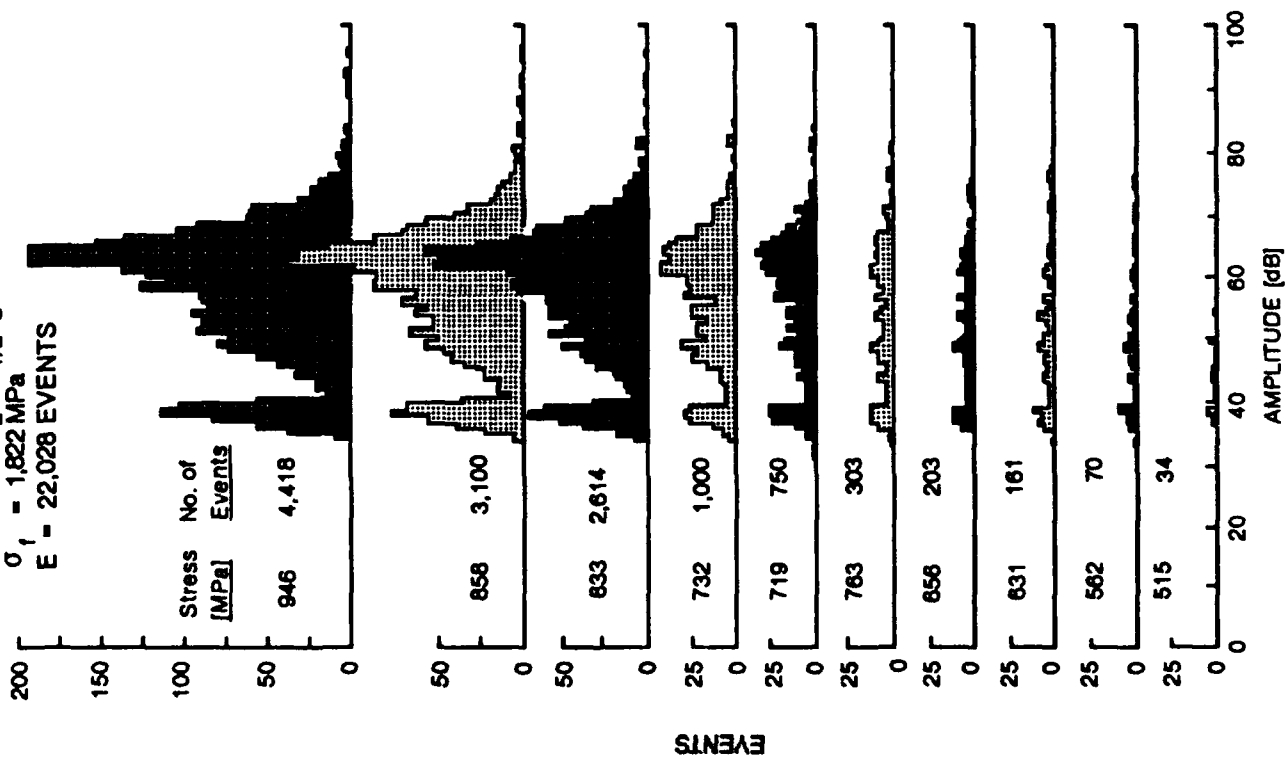


Figure 5.9. Location distribution histograms of events (recorded with the D/E AE system) accumulated at different load ranges during quasi-static loading of a double-edge notched $[90_2/0_2/90]_s$ graphite/epoxy laminate.

a. SPEC NO. 3 - C9/2
 LAY UP : $[0_2/90_{1/2}]_s$
 $\sigma_f = 1,822 \text{ MPa}$
 $E = 22,028 \text{ EVENTS}$



b. SPEC NO. 4 - A8/1
 LAY UP : $[90_2/0_{1/2}]_s$
 $\sigma_f = 400 \text{ MPa}$
 $E = 5,921 \text{ EVENTS}$

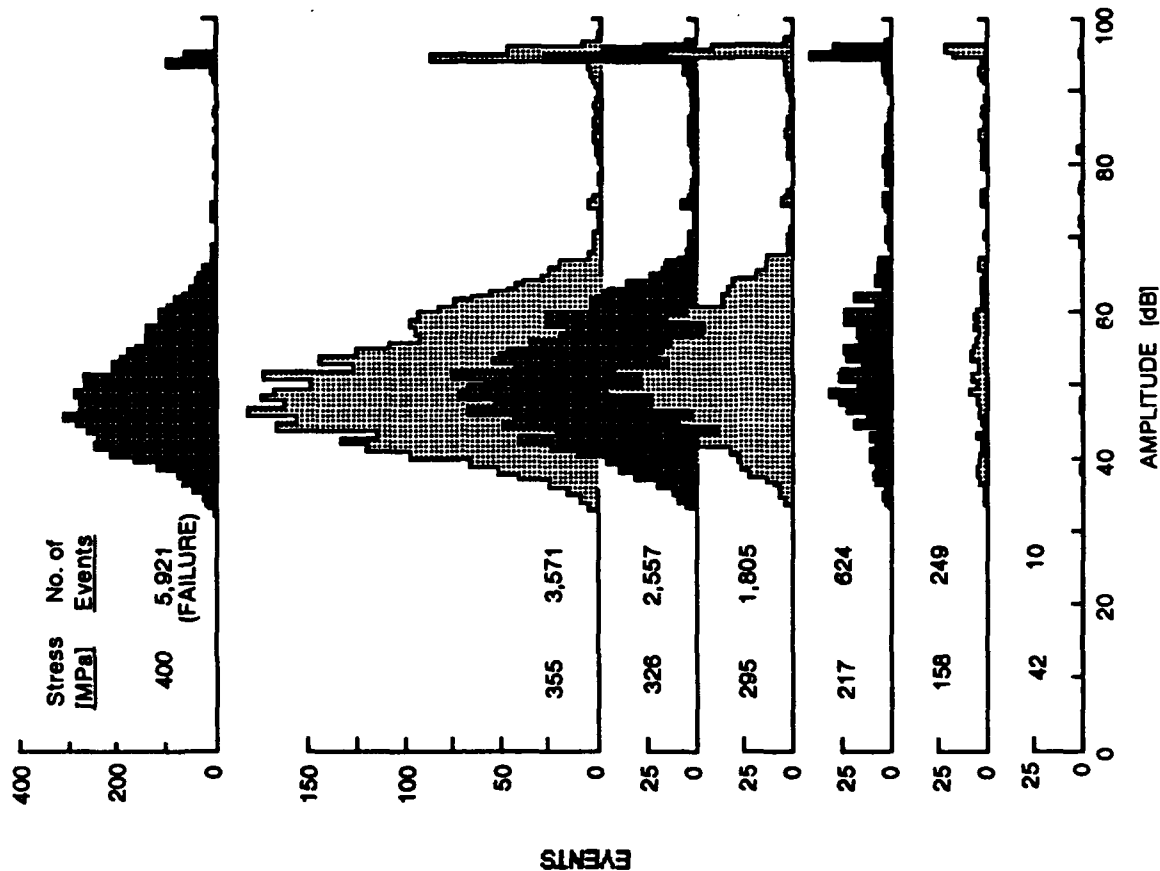
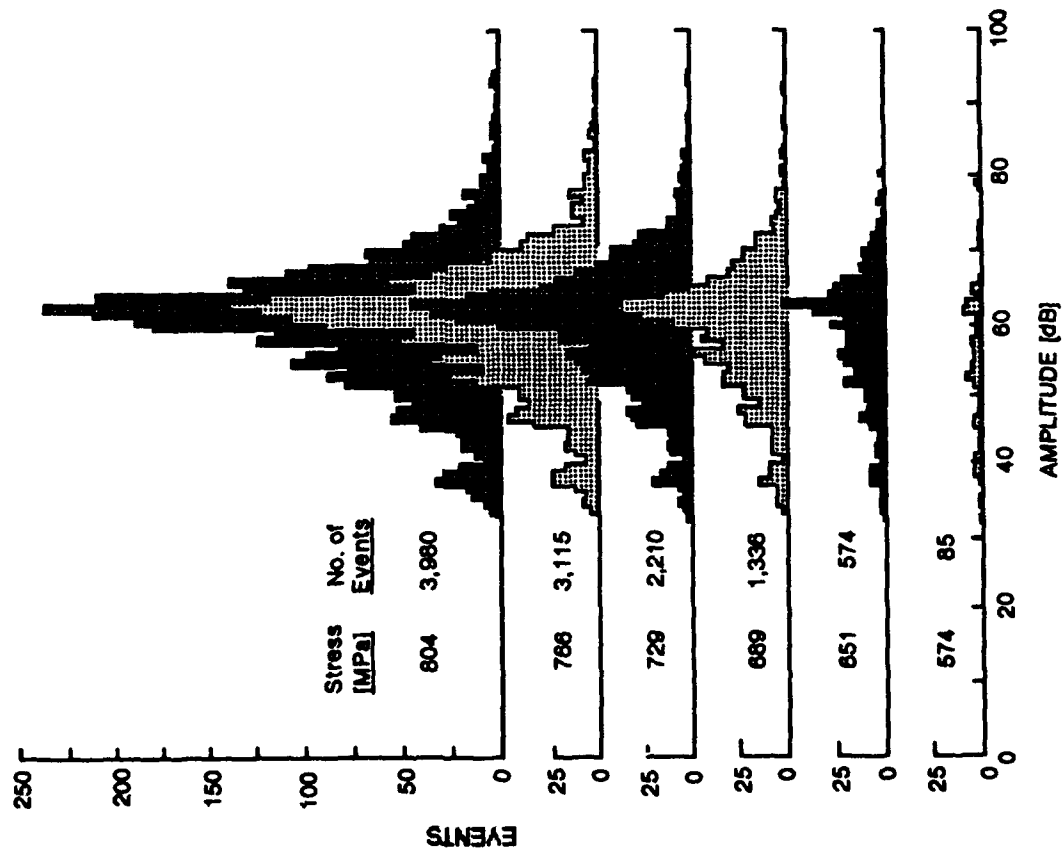


Figure 5.10. Amplitude distribution histograms of events (recorded with the D/E AE system) accumulated at different load ranges during quasi-static

c. SPEC NO. 4 - C2/2
 LAY UP: $[0_2/90/0]_s$
 $\sigma_1 = 1,664 \text{ MPa}$
 $E = 28,133 \text{ EVENTS}$



d. SPEC NO. 6 - A8/1
 LAY UP: $[90_2/0/90]_s$
 $\sigma_1 = 489 \text{ MPa}$
 $E = 7,565 \text{ EVENTS}$

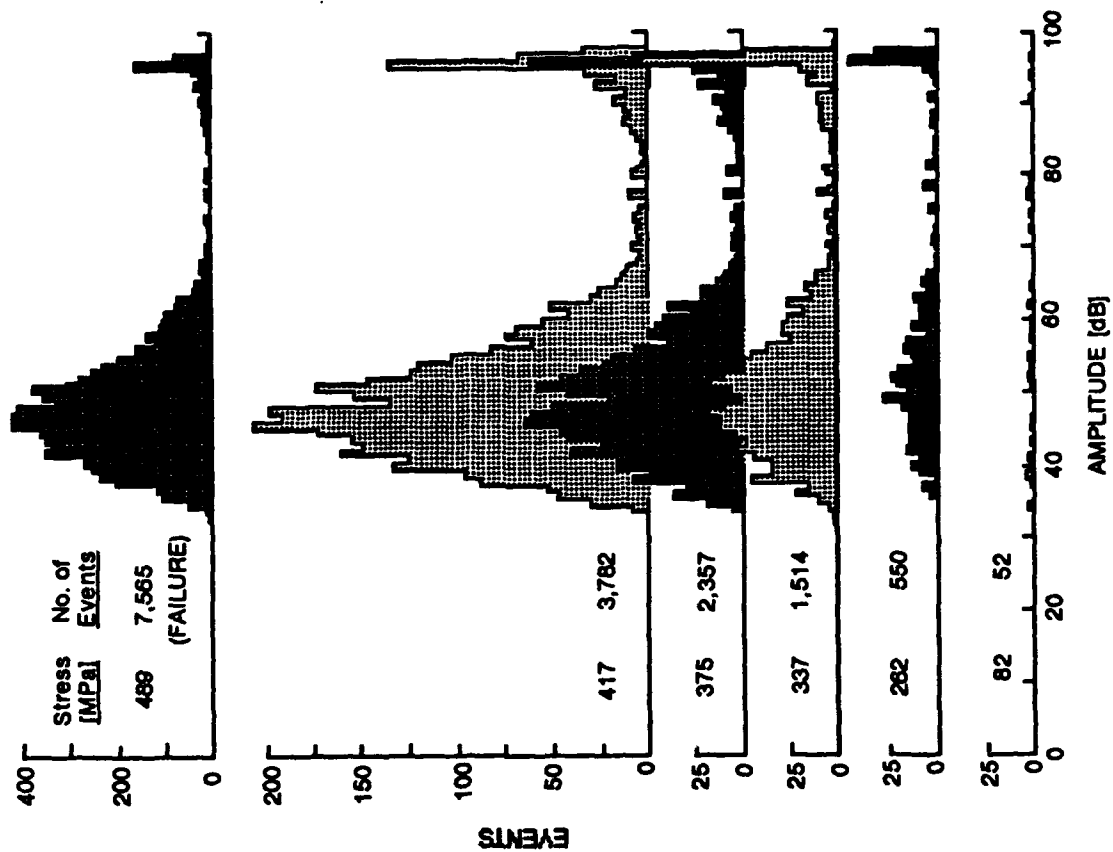
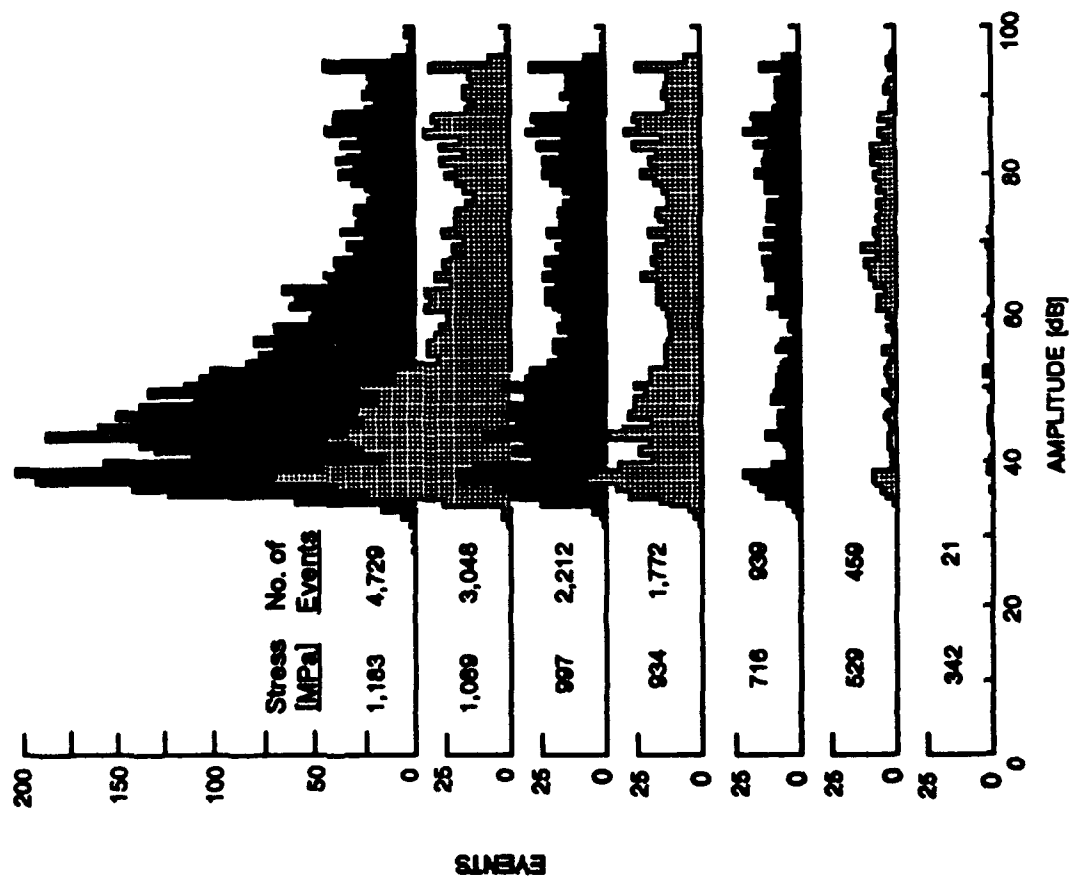


Figure 5.10. Continued.

g. SPEC NO. 5-D4/2
 LAY UP: $[0_2/90_2/0]_s$
 $\sigma_1 = 1,425 \text{ MPa}$
 $E = 15,831 \text{ EVENTS}$



f. SPEC NO. 3-A6/1
 LAY UP: $[90_2/0_2/90]_s$
 $\sigma_1 = 873 \text{ MPa}$
 $E = 22,346 \text{ EVENTS}$

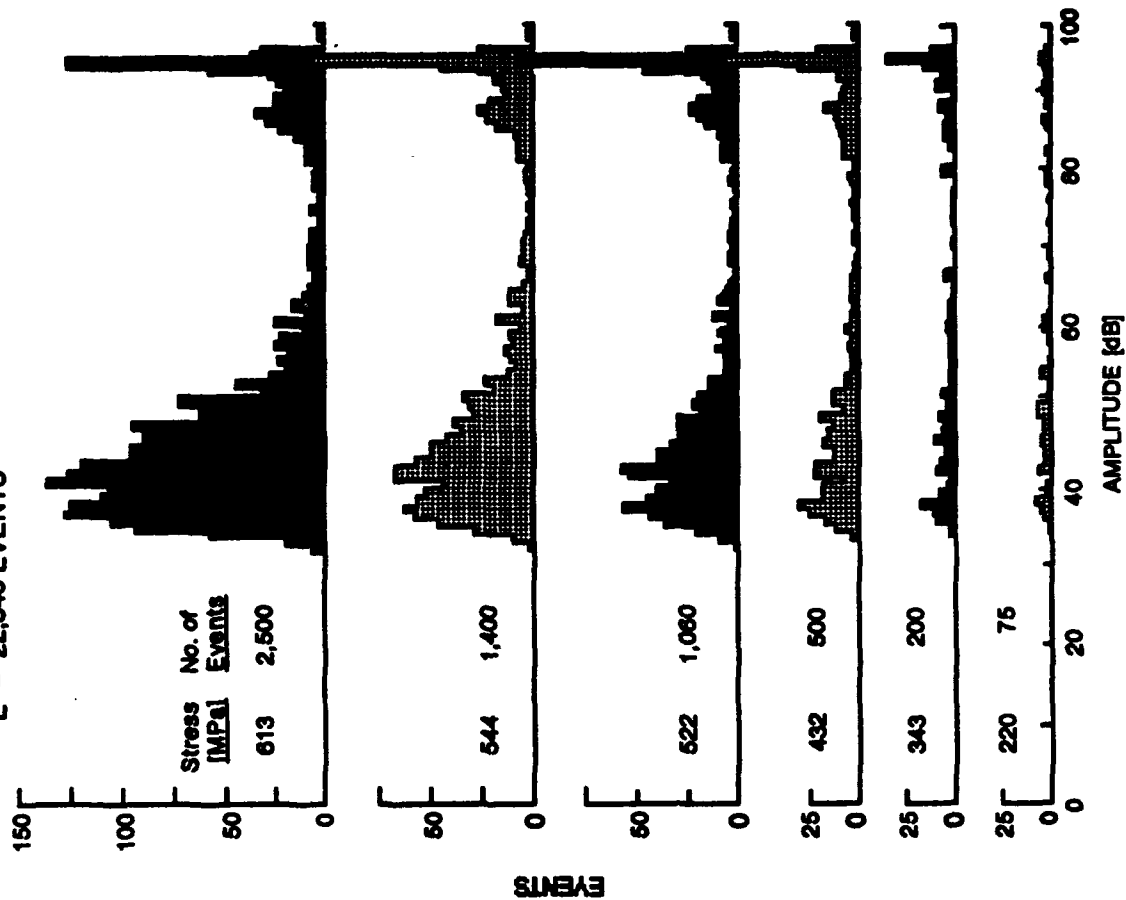


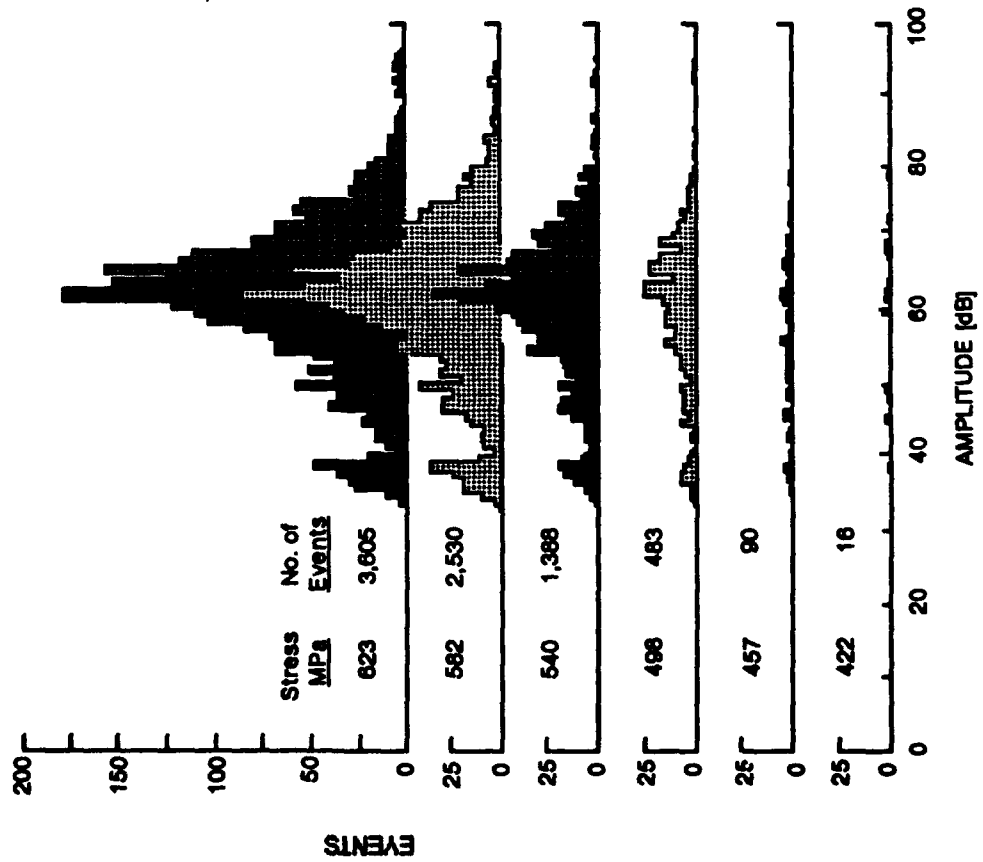
Figure 5.10. Continued.

g. SPEC NO. 6 - C7/1

LAYUP: [0/90/0/90]_{1/2}s

σ_1 = 1,327 MPa

E = 24,406 EVENTS



h. SPEC NO. 5 - B6/1

LAYUP: [90/0/90/0]_{1/2}s

σ_1 = 797 MPa

E = 20,884 EVENTS

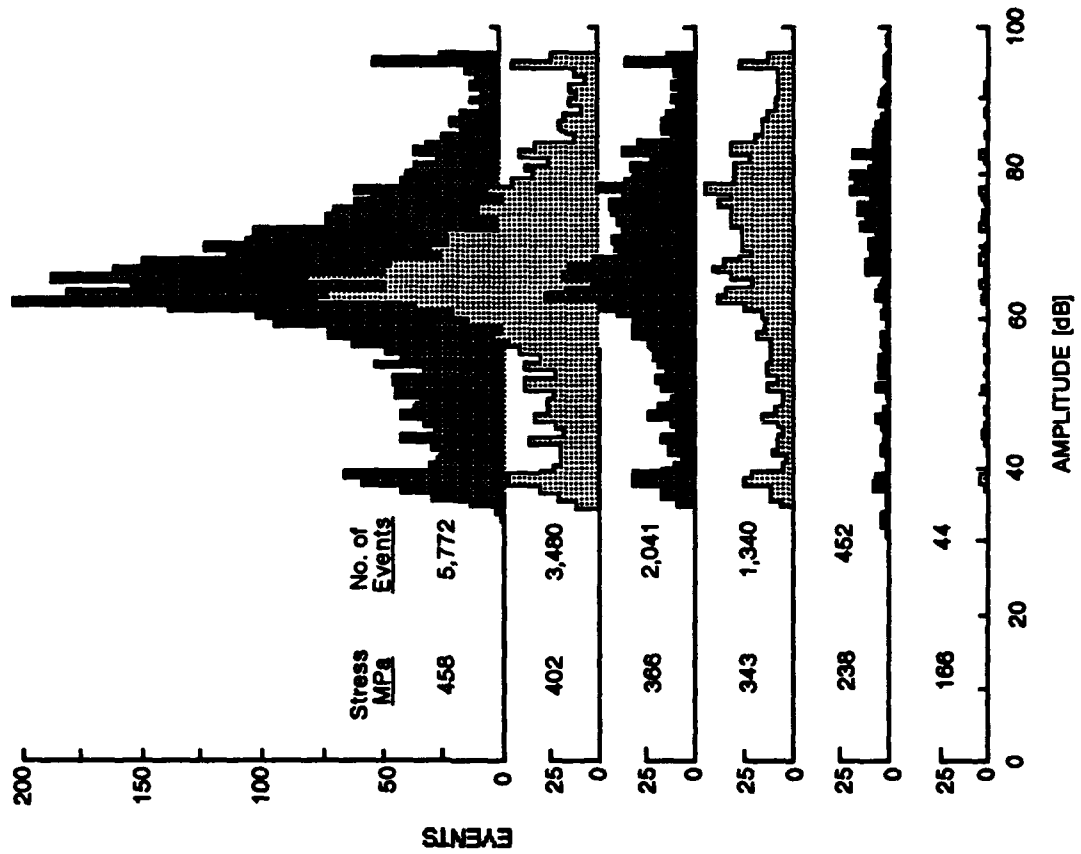


Figure 5.10. Continued.

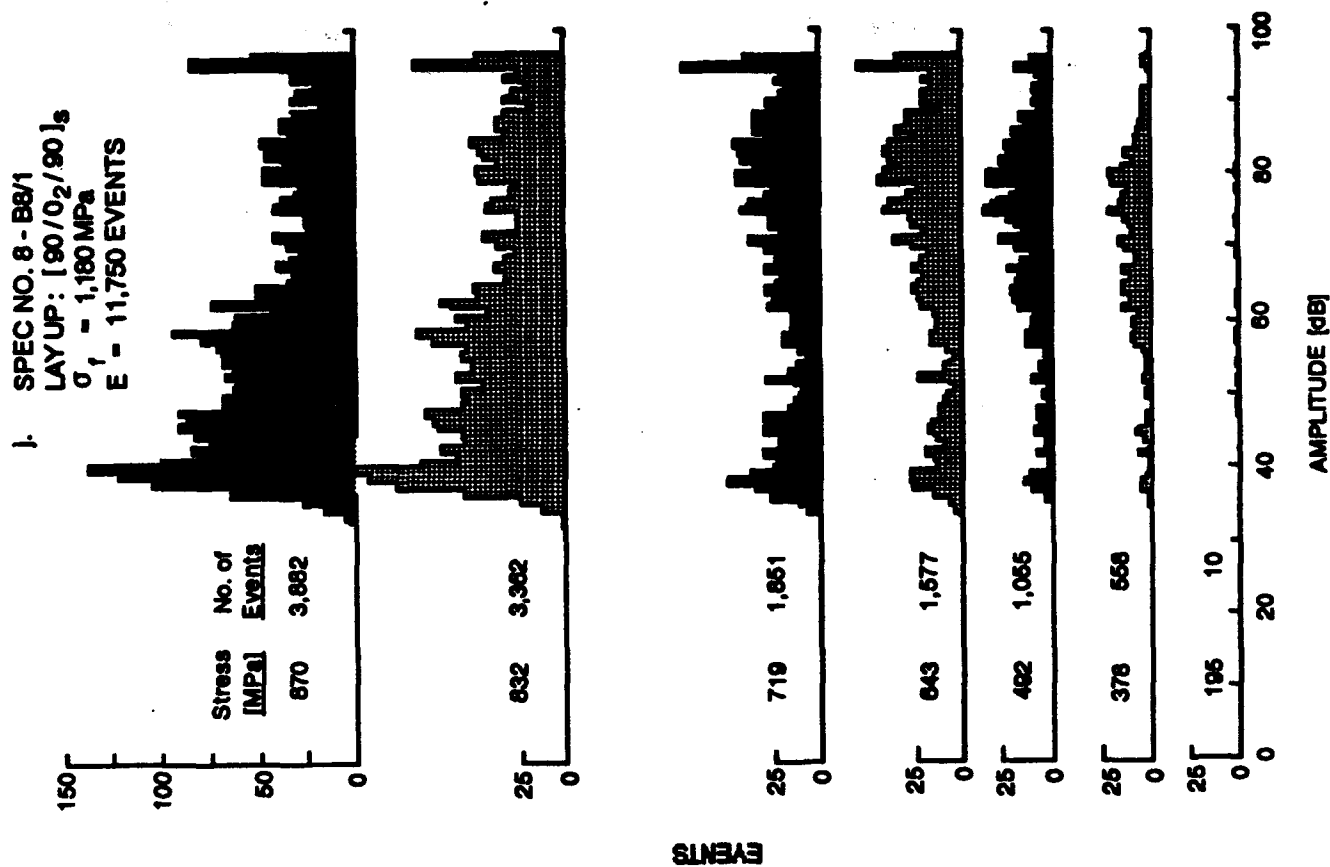
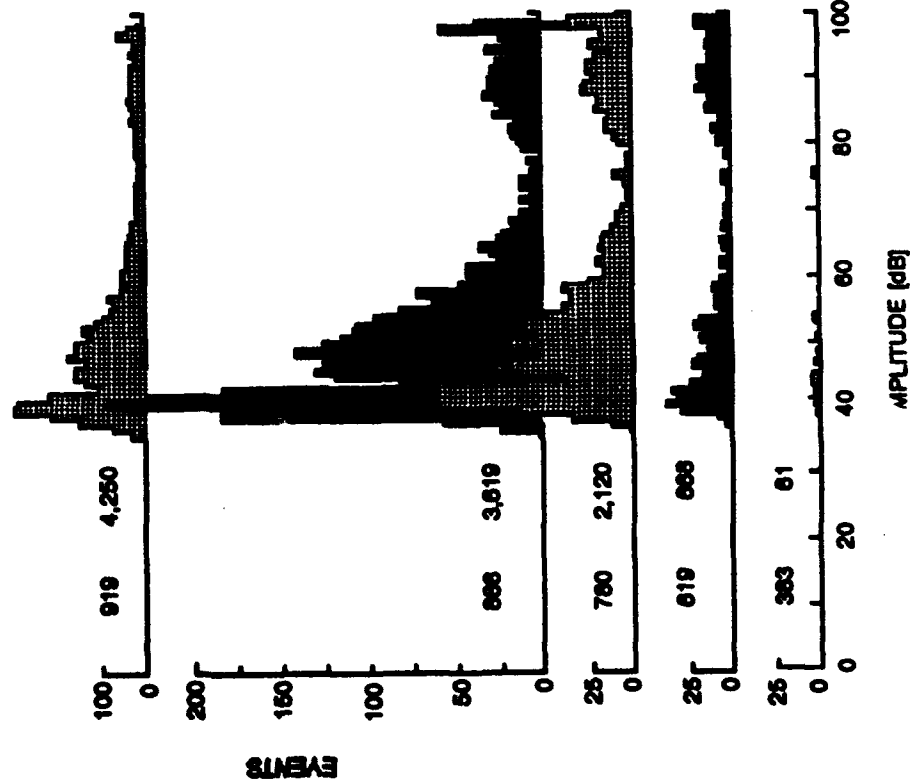
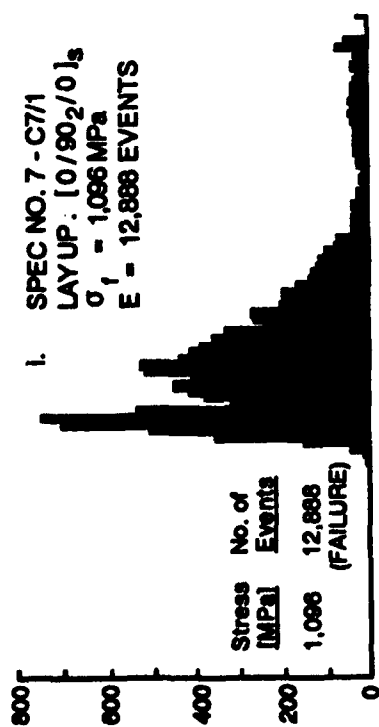
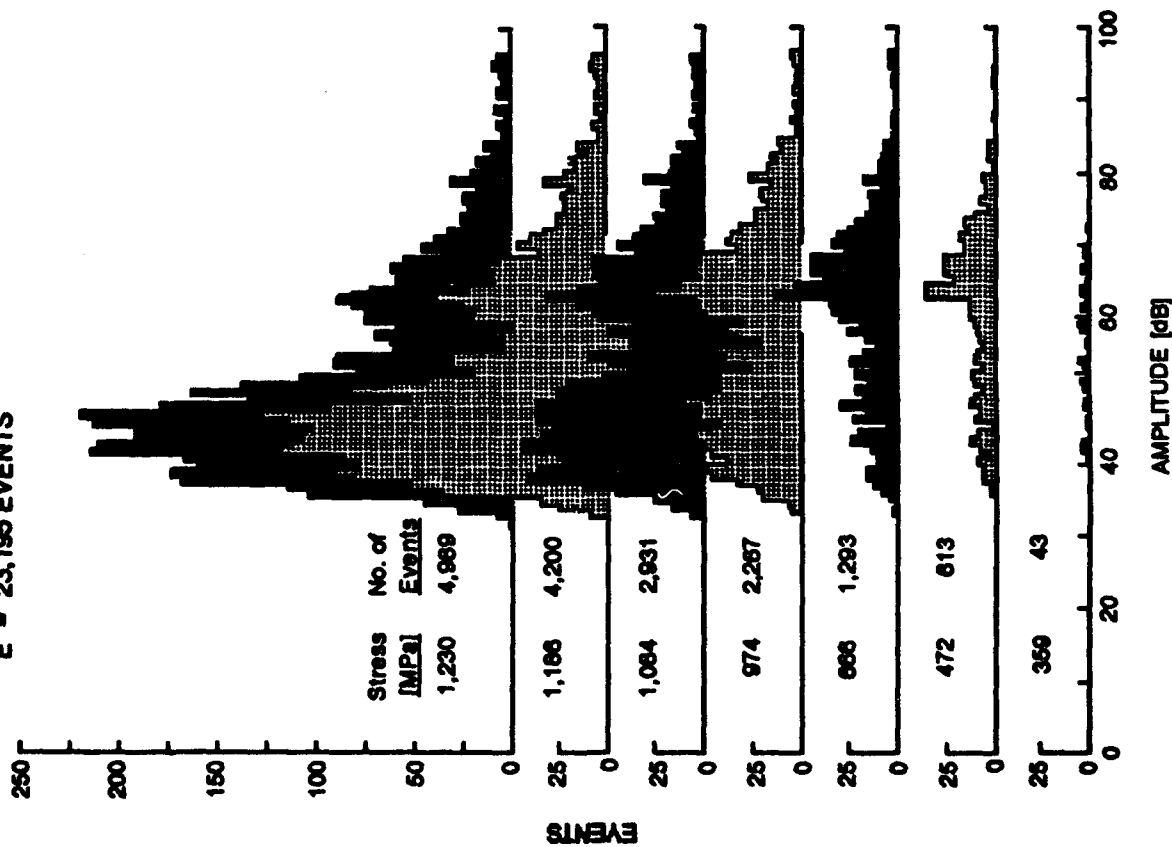


Figure 5.10. Continued.

k. SPEC. NO. 8 - C3/2
LAYUP: $[0_2/90]_s$
 $\sigma_1 = 1,634 \text{ MPa}$
E = 23,195 EVENTS



l. SPEC. NO. 7 - A5/1
LAYUP: $[90_2/0]_s$
 $\sigma_1 = 731 \text{ MPa}$
E = 20,196 EVENTS

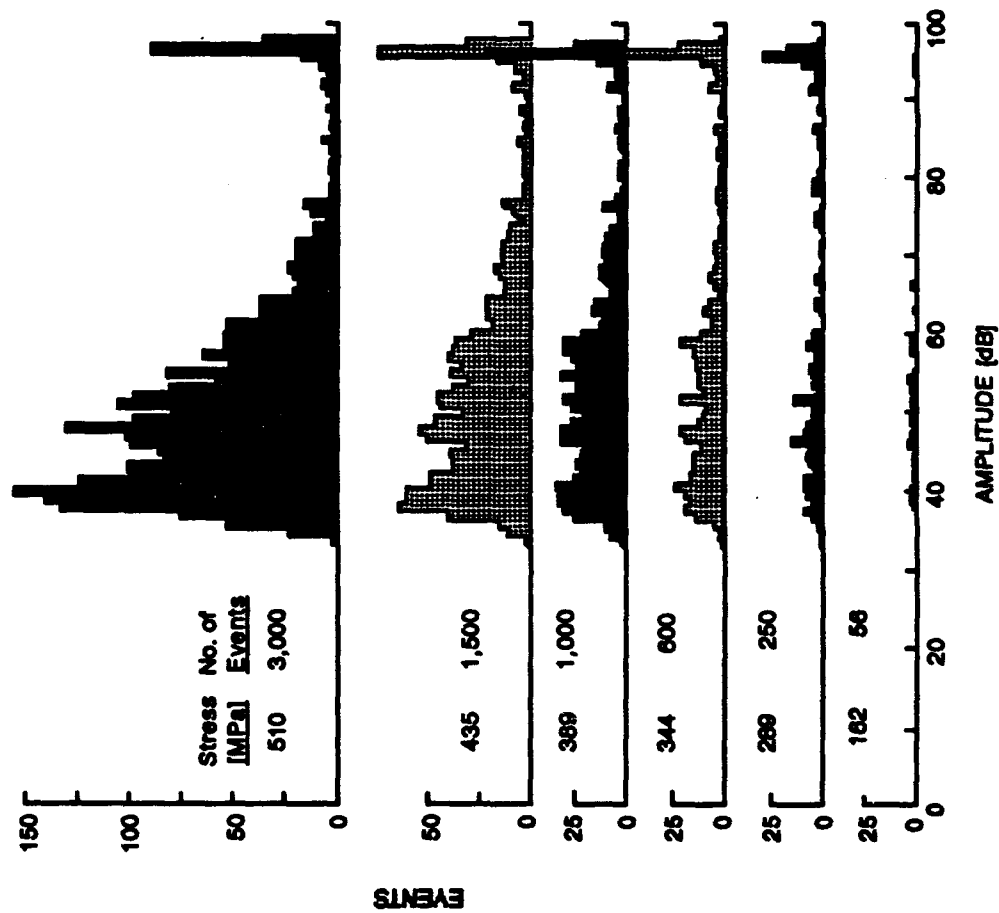
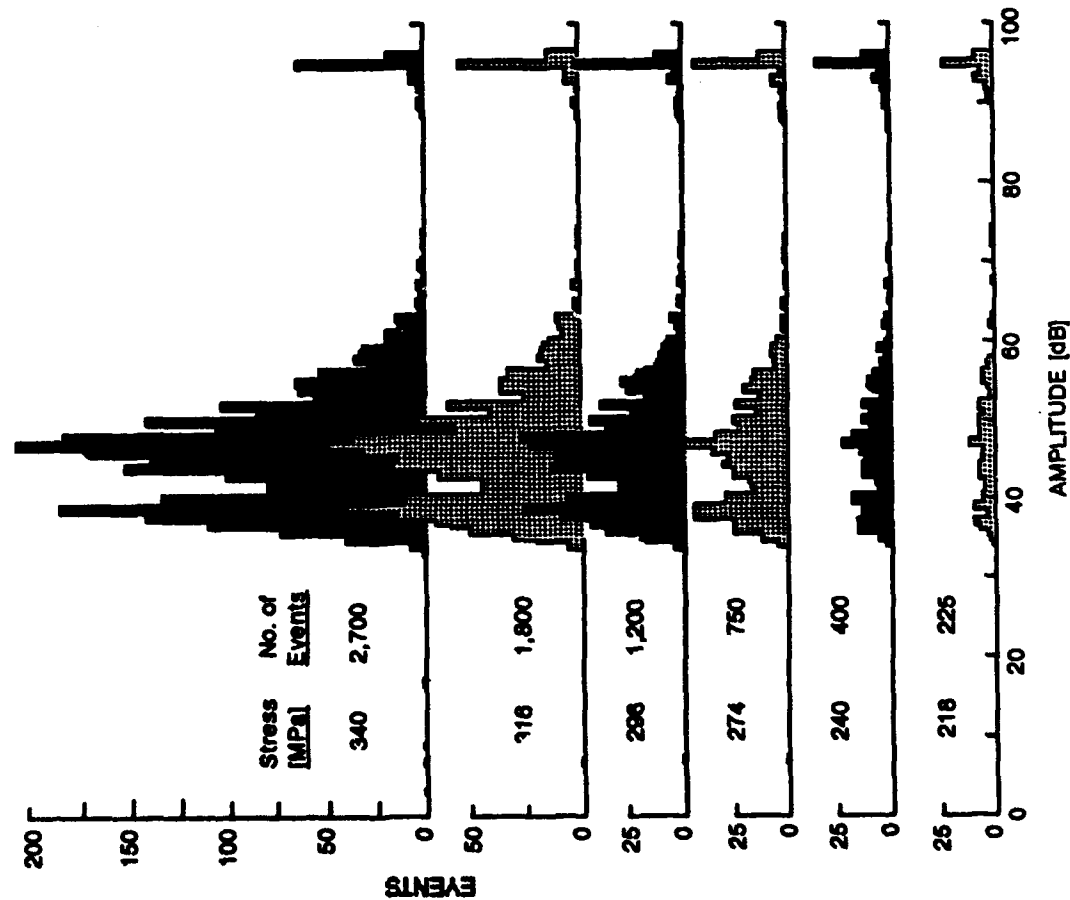


Figure 5.10. Concluded.

a. SPEC NO. 4 - B4/2
 LAY UP: $[90_2/0_{1/2}]_s$
 $\sigma_1 = 458 \text{ MPa}$
 $E = 18,213 \text{ EVENTS}$



b. SPEC NO. 4 - A8/1
 LAY UP: $[90_2/0_{1/2}]_s$
 $\sigma_1 = 400 \text{ MPa}$
 $E = 5,921 \text{ EVENTS}$

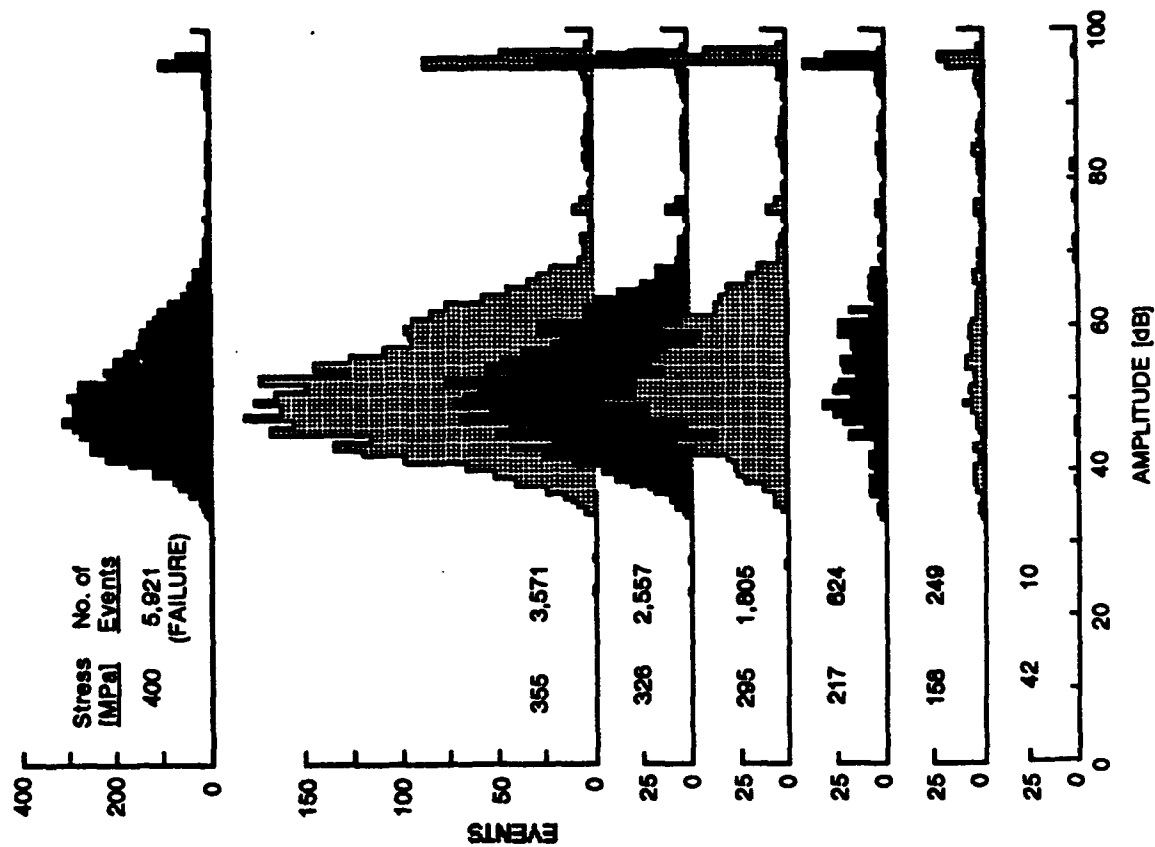
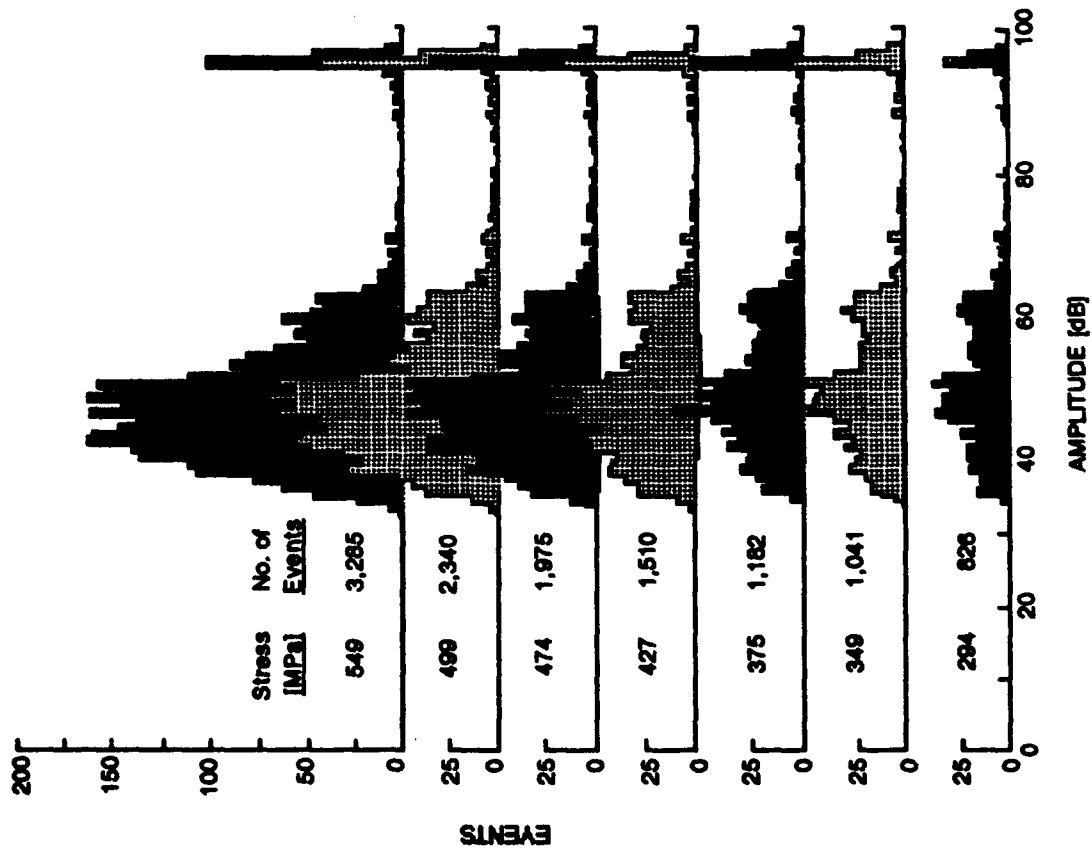


Figure 5.11. Amplitude distribution histograms of events (recorded with the D/E AE system) accumulated at different load ranges during quasi-static loading of selected

c. SPEC NO. 7-B5/1
 LAYUP: [90₂/0]_s
 $\sigma_1 = 732 \text{ MPa}$
 $E = 12,703 \text{ EVENTS}$



d. SPEC NO. 7-A5/1
 LAYUP: [90₂/0]_s
 $\sigma_1 = 731 \text{ MPa}$
 $E = 20,196 \text{ EVENTS}$

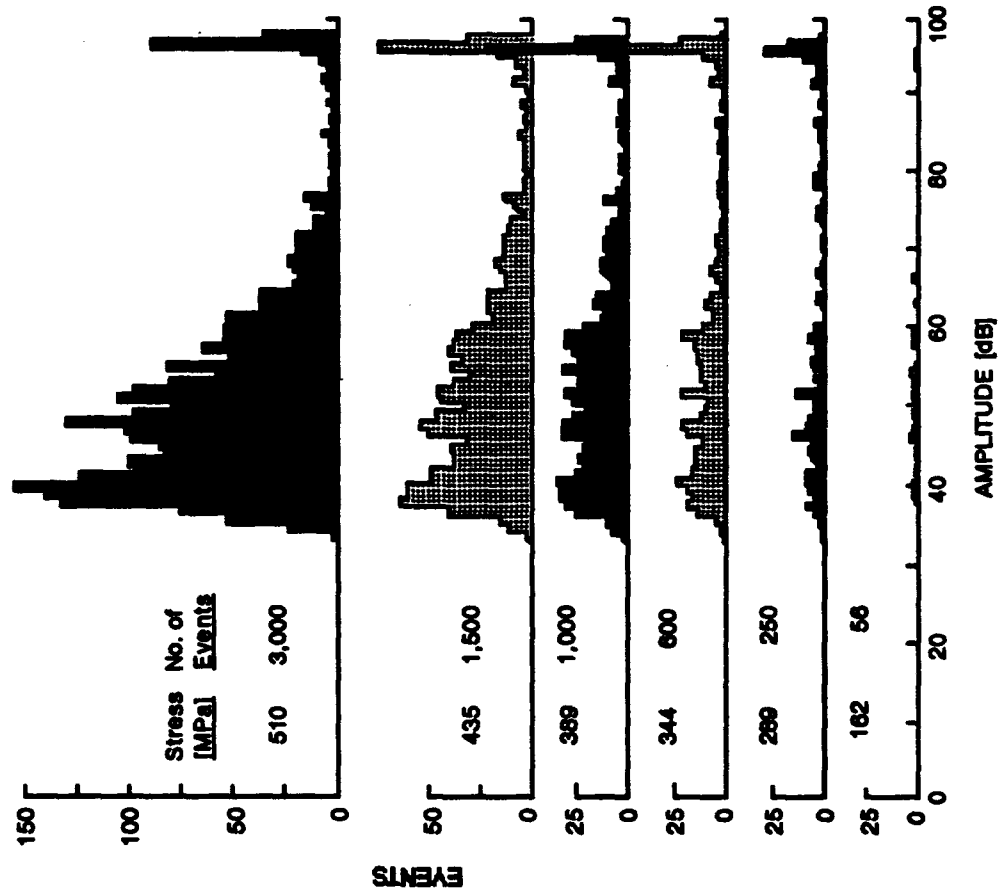
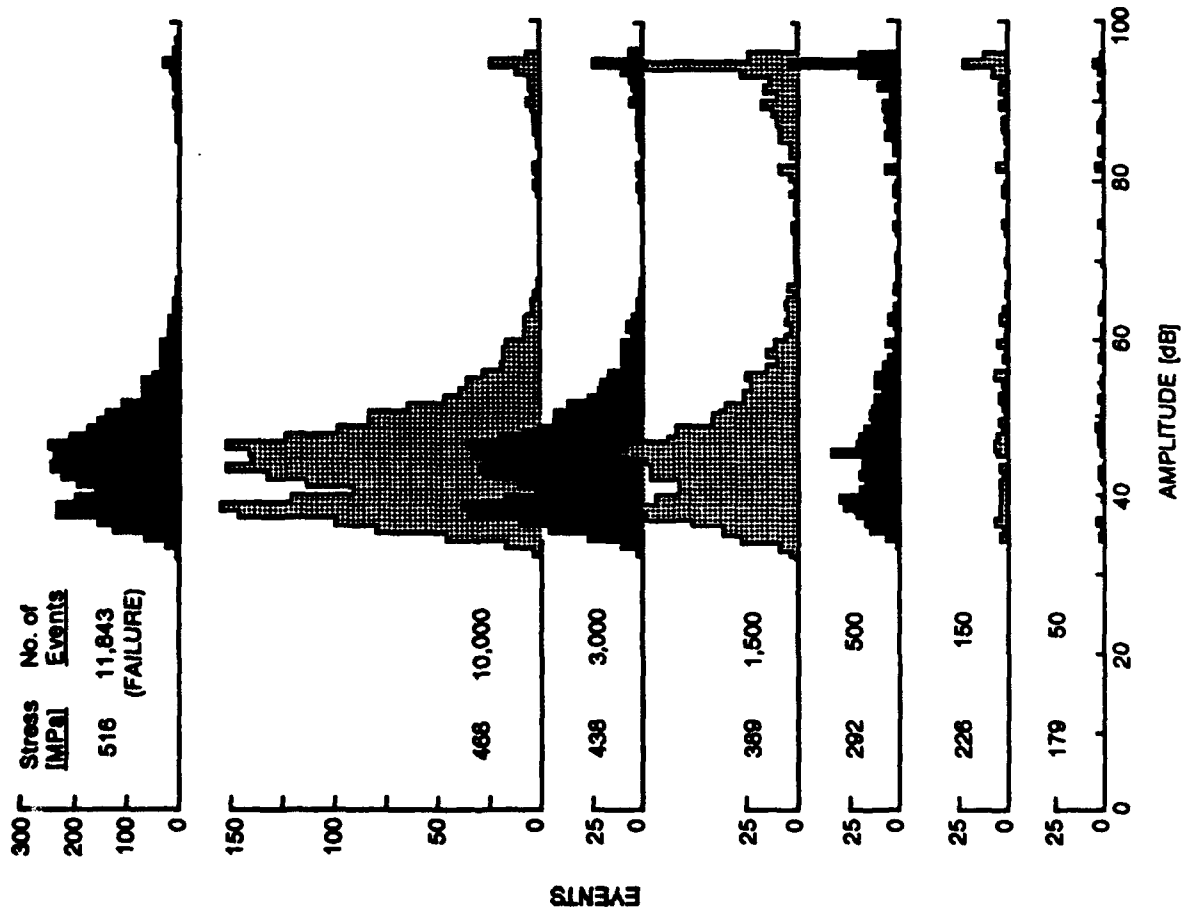


Figure 5.11. Continued.

e. SPEC NO. 6 - A4/2
 LAY UP: [90₂/0/90]_s
 σ_1 = 516 MPa
 E = 11,843 EVENTS



f. SPEC NO. 6 - A8/1
 LAY UP: [90₂/0/90]_s
 σ_1 = 489 MPa
 E = 7,565 EVENTS

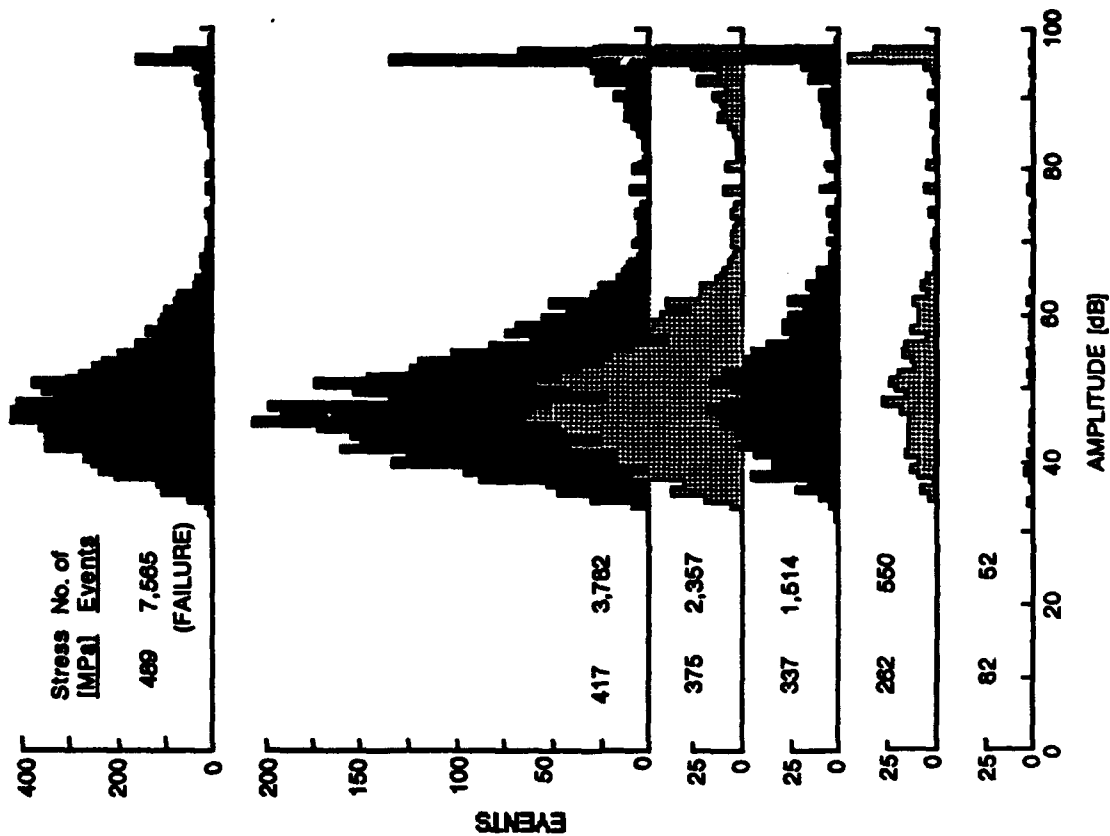


Figure 5.11. Concluded.

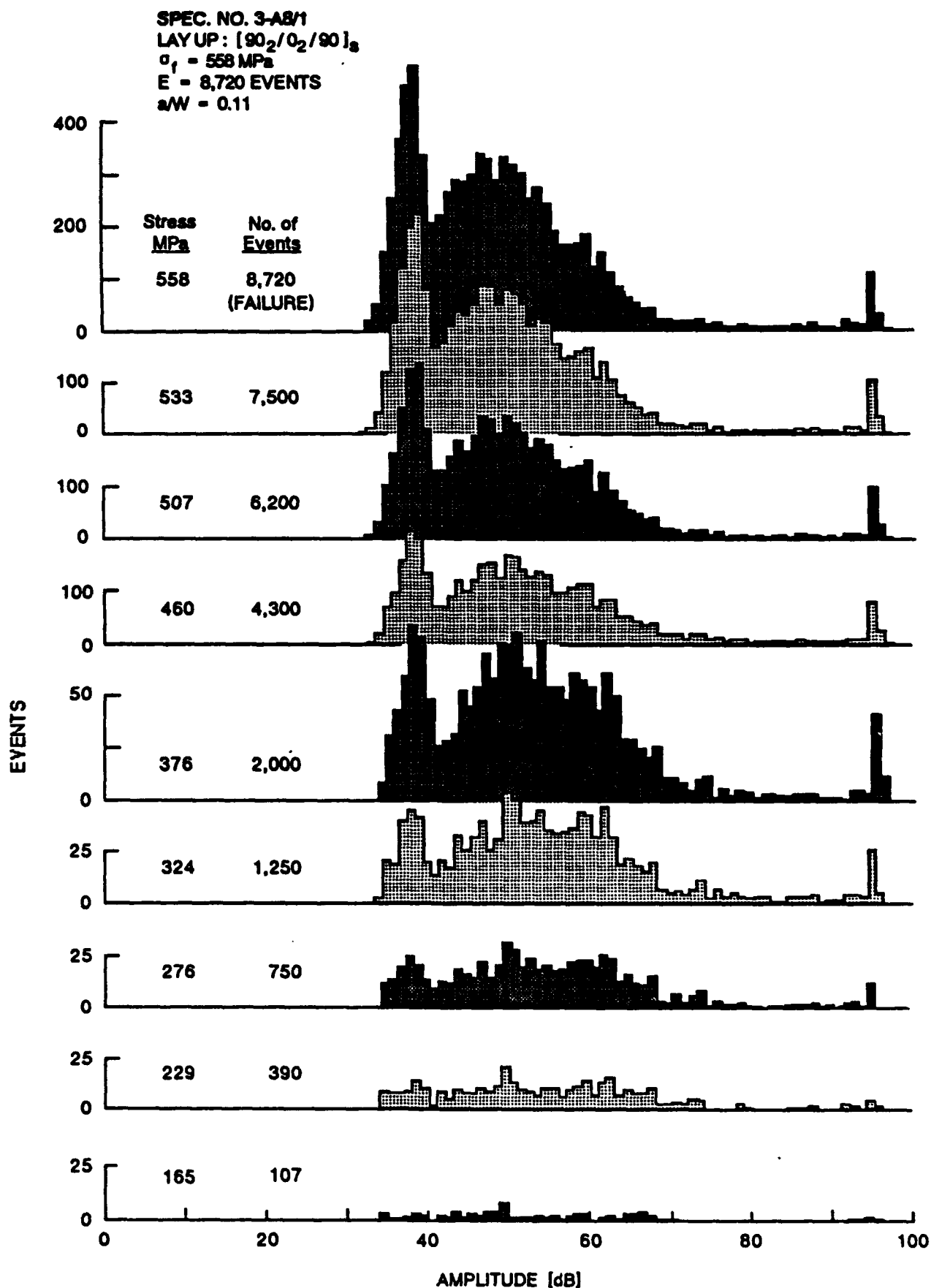
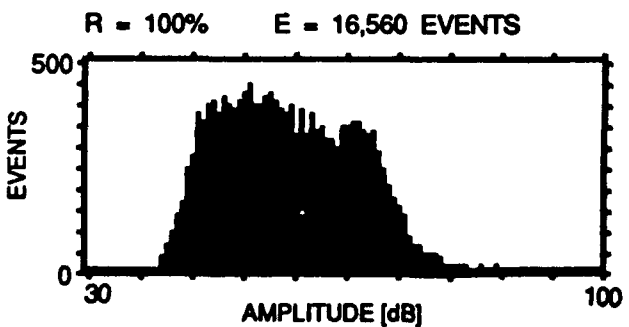
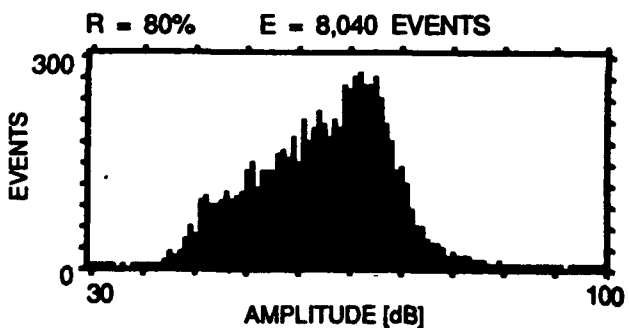
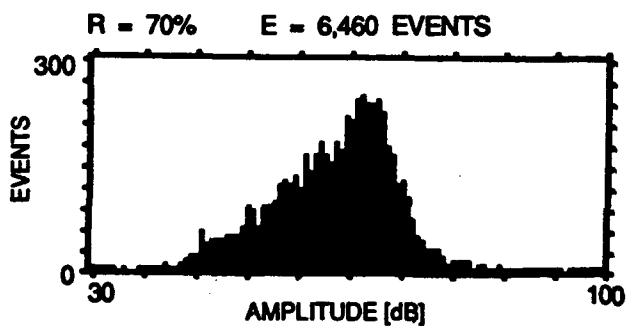
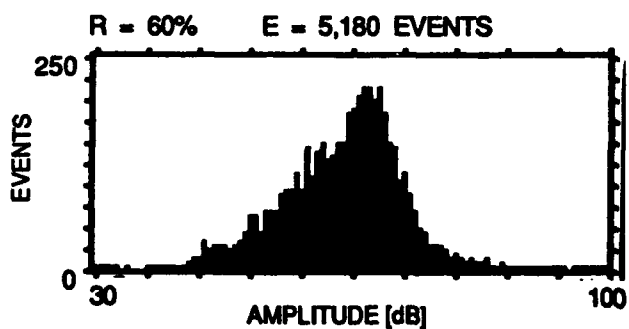
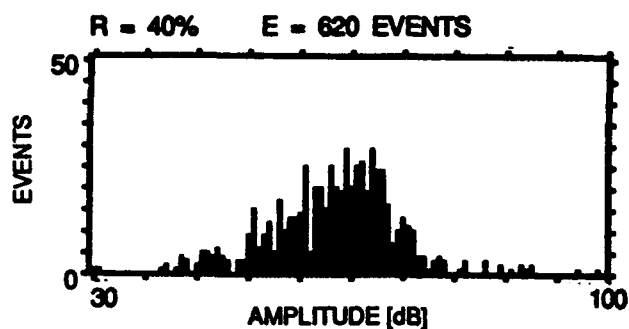


Figure 5.12. Amplitude distribution histograms of events (recorded with the D/E AE system) accumulated at different load ranges during quasi-static loading of the same double-edge notched $[90_2/0_2/90]_s$ graphite/epoxy laminate shown in Figure 5.9. 170

(a) SPEC. NO. 3-C9/2 $\sigma_1 = 1,822 \text{ MPa}$
LAY-UP: $[0_2/90_{1/2}]_s$ $E = 16,560 \text{ EVENTS}$



(b) SPEC. NO. 4-A8/1 $\sigma_1 = 400 \text{ MPa}$
LAY-UP: $[90_2/0_{1/2}]_s$ $E = 4,381 \text{ EVENTS}$

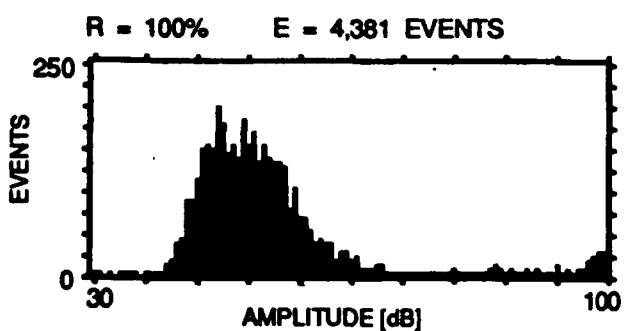
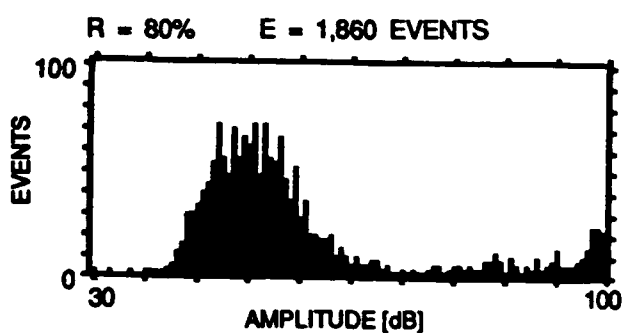
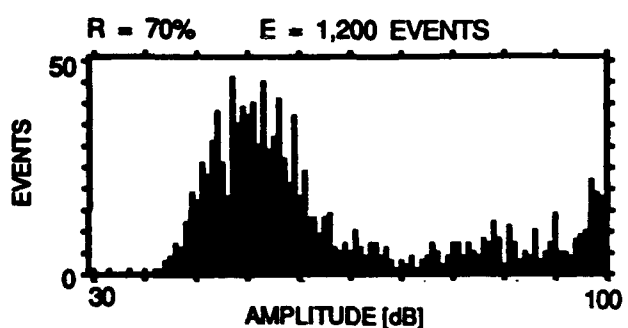
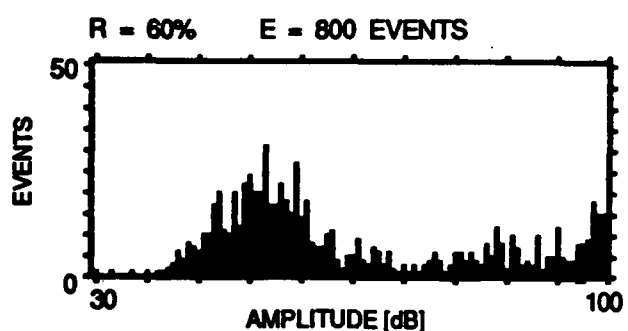
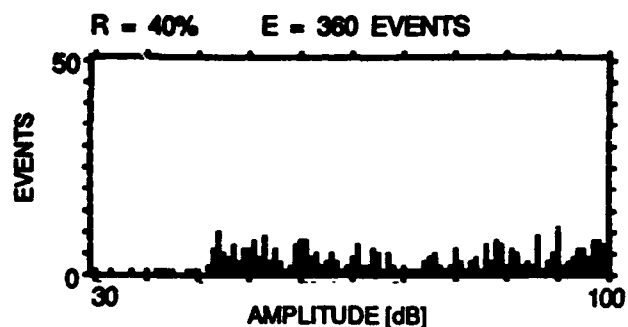
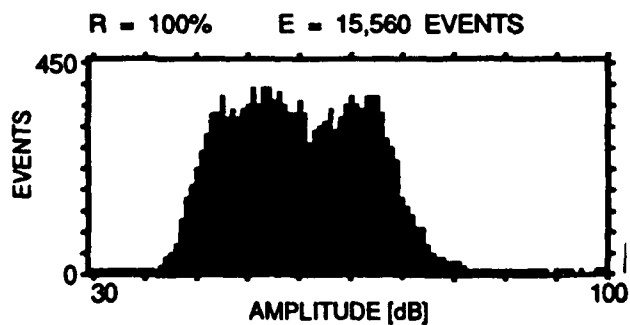
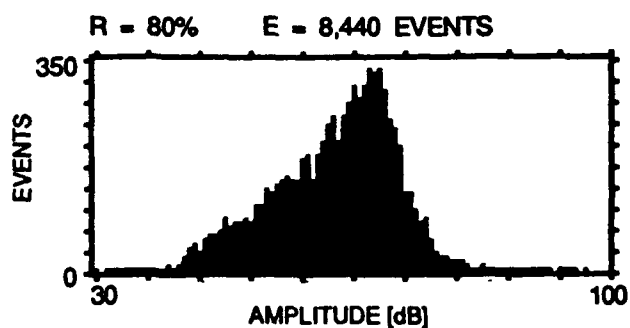
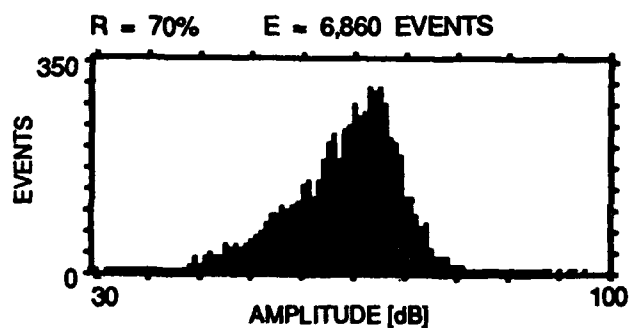
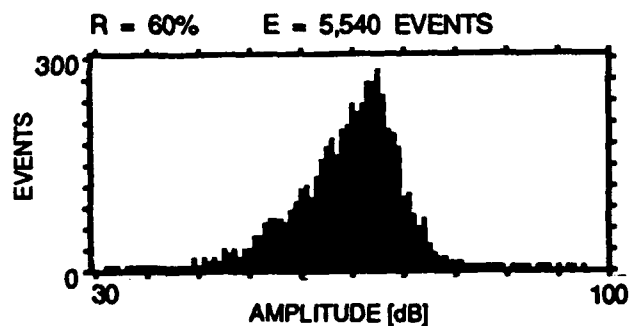
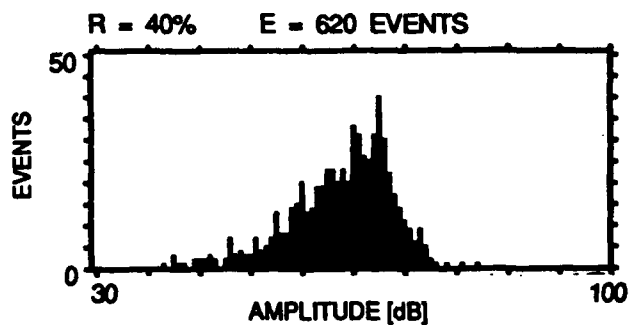


Figure 5.13. Amplitude distribution histograms of events (recorded with the PAC AE system) accumulated at different load ranges during quasi-static loading to failure of 12 different cross-ply graphite/epoxy laminates. Each Figure shows two laminates having reversed stacking sequence.

(c) SPEC. NO. 4-C2/2 $\sigma_f = 1,664$ MPa
LAY-UP: $[0_2/90/0]_s$ E = 15,560 EVENTS



(d) SPEC. NO. 6-A8/1 $\sigma_f = 489$ MPa
LAY-UP: $[90_2/0/90]_s$ E = 4,957 EVENTS

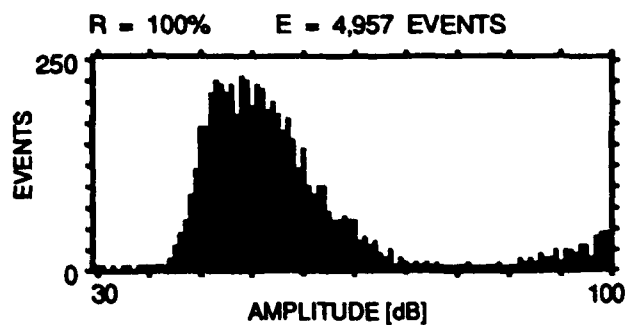
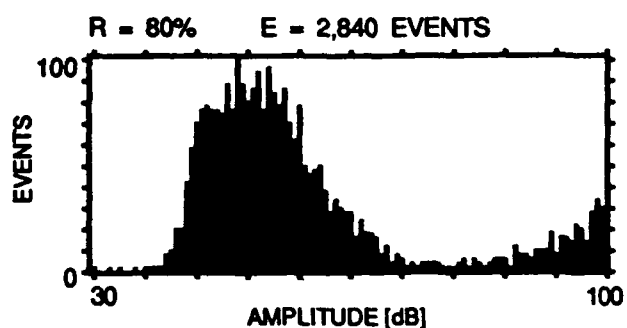
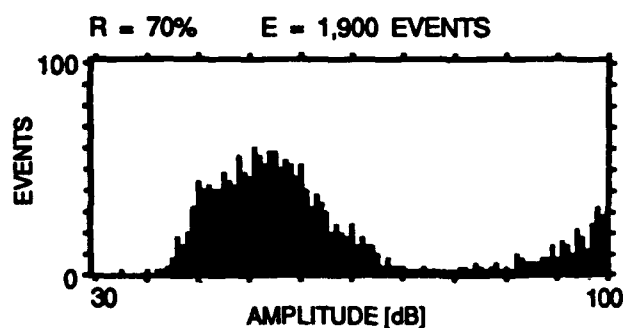
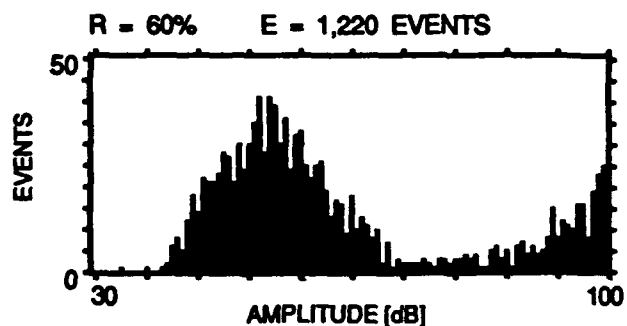
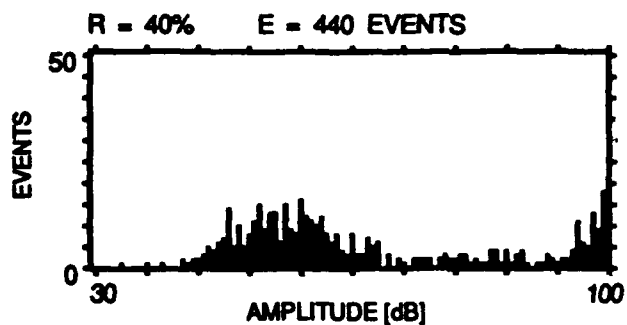
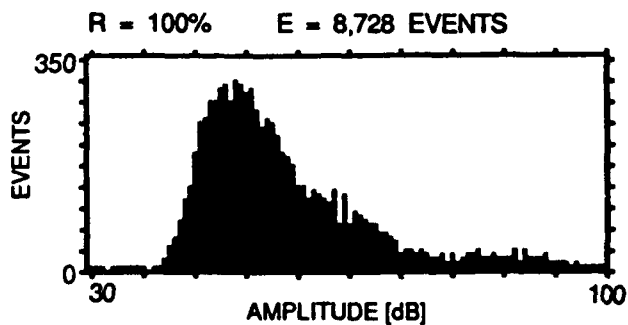
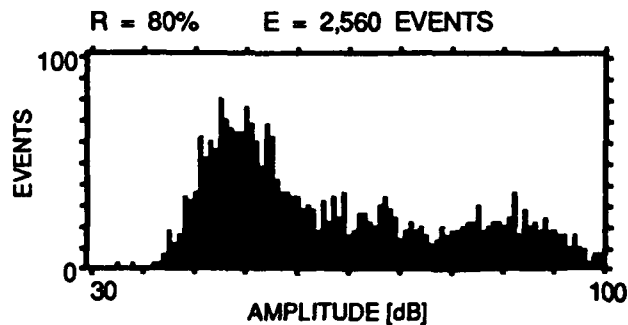
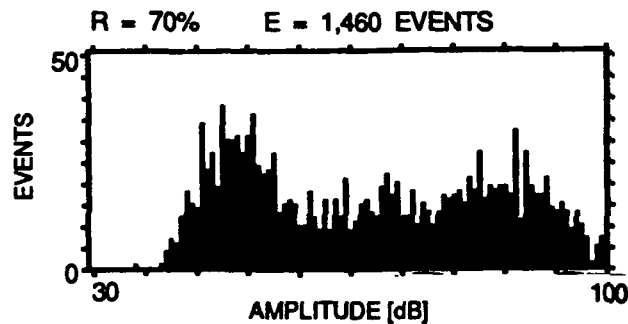
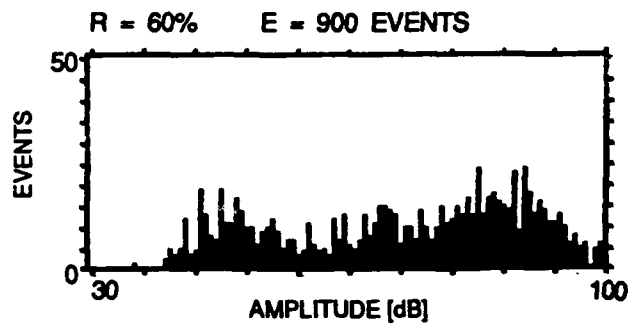
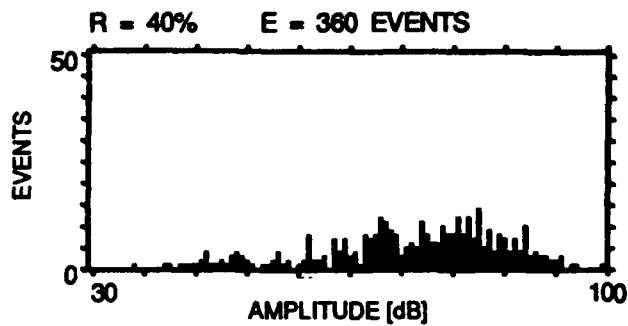


Figure 5.13. Continued.

(e) SPEC. NO. 5-D4/2 $\sigma_f = 1,425$ MPa
LAY-UP: $[0_2/90_2/0]_8$ E = 8,728 EVENTS



(f) SPEC. NO. 3-A10/2 $\sigma_f = 989$ MPa
LAY-UP: $[90_2/0_2/90]_8$ E = 12,070 EVENTS

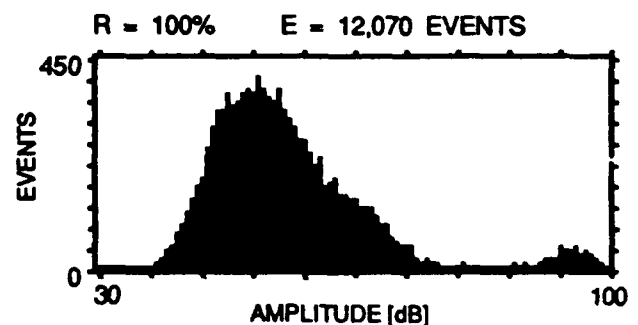
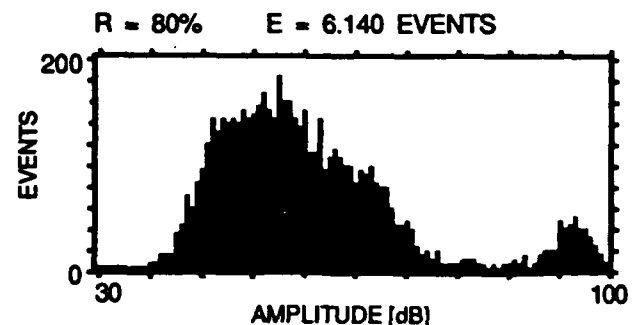
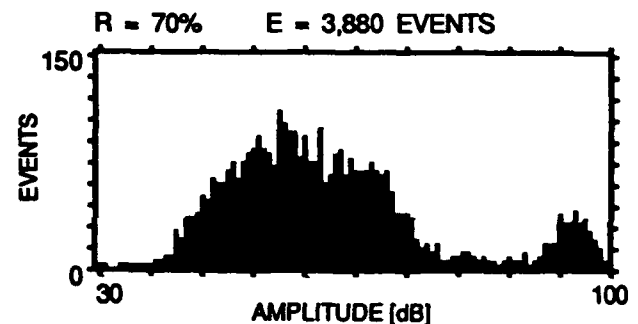
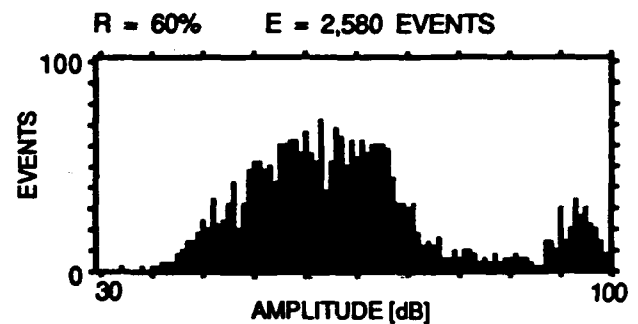
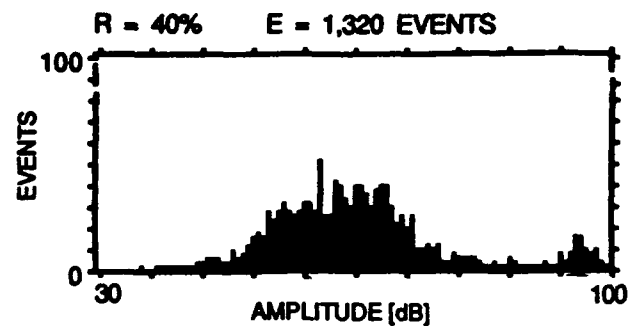


Figure 5.13. Continued.

(g) SPEC. NO. 6-C7/1 $\sigma_f = 1,327 \text{ MPa}$ (h) SPEC. NO. 5-B8/1 $\sigma_f = 797 \text{ MPa}$
 LAY-UP: $[0/90/0/90]_{1/2}$ E = 14,841 EVENTS LAY-UP: $[90/0/90/0]_{1/2}$ E = 12,871 EVENTS

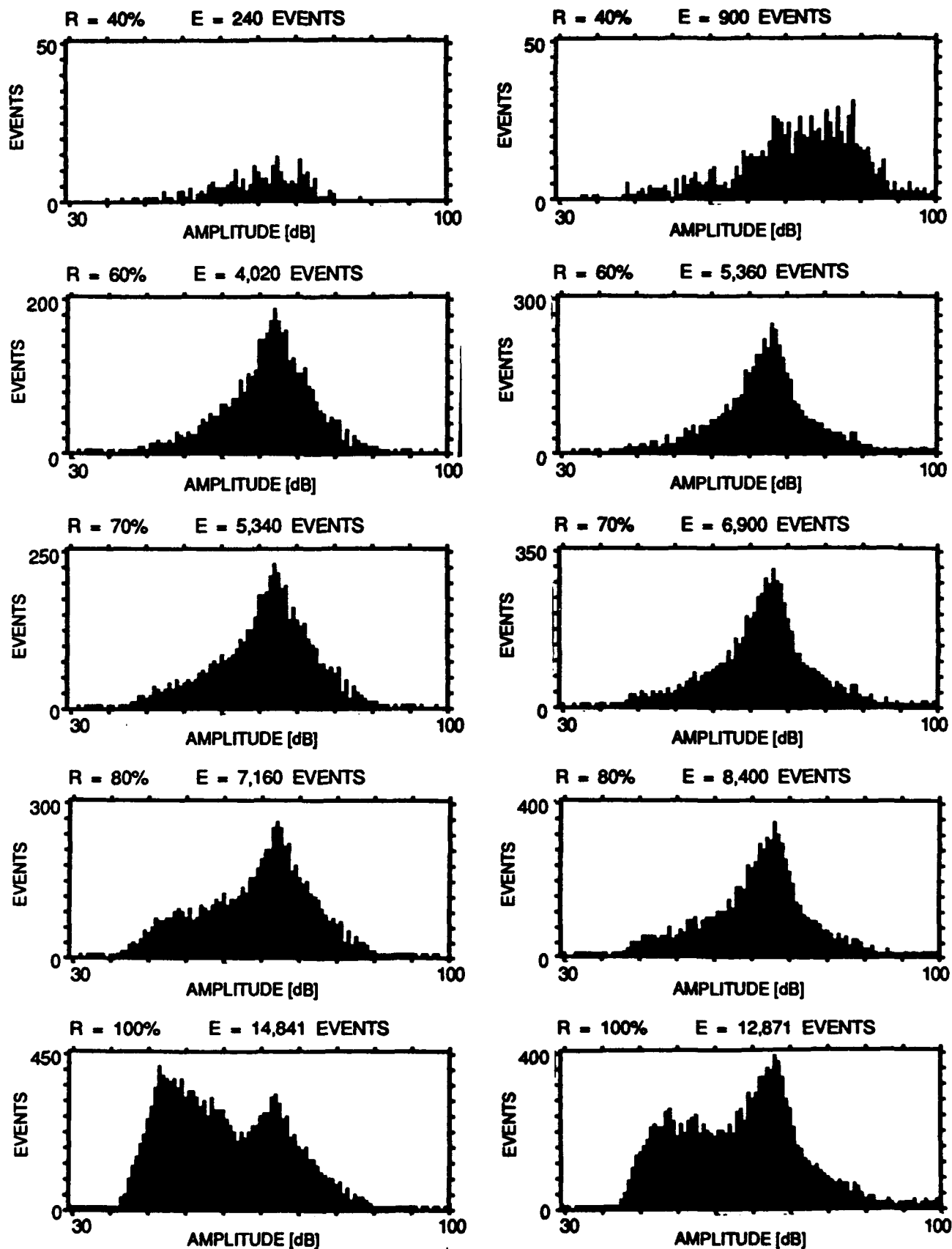
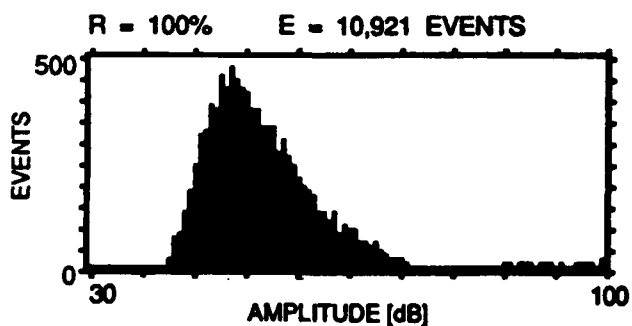
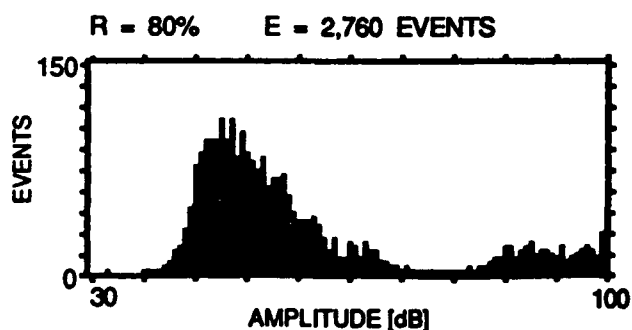
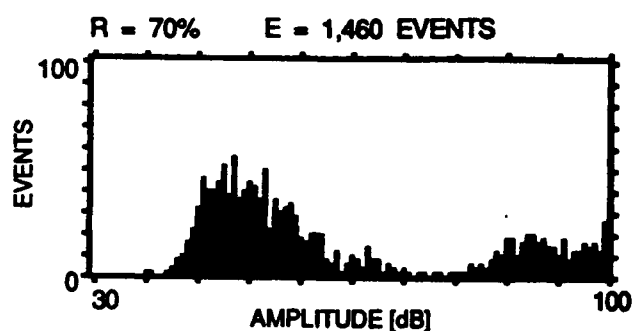
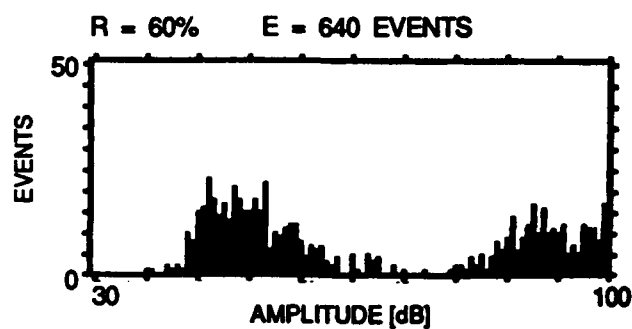
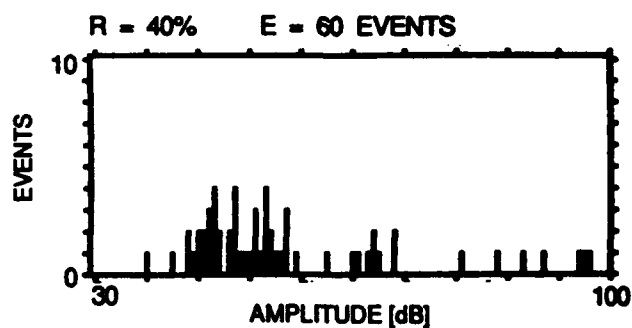


Figure 5.13. Continued.

(I) SPEC. NO. 7-C7/1 $\sigma_f = 1,096 \text{ MPa}$
LAY-UP: $[0_2/90/0]_s$ E = 10,921 EVENTS



(II) SPEC. NO. 8-B8/1 $\sigma_f = 1,180 \text{ MPa}$
LAY-UP: $[90_2/0/90]_s$ E = 7,182 EVENTS

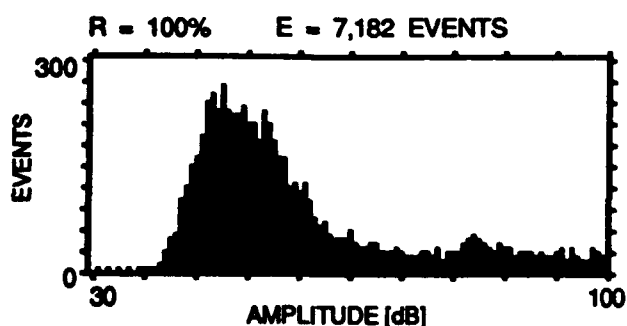
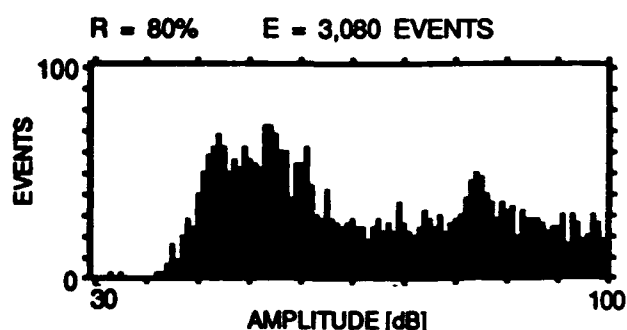
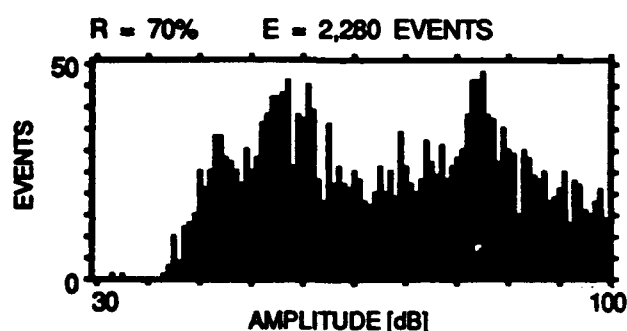
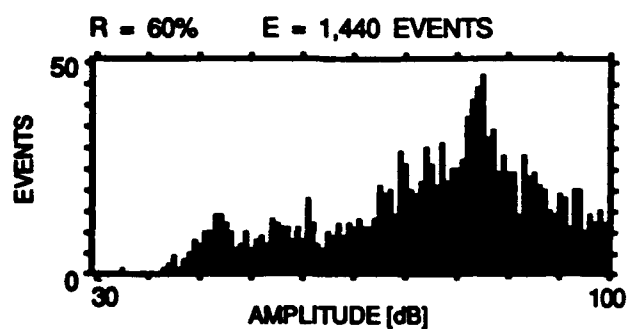
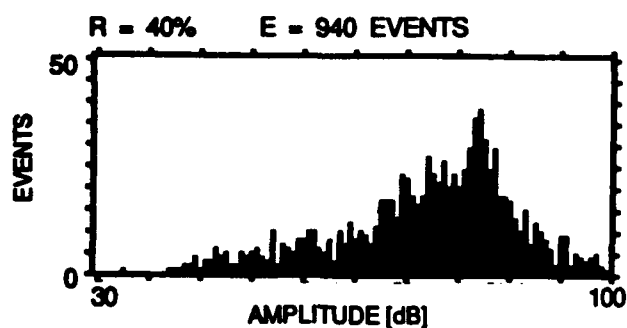


Figure 5.13. Continued.

(k) SPEC. NO. 8-C10/2 $\sigma_f = 1,537 \text{ MPa}$
 LAY-UP: $[0_2/90]_s$ $E = 13,035 \text{ EVENTS}$

(l) SPEC. NO. 7-B5/1 $\sigma_f = 732 \text{ MPa}$
 LAY-UP: $[90_2/0]_s$ $E = 19,721 \text{ EVENTS}$

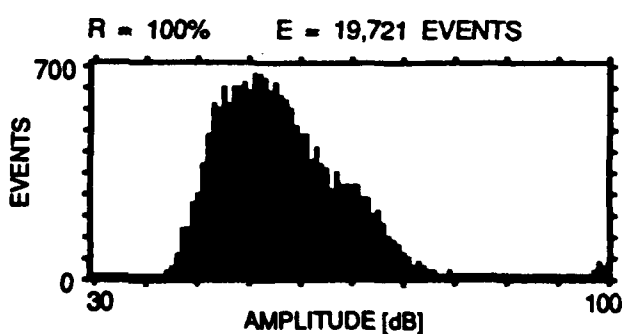
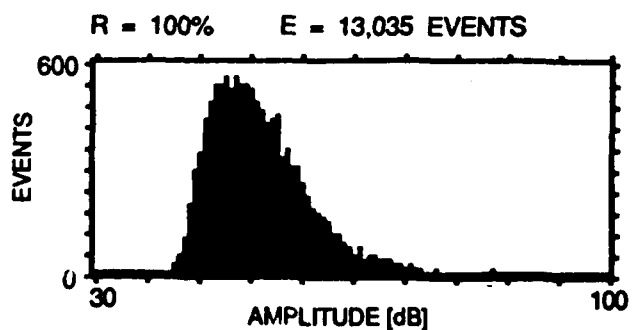
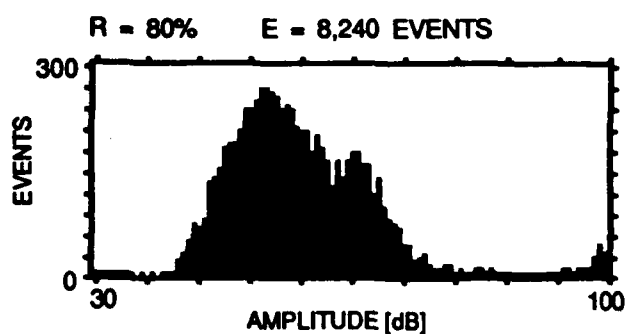
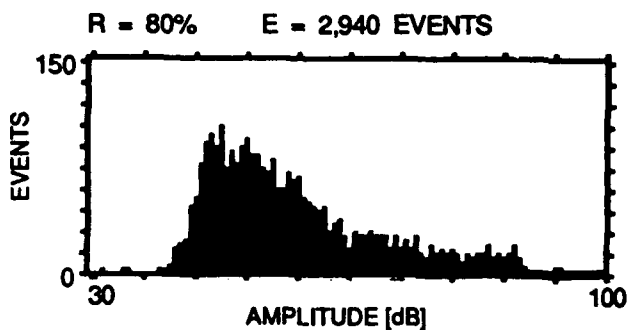
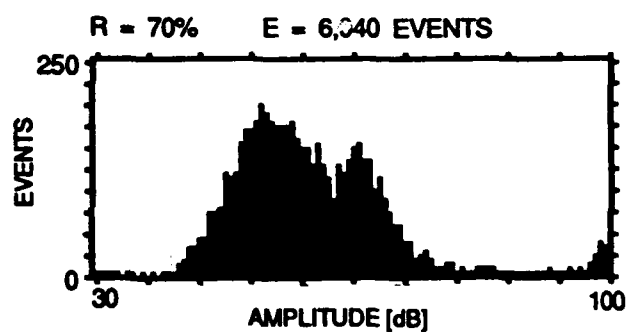
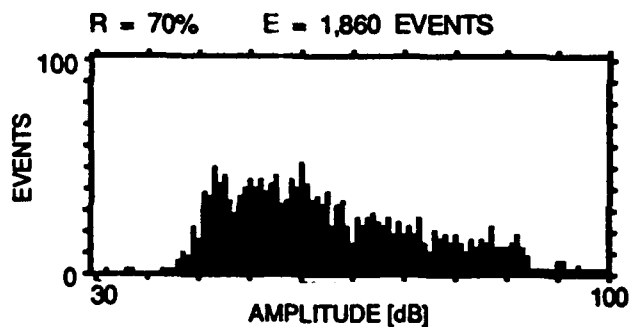
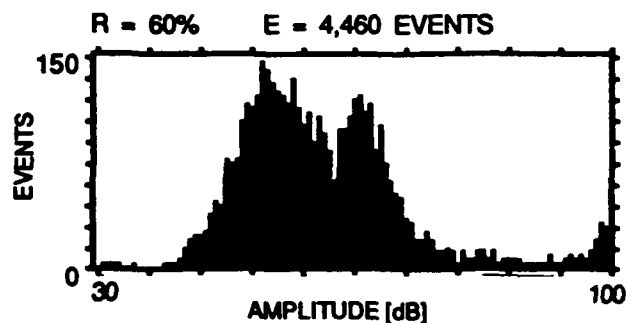
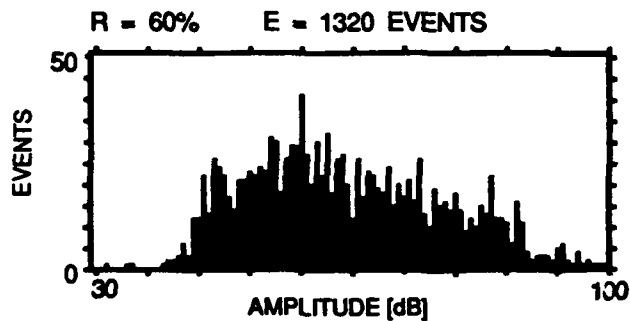
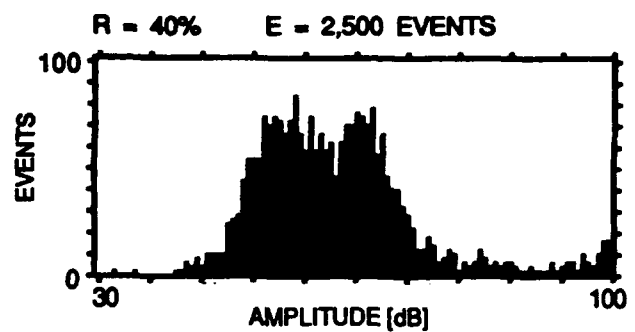
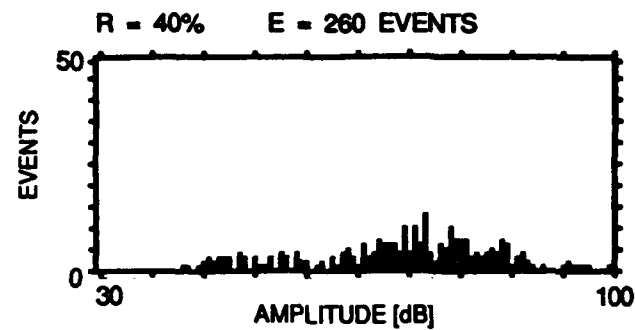


Figure 5.13. Concluded.

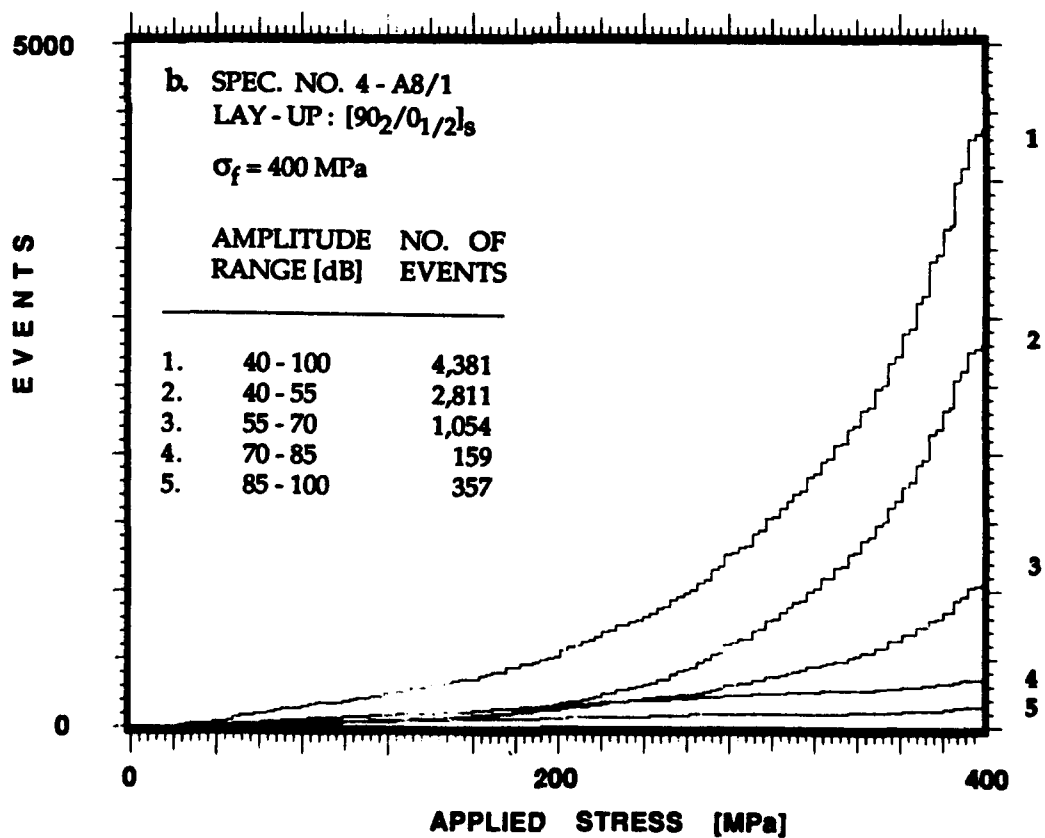
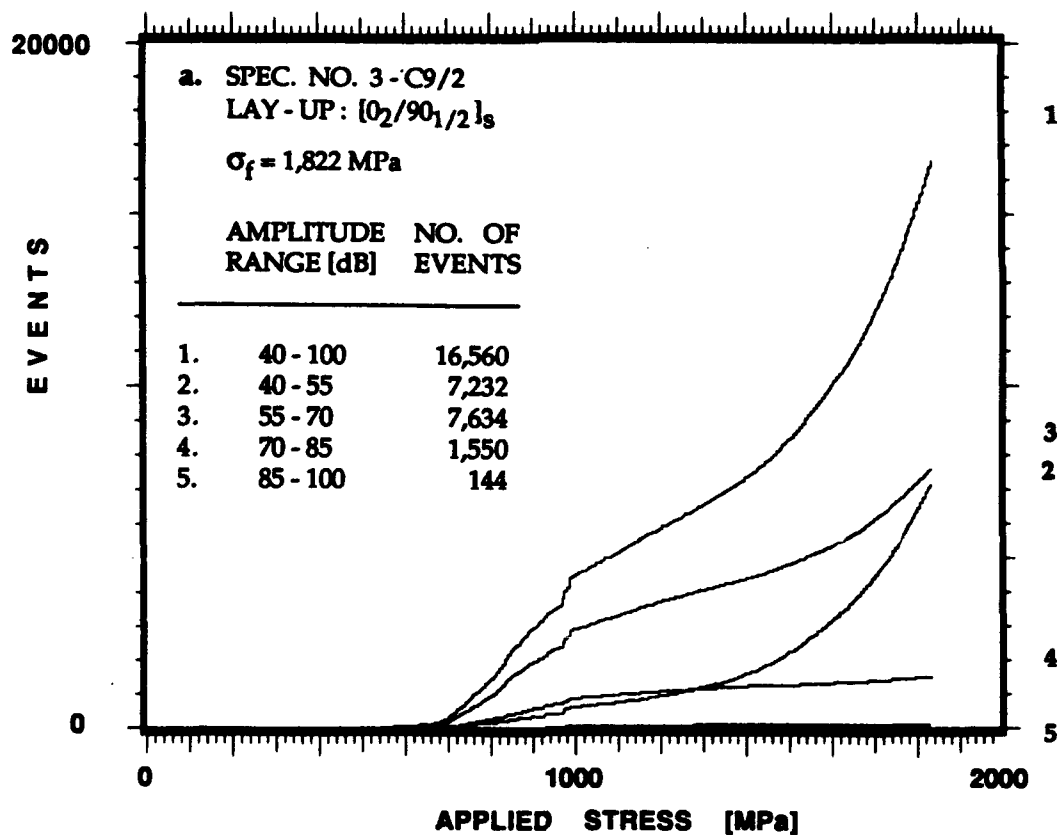


Figure 5.14. Events of different amplitude ranges accumulated (recorded with the PAC AE system) during quasi-static loading to failure as a function of far-field applied stress for 12 different cross-ply graphite/epoxy laminates. Each Figure shows two laminates having reversed stacking sequence.

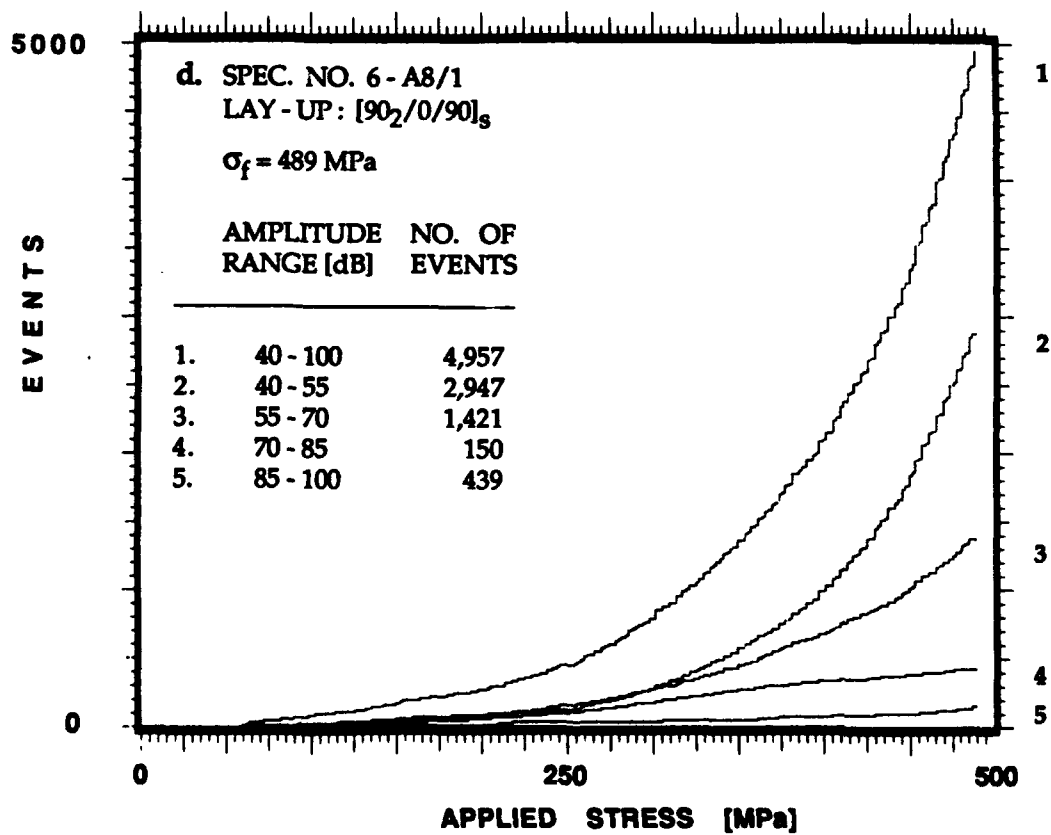
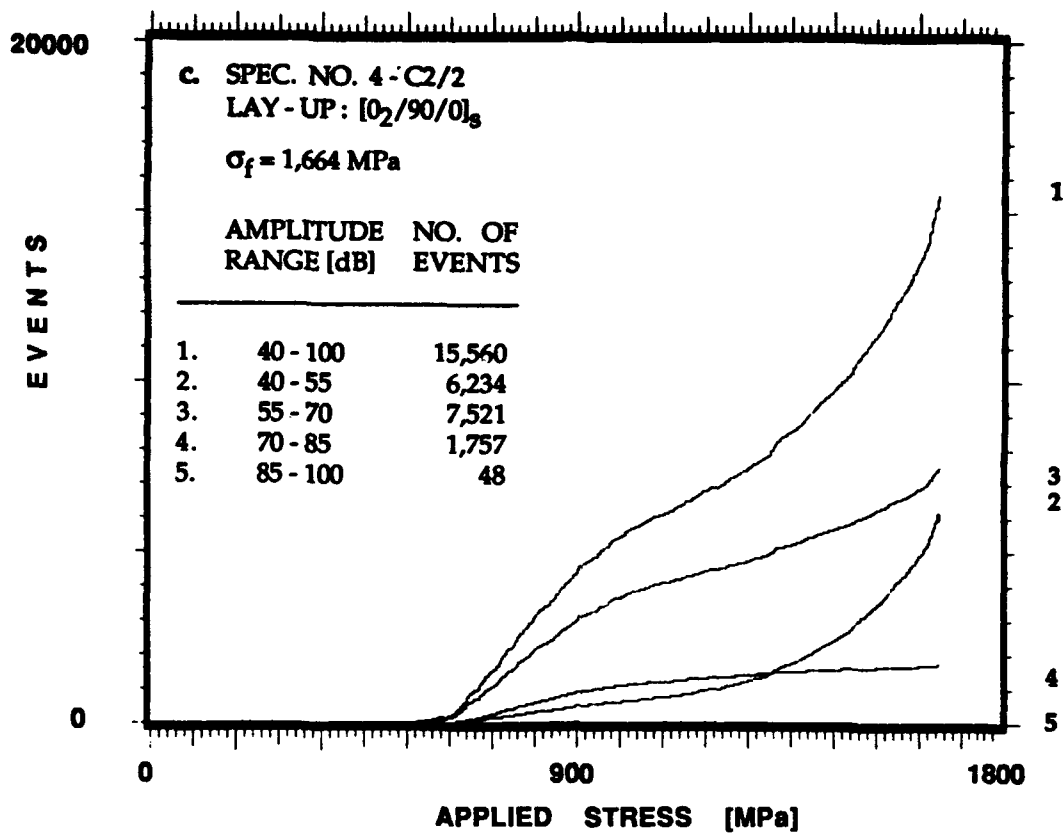


Figure 5.14. Continued.

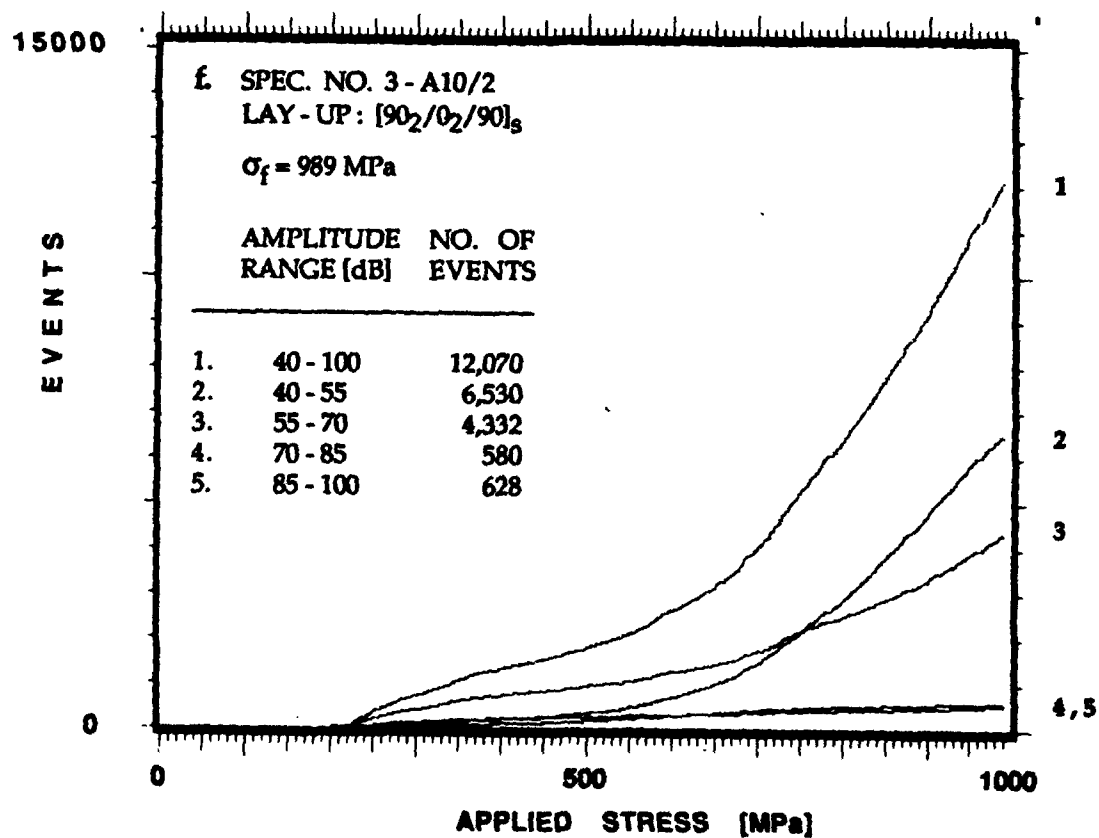
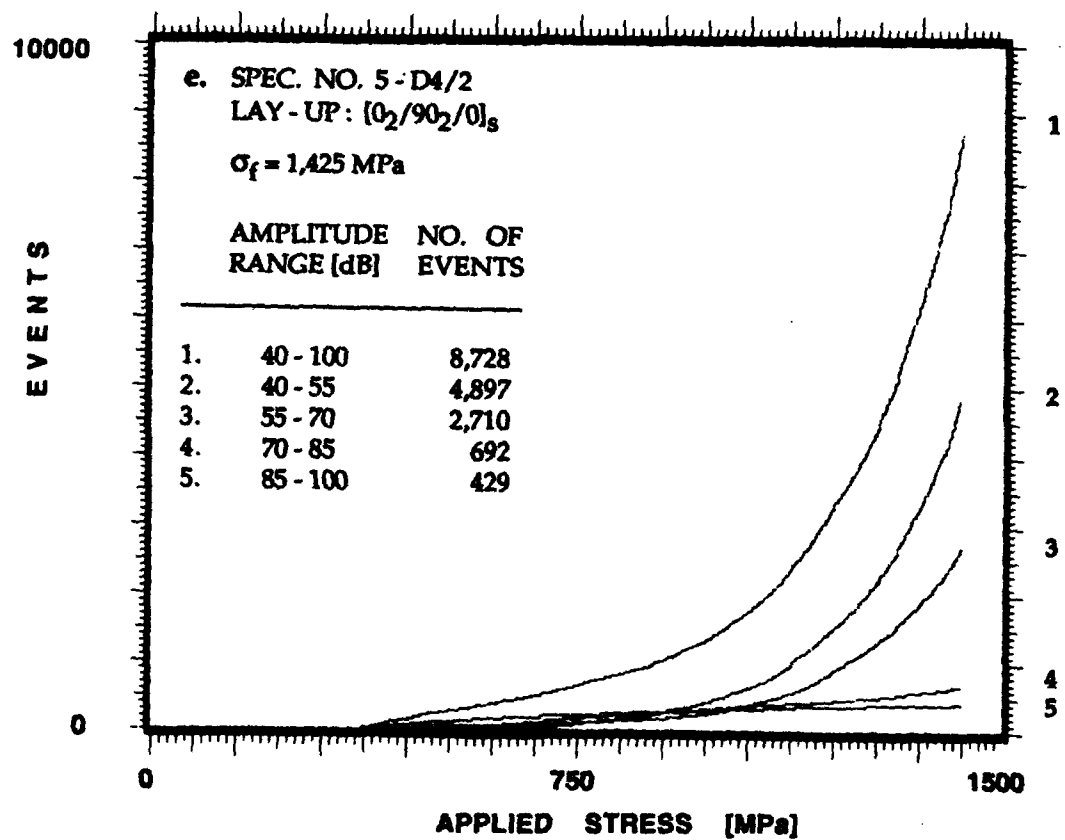


Figure 5.14. Continued.

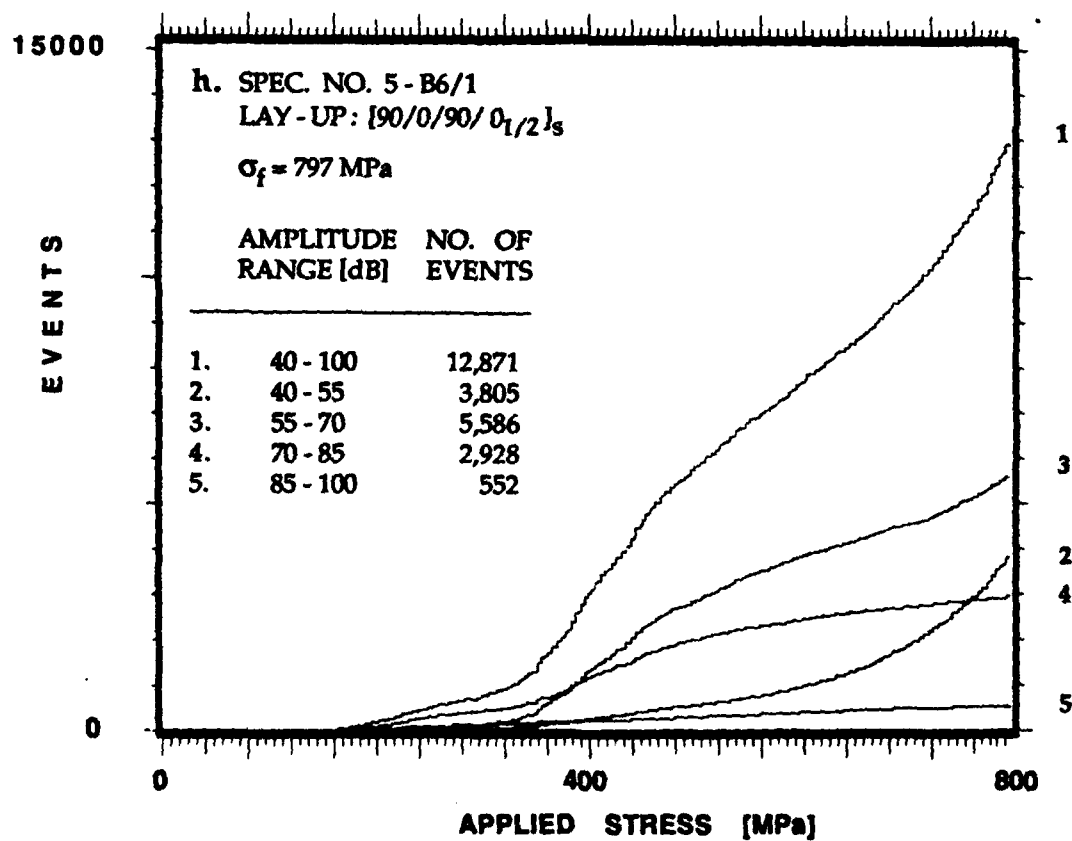
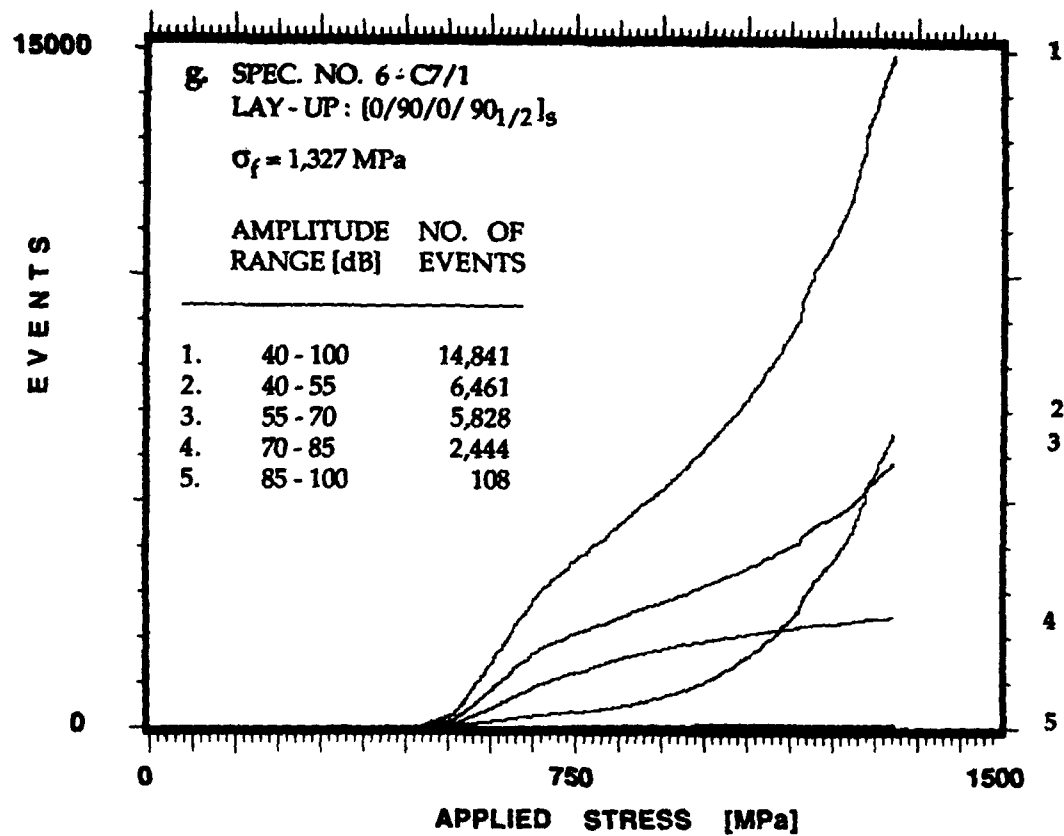


Figure 5.14. Continued.

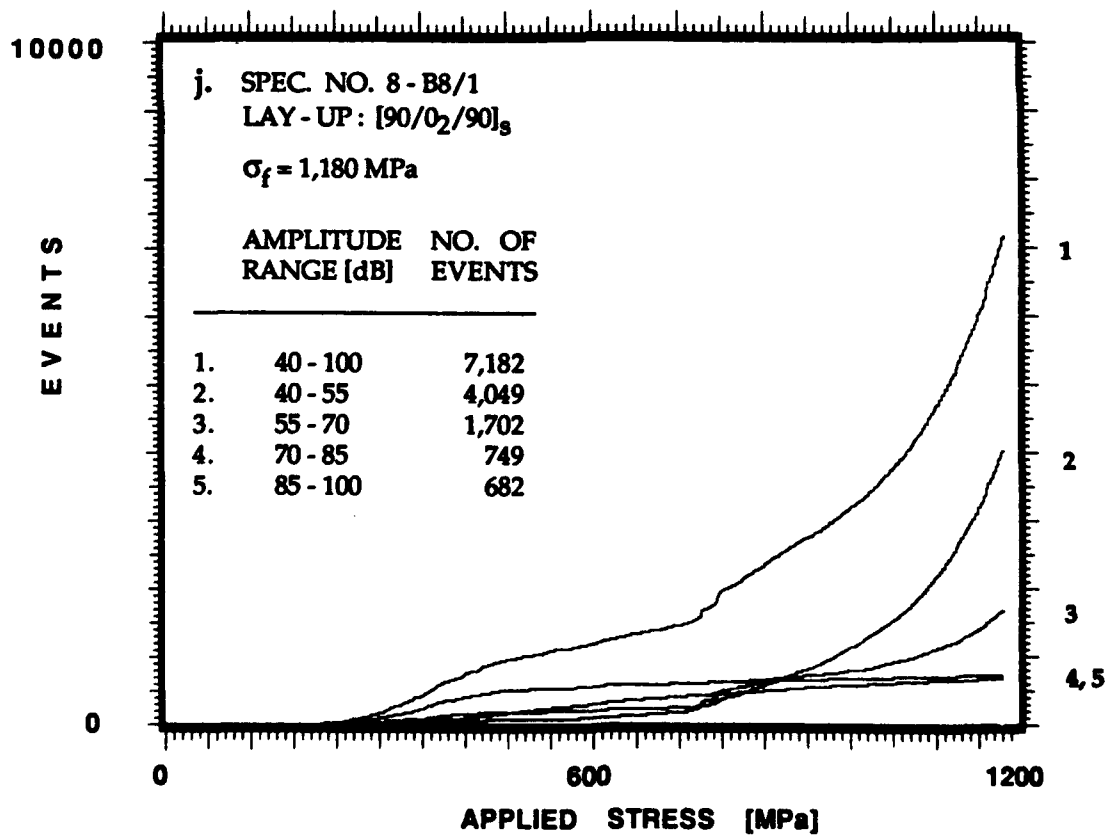
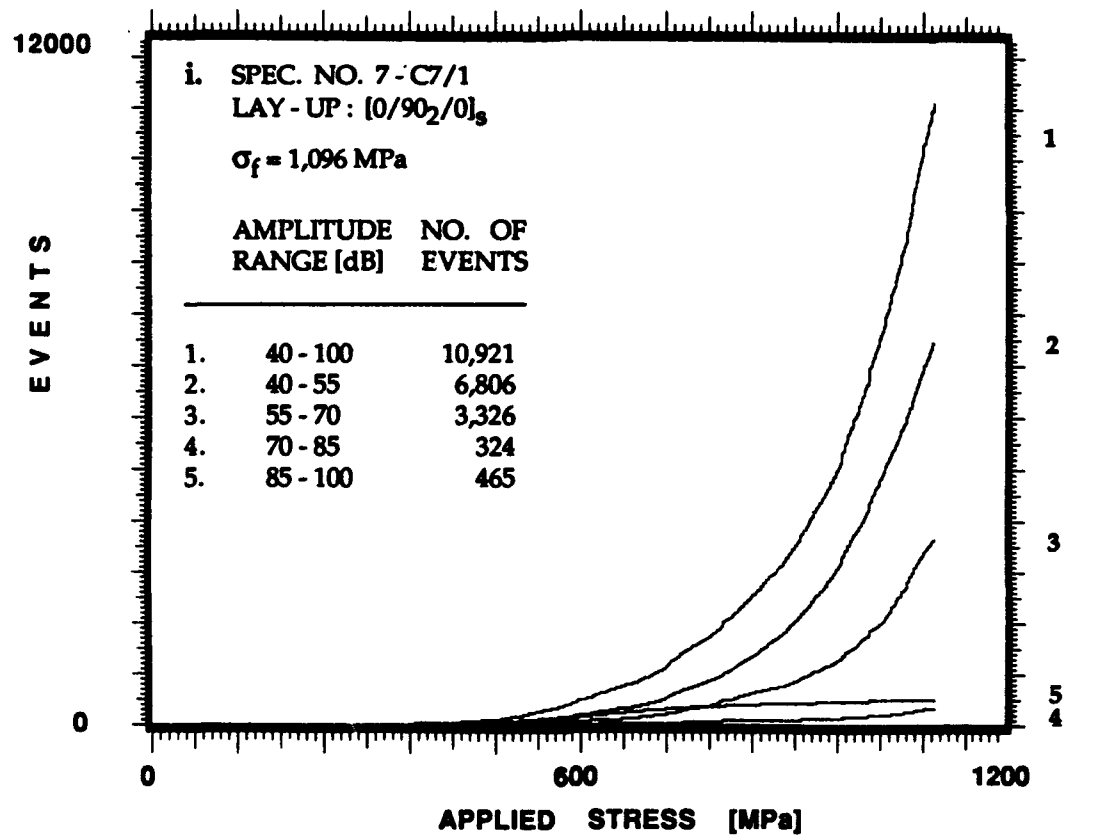


Figure 5.14. Continued.

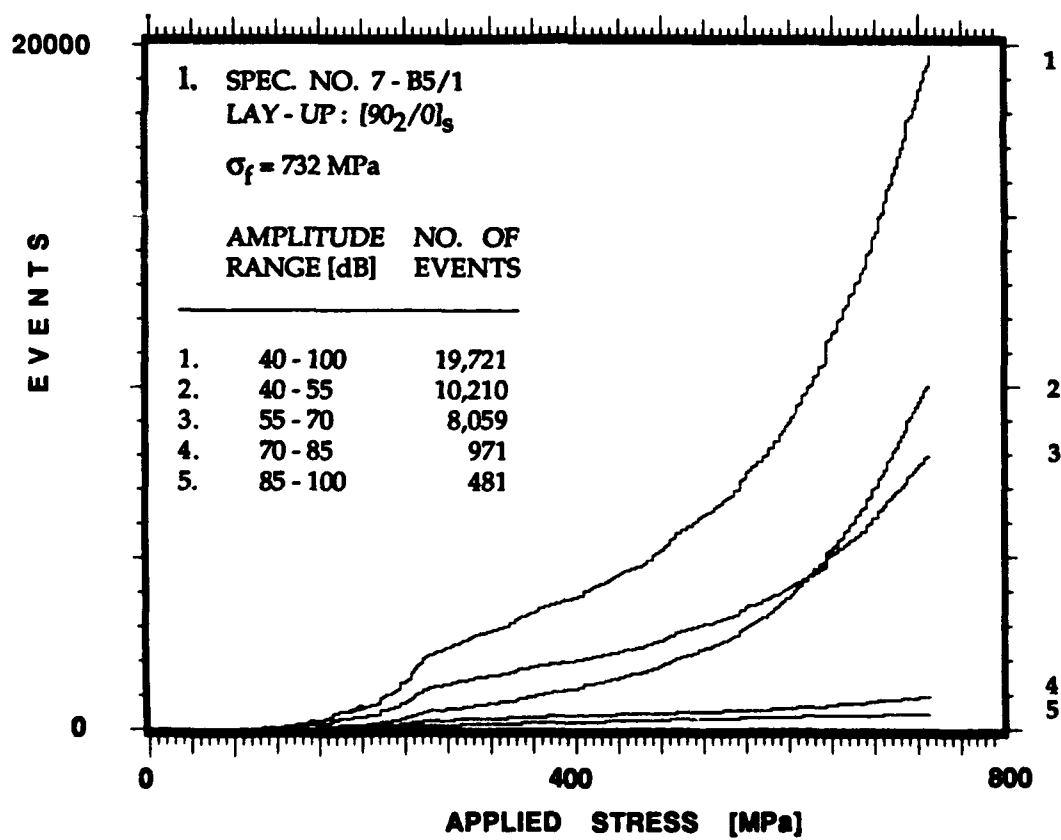
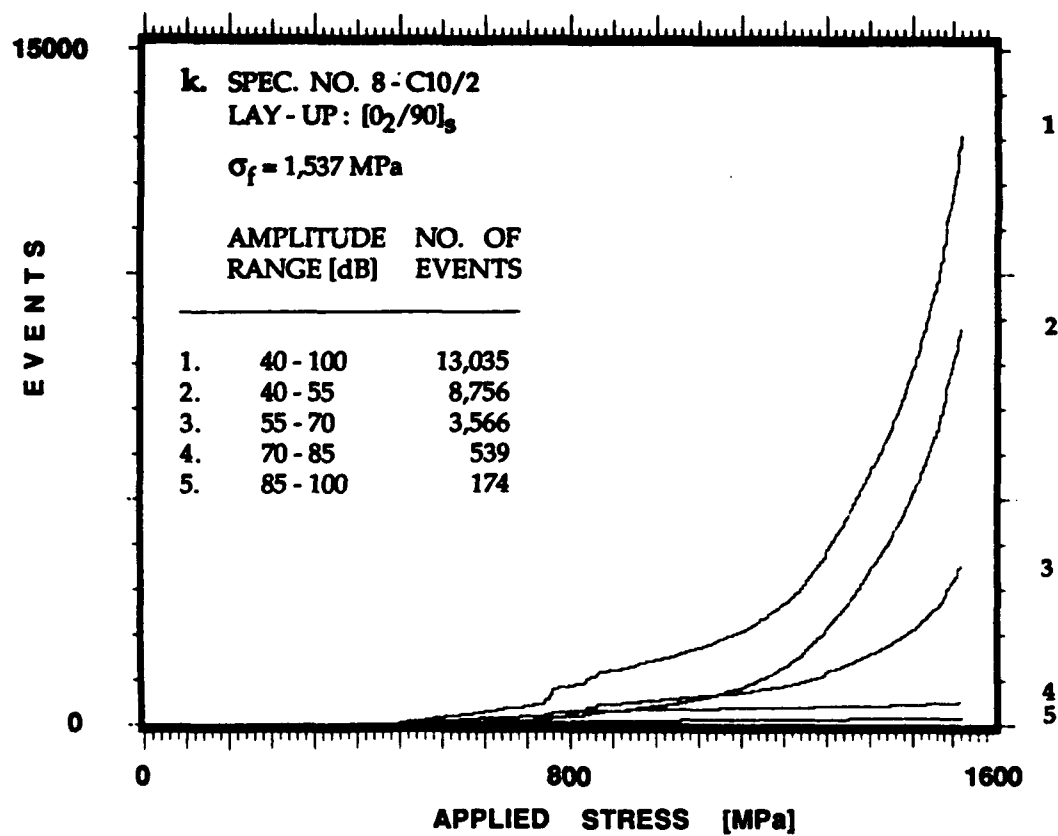


Figure 5.14. Concluded.

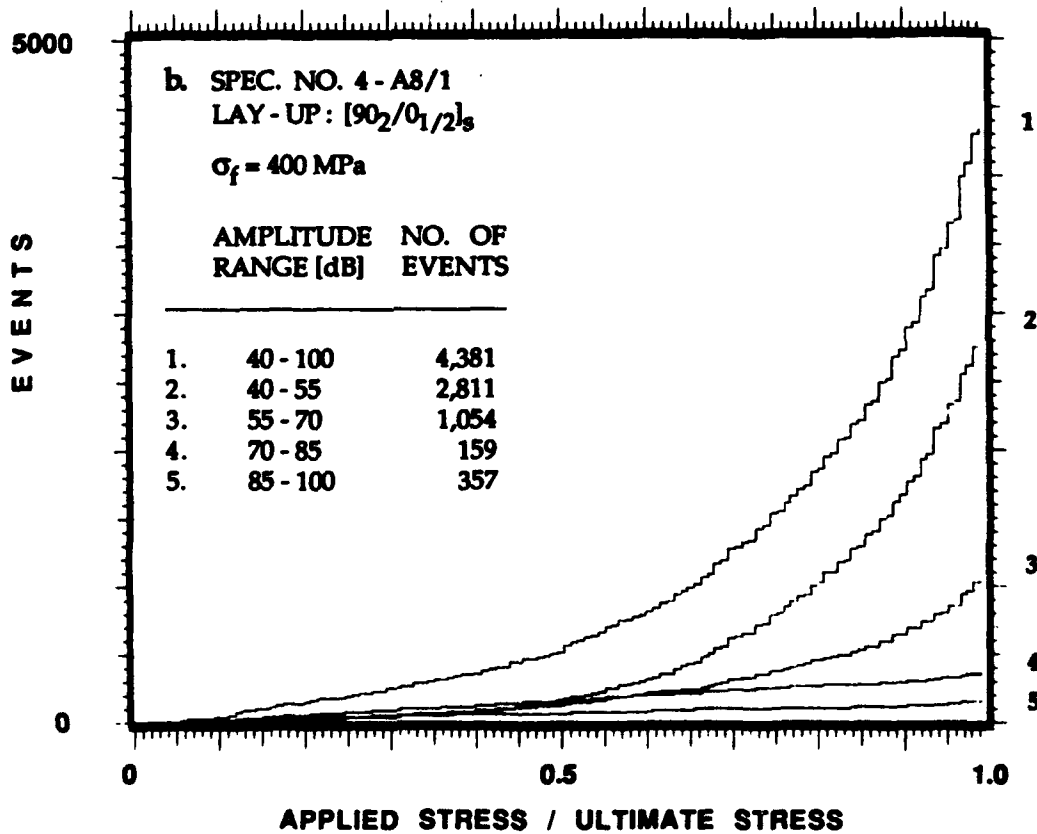
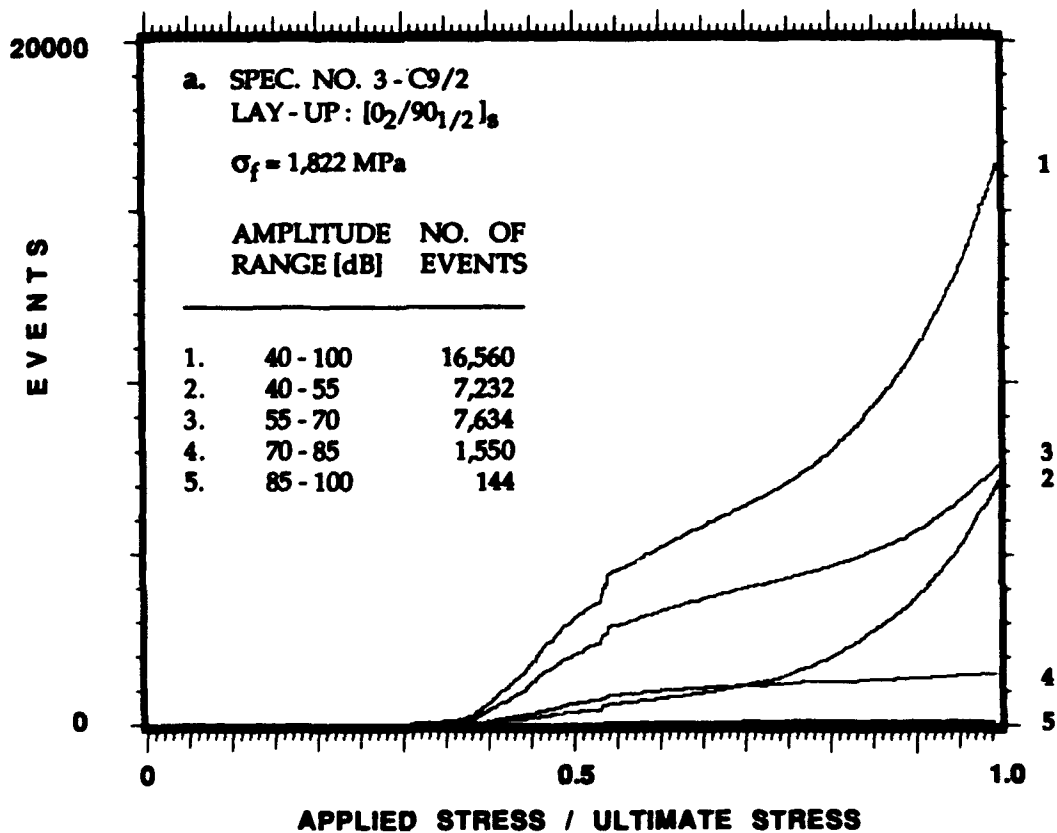


Figure 5.15. Events of different amplitude ranges (recorded with the PAC AE system) accumulated during quasi-static loading to failure as a function of far-field applied stress-to-ultimate stress ratio for 12 different cross-ply graphite/epoxy laminates. Each Figure shows two laminates having reversed stacking sequence.

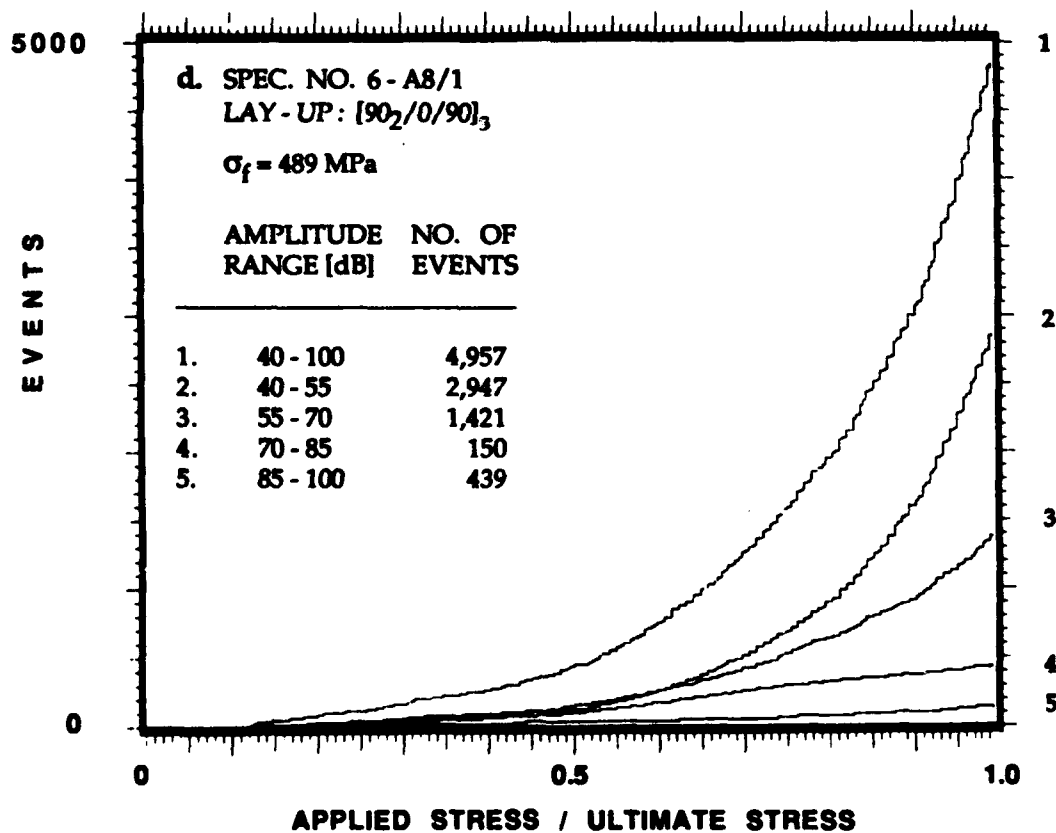
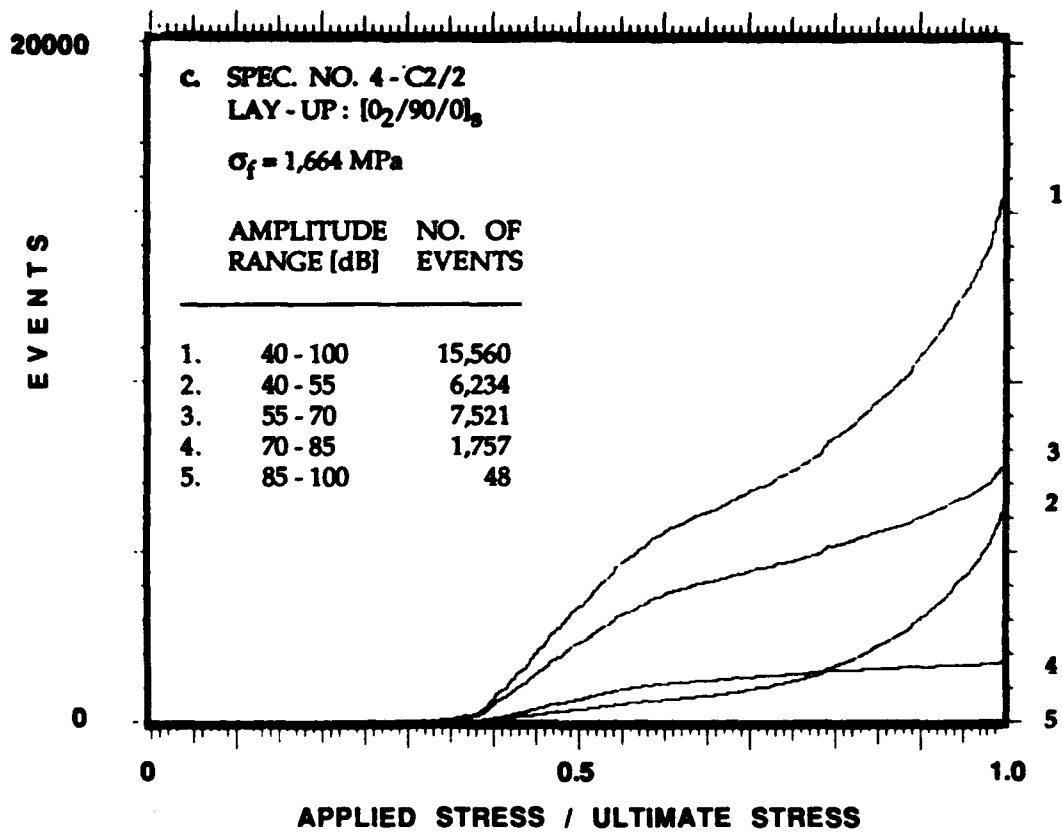


Figure 5.15. Continued.

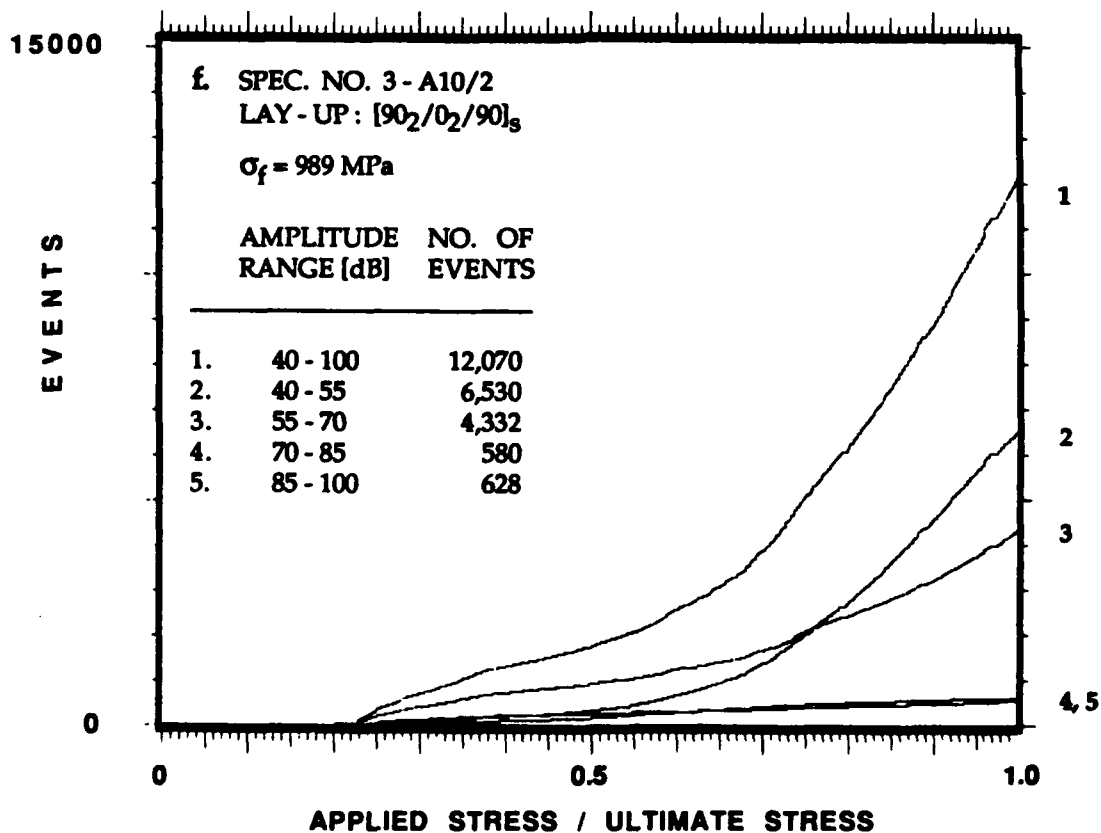
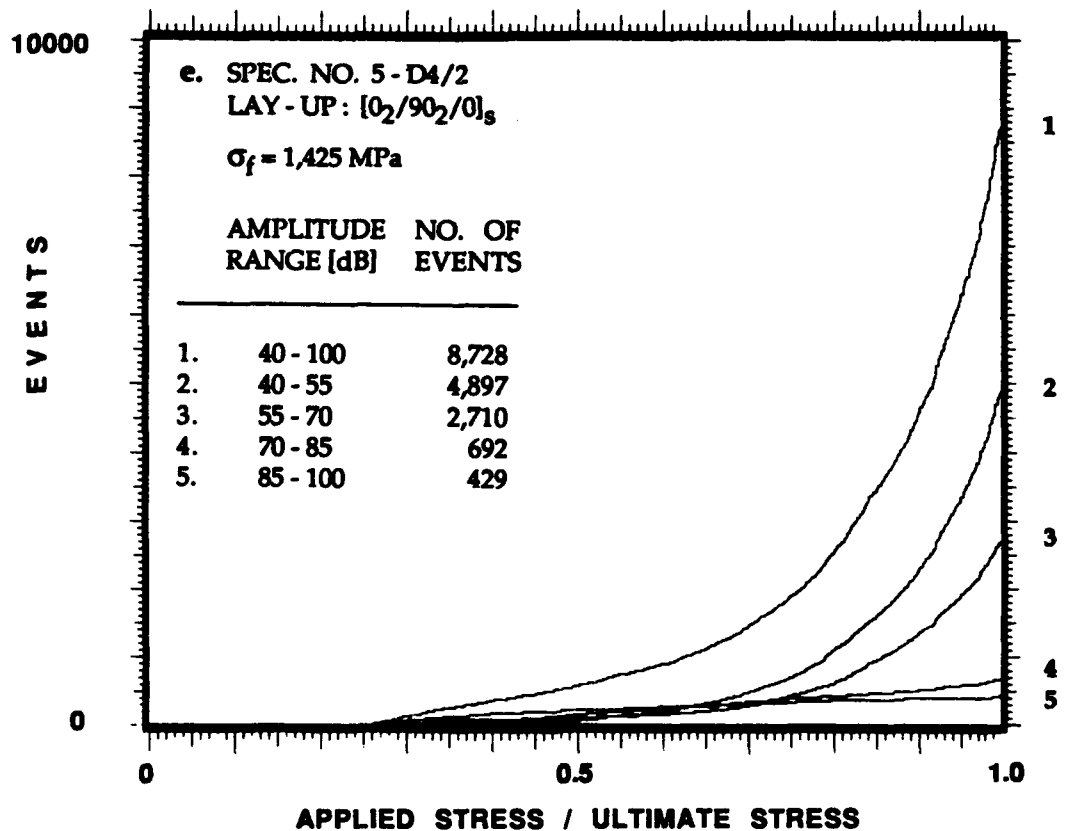


Figure 5.15. Continued.

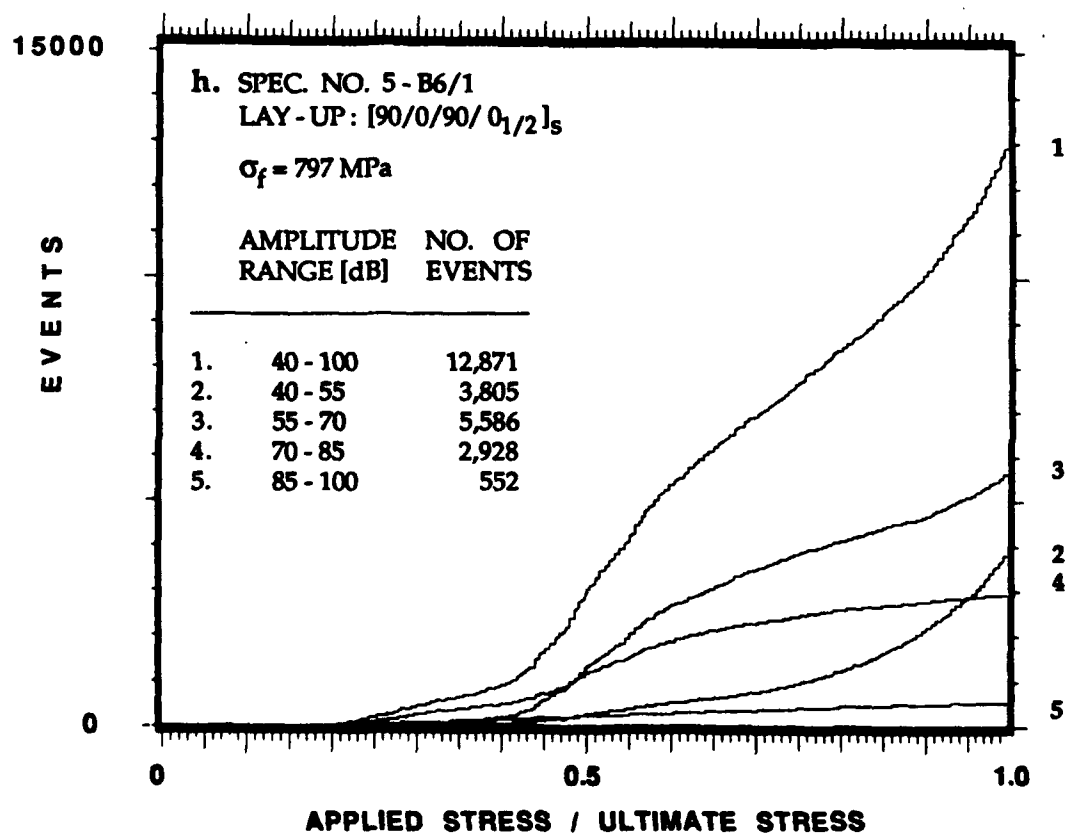
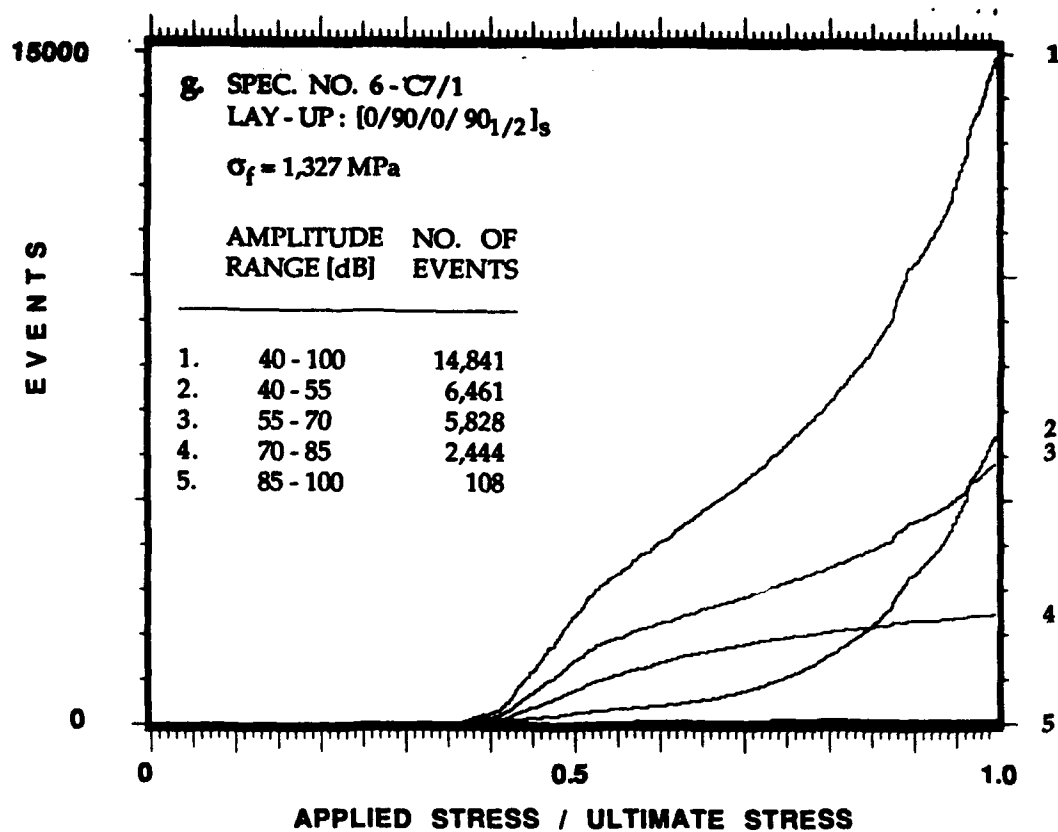


Figure 5.15. Continued.

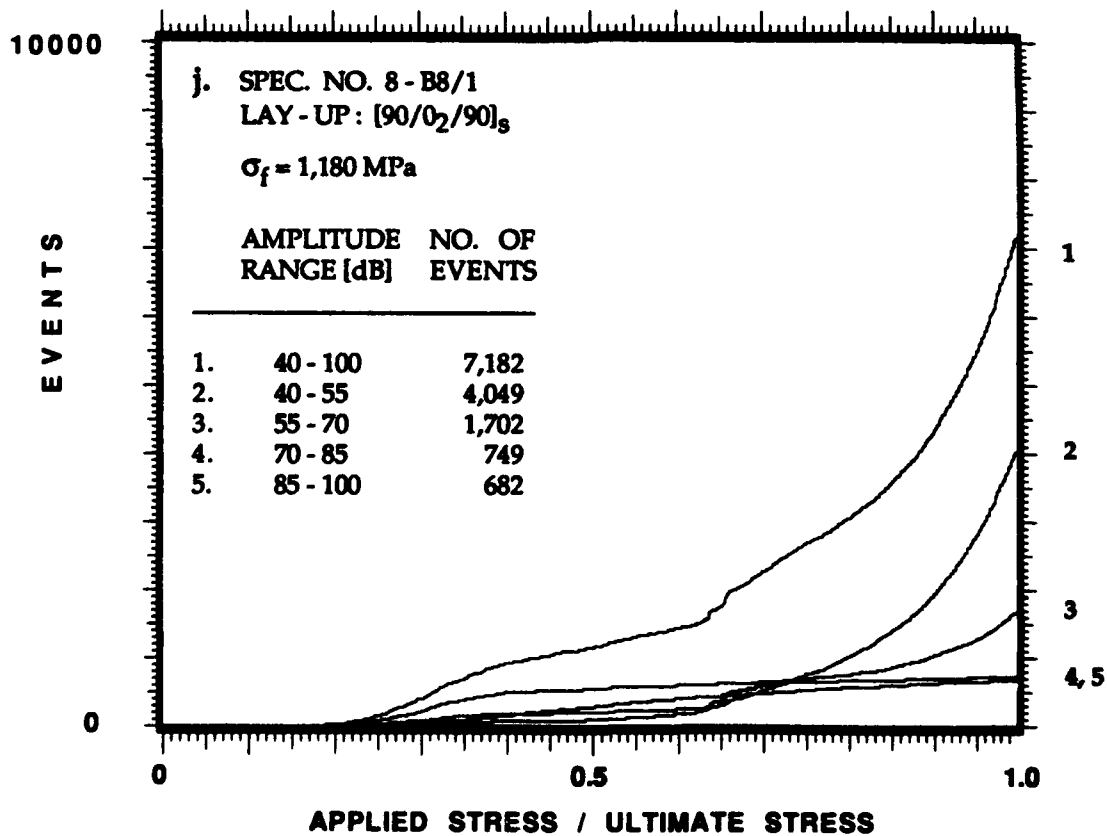
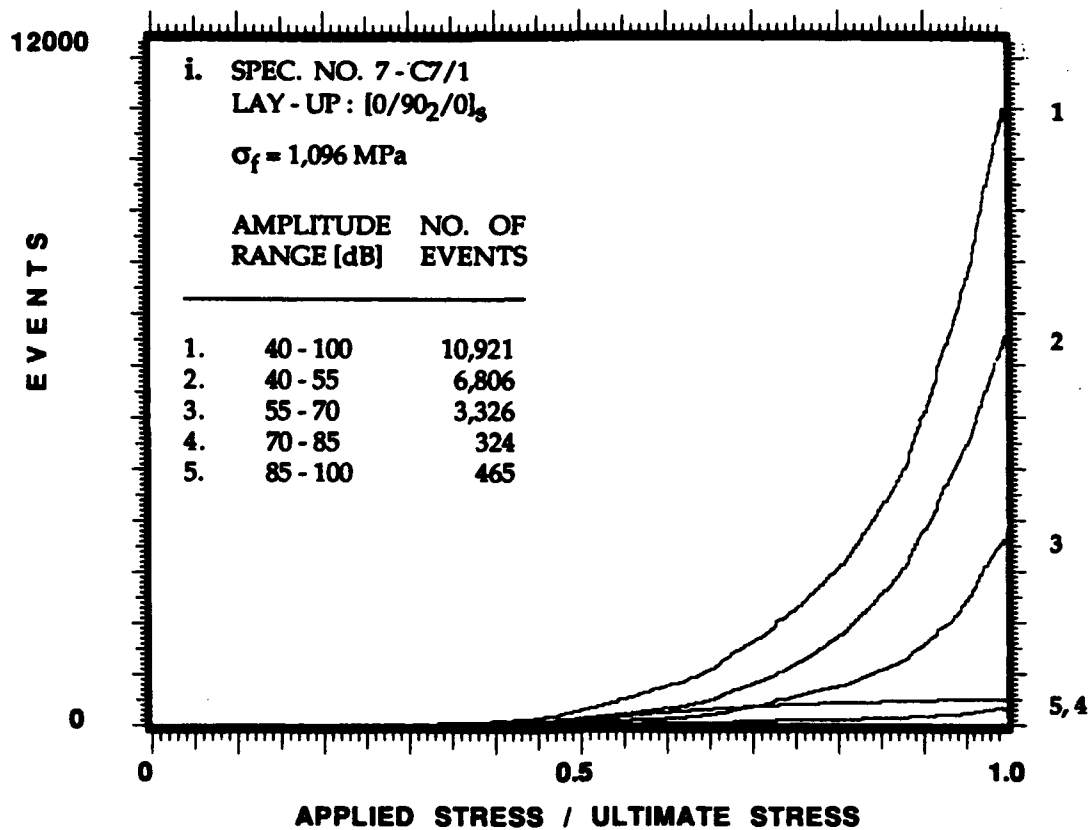


Figure 5.15. Continued.

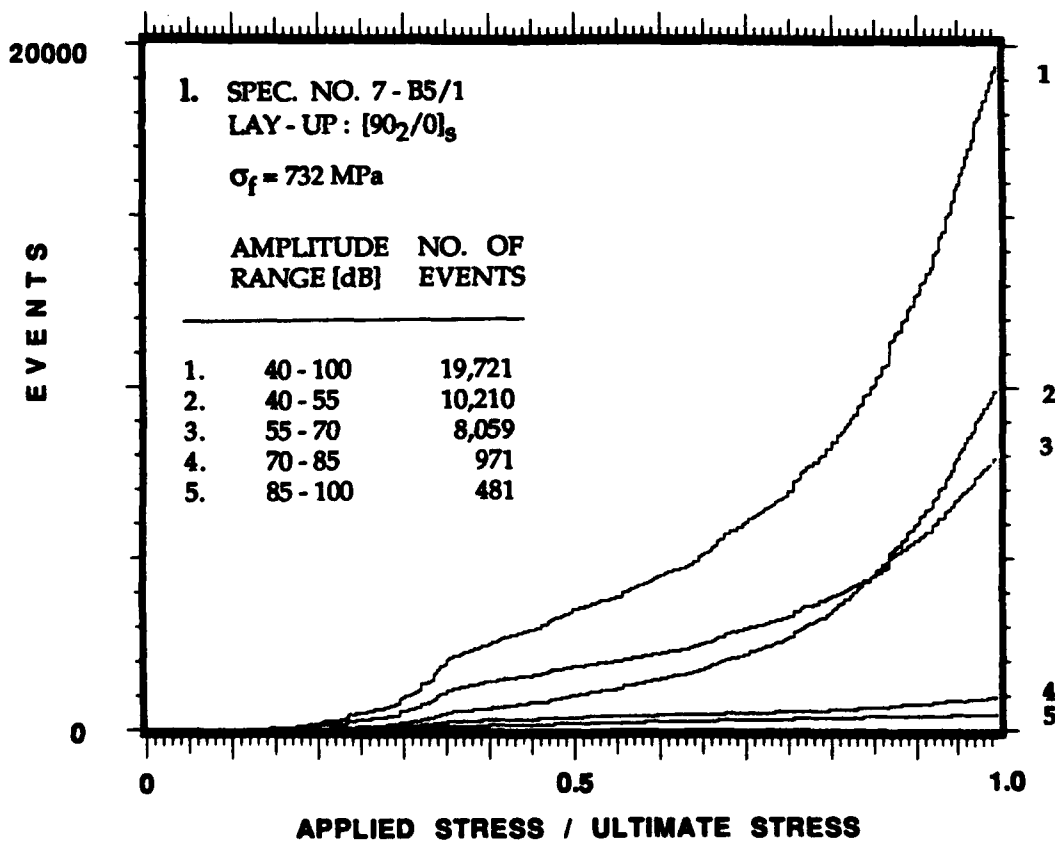
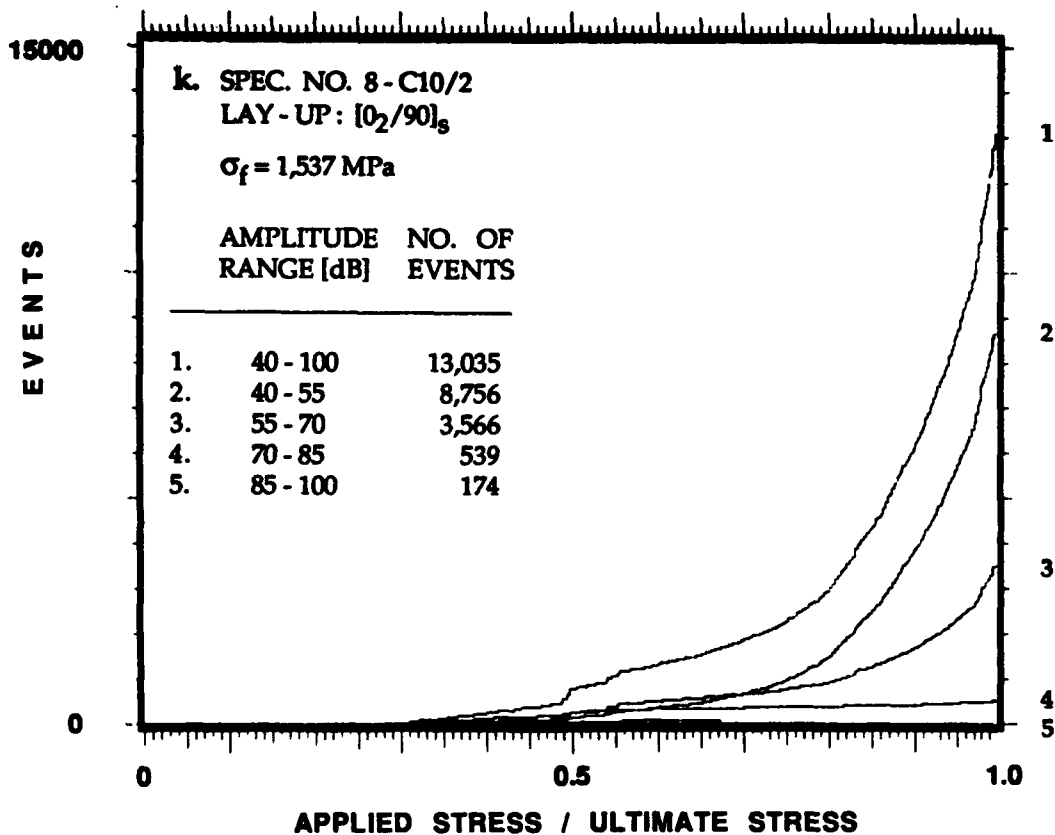


Figure 5.15. Concluded.

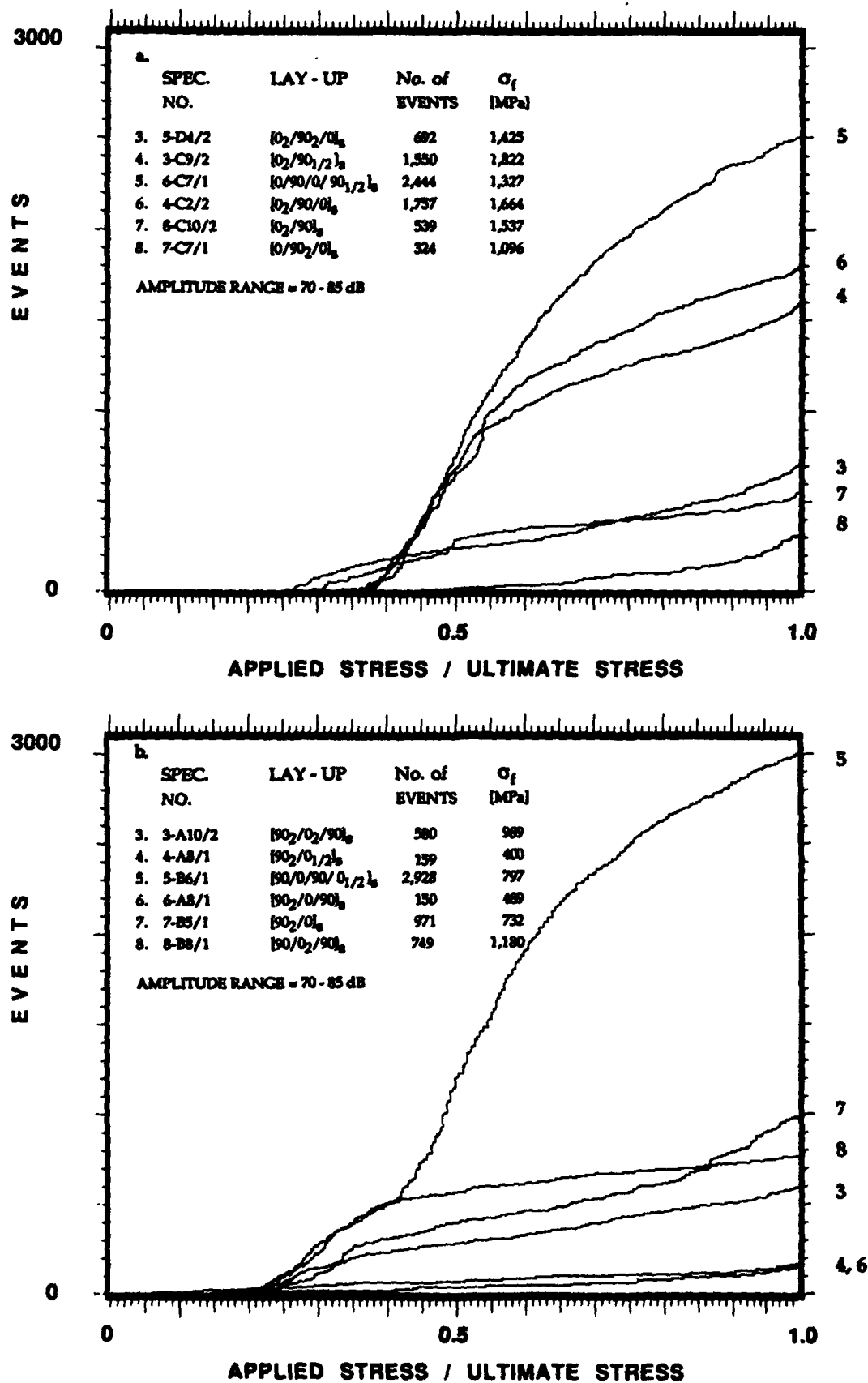


Figure 5.16. Events of 70 dB to 85 dB amplitude range (recorded with the PAC AE system) accumulated during quasi-static loading to failure as a function of far-field applied stress for 12 different cross-ply graphite/epoxy laminates: (a) laminates having external 0° plies (Group I); and (b) laminates having external 90° plies (Group II).

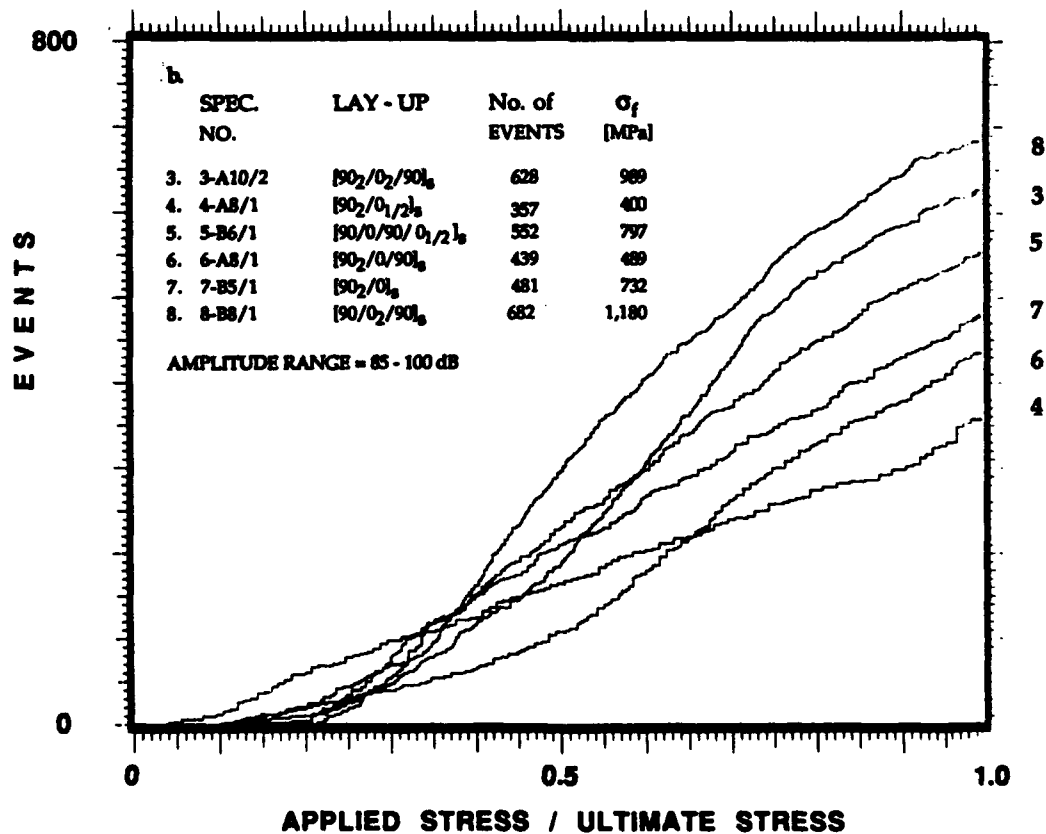
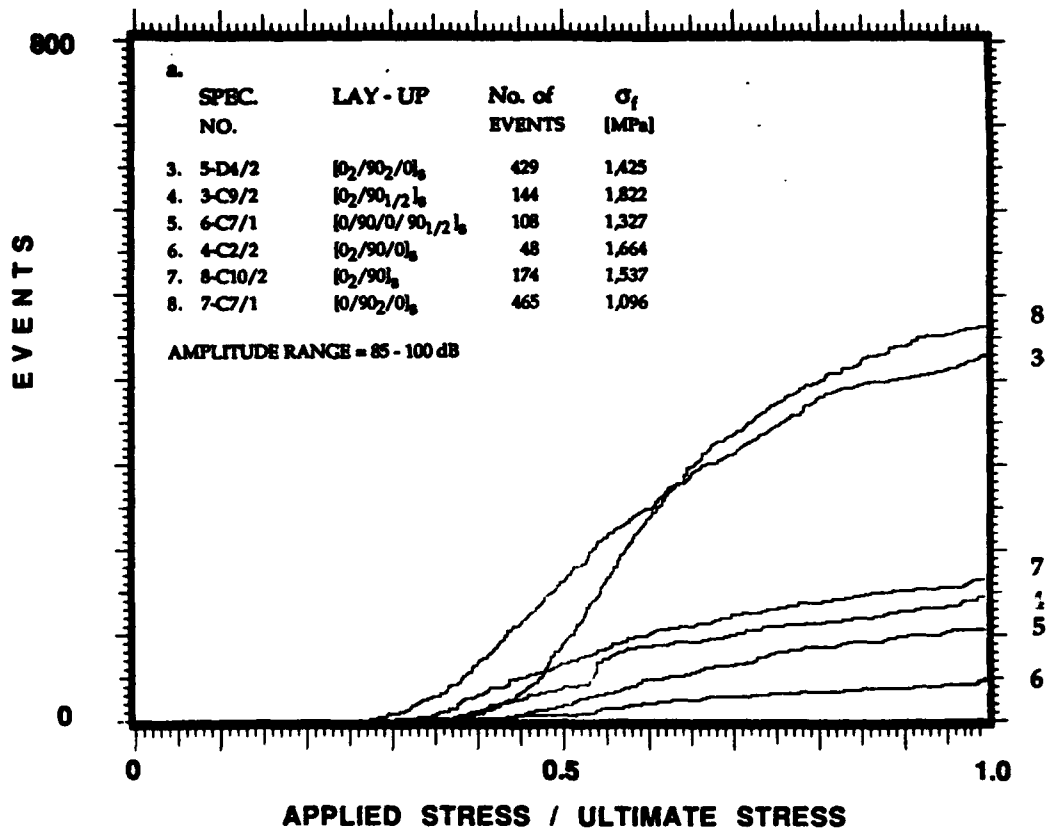


Figure 5.17. Events of 85 dB to 100 dB amplitude range (recorded with the PAC AE system) accumulated during quasi-static loading to failure as a function of far-field applied stress for 12 different cross-ply graphite/epoxy laminates: (a) laminates having external 0° plies (Group I); and (b) laminates having external 90° plies (Group II).

(a) SPEC. NO. 4-C2/2 $\sigma_f = 1,664$ MPa
LAY-UP: $[0_2/90/0]_s$ E = 15,560 EVENTS

(b) SPEC. NO. 6-A8/1 $\sigma_f = 489$ MPa
LAY-UP: $[90_2/0/90]_s$ E = 4,957 EVENTS

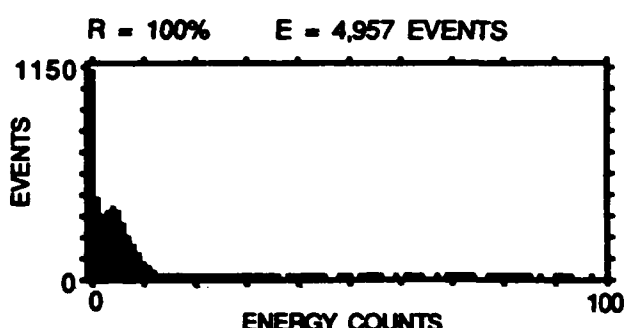
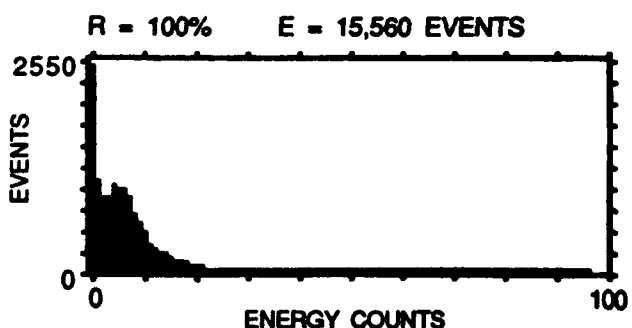
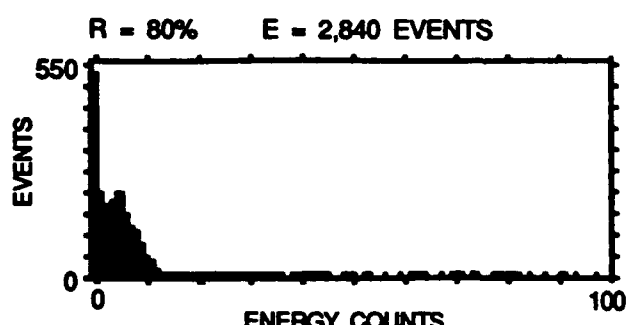
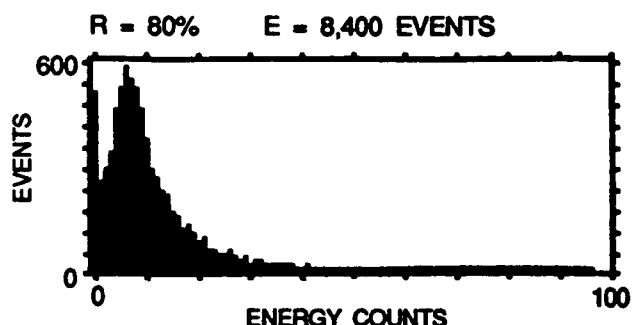
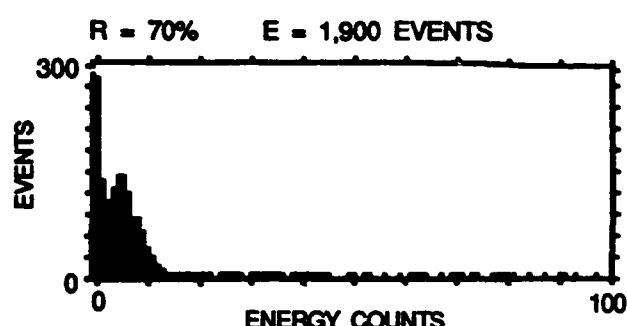
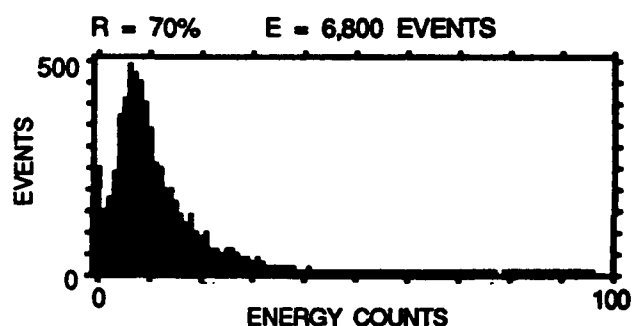
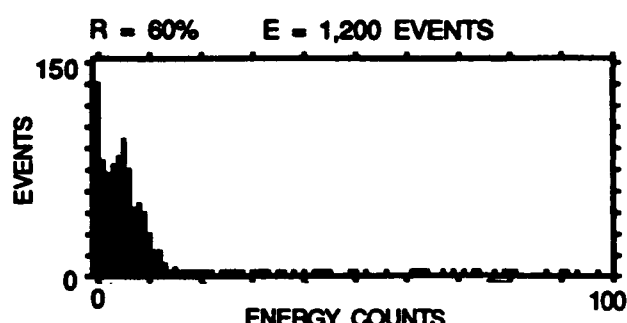
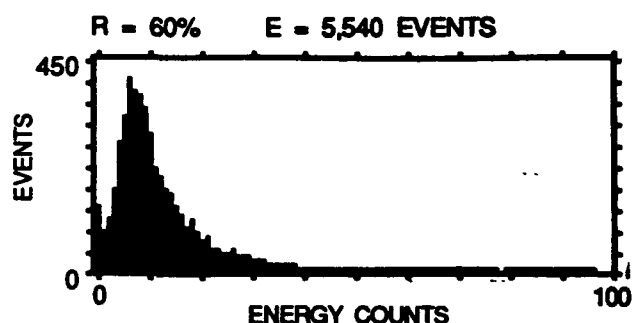
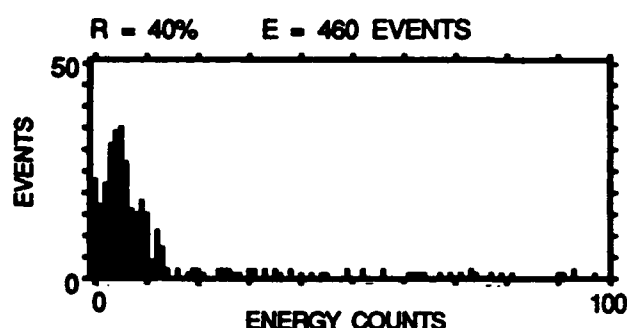
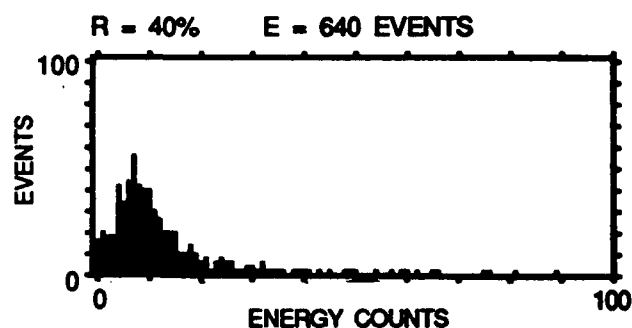
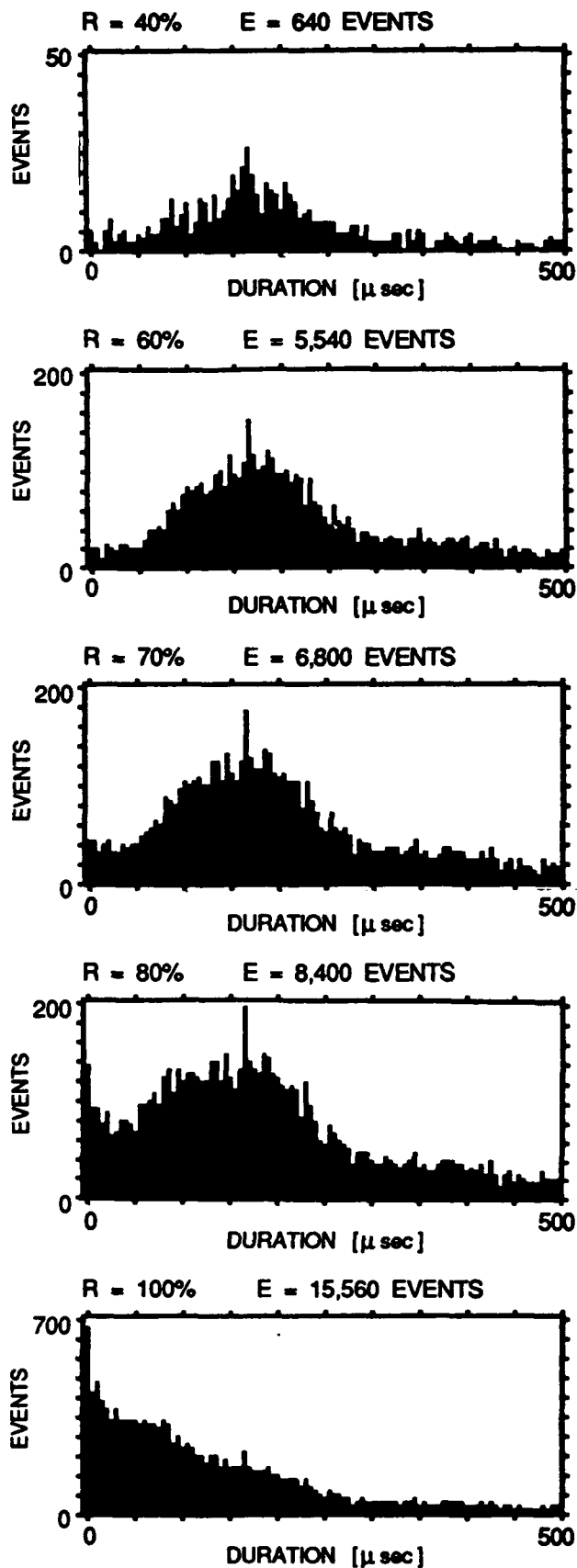


Figure 5.18. Energy-counts, duration, and counts per event distribution histograms of events (recorded with the PAC AE system) accumulated at different load ranges during quasi-static loading to failure for two selected cross-ply graphite/epoxy laminates having reversed stacking sequence.

(c) SPEC. NO. 4-C2/2 $\sigma_f = 1,664 \text{ MPa}$
 LAY-UP: $[0_2/90/0]_s$ $E = 15,560 \text{ EVENTS}$



(d) SPEC. NO. 6-A8/1 $\sigma_f = 489 \text{ MPa}$
 LAY-UP: $[90_2/0/90]_s$ $E = 4,957 \text{ EVENTS}$

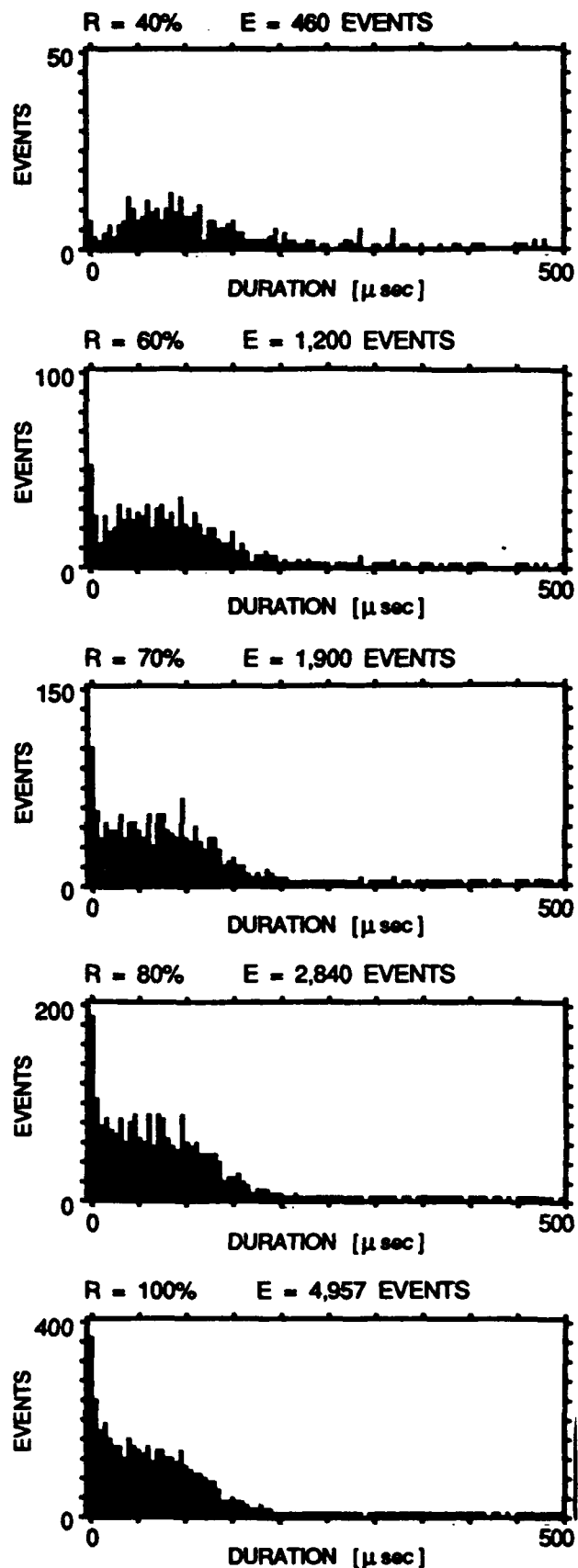


Figure 5.18. Continued.

(e) SPEC. NO. 4-C2/2 $\sigma_f = 1,664 \text{ MPa}$
 LAY-UP: $[0_2/90/0]_s$ $E = 15,560 \text{ EVENTS}$

(f) SPEC. NO. 6-A8/1 $\sigma_f = 489 \text{ MPa}$
 LAY-UP: $[90_2/0/90]_s$ $E = 4,957 \text{ EVENTS}$

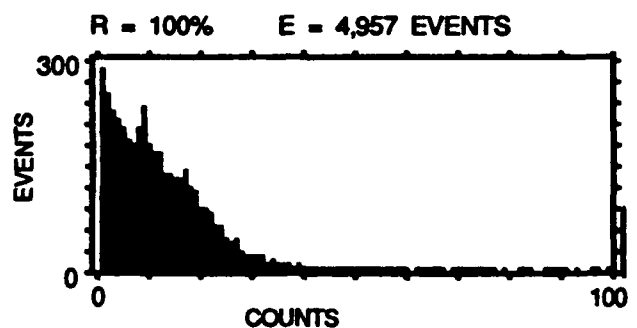
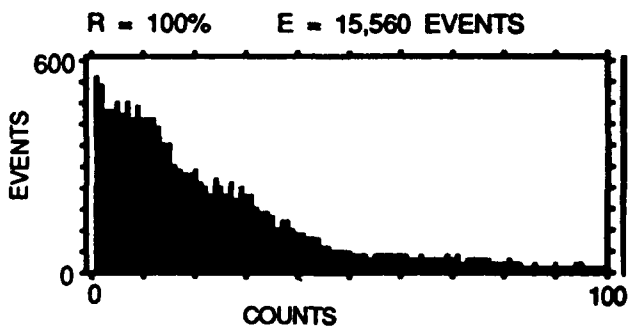
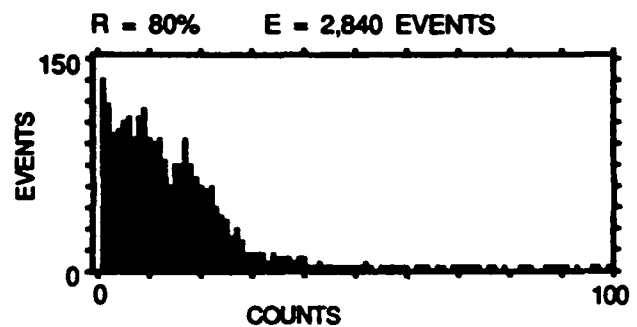
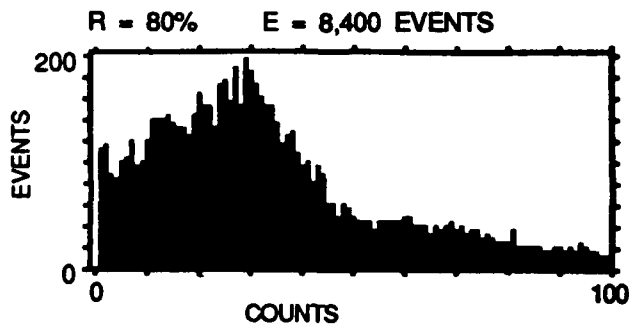
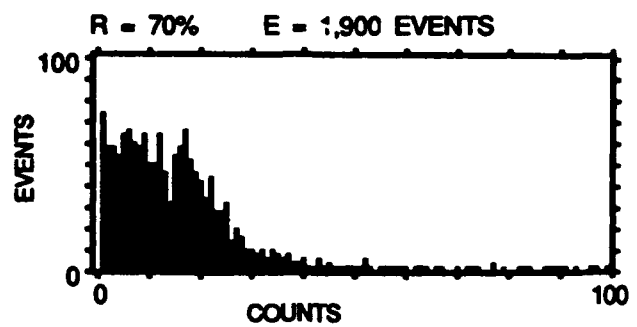
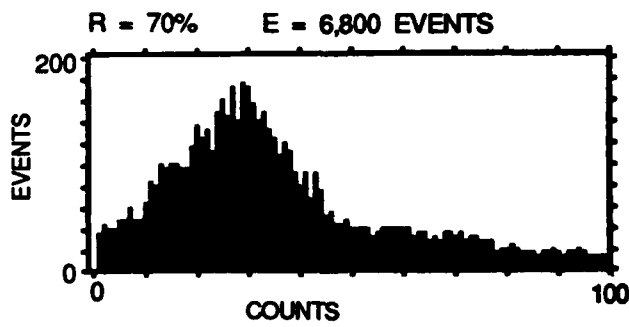
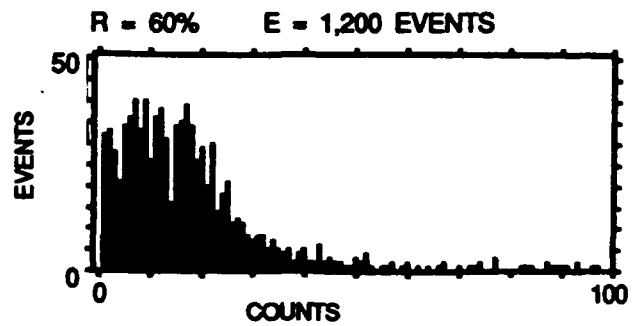
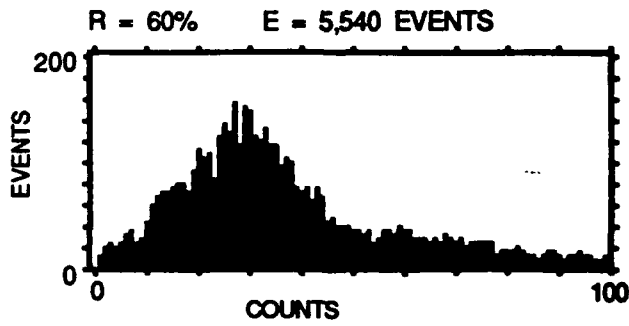
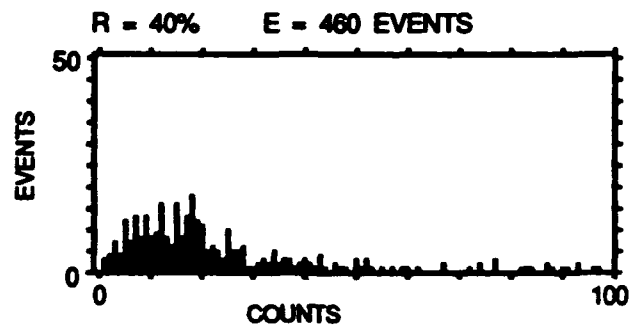
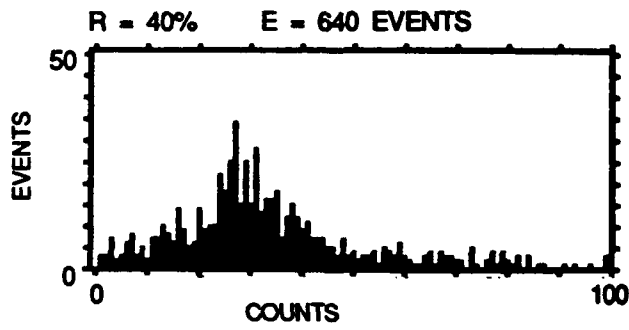


Figure 5.18. Concluded.

SPEC. NO. 4-C2/2
 LAY-UP: $[0_2/90/0]_s$
 $\sigma_f = 1,664 \text{ MPa}$
 $E = 15,560 \text{ EVENTS}$

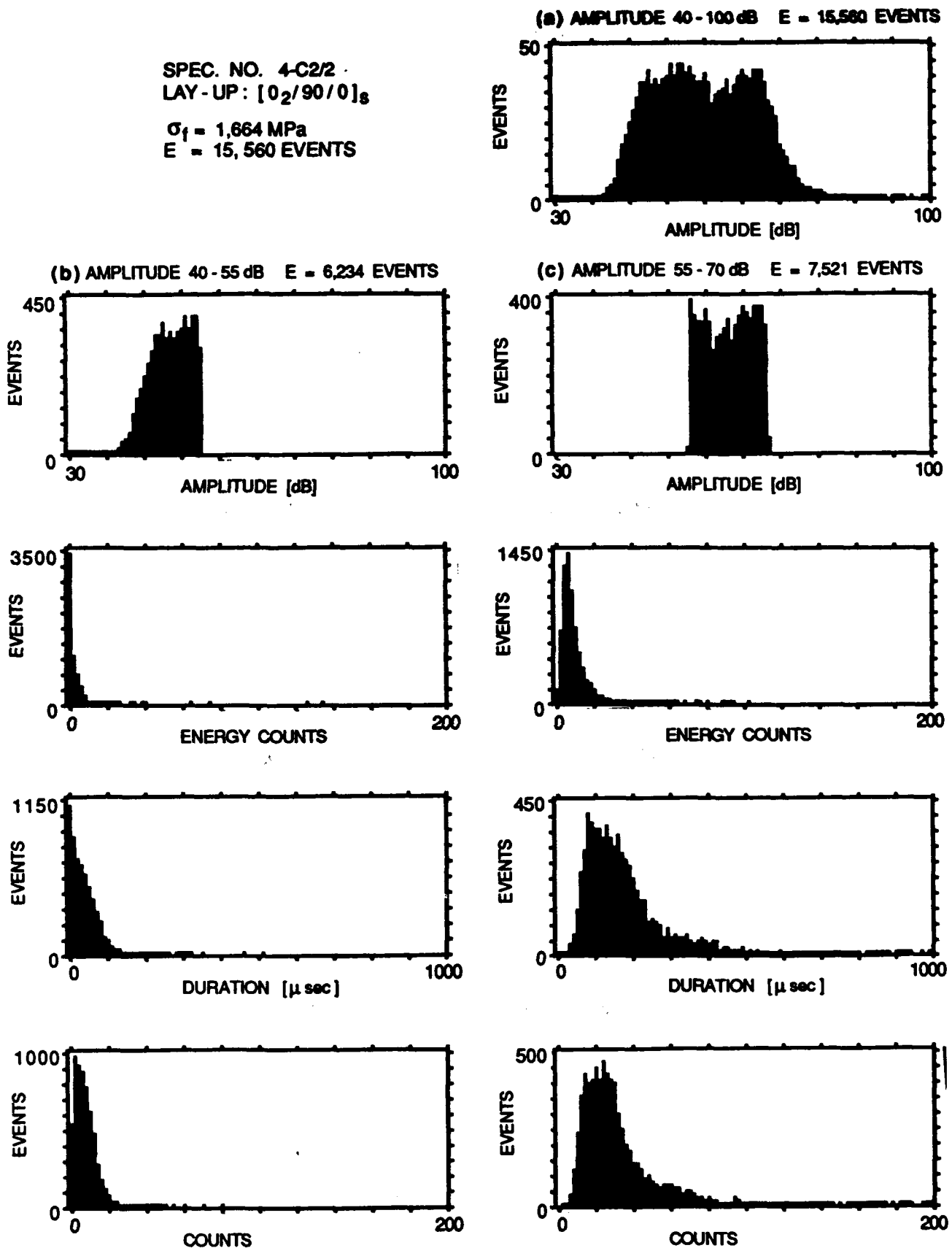


Figure 5.19. Intensity distribution histograms (I.D.H.) of events (recorded with the PAC AE system) accumulated during quasi-static loading to failure in a $[0_2/90/0]_s$ graphite/epoxy laminate: (a) amplitude distribution histogram (A.D.H.) of all the events accumulated; (b) (c) (d) and (e) I.D.H. of events having four different amplitude ranges; (f) A.D.H. events having 55 dB to 70 dB; (g) and (h) I.D.H. of events shown in distribution (f) having below and above 20 energy-counts, respectively.

SPEC. NO. 4-C2/2
LAY-UP: $[0_2/90/0]_8$

$\sigma_f = 1,664 \text{ MPa}$
 $E = 15,560 \text{ EVENTS}$

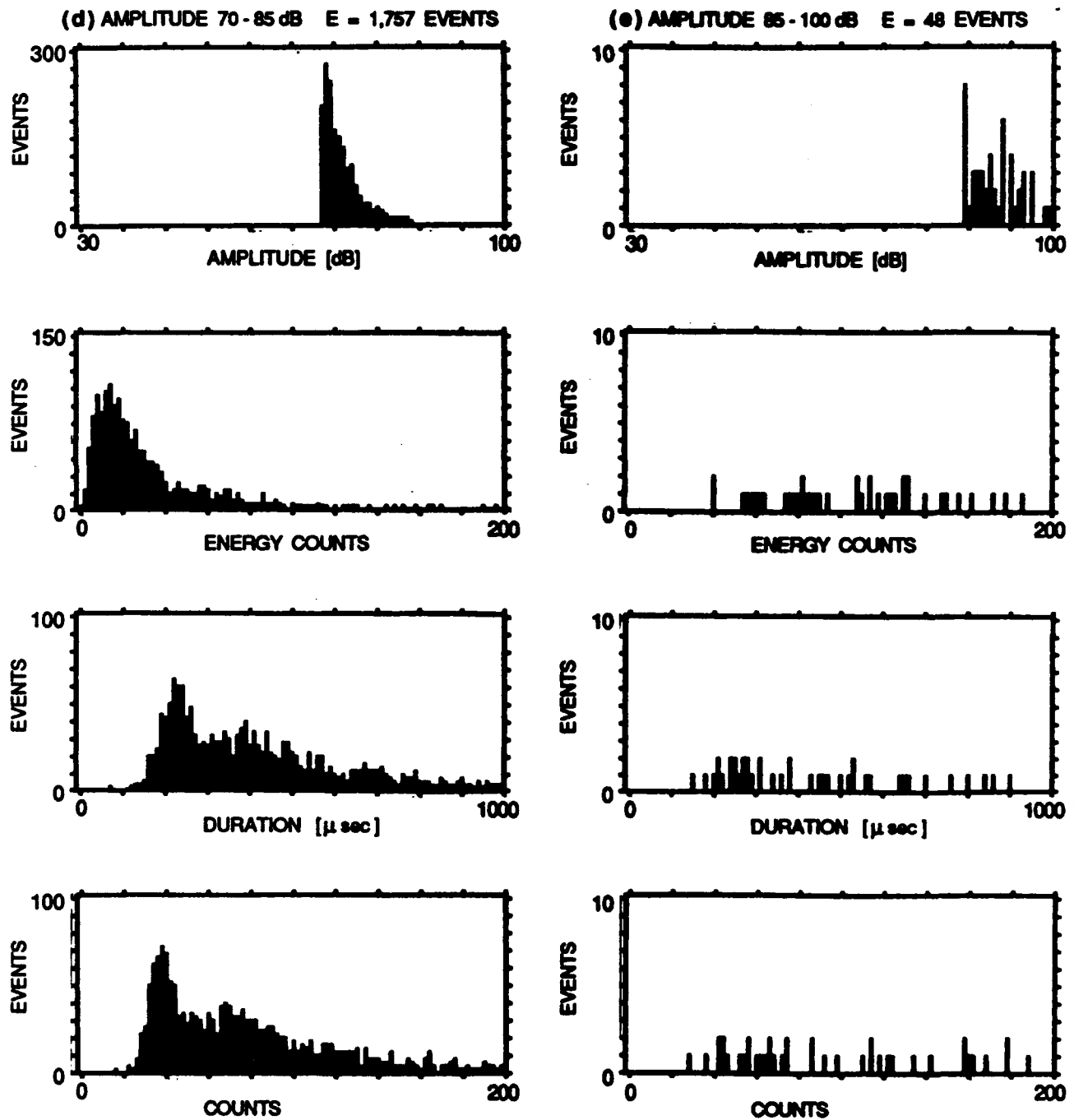
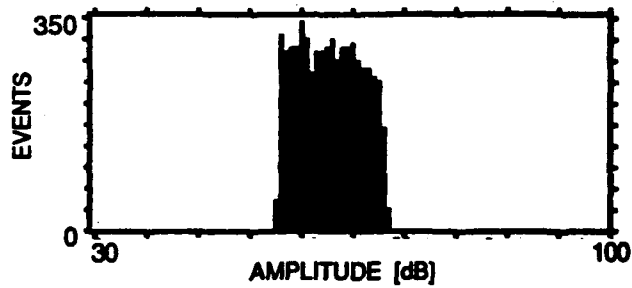


Figure 5.19. Continued.

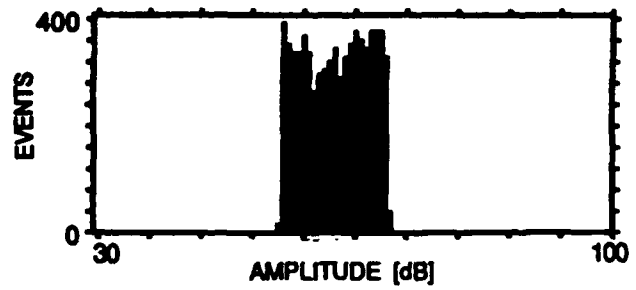
SPEC. NO. 4-C2/2
LAY-UP: [0₂/90/0]_s

$\sigma_f = 1,664 \text{ MPa}$
 $E = 15,560 \text{ EVENTS}$

(g) AMPLITUDE 55 - 70 dB ENERGY = 1 - 20
 $E = 6,157 \text{ EVENTS}$



(f) AMPLITUDE 55 - 70 dB $E = 7,521 \text{ EVENTS}$



(h) AMPLITUDE 55 - 70 dB ENERGY = 21 - 5,000
 $E = 319 \text{ EVENTS}$

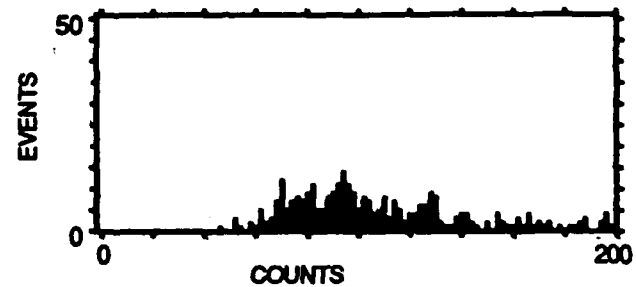
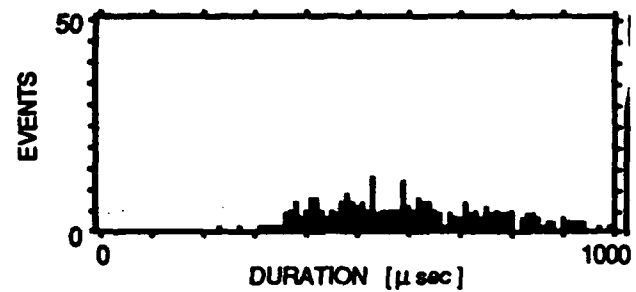
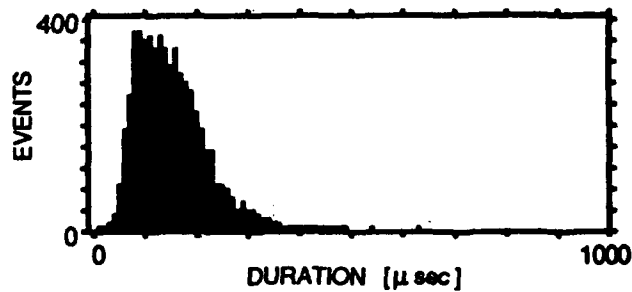
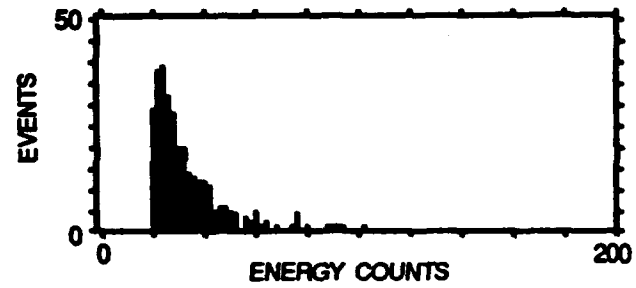
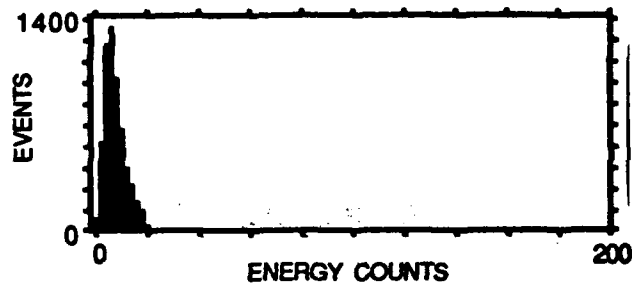
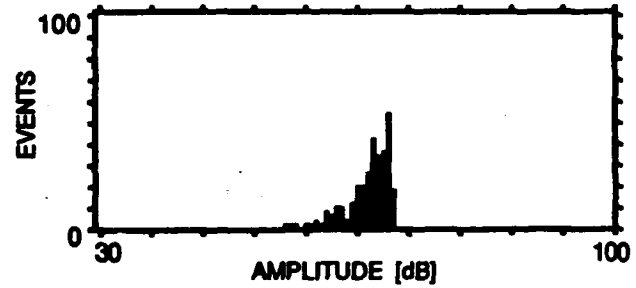


Figure 5.19. Concluded.

SPEC. NO. 6-A8/1
 LAY-UP: $[90_2/0/90]_s$
 $\sigma_f = 489 \text{ MPa}$
 $E = 4,957 \text{ EVENTS}$

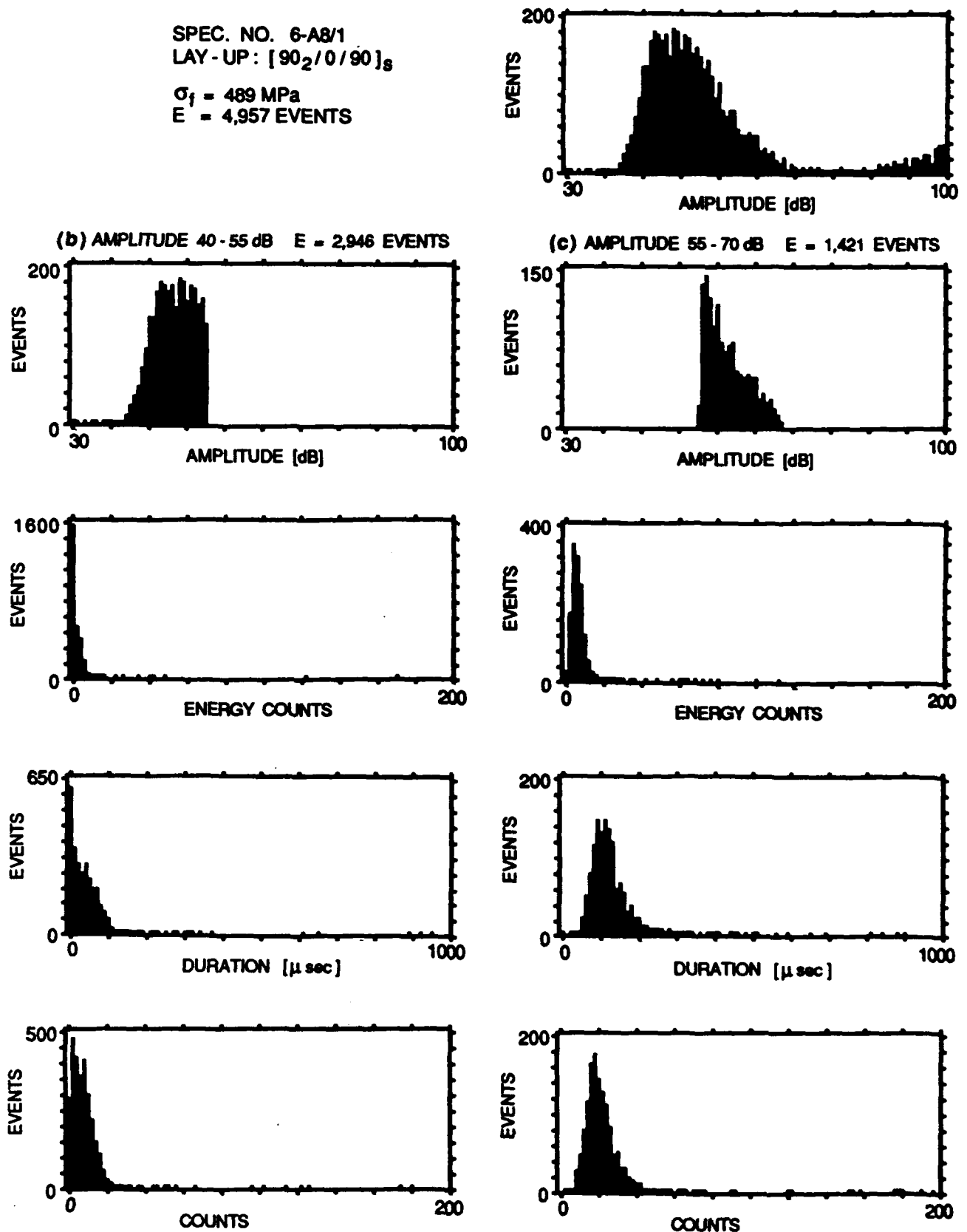


Figure 5.20. Intensity distribution histograms (I.D.H.) of events (recorded with the PAC AE system) accumulated during quasi-static loading to failure in a $[90_2/0/90]_s$ graphite/epoxy laminate: (a) amplitude distribution histogram (A.D.H.) of all the events accumulated; (b) (c) (d) and (e) I.D.H. of events having four different amplitude ranges; (f) A.D.H. events having 55 dB to 70 dB; (g) and (h) I.D.H. of events shown in distribution (f) having below and above 20 energy-counts, respectively.

SPEC. NO. 6-A8/1
LAY-UP: [90₂/0/90]_s

$\sigma_f = 489 \text{ MPa}$
 $E = 4,957 \text{ EVENTS}$

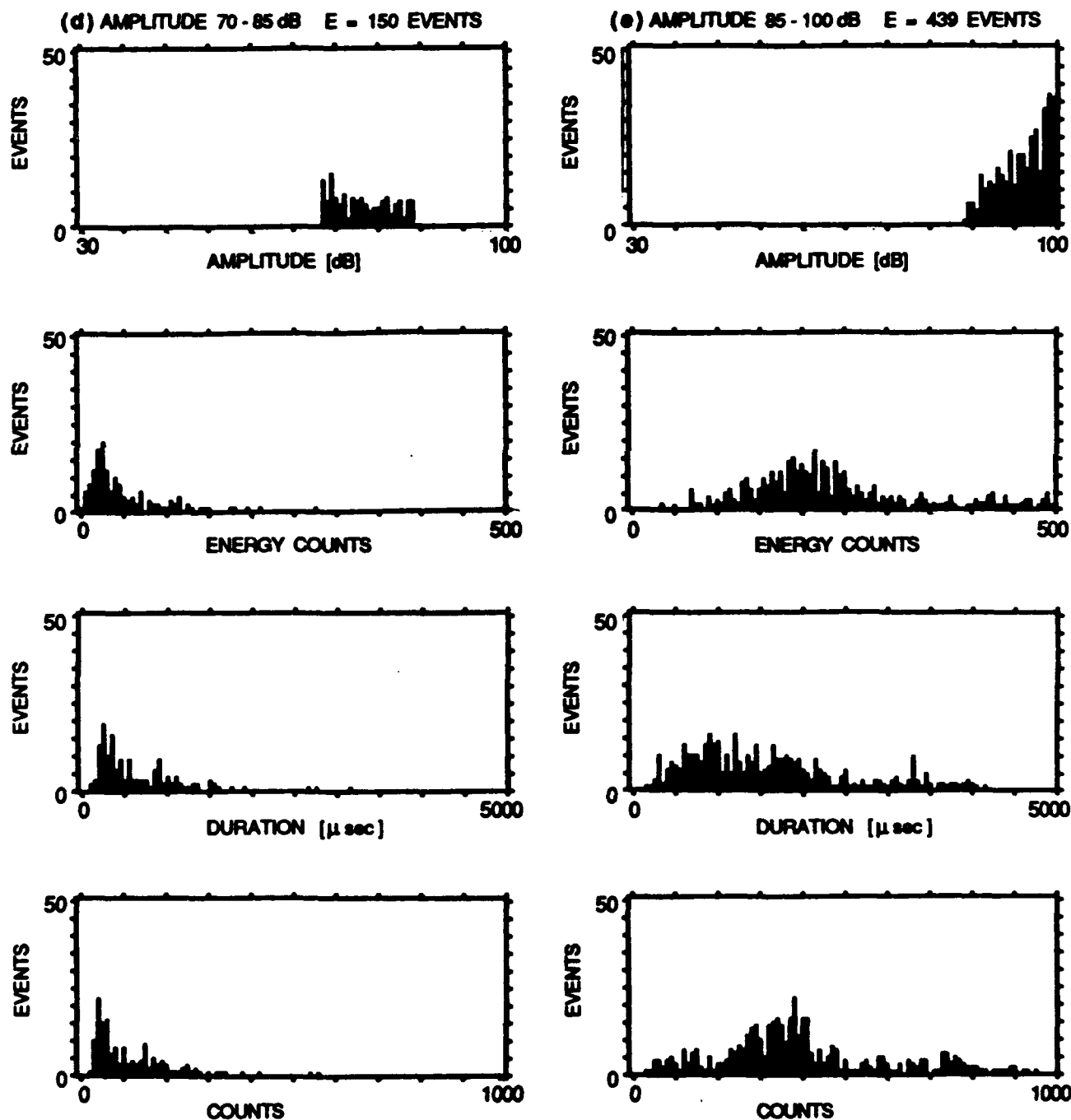


Figure 5.20. Continued.

SPEC. NO. 6-A8/1
 LAY-UP. [90₂/0/90]_s
 $\sigma_f = 489 \text{ MPa}$
 $E = 4,957 \text{ EVENTS}$

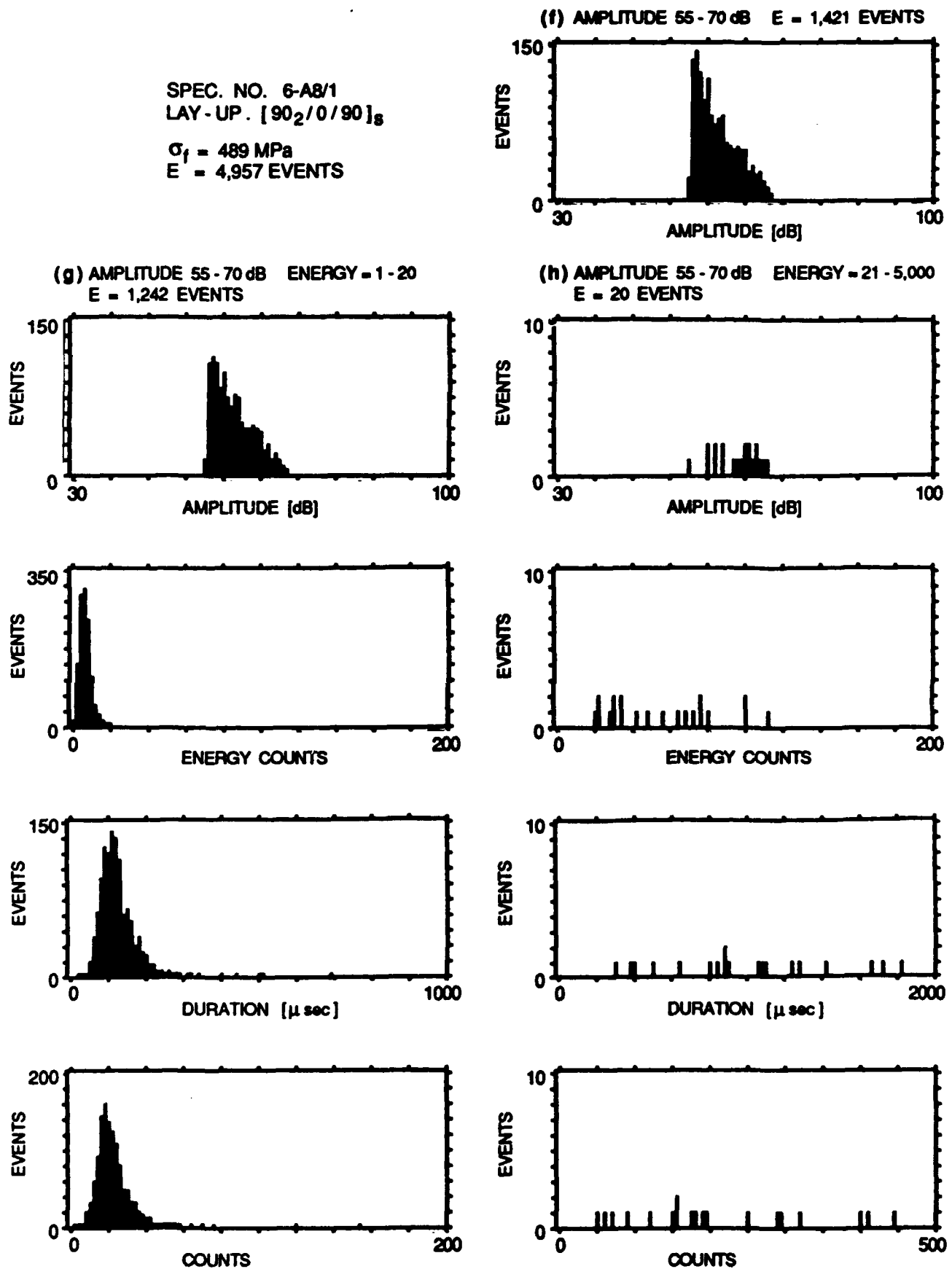


Figure 5.20. Concluded.

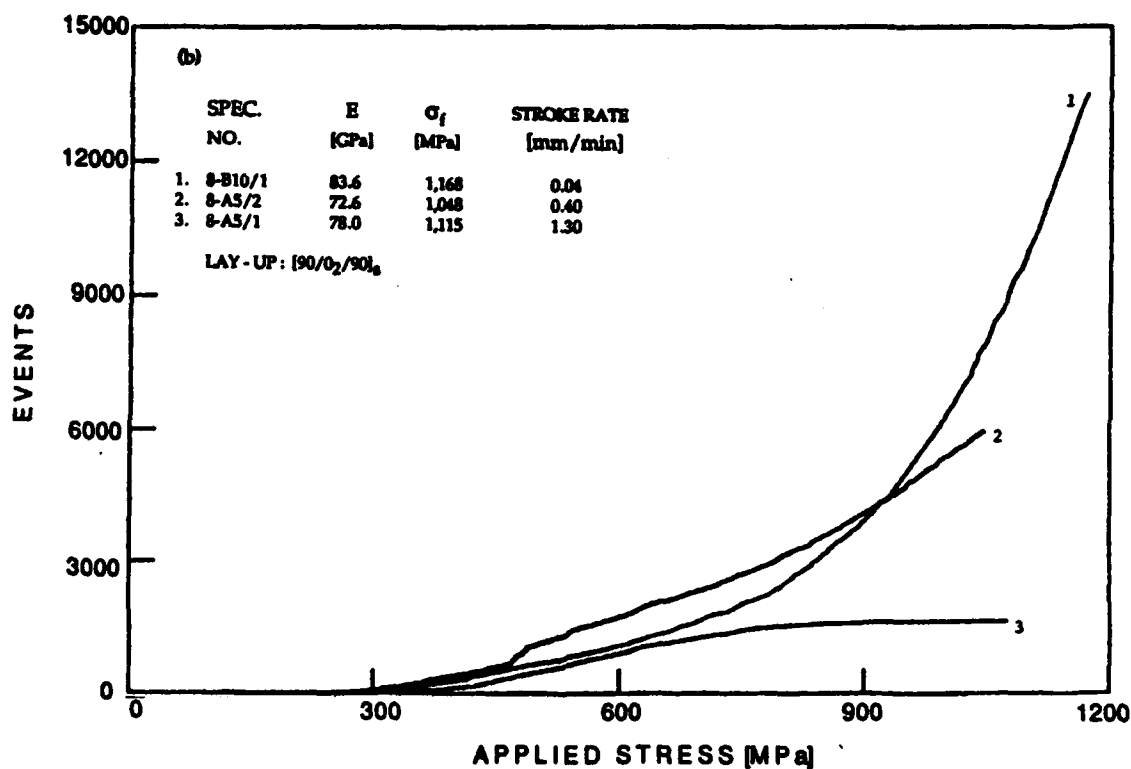
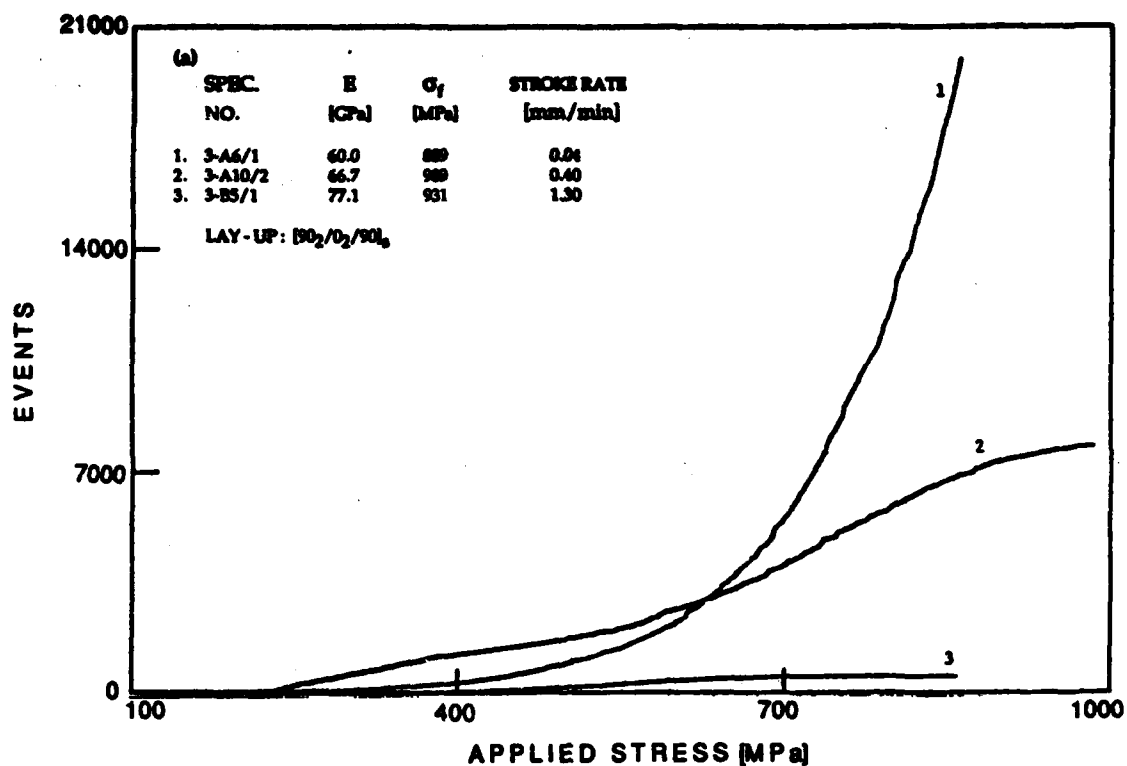


Figure 5.21. Events accumulated during quasi-static loading to failure (recorded with the D/E AE system) as a function of far-field applied stress for: (a) $[90_2/0_2/90]_s$; and (b) $[90/0_2/90]_s$ graphite/epoxy laminates subjected to three different stroke rates.

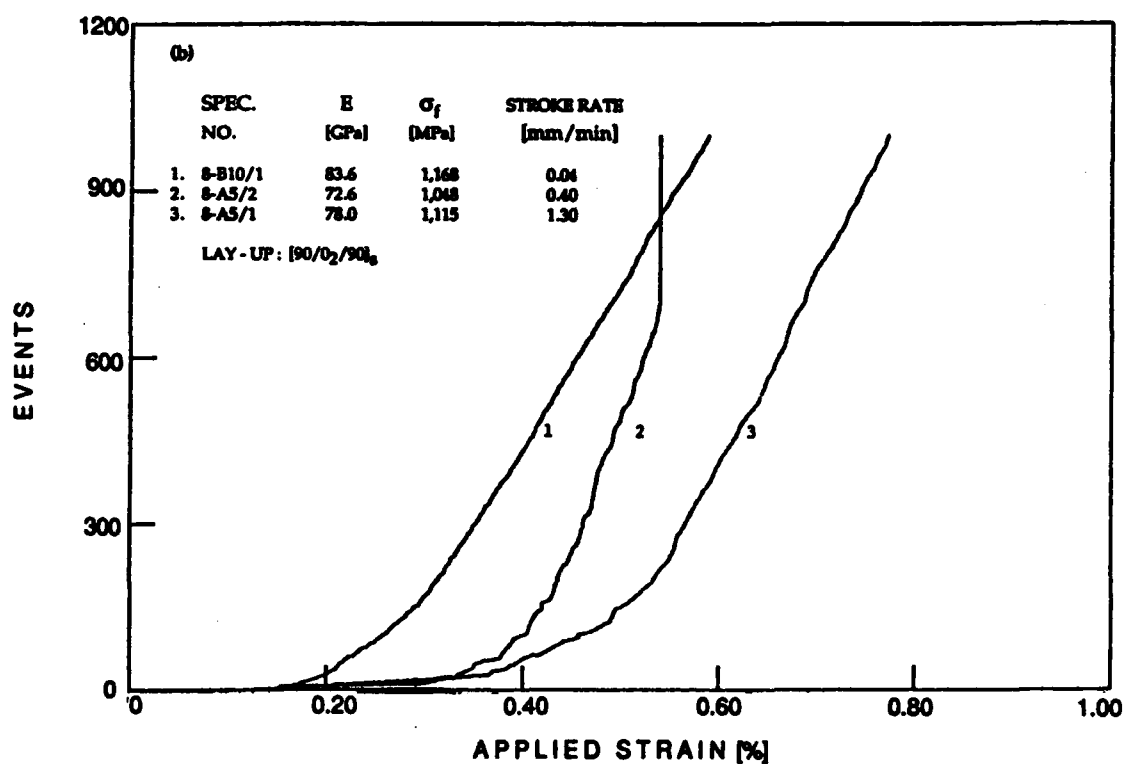
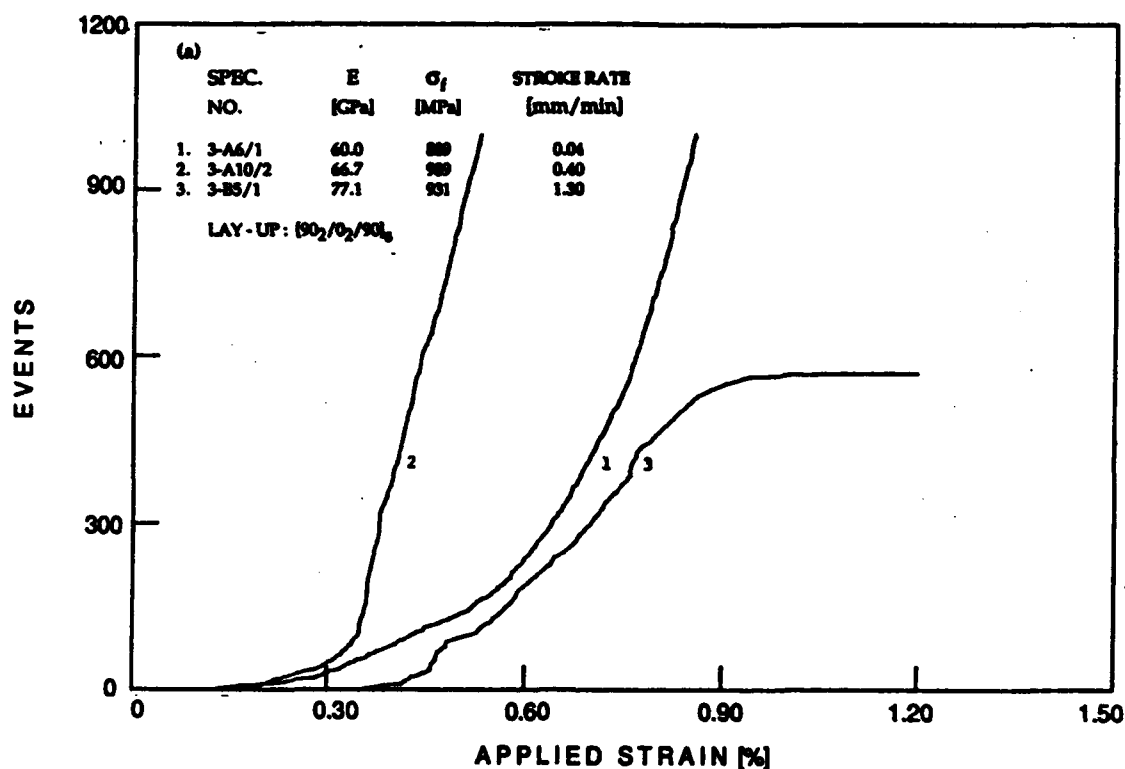
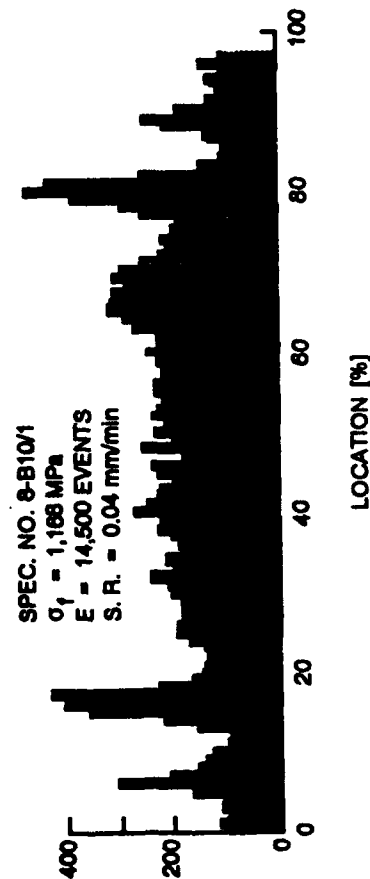
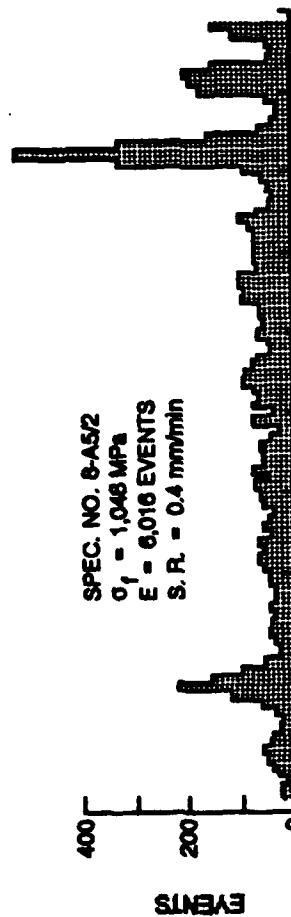
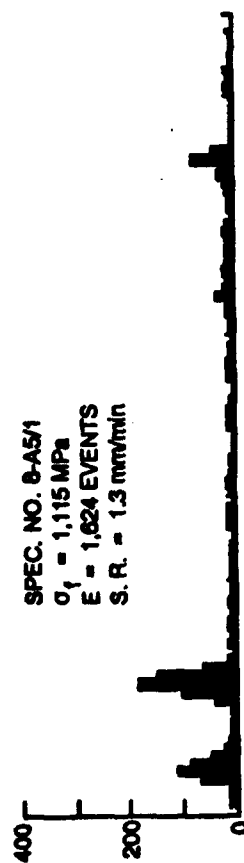


Figure 5.22. Events accumulated during quasi-static loading to failure (recorded with the D/E AE system) as a function of far-field applied strain for: (a) $[90_2/0_2/90]_s$; and (b) $[90/0_2/90]_s$ graphite/epoxy laminates subjected to three different stroke rates shown for the same specimens of Figure 5.21.

LAY UP: [90/0₂/90]_s



LAY UP: [90/0₂/90]_s

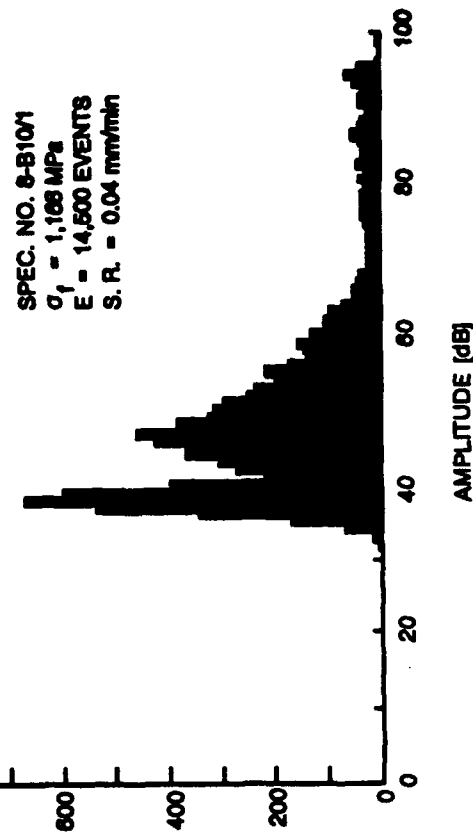
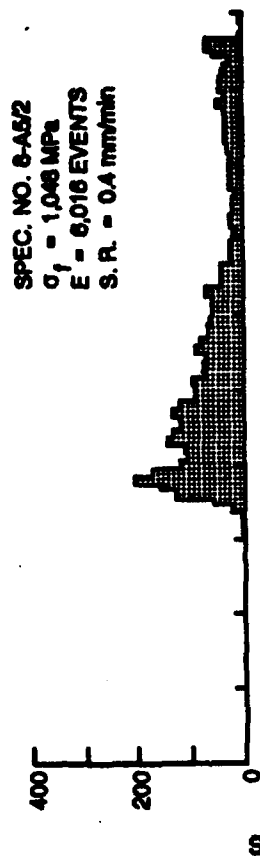
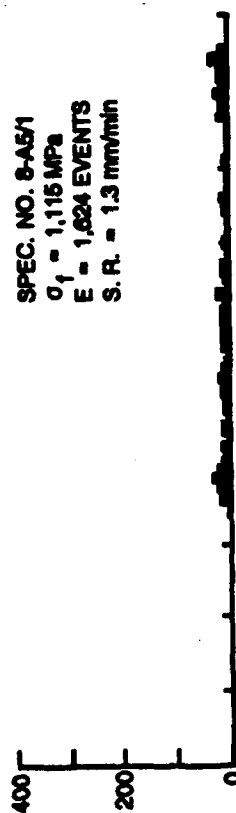


Figure 5.23. Location and amplitude distribution histograms of events (recorded with the D/E AE system) accumulated during quasi-static loading to failure of a [90/0₂/90]_s graphite/epoxy laminate subjected to three different stroke rates

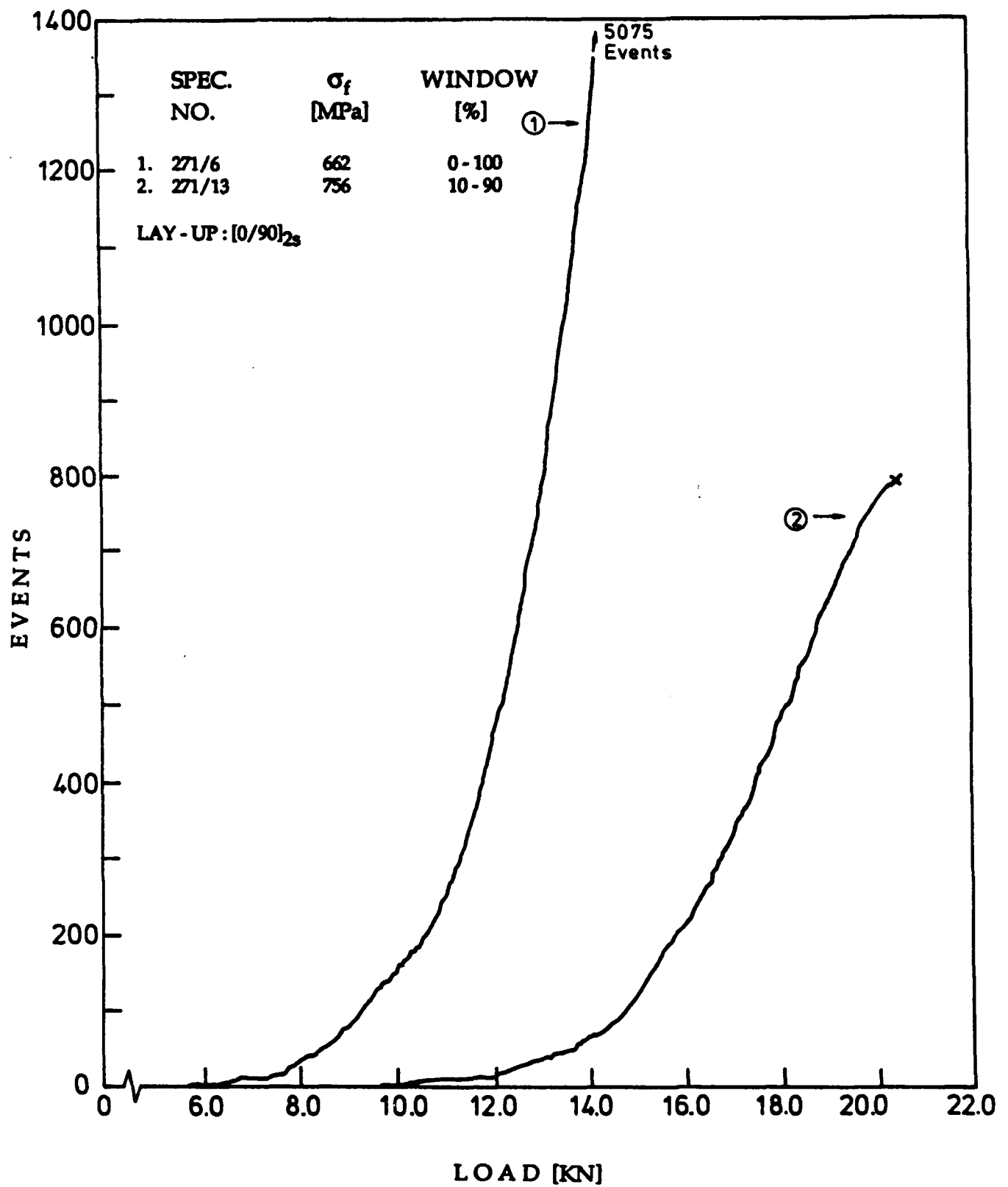


Figure 5.24. Events accumulated during quasi-static loading to failure (recorded with the D/E AE system) as a function of far-field applied stress for a [0/90]_{2s} graphite/epoxy laminate showing effect of spatial filtering on AE results.

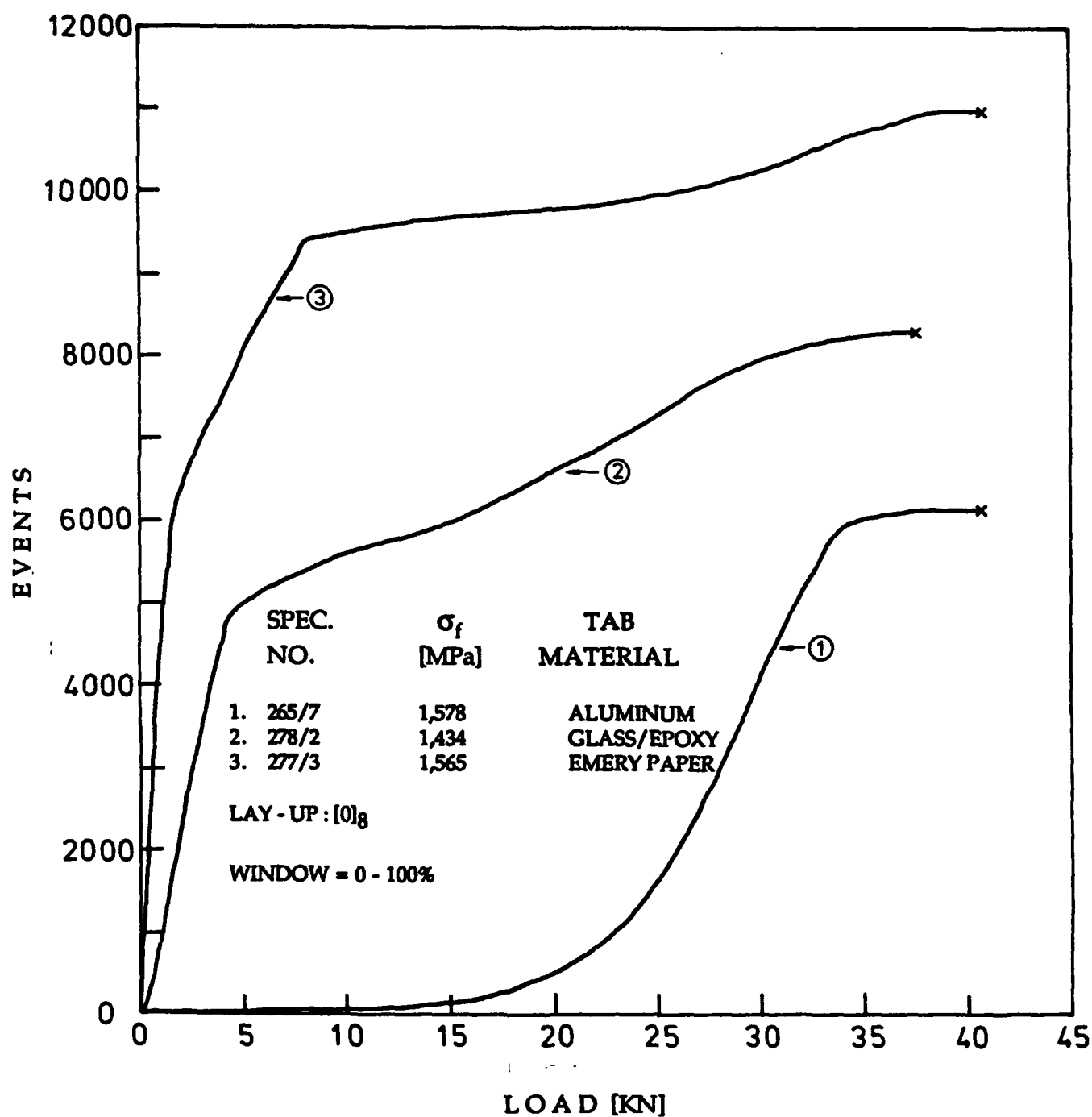


Figure 5.25. Events accumulated during quasi-static loading to failure (recorded with the D/E AE system) as a function of far-field applied stress for unidirectional graphite/epoxy laminate showing effect of specimen tabbing material on AE results.

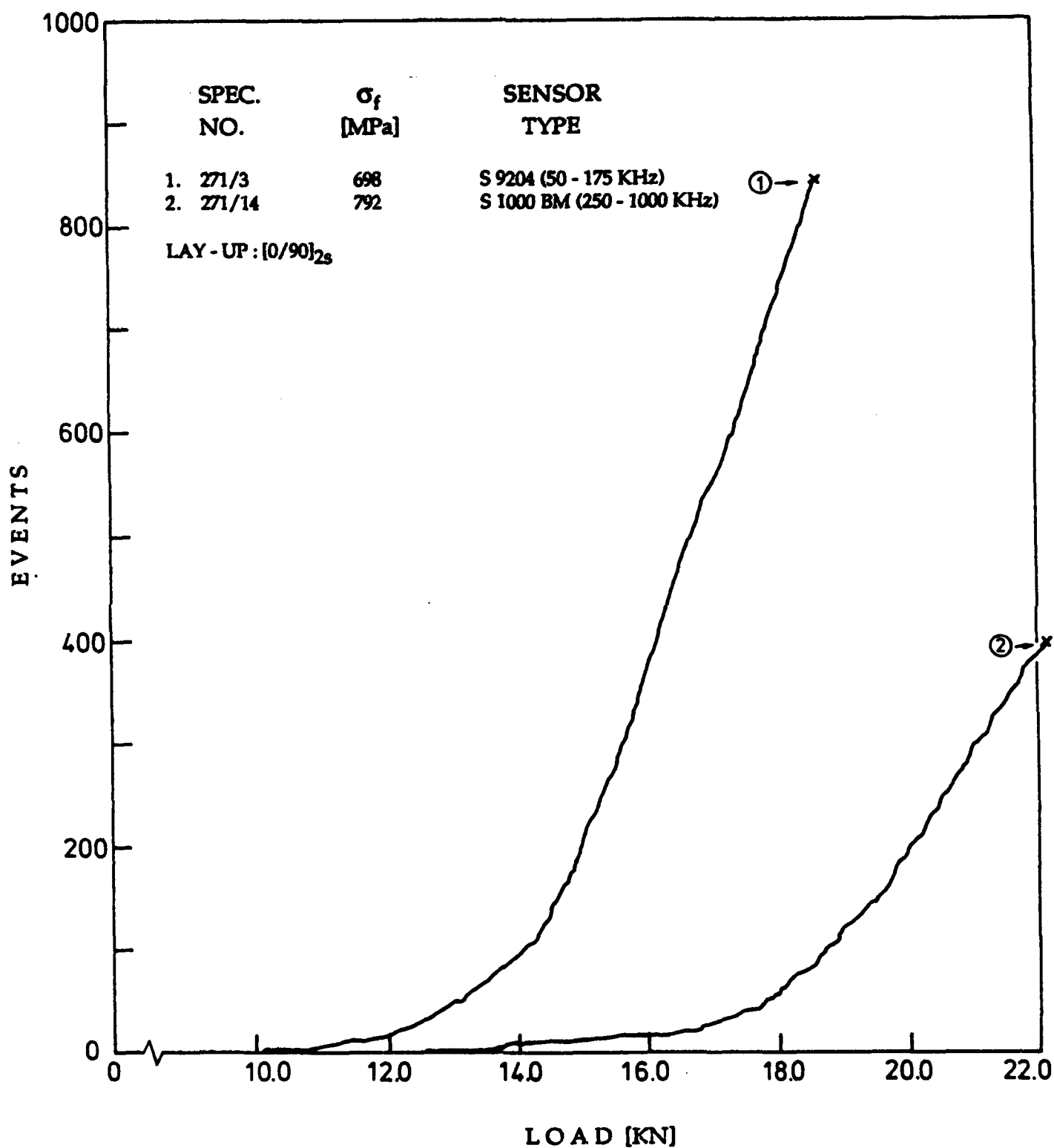


Figure 5.26. Events accumulated during quasi-static loading to failure (recorded with the D/E AE system) as a function of far-field applied stress for a $[0/90]_{2s}$ graphite/epoxy laminate showing effect sensor selection on AE results.

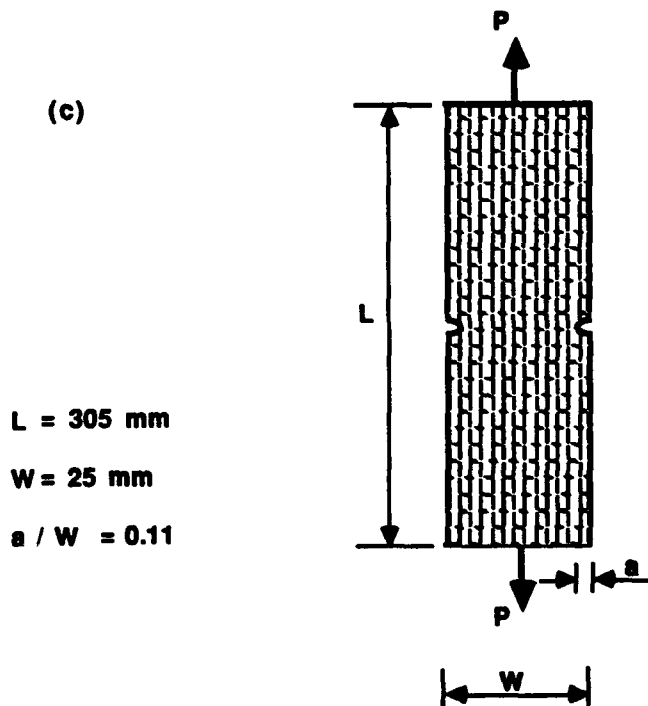
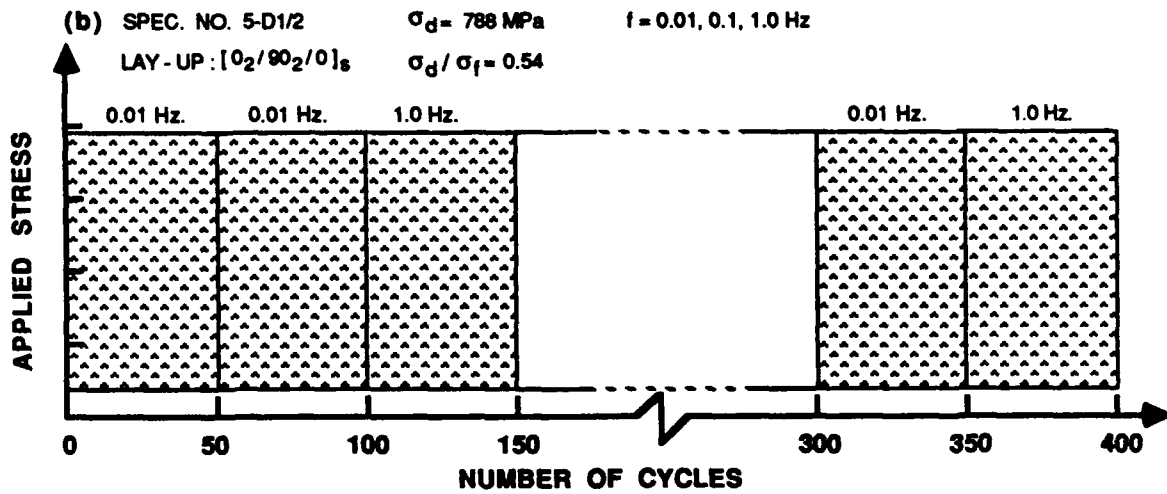
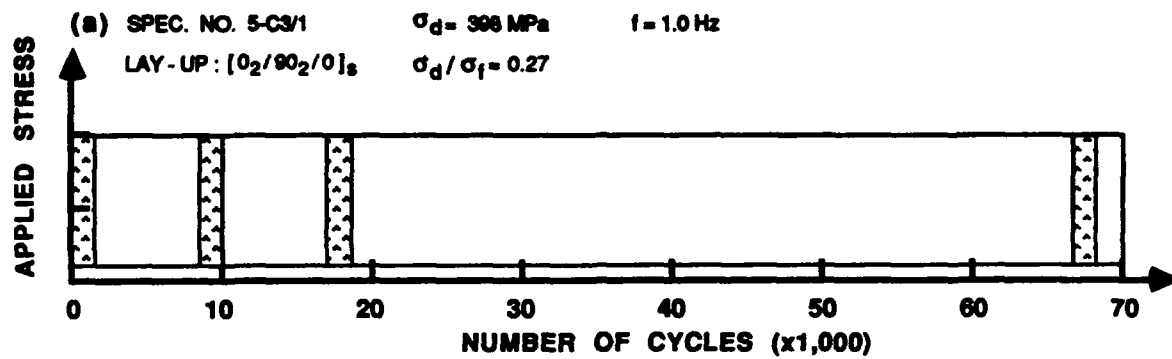


Figure 6.1 Schematics of loading sequences. Shaded areas indicate fatigue periods analyzed and discussed in this Section. All specimens were subjected to sinusoidal loading function at $R = 0.1$. Dynamic stress amplitude σ_d , loading frequency, f , and fatigue period, N , are indicated in each schematic.

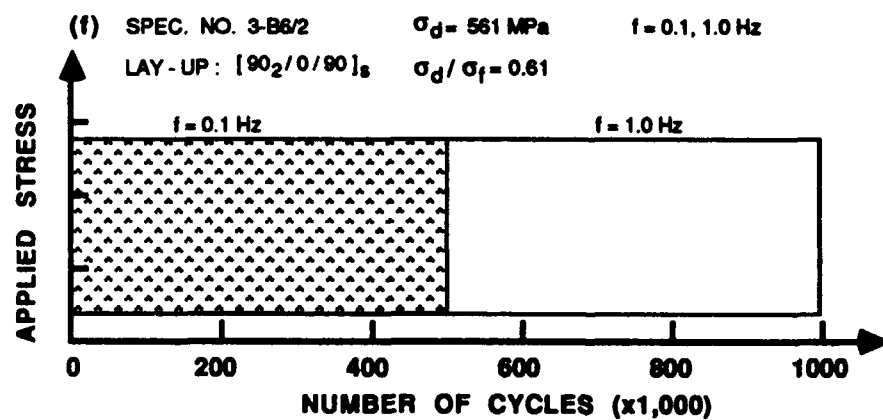
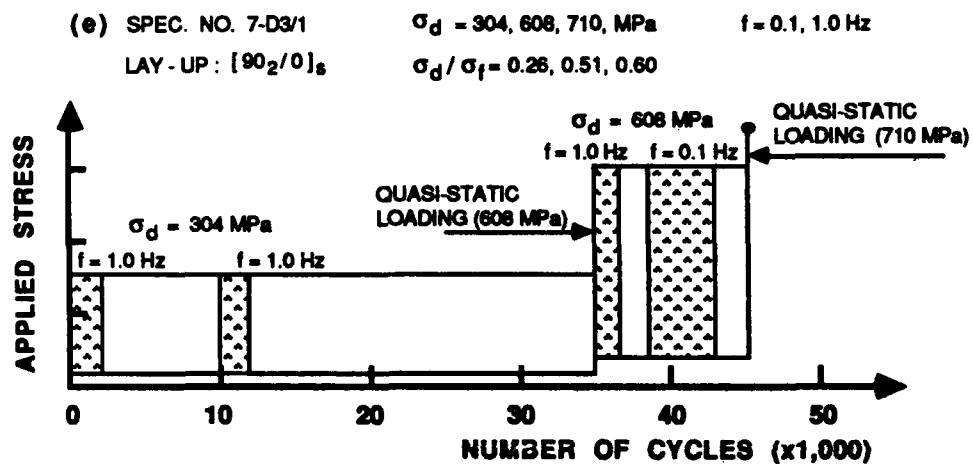
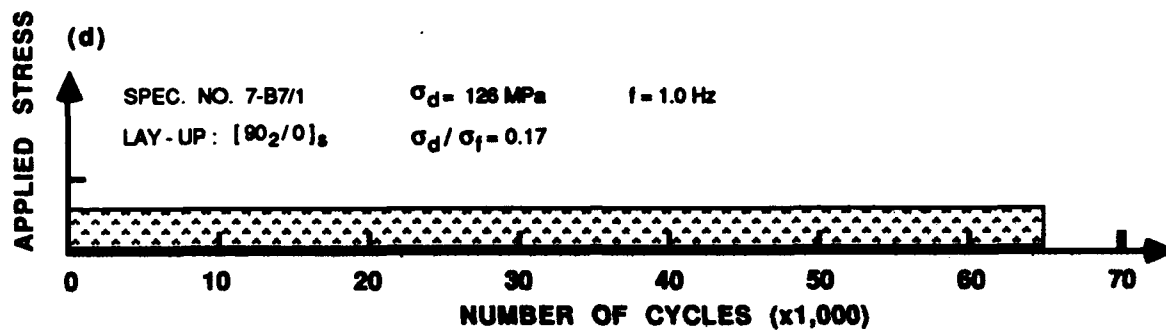


Figure 6.1. Continued.

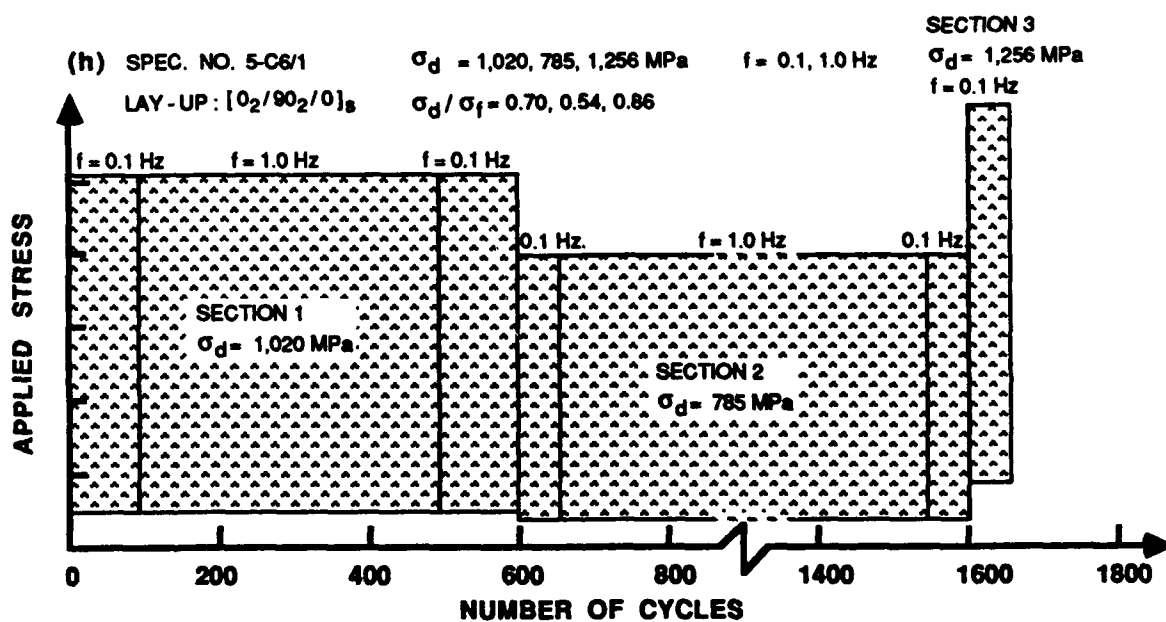
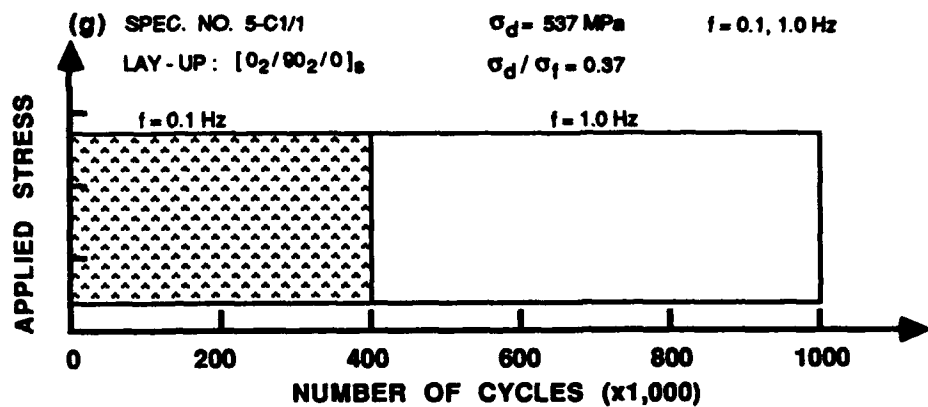


Figure 6.1. Concluded.

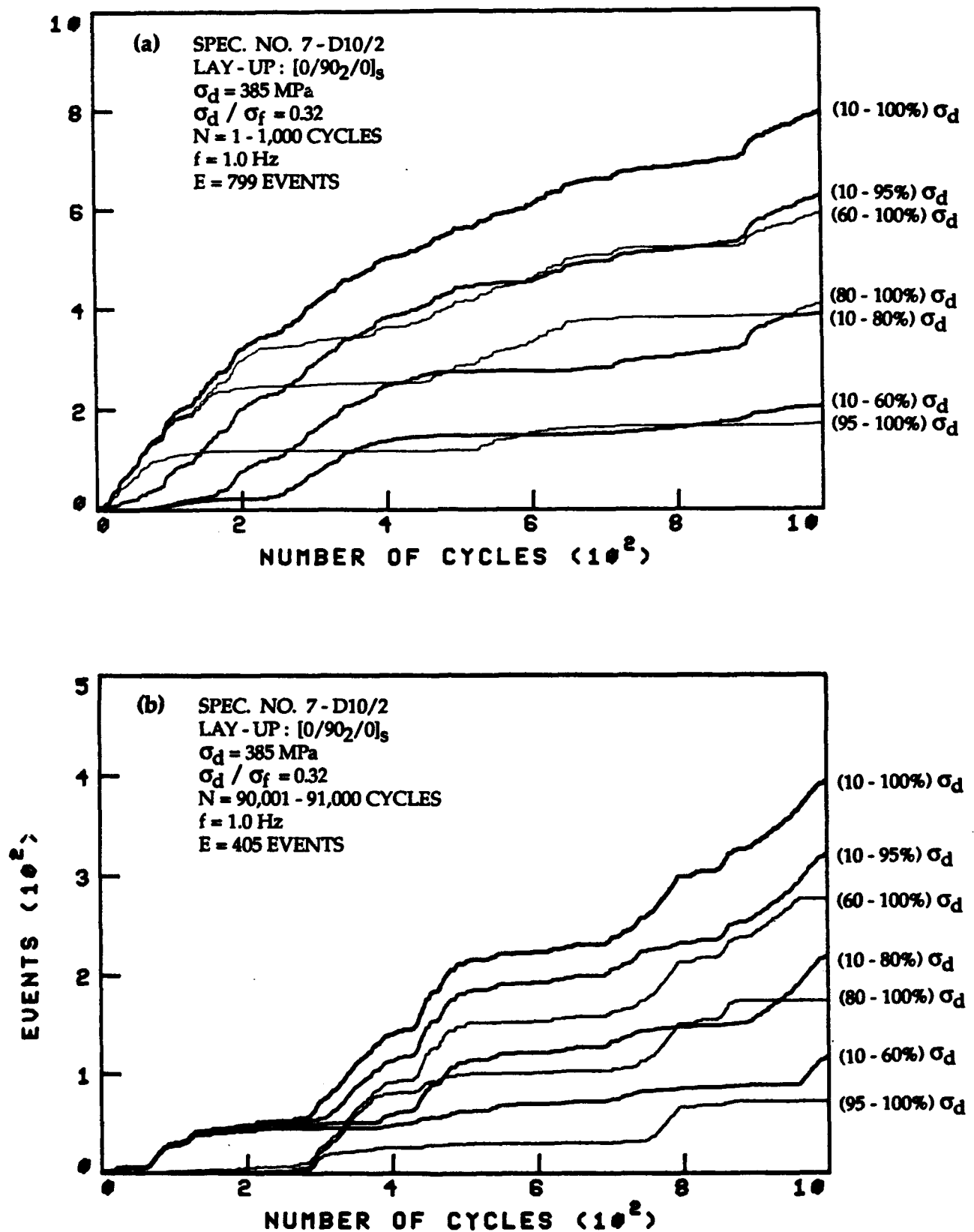


Figure 6.2. Accumulative events as a function of number of cycles, distinguishing among emission generated in seven different load ranges during selected periods of the fatigue loading of five representative specimens (results recorded with the D/E AE system). Most of the events occur at the lower load ranges.

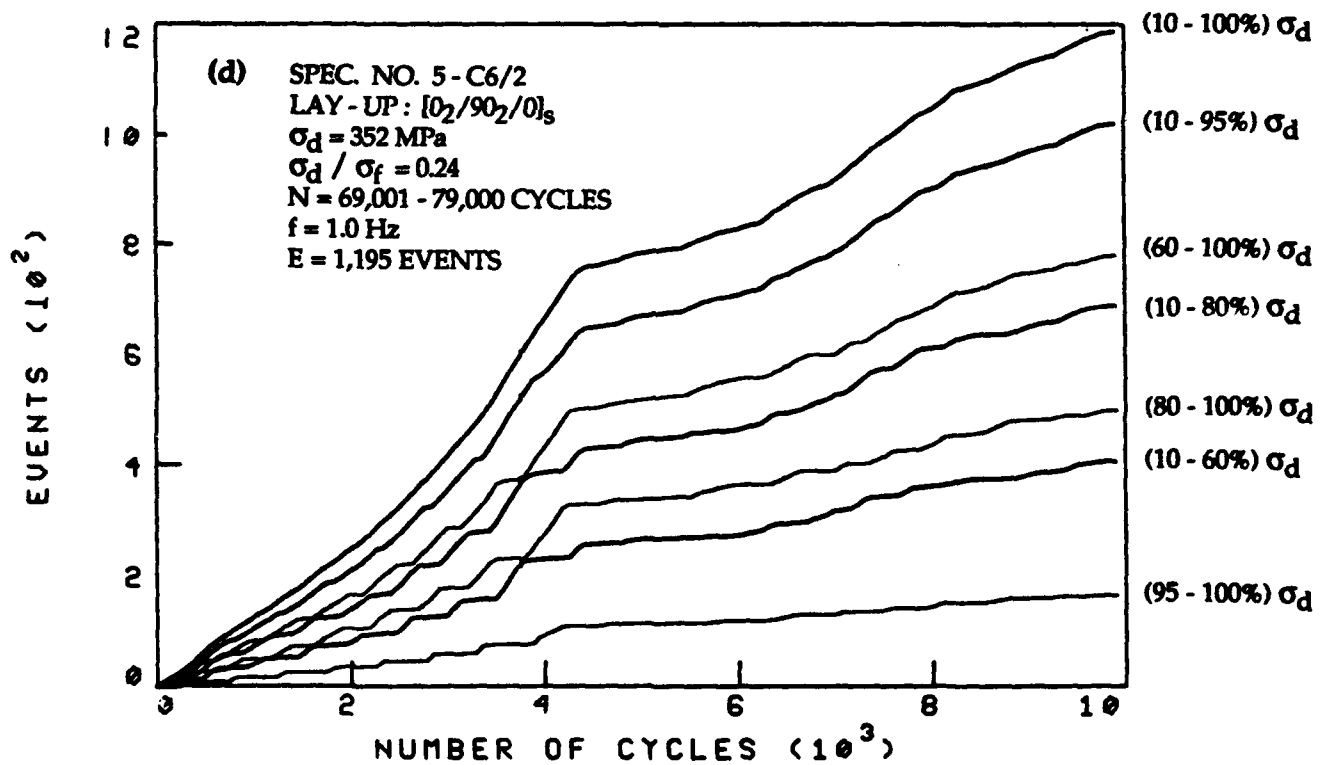
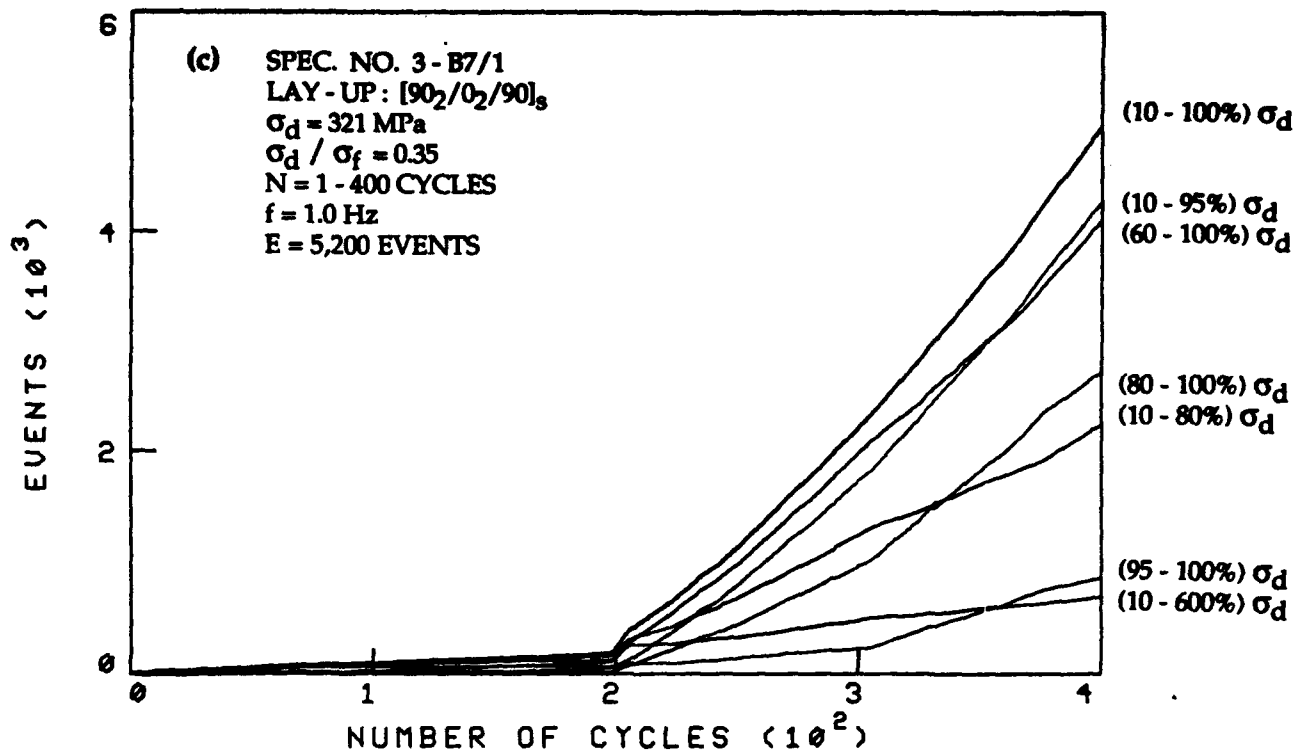


Figure 6.2. Continued.

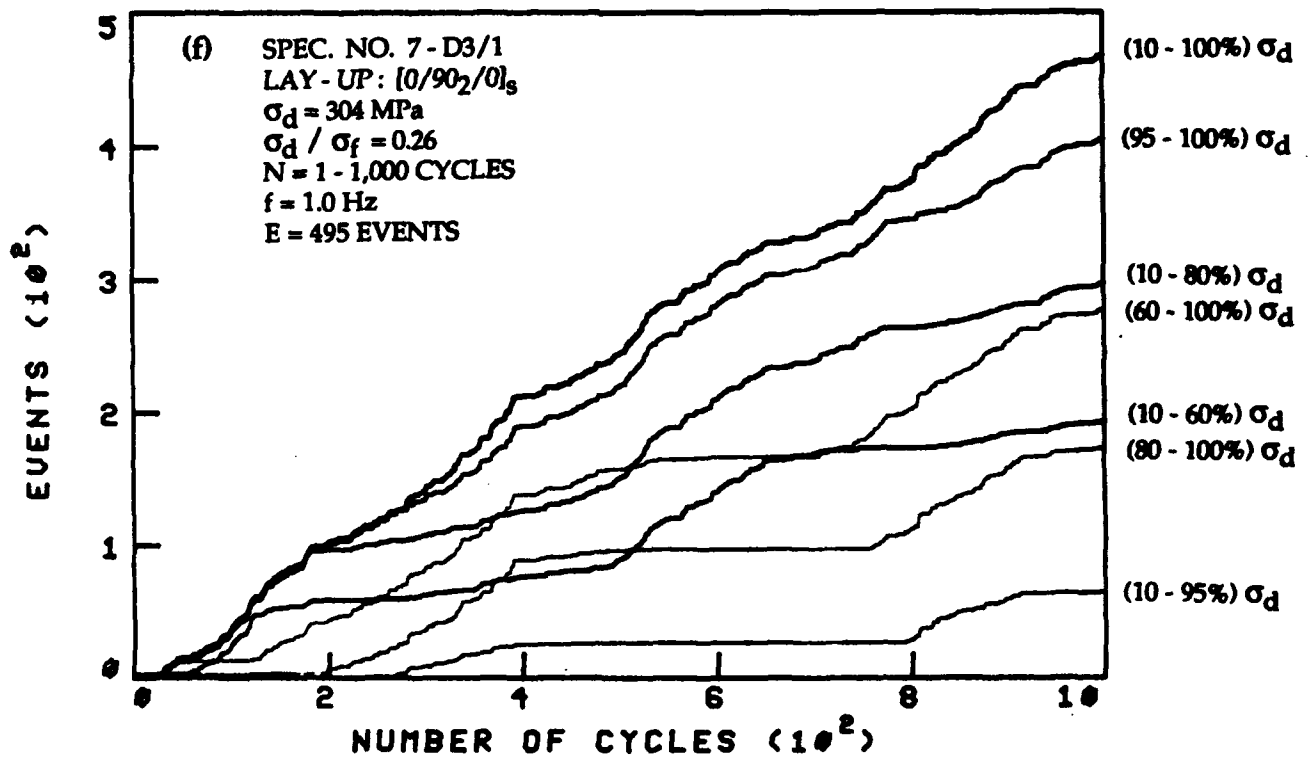
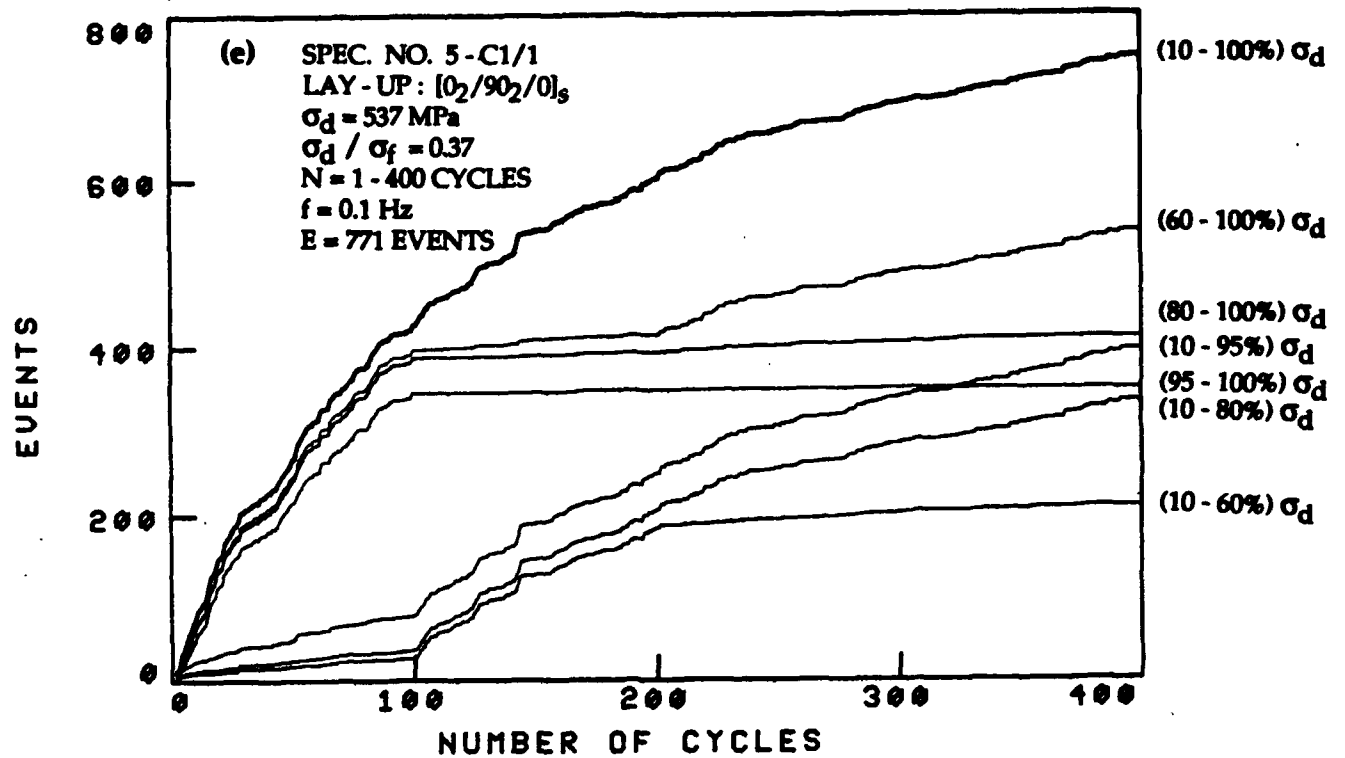


Figure 6.2. Concluded.

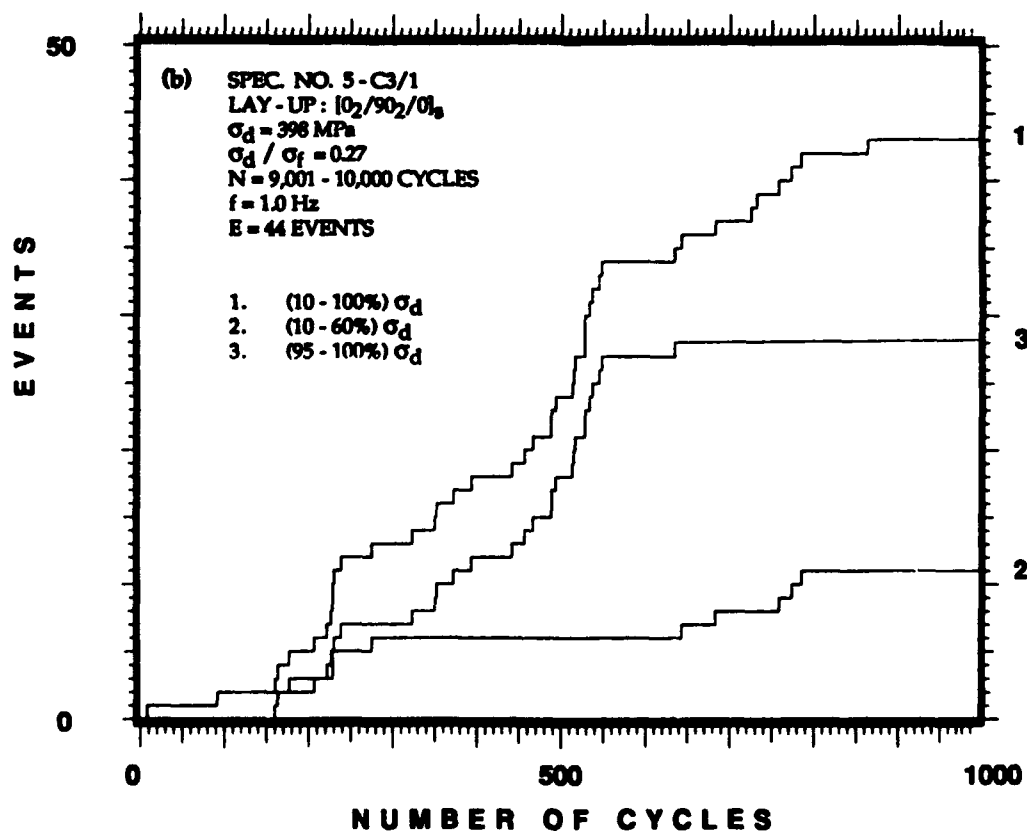
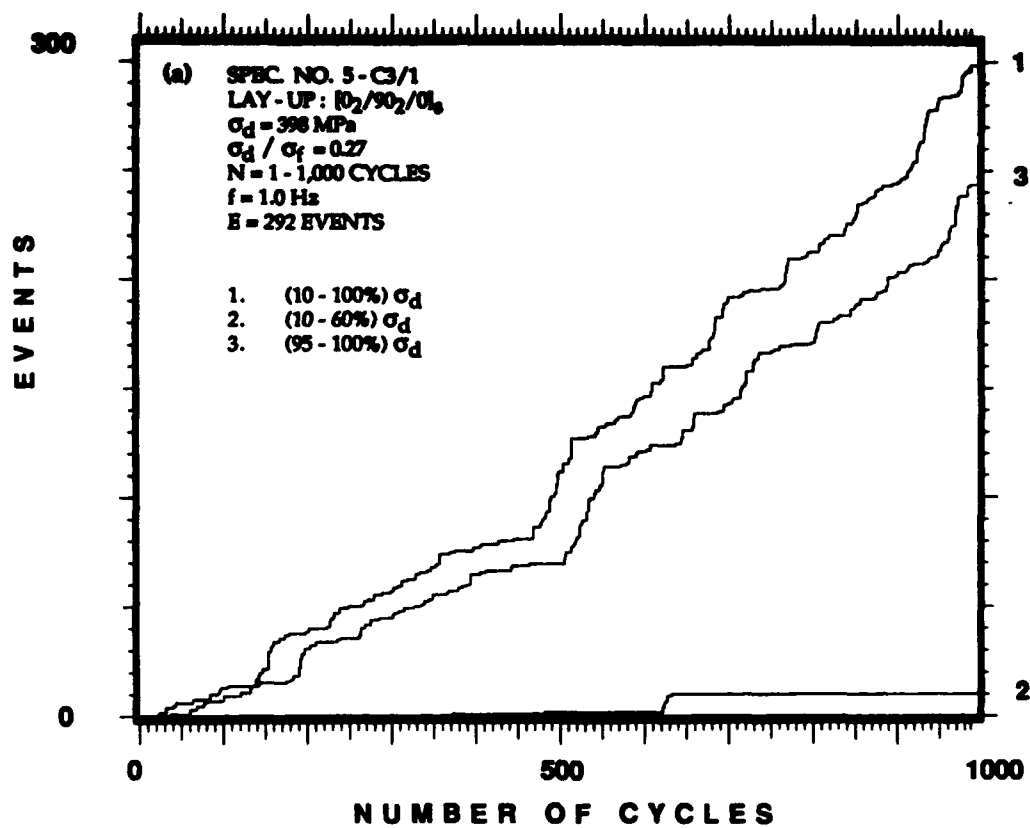


Figure 6.3. Accumulative events as a function of number of cycles, distinguishing among emission generated in three different load ranges during selected periods of the fatigue loading of four representative specimens (results recorded with the PAC AE system). Most of the events occur at the lower load ranges.

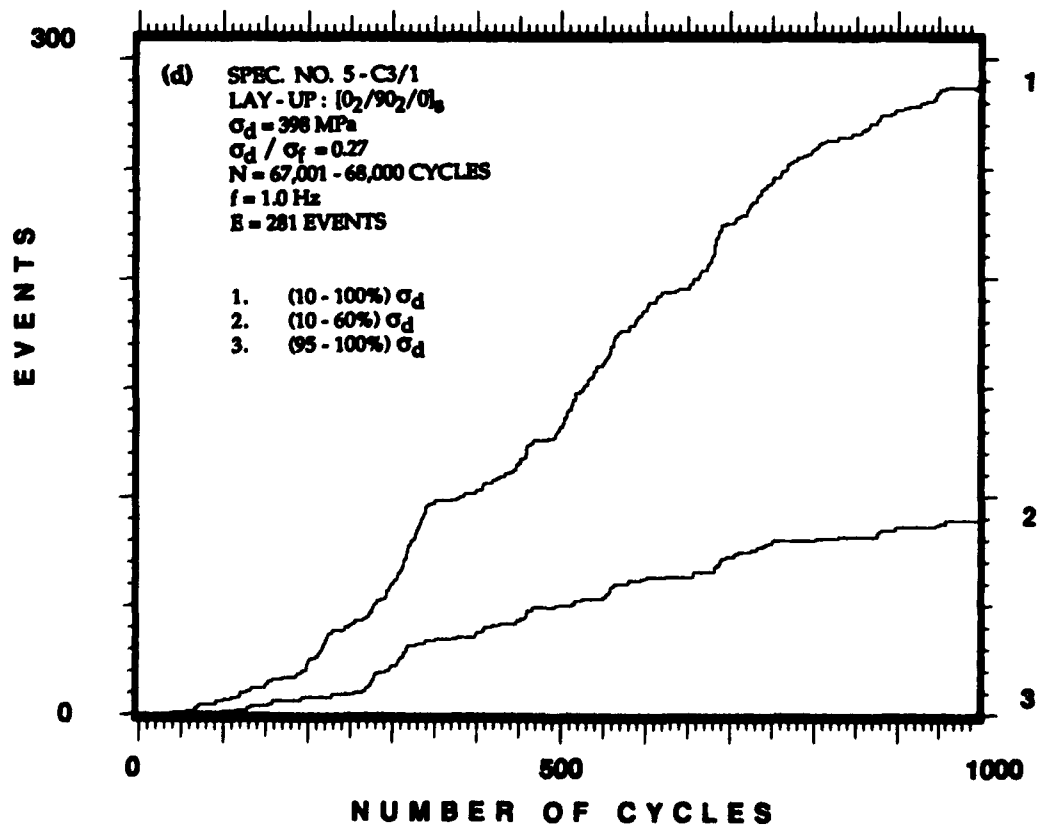
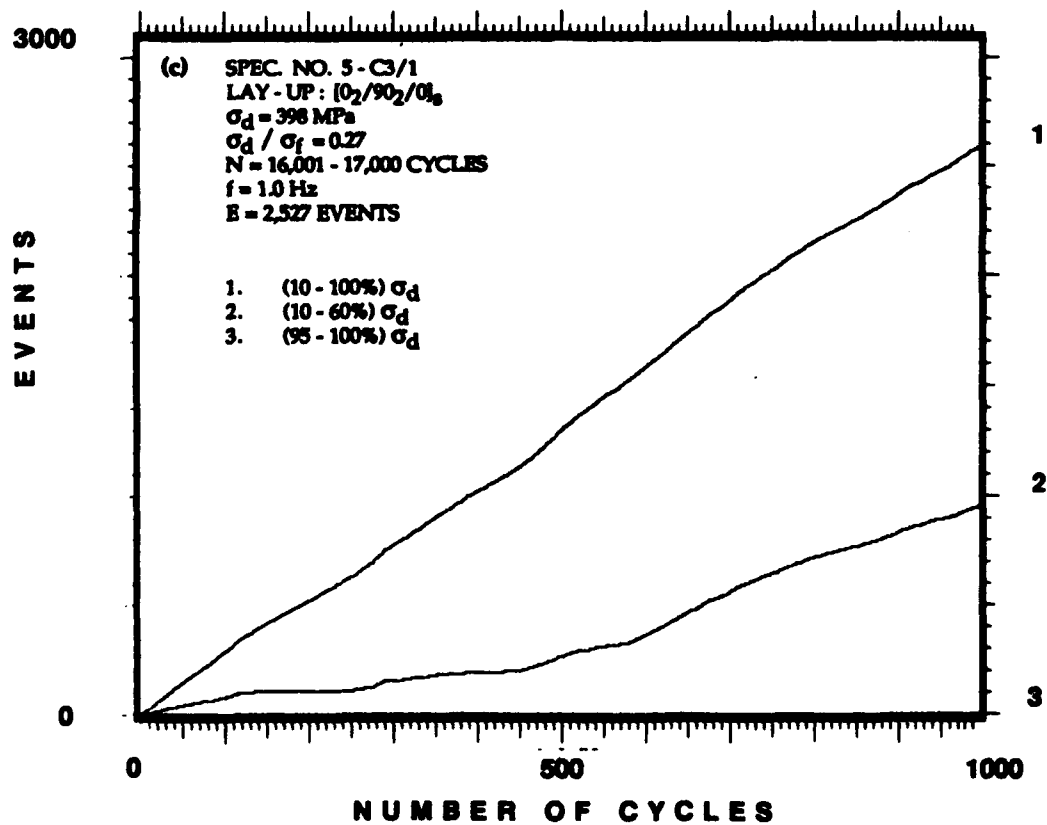


Figure 6.3. Continued.

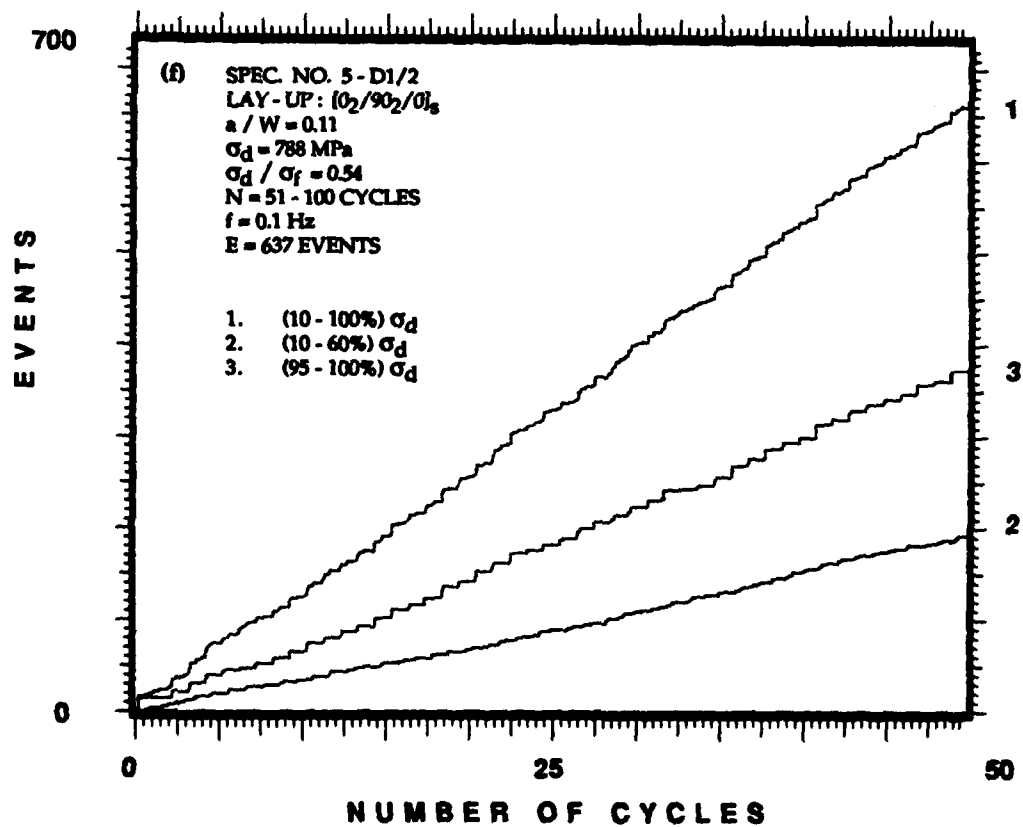
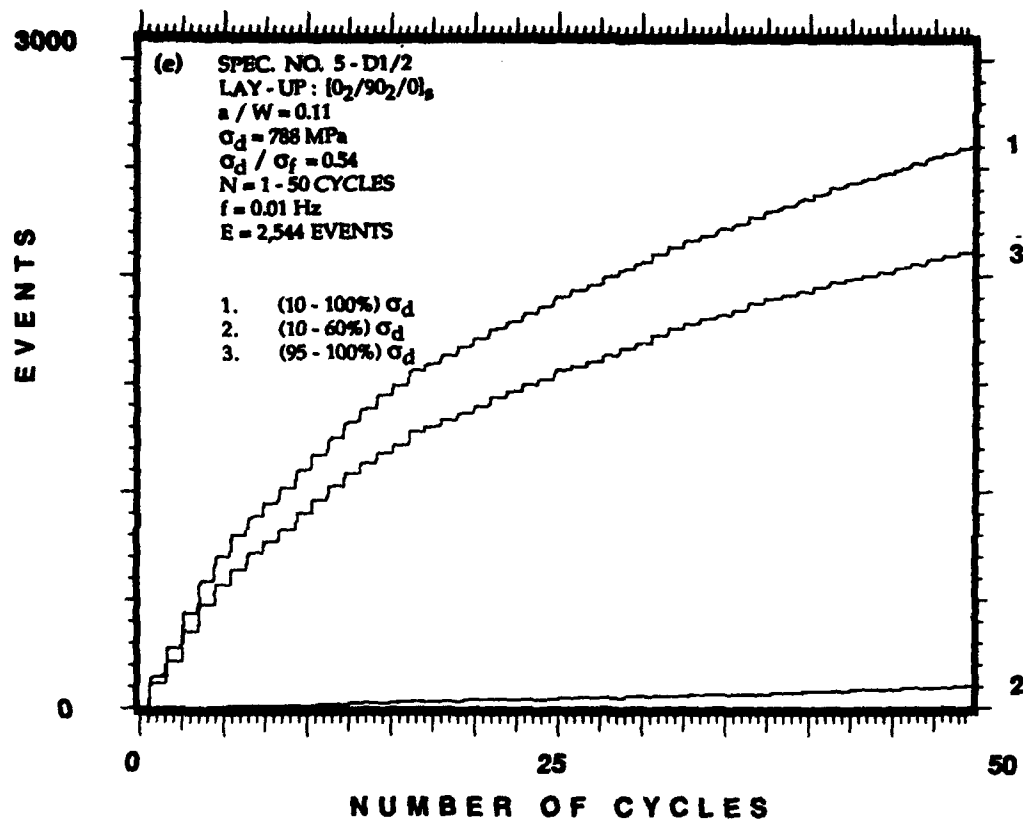


Figure 6.3. Continued.

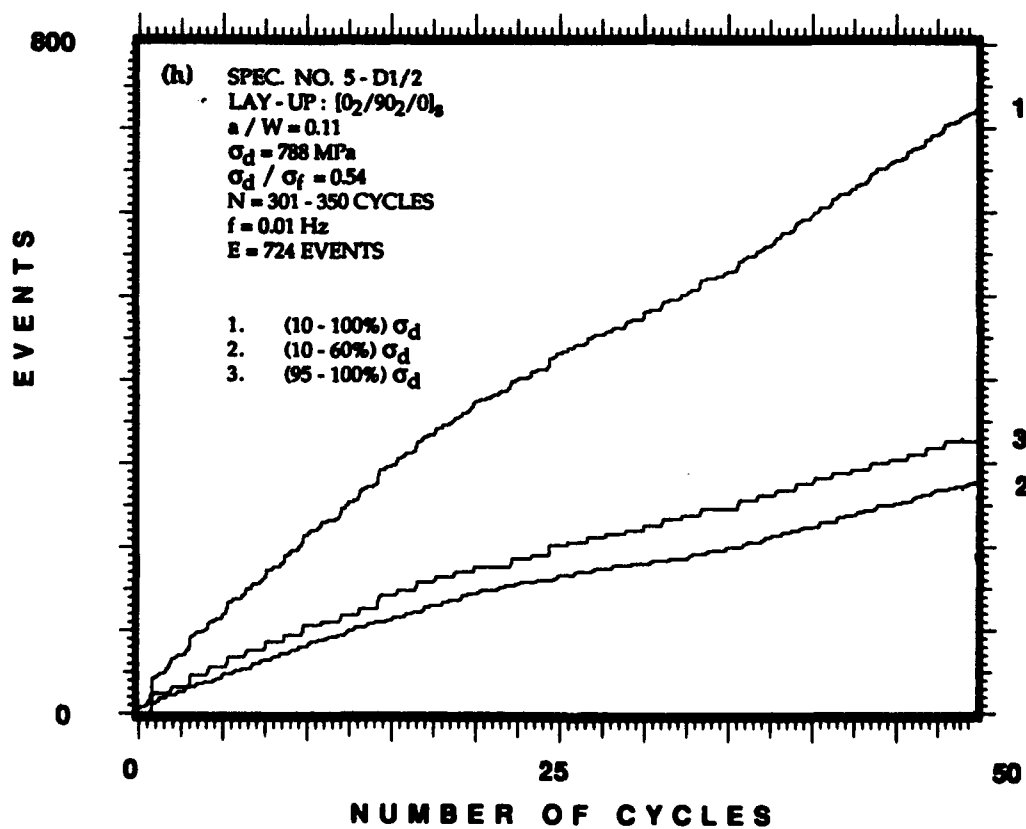
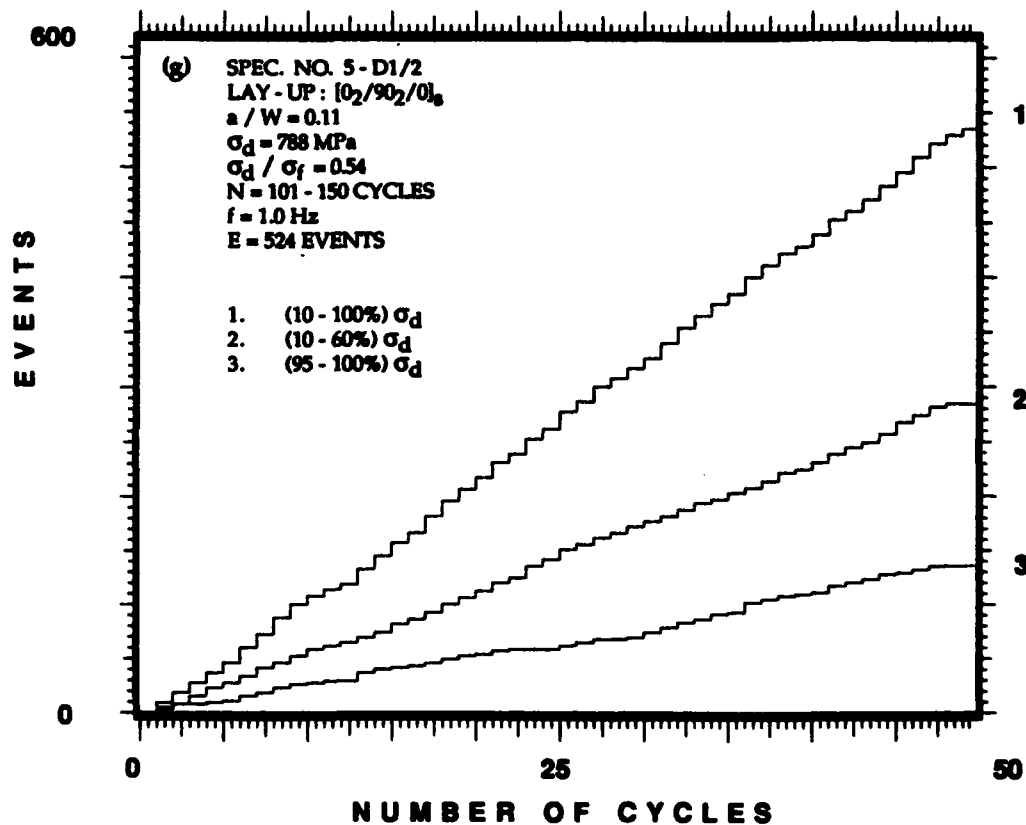


Figure 6.3. Continued.

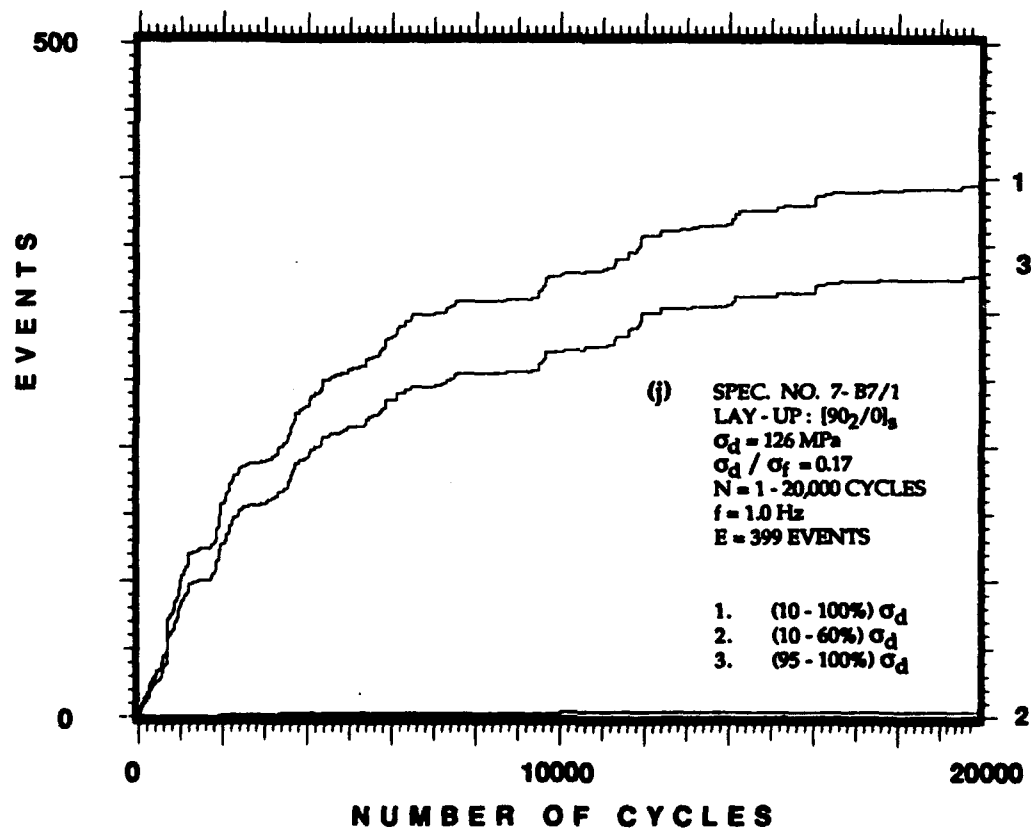
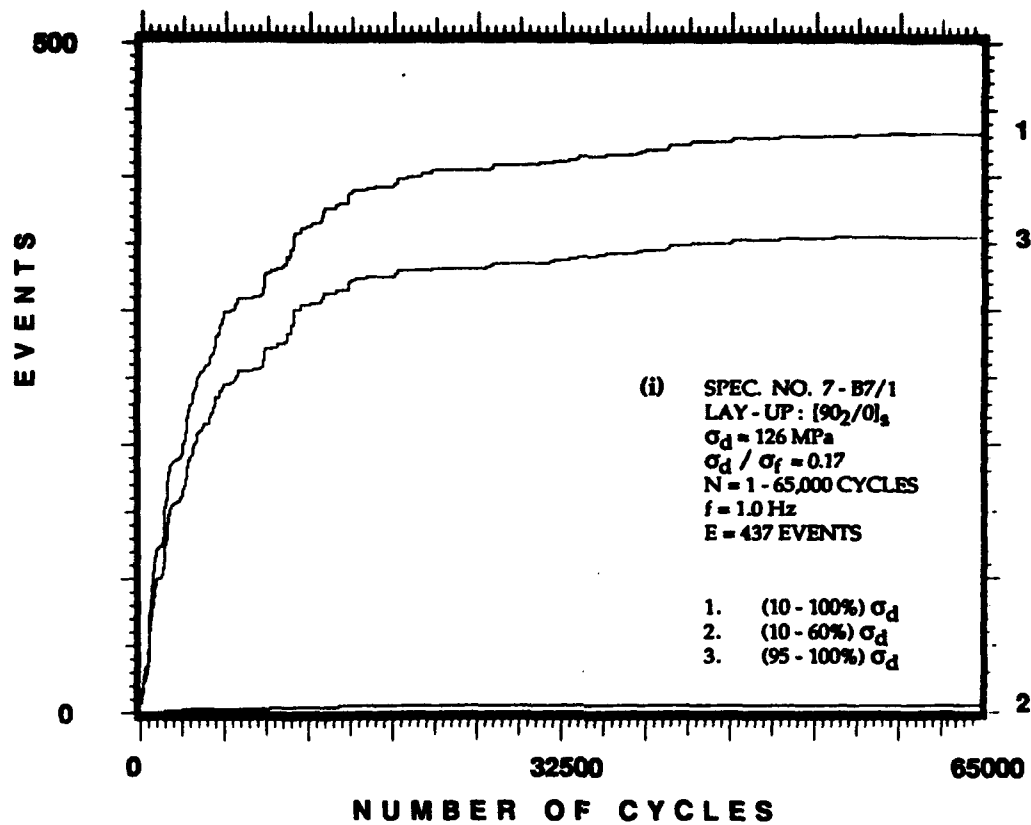


Figure 6.3. Continued.

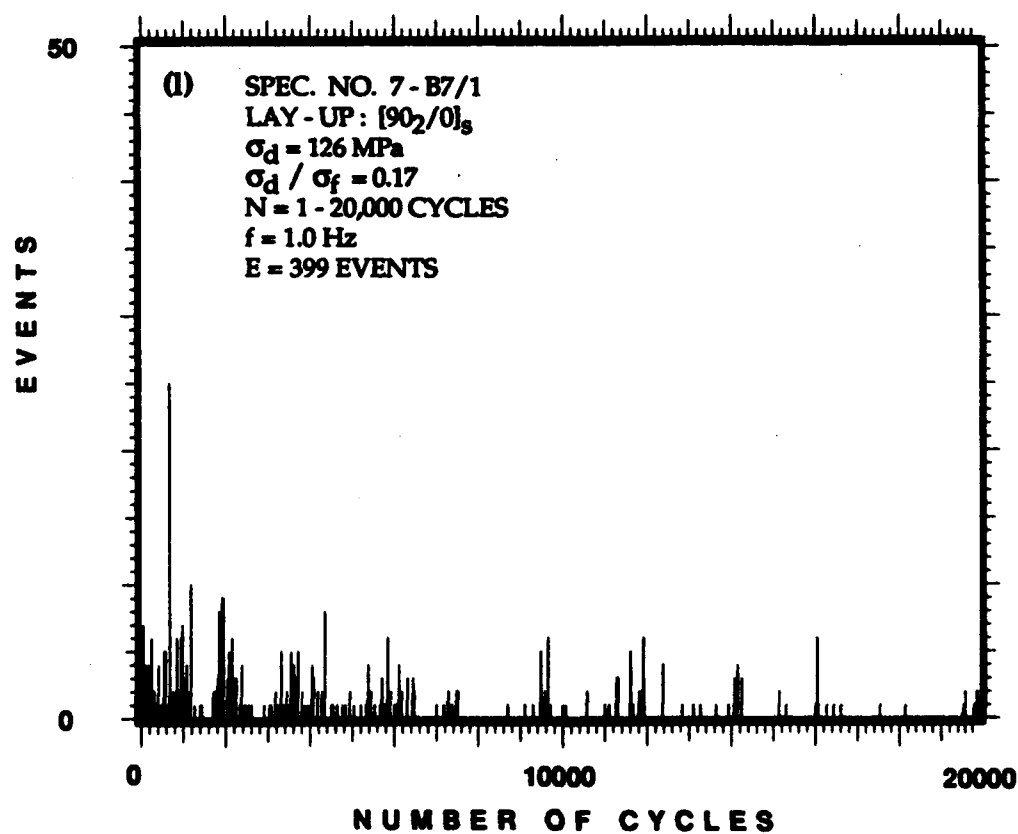
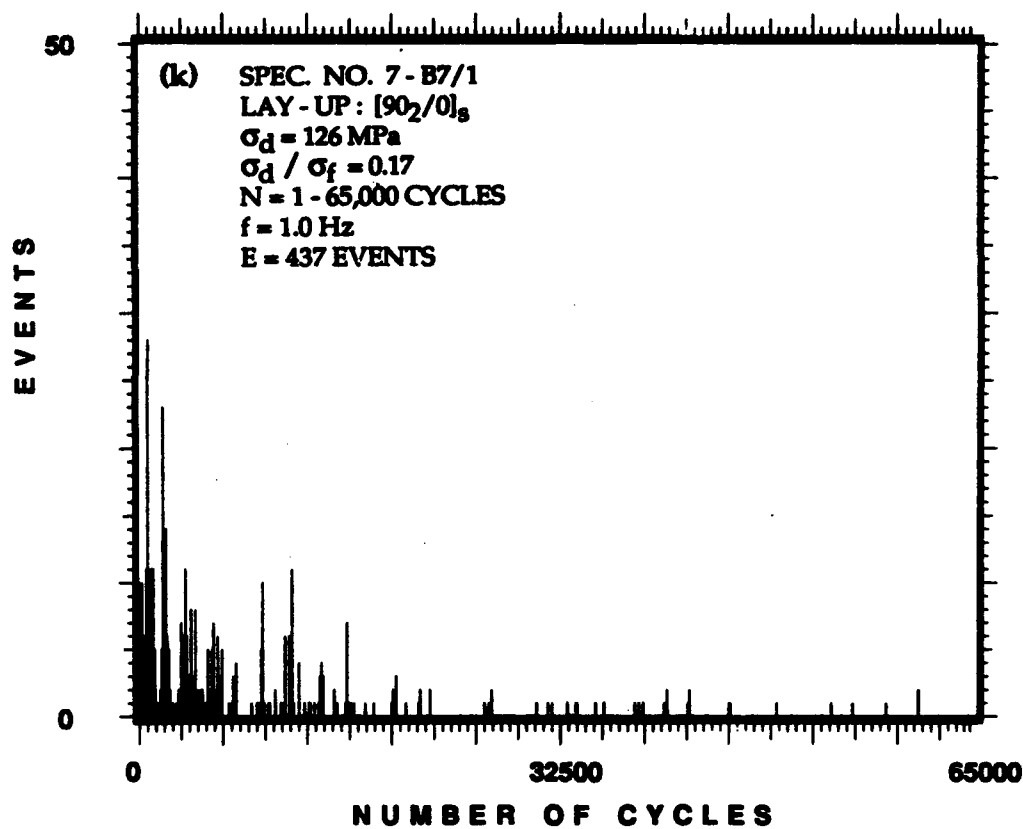


Figure 6.3. Concluded.

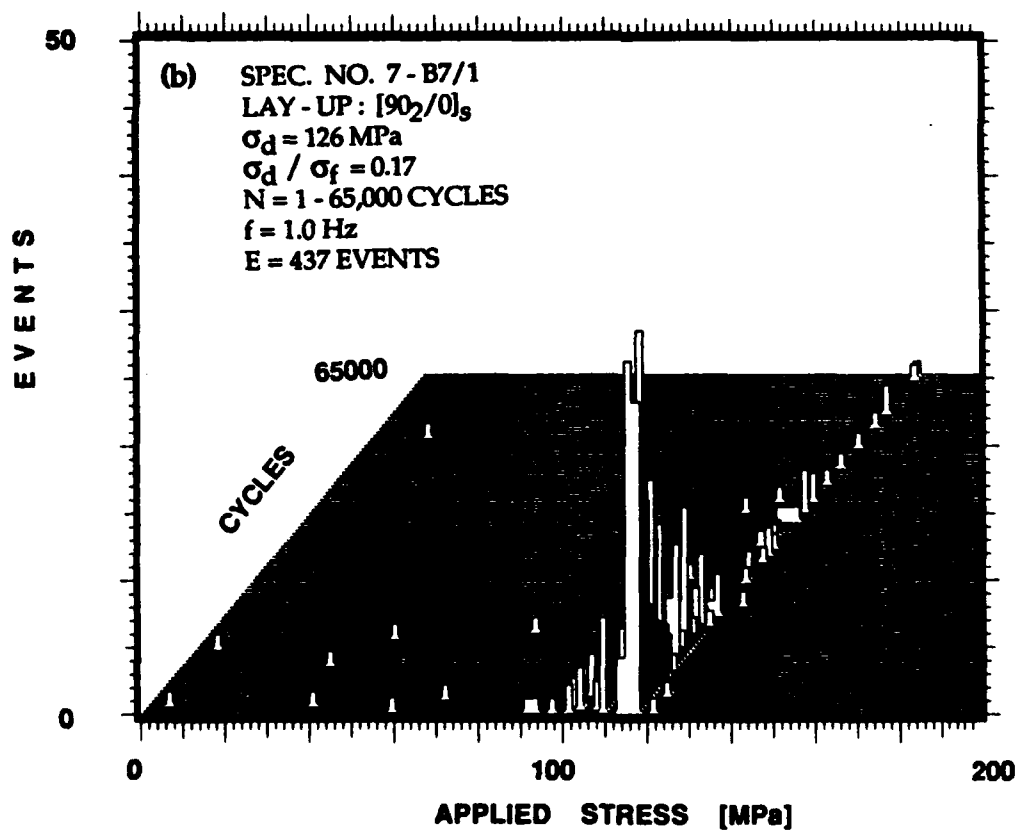
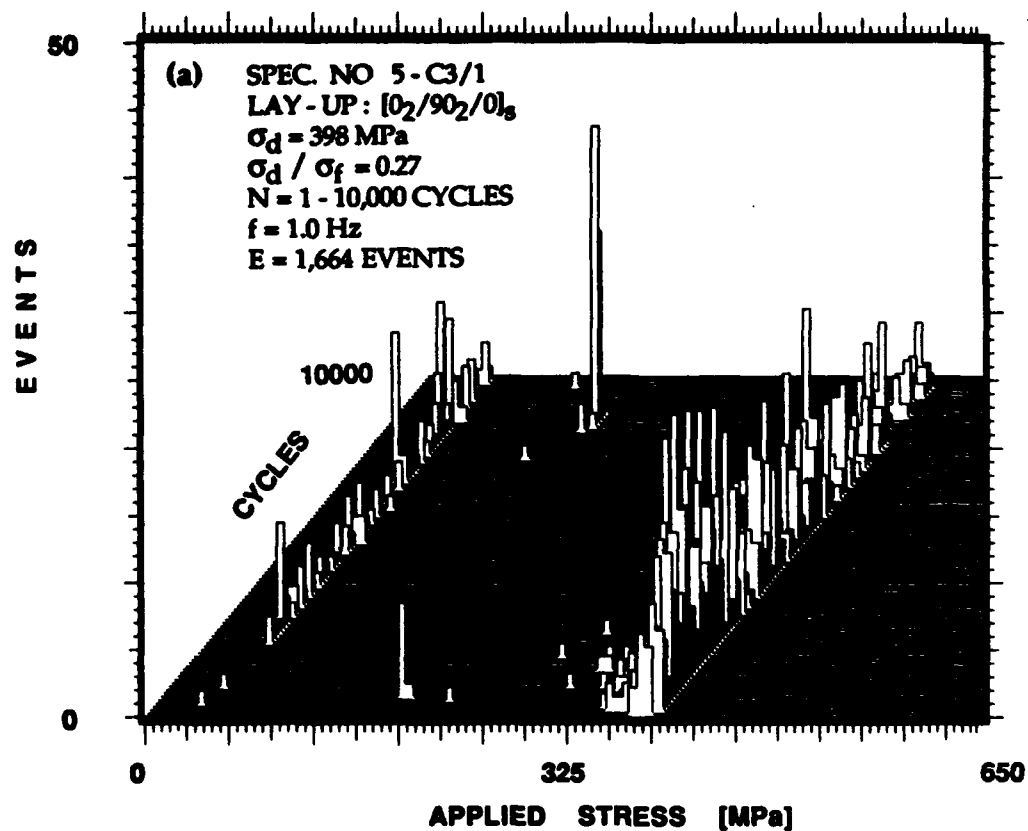


Figure 6.4. Three-dimensional plots of load and location distribution histograms of events recorded for two selected specimens.

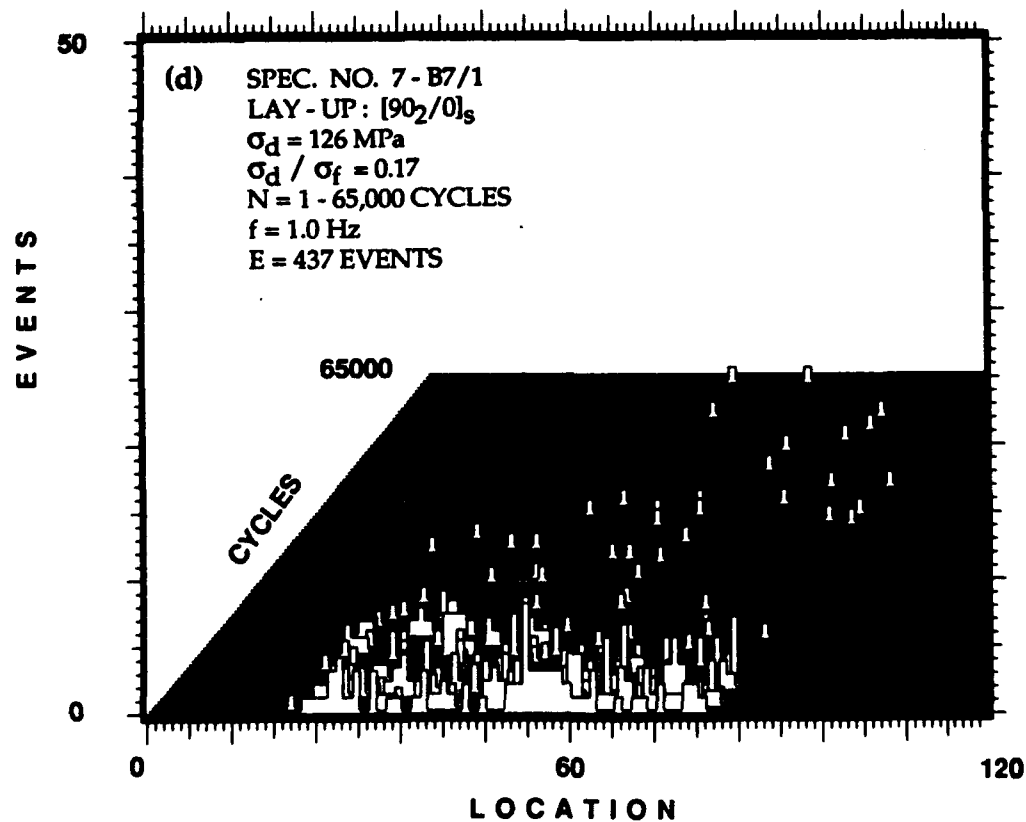
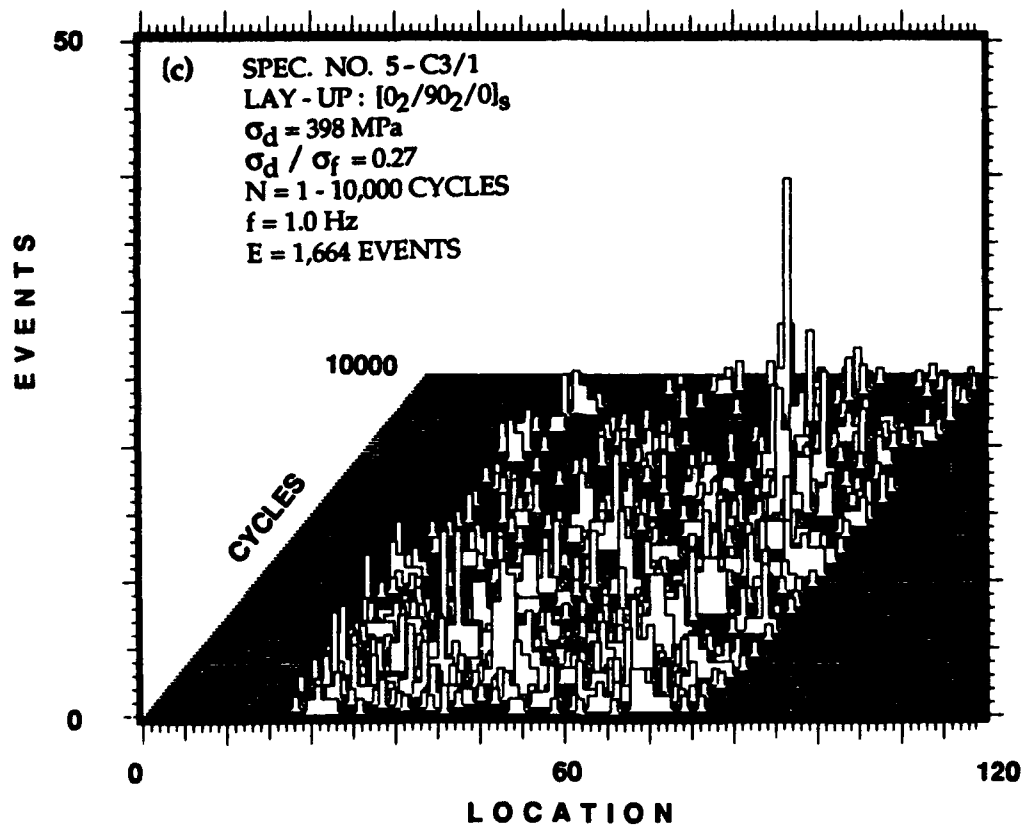


Figure 6.4. Concluded.

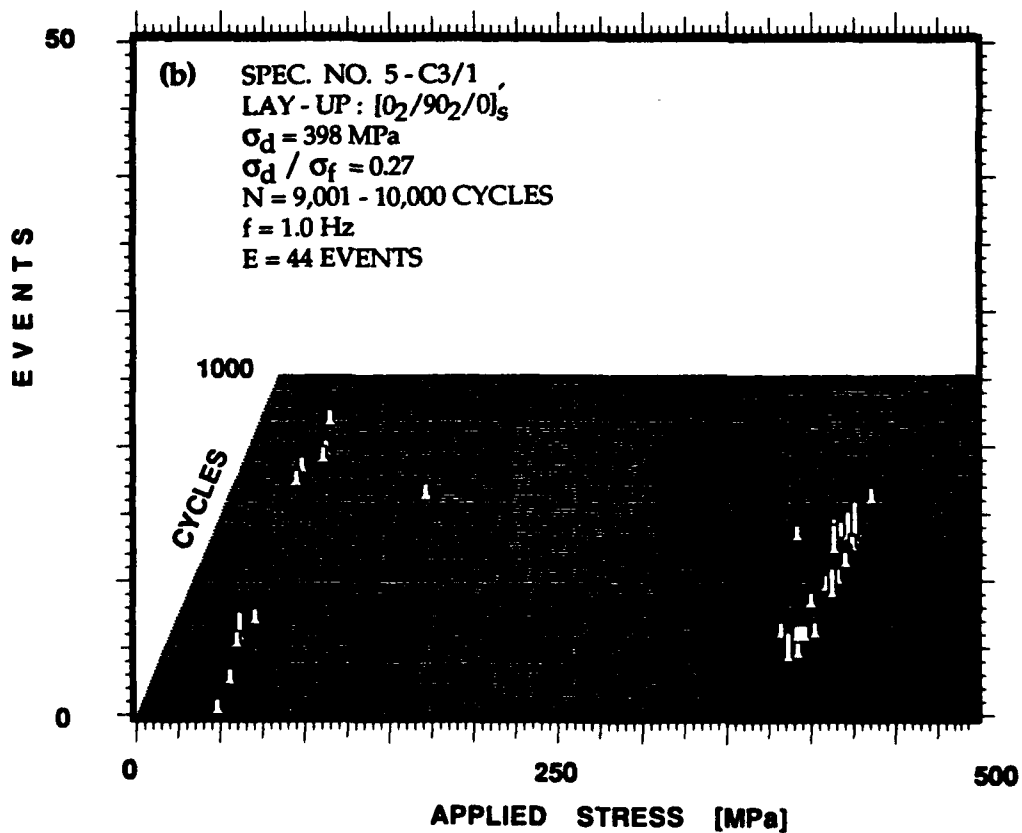
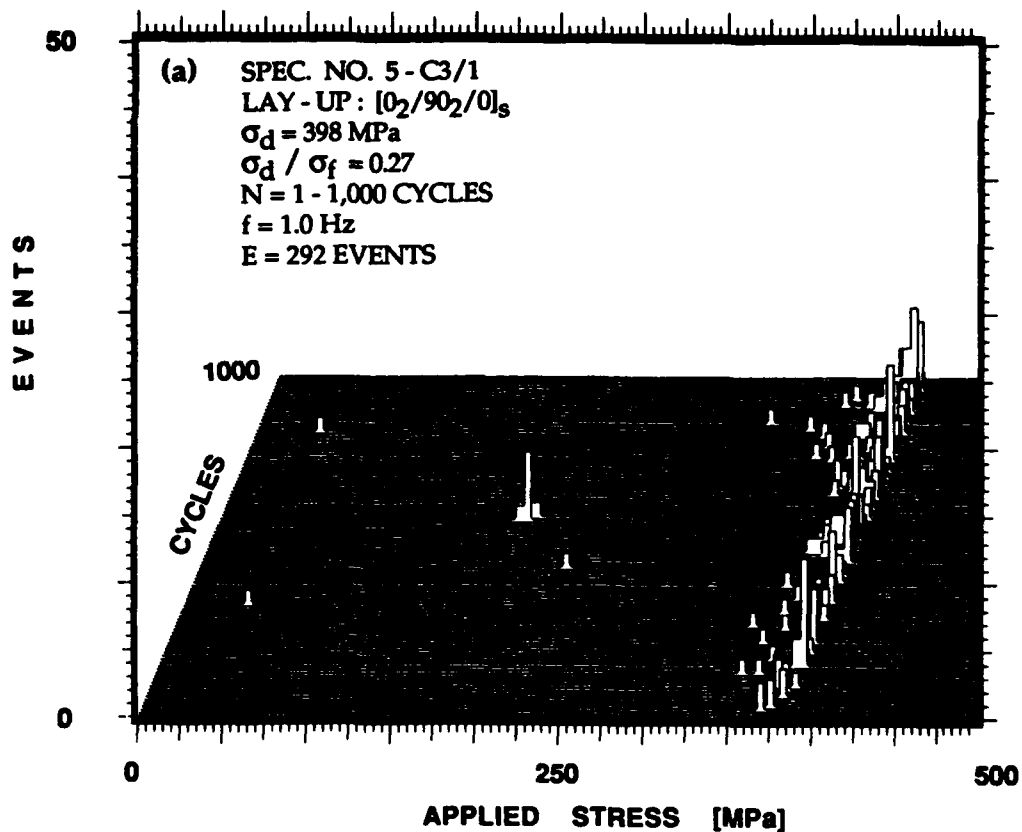


Figure 6.5. Three dimensional plots showing events as a function of load, generated during four different periods of the fatigue loading for three selected specimens. Initially, most of the events occur at the upper load range. At later stages events occur repeatedly at specific and low load levels indicating friction emission.

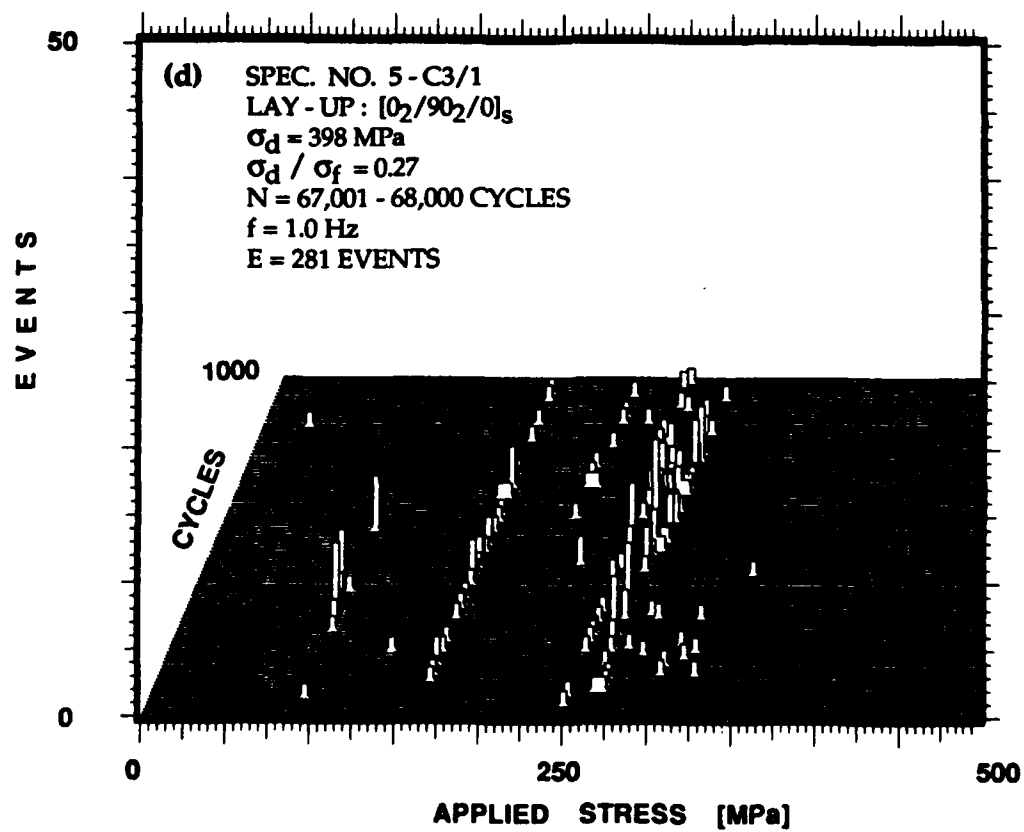
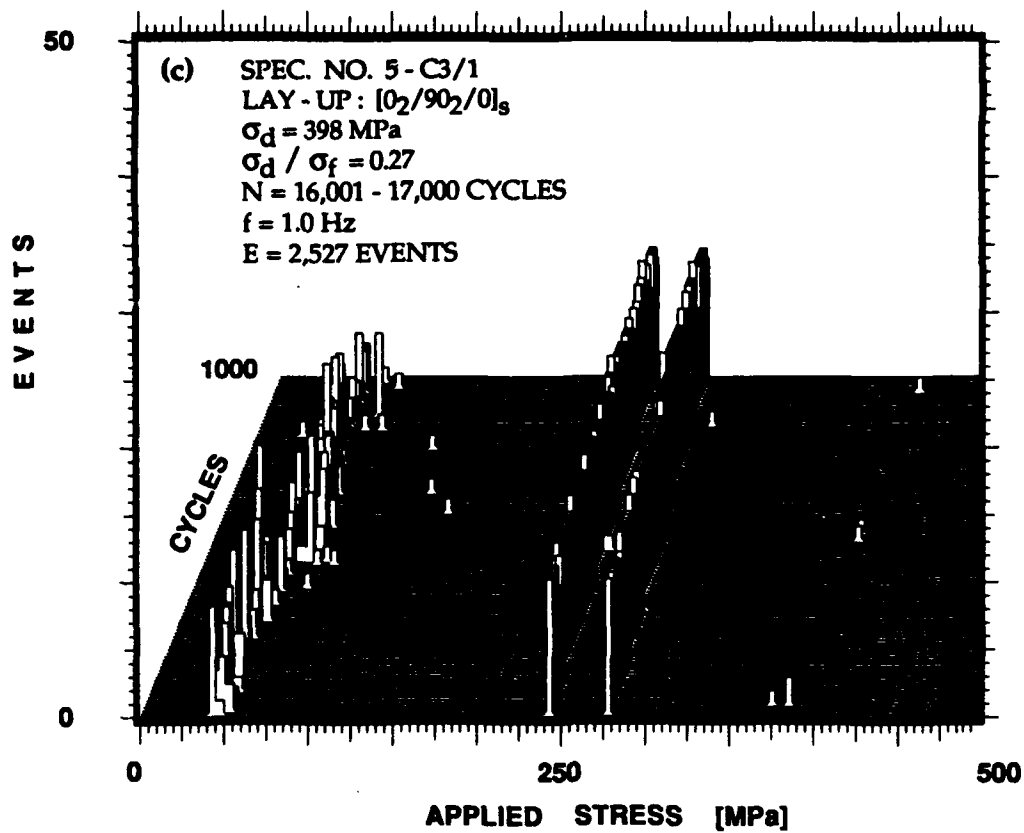


Figure 6.5. Continued.

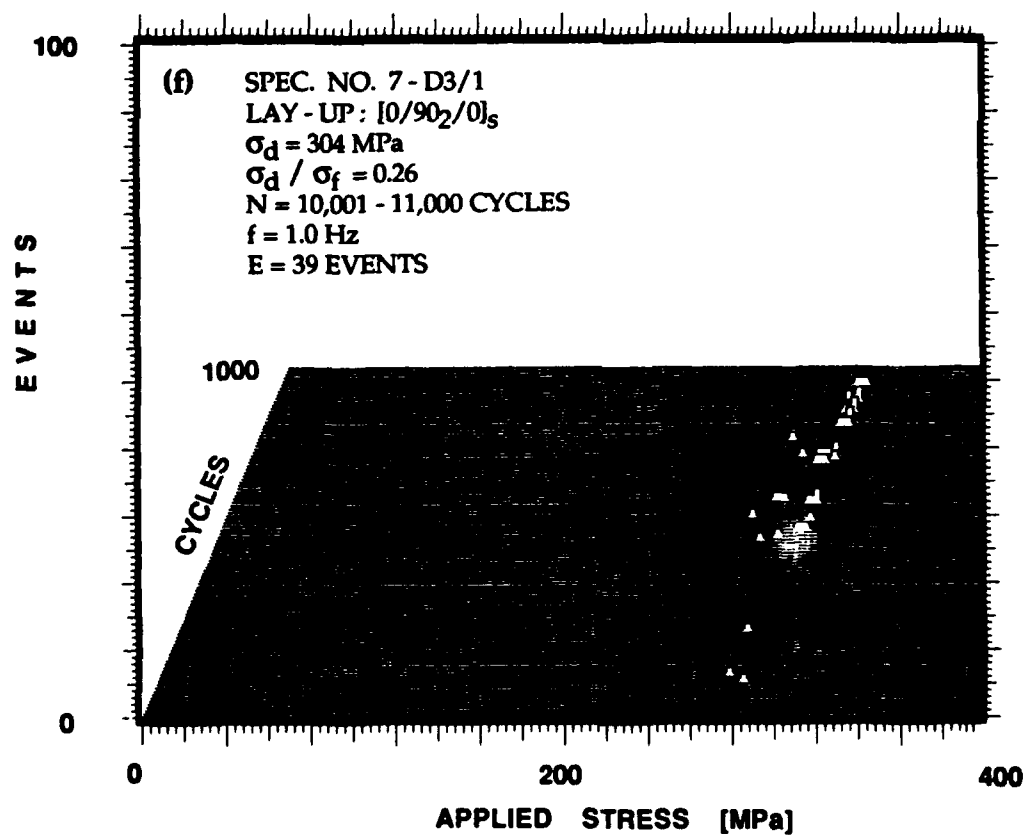
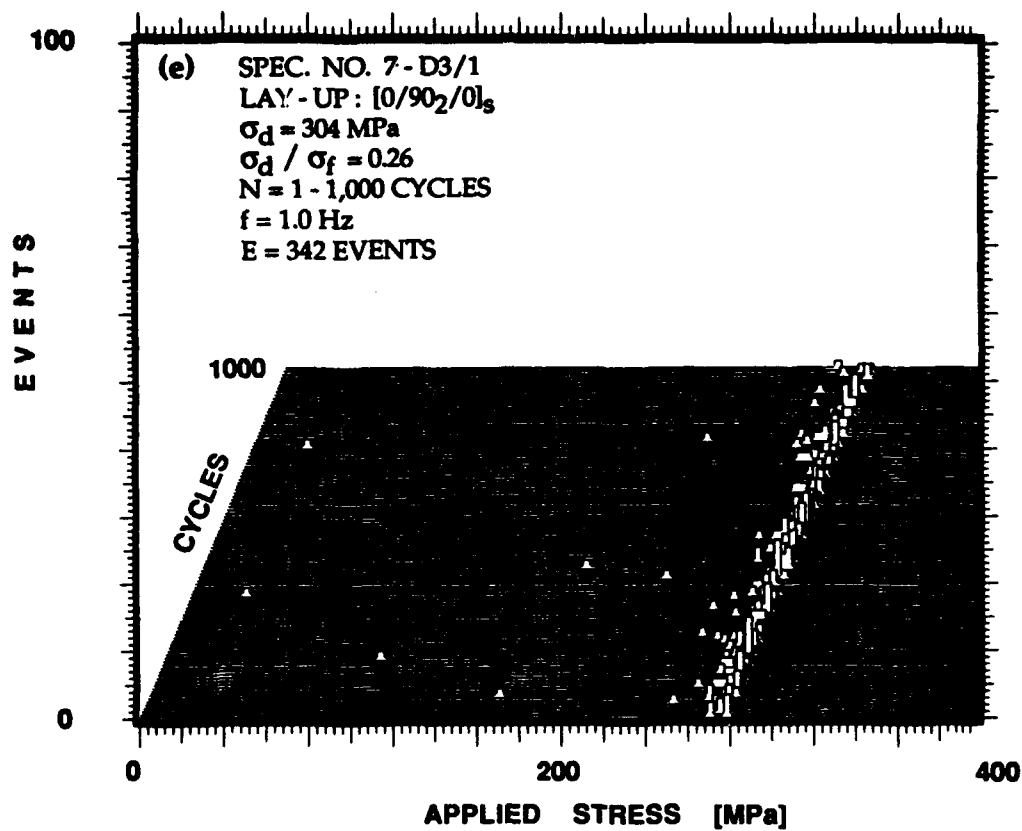


Figure 6.5. Continued.

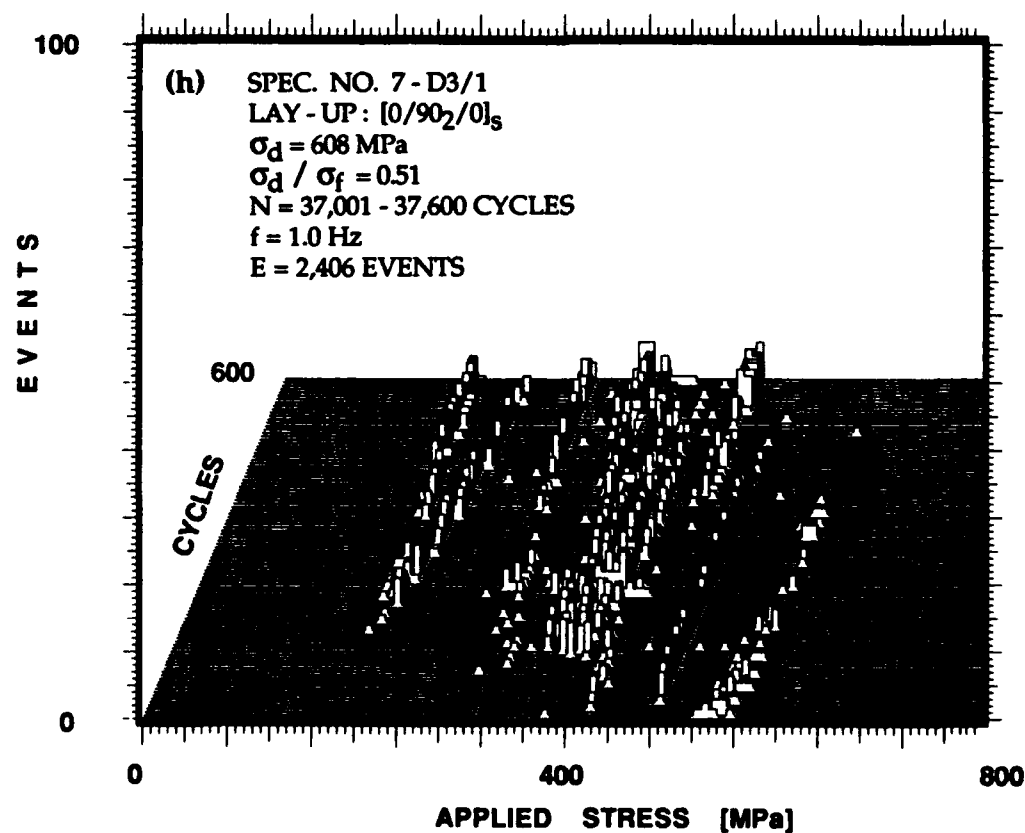
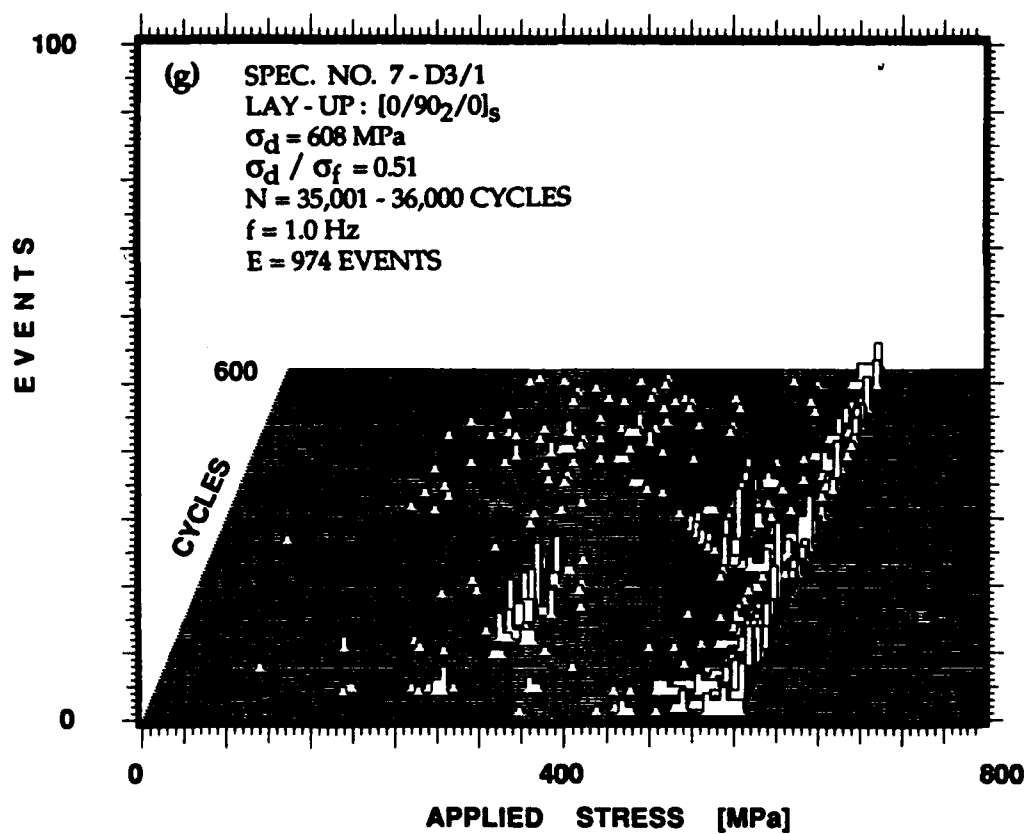


Figure 6.5. Continued.

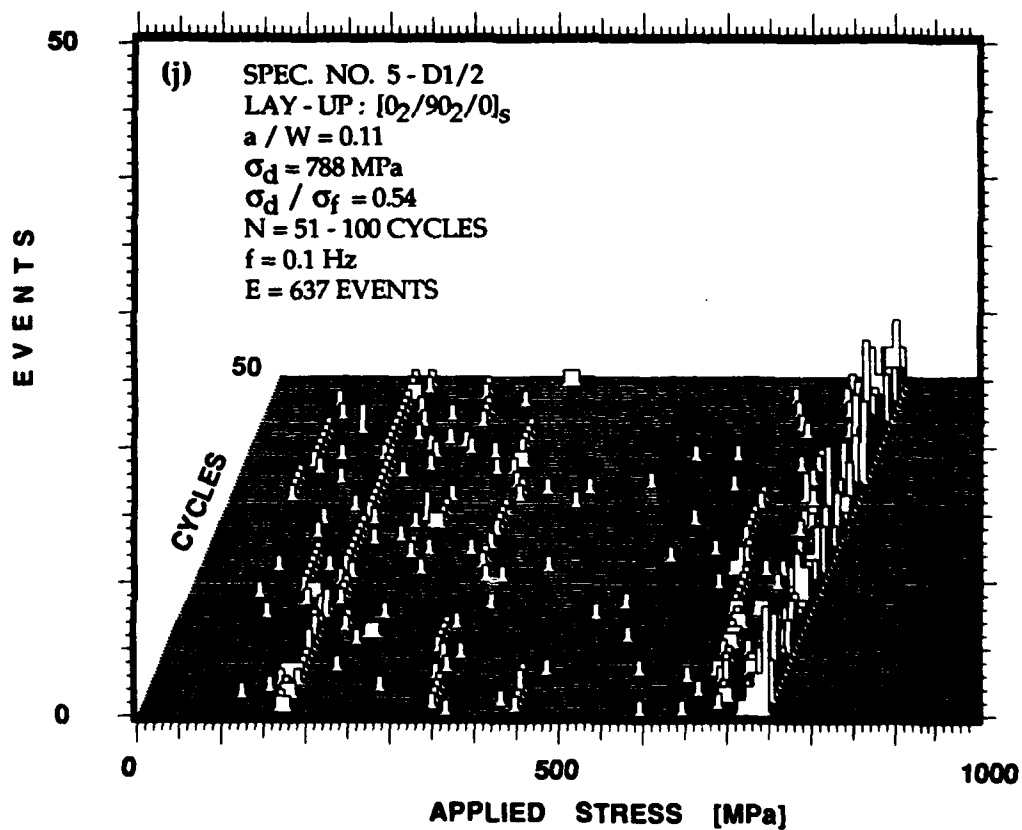
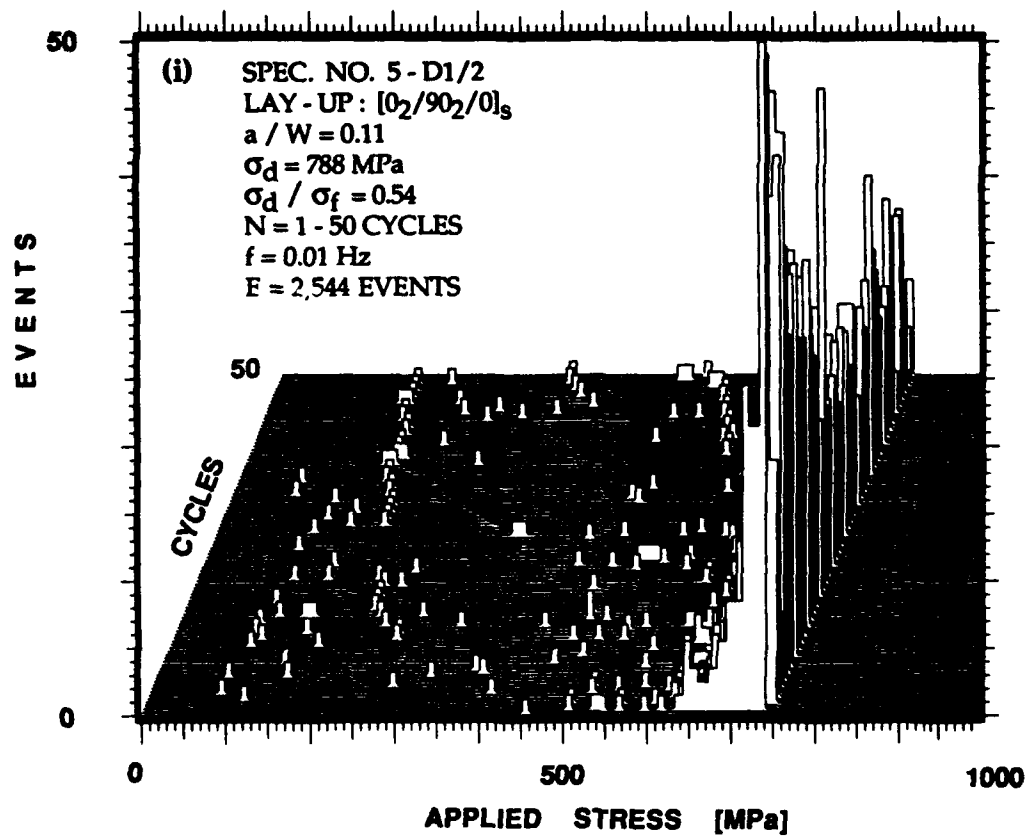


Figure 6.5. Continued.

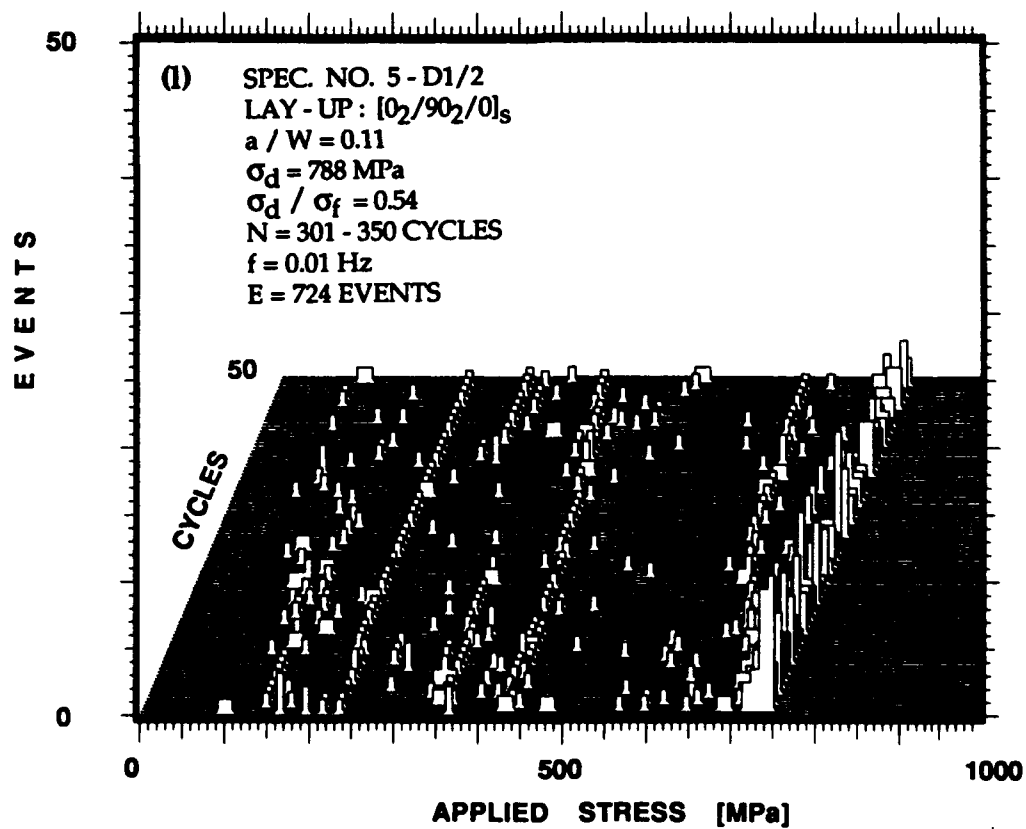
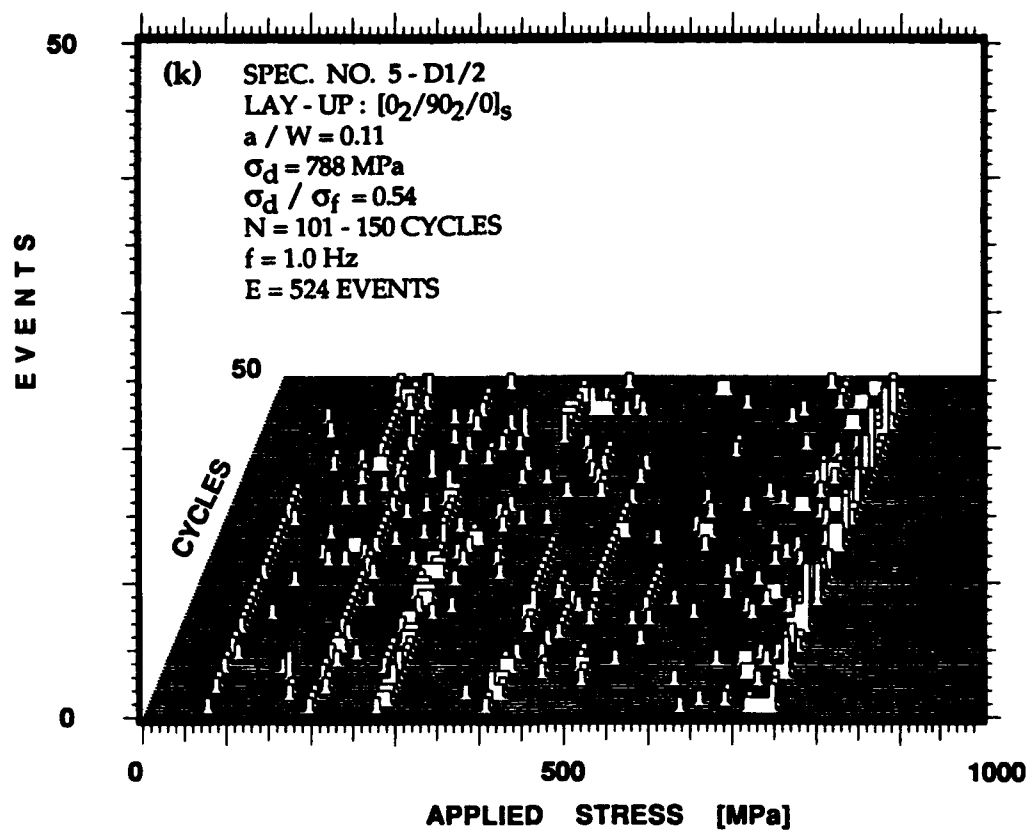


Figure 6.5. Concluded.

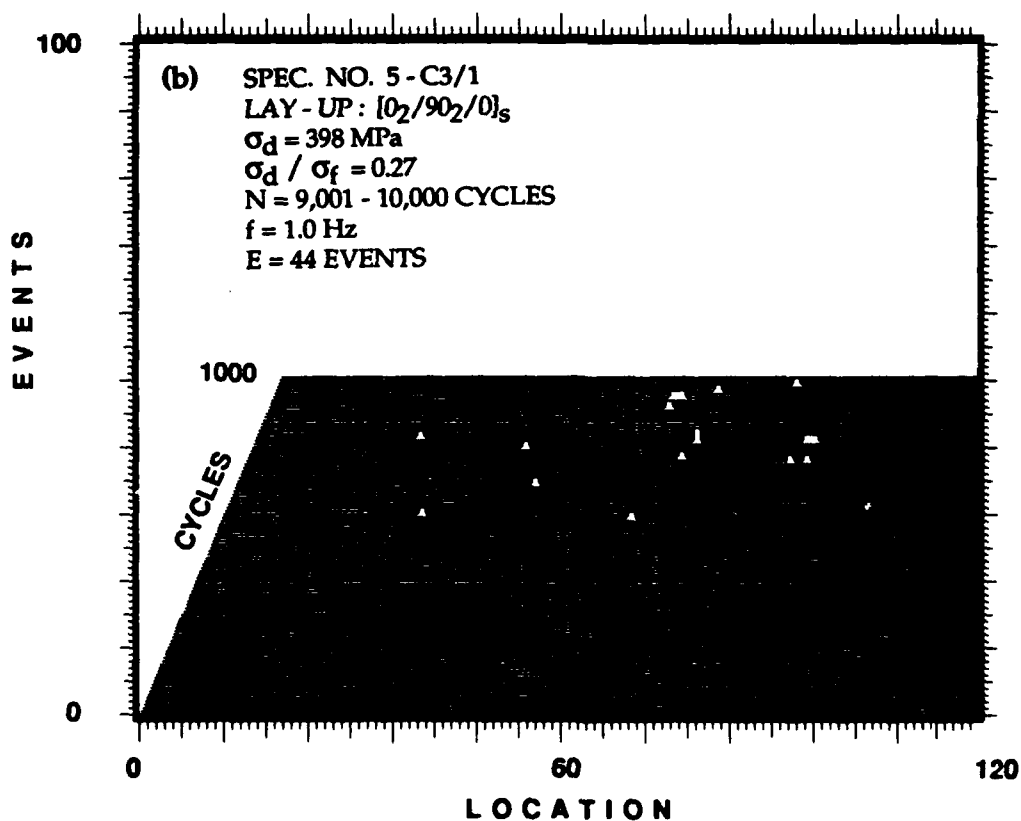
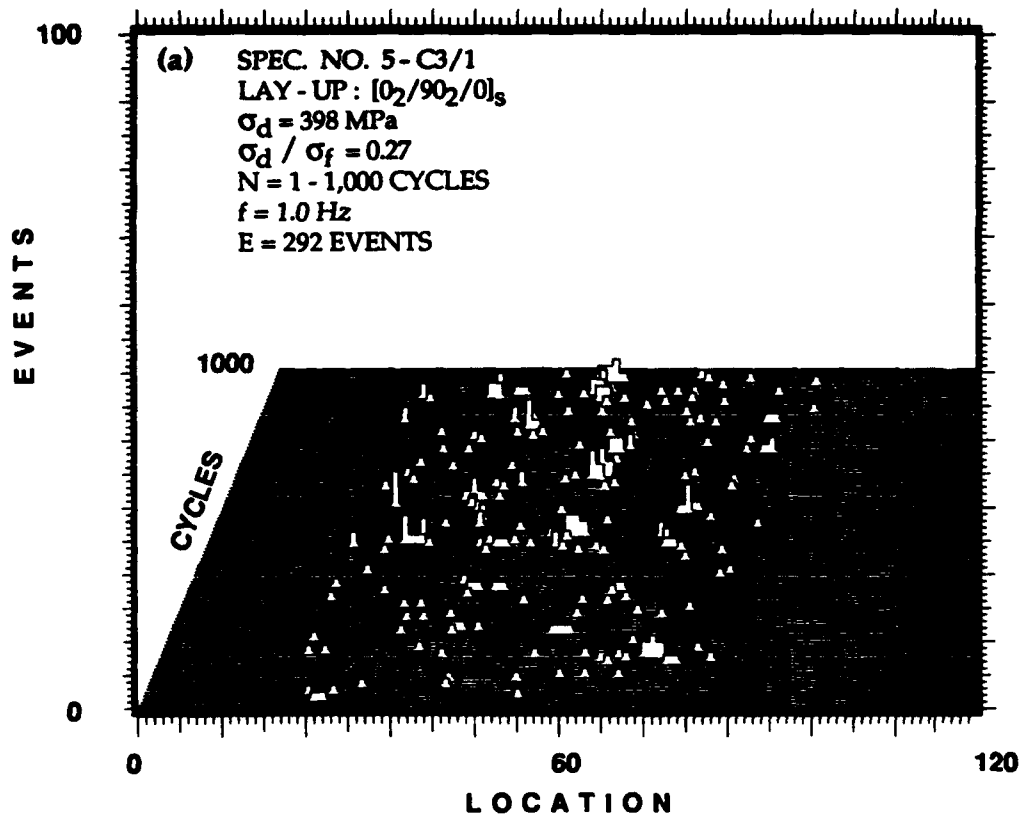


Figure 6.6. Three dimensional plots showing location distribution histograms of events generated during the same four periods of the fatigue loading and specimens shown in Figure 6.5. Initially, events occur throughout the specimens' length. At later periods, events occur repeatedly at the same locations indicating friction emission.

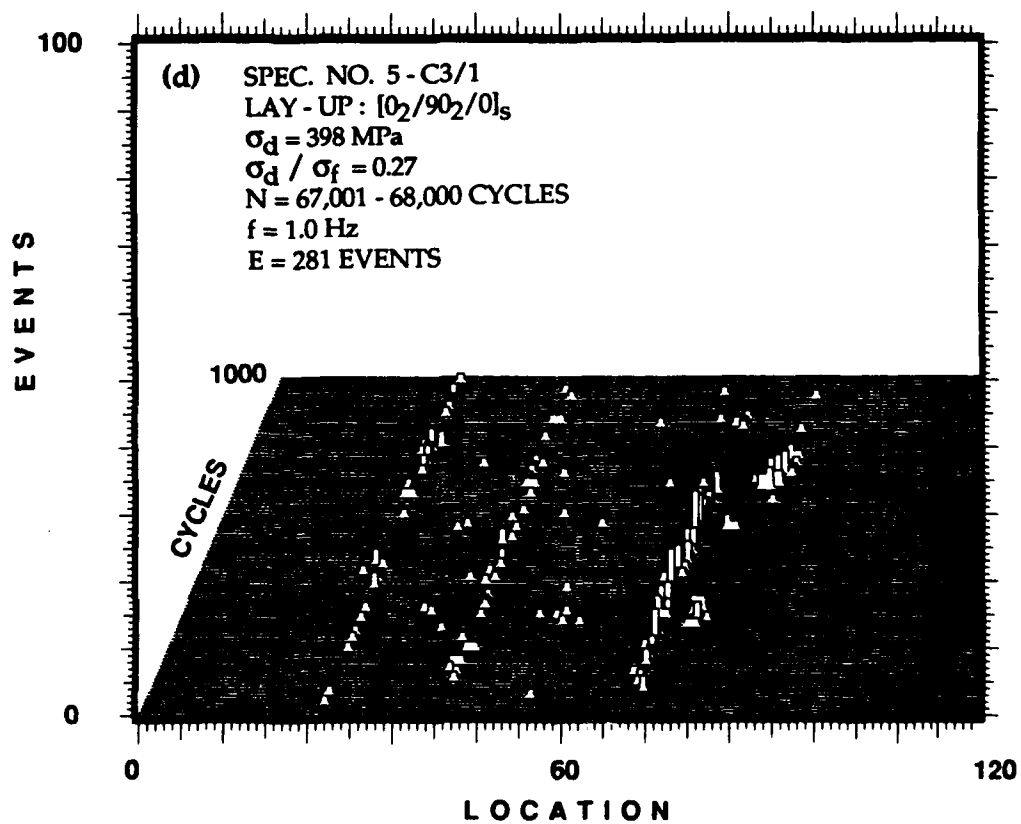
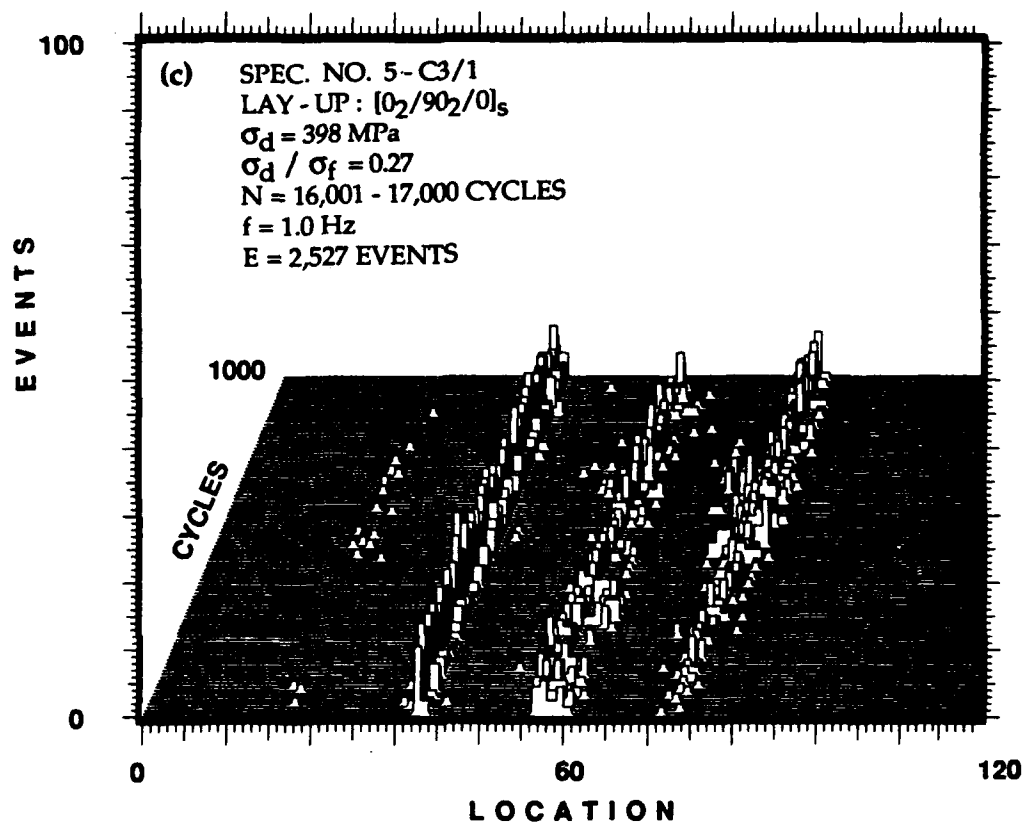


Figure 6.6. Continued.

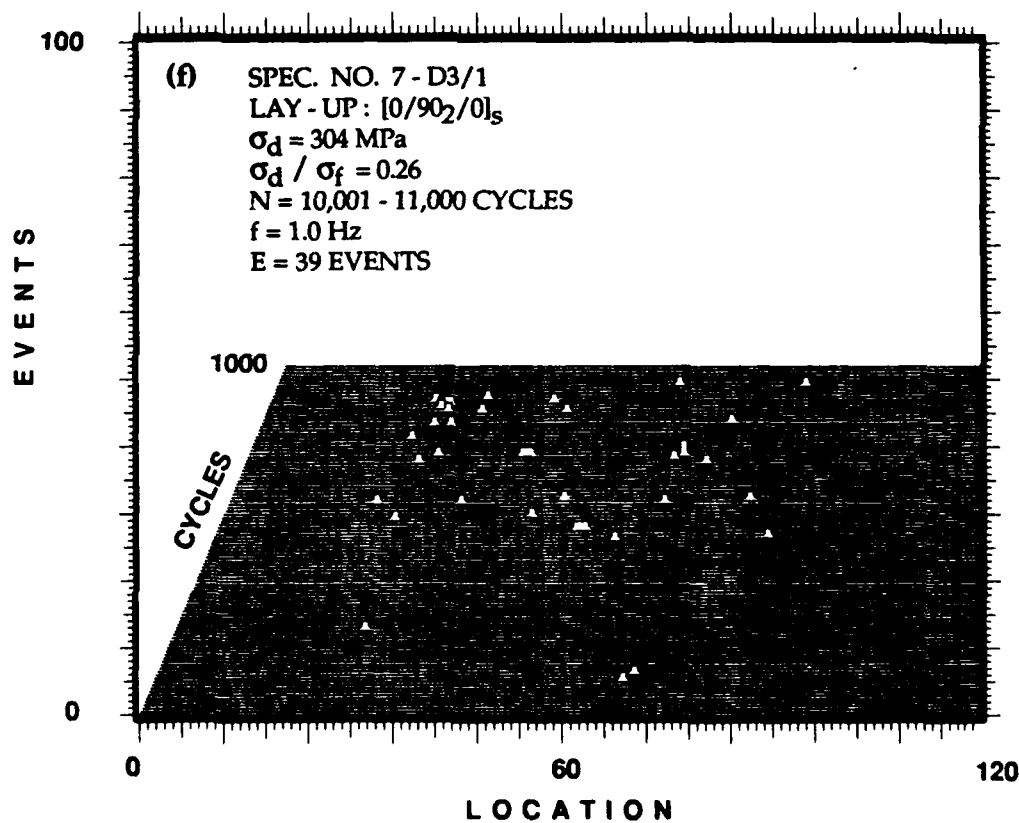
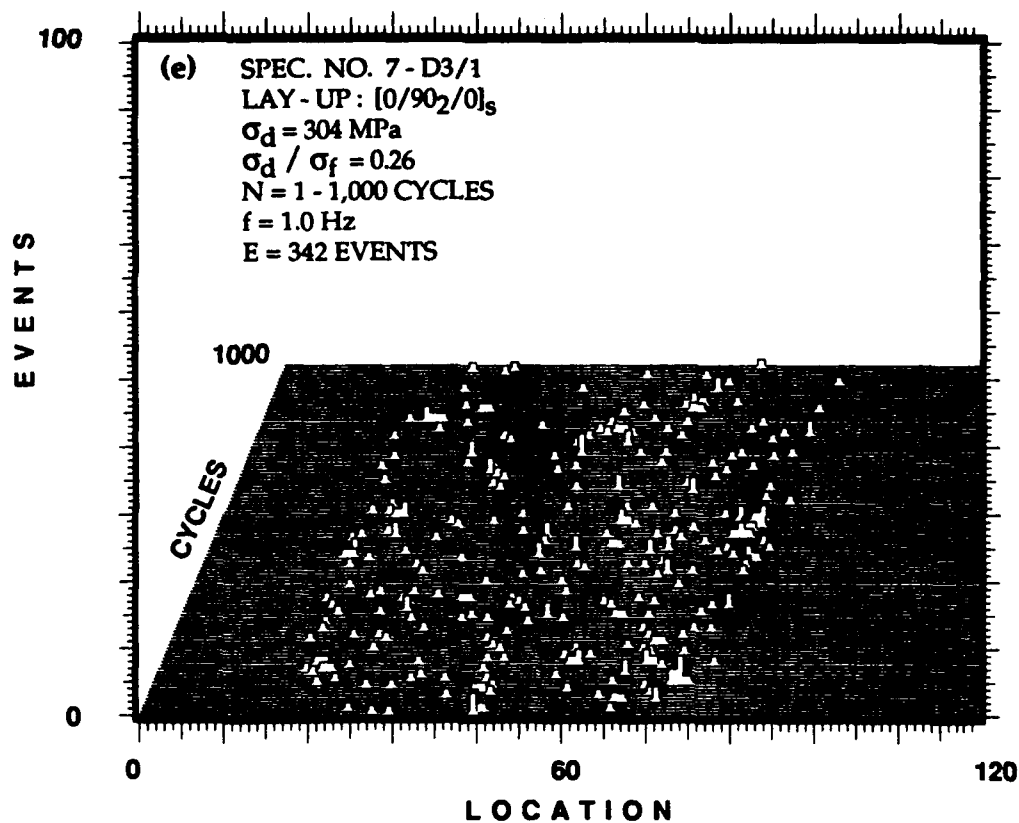


Figure 6.6. Continued.

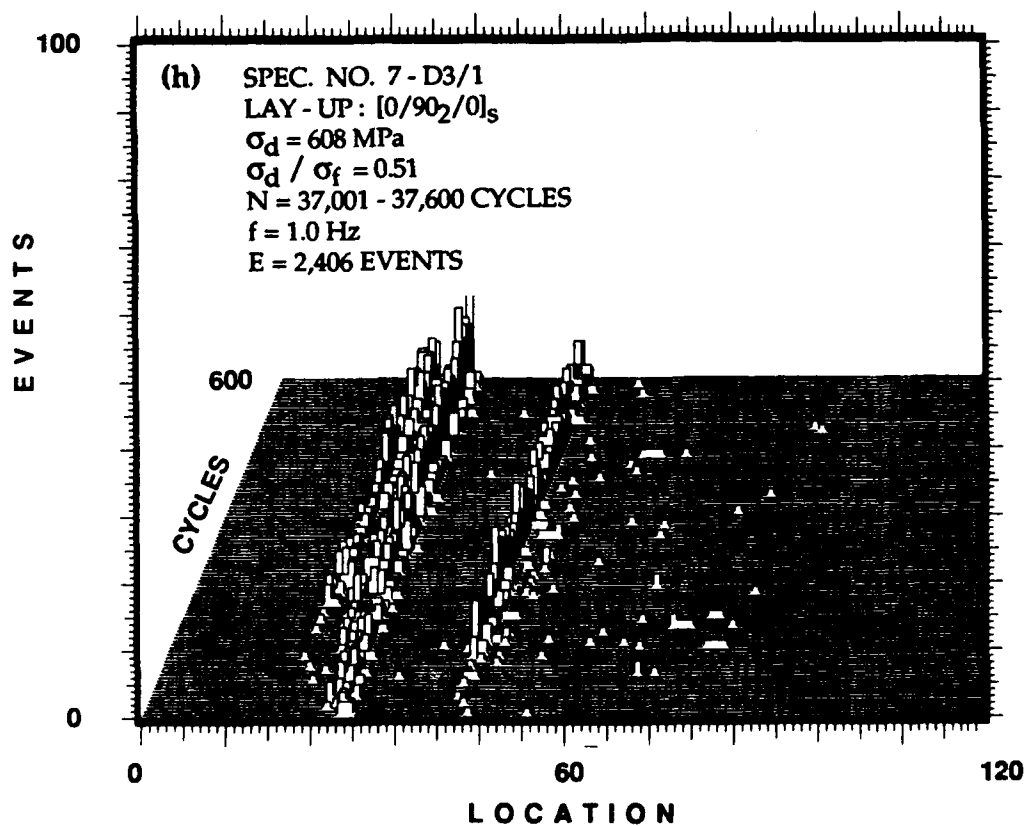
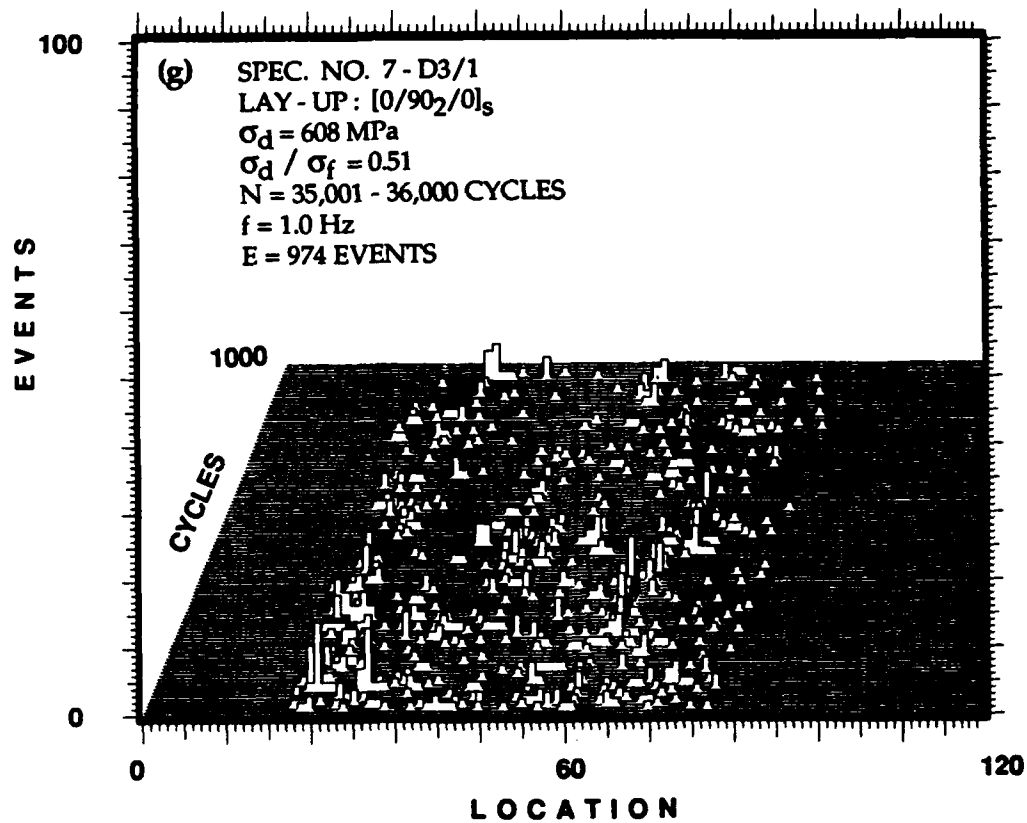


Figure 6.6. Continued.

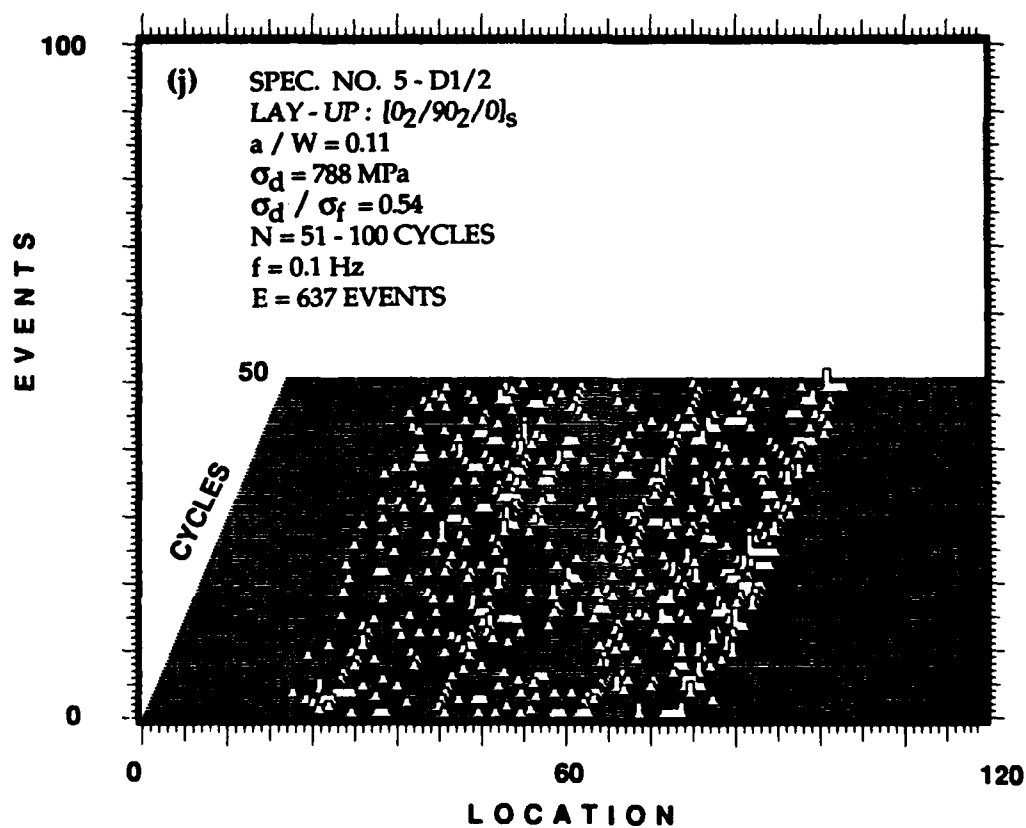
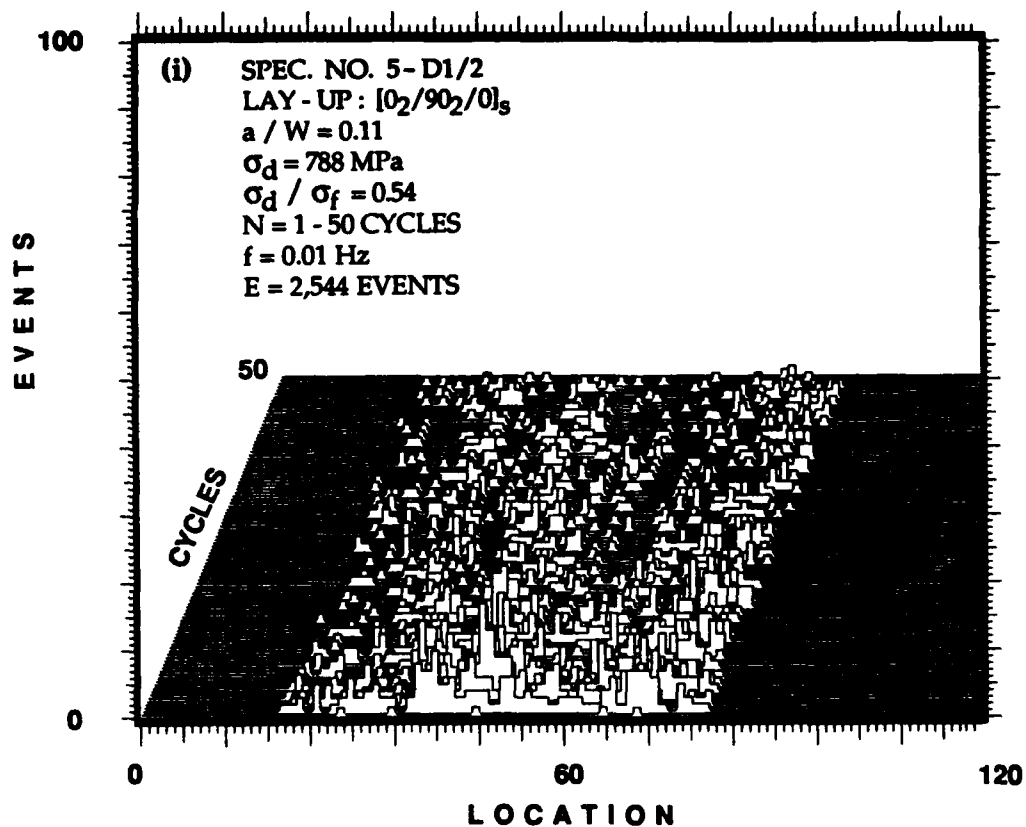


Figure 6.6. Continued.

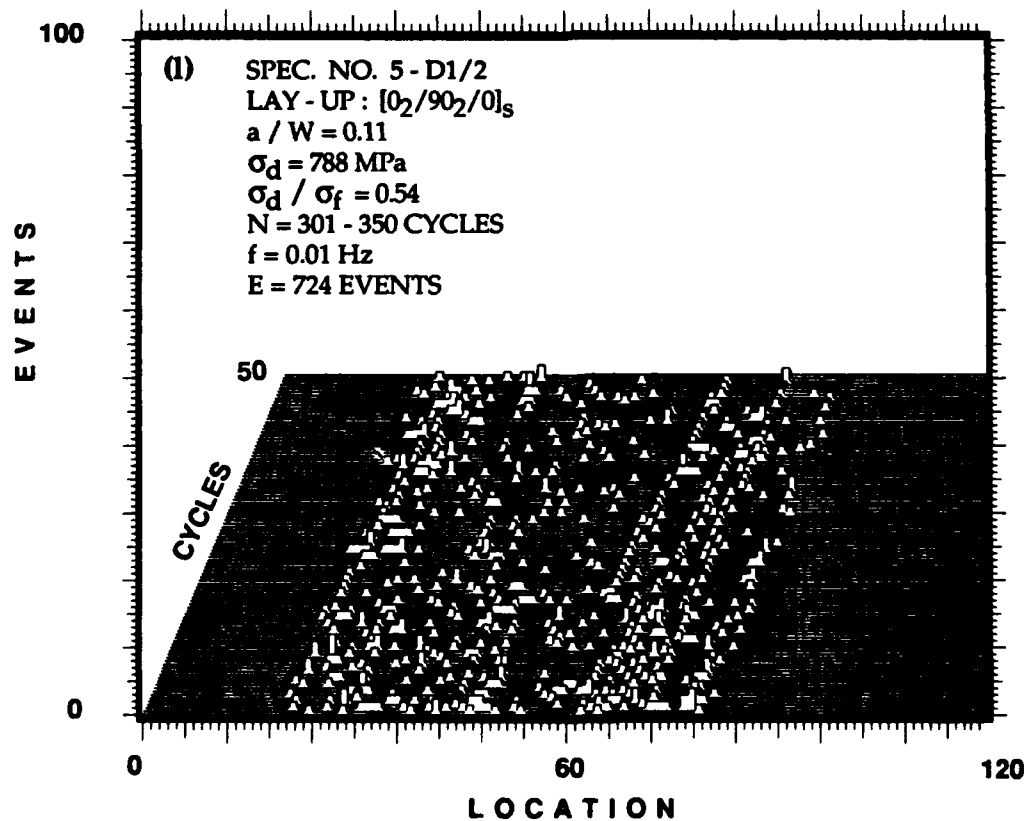
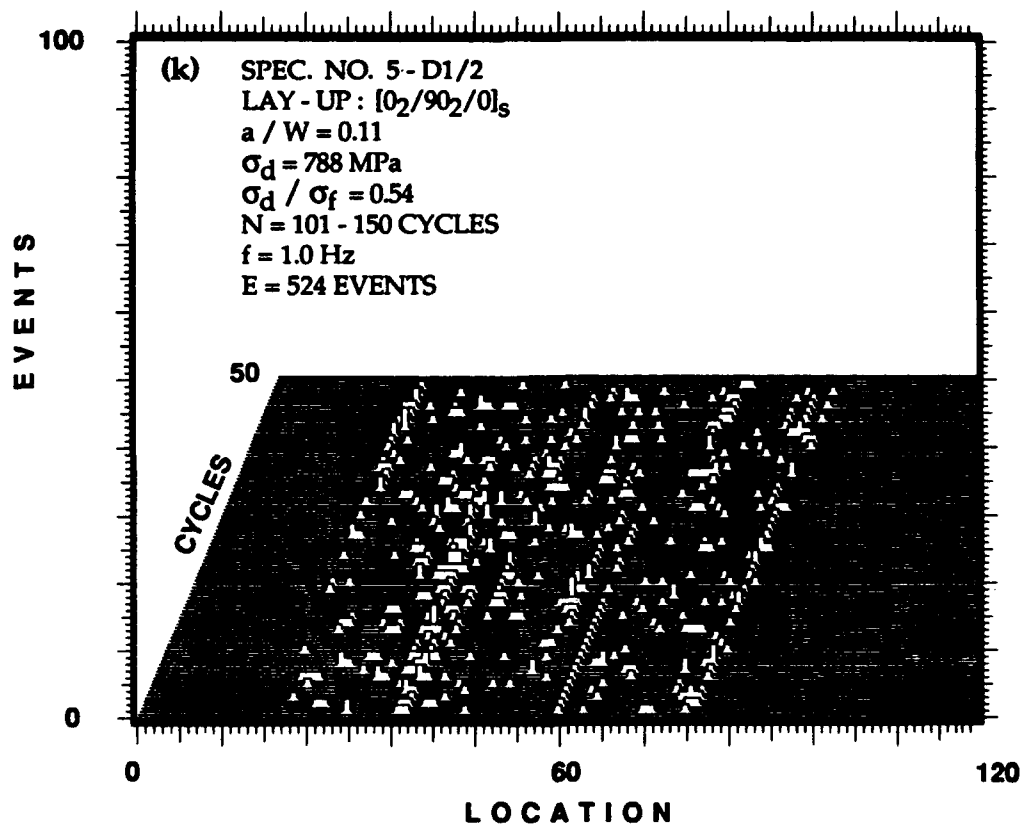


Figure 6.6. Concluded.

(a) SPEC. NO. 3-88/2 $\sigma_d = 581 \text{ MPa}$
 LAY-UP: $[90_2/0/90]_s$ $E = 2,128 \text{ EVENTS}$
 $N = 1-400 \text{ CYCLES}$
 $f = 0.1 \text{ Hz}$

(b) SPEC. NO. 5-C1/1 $\sigma_d = 537 \text{ MPa}$
 LAY-UP: $[0_2/90_2/0]_s$ $E = 389 \text{ EVENTS}$
 $N = 1-400 \text{ CYCLES}$
 $f = 0.1 \text{ Hz}$

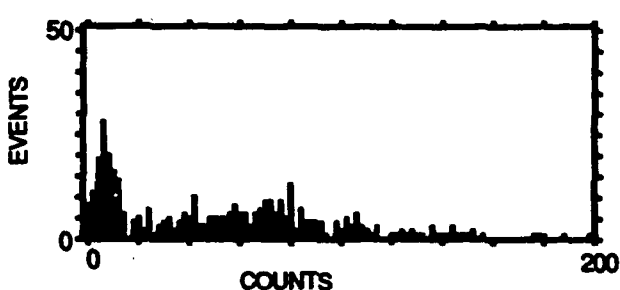
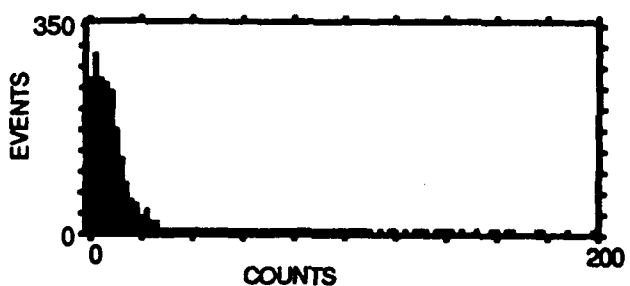
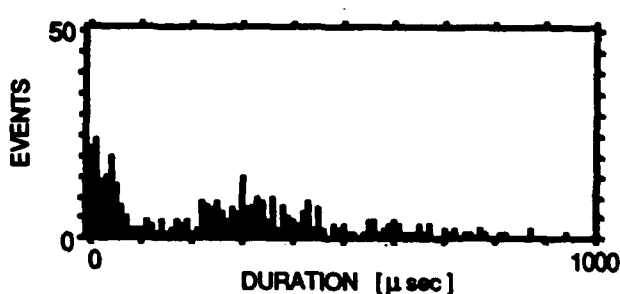
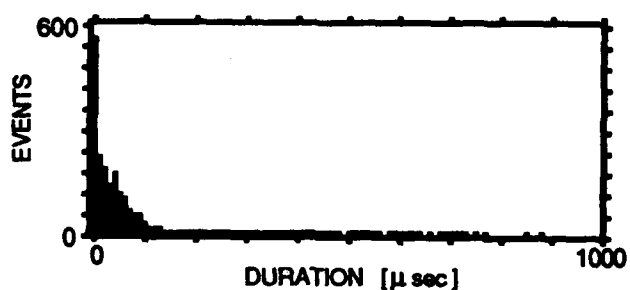
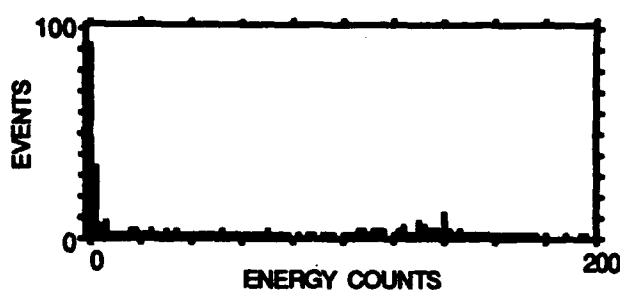
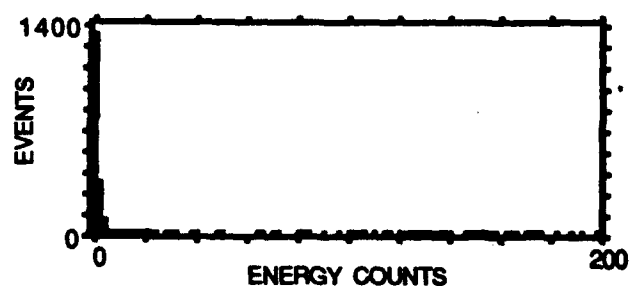
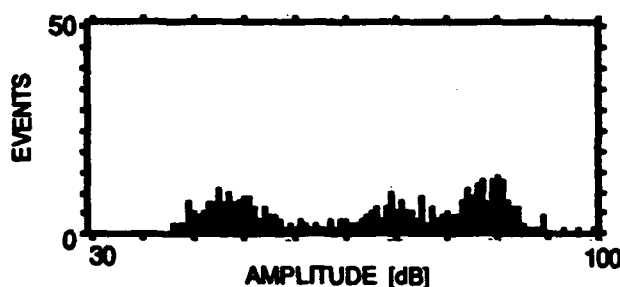
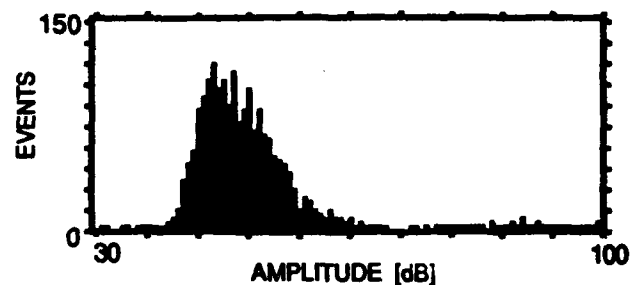
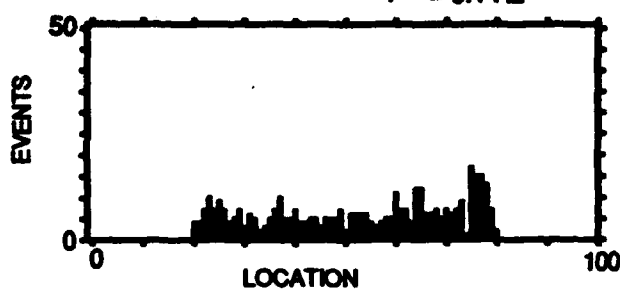


Figure 6.7. Acoustic emission event intensity and location distribution histograms for all the events accumulated during selected periods of the fatigue loading for four specimens. These distributions depend primarily on laminate configuration, dynamic stress amplitude, and the duration of the fatigue loading.

(c) SPEC. NO. 7-B7/1
LAY-UP: $[90_2/0]_8$

$\sigma_d = 126 \text{ MPa}$
 $E = 437 \text{ EVENTS}$
 $N = 1 - 65,000 \text{ CYCLES}$
 $f = 1.0 \text{ Hz}$

(d) SPEC. NO. 5-D1/2
LAY-UP: $[0_2/90_2/0]_8$
 $a/W = 0.11$

$\sigma_d = 788 \text{ MPa}$
 $E = 2,544 \text{ EVENTS}$
 $N = 1 - 50 \text{ CYCLES}$
 $f = 0.01 \text{ Hz}$

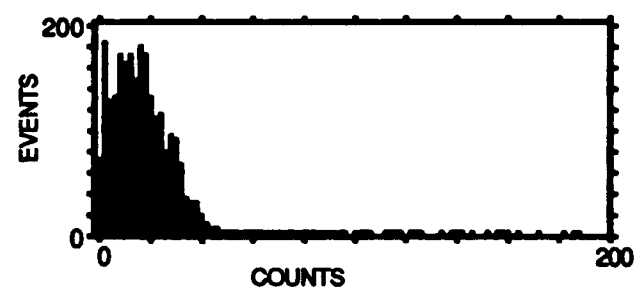
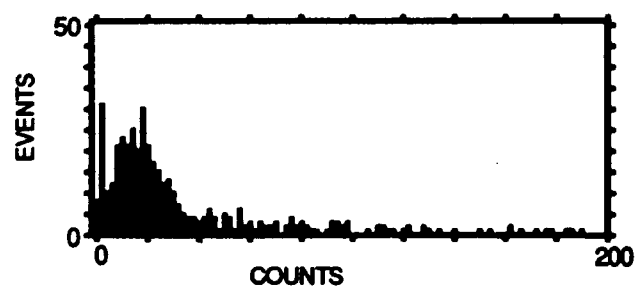
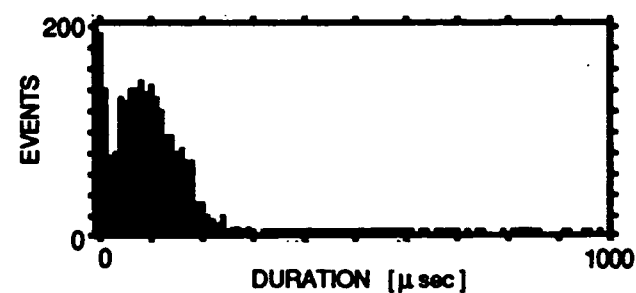
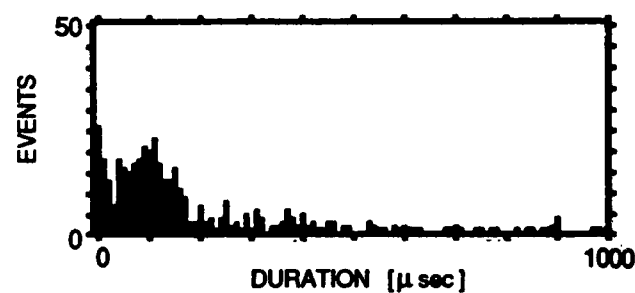
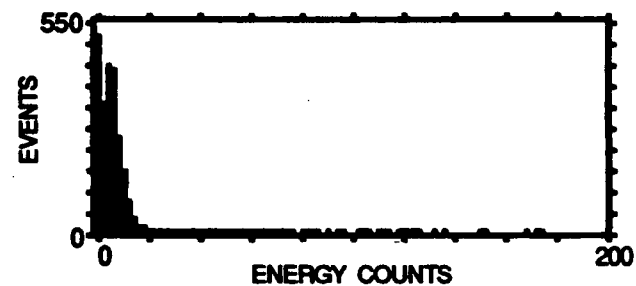
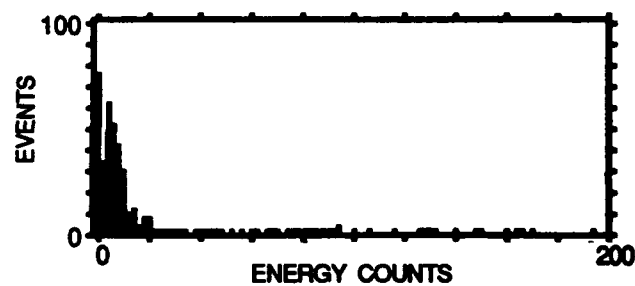
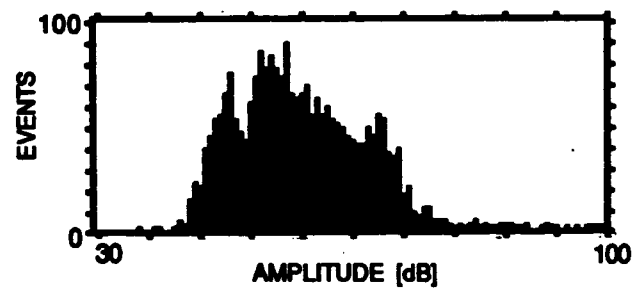
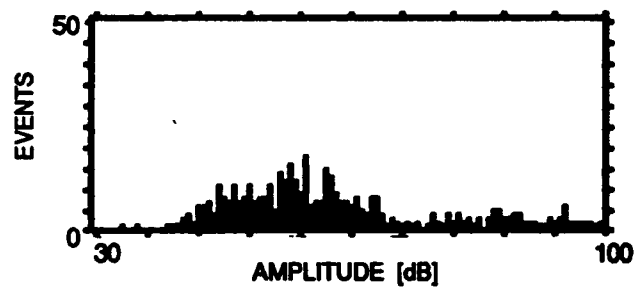
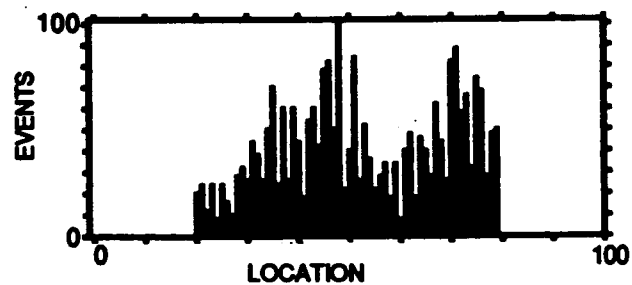


Figure 6.7. Concluded.

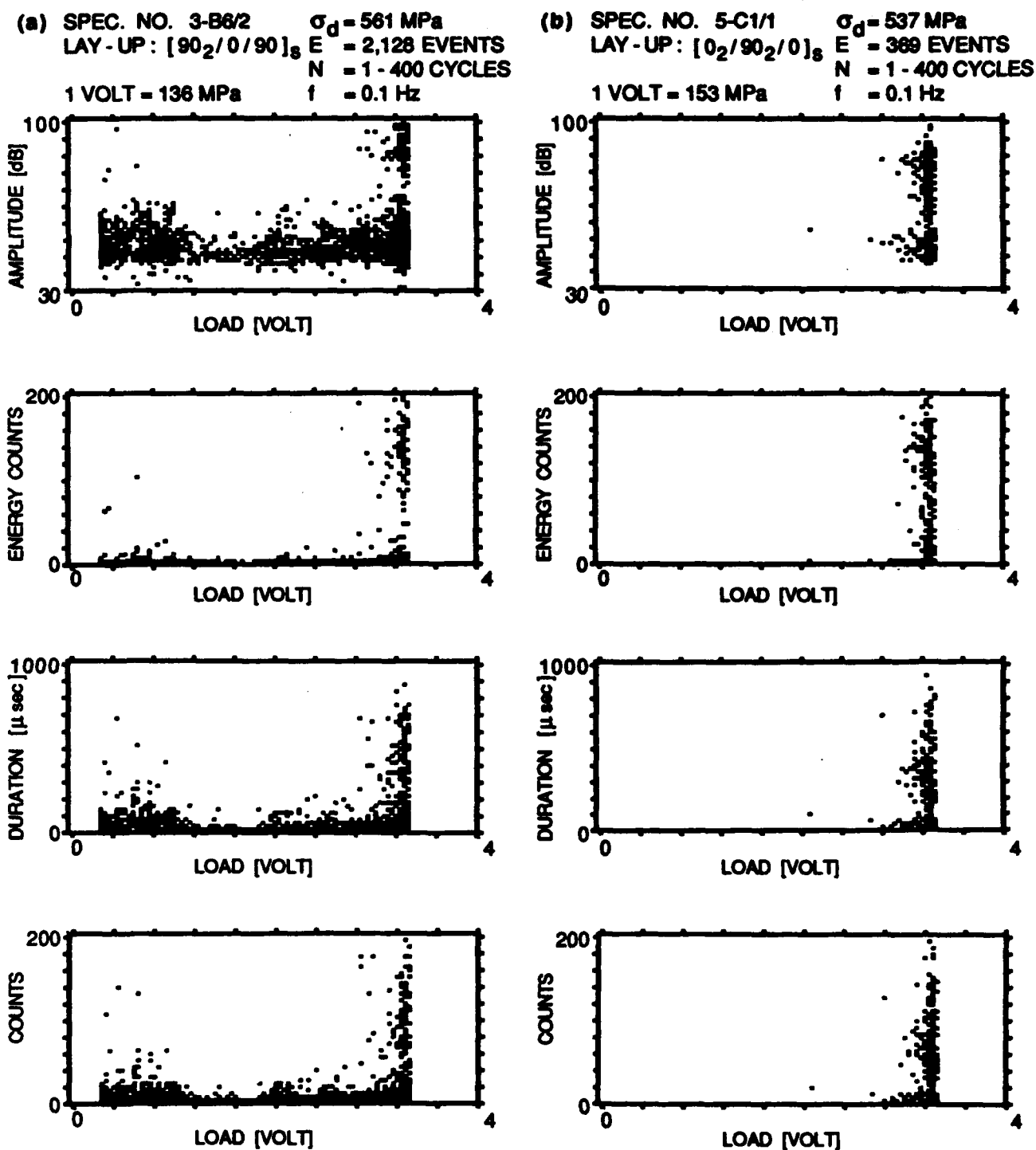


Figure 6.8. Intensities of events as a function of far-field applied stress for all the events accumulated during the same periods of the fatigue loading and specimens shown in Figure 6.7. Events occur throughout the entire load range. High intensity events occur only at the upper load range.

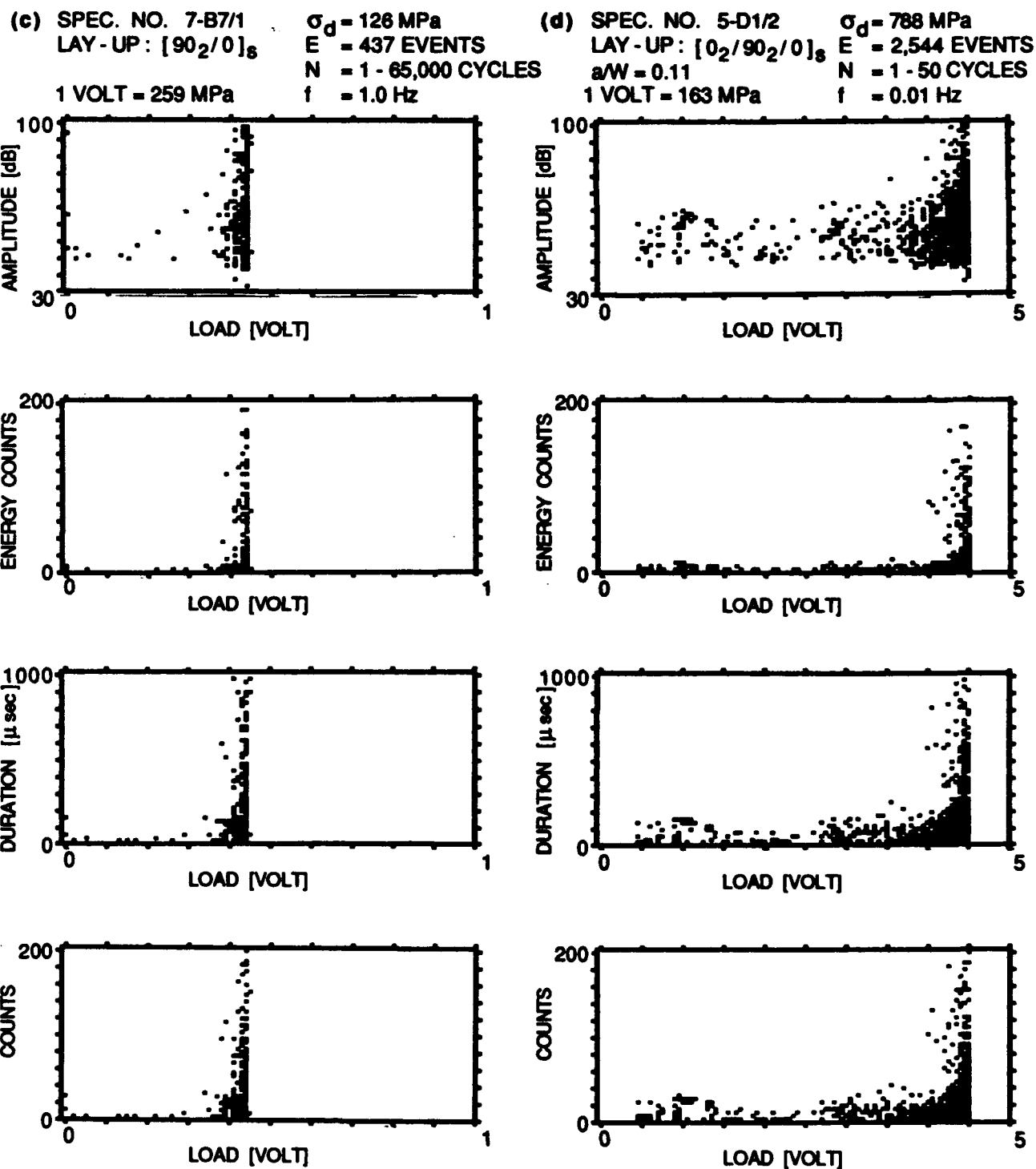
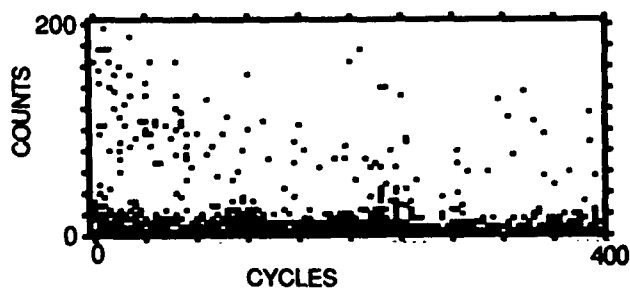
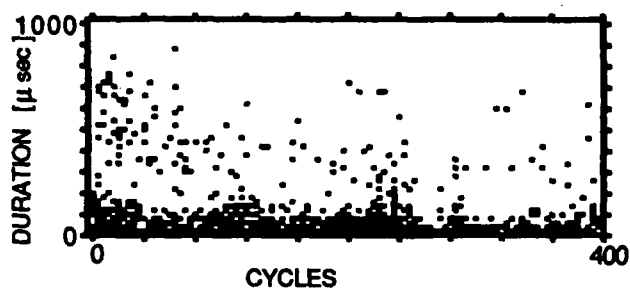
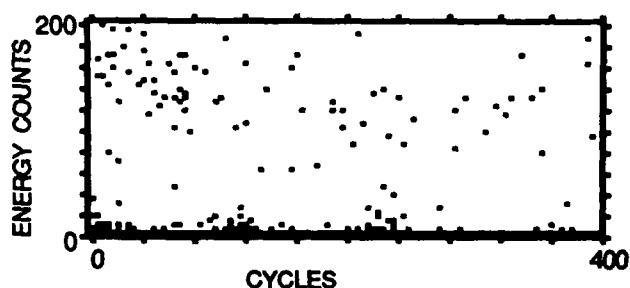
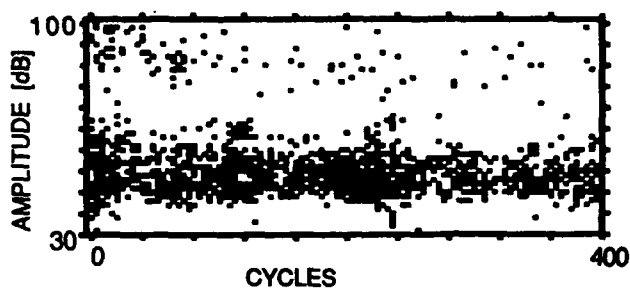


Figure 6.8. Concluded.

(a) SPEC. NO. 3-B6/2 $\sigma_d = 561$ MPa
 LAY-UP: $[90_2/0/90]_s$ E = 2,128 EVENTS
 N = 1-400 CYCLES
 f = 0.1 Hz



(b) SPEC. NO. 5-C1/1 $\sigma_d = 537$ MPa
 LAY-UP: $[0_2/90_2/0]_s$ E = 369 EVENTS
 N = 1-400 CYCLES
 f = 0.1 Hz

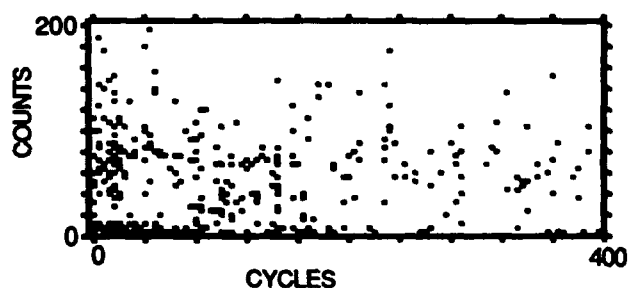
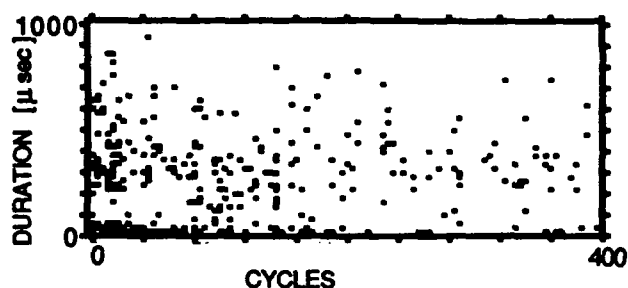
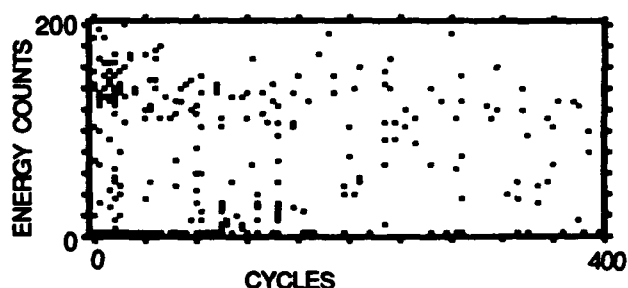
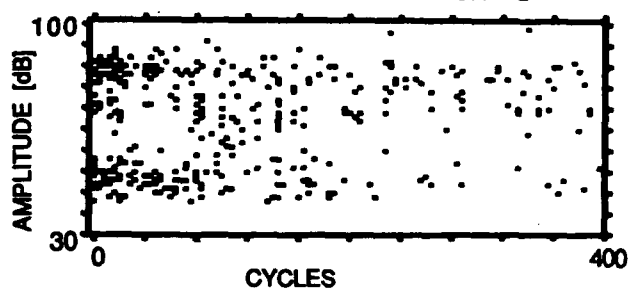
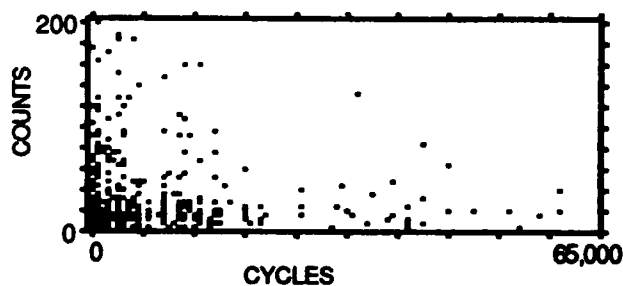
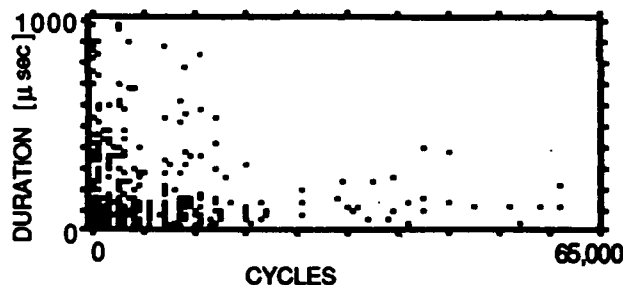
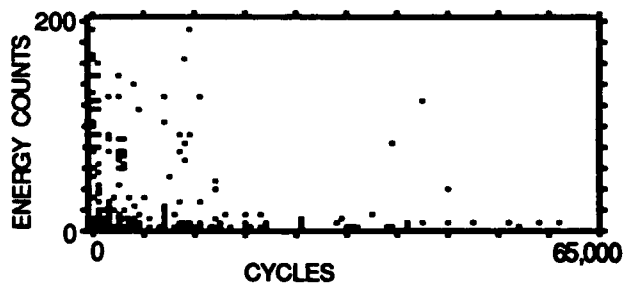
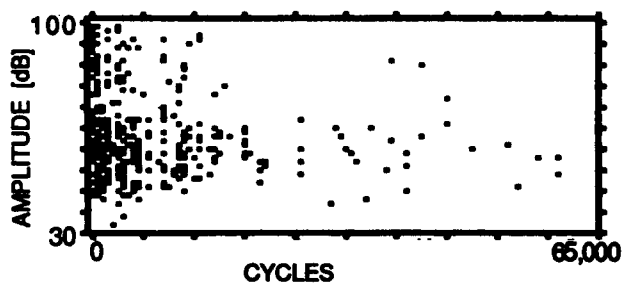


Figure 6.9. Intensities of events as a function of number of cycles for all the events accumulated during the same periods of the fatigue loading and specimens shown in Figures 6.7 and 6.8. Rate of events decreases with number of cycles.

(c) SPEC. NO. 7-B7/1 $\sigma_d = 126 \text{ MPa}$
 LAY-UP: $[90_2/0]_s$ E = 437 EVENTS
 N = 1 - 65,000 CYCLES
 f = 1.0 Hz



(d) SPEC. NO. 5-D1/2 $\sigma_d = 788 \text{ MPa}$
 LAY-UP: $[0_2/90_2/0]_s$ E = 2,544 EVENTS
 a/W = 0.11 N = 1 - 50 CYCLES
 f = 0.01 Hz

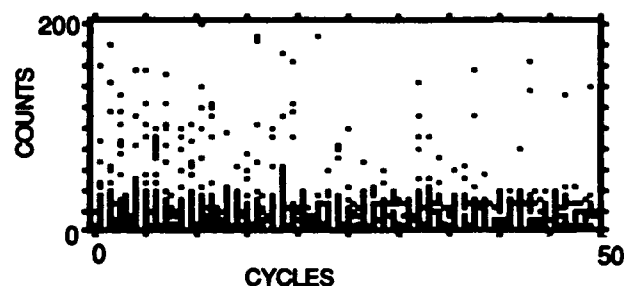
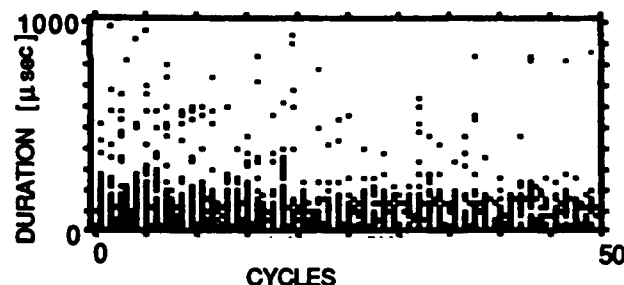
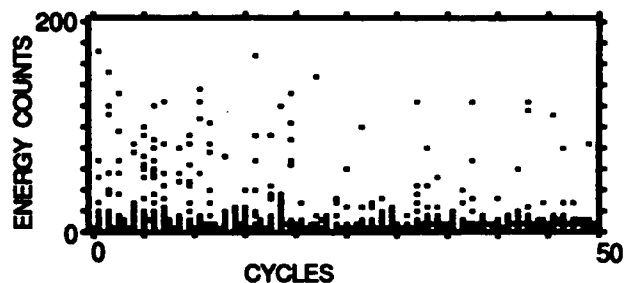
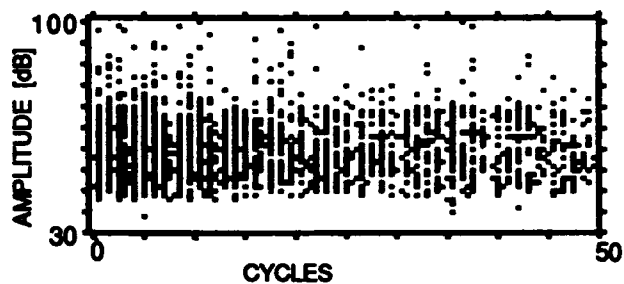


Figure 6.9. Concluded.

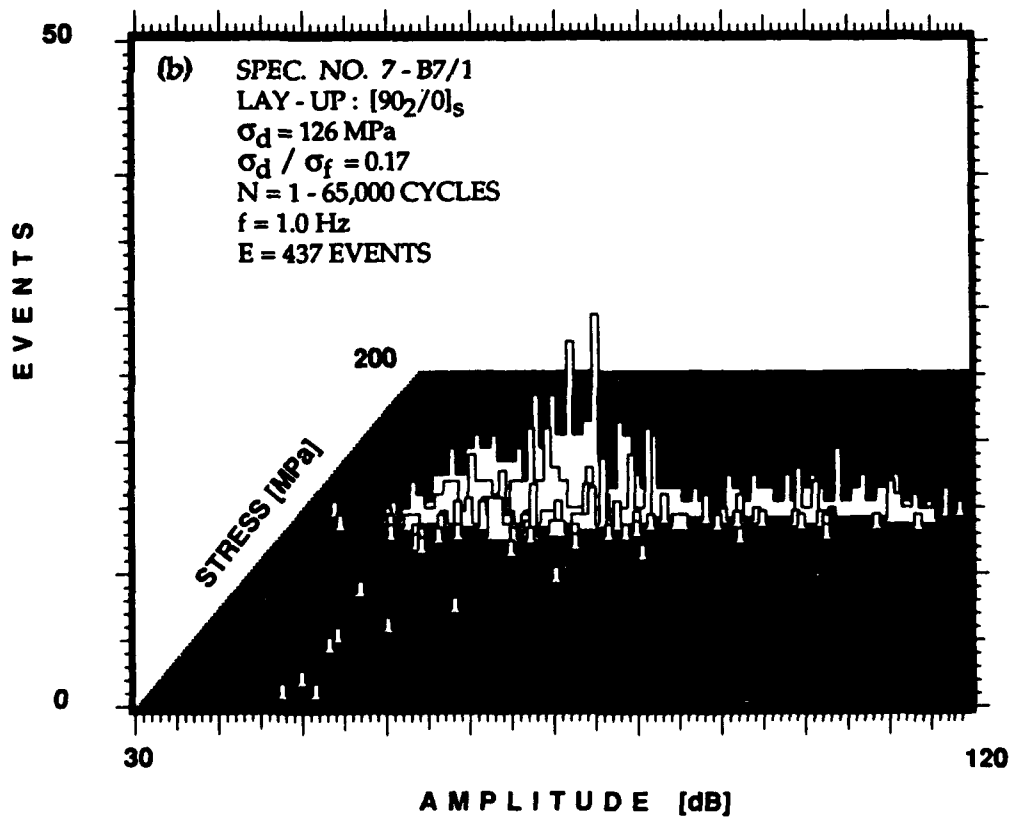
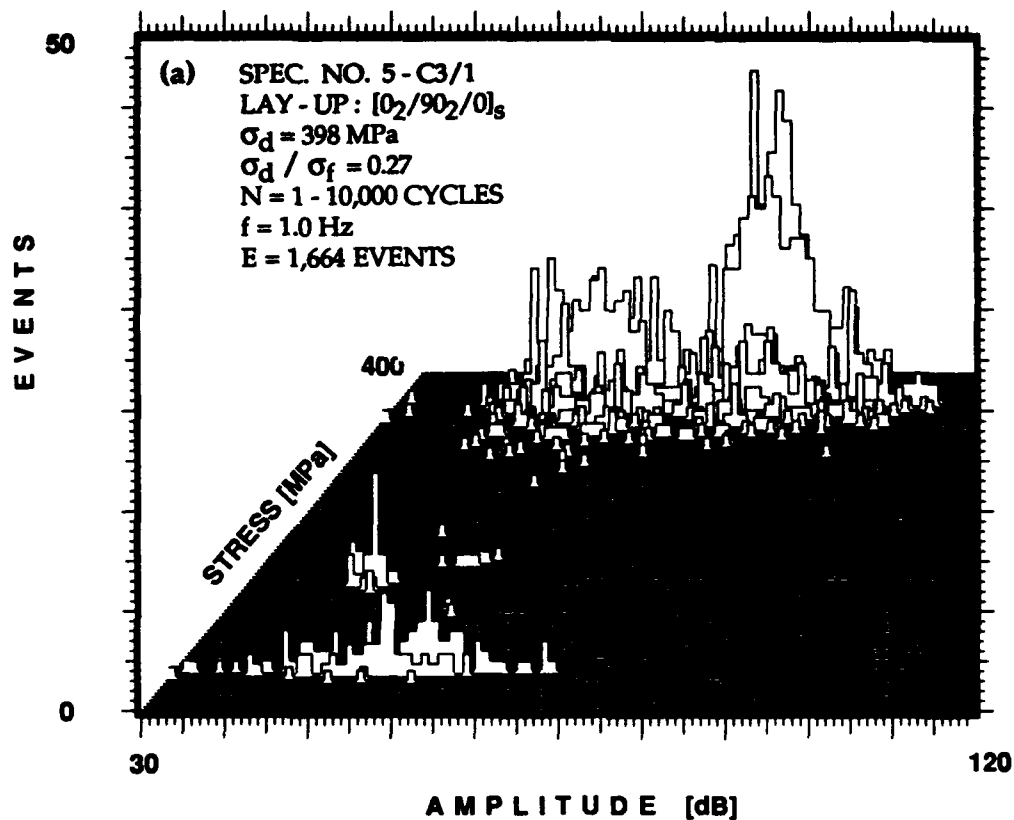


Figure 6.10. Three-dimensional plots of amplitude distribution histograms of events recorded for the same two specimens shown in Figure 6.4.

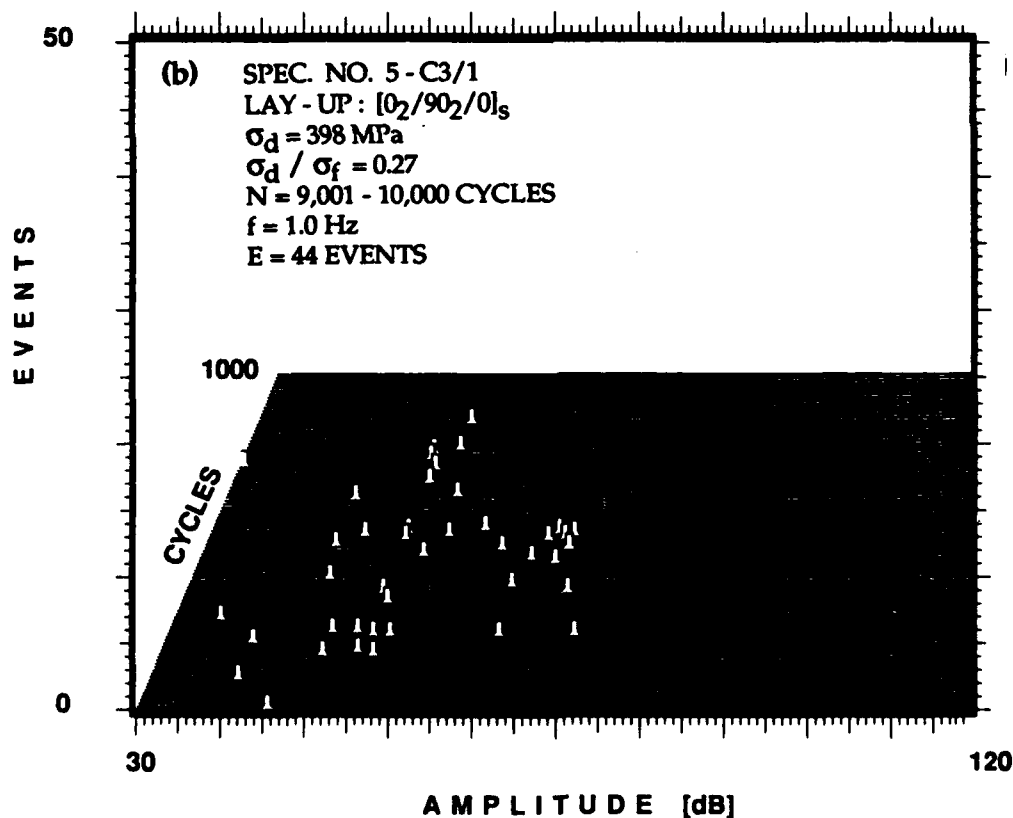
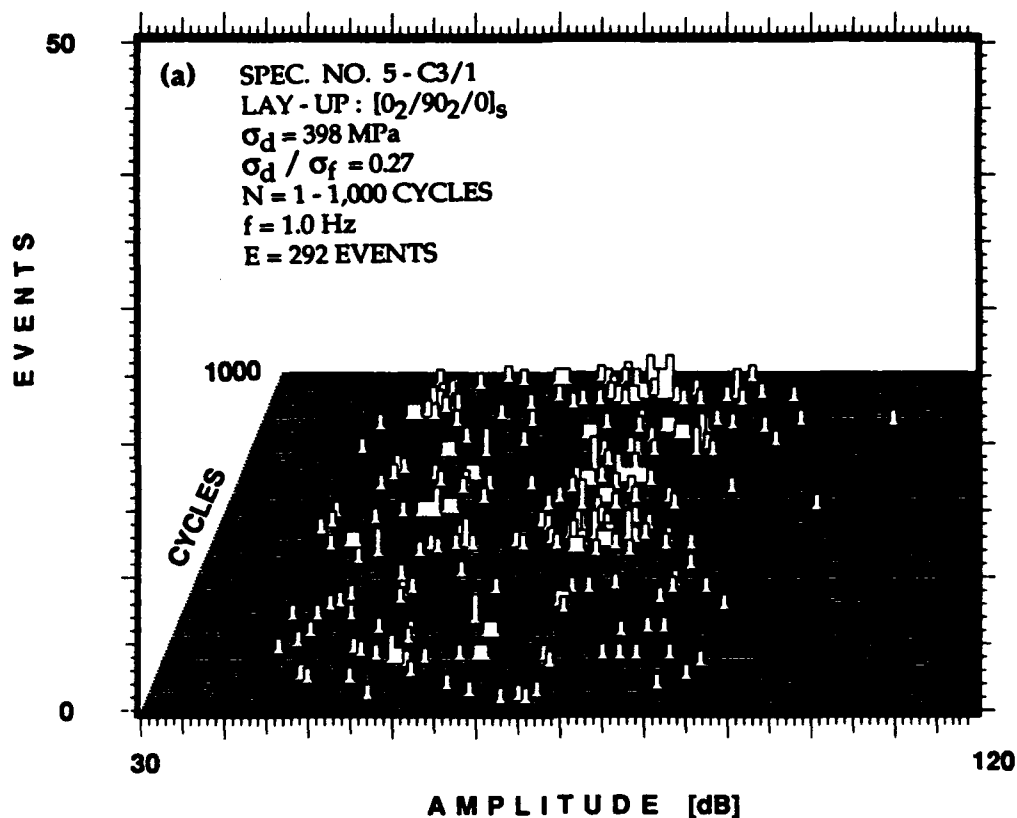


Figure 6.11. Three dimensional plots showing amplitude distribution histograms for all the events generated during the same periods of the fatigue loading and specimens shown in Figures 6.5 and 6.6. High amplitude events occur primarily during the initial periods of the fatigue loading. During the later periods most of the events are of low amplitude.

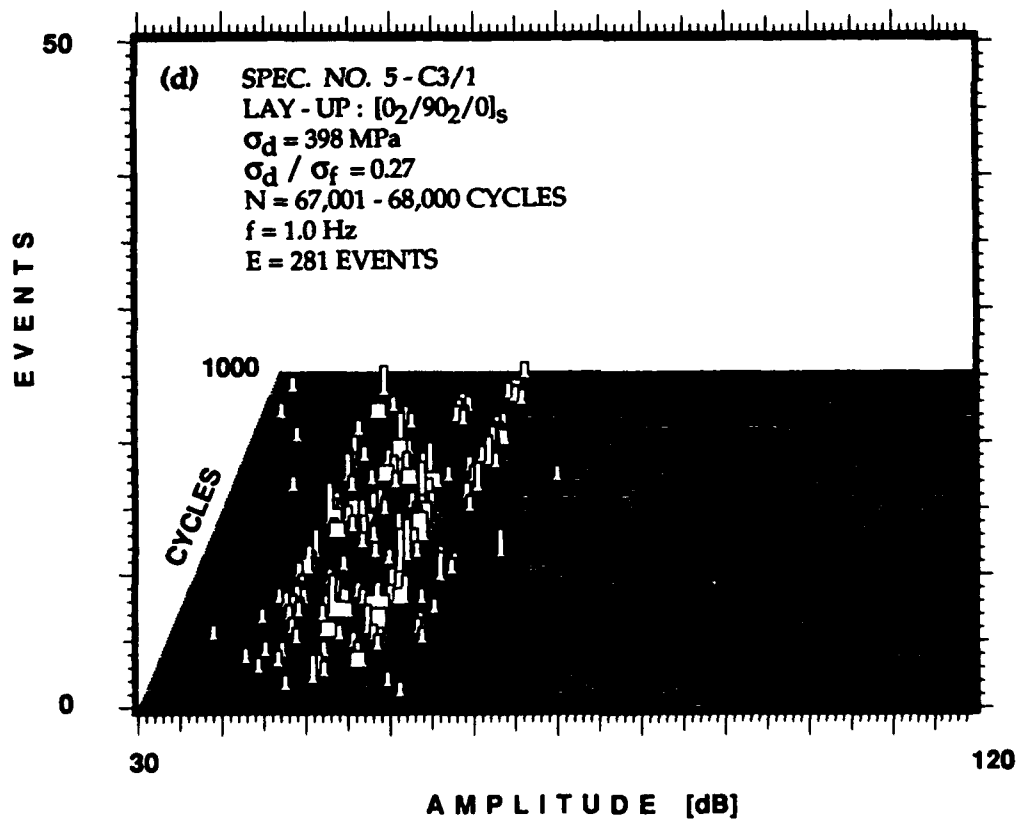
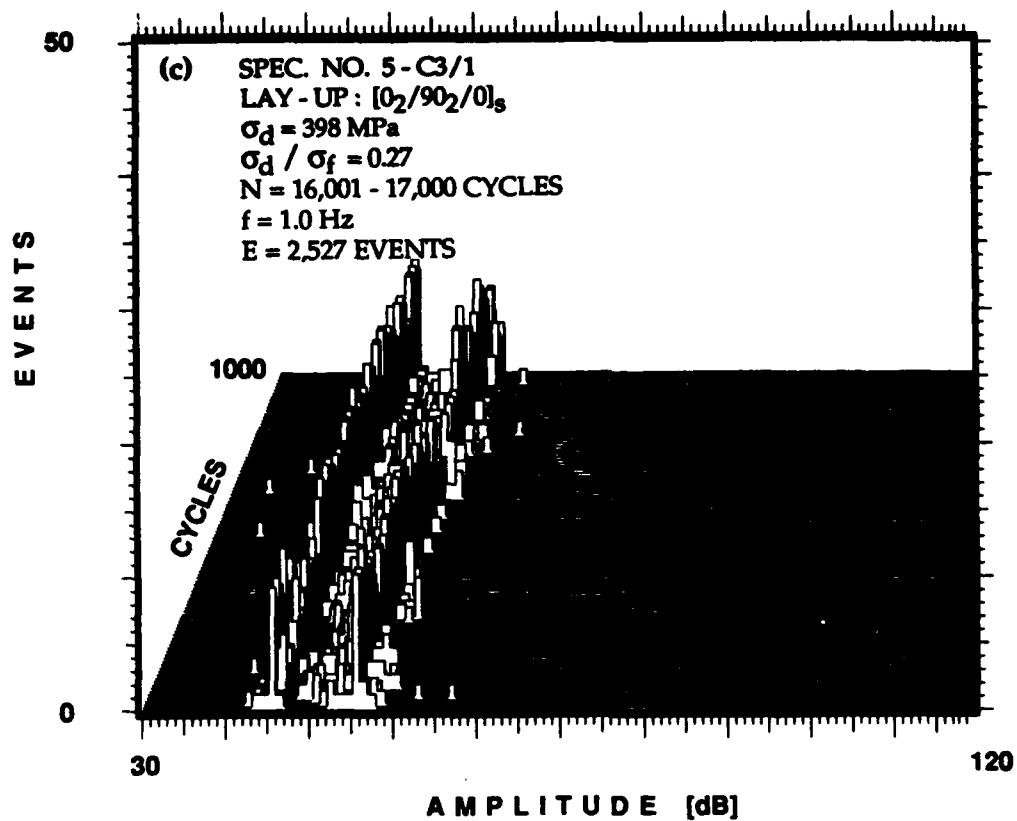


Figure 6.11. Continued.

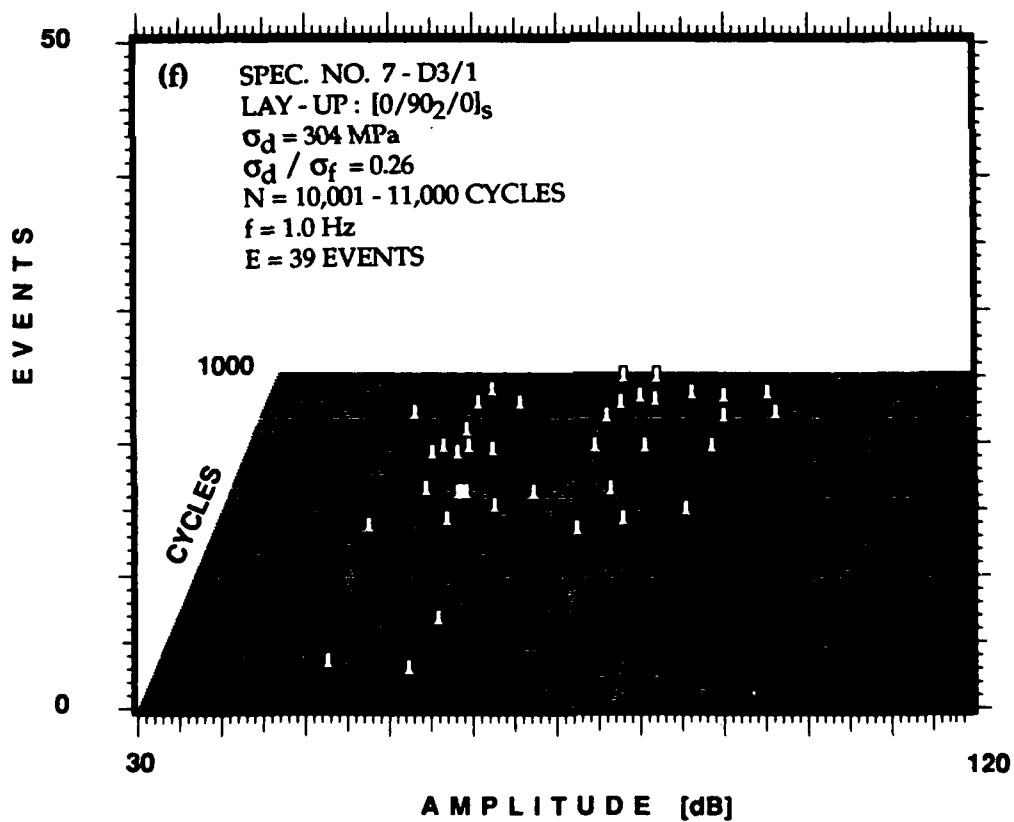
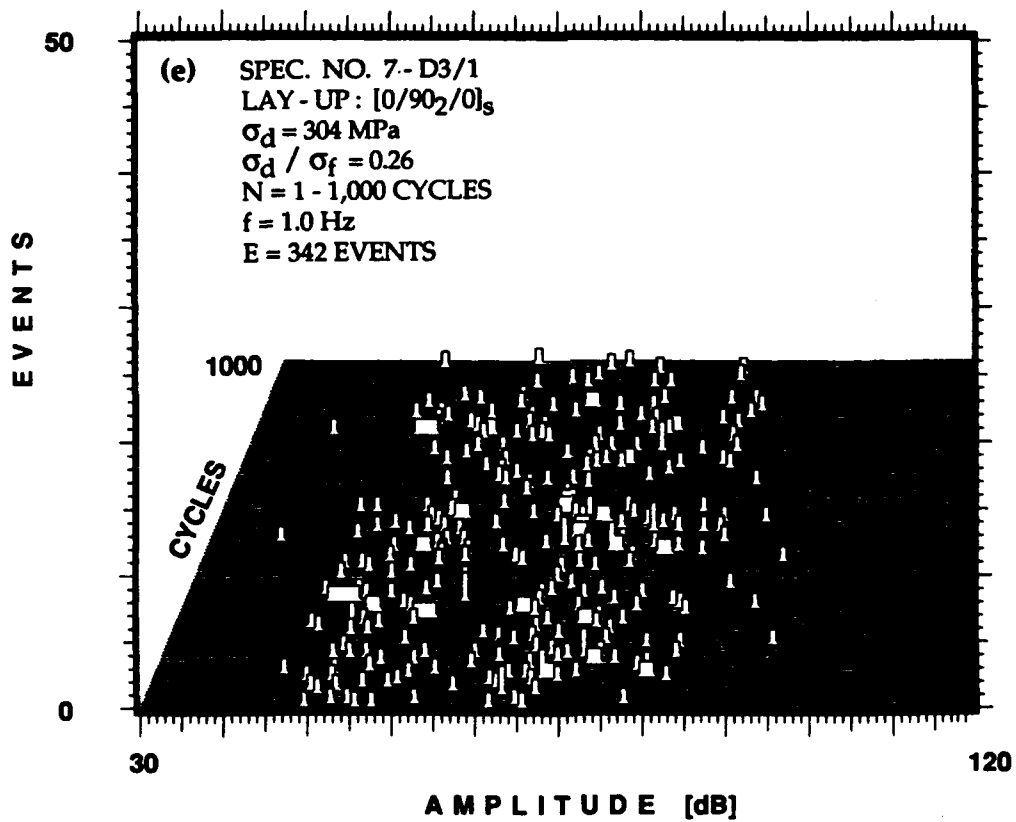


Figure 6.11. Continued.

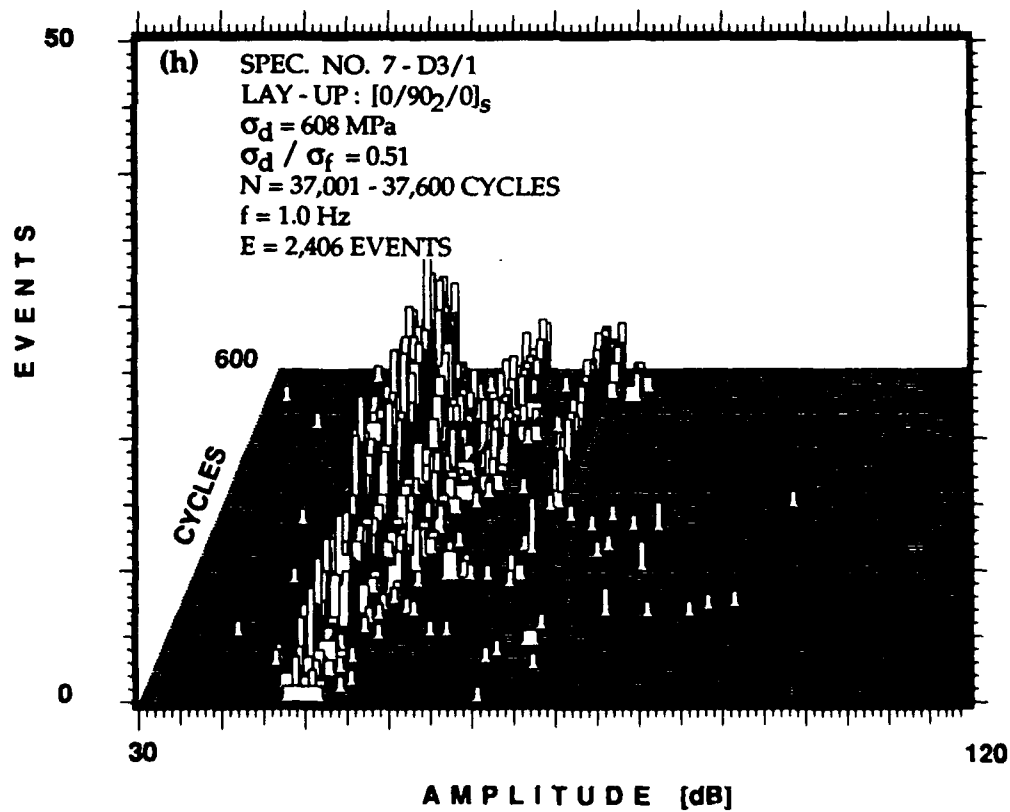
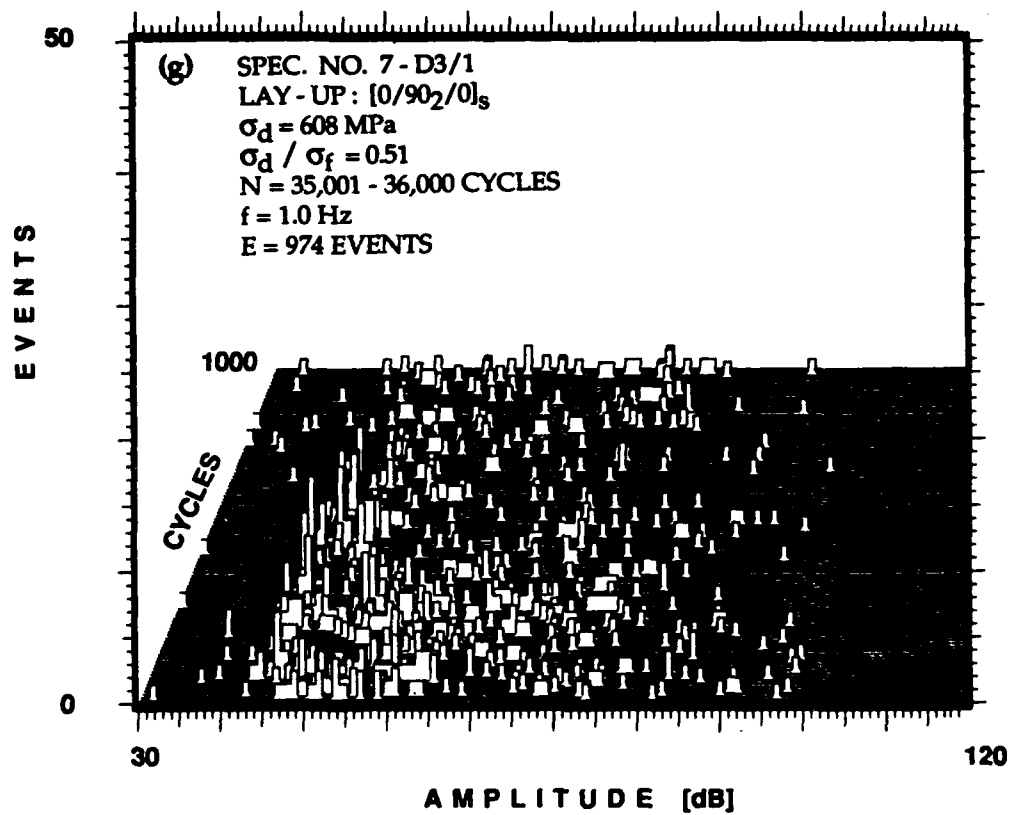


Figure 6.11. Continued.

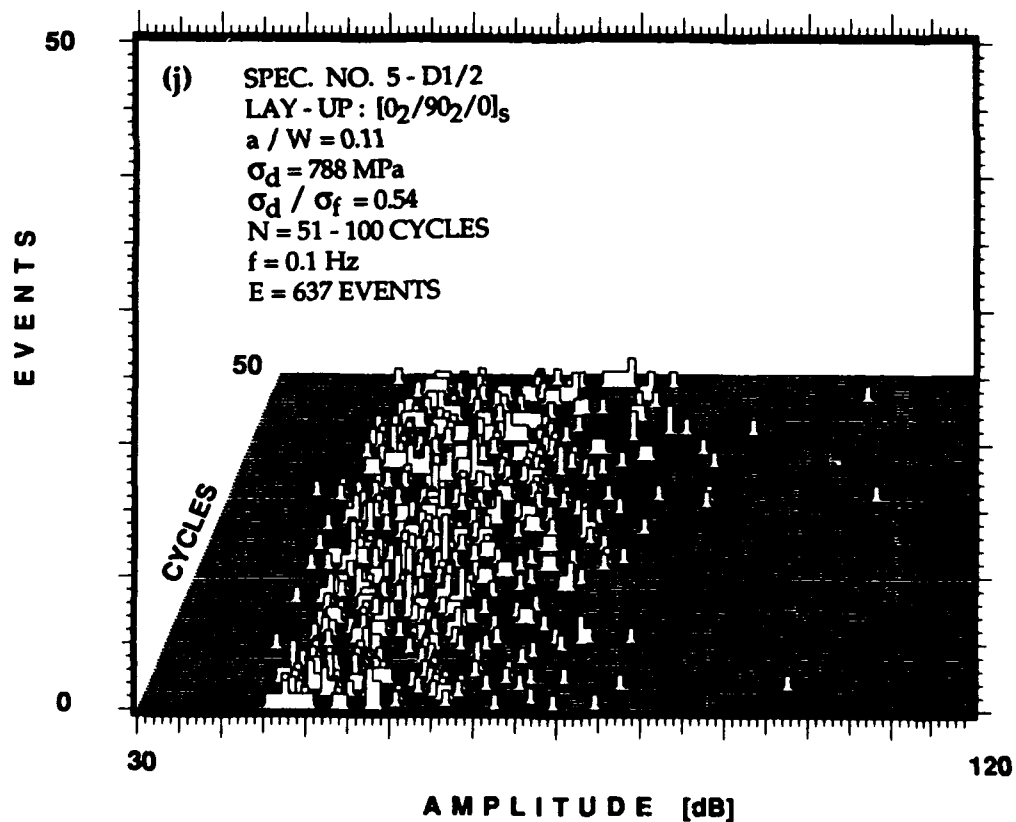
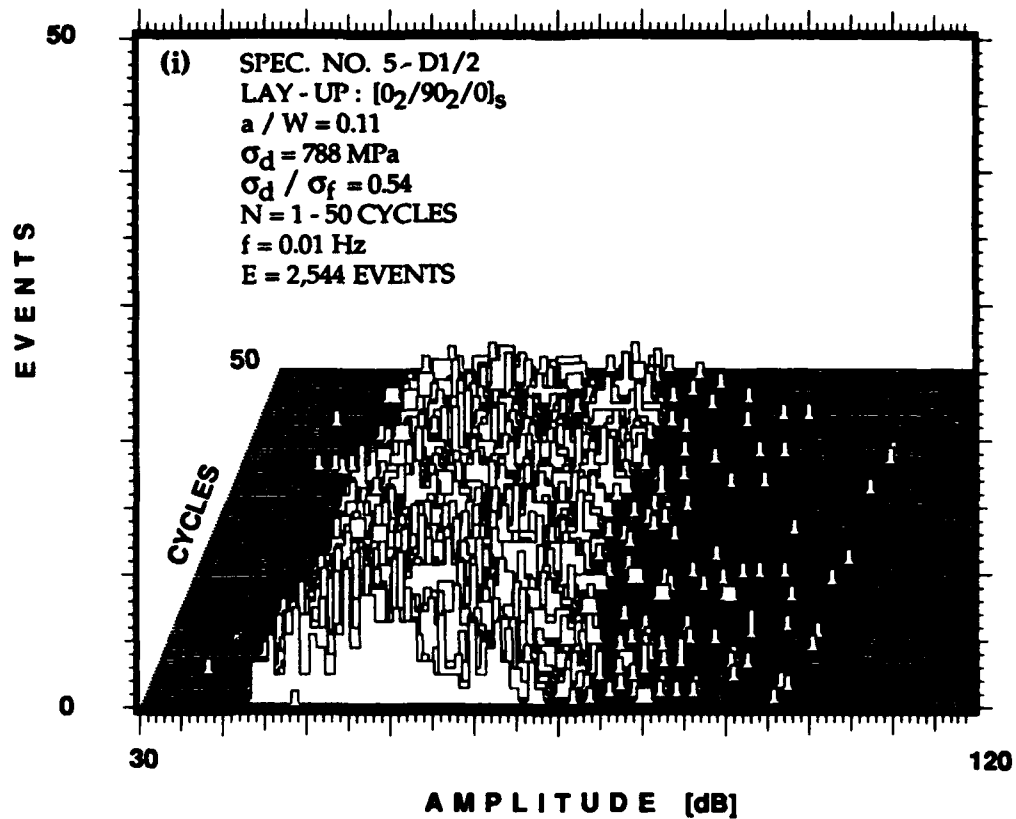


Figure 6.11. Continued.

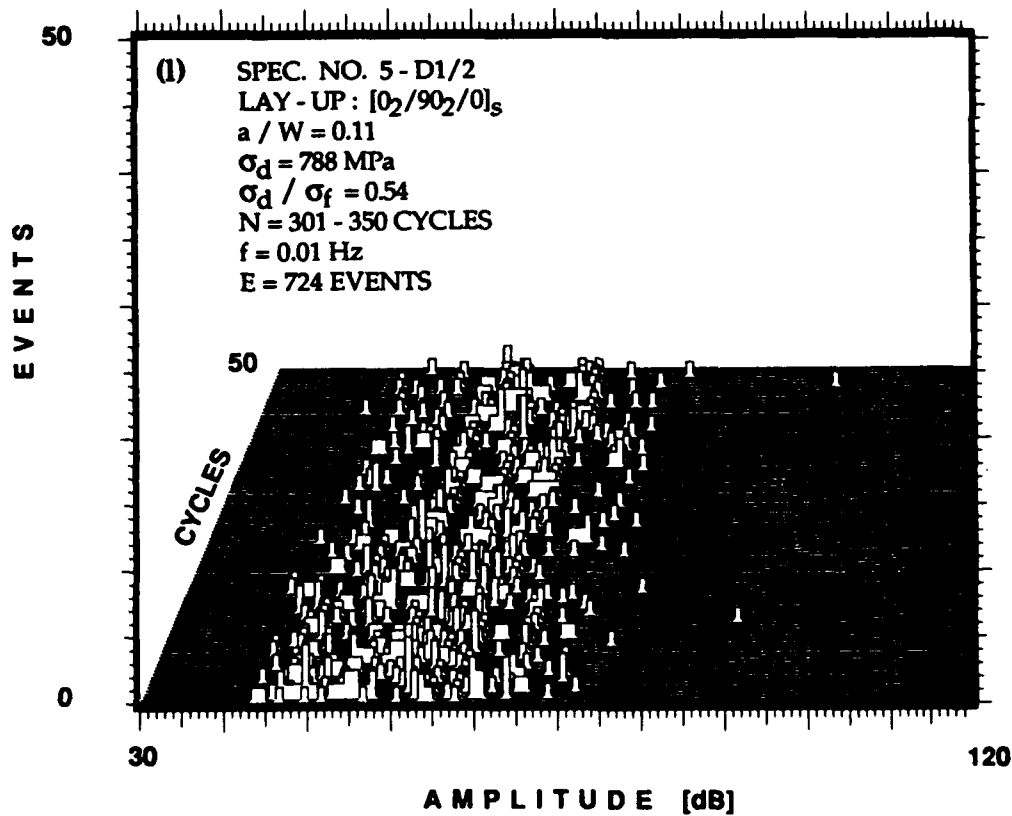
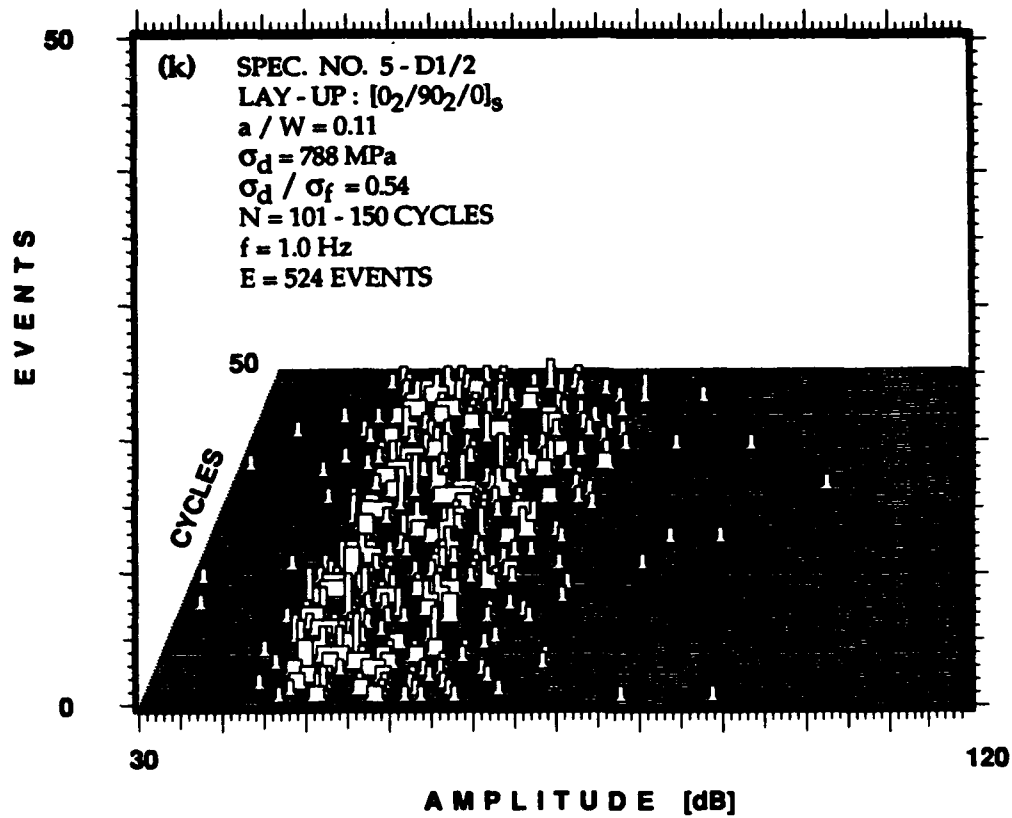


Figure 6.11. Concluded.

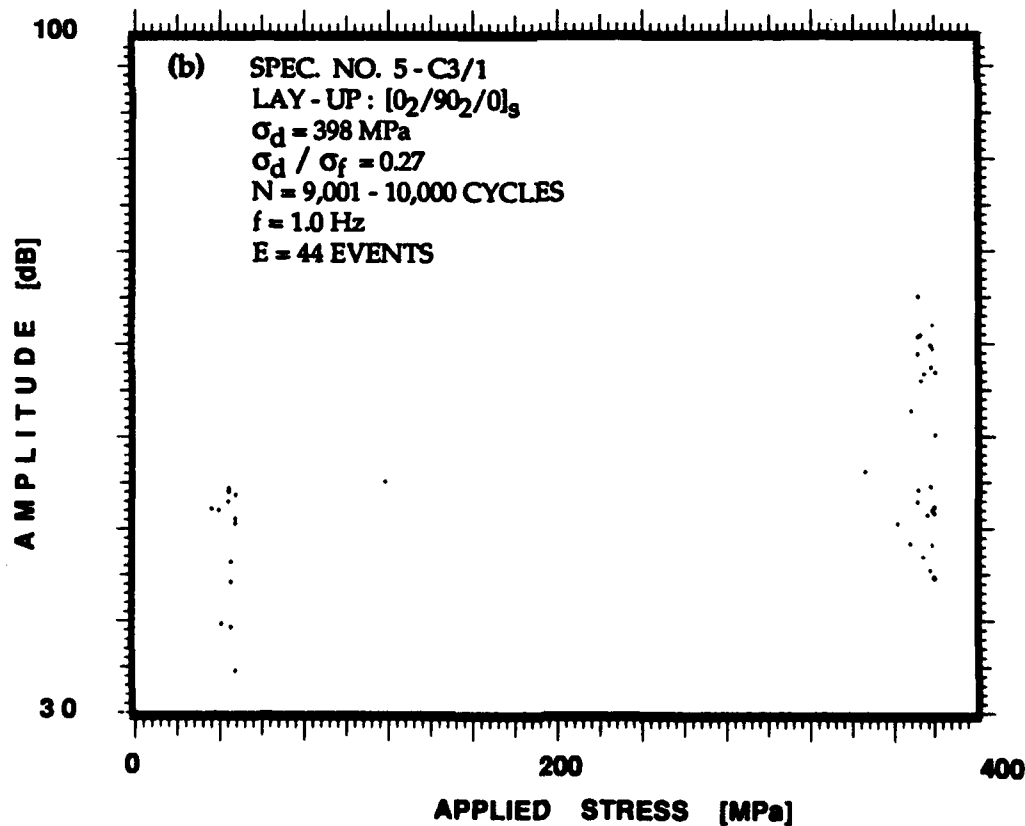
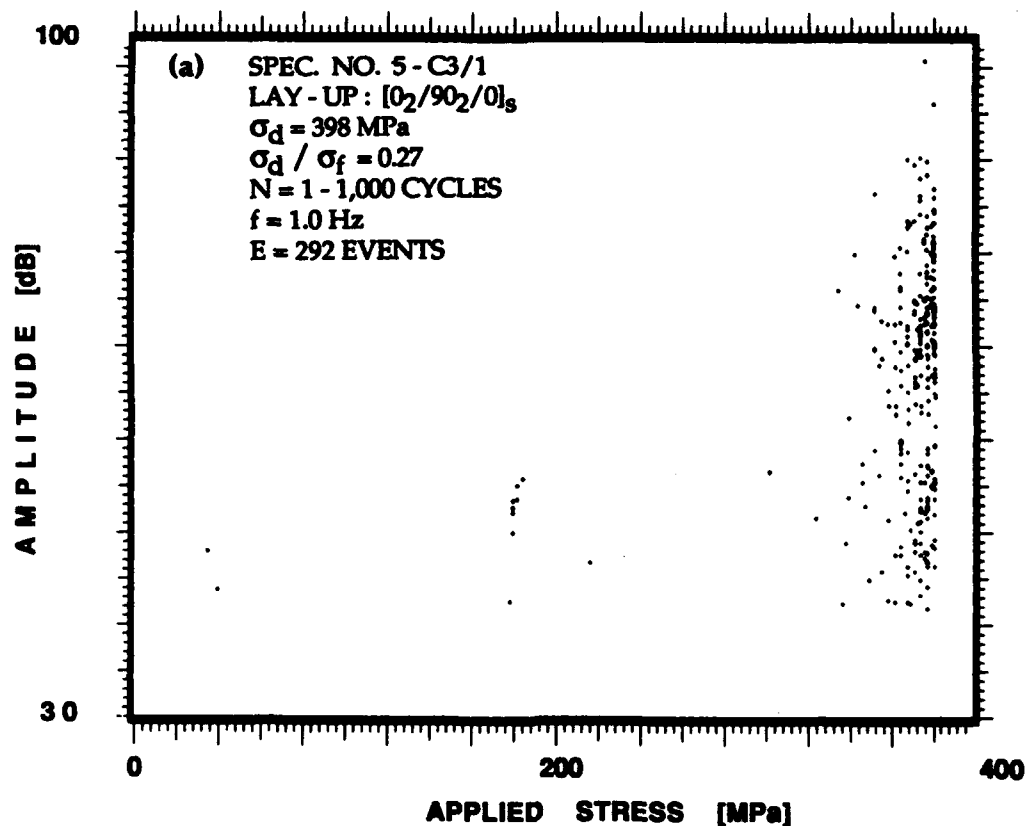


Figure 6.12. Intensities of events as a function of far-field applied stress for all the events accumulated during the same four periods of the fatigue loading and specimen shown in Figures 6.11a to 6.11d. Events occur throughout the entire load range. High intensity events occur only at the upper load range.

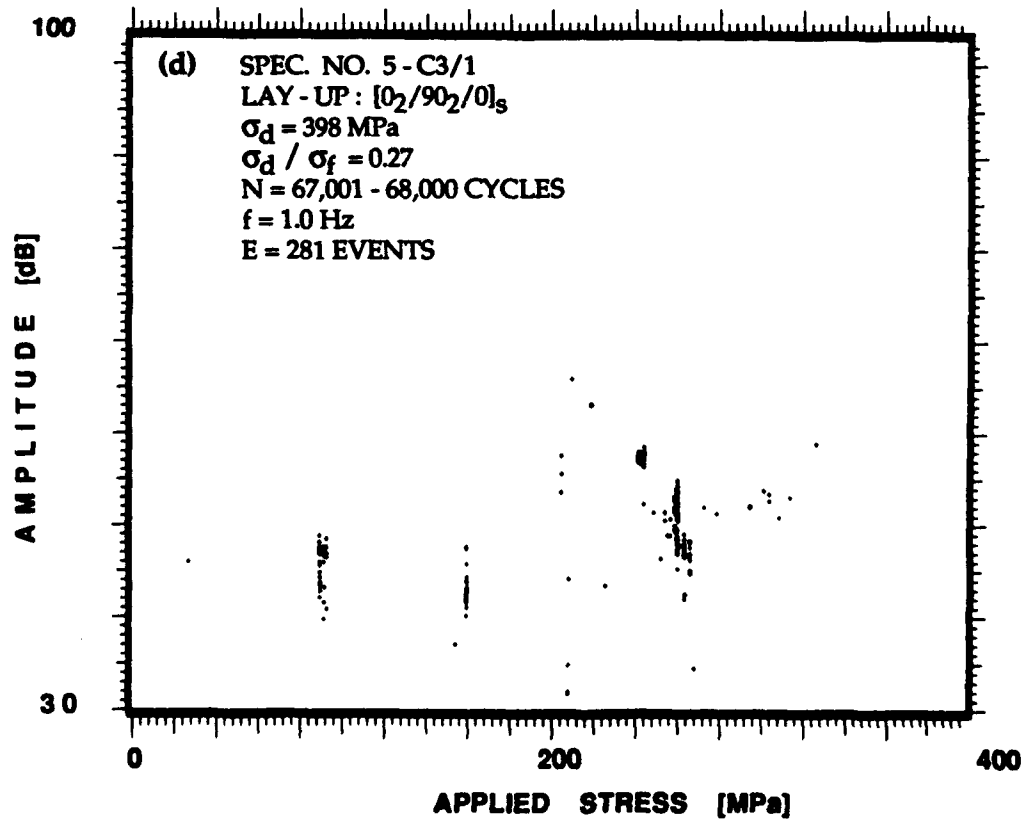
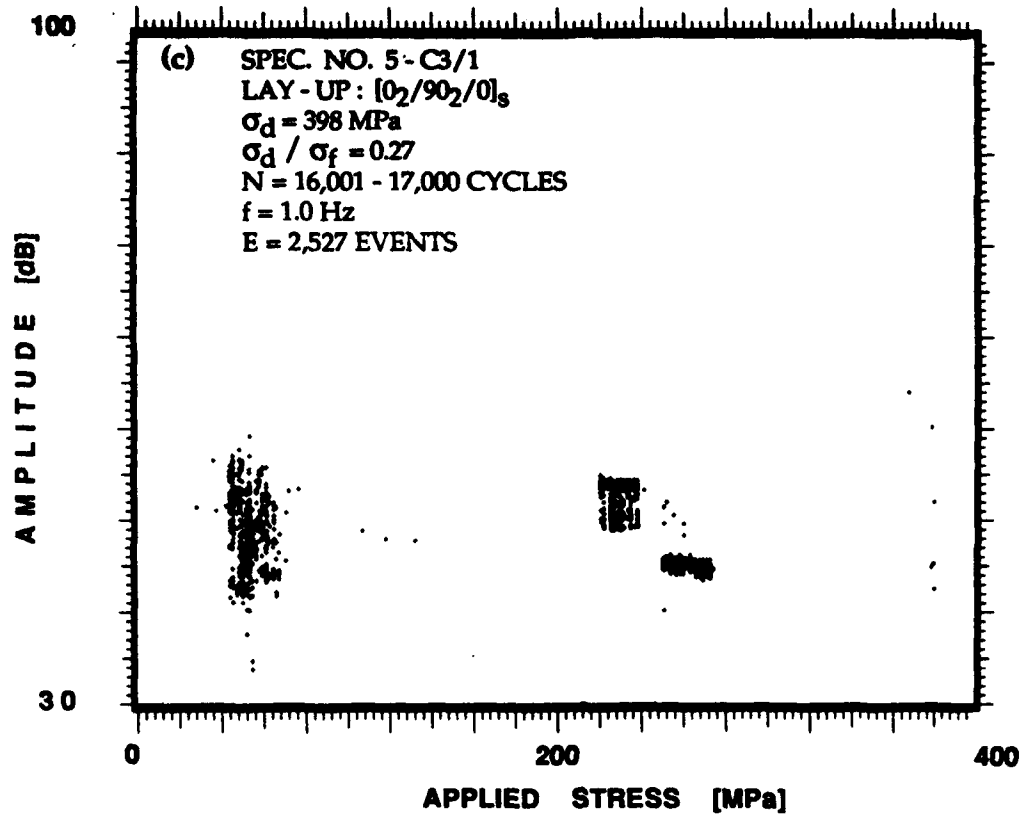


Figure 6.12. Continued.

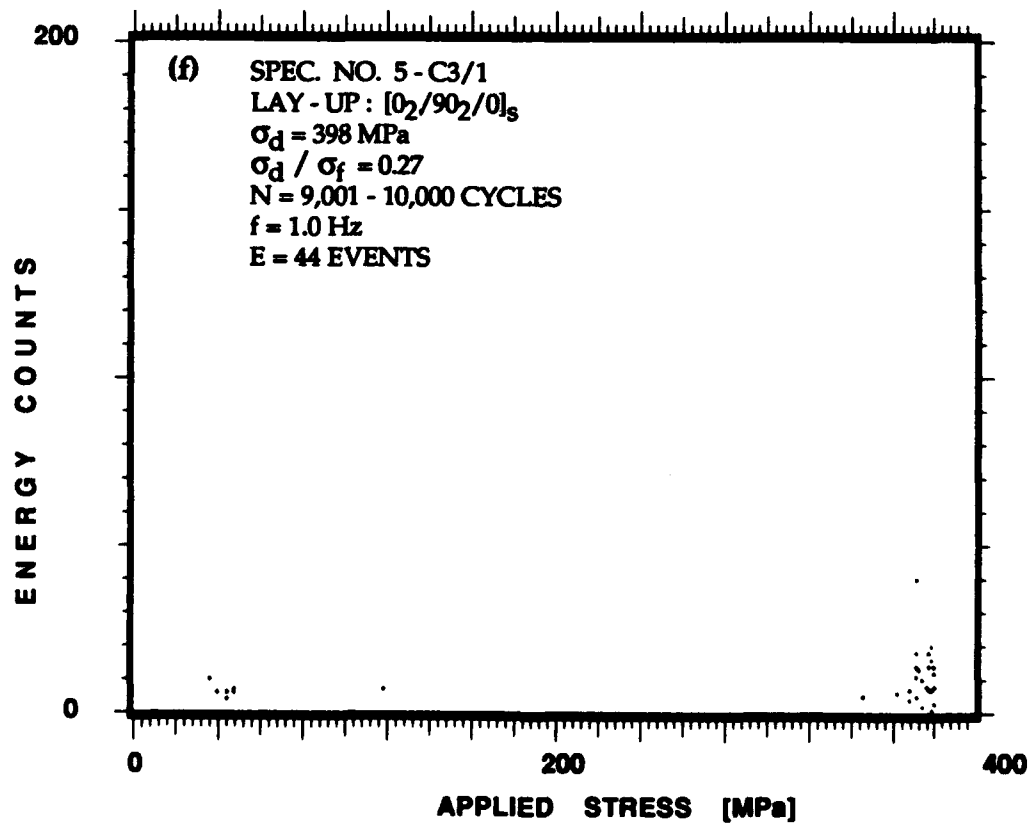
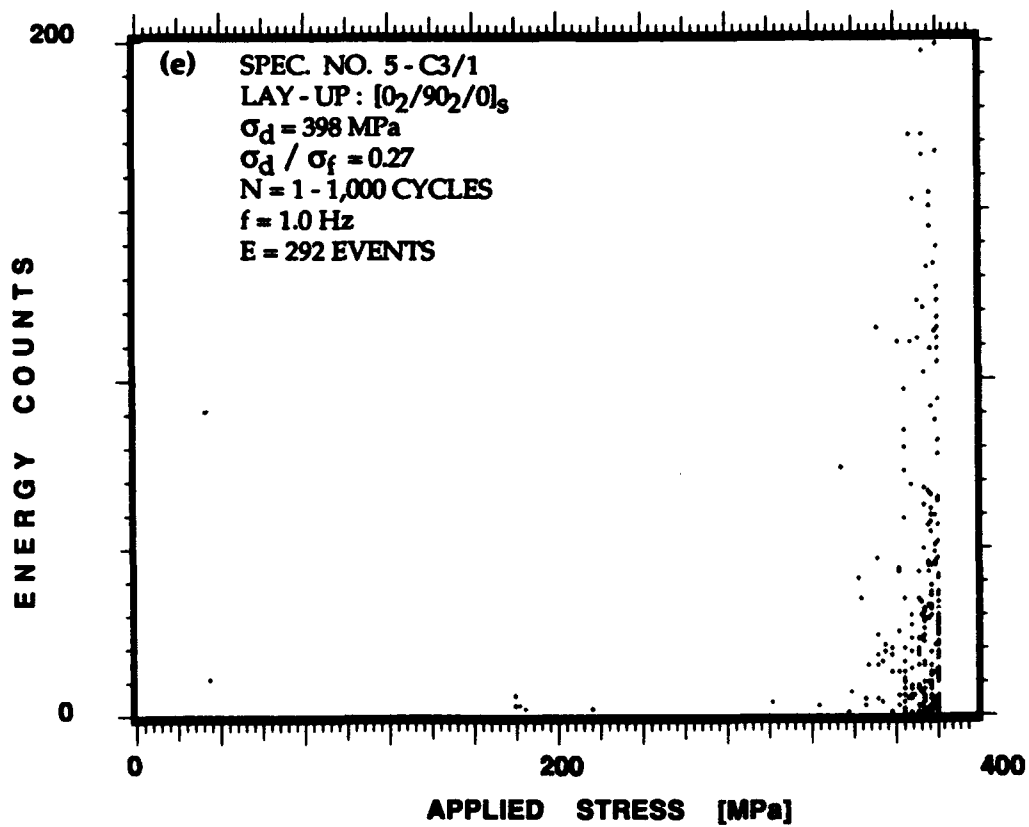


Figure 6.12. Continued.

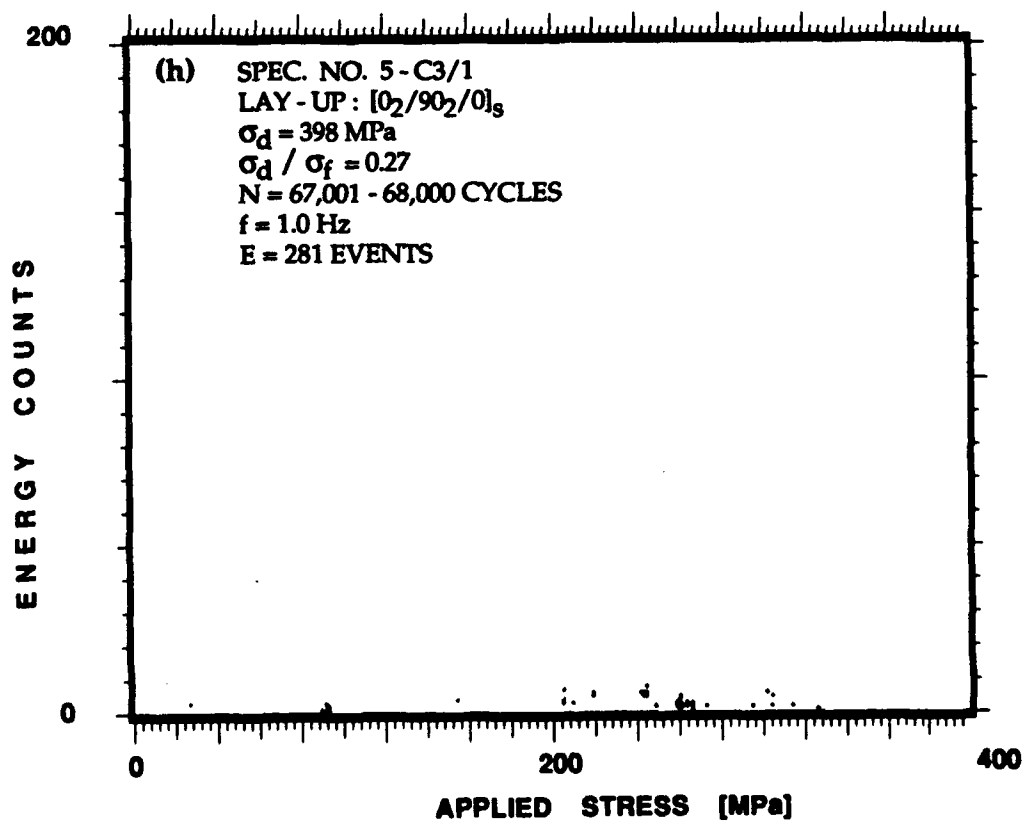
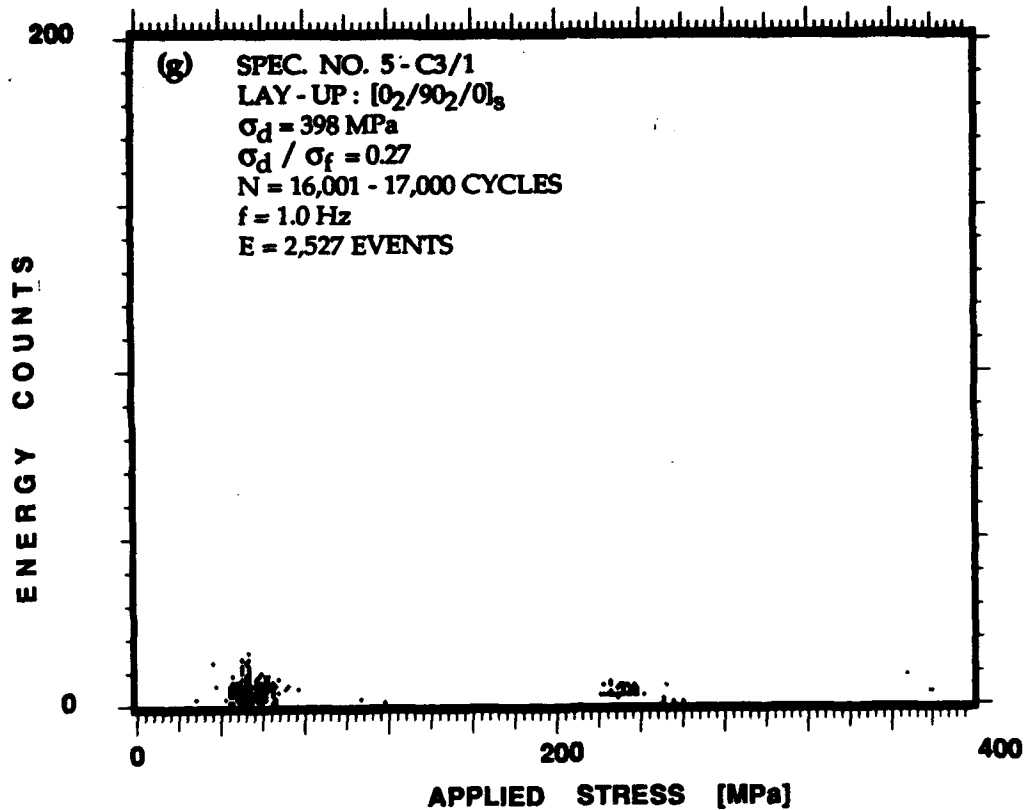


Figure 6.12. Continued.

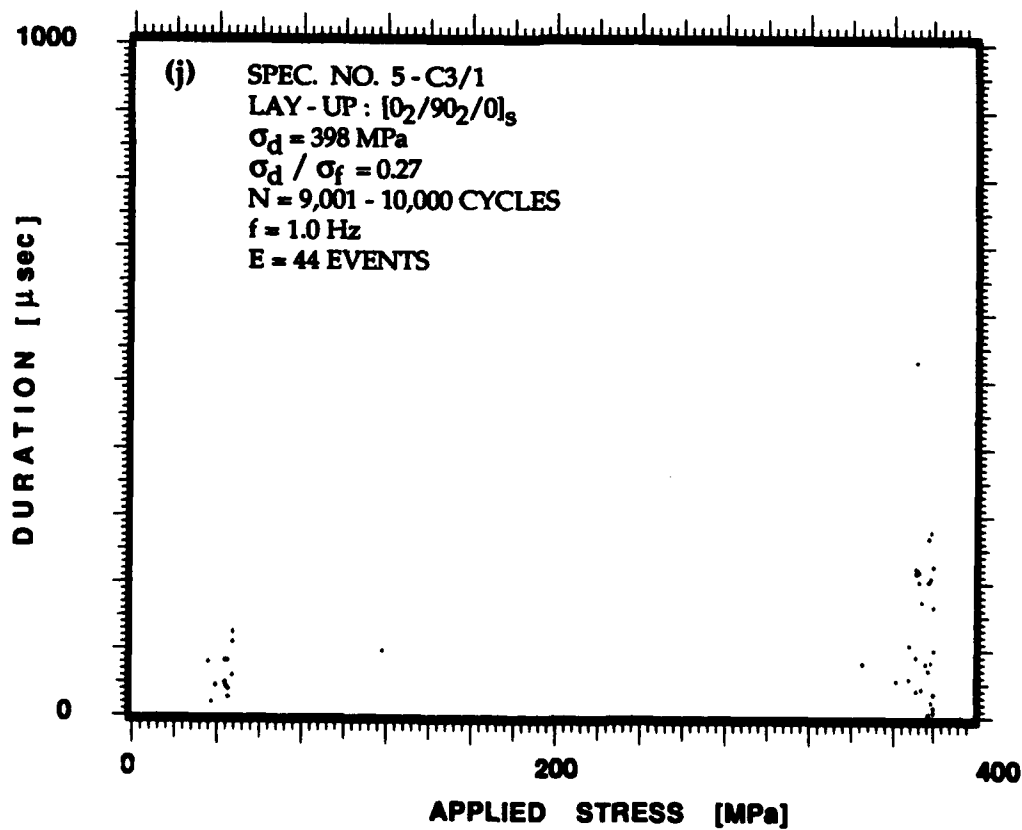
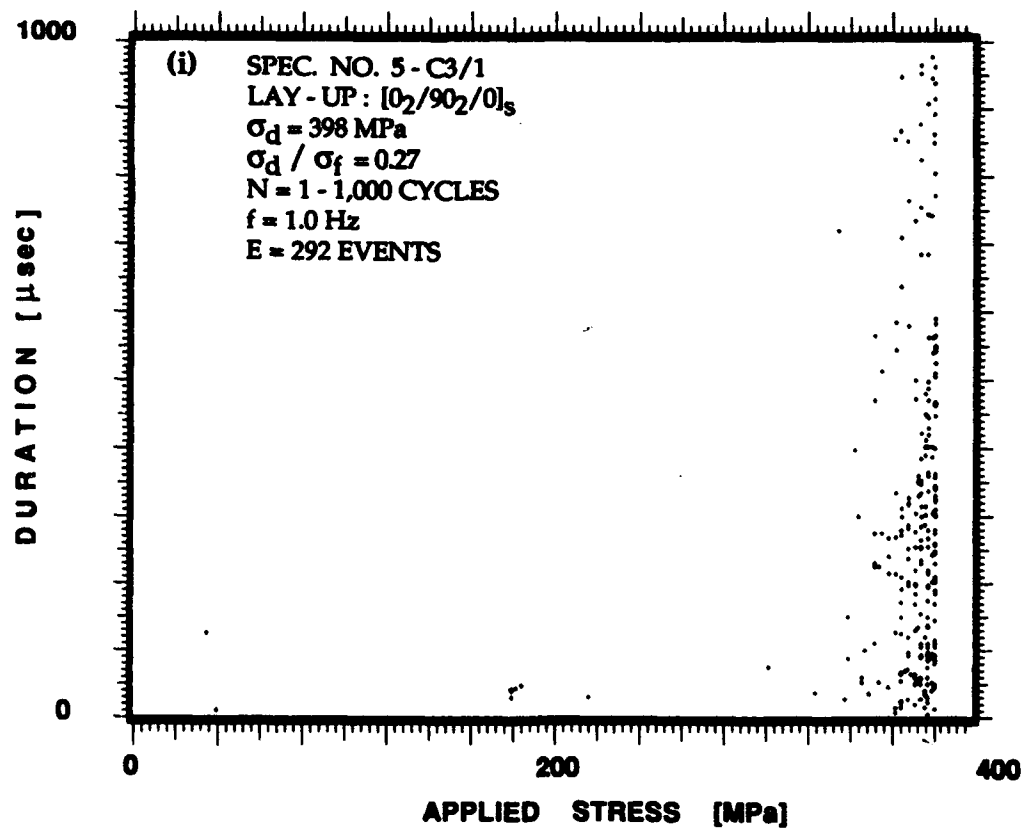


Figure 6.12. Continued.

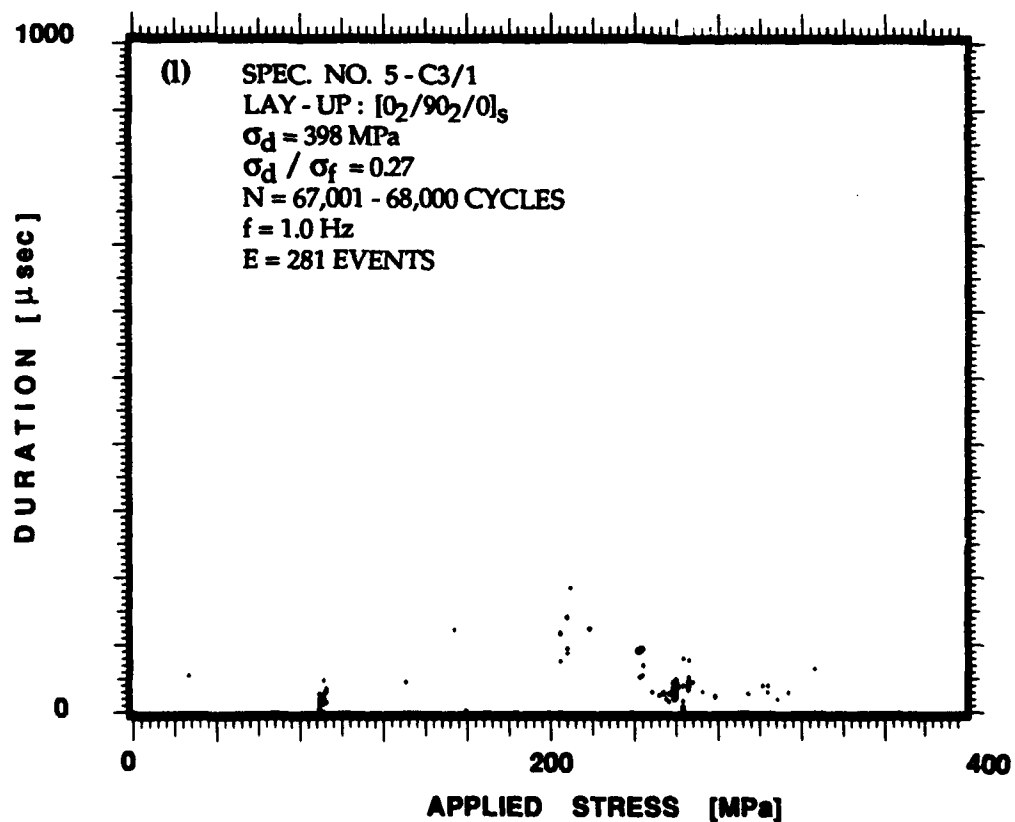
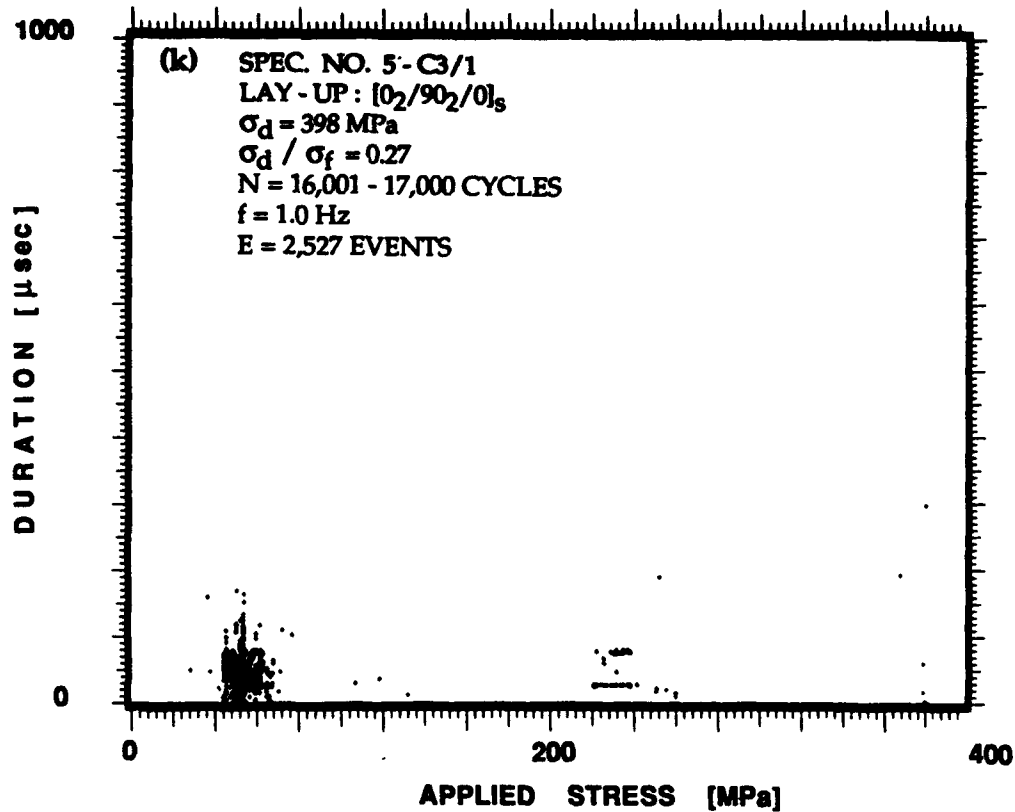


Figure 6.12. Continued.

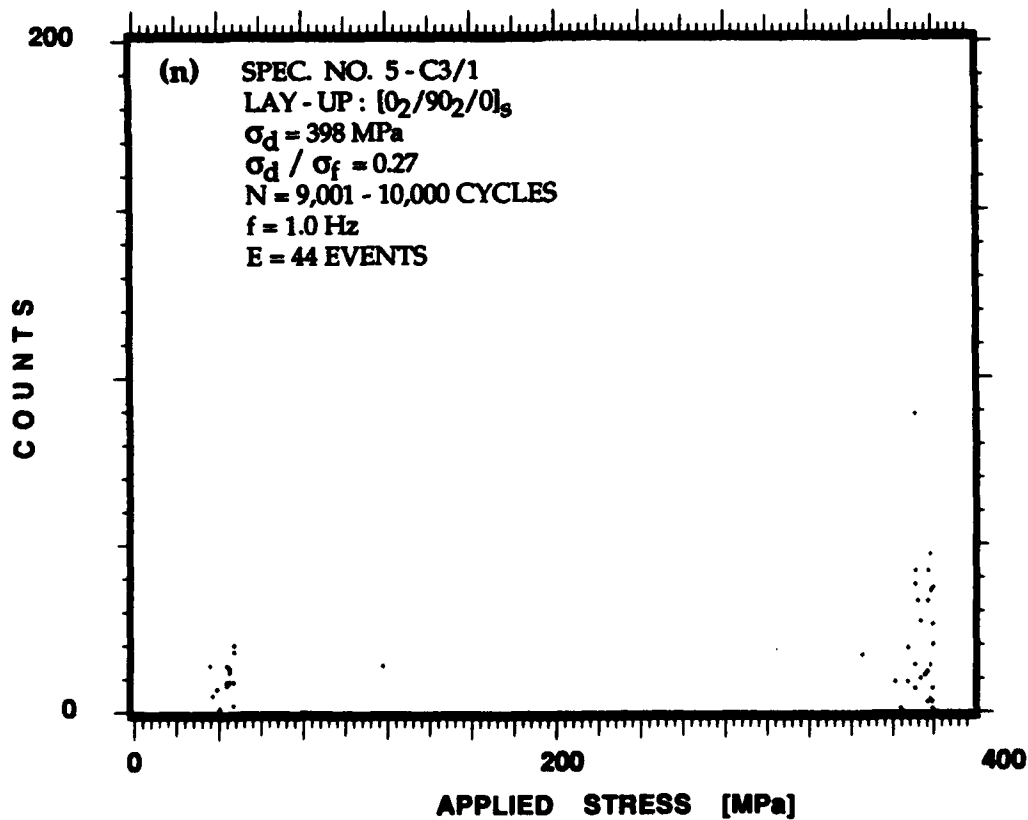
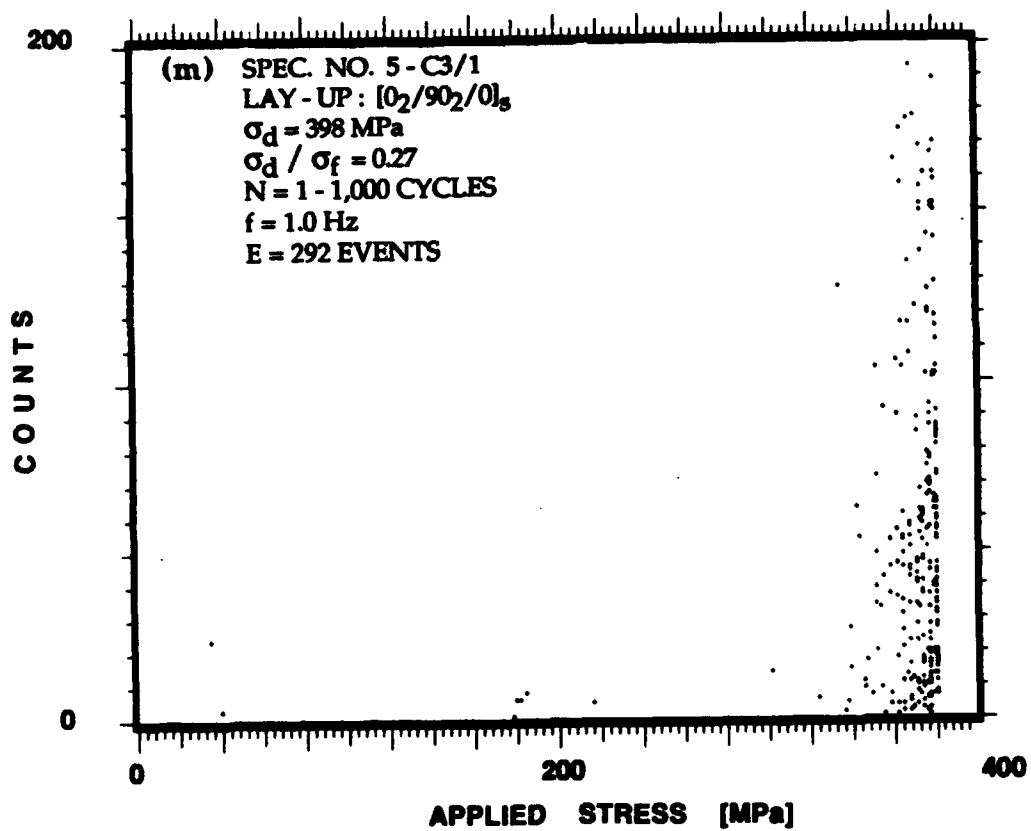


Figure 6.12. Continued.

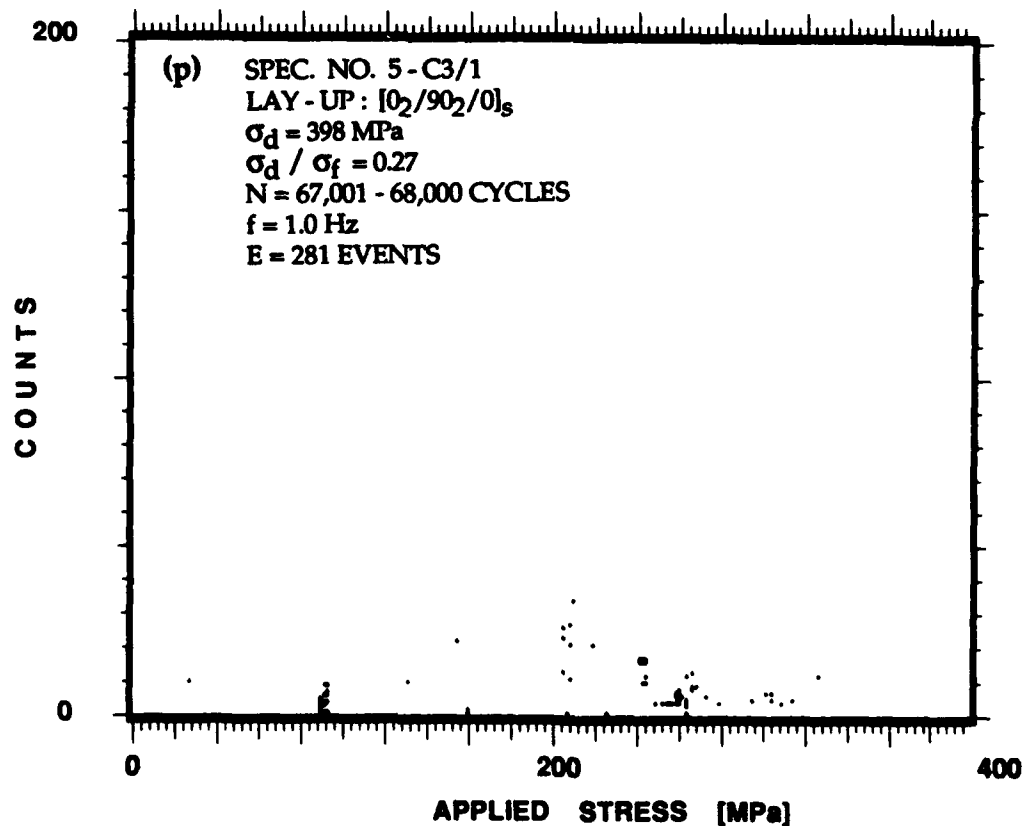
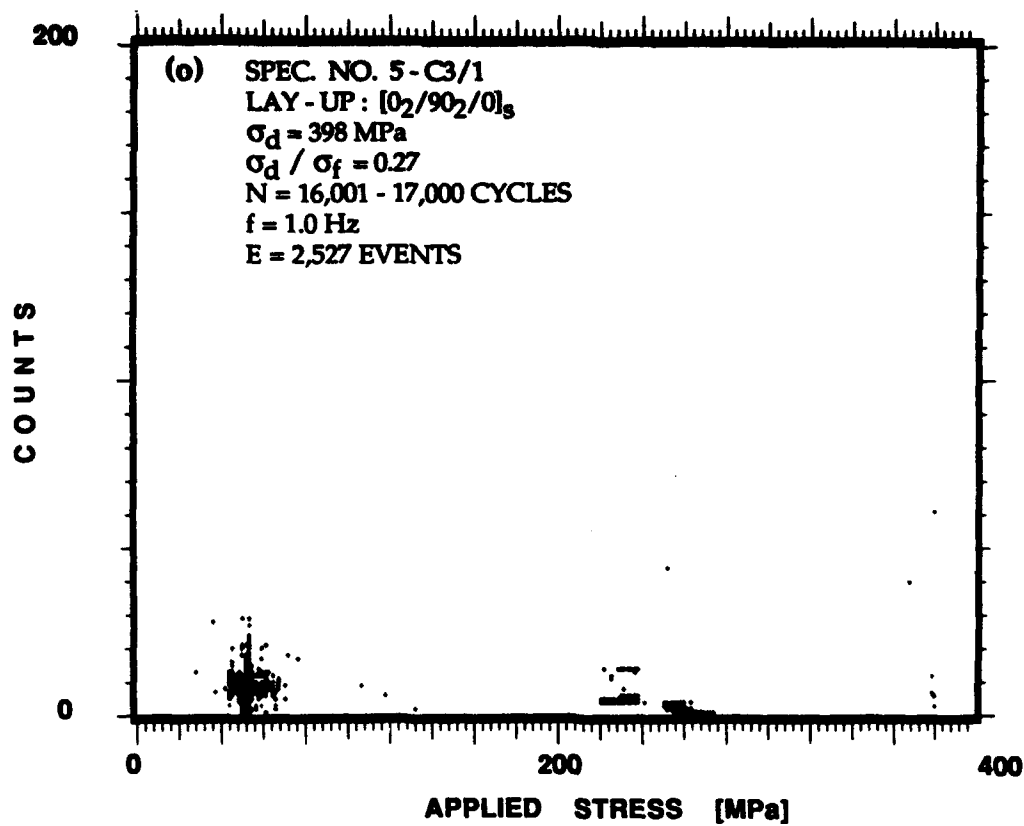


Figure 6.12. Concluded.

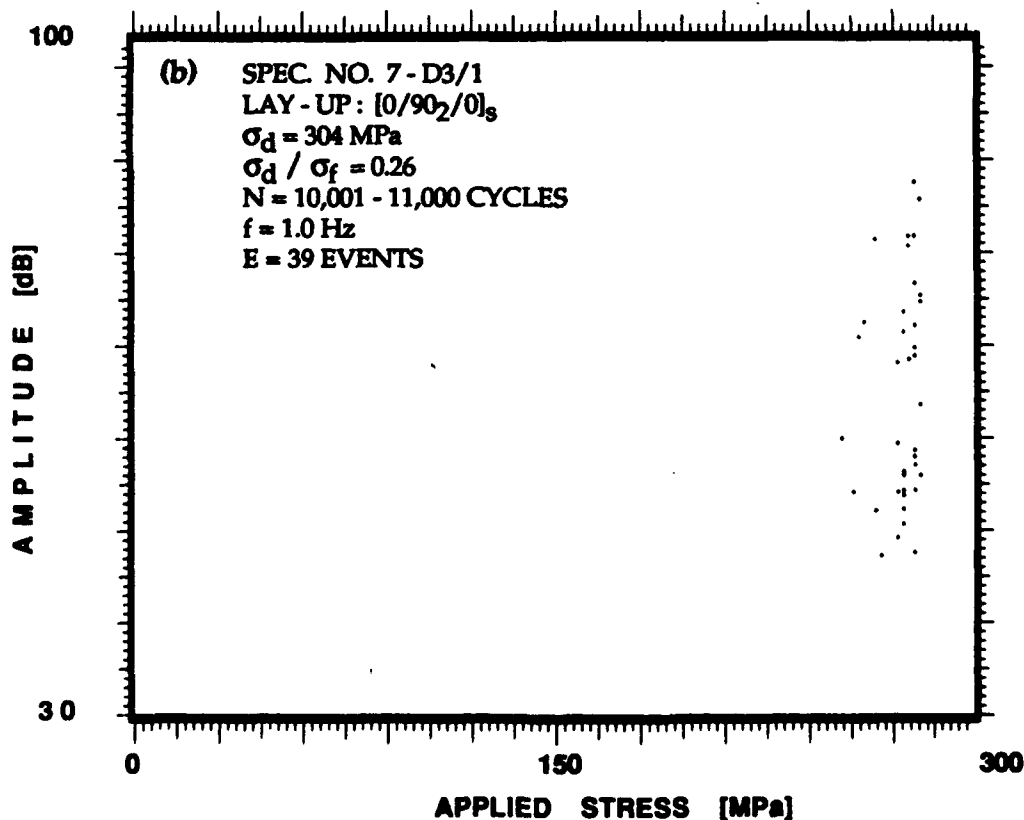
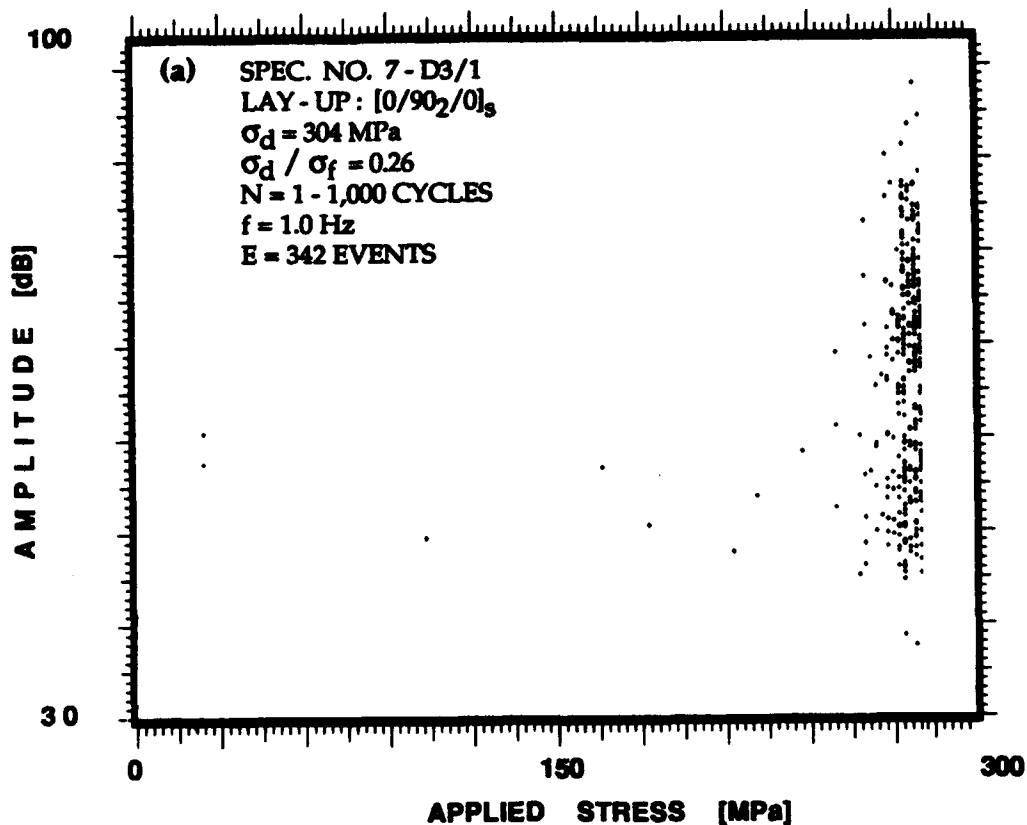


Figure 6.13. Intensities of events as a function of far-field applied stress for all the events accumulated during the same four periods of the fatigue loading and specimen shown in Figures 6.11e to 6.11h. Events occur throughout the entire load range. High intensity events occur only at the upper load range.

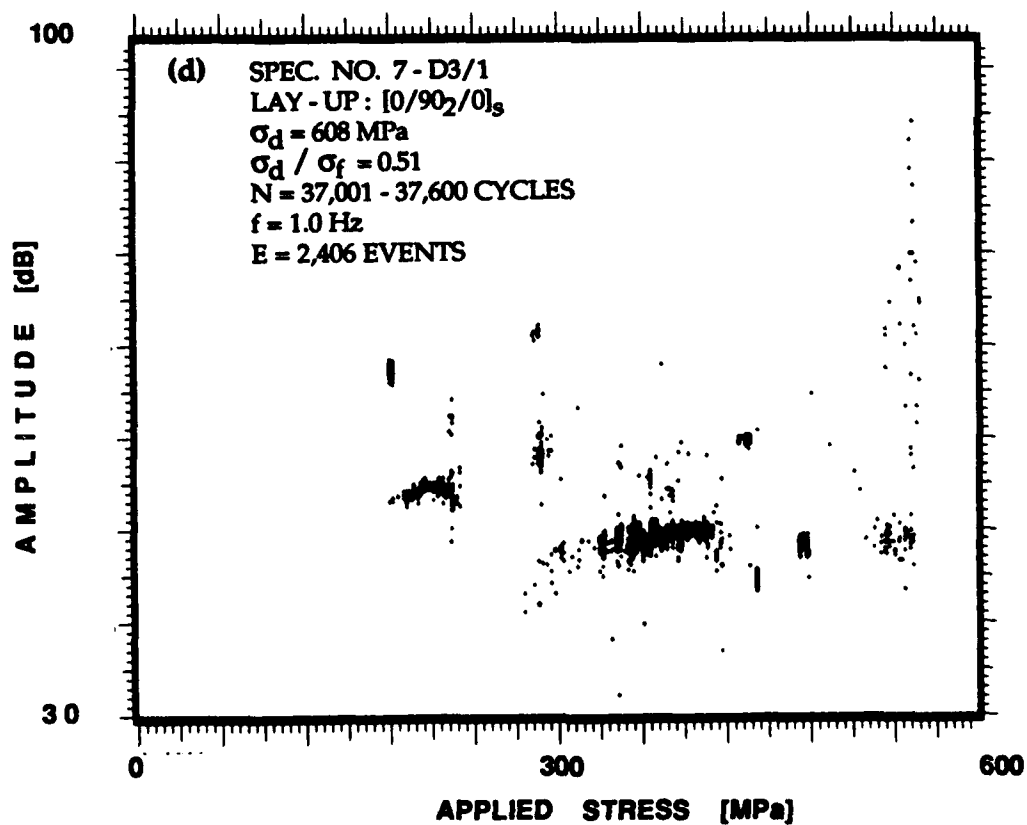
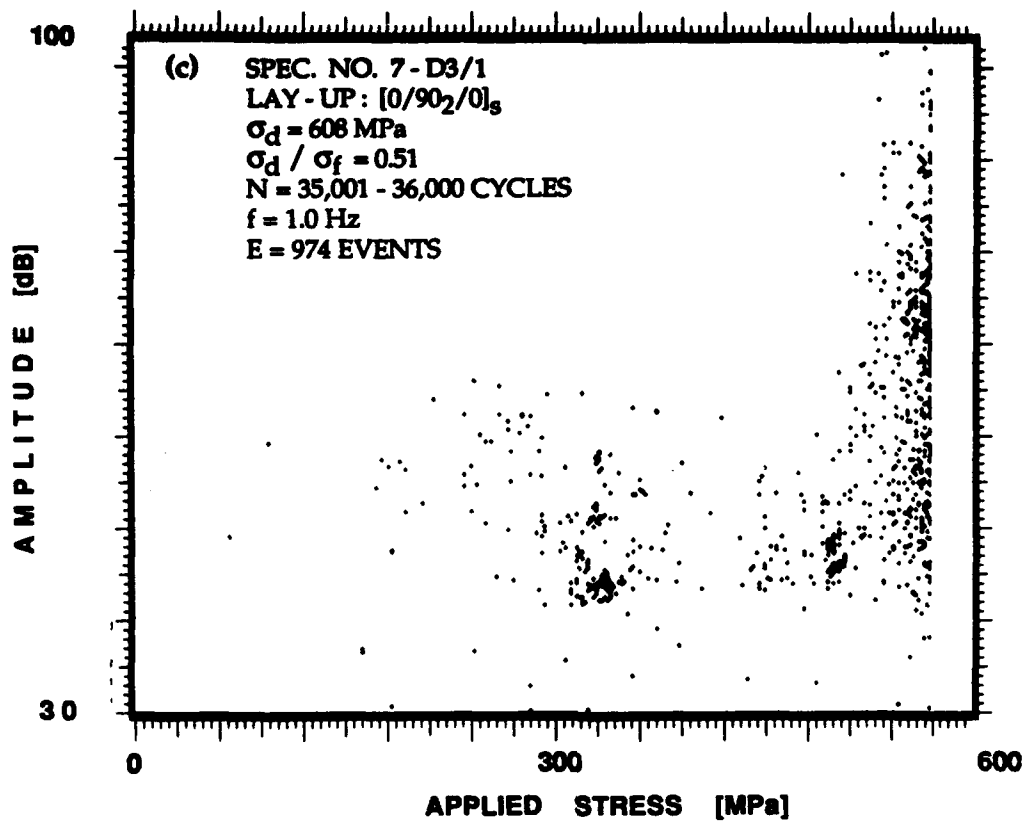


Figure 6.13. Continued.

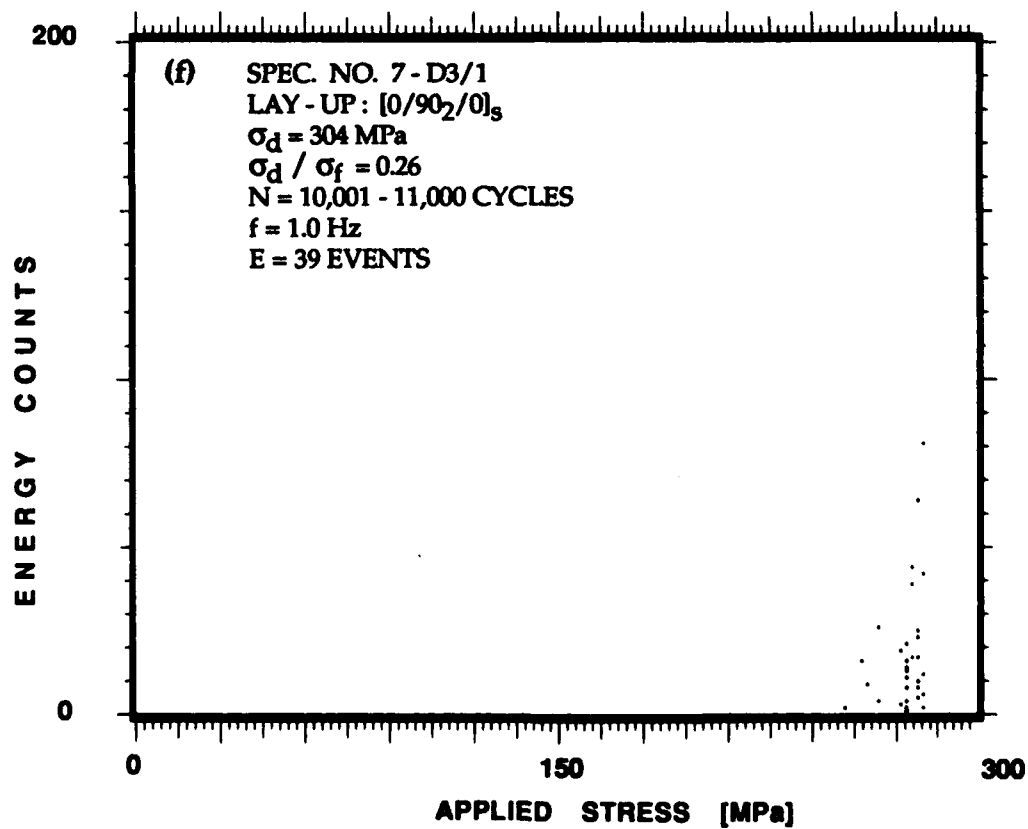
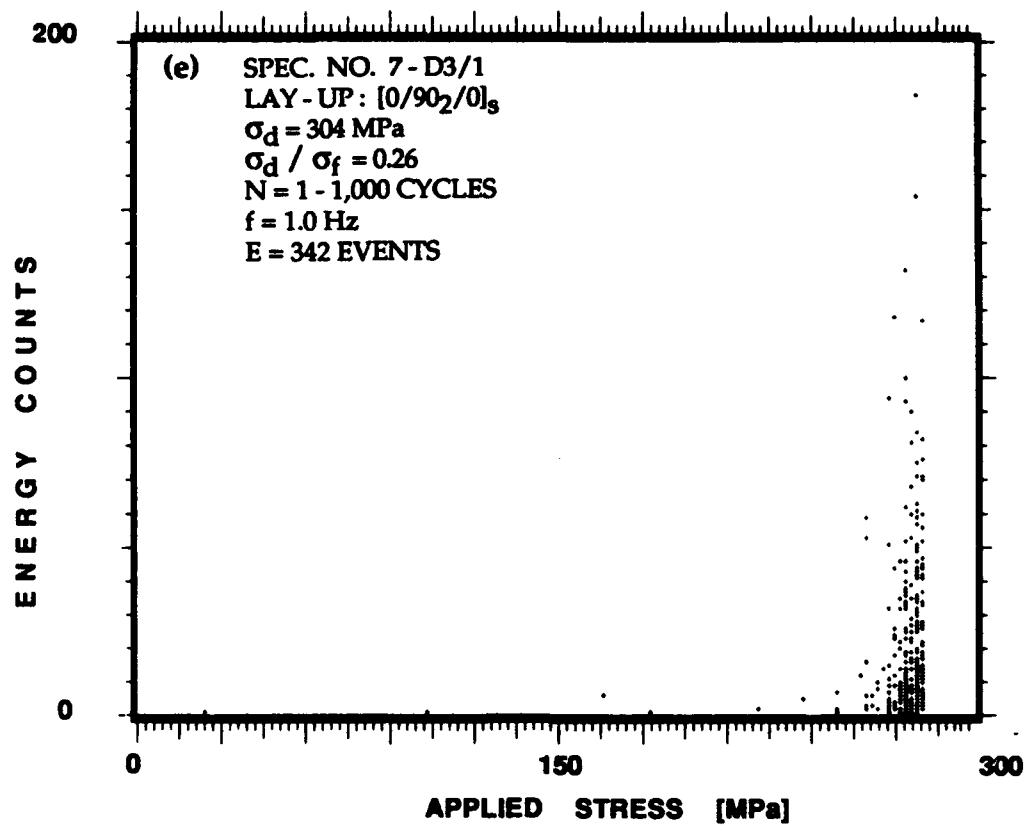


Figure 6.13. Continued.

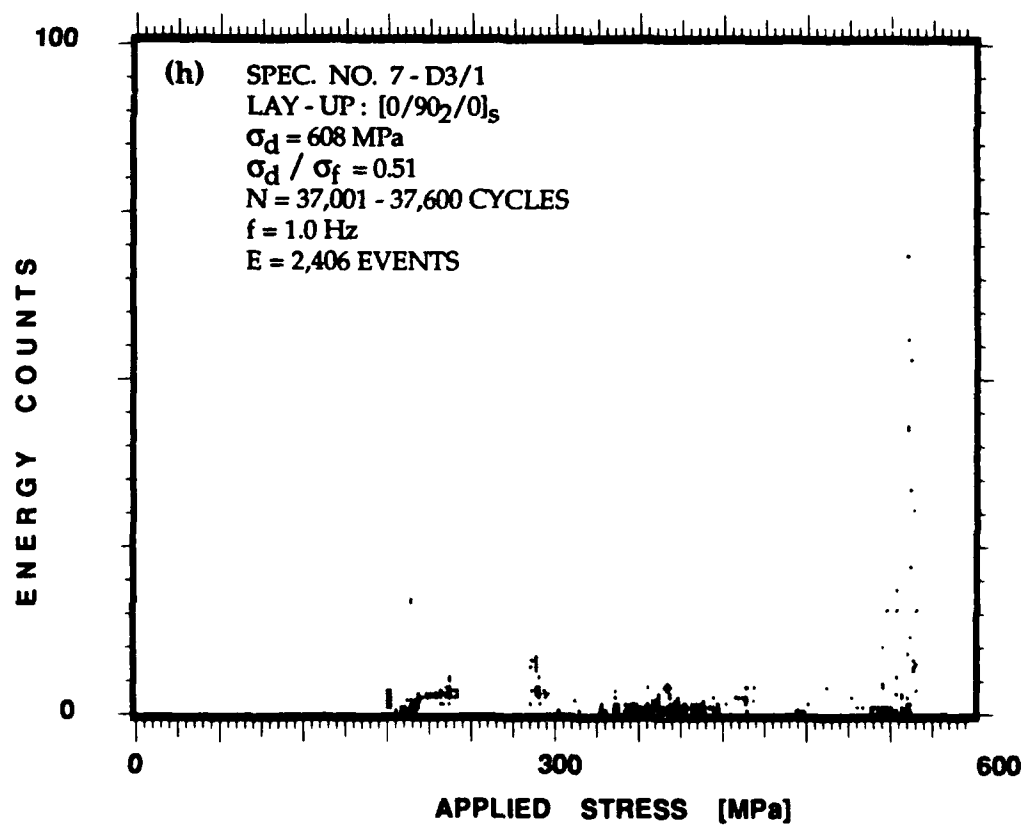
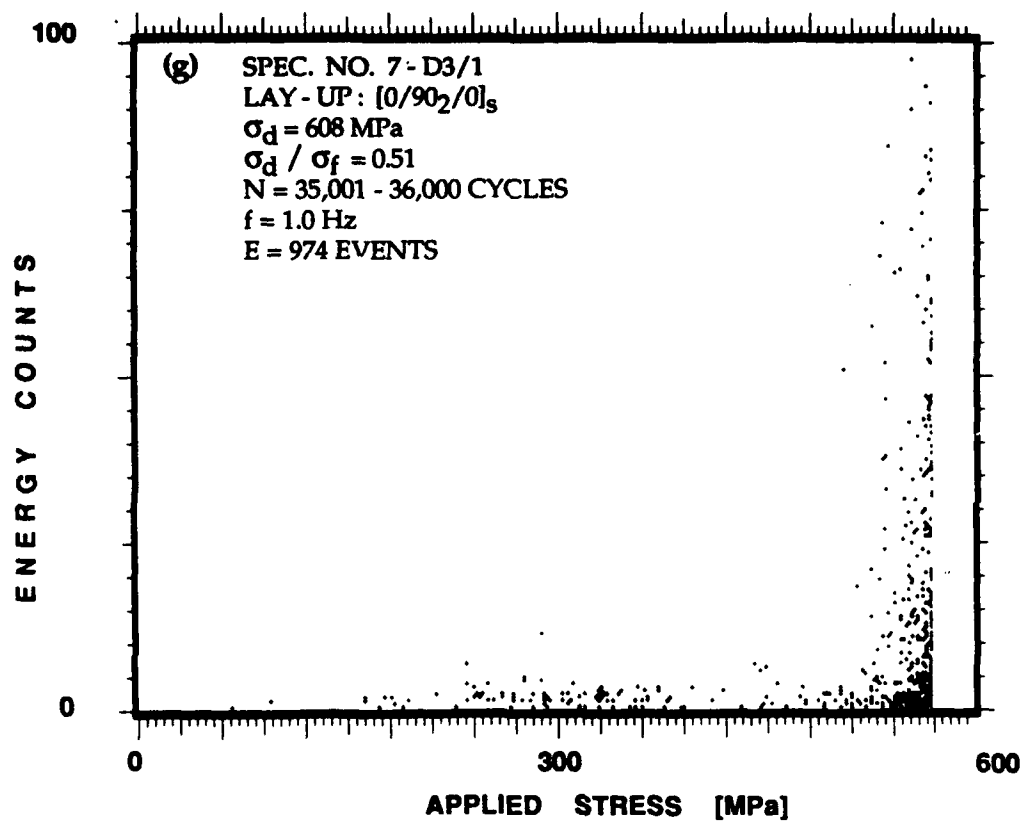


Figure 6.13. Continued.

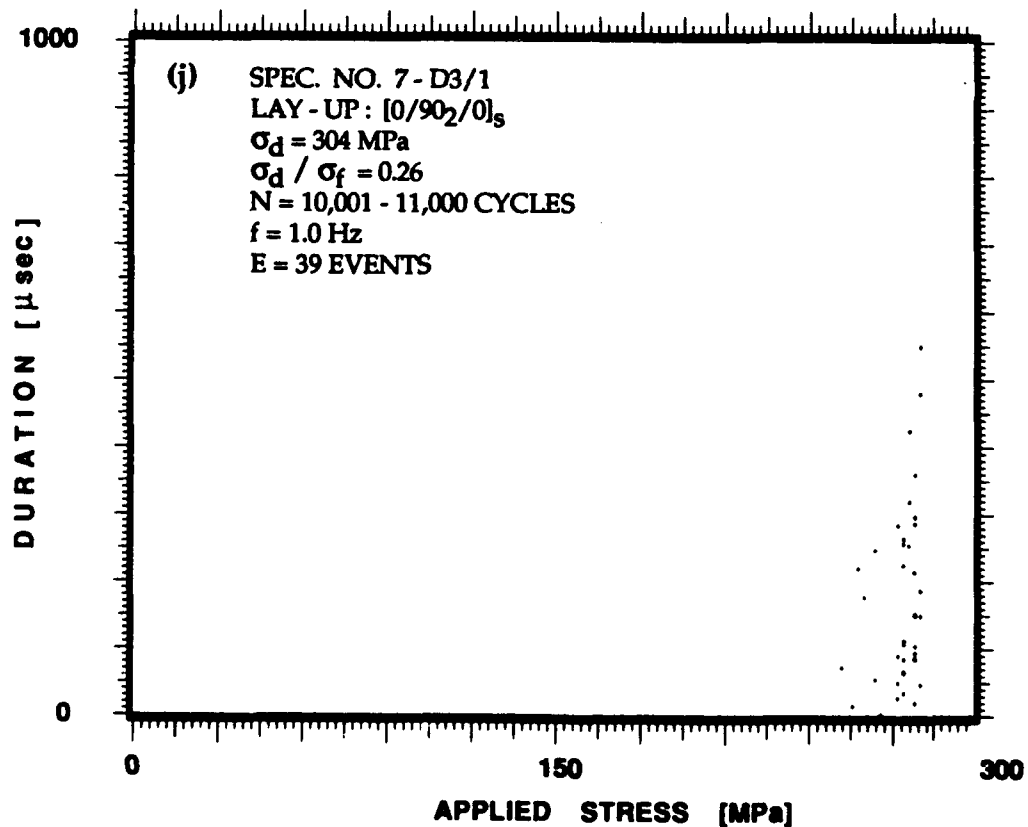
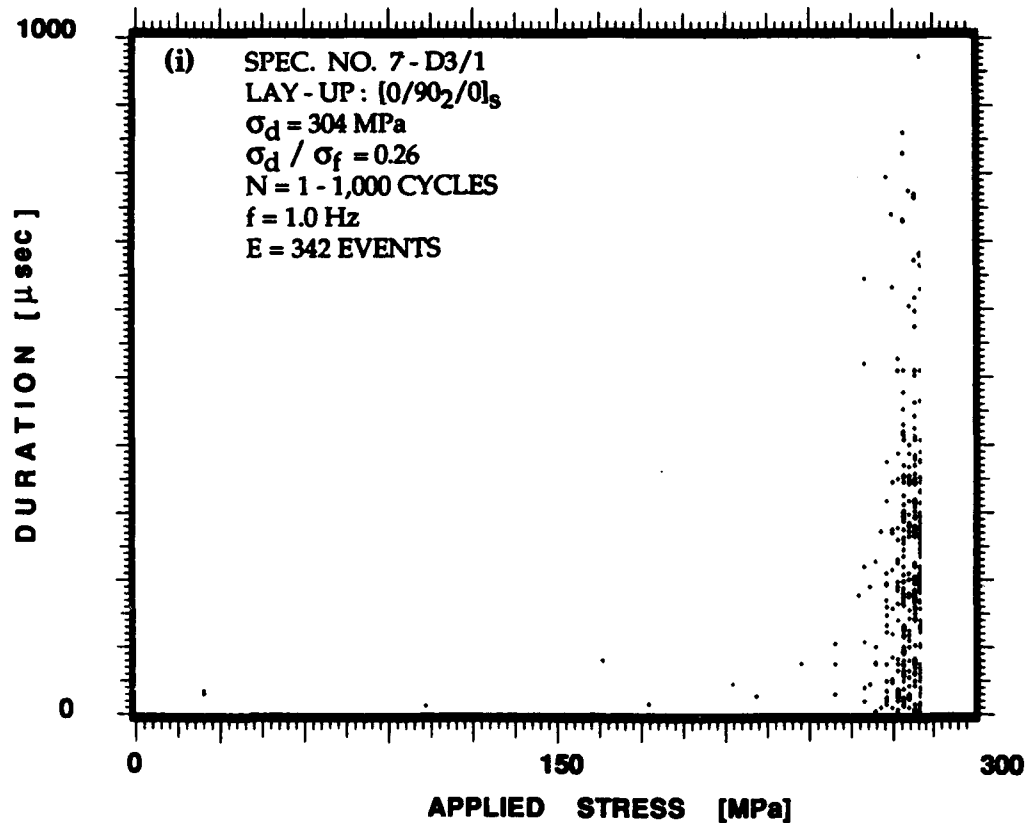


Figure 6.13. Continued.

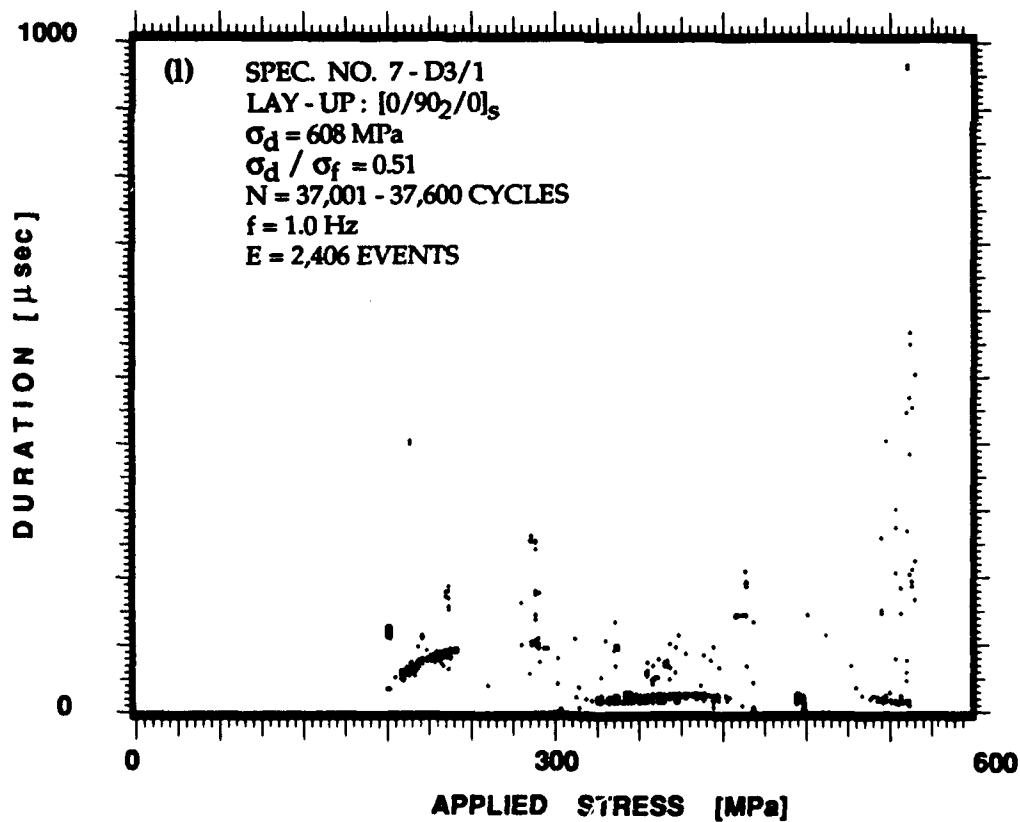
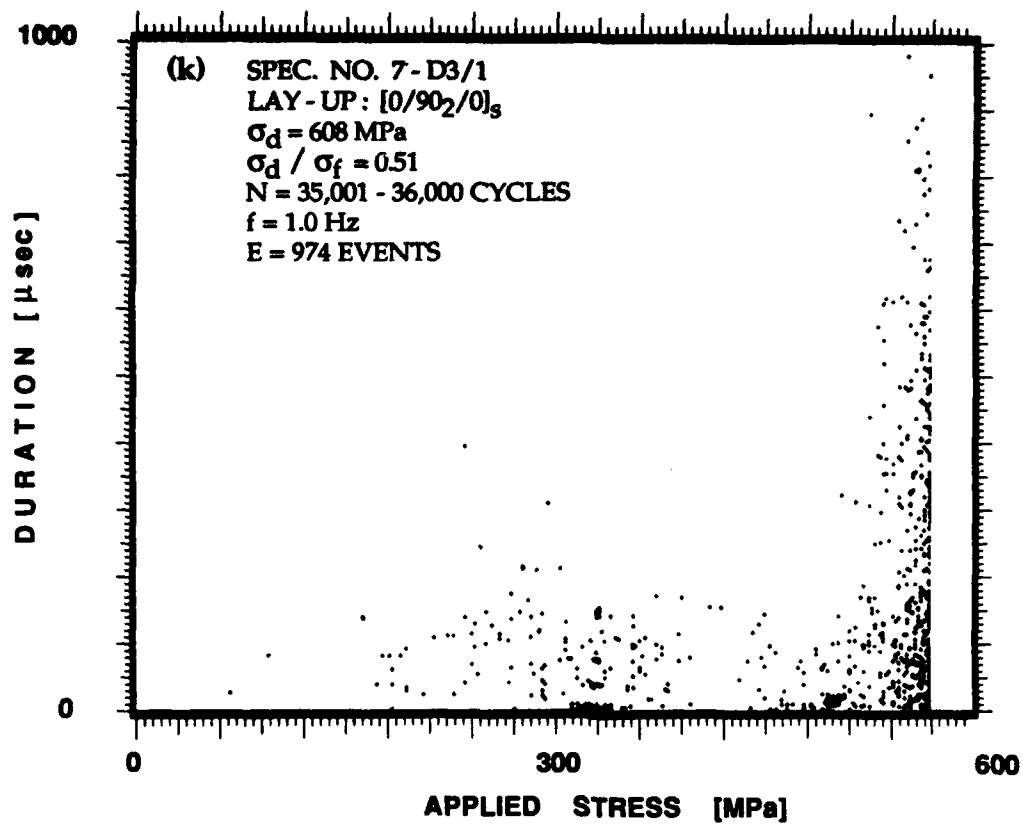


Figure 6.13. Continued.

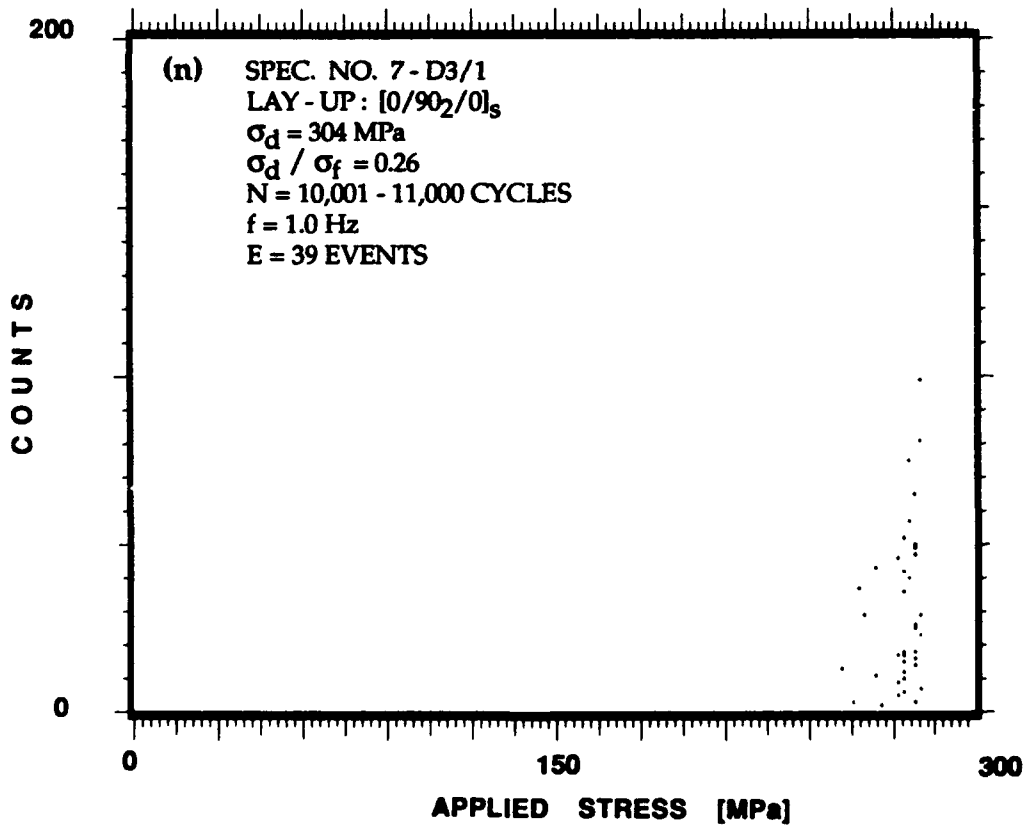
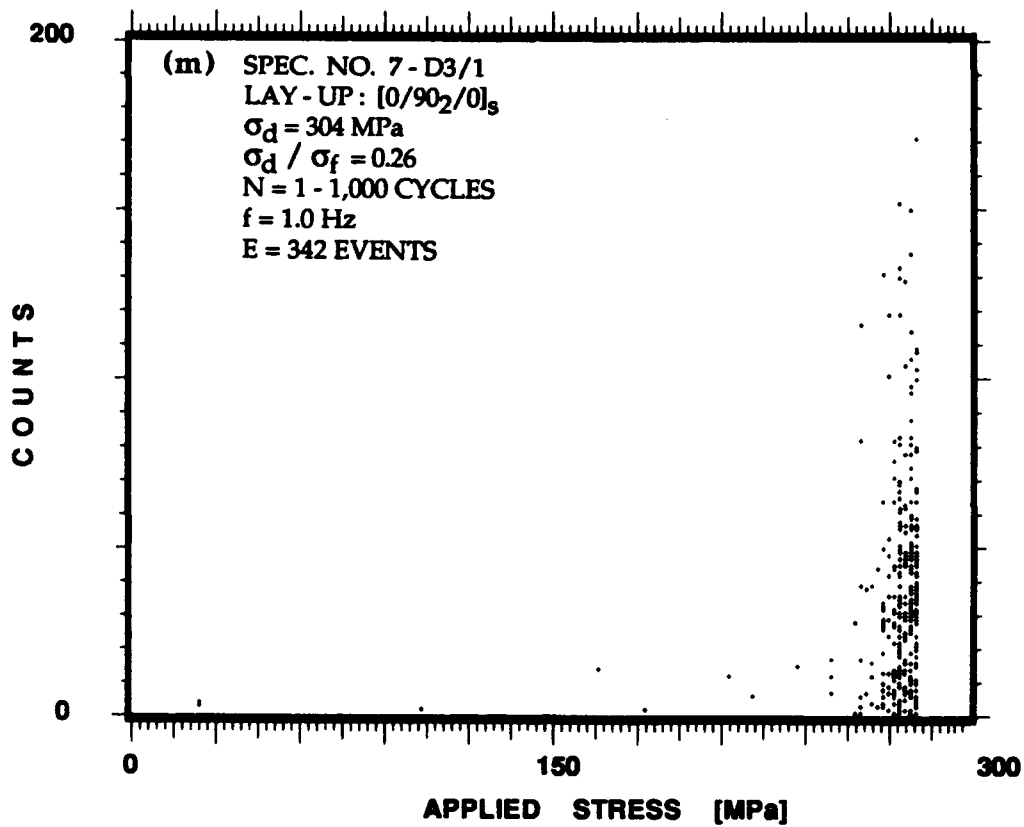


Figure 6.13. Continued.

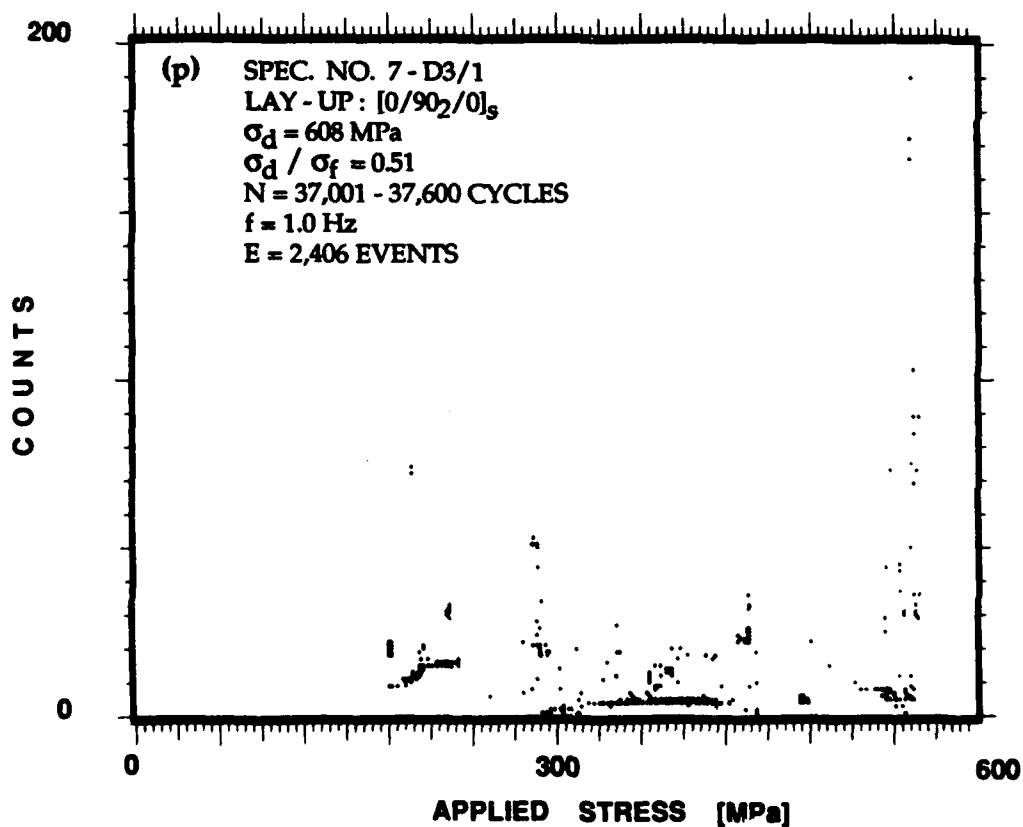
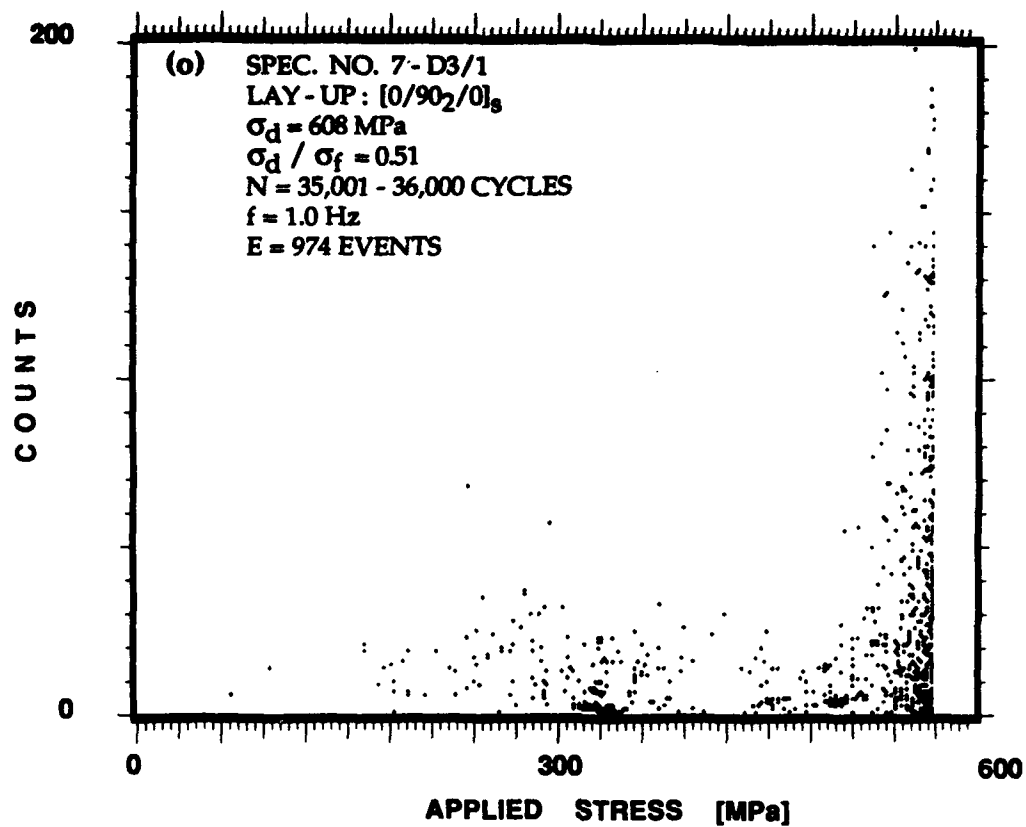


Figure 6.13. Concluded.

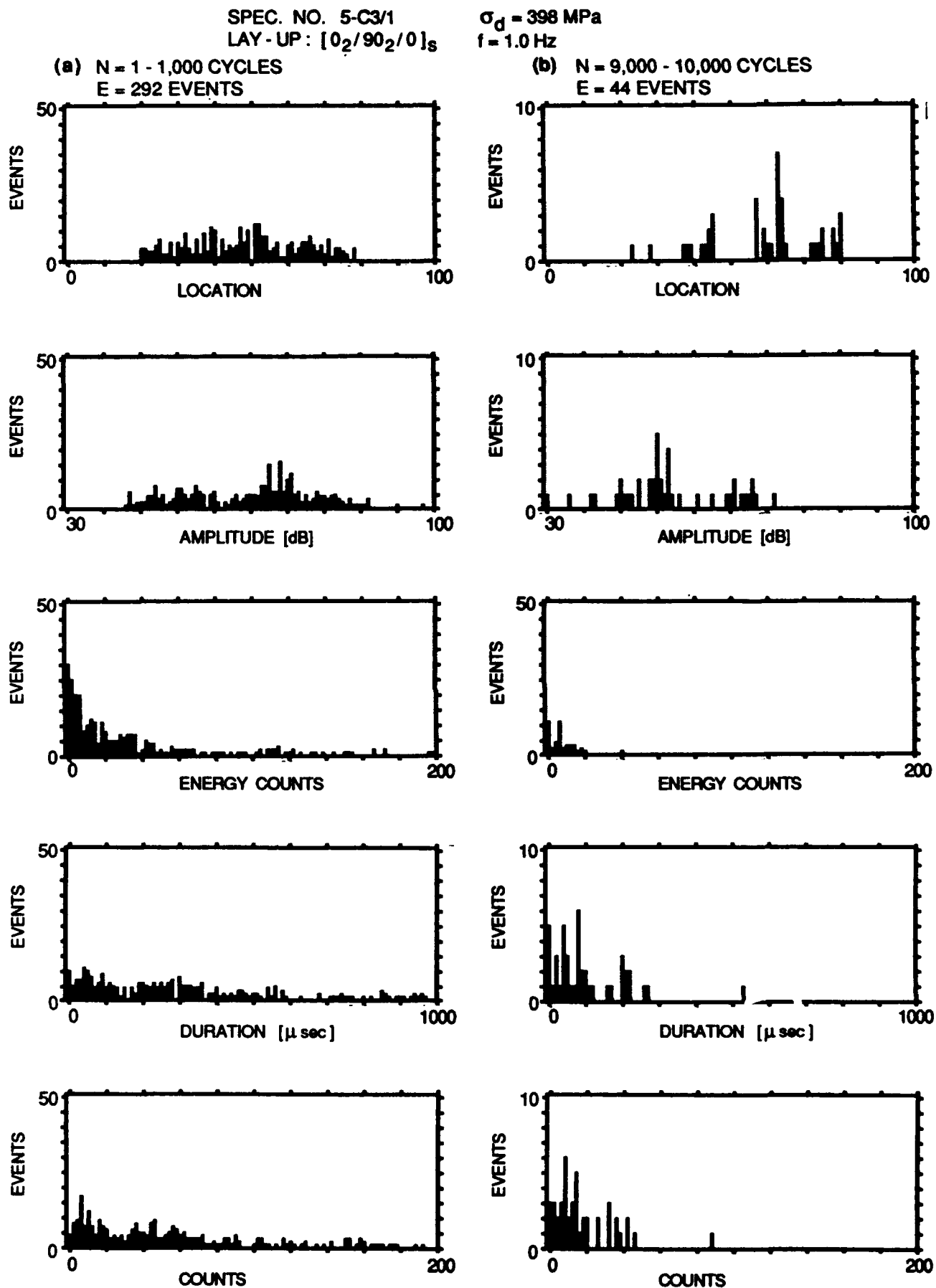


Figure 6.14. Acoustic emission event intensity and location distribution histograms for all the events accumulated during the same periods of the fatigue loading and specimen shown in Figures 6.11a to 6.11d. All distributions vary with the progression of the fatigue loading.

SPEC. NO. 5-C3/1
LAY-UP: $[0_2/90_2/0]_8$

$\sigma_d = 398 \text{ MPa}$
 $f = 1.0 \text{ Hz}$

(c) $N = 16,000 - 17,000 \text{ CYCLES}$
 $E = 2,527 \text{ EVENTS}$

(d) $N = 67,000 - 68,000 \text{ CYCLES}$
 $E = 281 \text{ EVENTS}$

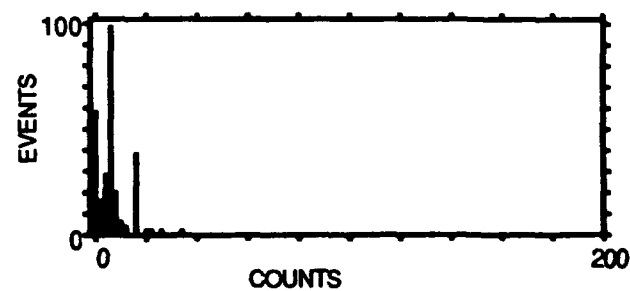
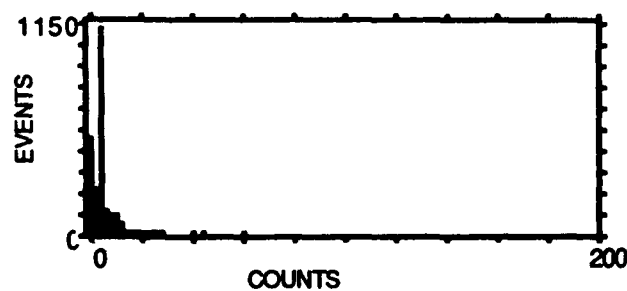
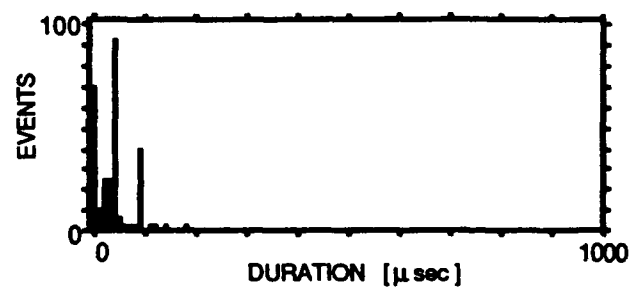
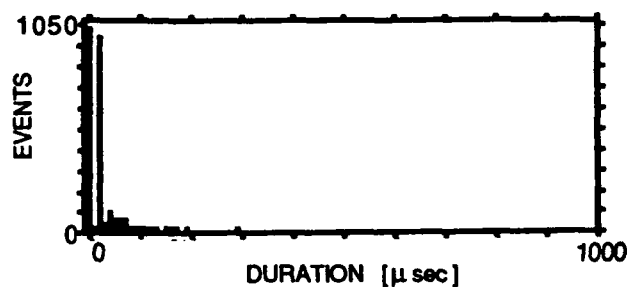
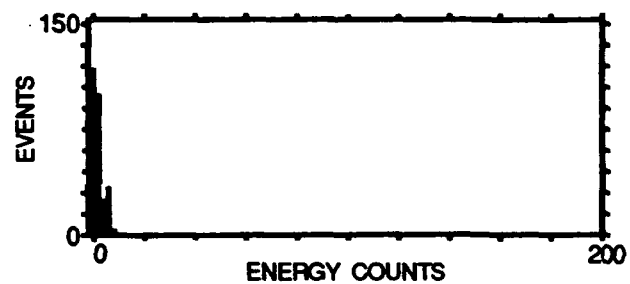
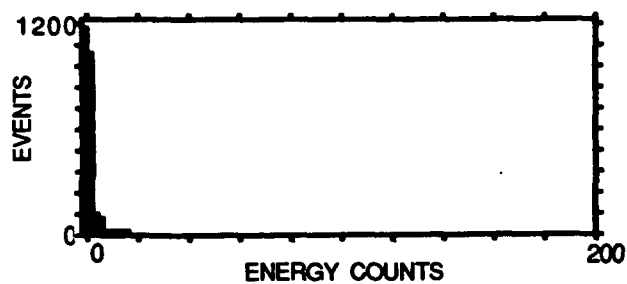
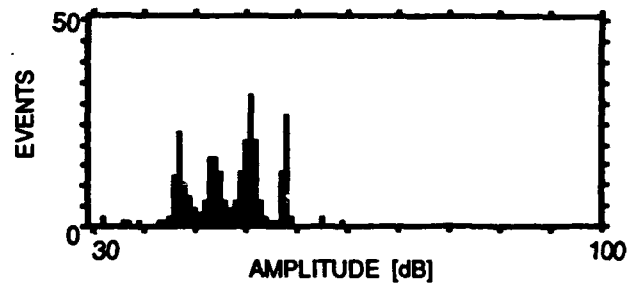
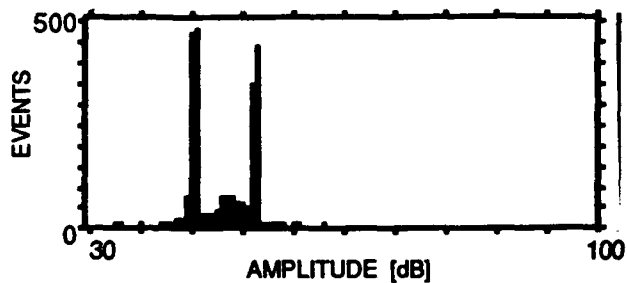
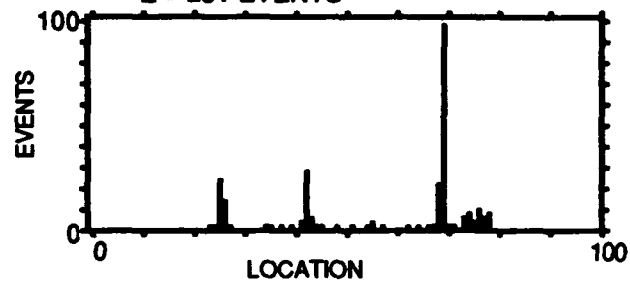
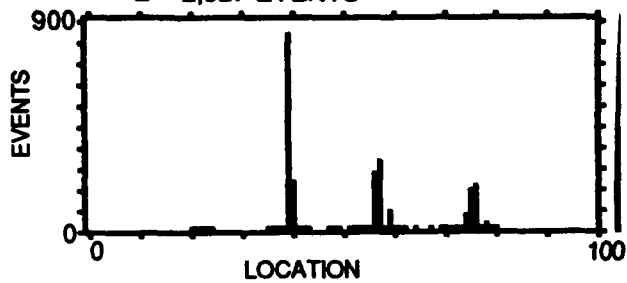


Figure 6.14. Concluded.

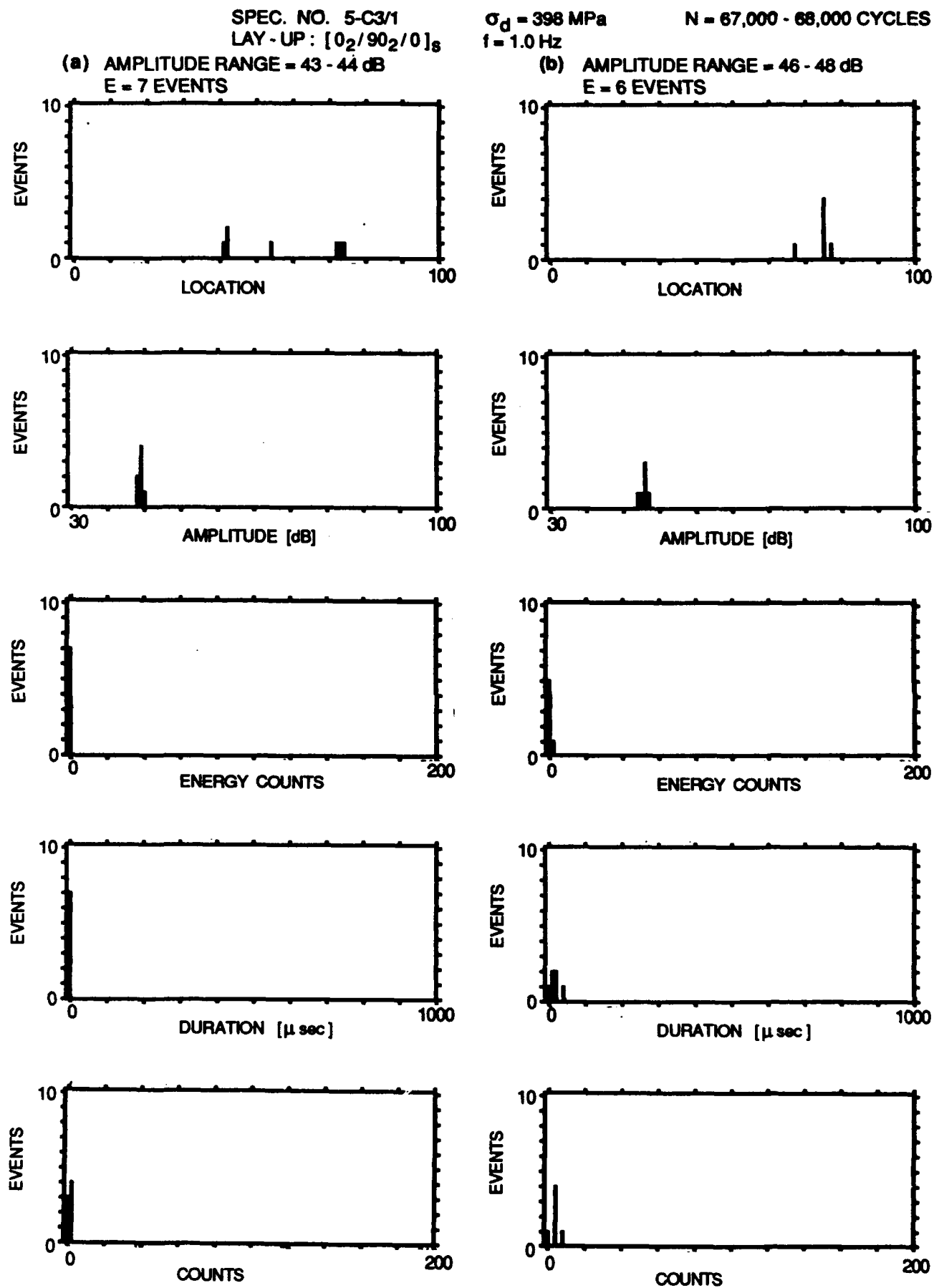


Figure 6.15. Acoustic emission event intensity and location distribution histograms for those events shown in Figure 6.14d that have four specific amplitude ranges. Events of specific amplitudes correlate with the other three intensities and they occur at specific locations.

SPEC. NO. 5-C3/1
LAY-UP: $[0_2/90_2/0]_8$

$\sigma_d = 398 \text{ MPa}$
 $f = 1.0 \text{ Hz}$

$N = 67,000 - 68,000 \text{ CYCLES}$

(c) AMPLITUDE RANGE = 51 - 53 dB
E = 63 EVENTS

(d) AMPLITUDE RANGE = 56 - 58 dB
E = 21 EVENTS

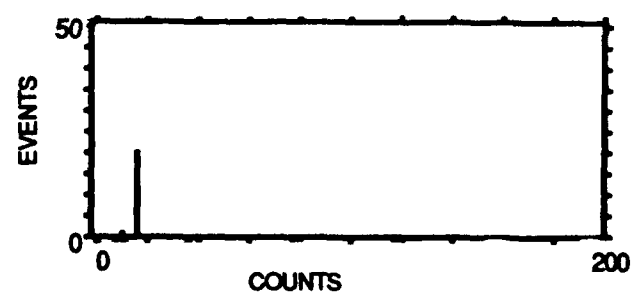
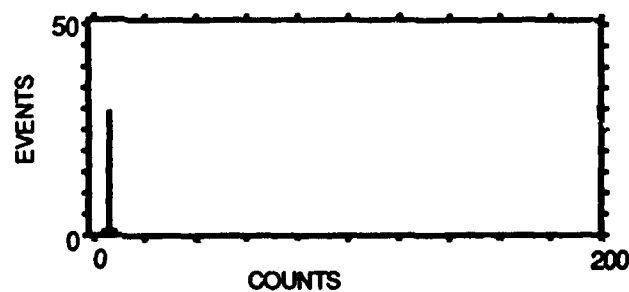
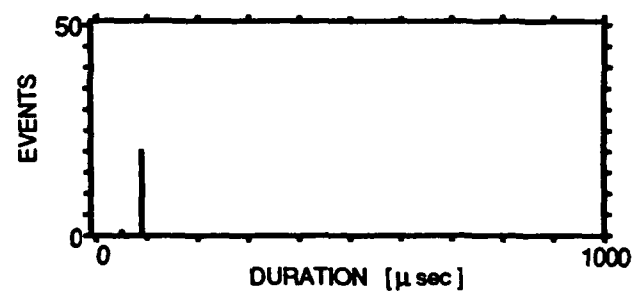
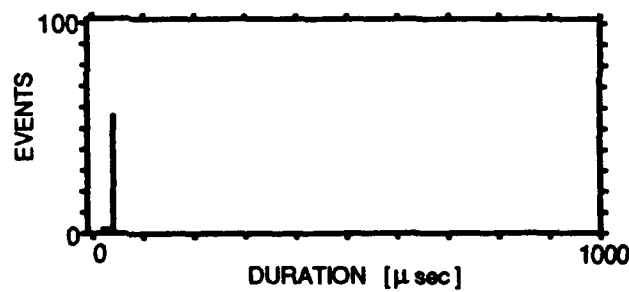
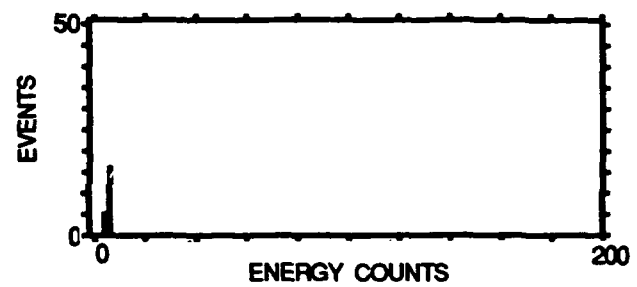
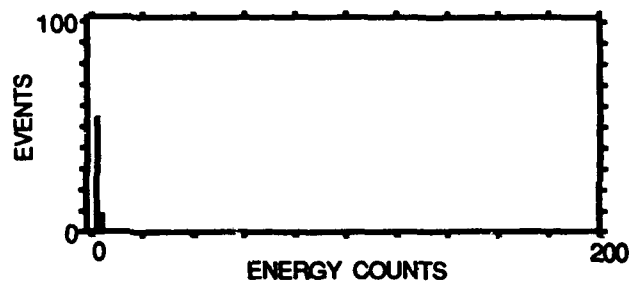
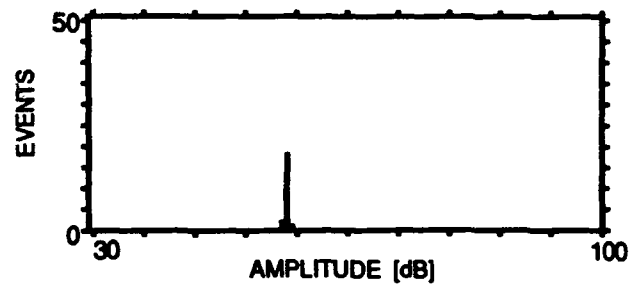
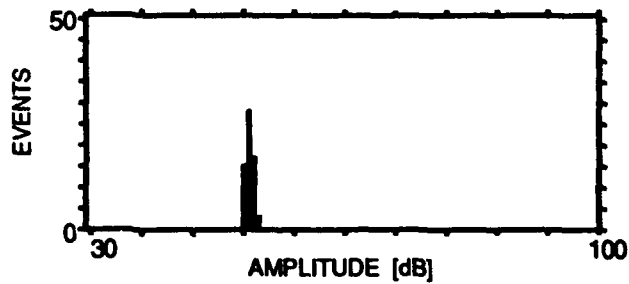
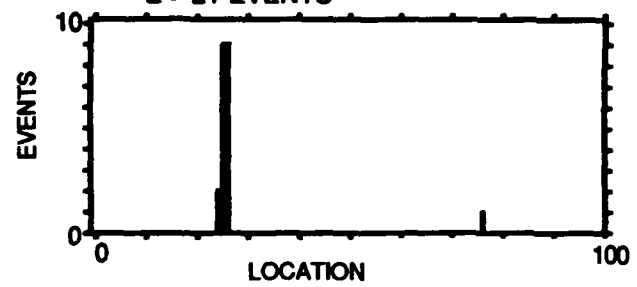
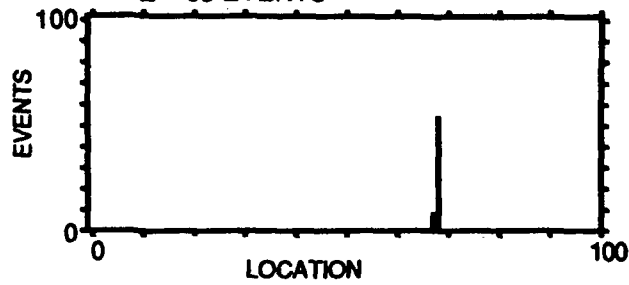


Figure 6.15. Concluded.

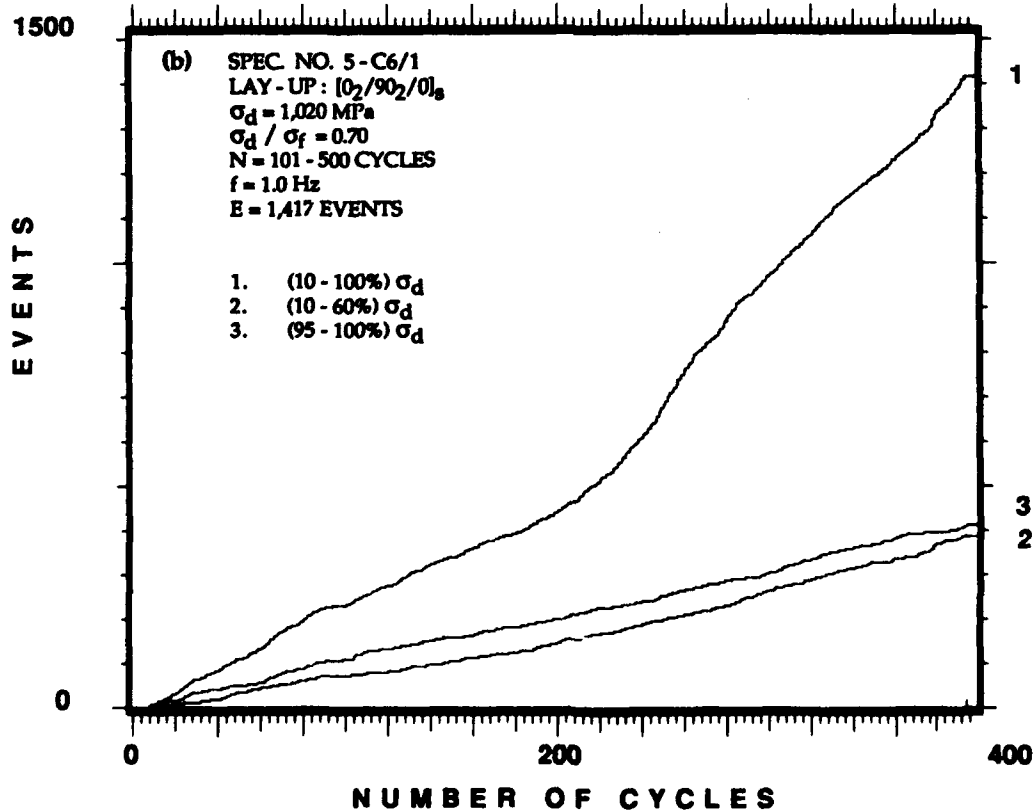
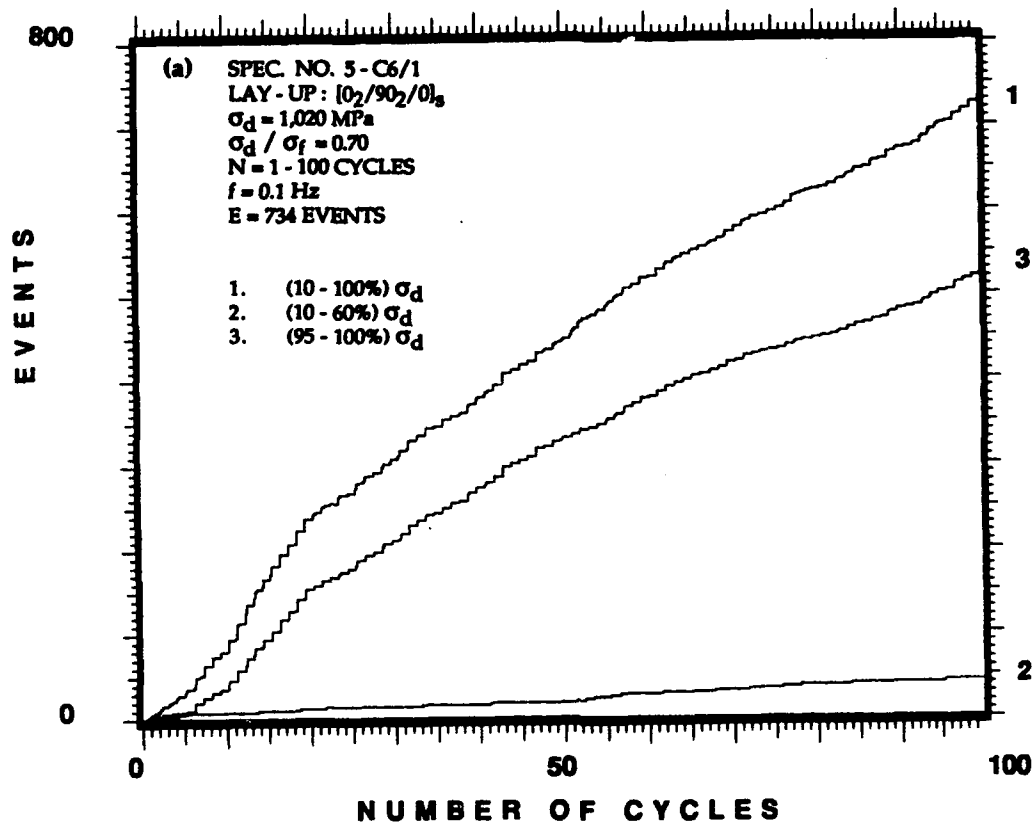


Figure 6.16. Accumulative events as a function of number of cycles, distinguishing among emission generated in three different load ranges during three consecutive periods of the fatigue loading of a $[0_2/90_2/0]_s$ laminate.

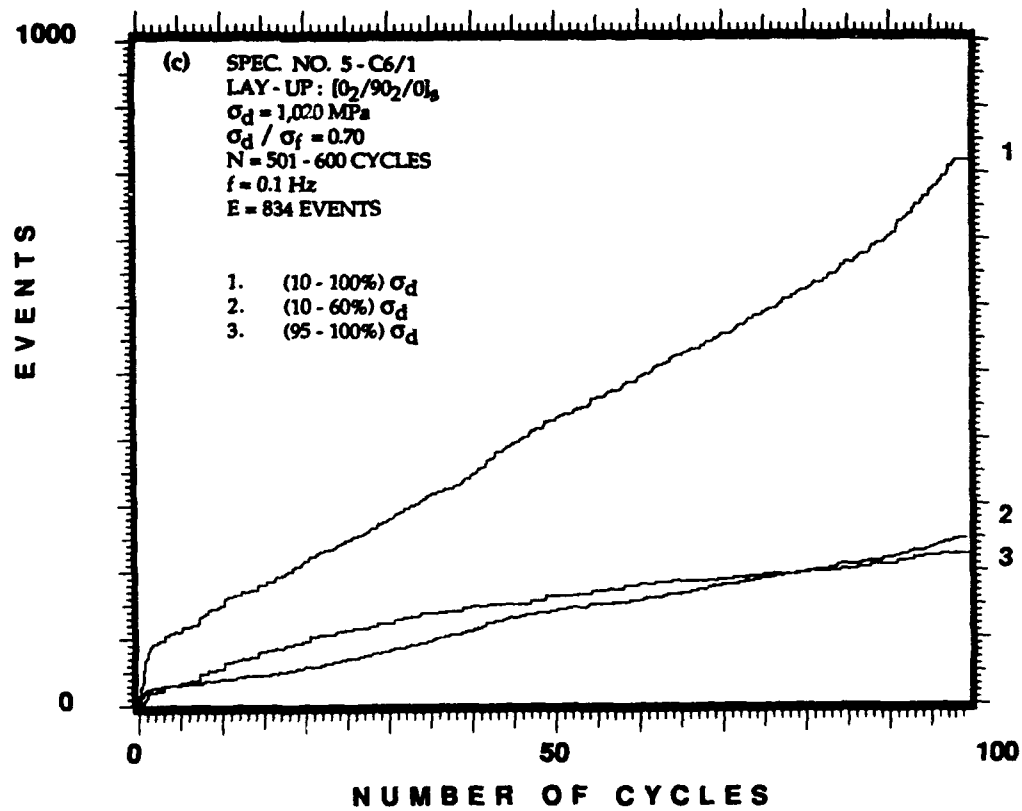


Figure 6.16. Concluded.

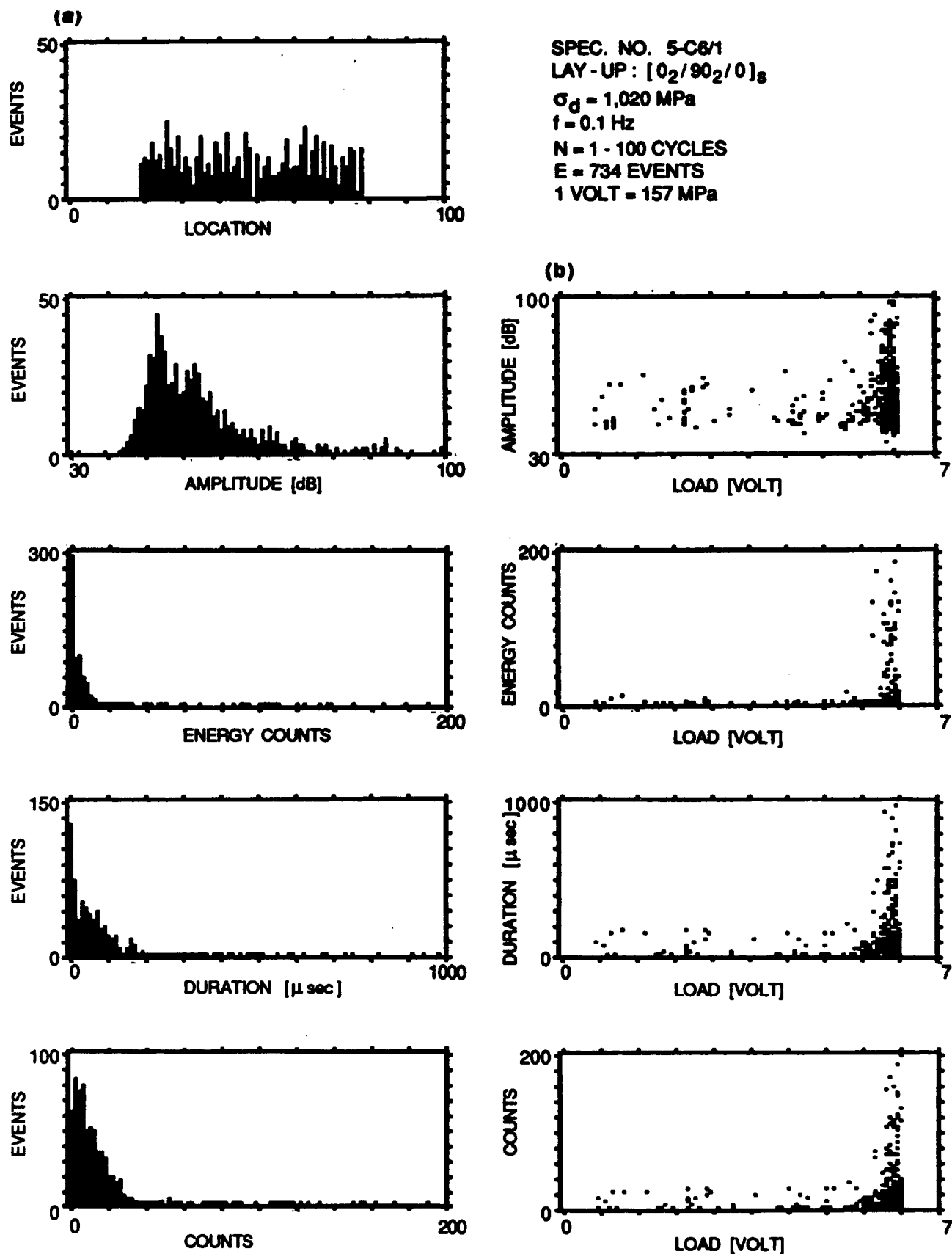
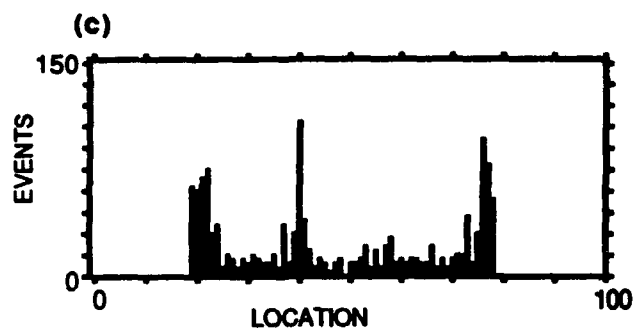


Figure 6.17. Acoustic emission event intensity and location distribution histograms and intensities of events as a function of far-field applied stress for all the events accumulated during the same periods of the fatigue loading and specimen shown in Figure 6.16. Events occur throughout the entire load range. High intensity events occur only at the upper load range.



SPEC. NO. 5-C6/1
LAY-UP: $[0_2/90_2/0]_s$
 $\sigma_d = 1,020$ MPa
 $f = 1.0$ Hz
N = 101 - 500 CYCLES
E = 1,417 EVENTS
1 VOLT = 157 MPa

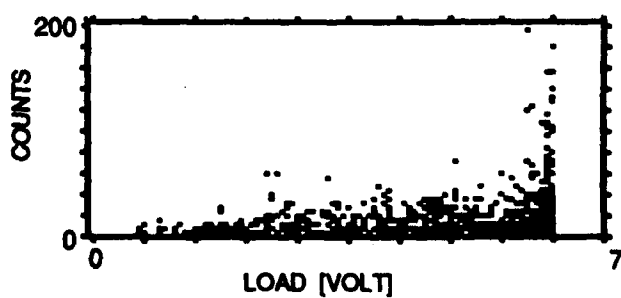
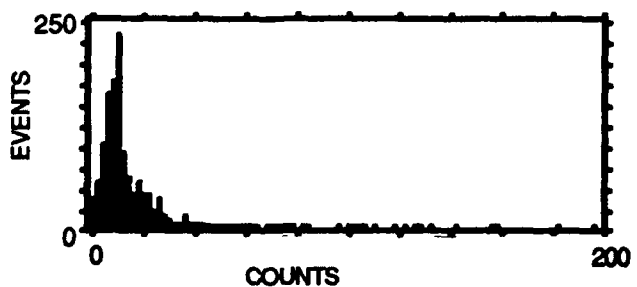
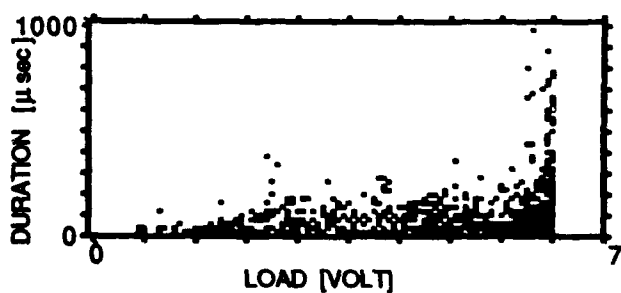
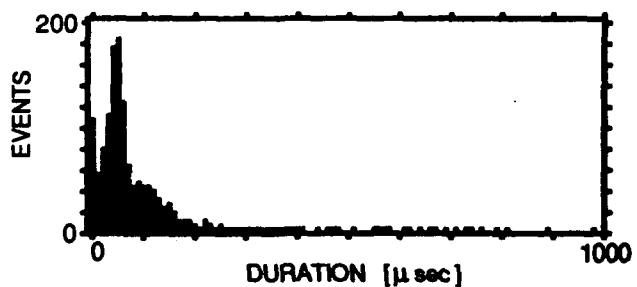
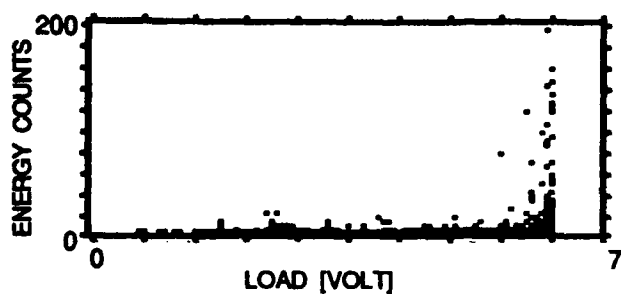
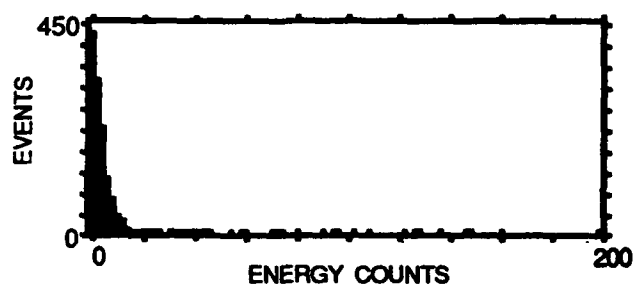
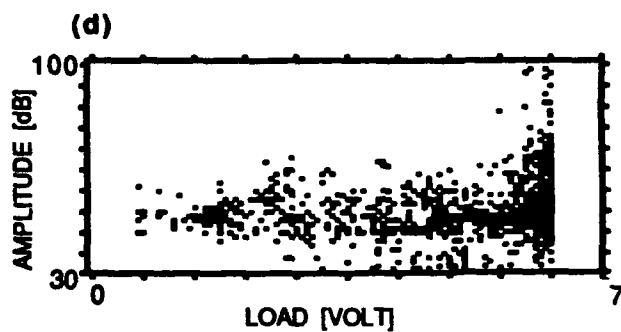
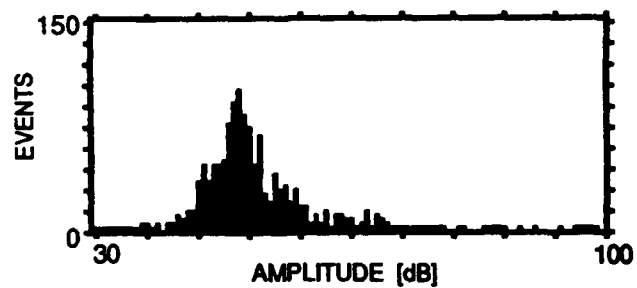
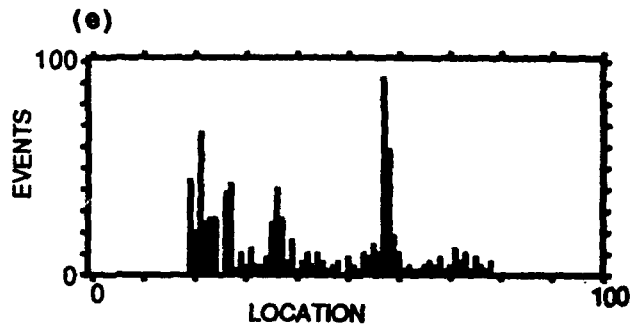


Figure 6.17. Continued.



SPEC. NO. 5-C6/1
 LAY-UP: $[0_2/90_2/0]_s$
 $\sigma_d = 1,020 \text{ MPa}$
 $f = 0.1 \text{ Hz}$
 $N = 501 - 600 \text{ CYCLES}$
 $E = 834 \text{ EVENTS}$
 $1 \text{ VOLT} = 157 \text{ MPa}$

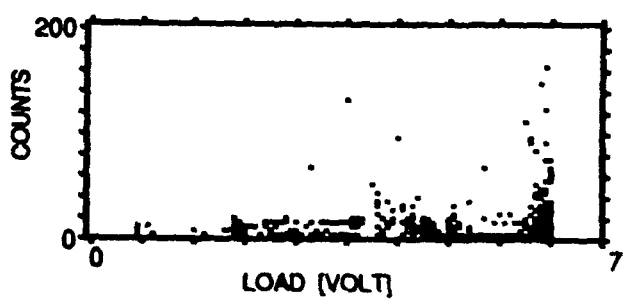
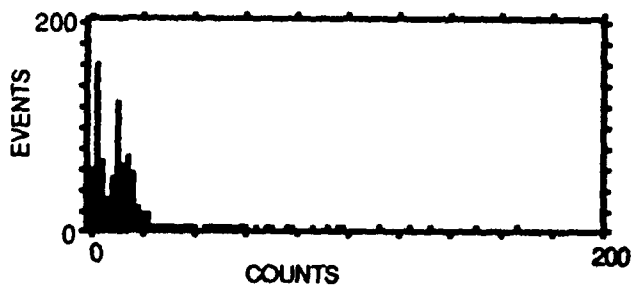
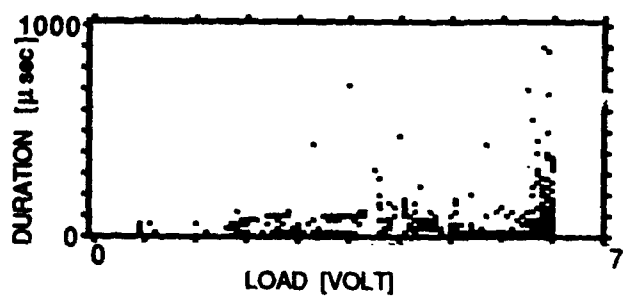
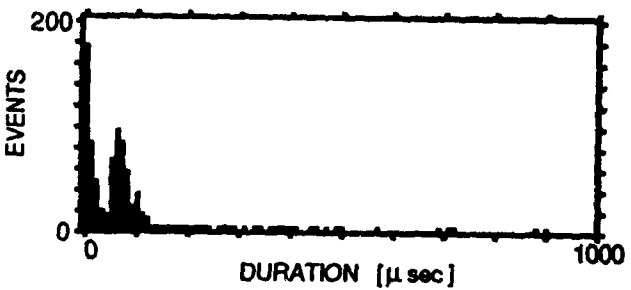
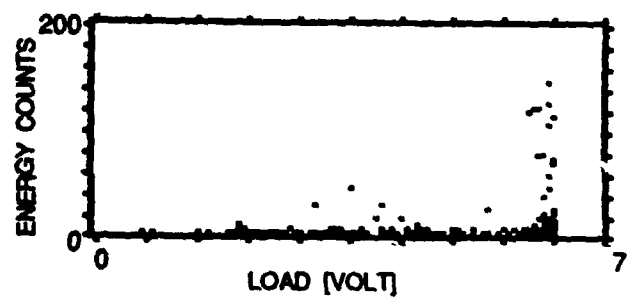
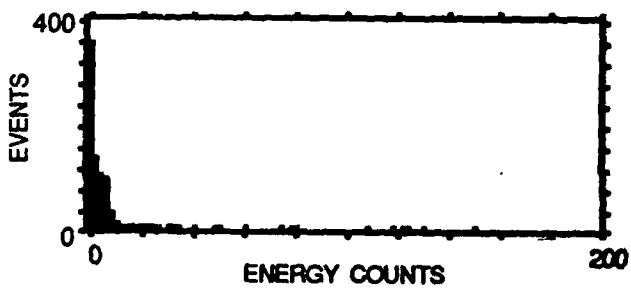
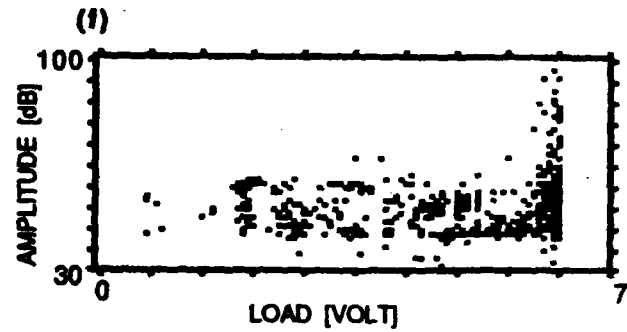
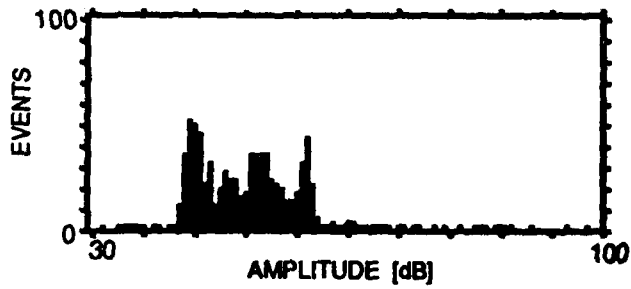
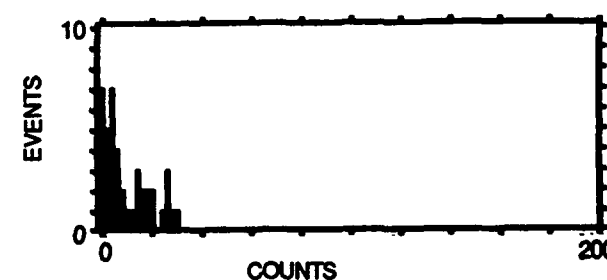
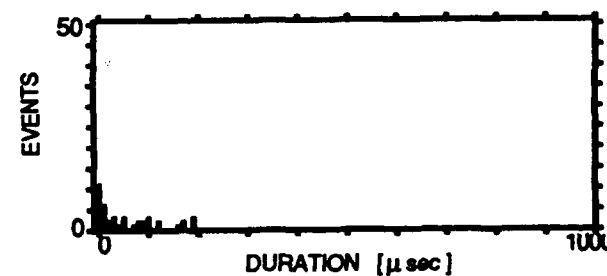
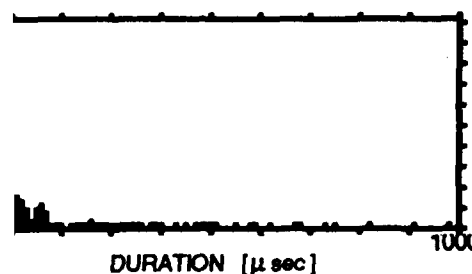
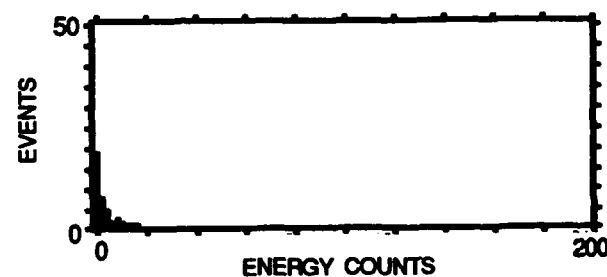
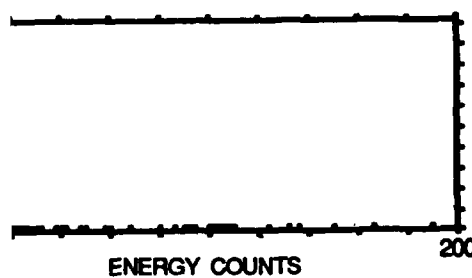
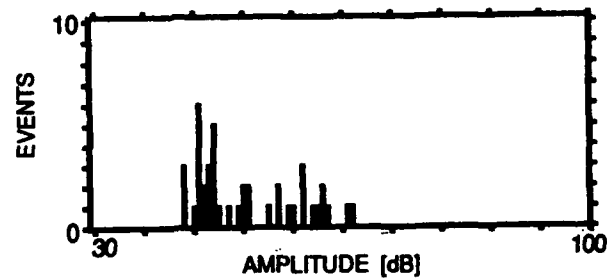
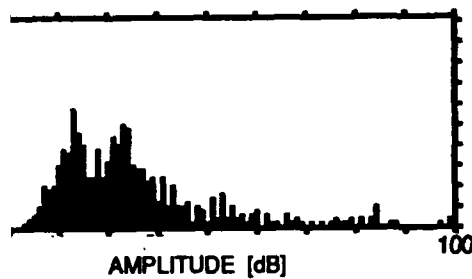
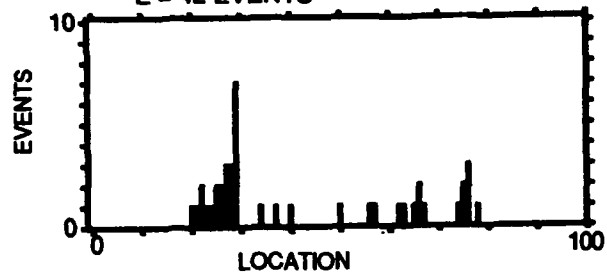
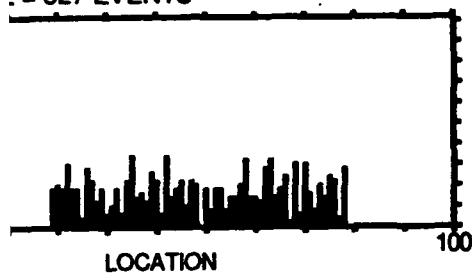


Figure 6.17. Concluded.

SPEC. NO. 5-C6/1
 LAY - UP : $[0_2/90_2/0]_s$
 LOAD RANGE = (95% - 100%) σ_d
 E = 527 EVENTS

$\sigma_d = 1,020$ MPa N = 1 - 100 CYCLES
 $f = 0.1$ Hz E = 734 EVENTS
 (b) LOAD RANGE = (10% - 60%) σ_d
 E = 42 EVENTS



6.18. Acoustic emission event intensity and location distribution histograms for events accumulated during the same periods of the fatigue loading and specimen shown in Figures 6.16 and 6.17: (a) events accumulated at the upper part of the load range; and (b) events accumulated at the lower part of the load range. Friction emission threshold (FRET) values can be assigned to friction generated emission.

SPEC. NO. 5-C8/1
LAY-UP: $[0_2/90_2/0]_s$

$\sigma_d = 1,020 \text{ MPa}$ $N = 101 - 500 \text{ CYCLES}$
 $f = 1.0 \text{ Hz}$ $E = 1,417 \text{ EVENTS}$

(c) LOAD RANGE = (95% - 100%) σ_d
 $E = 409 \text{ EVENTS}$

(d) LOAD RANGE = (10% - 60%) σ_d
 $E = 393 \text{ EVENTS}$

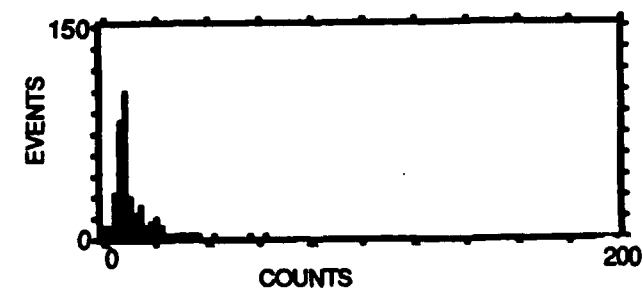
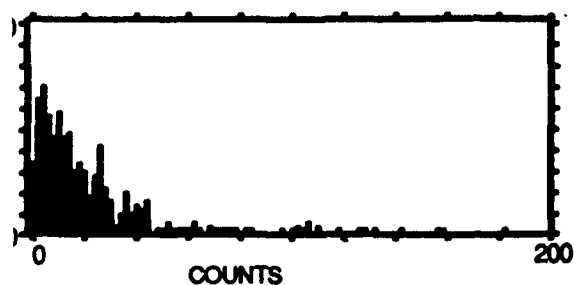
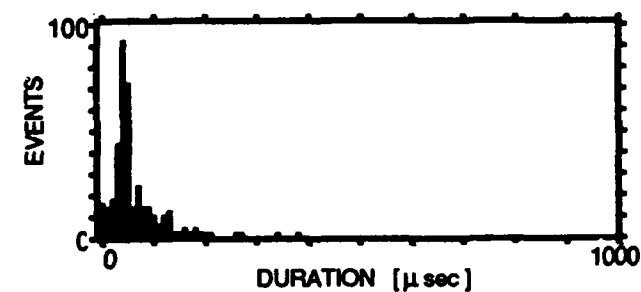
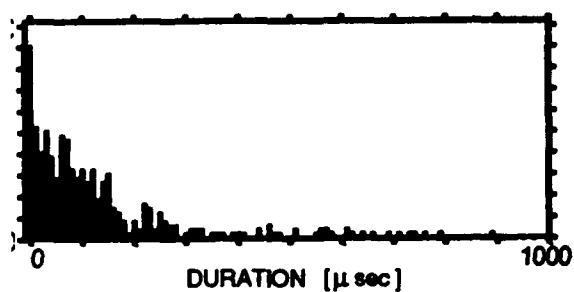
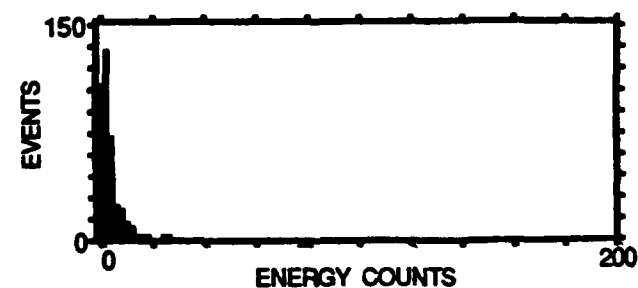
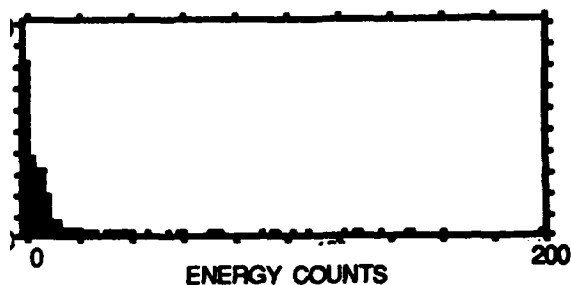
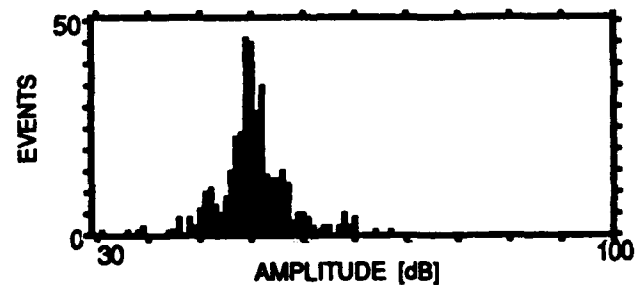
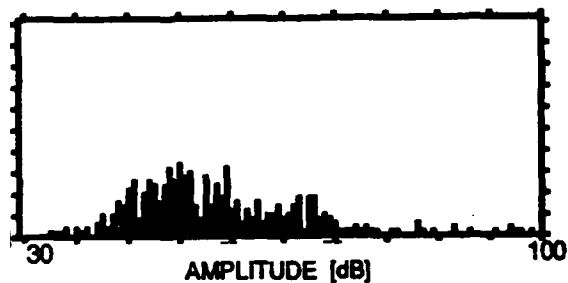
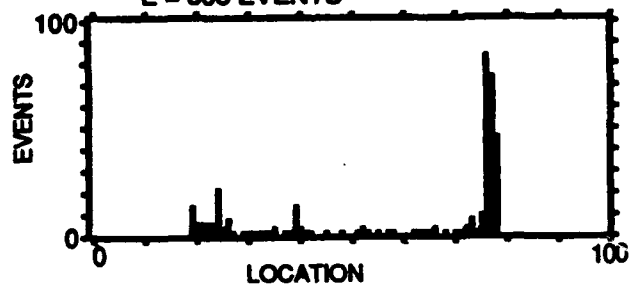
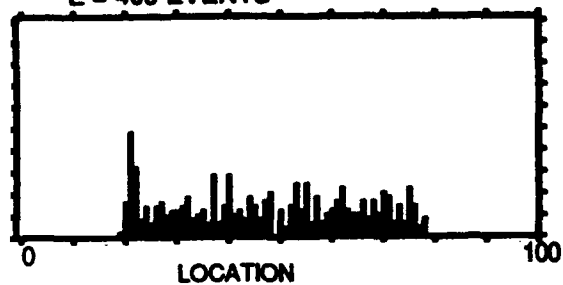
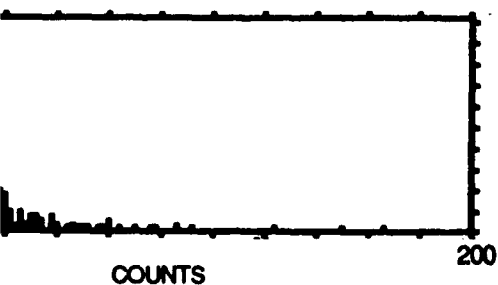
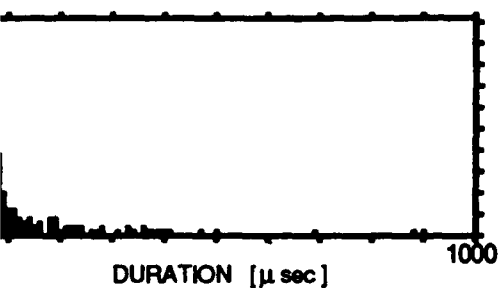
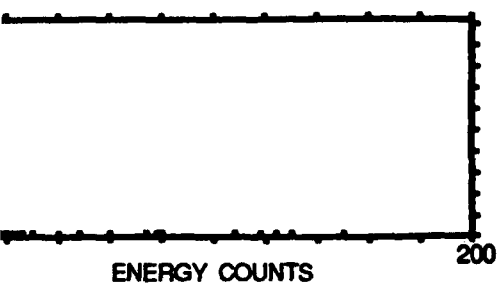
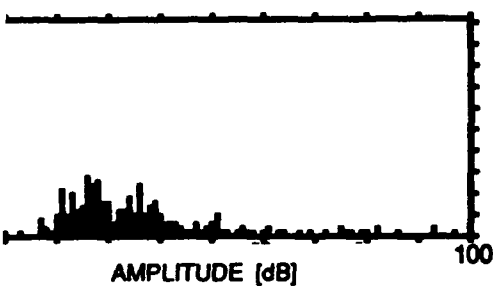
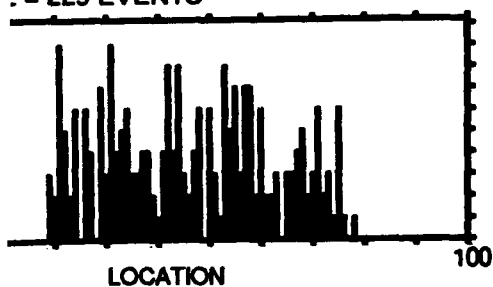
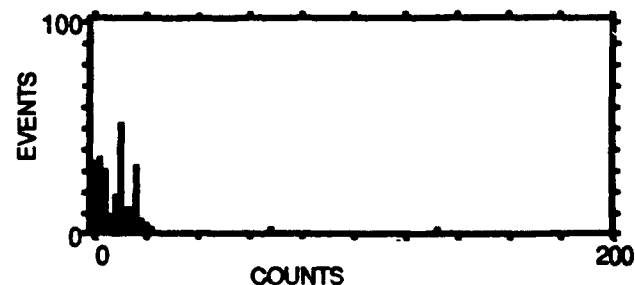
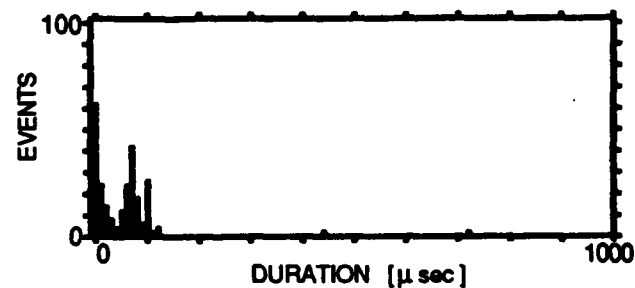
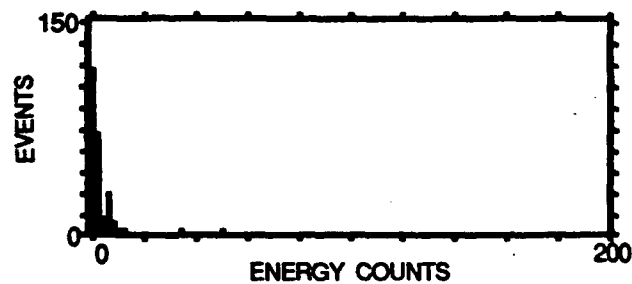
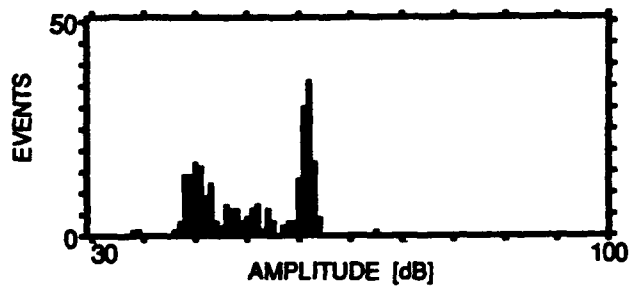
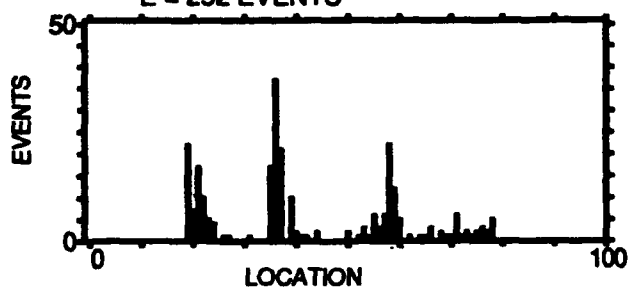


Figure 6.18. Continued.

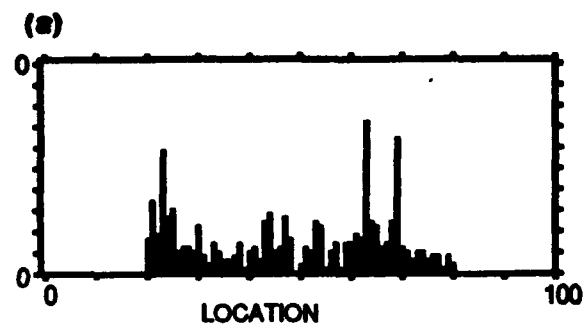
SPEC. NO. 5-C6/1
 LAY - UP : $[0_2/90_2/0]_S$
 LOAD RANGE = (95% - 100%) σ_d
 E = 229 EVENTS



$\sigma_d = 1,020$ MPa N = 501 - 600 CYCLES
 $f = 0.1$ Hz E = 834 EVENTS
 (f) LOAD RANGE = (10% - 60%) σ_d
 E = 252 EVENTS



6.18. Concluded.



SPEC. NO. 7-D3/1
 LAY-UP: $[0/90_2/0]_s$
 $\sigma_d = 608 \text{ MPa}$
 $f = 1.0 \text{ Hz}$
 $N = 35,000 - 36,000 \text{ CYCLES}$
 $E = 974 \text{ EVENTS}$
 $1 \text{ VOLT} = 203 \text{ MPa}$

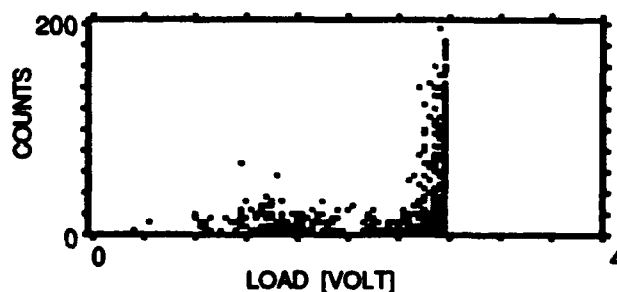
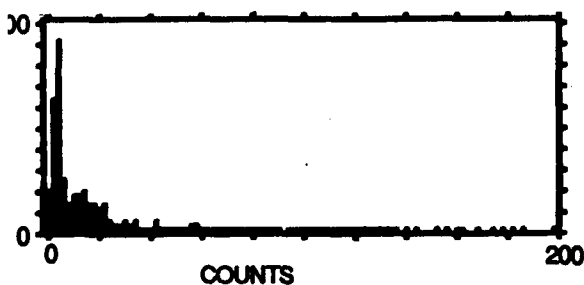
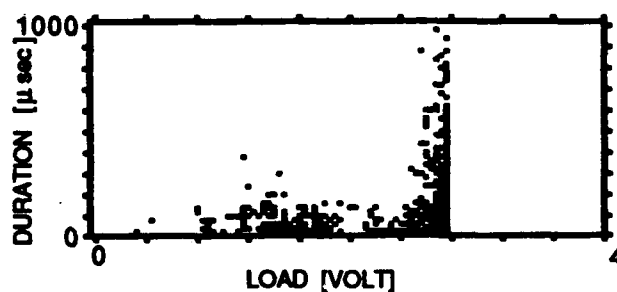
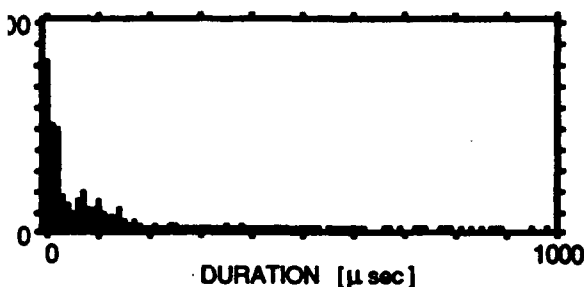
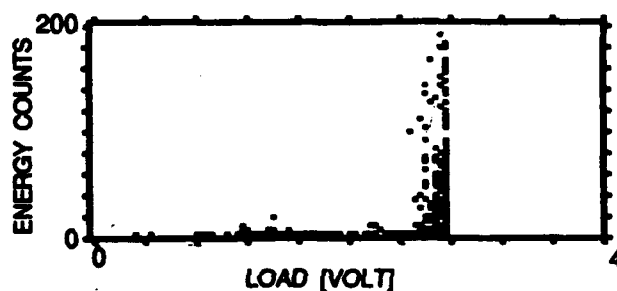
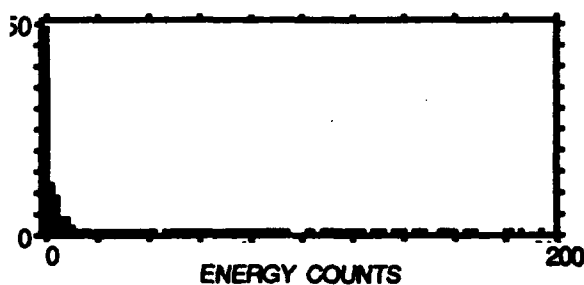
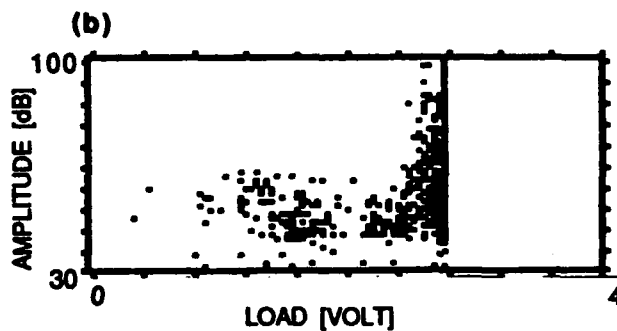
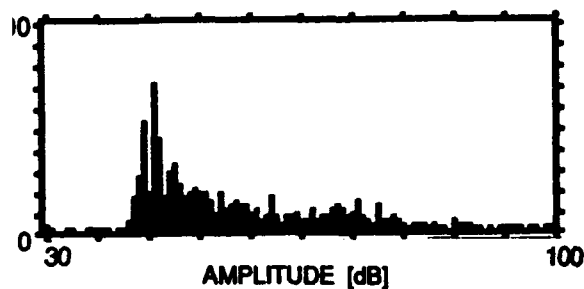
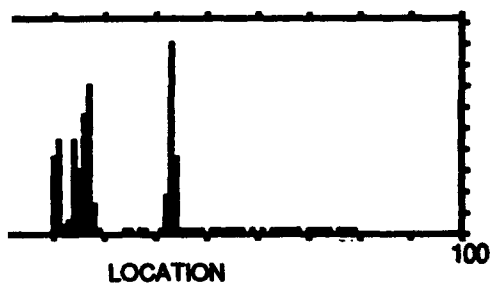
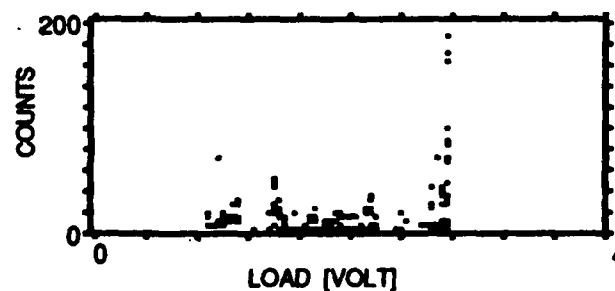
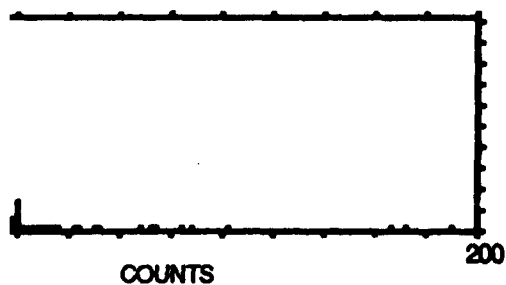
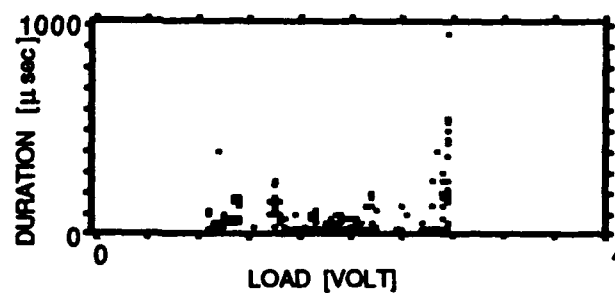
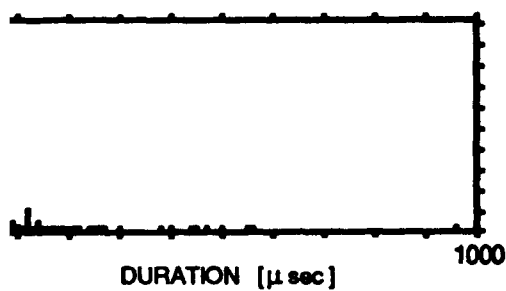
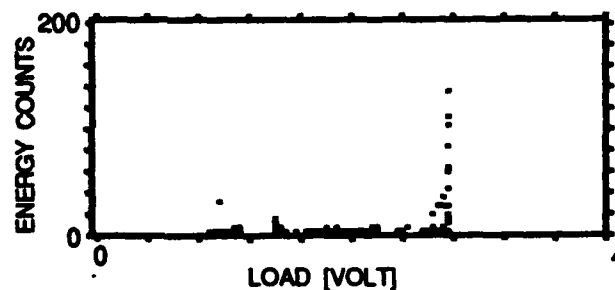
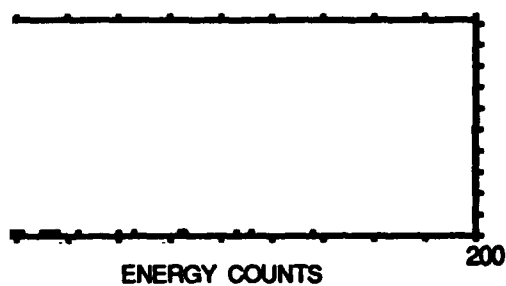
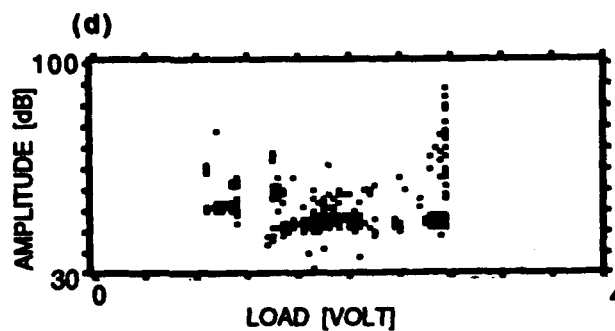
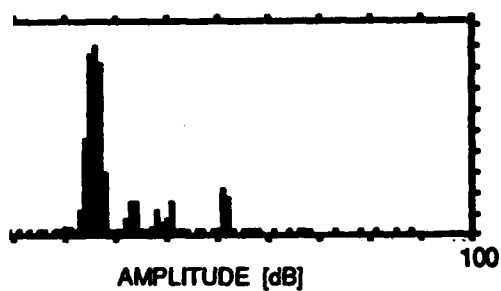


Figure 6.19. Acoustic emission event intensity and location distribution histograms and intensities of events as a function of far-field applied stress for all the events accumulated during the two selected periods of the fatigue loading and for the same specimen shown in Figures 6.11g and 6.11h. Events occur throughout the entire load range. High intensity events occur only at the upper load range.



SPEC. NO. 7-D3/1
 LAY-UP: $[0/90_2/0]_s$
 $\sigma_d = 608 \text{ MPa}$
 $f = 1.0 \text{ Hz}$
 $N = 37,000 - 37,600 \text{ CYCLES}$
 $E = 2,406 \text{ EVENTS}$
 $1 \text{ VOLT} = 203 \text{ MPa}$



6.19. Concluded.

SPEC. NO. 7-D3/1
LAY-UP: $[0/90_2/0]_8$

$\sigma_d = 600 \text{ MPa}$
 $f = 1.0 \text{ Hz}$

$N = 35,000 - 36,000 \text{ CYCLES}$
 $E = 974 \text{ EVENTS}$

(a) LOAD RANGE = (95% - 100%) σ_d
 $E = 438 \text{ EVENTS}$

(b) LOAD RANGE = (10% - 90%) σ_d
 $E = 205 \text{ EVENTS}$

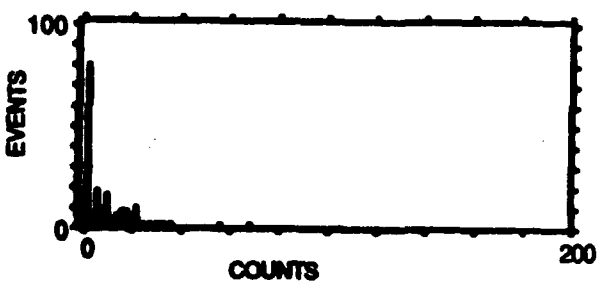
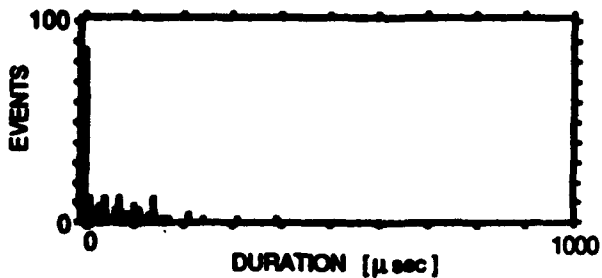
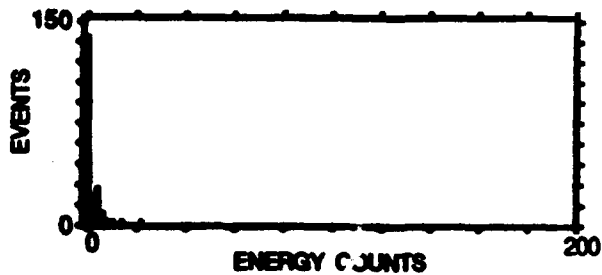
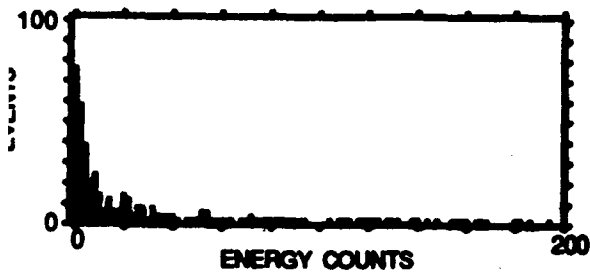
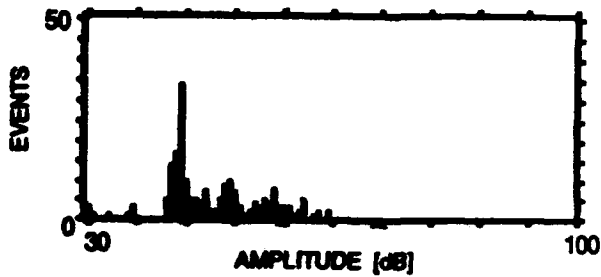
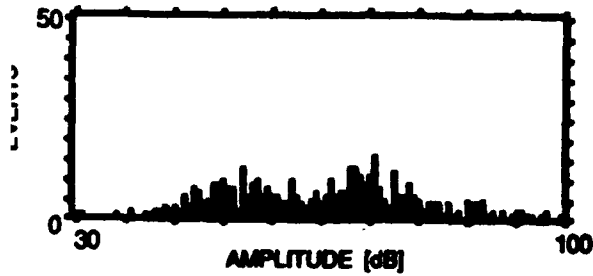
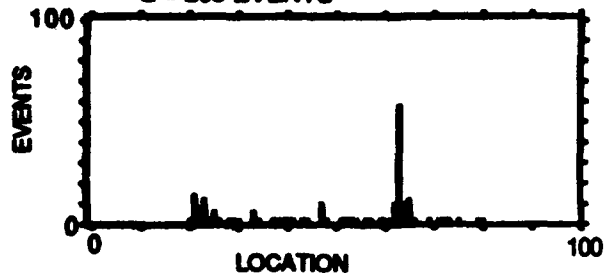
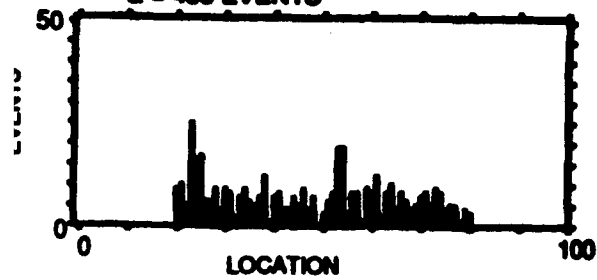


Figure 6.20. Acoustic emission event intensity and location distribution histograms for events accumulated during the same two periods of the fatigue loading and specimen shown in Figure 6.19. (a) events accumulated at the upper part of the load range; and (b) events accumulated at the lower part of the load range. Friction emission threshold (FRET) values can be assigned to friction generated emission.

SPEC. NO. 7-D3/1

LAY-UP: $[0/90_2/0]_8$

LOAD RANGE = (95% - 100%) σ_d

E = 74 EVENTS

$\sigma_d = 608 \text{ MPa}$

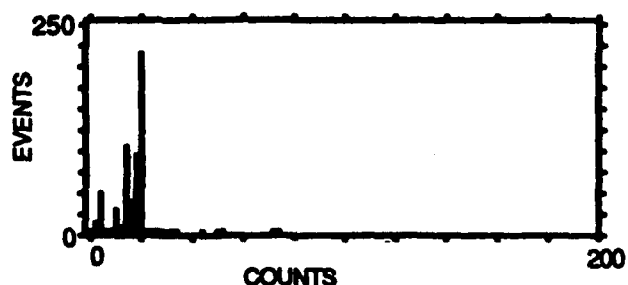
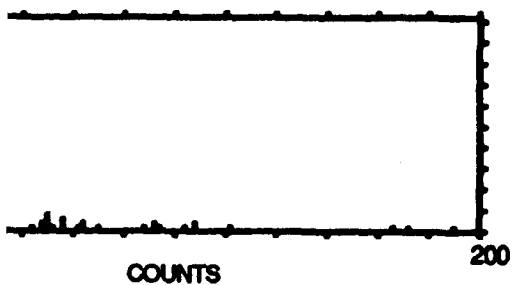
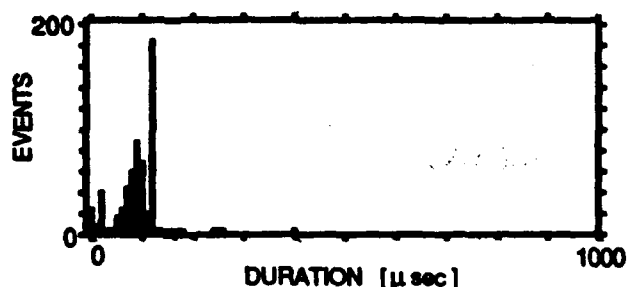
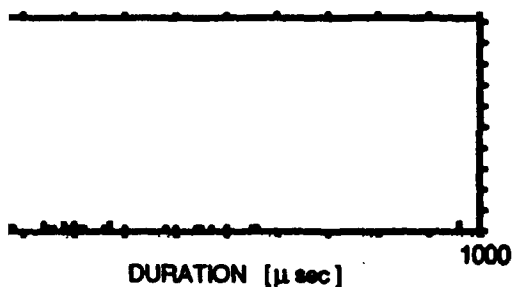
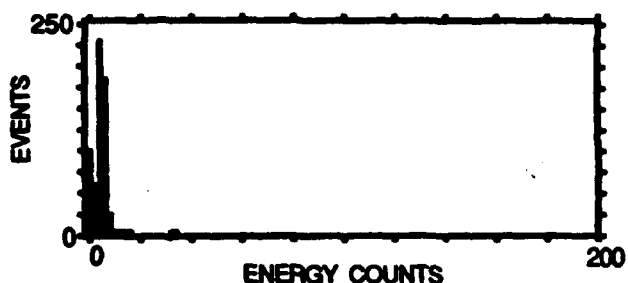
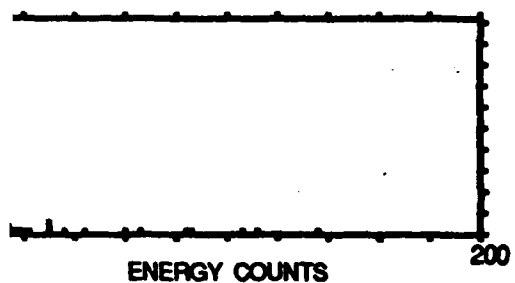
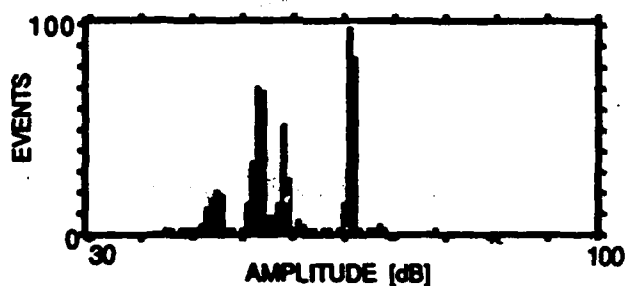
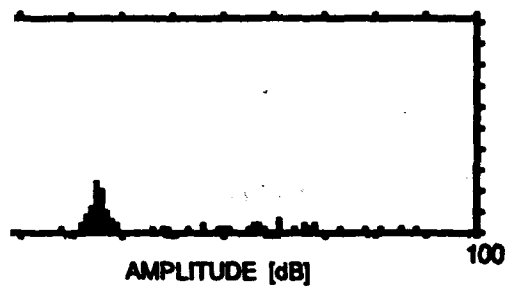
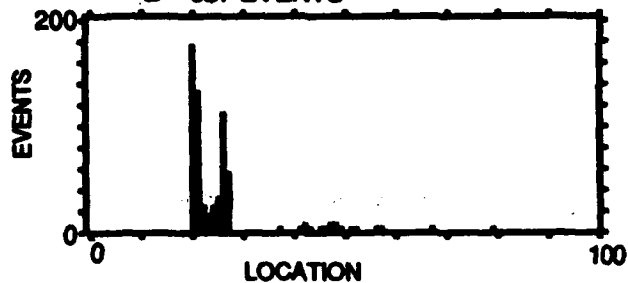
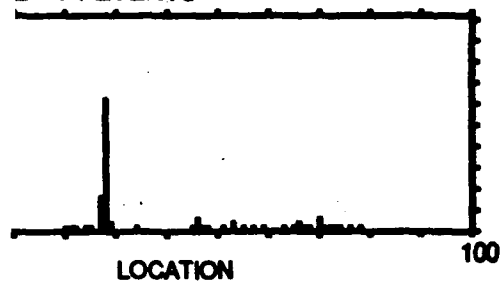
$f = 0.1 \text{ Hz}$

N = 37,000 - 37,600 CYCLES

E = 2,406 EVENTS

(d) LOAD RANGE = (10% - 60%) σ_d

E = 627 EVENTS



6.20. Concluded.

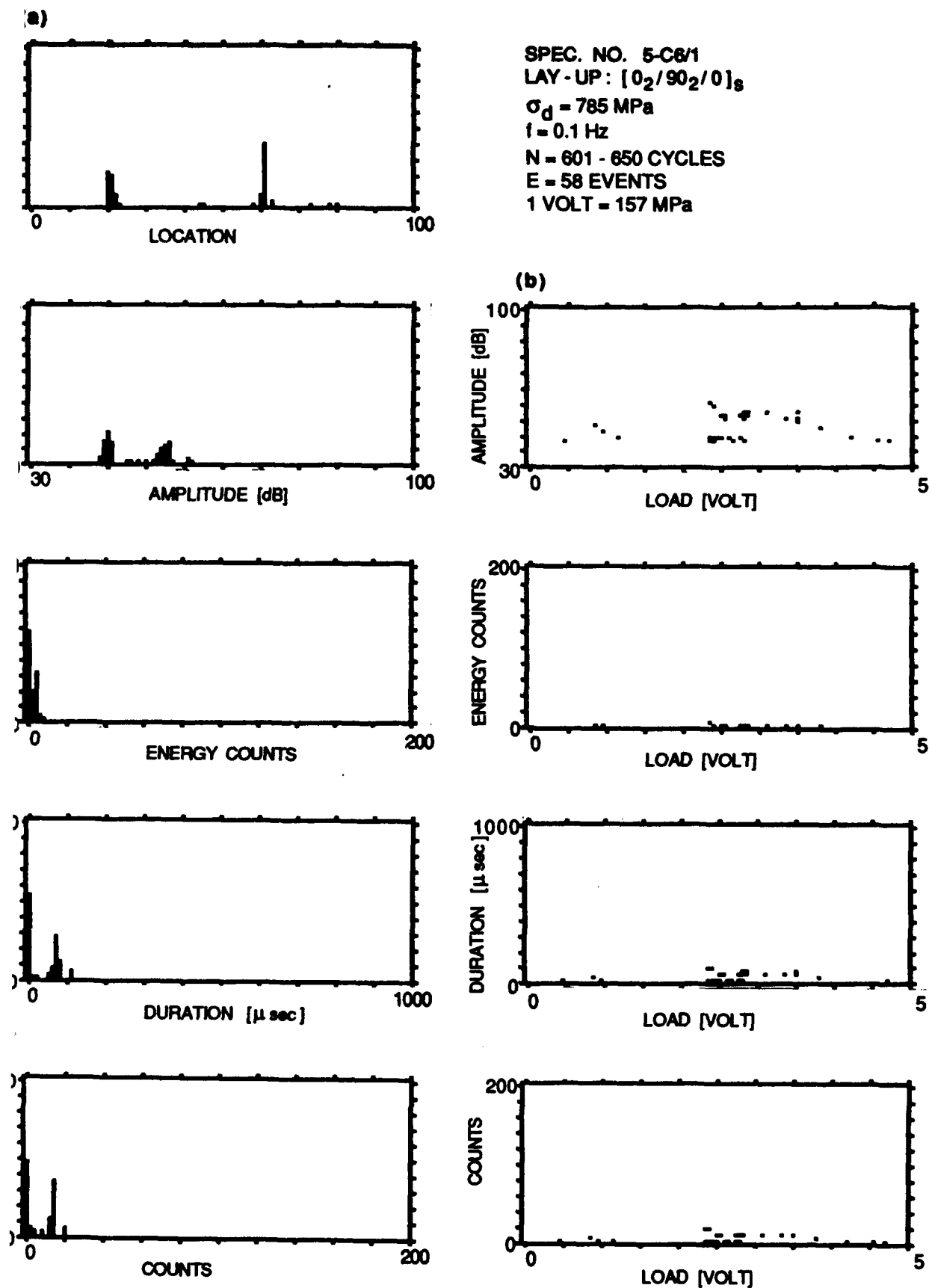


Figure 6.21. Acoustic emission event intensity and location distribution histograms and intensities of events as a function of far-field applied stress for all the events accumulated during three consecutive periods of the fatigue loading for the same specimen shown in Figure 6.18 at a lower dynamic stress amplitude. Events occur throughout the entire load range. All events are of low intensity indicating emission generated solely by grating.



SPEC. NO. 5-C6/1
 LAY-UP: $[0_2/90_2/0]_s$
 $\sigma_d = 785 \text{ MPa}$
 $f = 1.0 \text{ Hz}$
 $N = 651 - 1,550 \text{ CYCLES}$
 $E = 999 \text{ EVENTS}$
 $1 \text{ VOLT} = 157 \text{ MPa}$

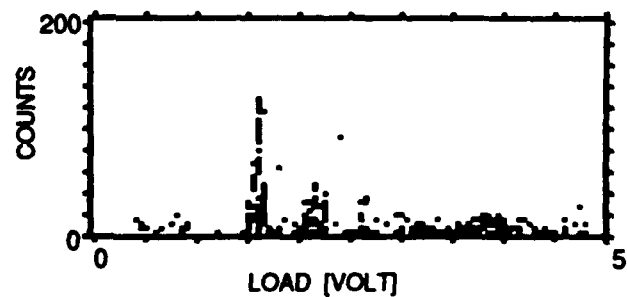
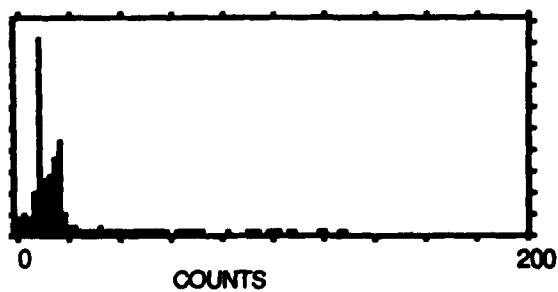
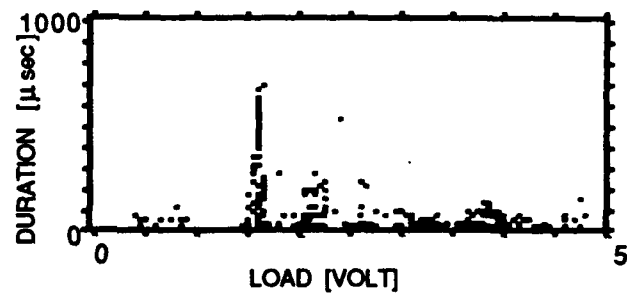
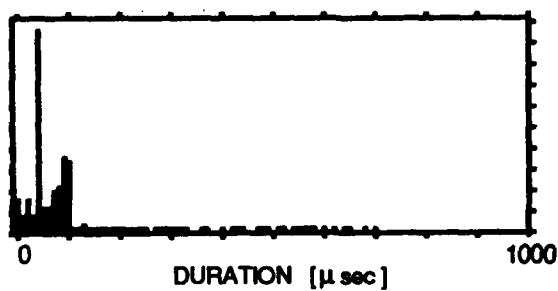
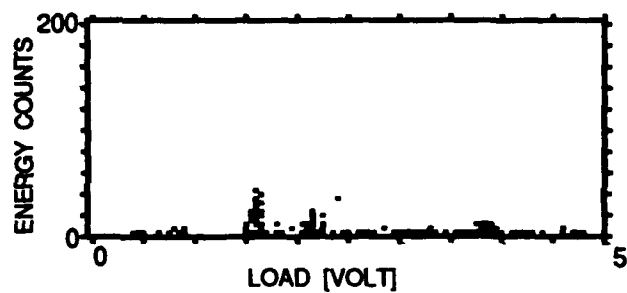
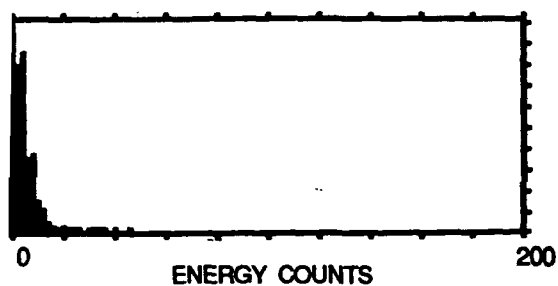
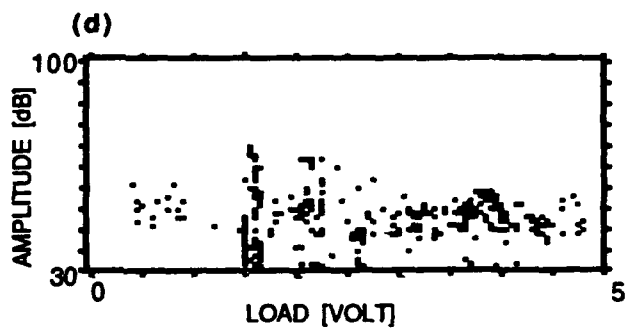
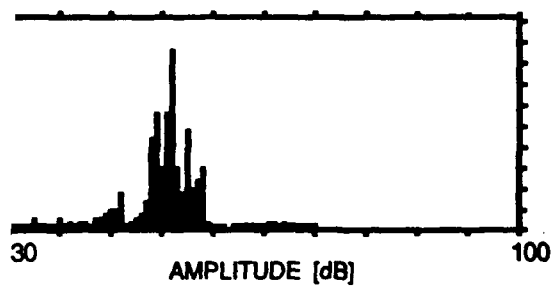


Figure 6.21. Continued.

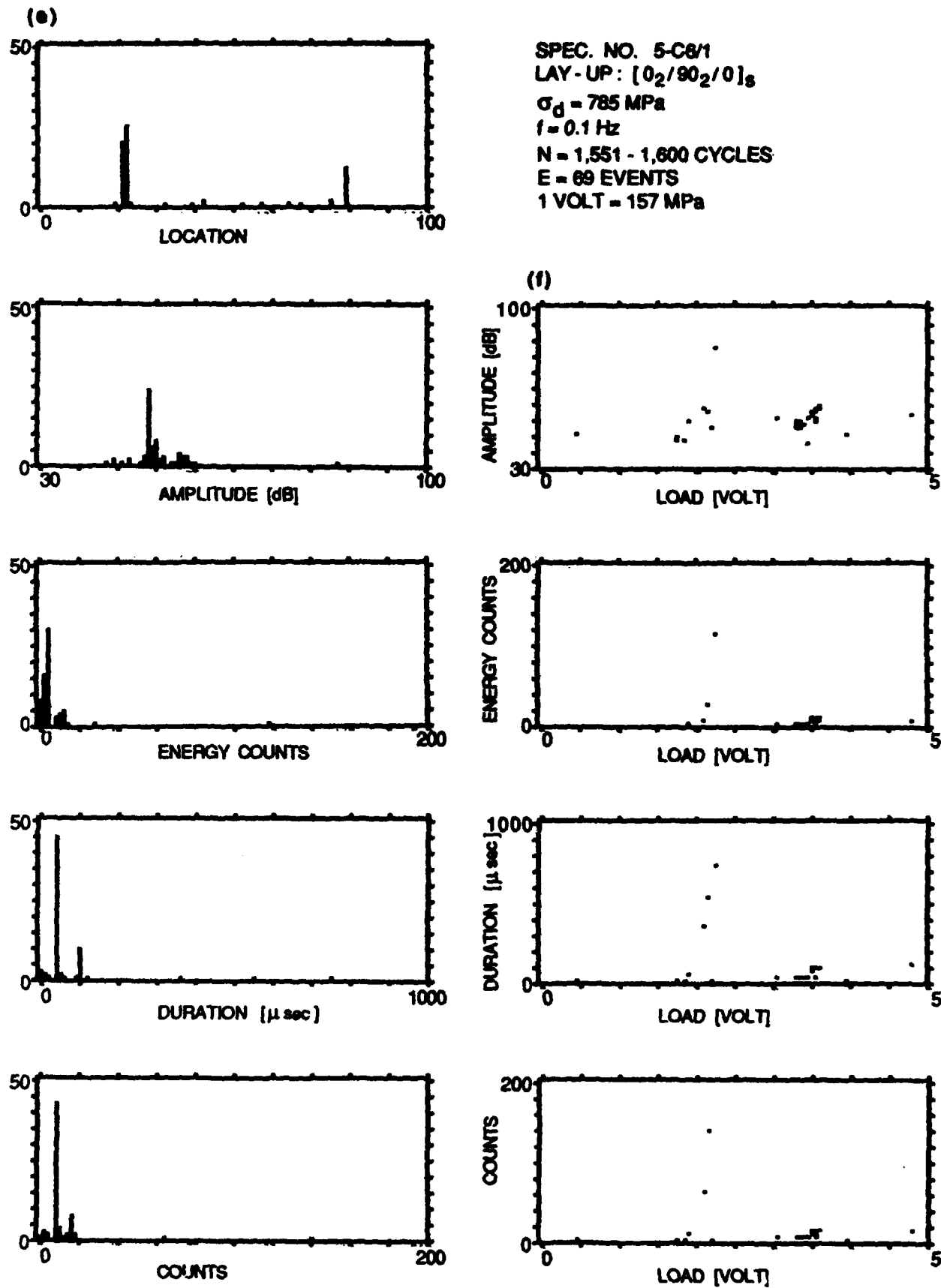
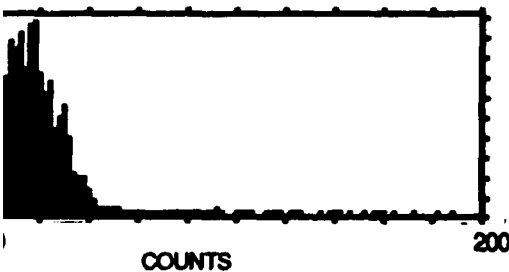
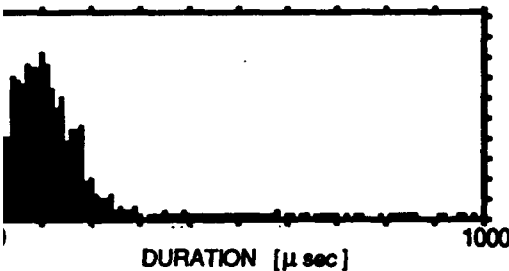
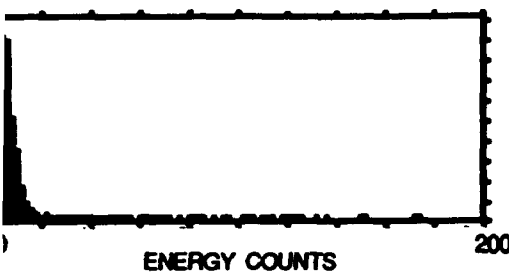
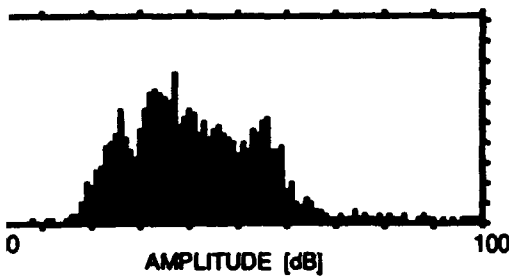
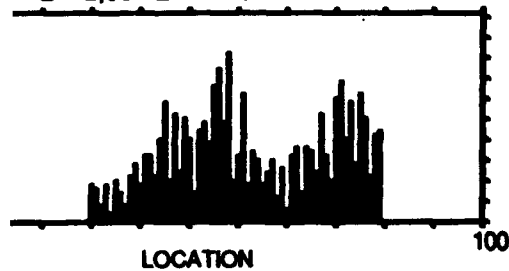
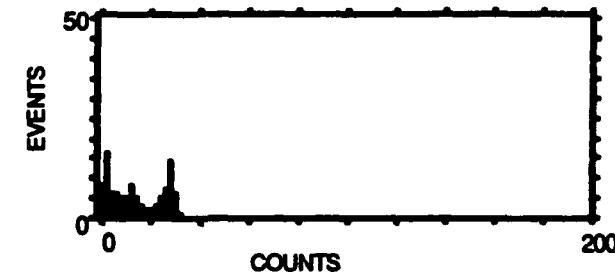
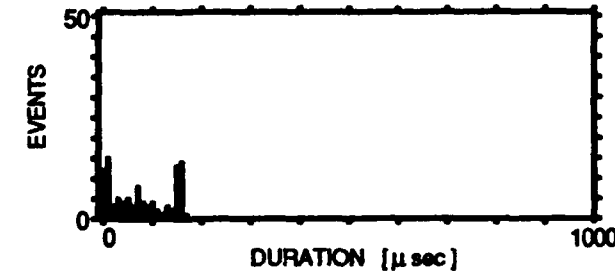
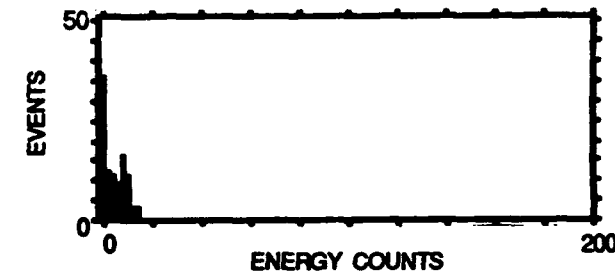
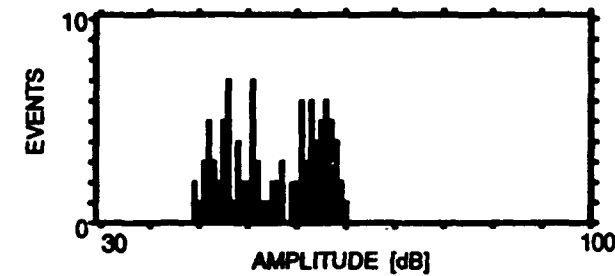


Figure 6.21. Concluded.

SPEC. NO. 5-D1/2
LAY-UP: $[0_2/90_2/0]_s$
(a) LOAD RANGE = (95% - 100%) σ_d
E = 2,061 EVENTS



$C_d = 100 \text{ mPa}$ $N = 1-50 \text{ CYCLES}$
 $f = 0.01 \text{ Hz}$ $E = 2,544 \text{ EVENTS}$
(b) LOAD RANGE = (10% - 60%) σ_d
E = 102 EVENTS

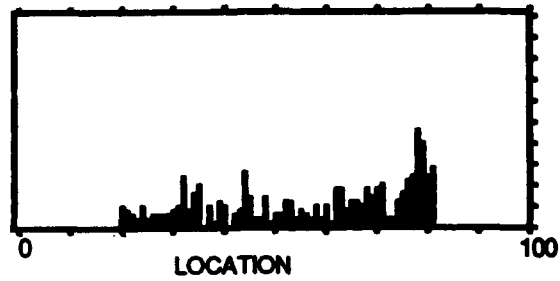


re 6.22. Acoustic emission event intensity and location distribution histograms and intensities of events as a function of far-field applied stress for the same specimen and the same four 100-cycle periods of the fatigue loading shown in Figures 6.3e to 6.3h: (a) (c) (e) and (g) for events accumulated at the upper part of the load range; and (b) (d) (f) and (h) for events accumulated at the lower part of the load range. Friction emission threshold (FRET) values can be assigned to friction generated emission.

SPEC. NO. 5-D1/2

LAY-UP: $[0_2/90_2/0]_s$

(c) LOAD RANGE = (95% - 100%) σ_d
E = 359 EVENTS



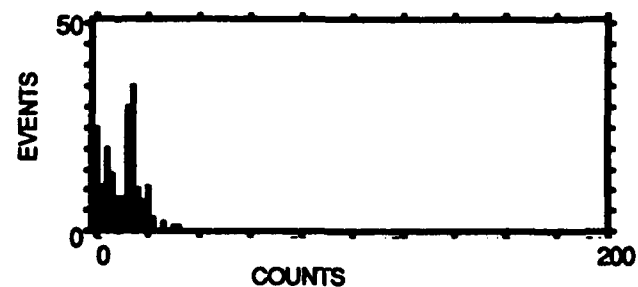
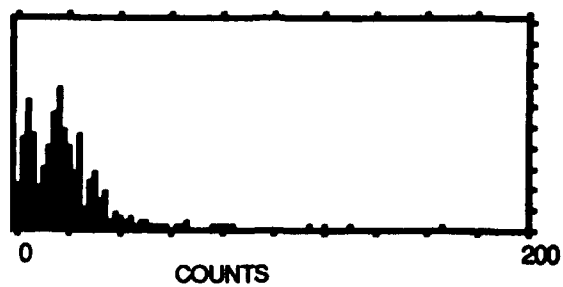
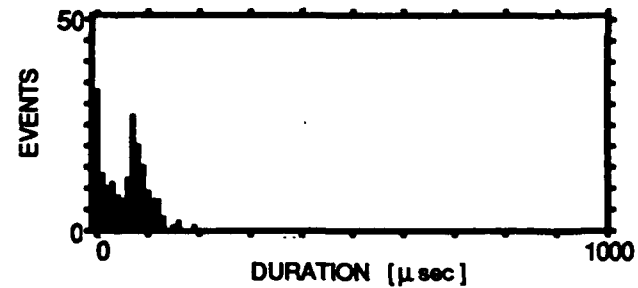
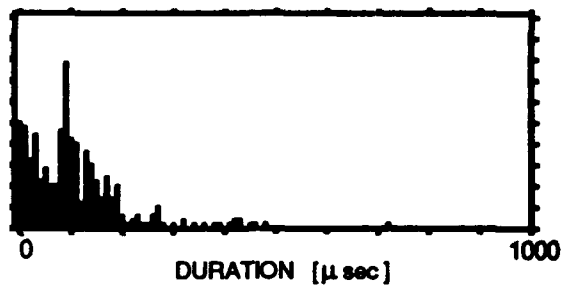
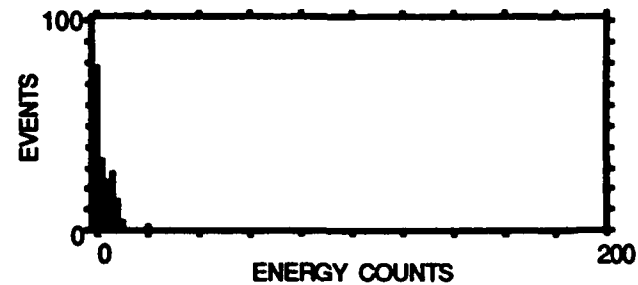
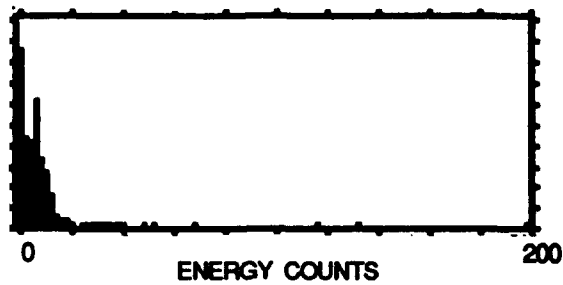
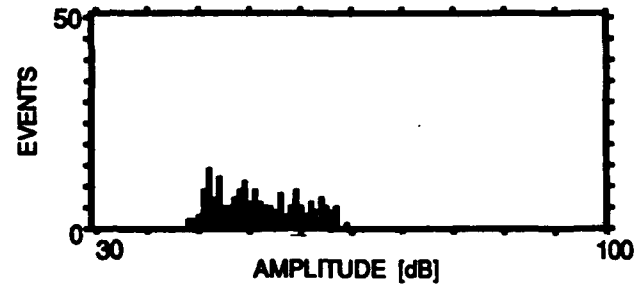
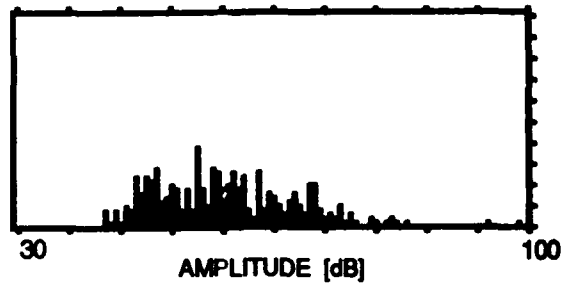
$\sigma_d = 788 \text{ MPa}$

$f = 0.1 \text{ Hz}$

N = 51 - 100 CYCLES

E = 637 EVENTS

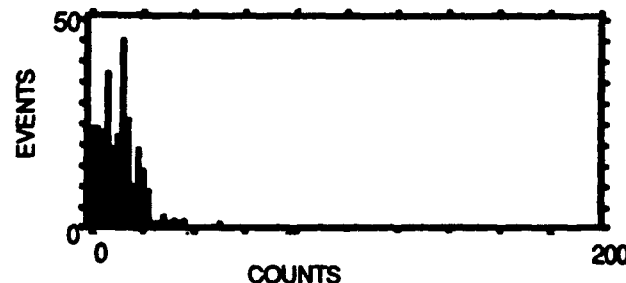
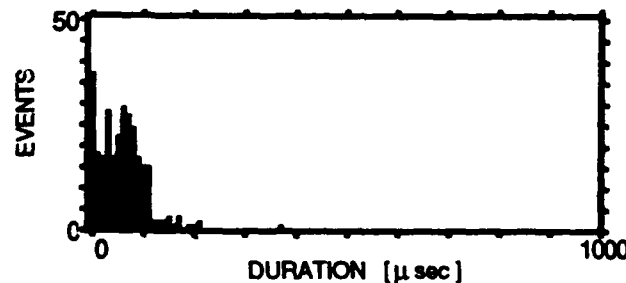
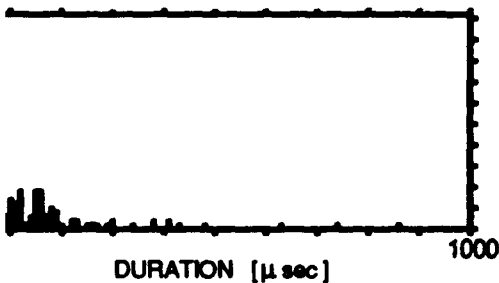
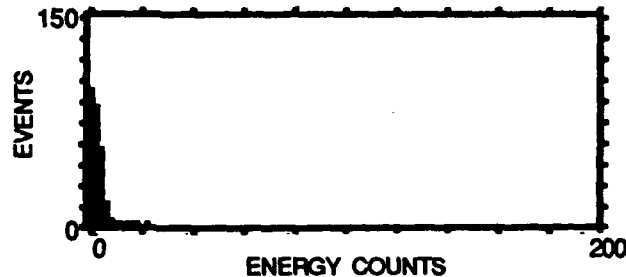
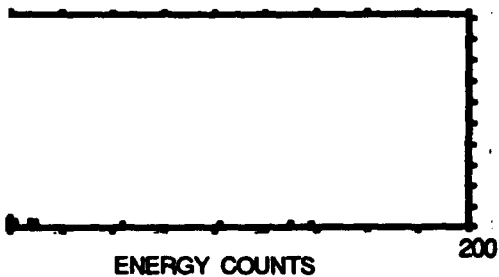
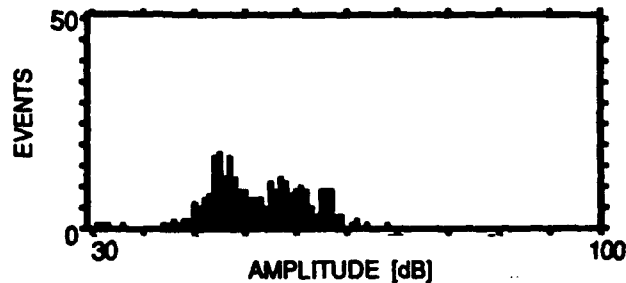
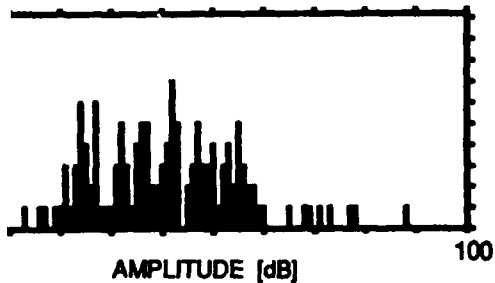
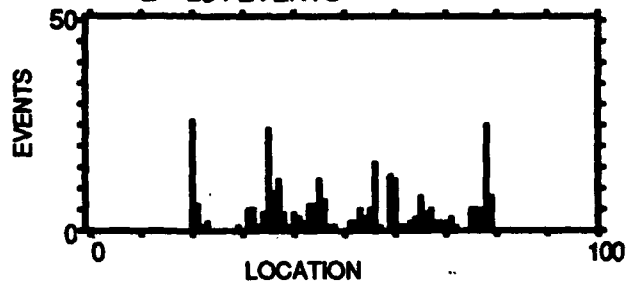
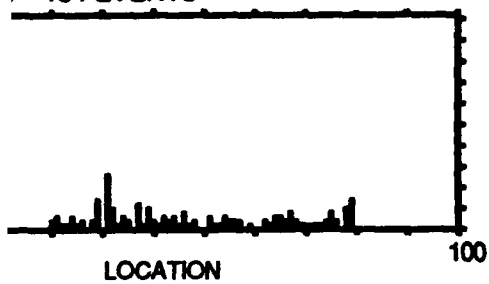
(d) LOAD RANGE = (10% - 60%) σ_d
E = 186 EVENTS



ure 6.22. Continued.

SPEC. NO. 5-D1/2
 LAY - UP : $[0_2/90_2/0]_s$
 LOAD RANGE = (95% - 100%) σ_d
 E = 134 EVENTS

$\sigma_d = 788 \text{ MPa}$ $N = 101 - 150 \text{ CYCLES}$
 $f = 1.0 \text{ Hz}$ $E = 524 \text{ EVENTS}$
 (f) LOAD RANGE = (10% - 60%) σ_d
 E = 284 EVENTS



5.22. Continued.

SPEC. NO. 5-D1/2

LAY-UP: $[0_2/90_2/0]_8$

) LOAD RANGE = (95% - 100%) σ_d
E = 330 EVENTS

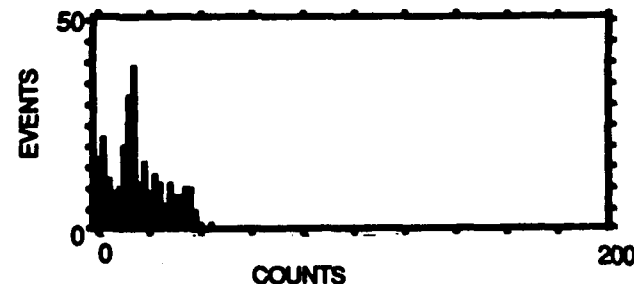
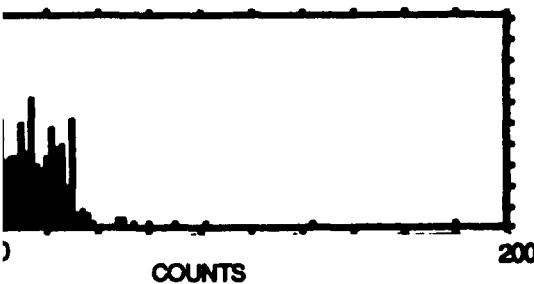
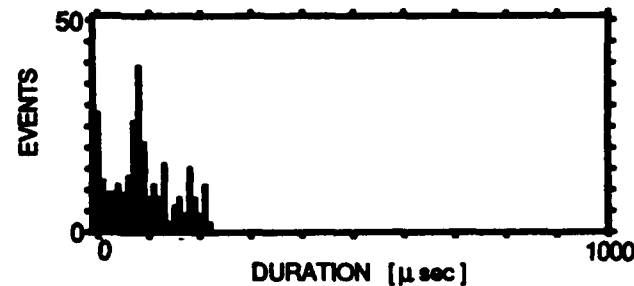
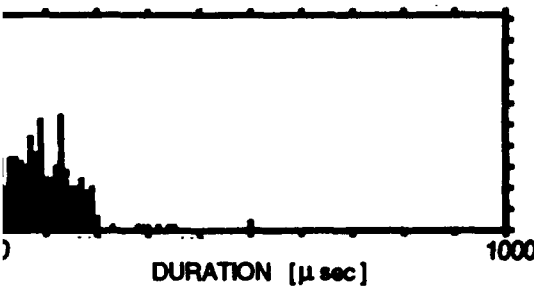
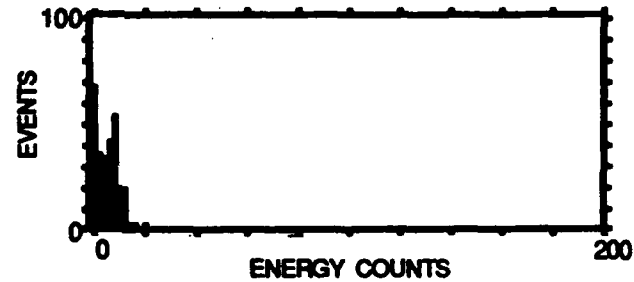
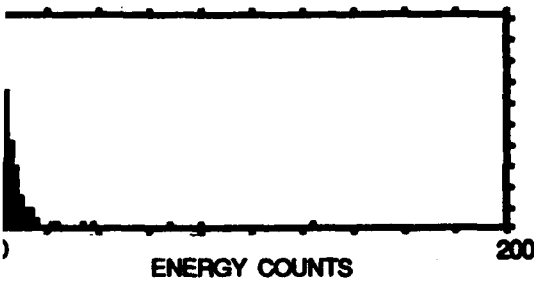
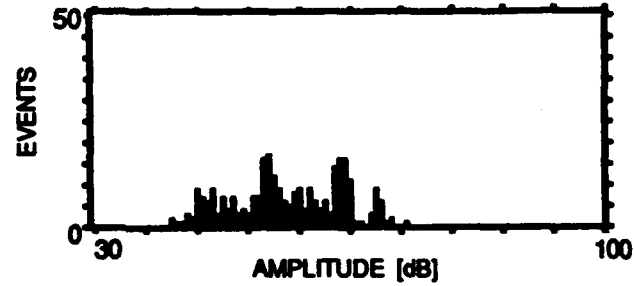
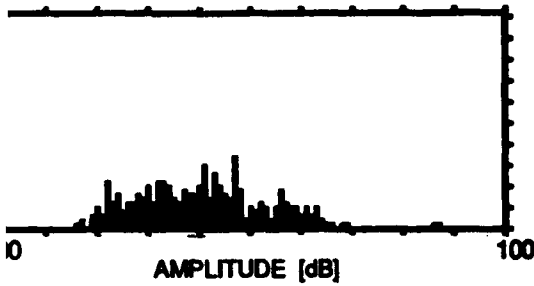
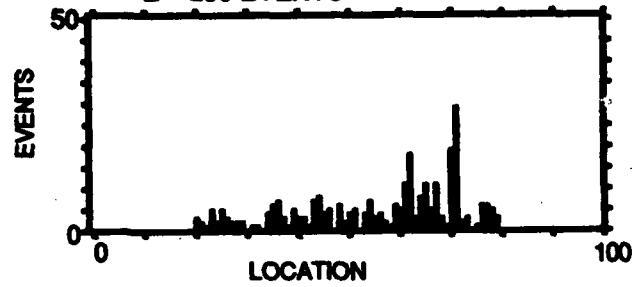
$\sigma_d = 788 \text{ MPa}$

$f = 0.01 \text{ Hz}$

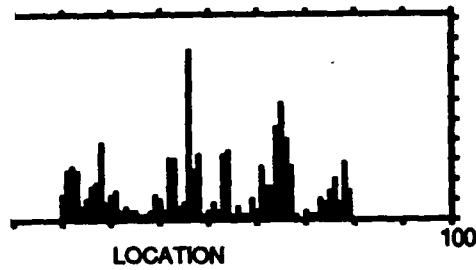
N = 301 - 350 CYCLES

E = 724 EVENTS

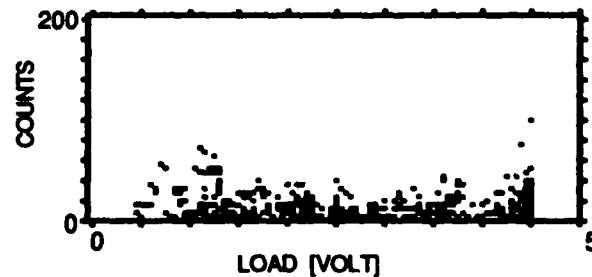
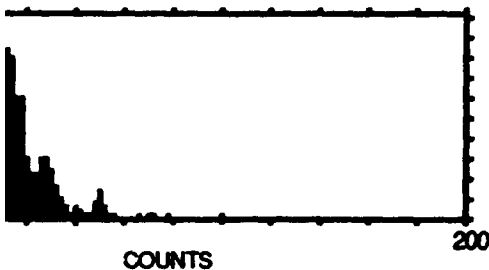
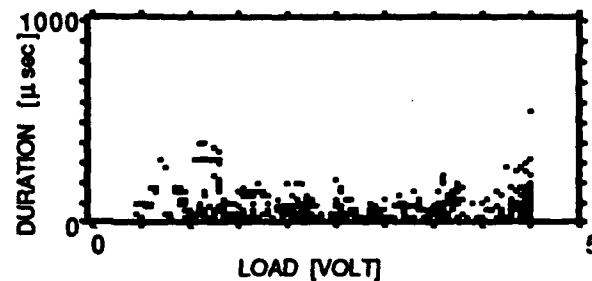
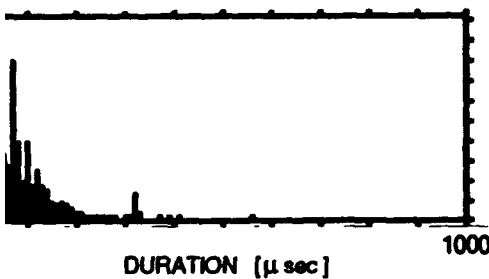
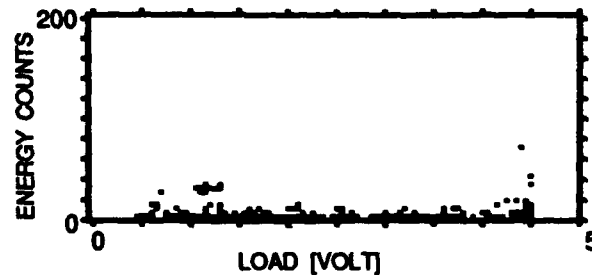
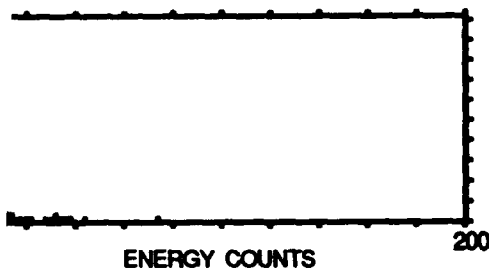
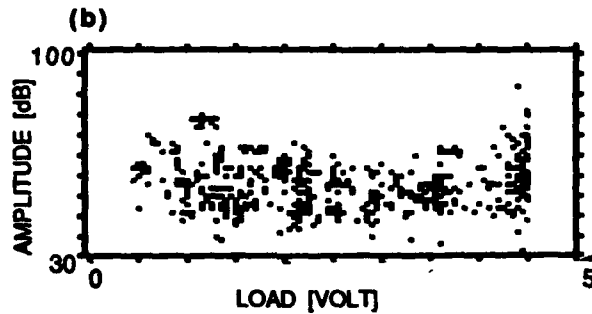
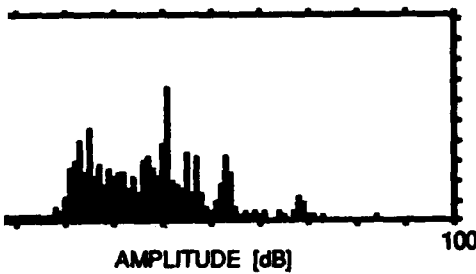
(h) LOAD RANGE = (10% - 60%) σ_d
E = 280 EVENTS



are 6.22. Concluded.



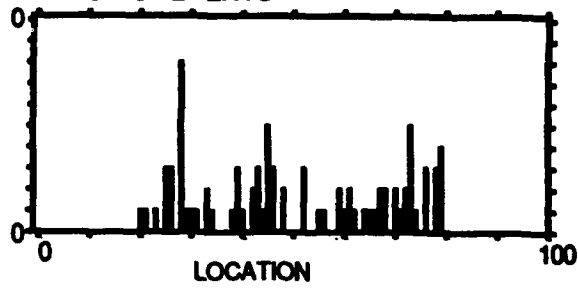
SPEC. NO. 5-D1/2
 LAY-UP: $[0_2/90_2/0]_8$
 $\sigma_d = 788 \text{ MPa}$
 $f = 1.0 \text{ Hz}$
 $N = 351 - 400 \text{ CYCLES}$
 $E = 954 \text{ EVENTS}$
 $1 \text{ VOLT} = 163 \text{ MPa}$



e 6.23. Acoustic emission event intensity and location distribution histograms and intensities of events as a function of far-field applied stress for events accumulated during a 50-cycle period of the fatigue loading showing: (a) and (b) all the events accumulated; (c) and (d) events accumulated at the upper and the lower parts of the load range, respectively; (e) and (f) events of amplitude range of 75 dB to 80 dB. Results show effect of loading frequency and state-of-damage on the intensity of friction emission.

SPEC. NO. 5-D1/2
LAY-UP: $[0_2/90_2/0]_8$

(c) LOAD RANGE = (95% - 100%) σ_d
E = 84 EVENTS



$\sigma_d = 788 \text{ MPa}$
 $f = 1.0 \text{ Hz}$

N = 351 - 400 CYCLES
E = 954 EVENTS

(d) LOAD RANGE = (10% - 60%) σ_d
E = 614 EVENTS

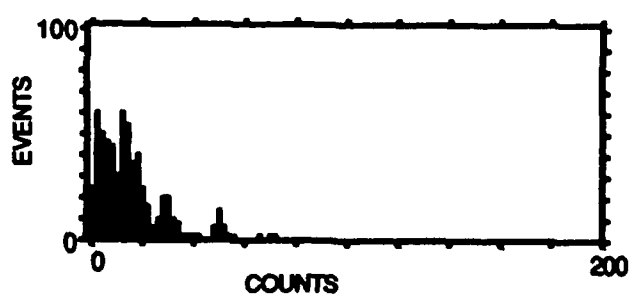
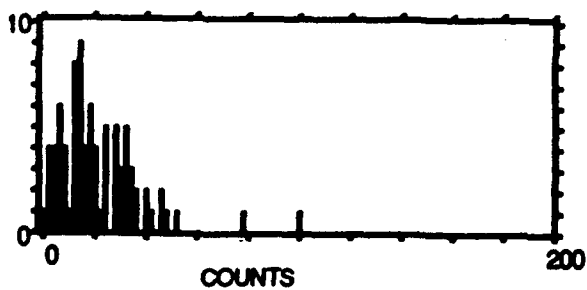
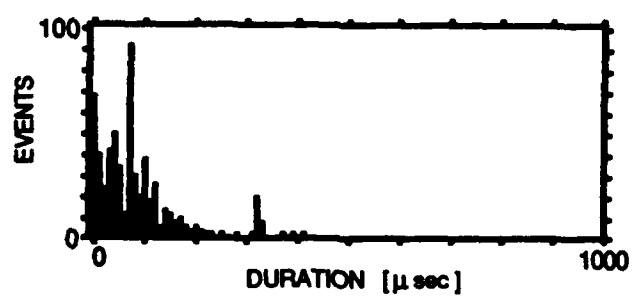
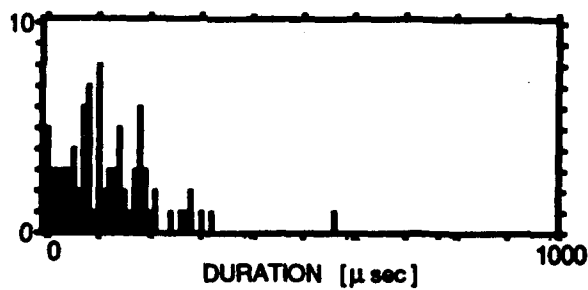
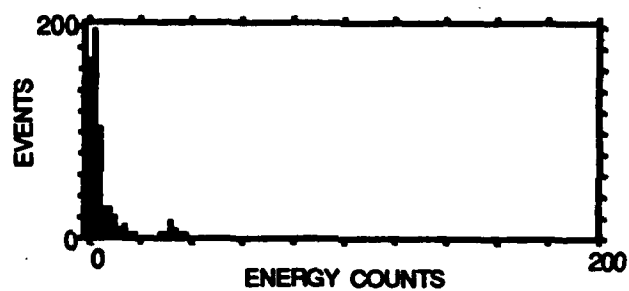
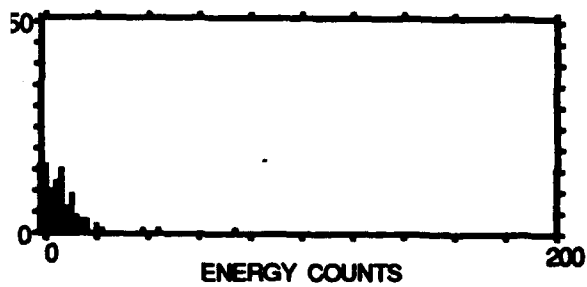
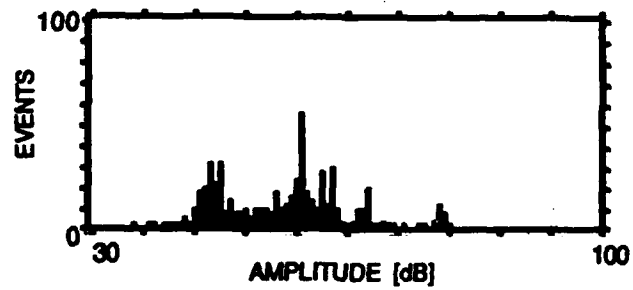
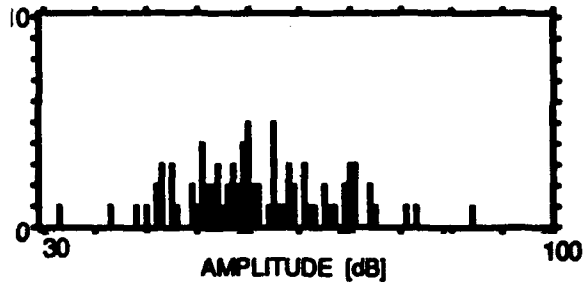
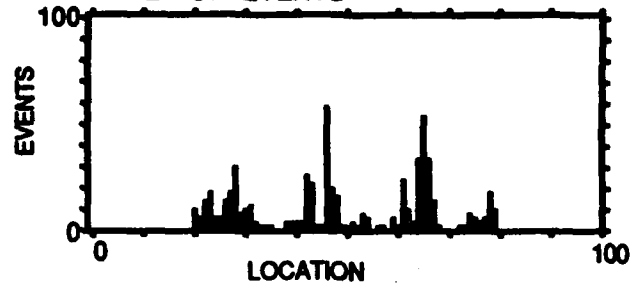
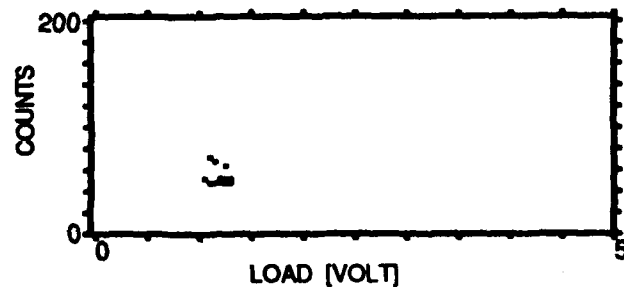
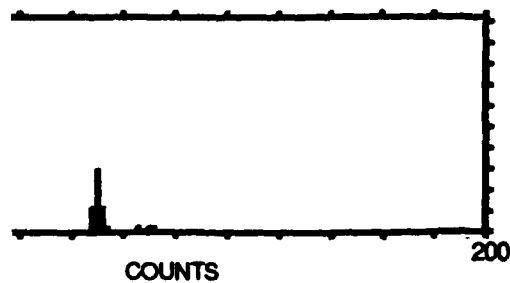
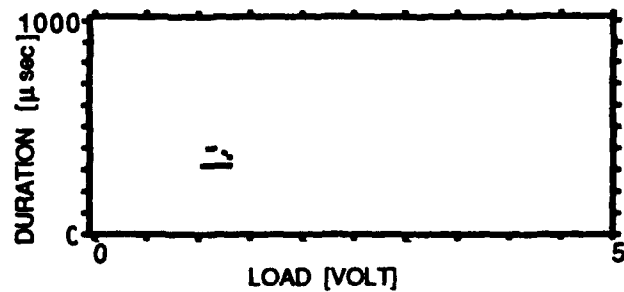
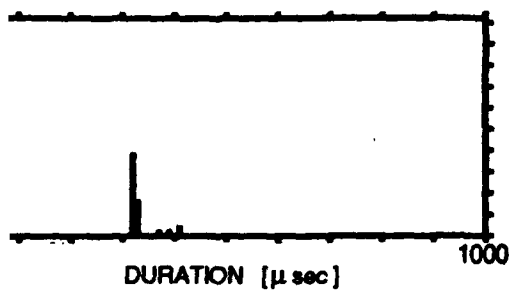
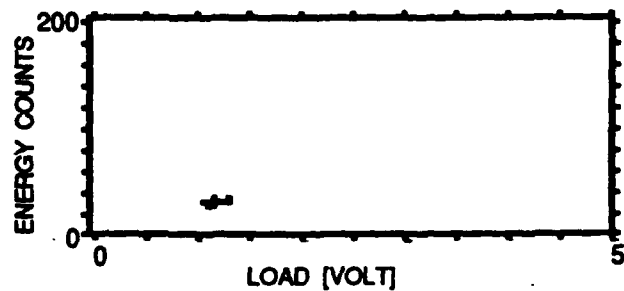
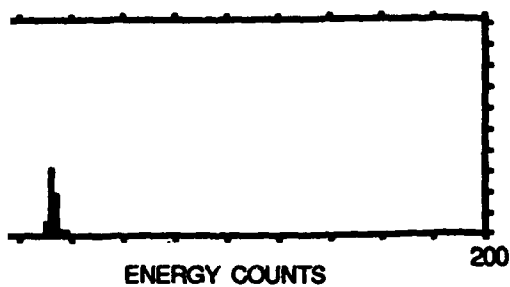
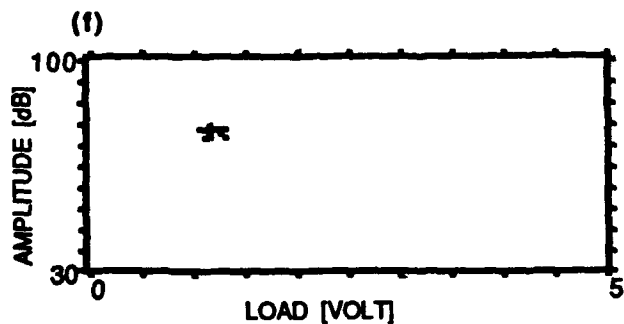
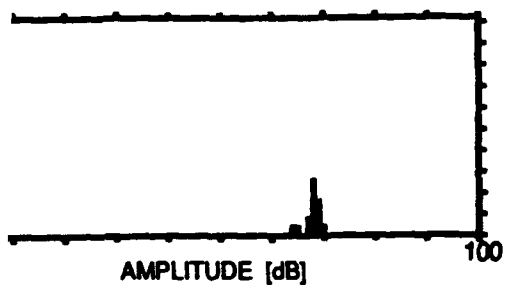


Figure 6.23. Continued.



SPEC. NO. 5-D1/2
 LAY-UP: $[0_2/90_2/0]_s$
 $\sigma_d = 788 \text{ MPa}$
 $f = 1.0 \text{ Hz}$
 $N = 351 - 400 \text{ CYCLES}$
 $E = 31 \text{ EVENTS}$
 $1 \text{ VOLT} = 163 \text{ MPa}$
 AMPLITUDE RANGE = 75 - 80 dB



6.23. Concluded.

SPEC. NO. 7-D10/1
LAY-UP: $[0/90_2/0]_8$

$\sigma_d = 385 \text{ MPa}$
 $f = 1.0 \text{ Hz}$
1 VOLT = 203 MPa

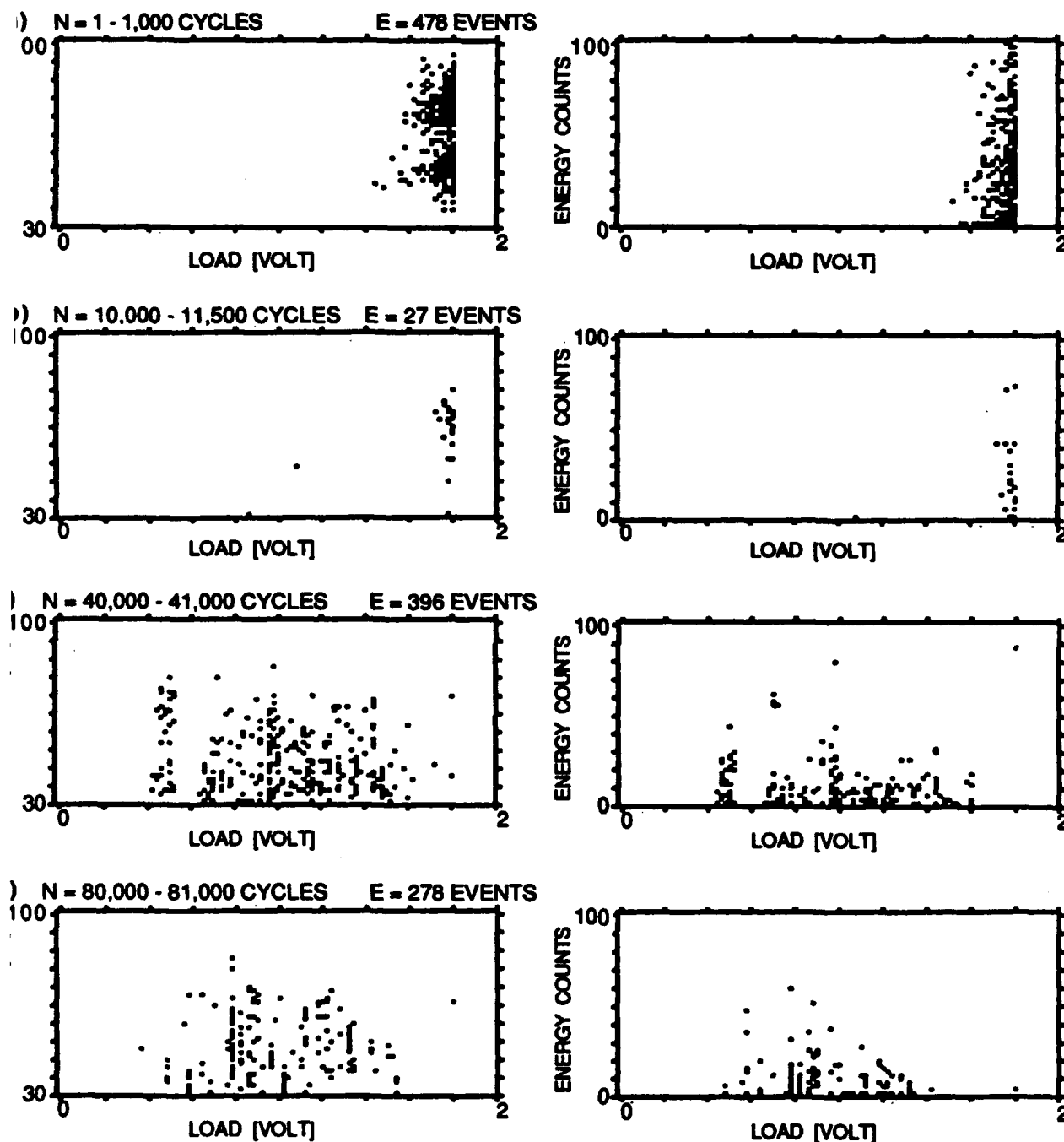
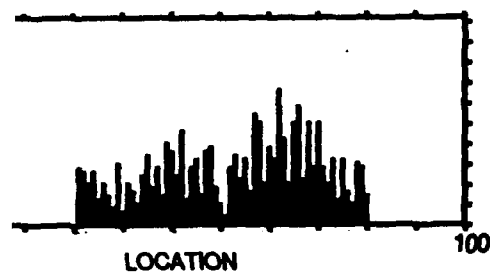
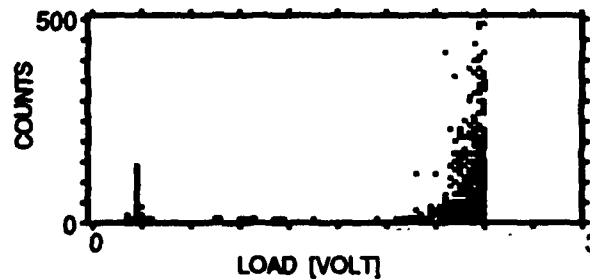
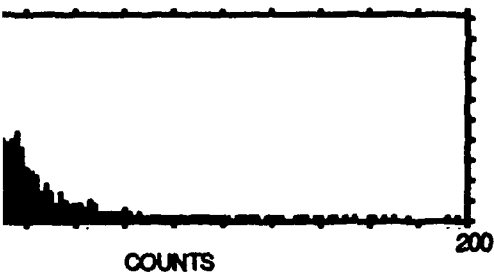
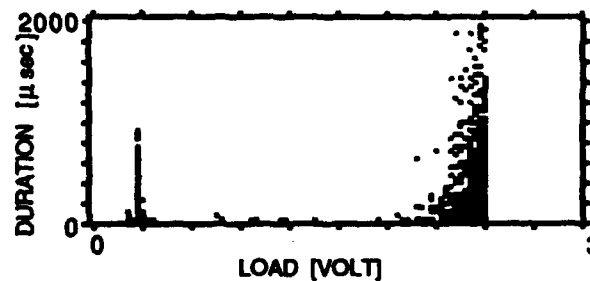
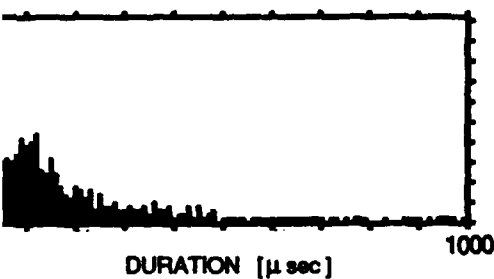
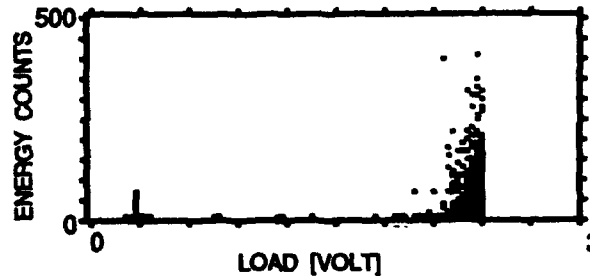
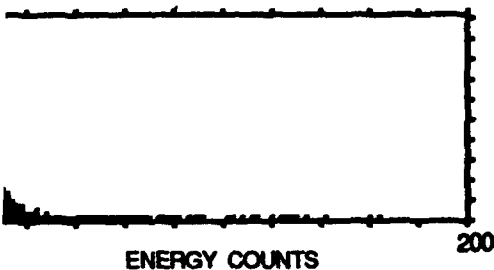
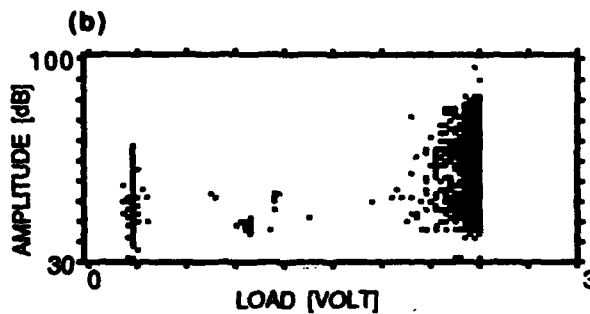
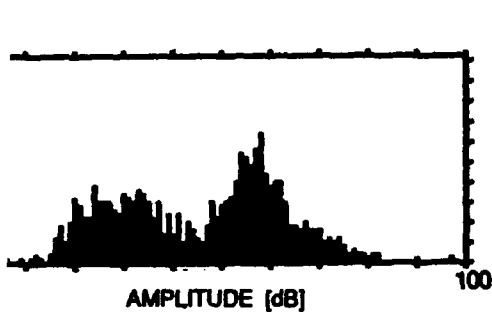


Figure 6.24. Intensities of events as a function of far-field applied stress for all the events accumulated during four selected periods of the fatigue loading for the same specimen shown in Figures 6.2a and 6.2b. High intensity events occur throughout the lower load range showing the effect of loading frequency and state-of-damage on the intensity of friction emission.



SPEC. NO. 5-C3/1
 LAY-UP: $[0_2/90_2/0]_s$
 $\sigma_d = 398 \text{ MPa}$
 $f = 1.0 \text{ Hz}$
 $N = 1 - 10,000 \text{ CYCLES}$
 $E = 1,644 \text{ EVENTS}$
 $1 \text{ VOLT} = 159 \text{ MPa}$



6.25. Acoustic emission event intensity histograms and intensities of events as a function of far-field applied stress for all the events accumulated during the first 10,000-cycle period of the fatigue loading of the same specimen shown in Figures 6.4a, 6.4c, and 6.10a. High intensity events occur also at the lowest load range, indicating the occurrence of trains of events.

SPEC. NO. 5 - C3/1
 LAY - UP : $[0_2/90_2/0]_s$
 $\sigma_d = 398 \text{ MPa}$
 $\sigma_d / \sigma_f = 0.27$

$N = 16,001 - 17,000 \text{ CYCLES}$
 $f = 1.0 \text{ Hz}$
 $E = 2,527 \text{ EVENTS}$

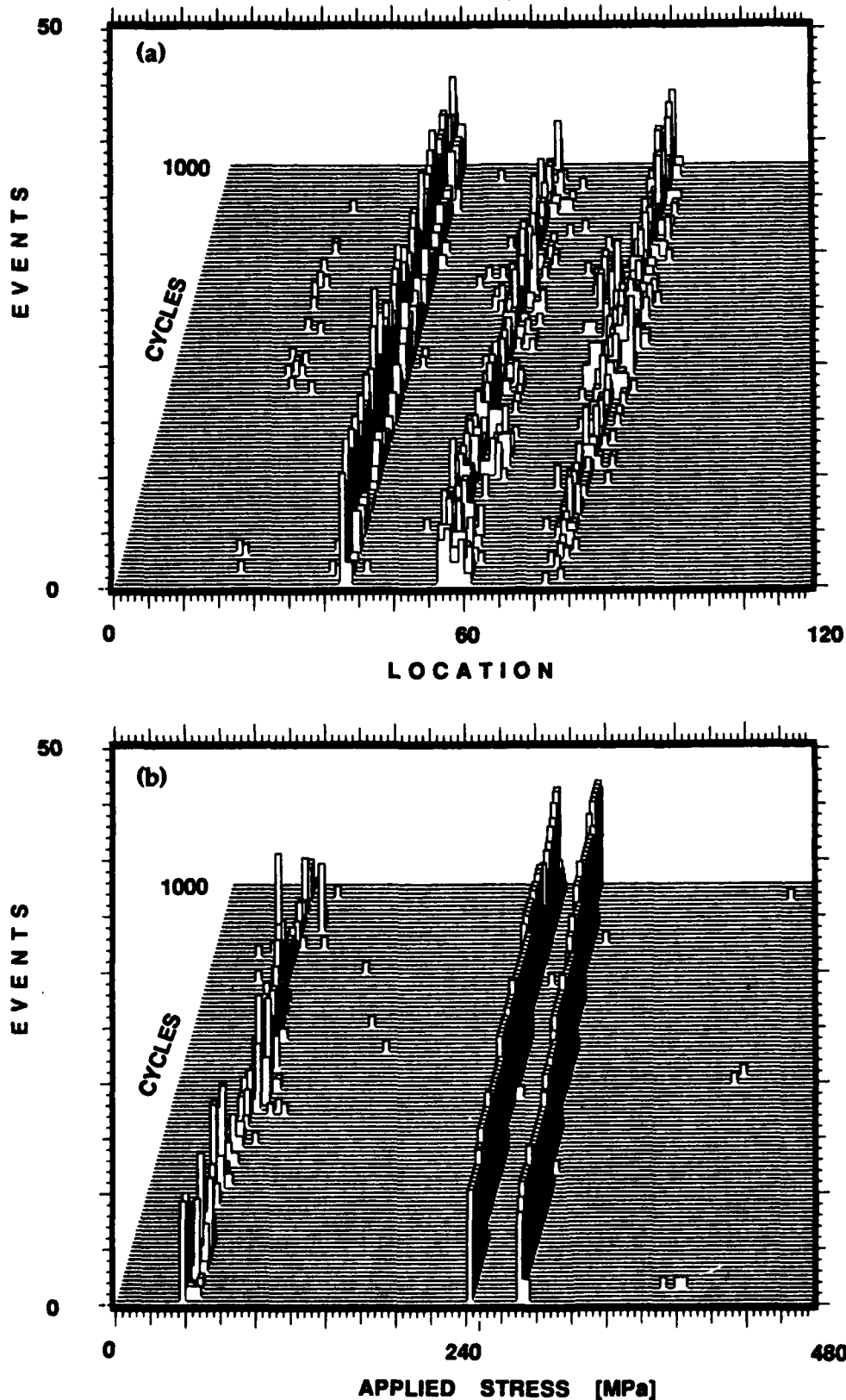


Figure 6.26. Three-dimensional plots of load and location distribution histograms of events recorded for the same specimen and fatigue period shown in Figure 6.3c. Results show that emission is generated repeatedly at specific load levels and at specific sites along the specimen.

SPEC. NO. 5 - C3/1
 LAY - UP : $[0_2/90_2/0]_s$
 $\sigma_d = 398 \text{ MPa}$

$\sigma_d / \sigma_f = 0.27$
 $N = 16,001 - 17,000 \text{ CYCLES}$
 $f = 1.0 \text{ Hz}$

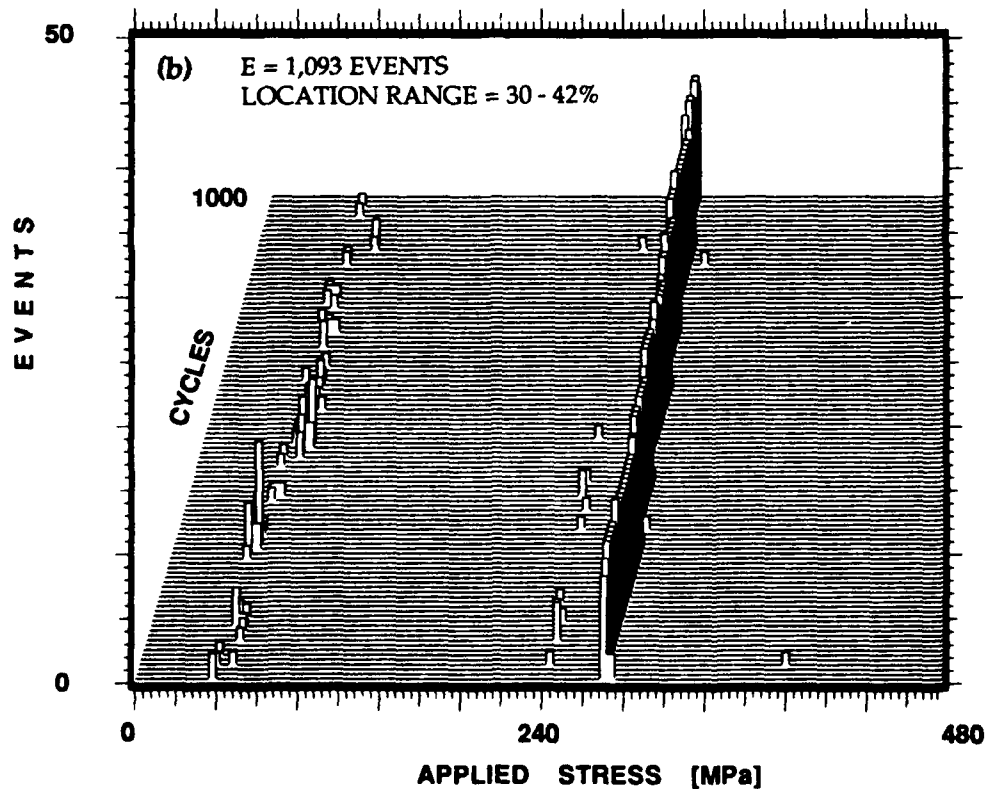
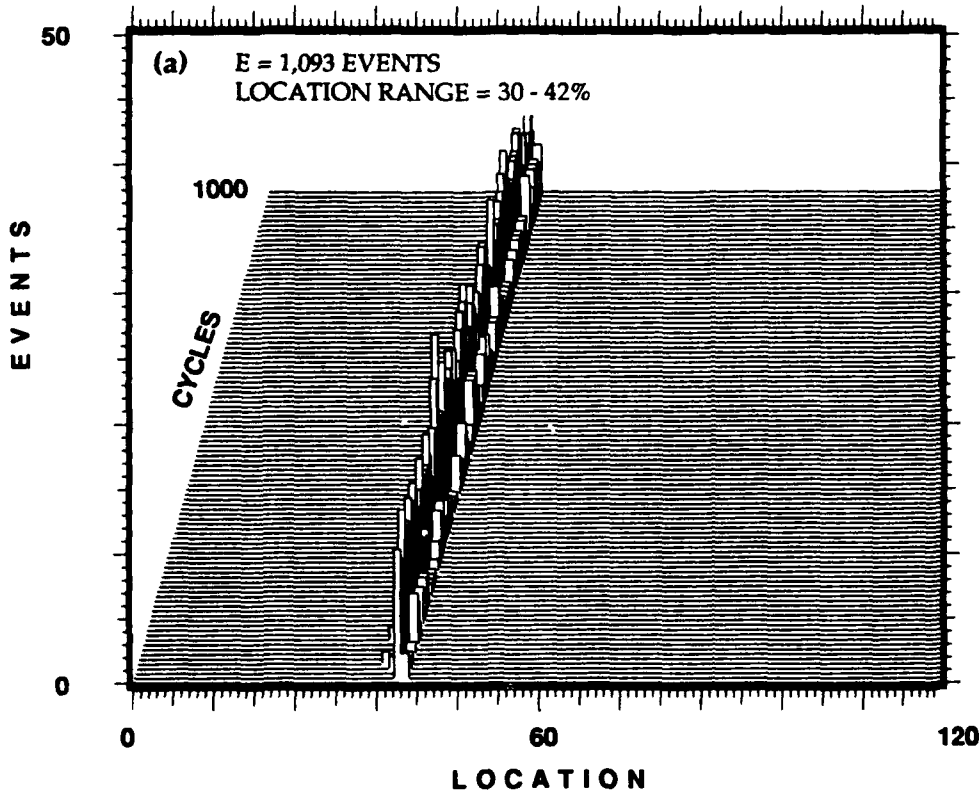


Figure 6.27. Three-dimensional plots of location and load distribution histograms of events generated within the location range of 30-42 percent of the specimen's gage length shown in Figure 6.26. Events which are generated at a specific location are also generated at specific load levels.

SPEC. NO. 5 - C3/1
 LAY - UP: $[0_2/90_2/0]_s$
 $\sigma_d = 398 \text{ MPa}$

$\sigma_d / \sigma_f = 0.27$
 $N = 16,001 - 17,000 \text{ CYCLES}$
 $f = 1.0 \text{ Hz}$

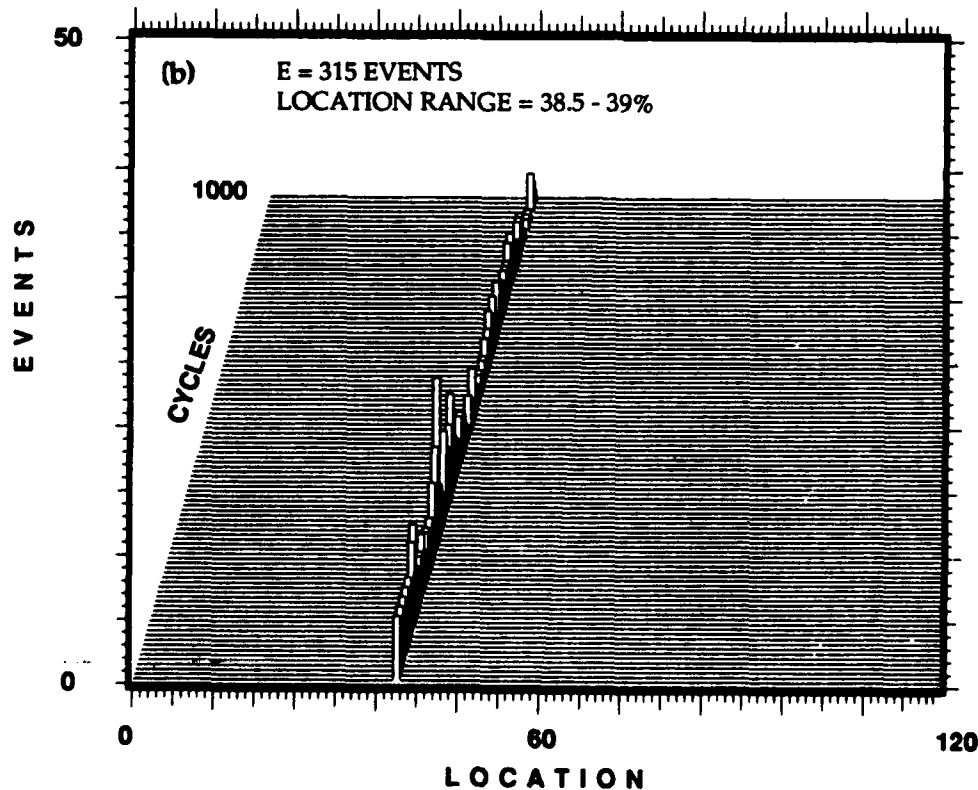
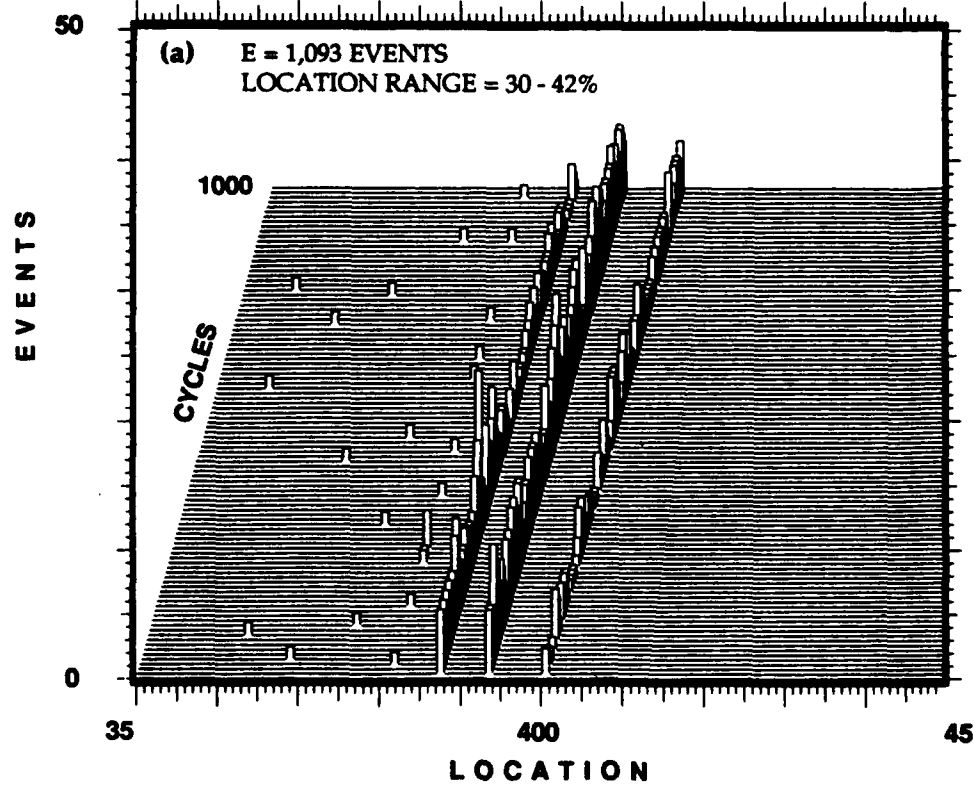


Figure 6.28. Three-dimensional plots of location distribution histograms of events generated within the location range of 30-42 percent of the specimen's gage length: (a) detailed plot of the distribution shown in Figure 6.27a; (b), (c), and (d) location distribution histograms of the events generated within three specific different location ranges.

SPEC. NO. 5 - C3/1
 LAY - UP : $[0_2/90_2/0]_s$
 $\sigma_d = 398 \text{ MPa}$

$\sigma_d / \sigma_f = 0.27$
 $N = 16,001 - 17,000 \text{ CYCLES}$
 $f = 1.0 \text{ Hz}$

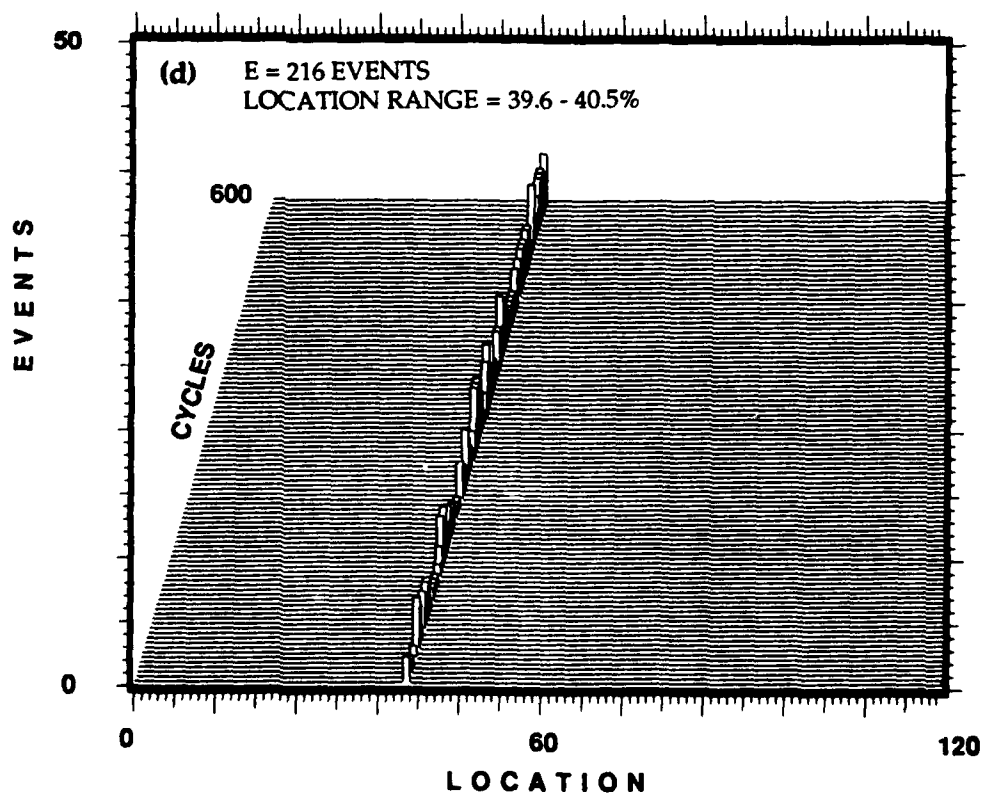
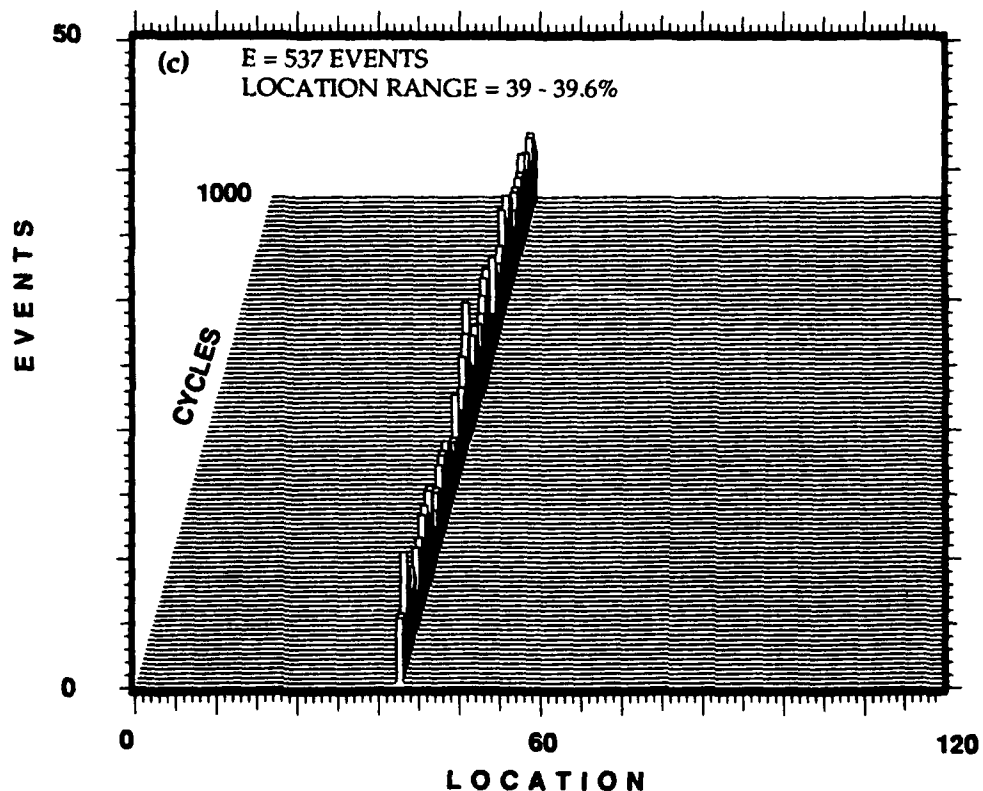


Figure 6.28. Concluded.

SPEC. NO. 5 - C3/1
 LAY - UP: $[0_2/90_2/0]_s$
 $\sigma_d = 398 \text{ MPa}$

$\sigma_d / \sigma_f = 0.27$
 $N = 16,001 - 17,000 \text{ CYCLES}$
 $f = 1.0 \text{ Hz}$

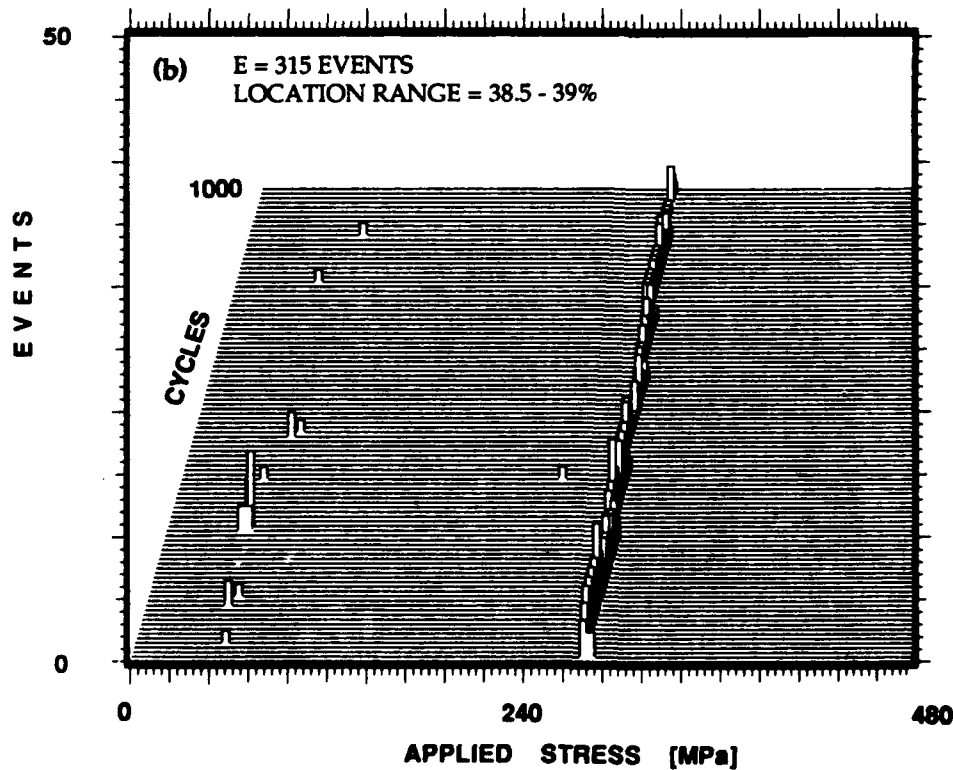
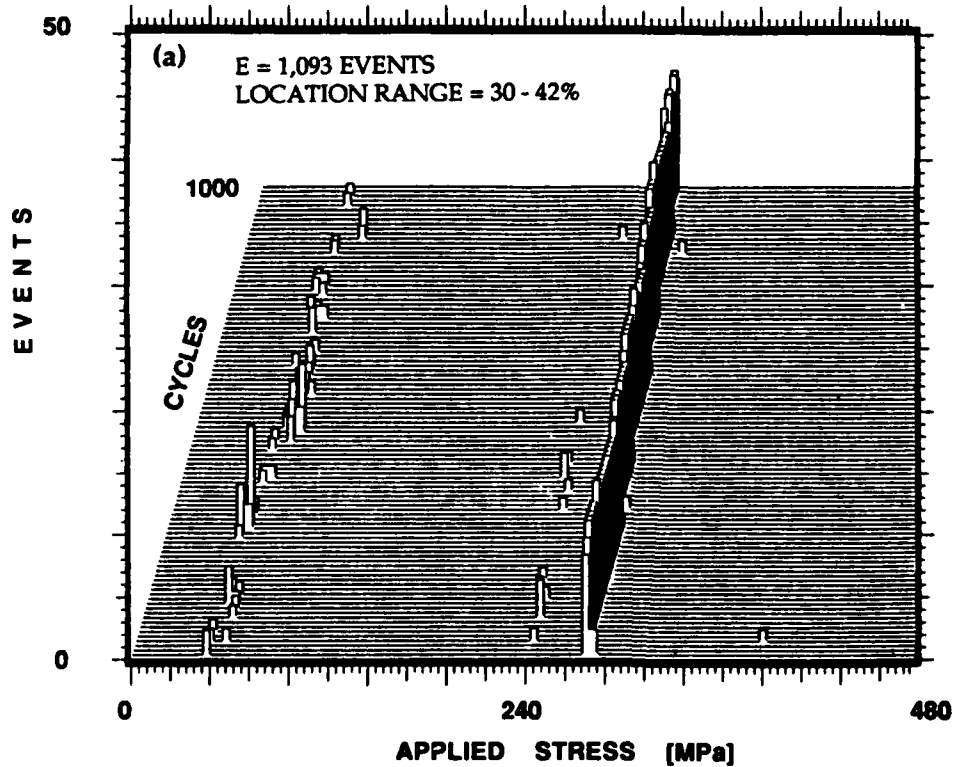


Figure 6.29. Three-dimensional plots of load distribution histograms of events generated within the location range of 30-42 percent of the specimen's gage length: (a) load distribution histograms of the events shown in Figure 6.28a; (b), (c), and (d) load distribution histograms of the events generated within the three specific location ranges shown in Figures 6.28b, 6.28c, and 6.28d, respectively. Events which are generated at a specific location are also generated at specific load levels.

SPEC. NO. 5 - C3/1
 LAY - UP : $[0_2/90_2/0]_s$
 $\sigma_d = 398 \text{ MPa}$

$\sigma_d / \sigma_f \approx 0.27$
 $N = 16,001 - 17,000 \text{ CYCLES}$
 $f = 1.0 \text{ Hz}$

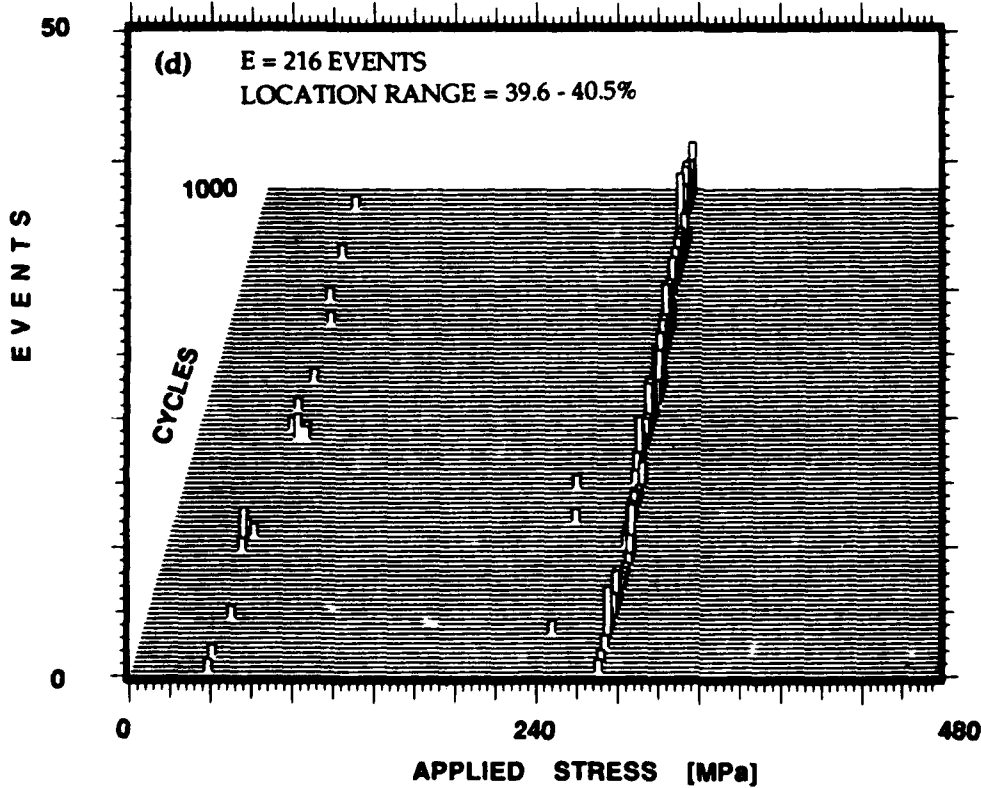
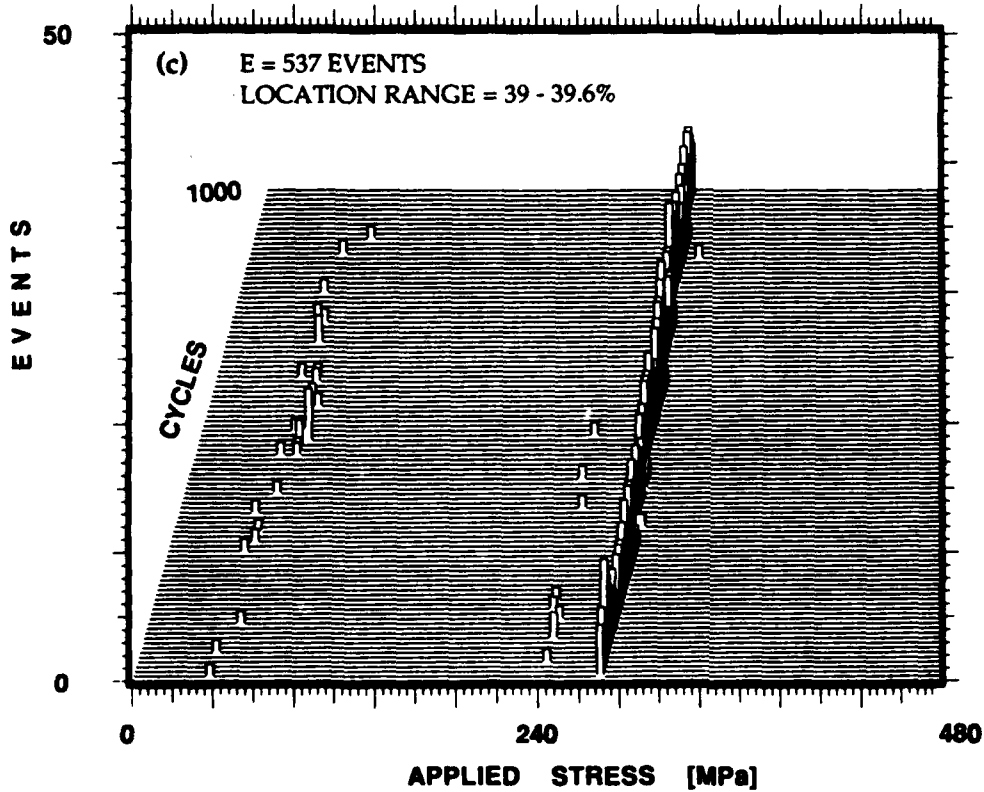


Figure 6.29. Concluded.

SPEC. NO. 5 - C3/1
 LAY - UP : $[0_2/90_2/0]_s$
 $\sigma_d = 398 \text{ MPa}$

$\sigma_d / \sigma_f = 0.27$
 $N = 16,001 - 17,000 \text{ CYCLES}$
 $f = 1.0 \text{ Hz}$

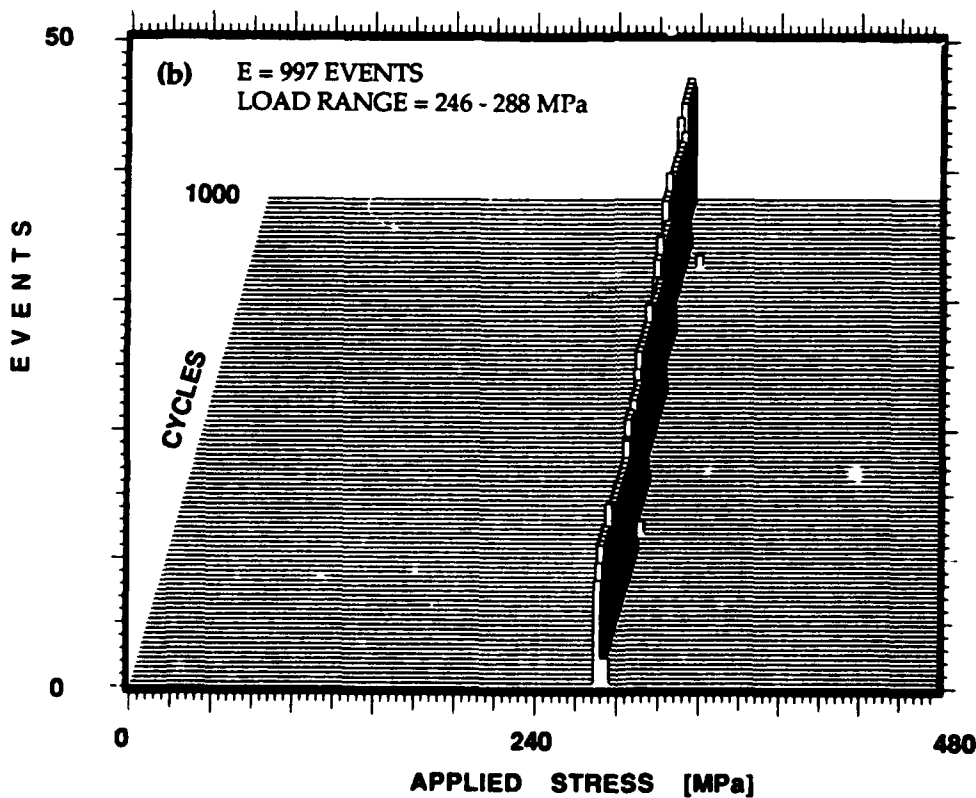
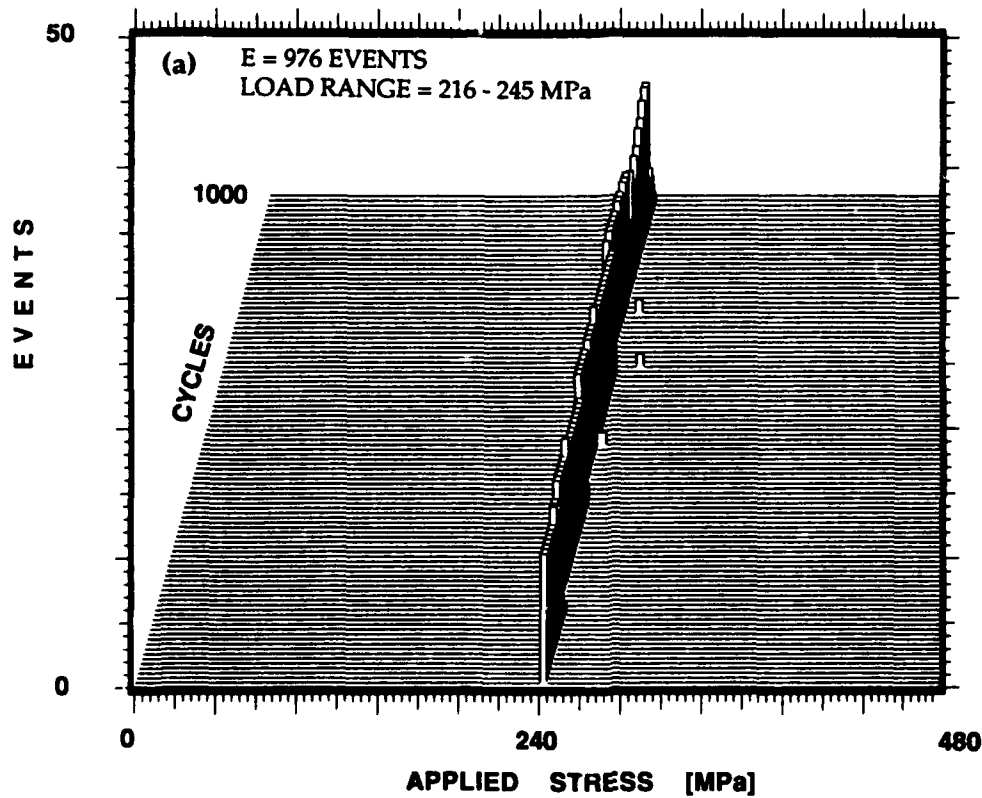


Figure 6.30. Three-dimensional plots of load and location distribution histograms of events generated within 60-68 percent of the dynamic stress amplitude shown in Figure 6.26b. Events which are generated at a specific load level are also generated at specific sites along the specimen.

SPEC. NO. 5 - C3/1
 LAY - UP : $[0_2/90_2/0]_s$
 $\sigma_d = 398 \text{ MPa}$

$\sigma_d / \sigma_f = 0.27$
 $N = 16,001 - 17,000 \text{ CYCLES}$
 $f = 1.0 \text{ Hz}$

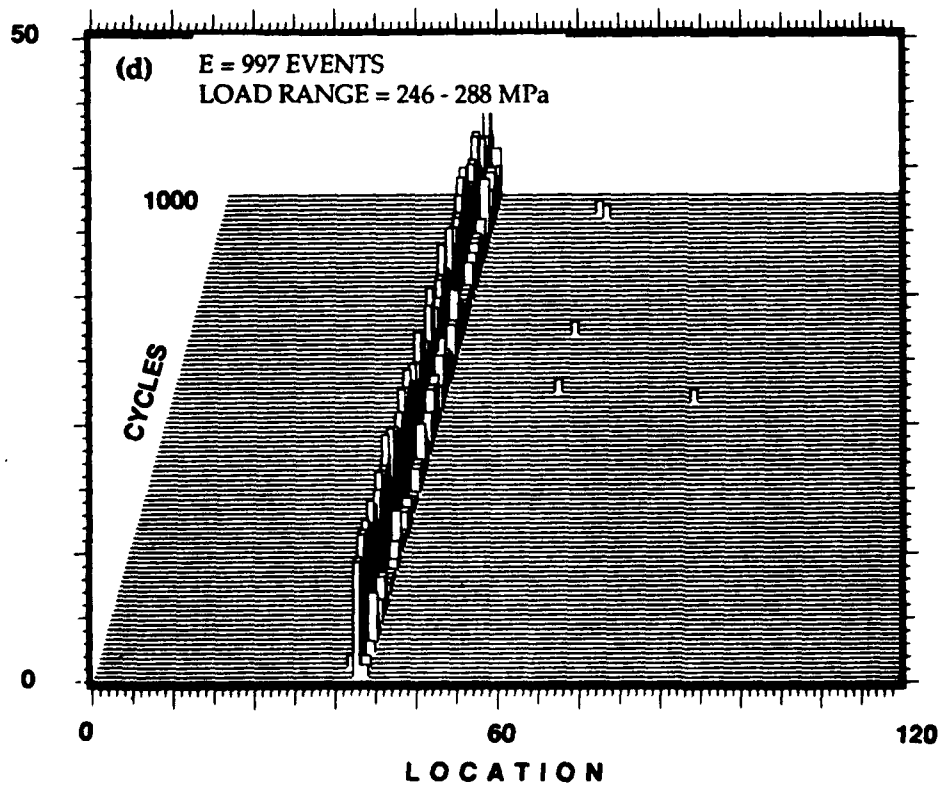
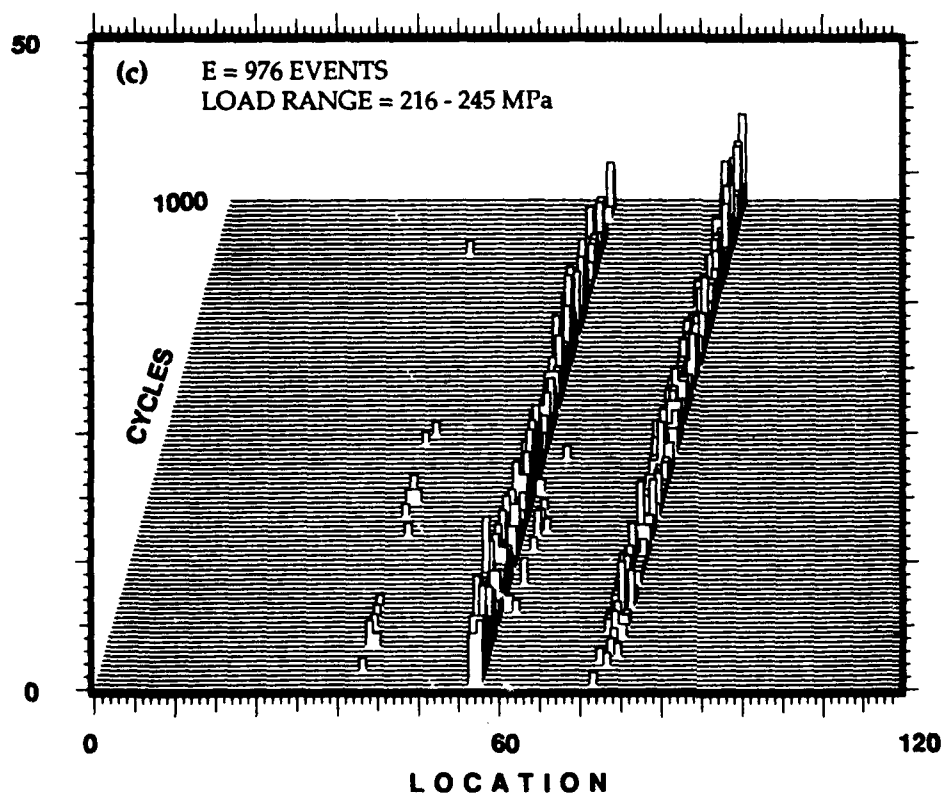


Figure 6.30. Concluded.

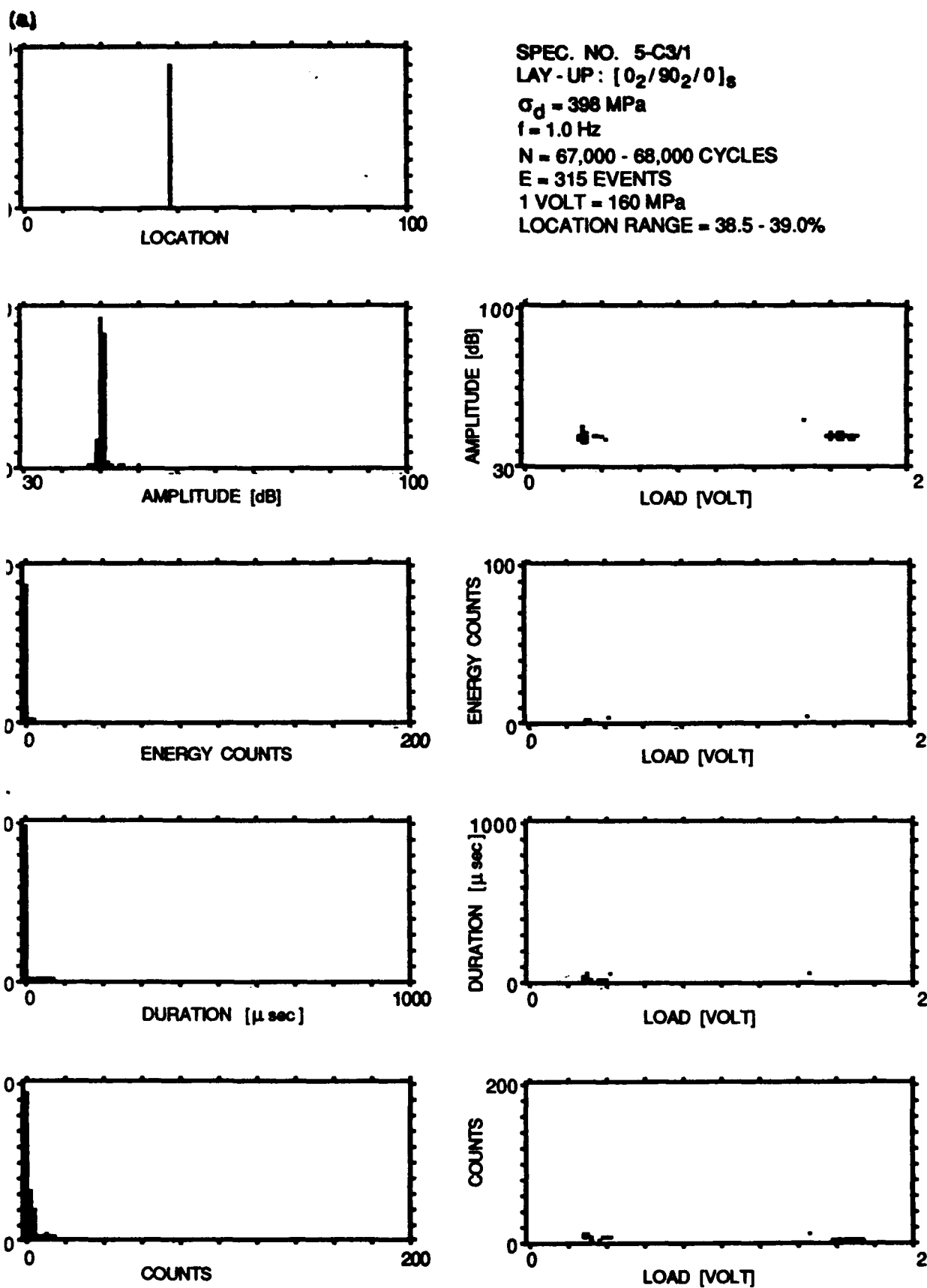
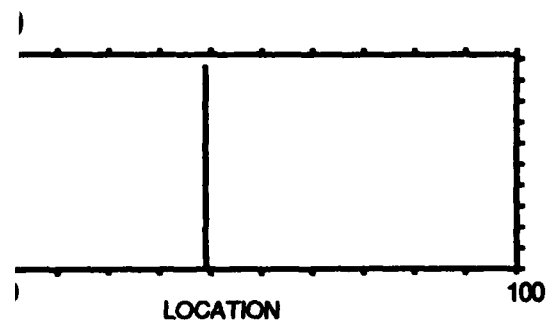
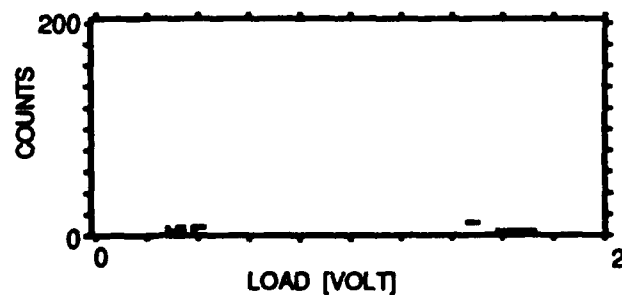
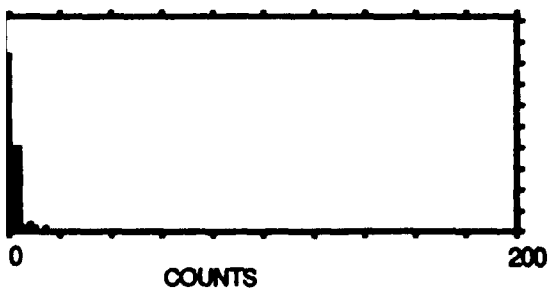
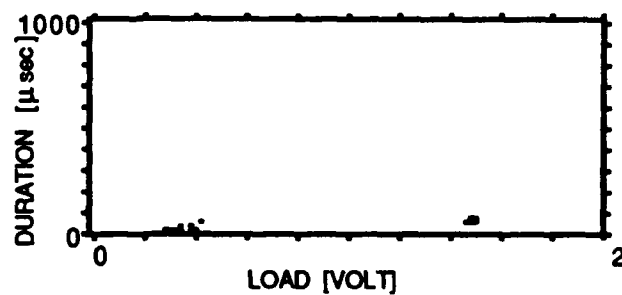
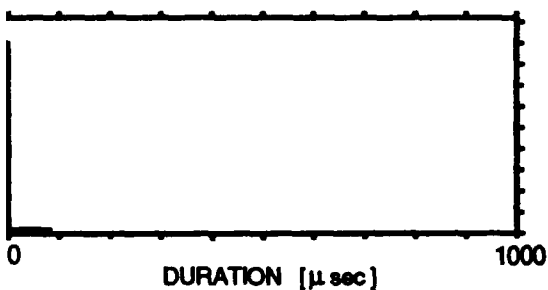
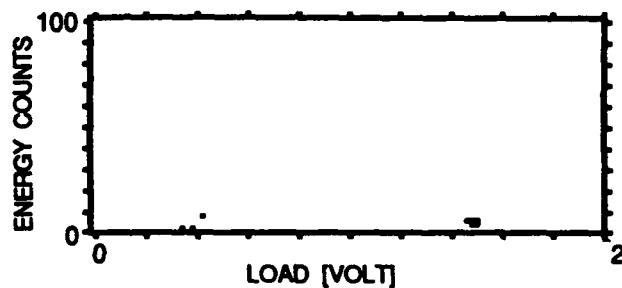
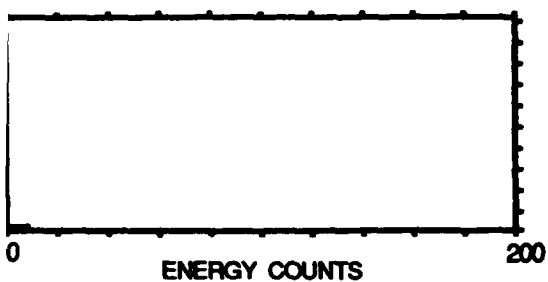
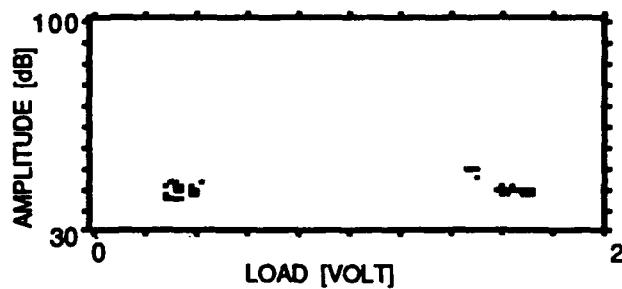
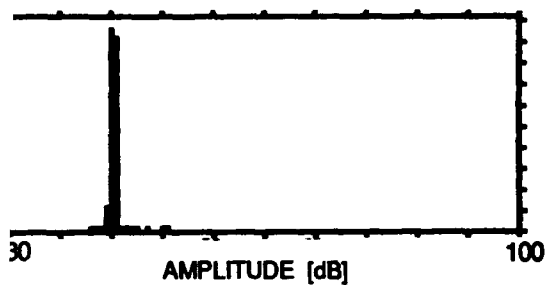


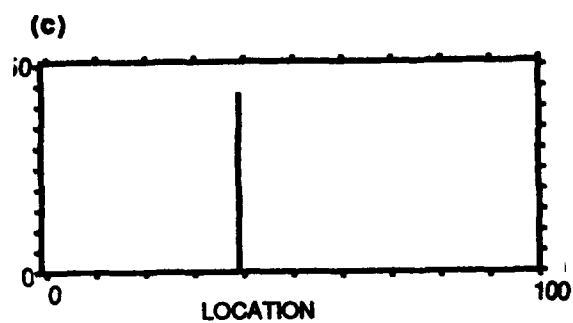
Figure 6.31. Acoustic emission event intensity and location distribution histograms and intensities of events as a function of far-field applied stress for all the events accumulated within: (a), (b), and (c) the three location ranges shown in Figures 6.28b, 6.28c, and 6.28d, respectively; (d) and (e) the two load ranges shown in Figure 6.30a and 6.30b respectively. Events which are generated repeatedly at the same location and load ranges are all of specific and low intensities.



SPEC. NO. 5-C3/1
 LAY - UP : $[0_2/90_2/0]_s$
 $\sigma_d = 398 \text{ MPa}$
 $f = 1.0 \text{ Hz}$
 $N = 67,000 - 68,000 \text{ CYCLES}$
 $E = 537 \text{ EVENTS}$
 $1 \text{ VOLT} = 160 \text{ MPa}$
 LOCATION RANGE = 39.0- 39.6%



ure 6.31. Continued.



SPEC. NO. 5-C3/1
 LAY-UP: $[0_2/90_2/0]_s$
 $\sigma_d = 398 \text{ MPa}$
 $f = 1.0 \text{ Hz}$
 $N = 67,000 - 68,000 \text{ CYCLES}$
 $E = 216 \text{ EVENTS}$
 $1 \text{ VOLT} = 160 \text{ MPa}$
 LOCATION RANGE = 39.6 - 40.5%

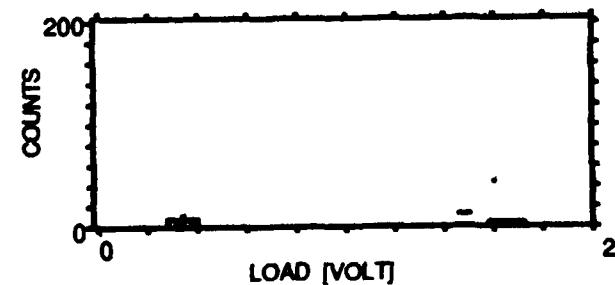
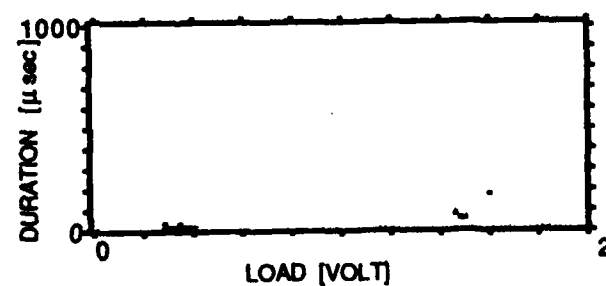
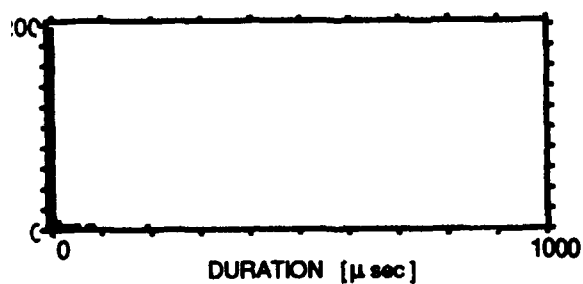
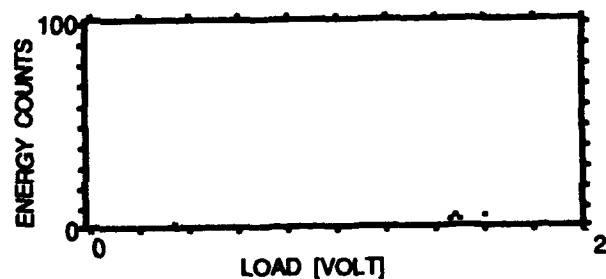
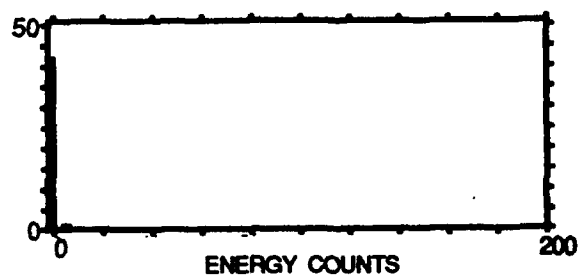
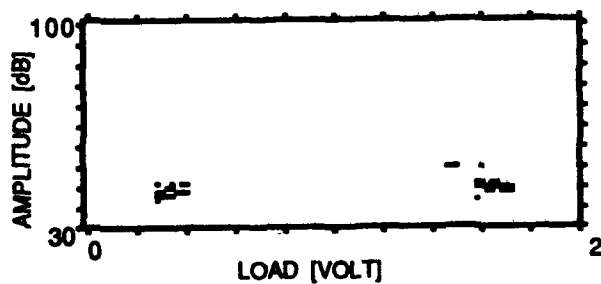
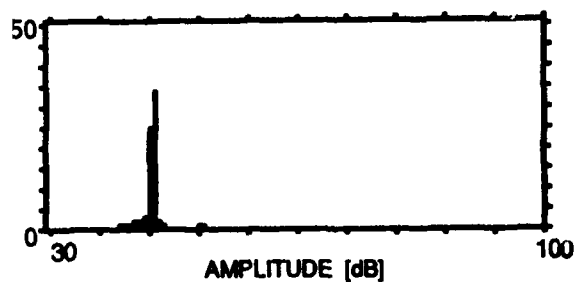
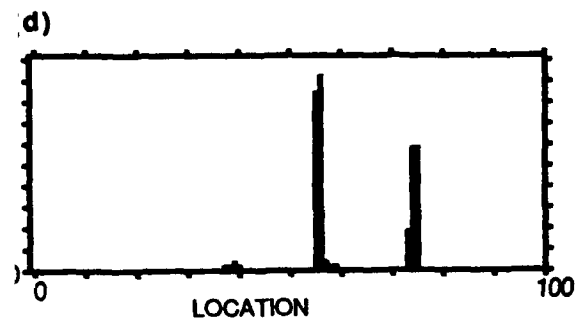


Figure 6.31. Continued.



SPEC. NO. 5-C3/1
 LAY - UP : $[0_2/90_2/0]_s$
 $\sigma_d = 398$ MPa
 $f = 1.0$ Hz
 $N = 67,000 - 68,000$ CYCLES
 $E = 976$ EVENTS
 1 VOLT = 160 MPa
 LOAD RANGE = 215 - 244 MPa

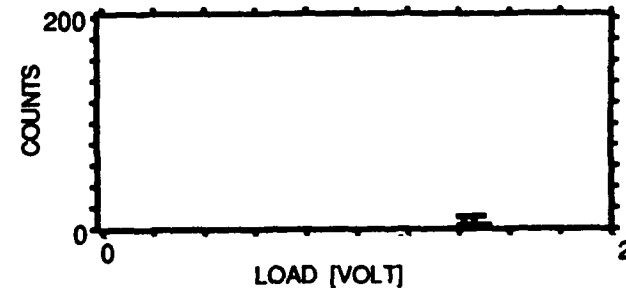
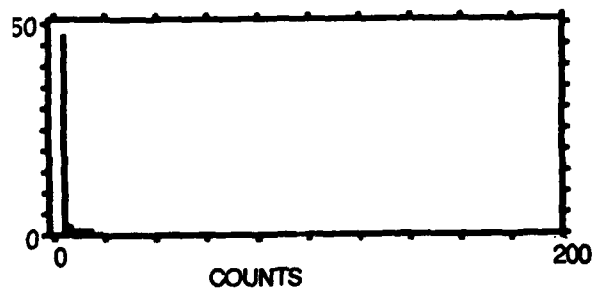
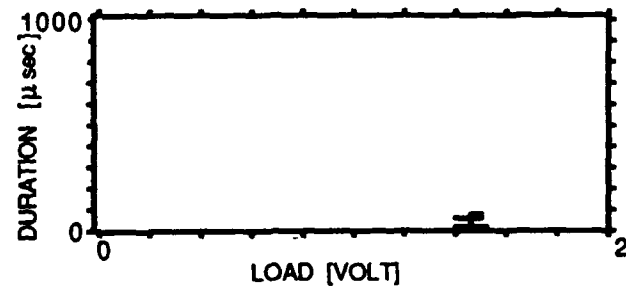
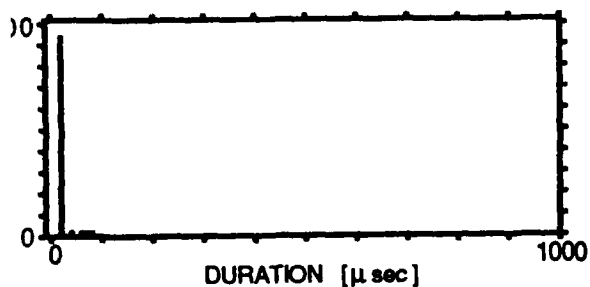
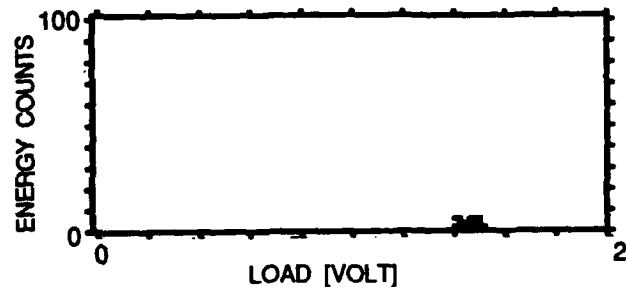
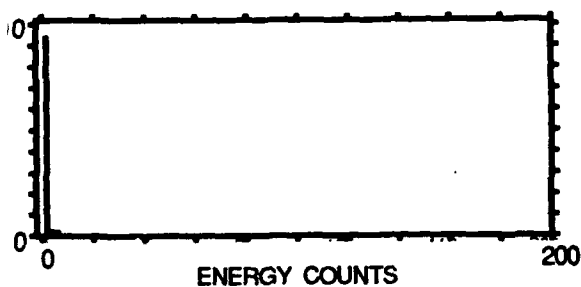
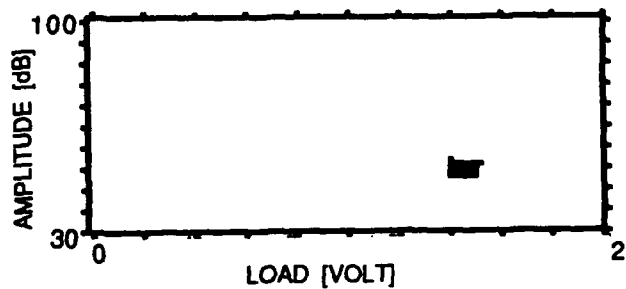
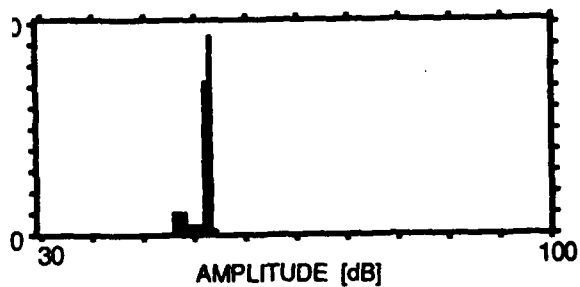


Figure 6.31. Continued.

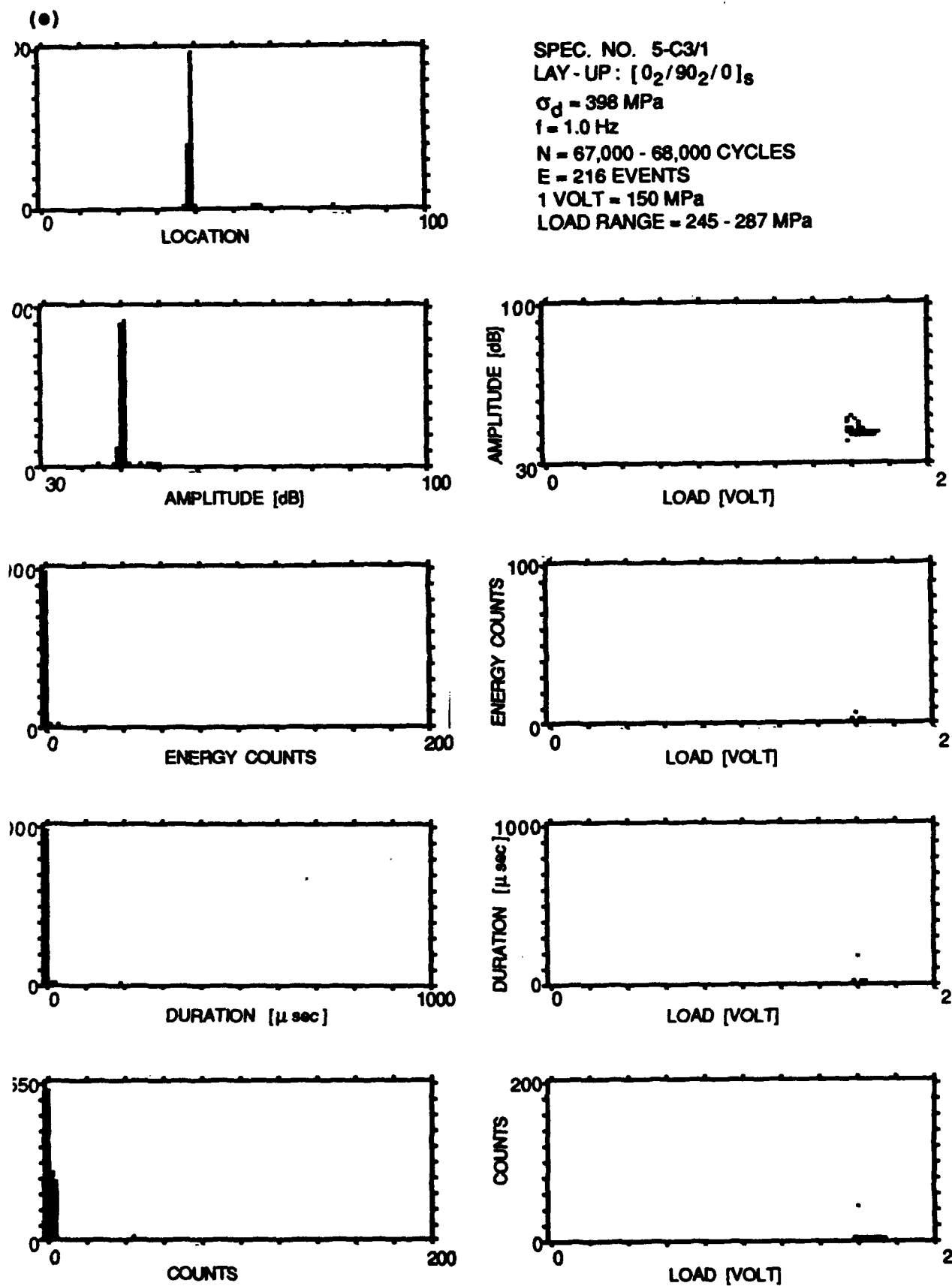


Figure 6.31. Concluded.

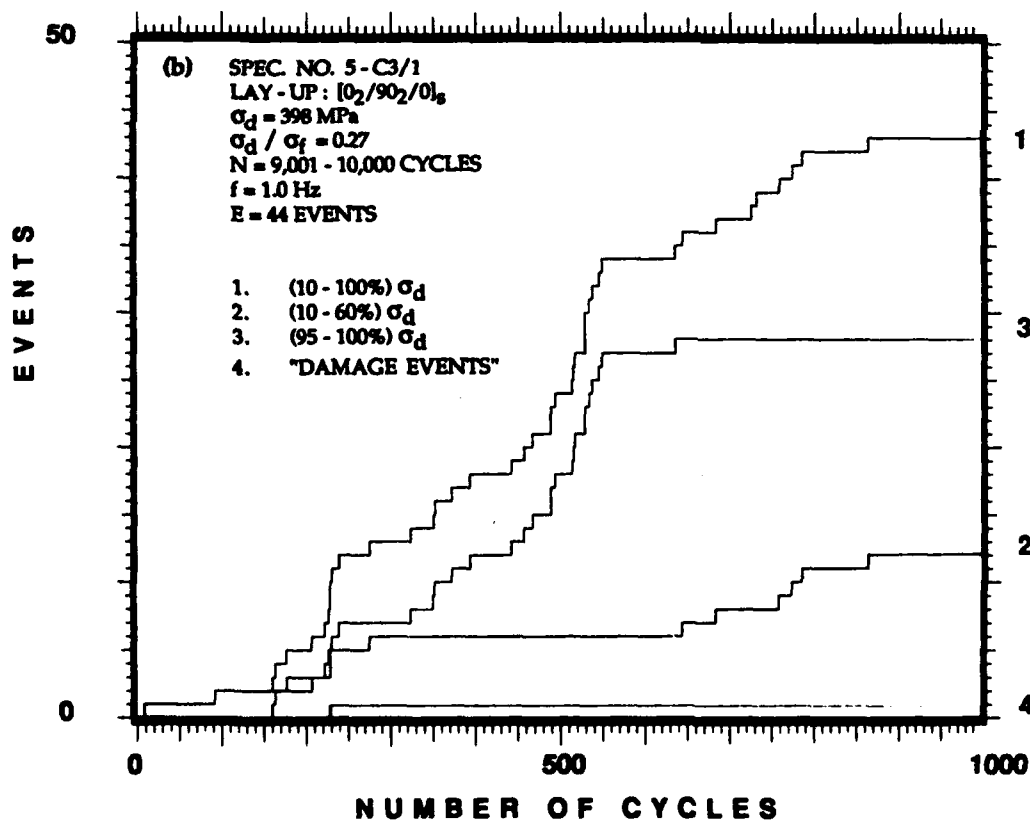
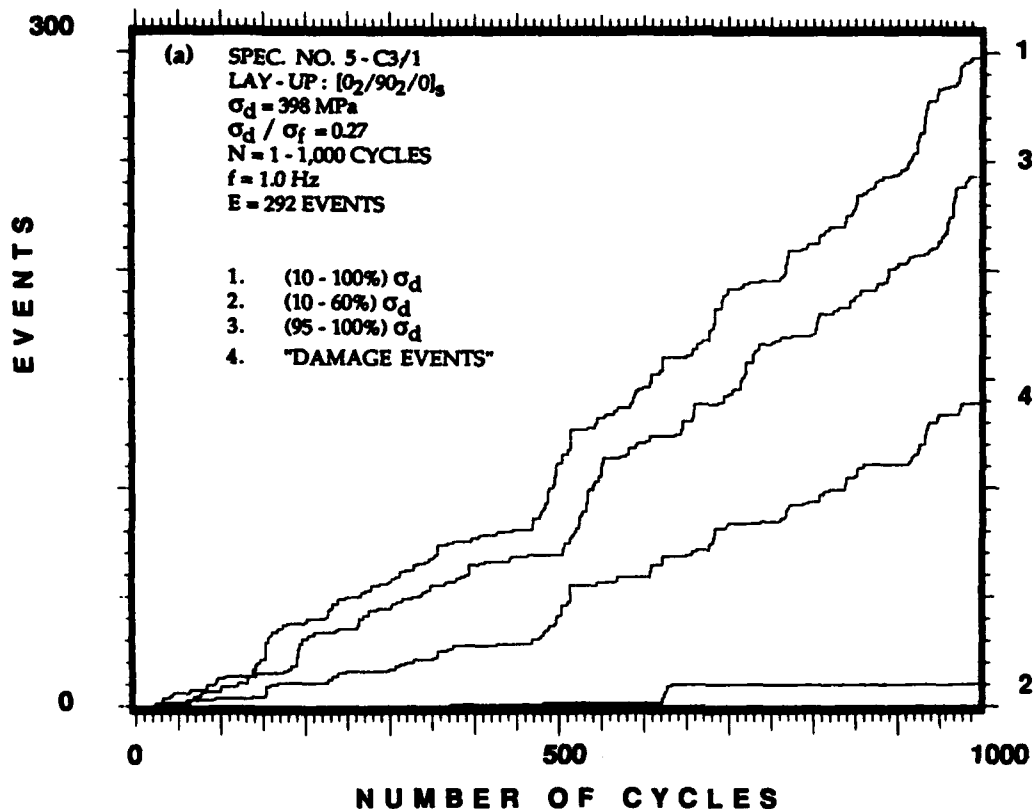
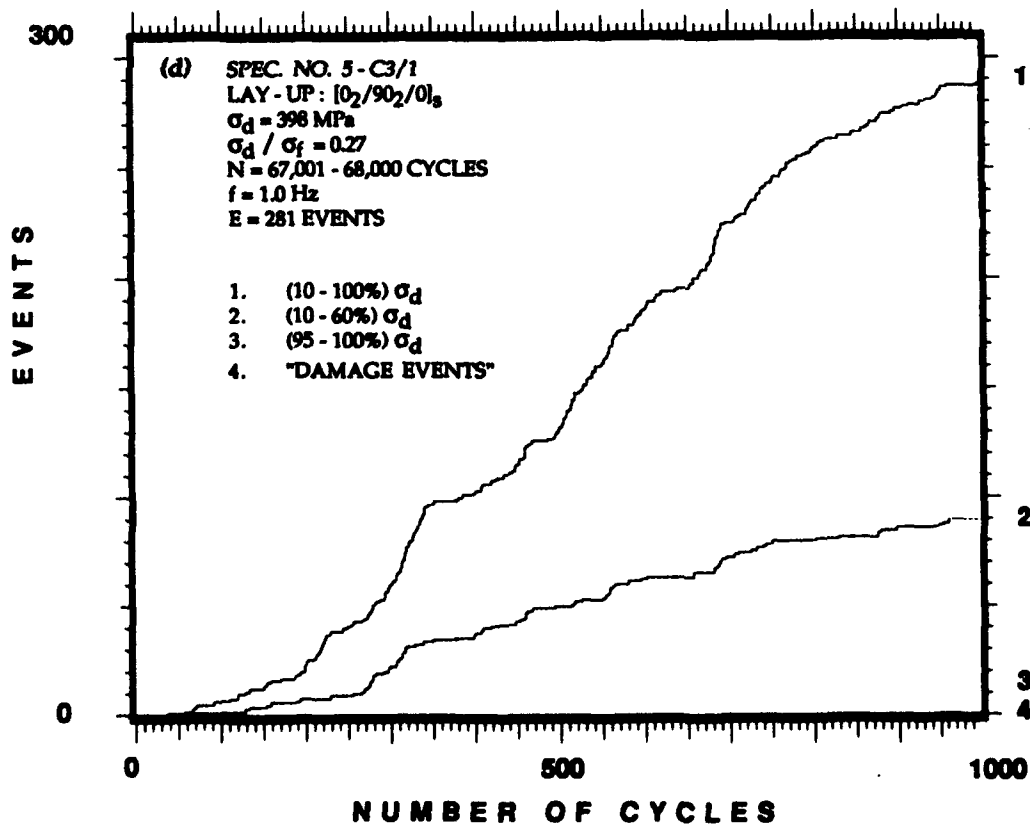
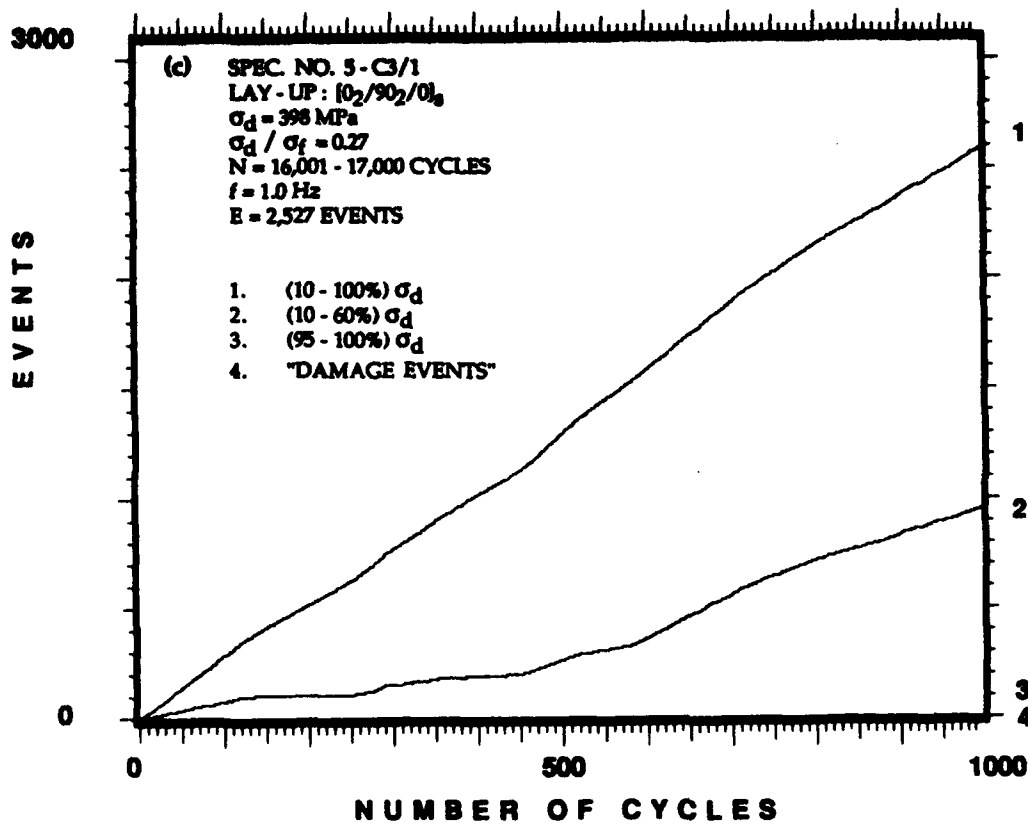


Figure 6.32. Accumulative events as a function of number of cycles, distinguishing among emission generated in three different load ranges (curves No. 1-3) and derived damage (DD) curve for all the events generated (curve No. 4) during selected periods of the fatigue loading of three representative specimens. The amount of emission caused by actual damage accumulation is significantly smaller than the total emission generated during fatigue loading.



gure 6.32. Continued.

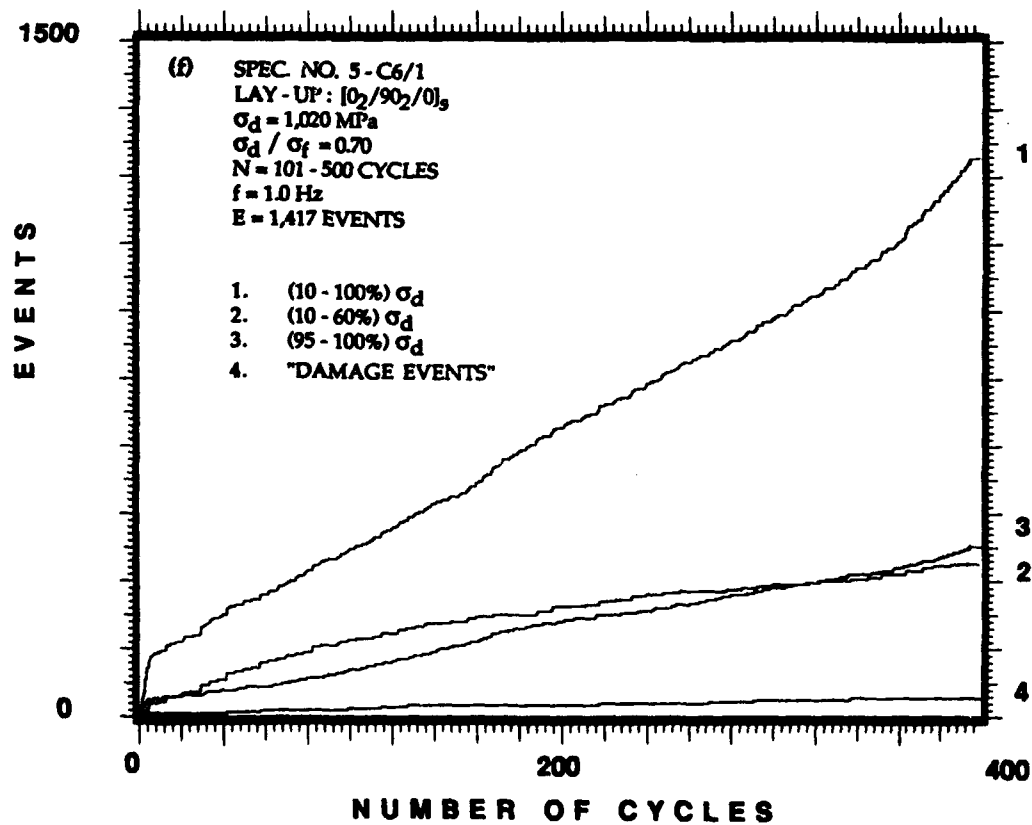
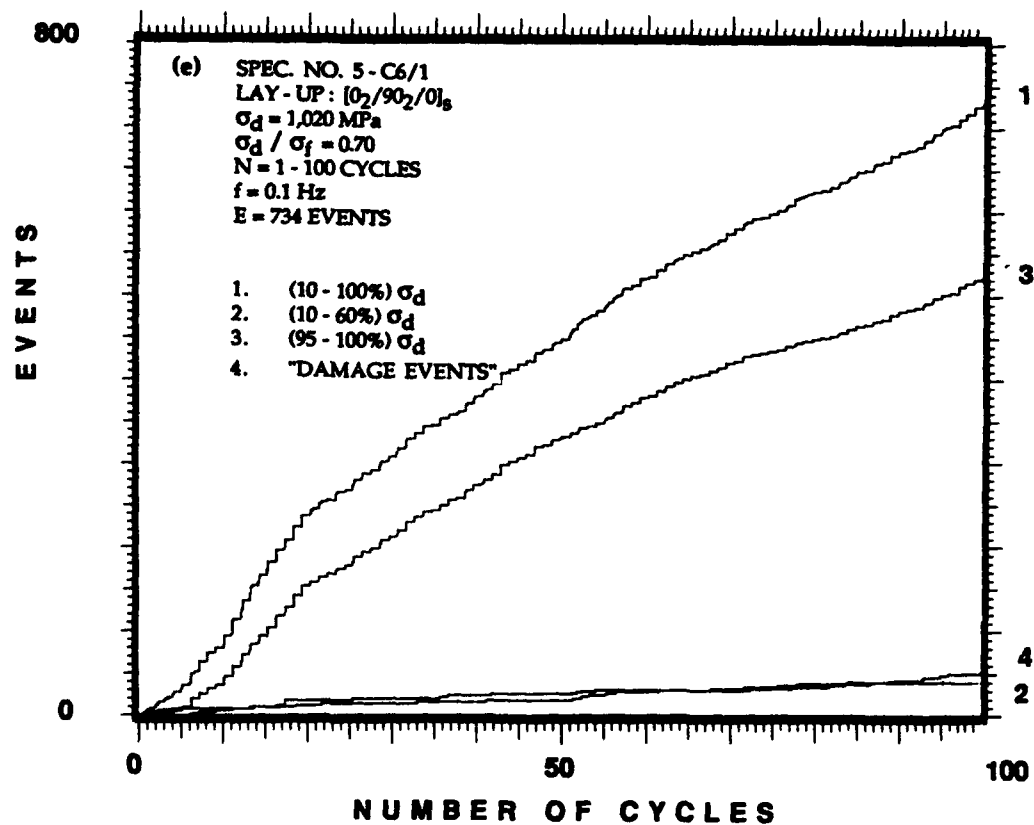


Figure 6.32. Continued.

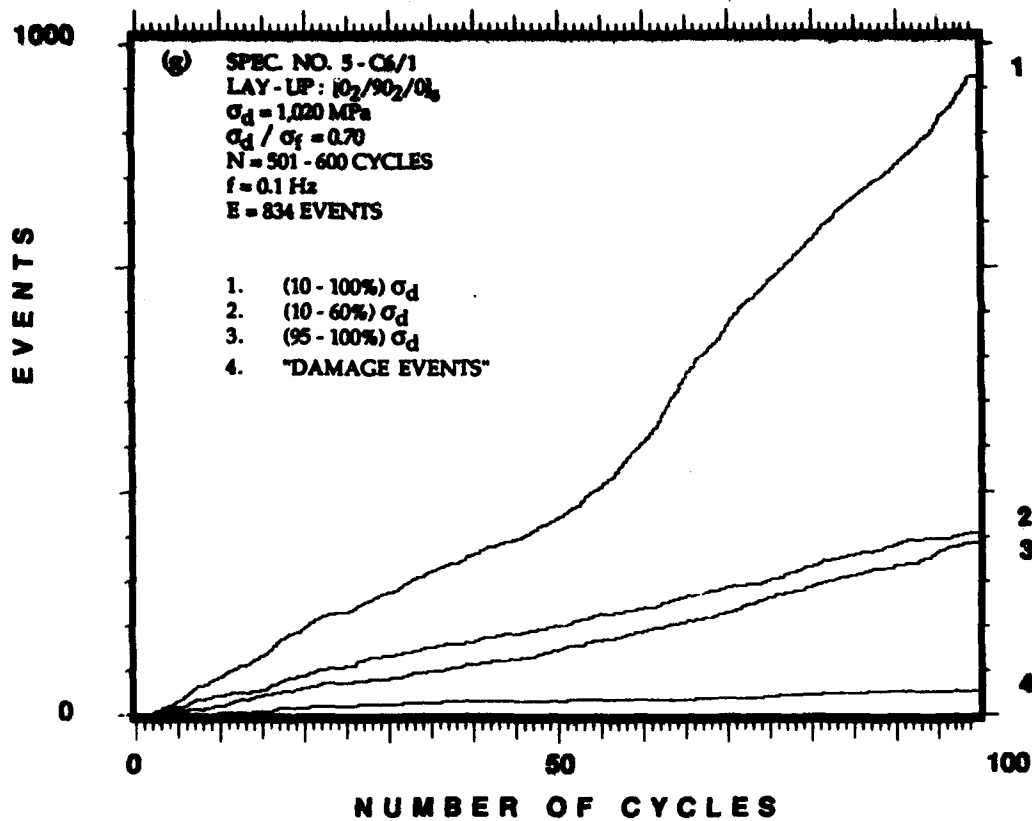


Figure 6.32. Continued.

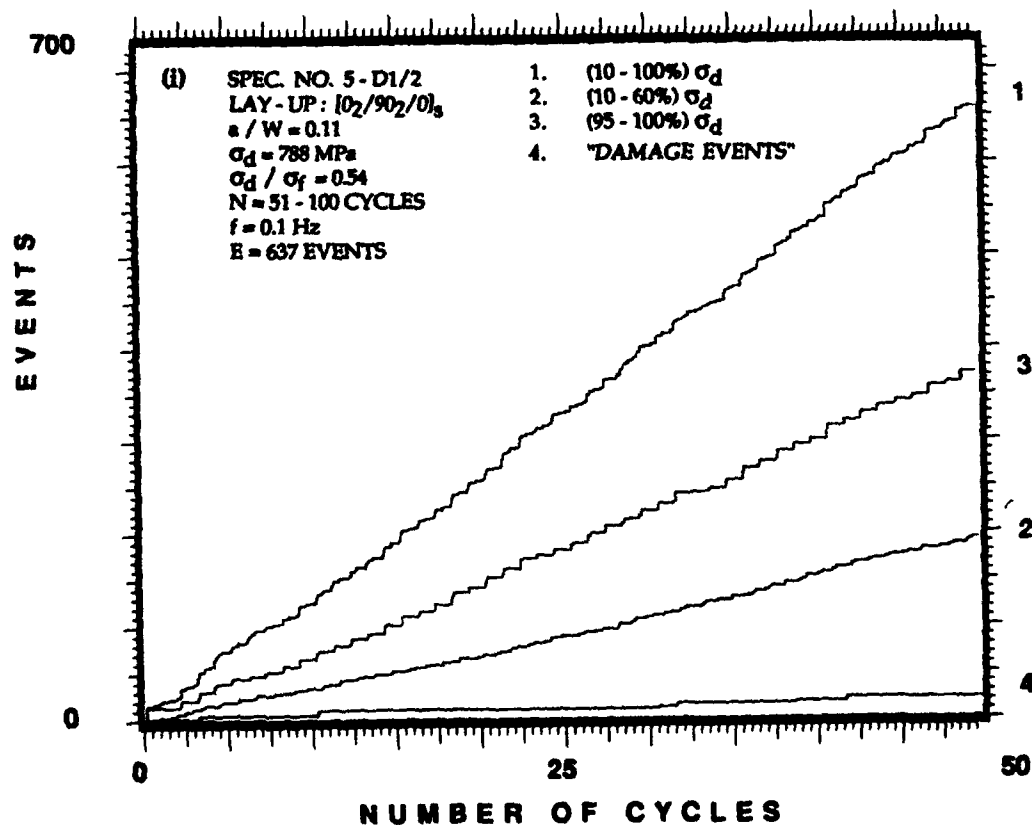
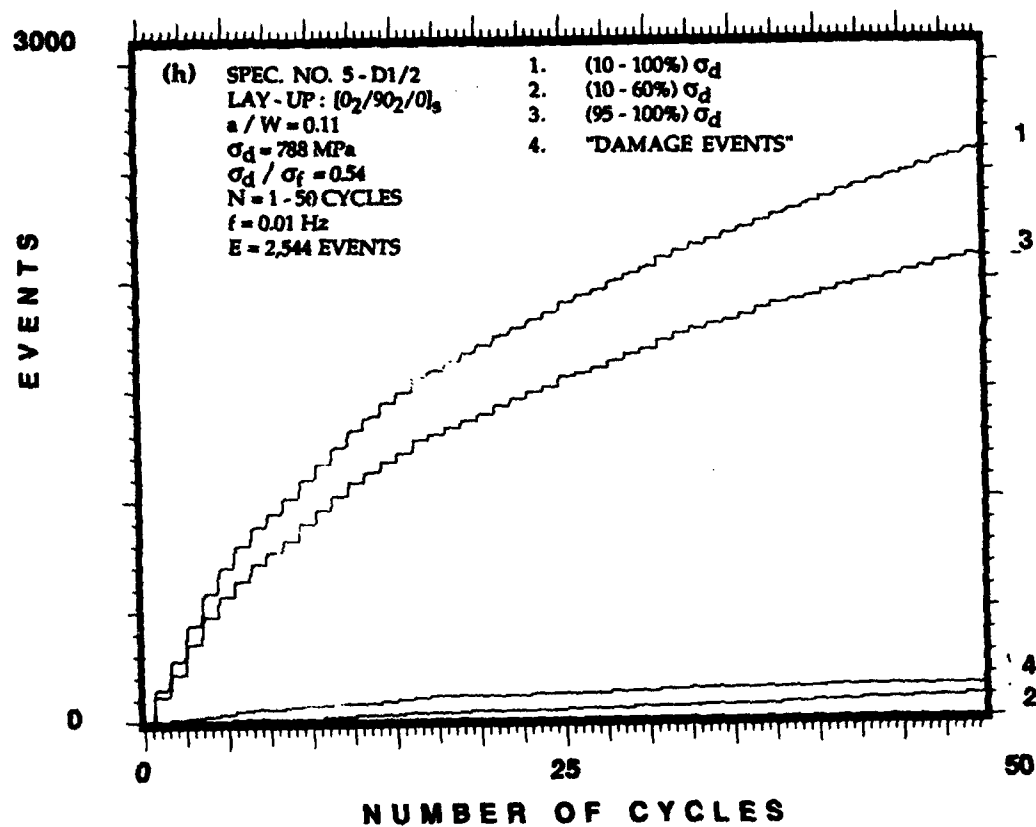


Figure 6.32. Continued.

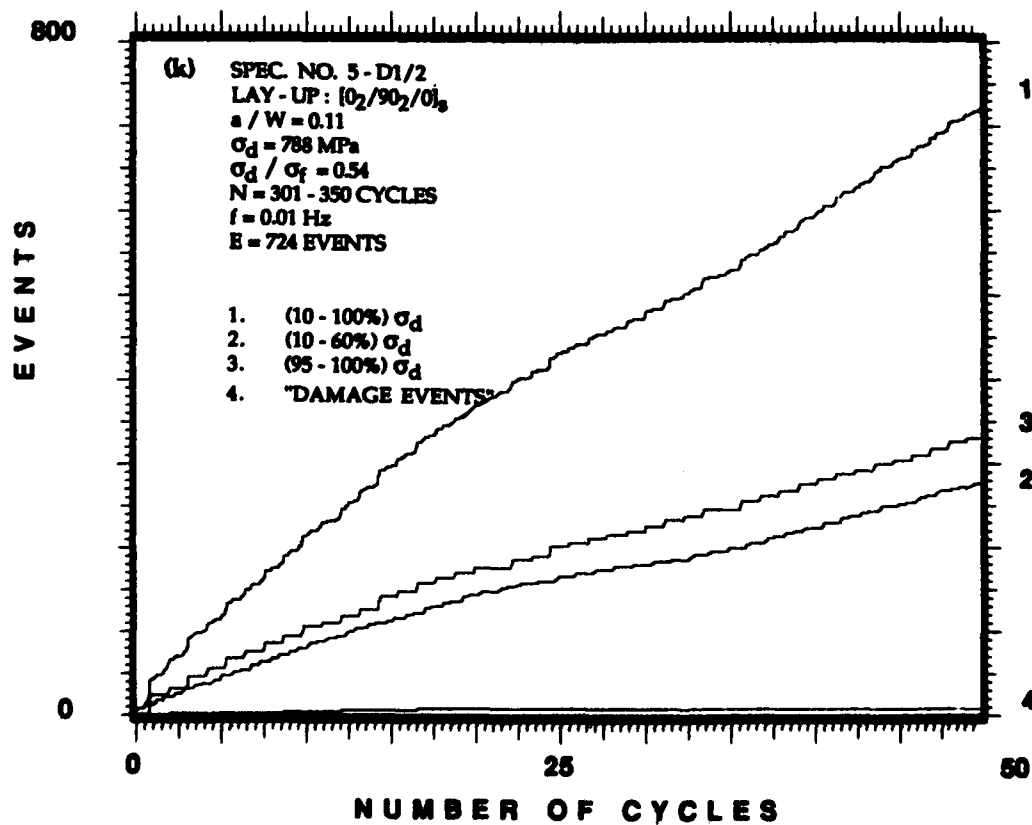
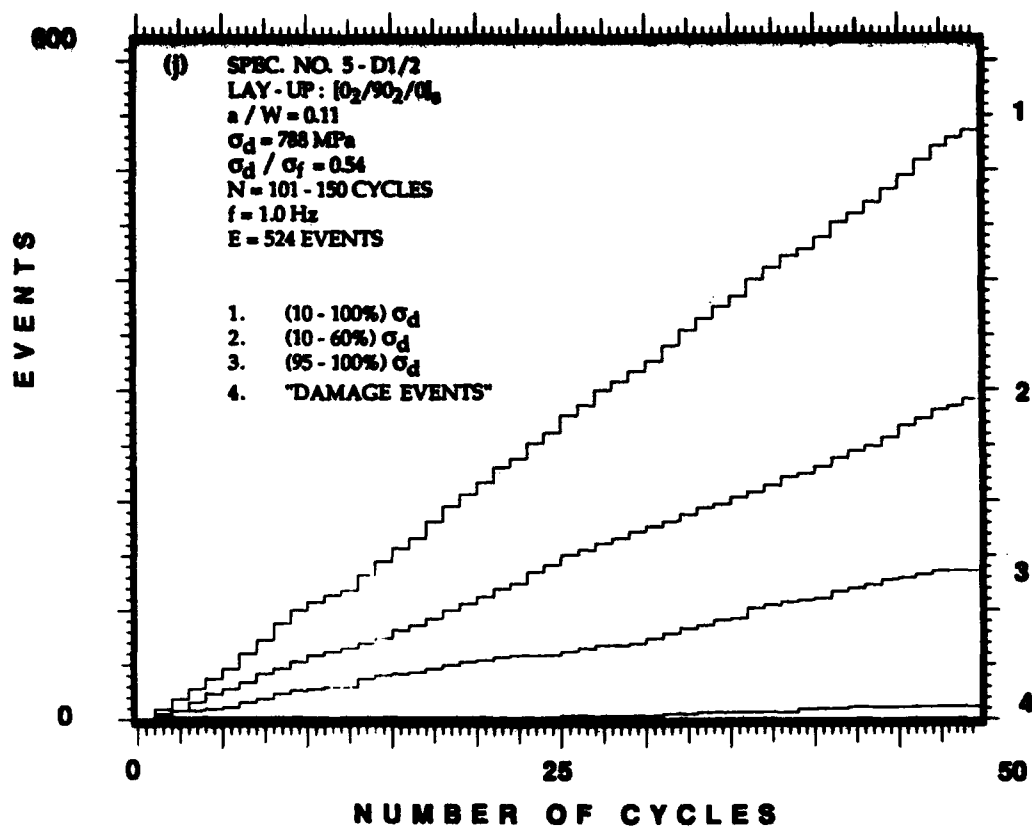


Figure 6.32. Concluded.

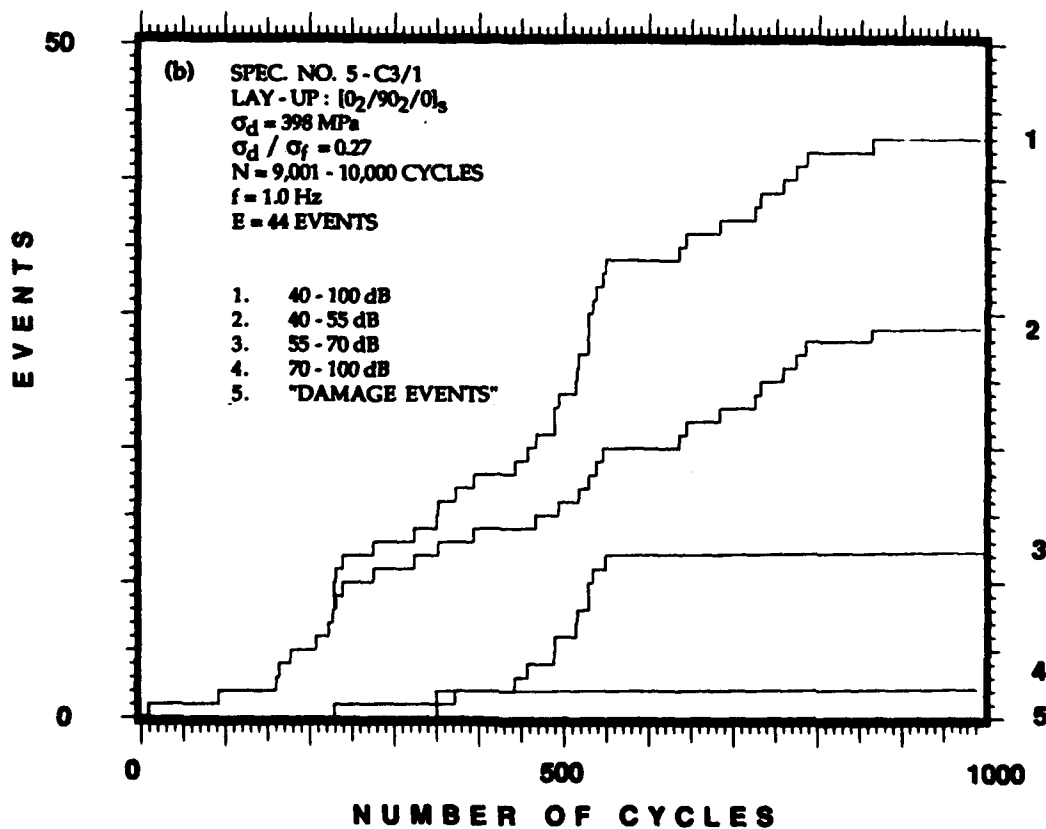
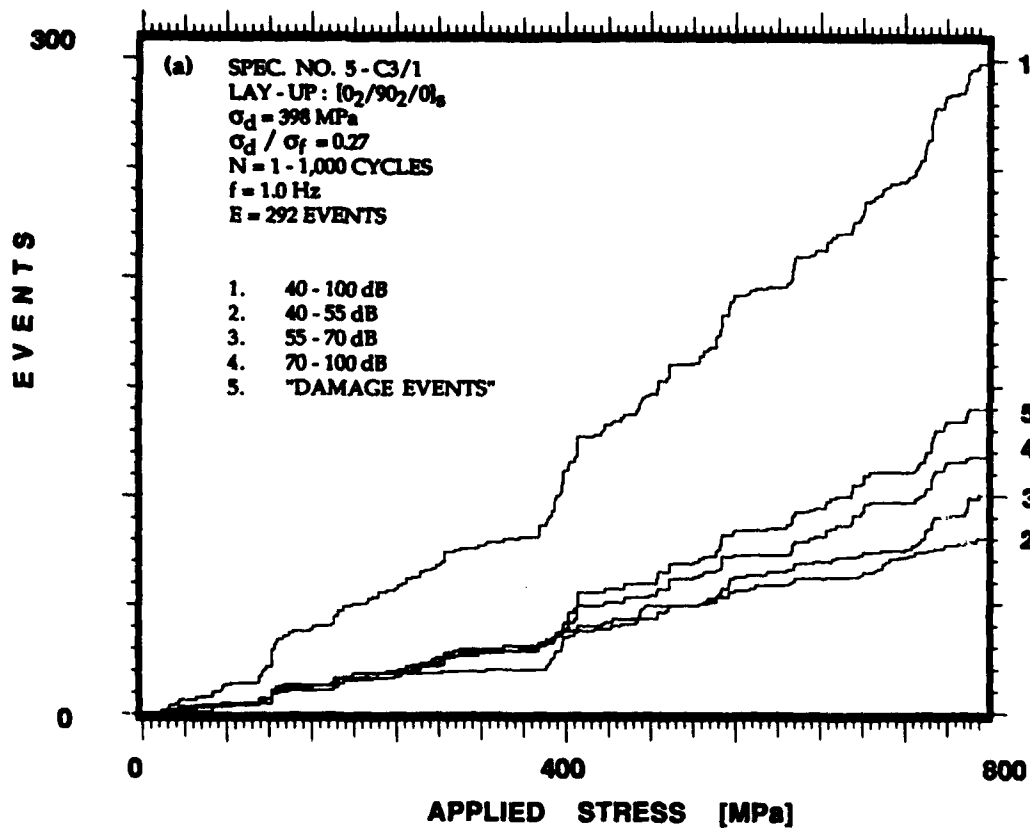


Figure 6.33. Accumulative events of four different amplitude ranges (curves No. 1-4) and derived damage (DD) curve for all the events generated (curve No. 5) plotted as a function of number of cycles for the same three specimens and fatigue periods shown in Figure 6.32. The number of "damage events" is similar to that of high amplitude events.

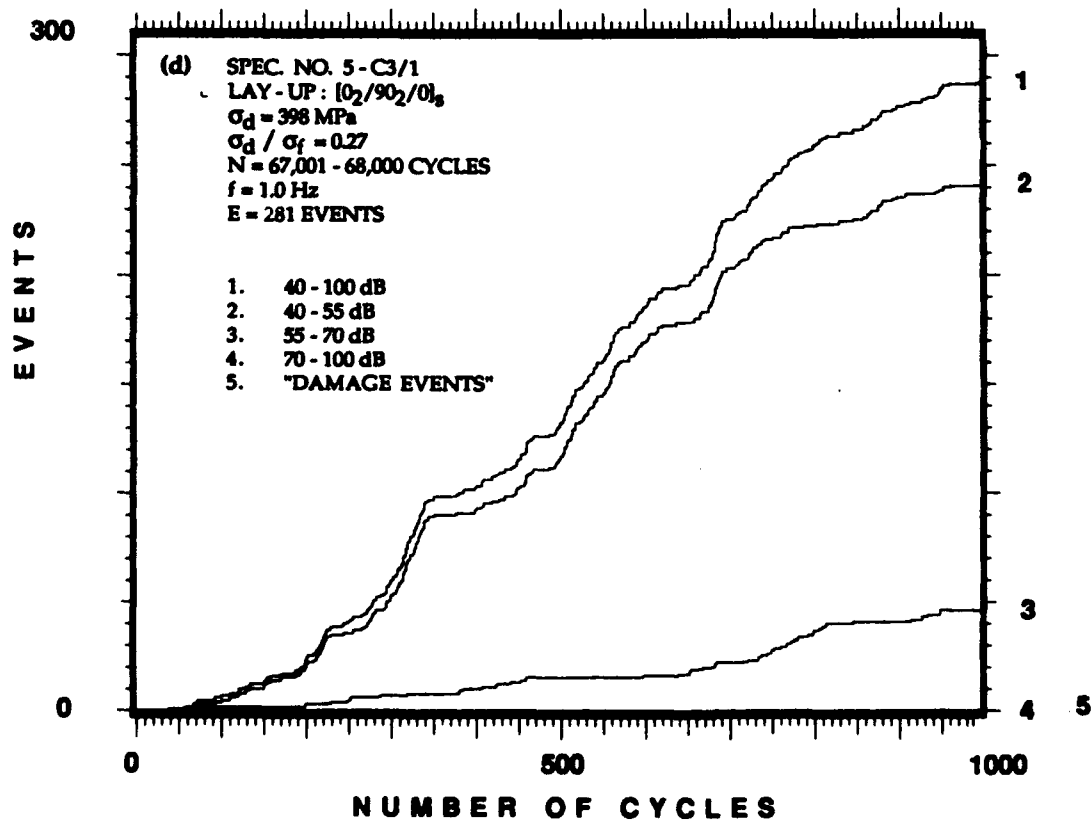
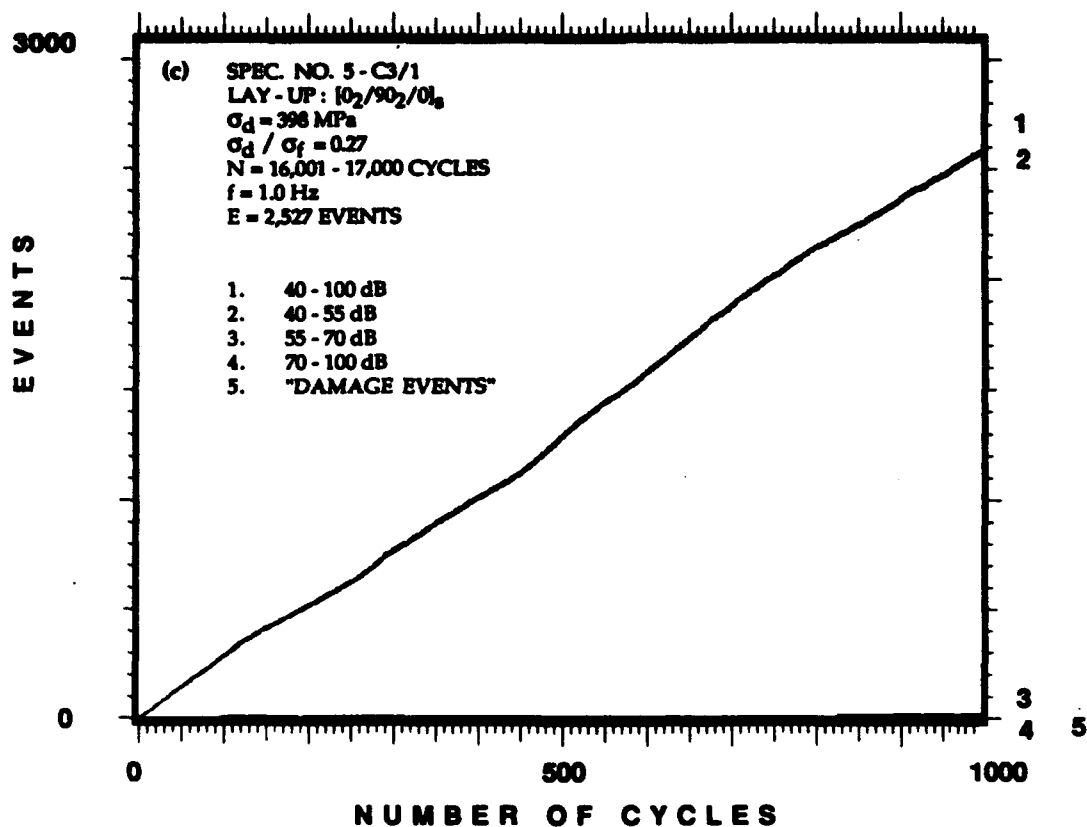


Figure 6.33. Continued.

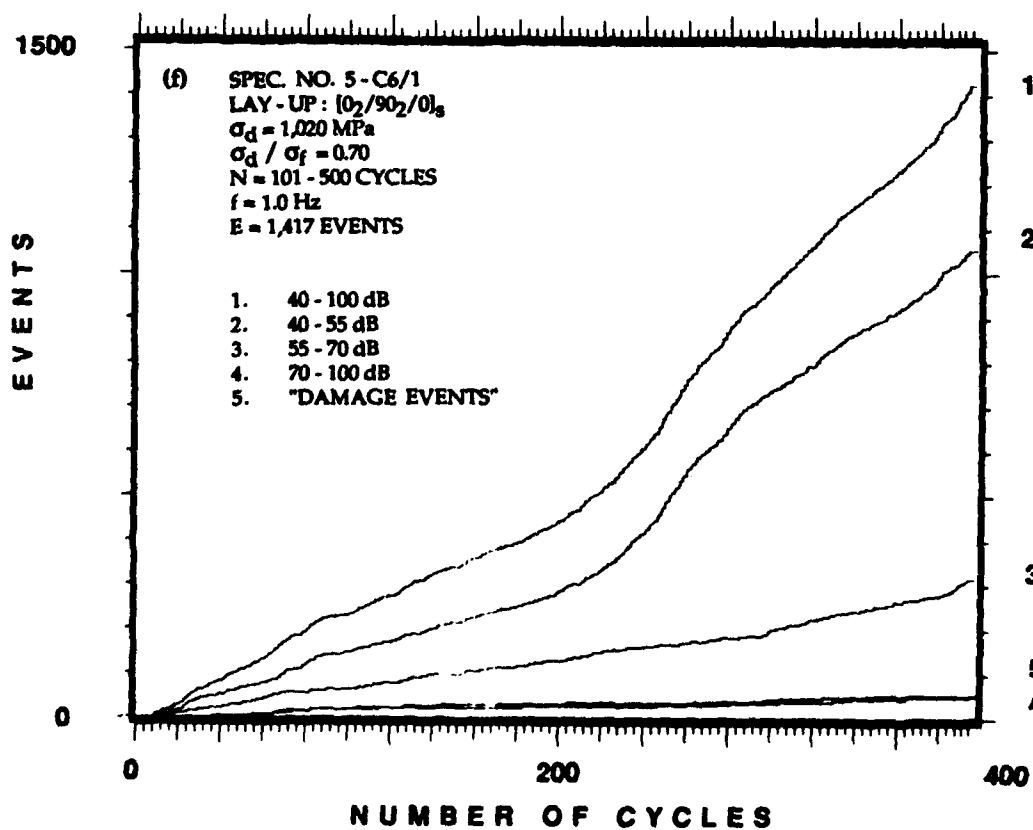
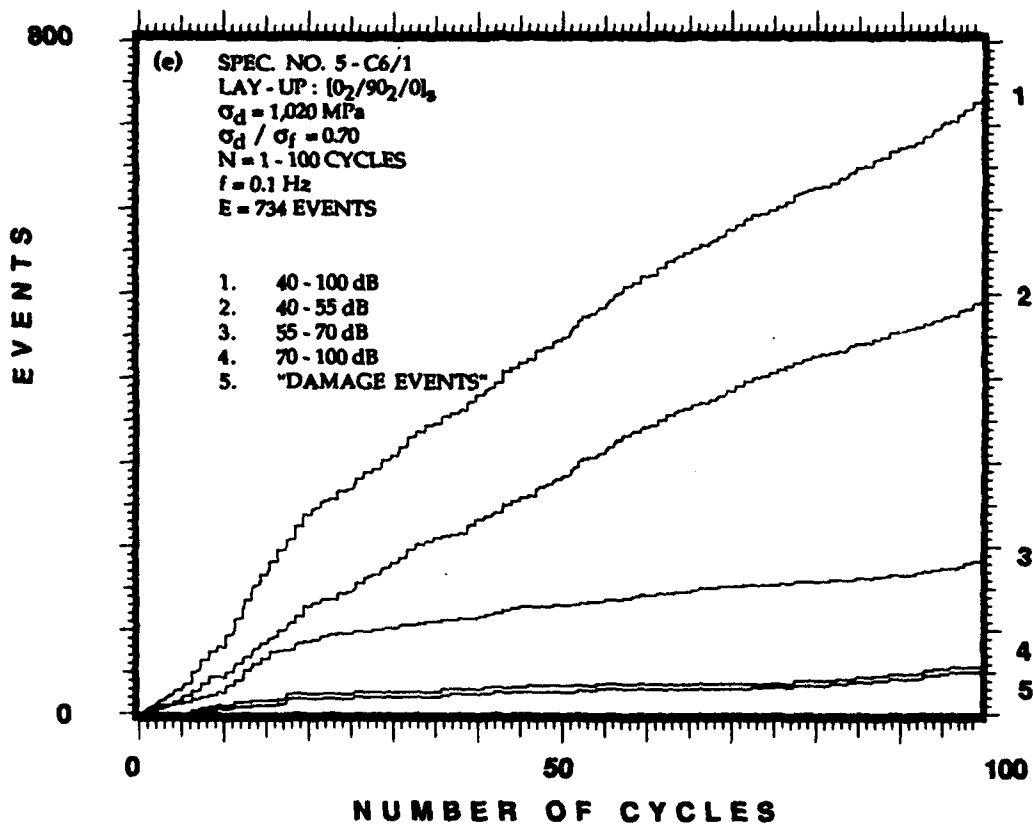


Figure 6.33. Continued.

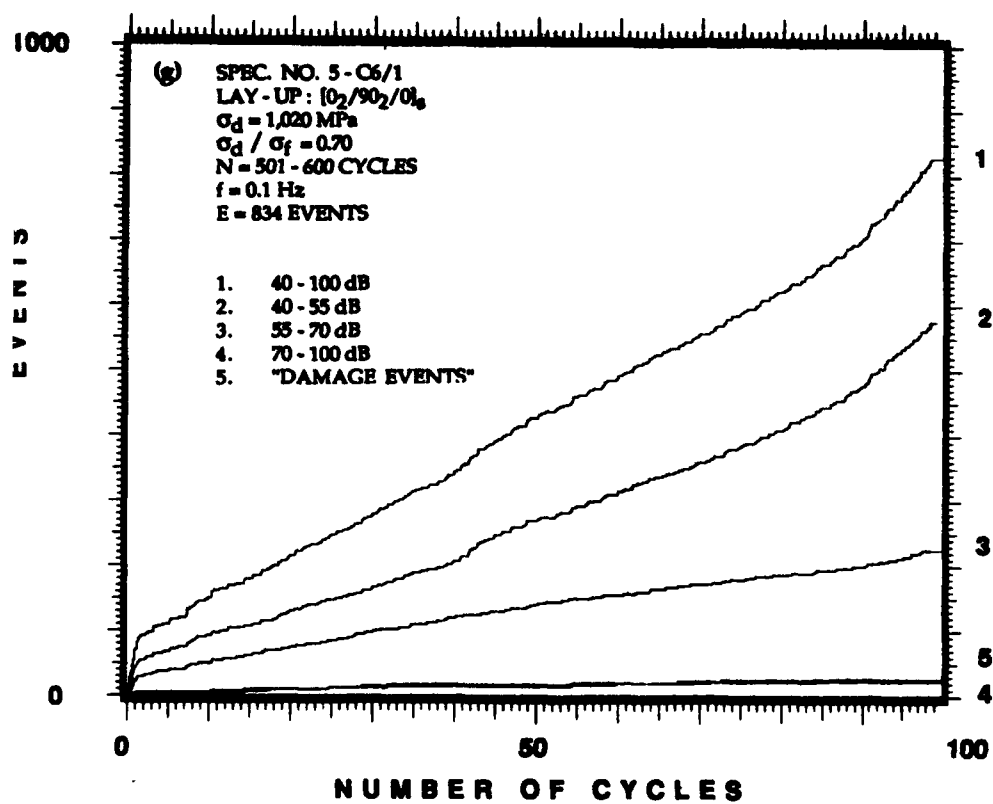


Figure 6.33. Continued.

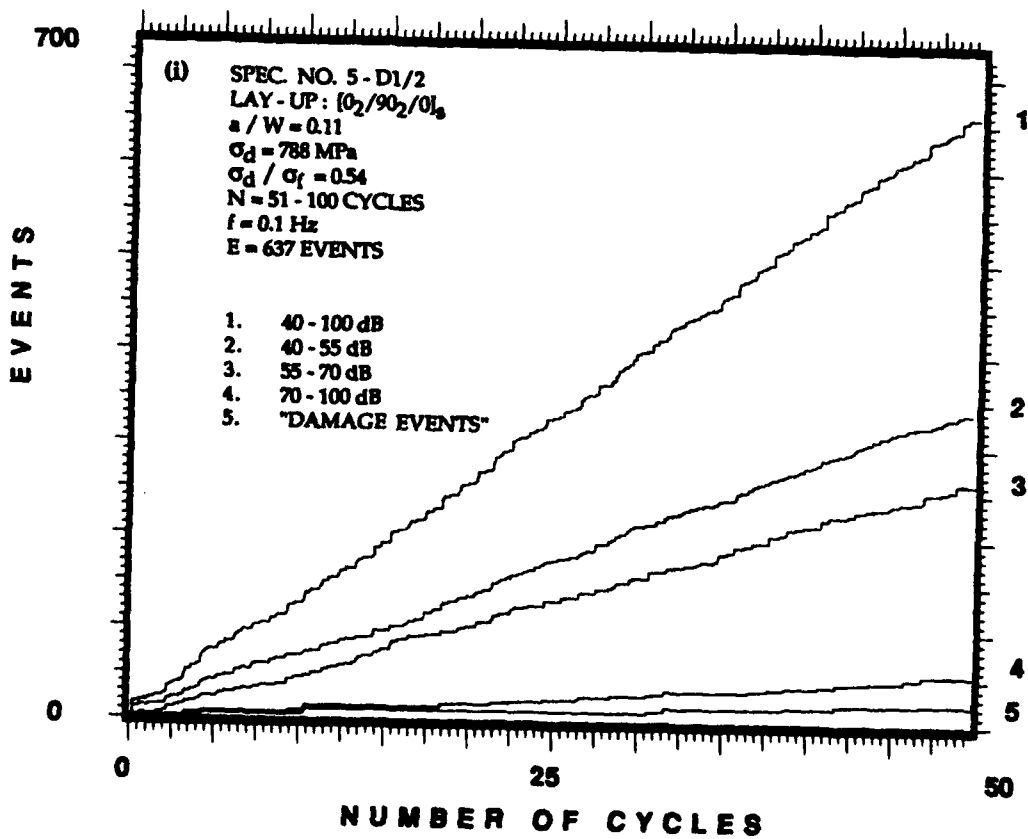
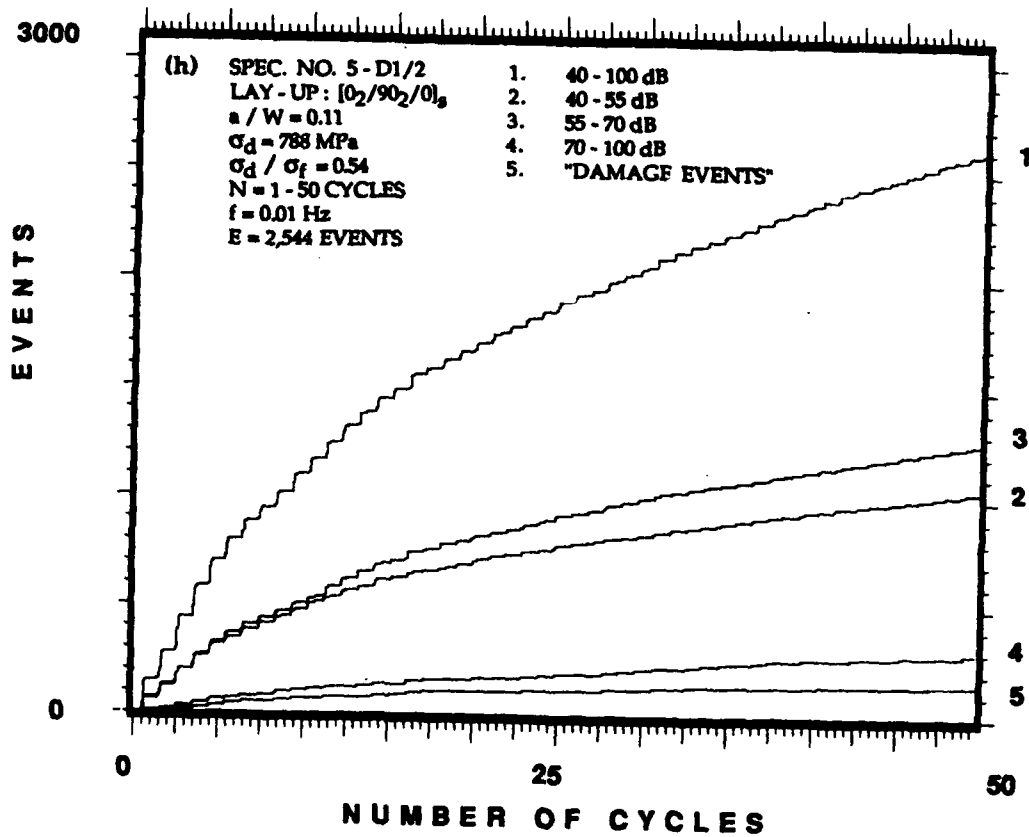


Figure 6.33. Continued.

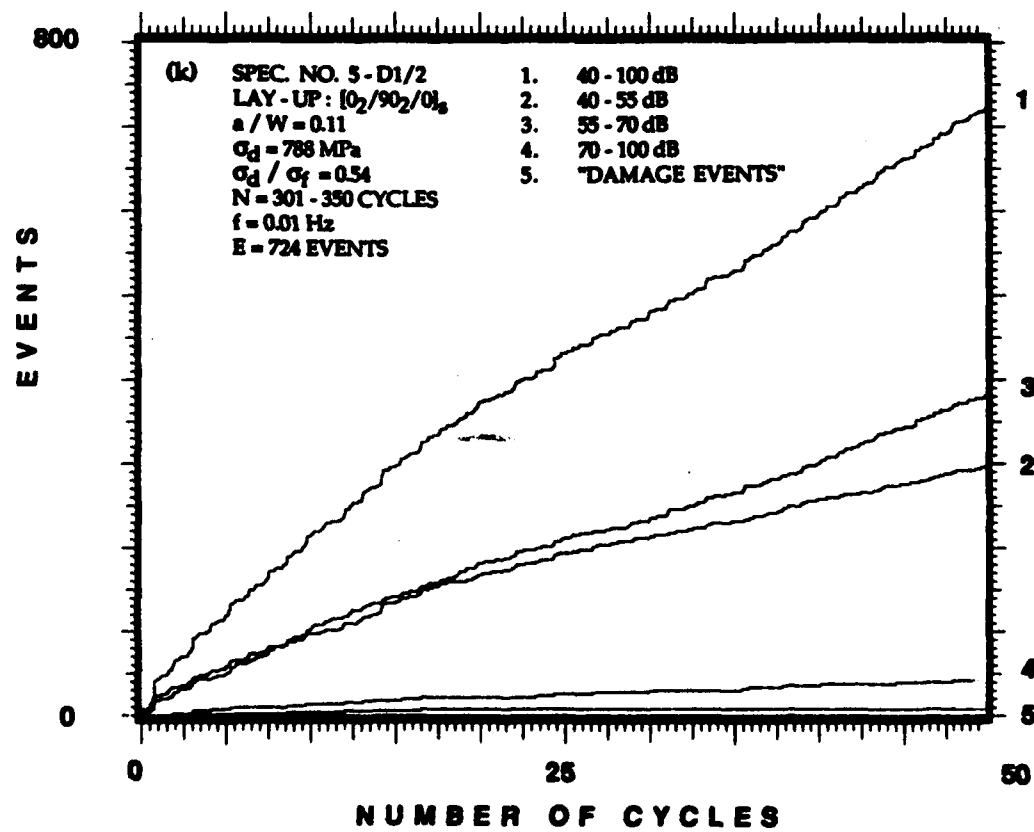
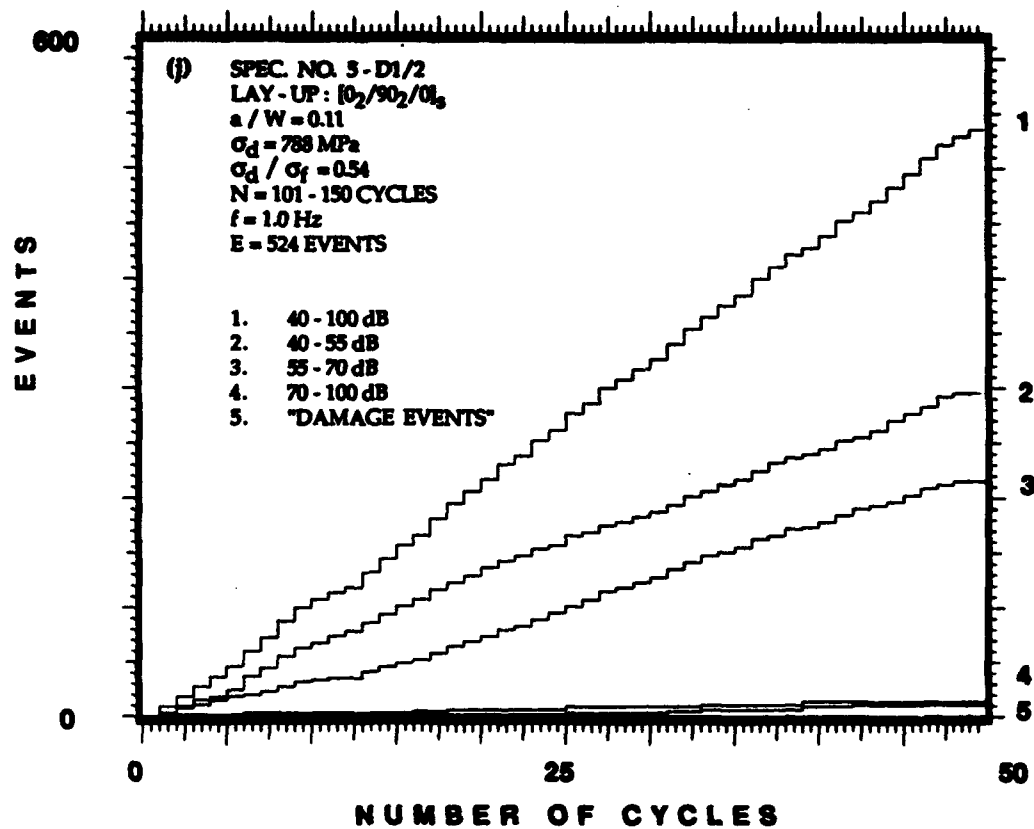


Figure 6.33. Concluded.

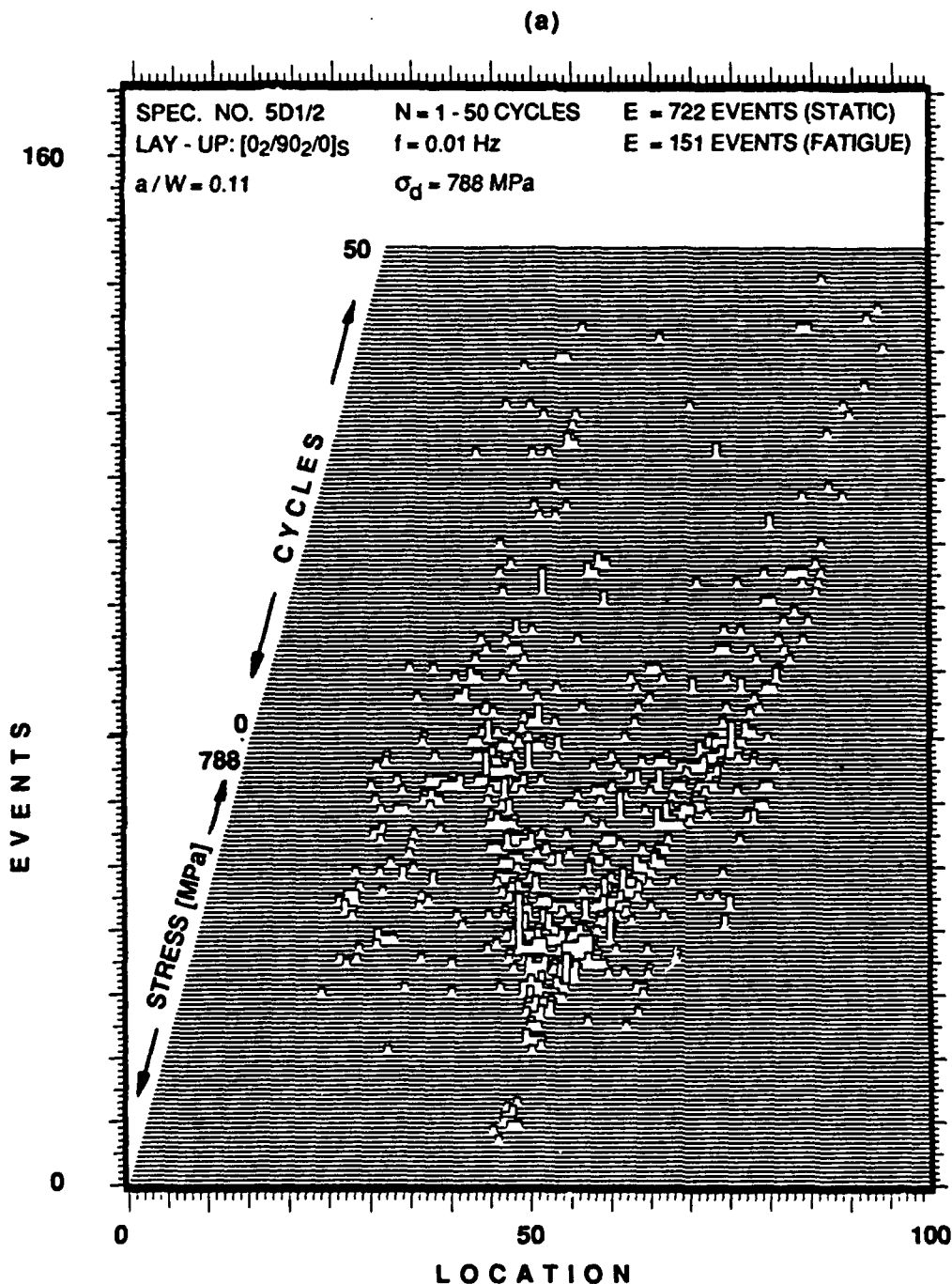


Figure 6.34. Location distribution histograms of events recorded during the first quasi-static load cycle and during the subsequent first 50 cycles of the fatigue loading for the same specimen shown in Figures 6.3e, 6.5i, and 6.6i. The plots are for: (a) only the events generated by damage; and (b) all the events generated (see curves No. 4 and 1 in Figure 6.32h, respectively).

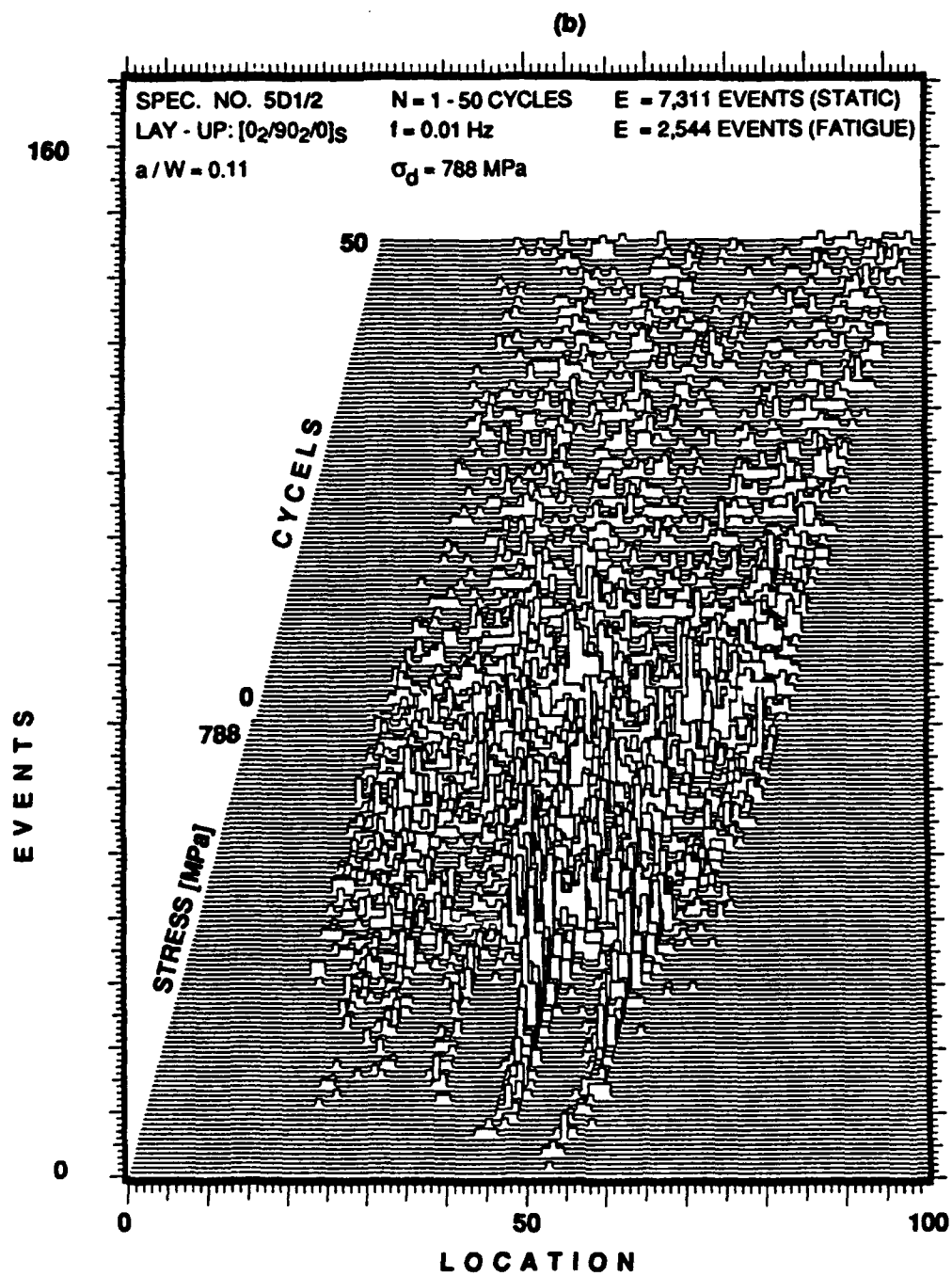


Figure 6.34. Concluded.

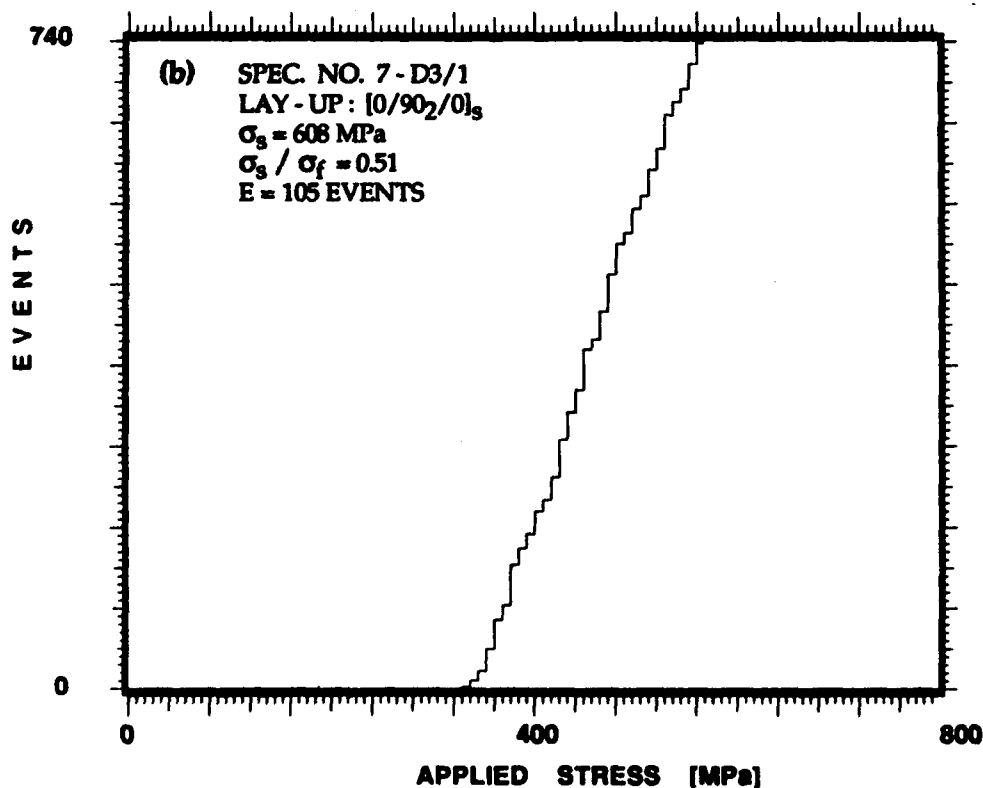
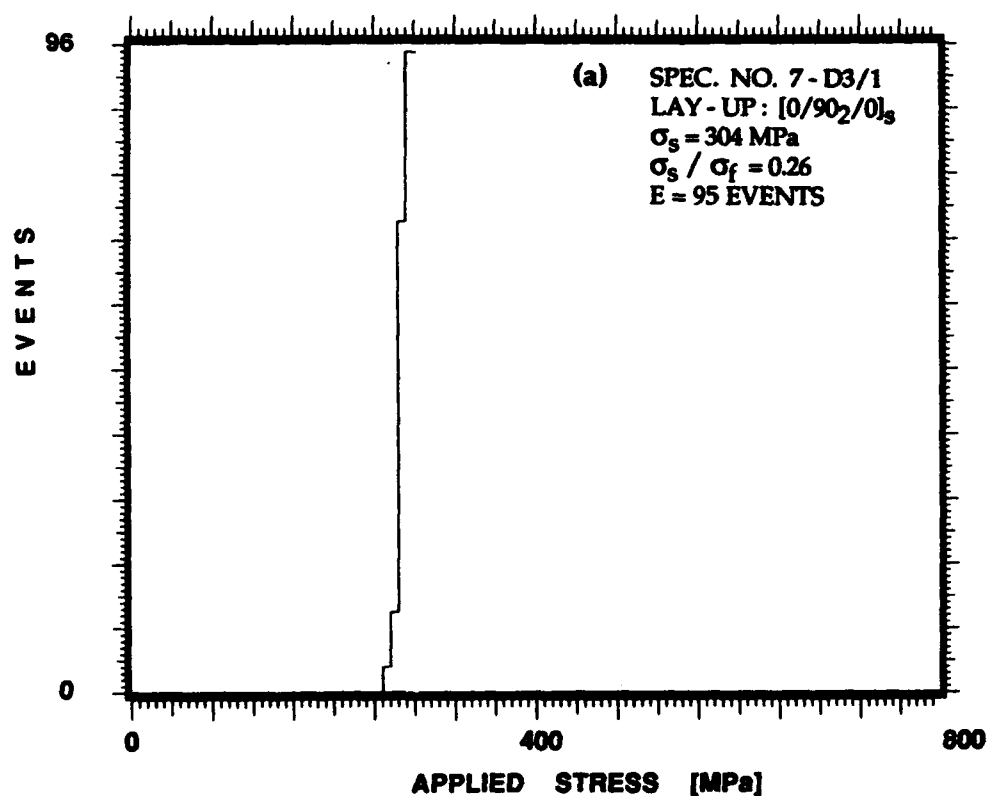


Figure 6.35. Accumulative events as a function of far-field applied stress of events generated during three post-fatigue quasi-static loadings of a $[0/90_2/0]_s$ laminate subjected to the loading sequence shown in Figure 6.1e: (a), (b), and (c) events generated during each of the three loadings; and (d) comparison among the three loadings. Results show that fatigue loading has a delay effect on the emission initiation load and the rate of events accumulation. 316

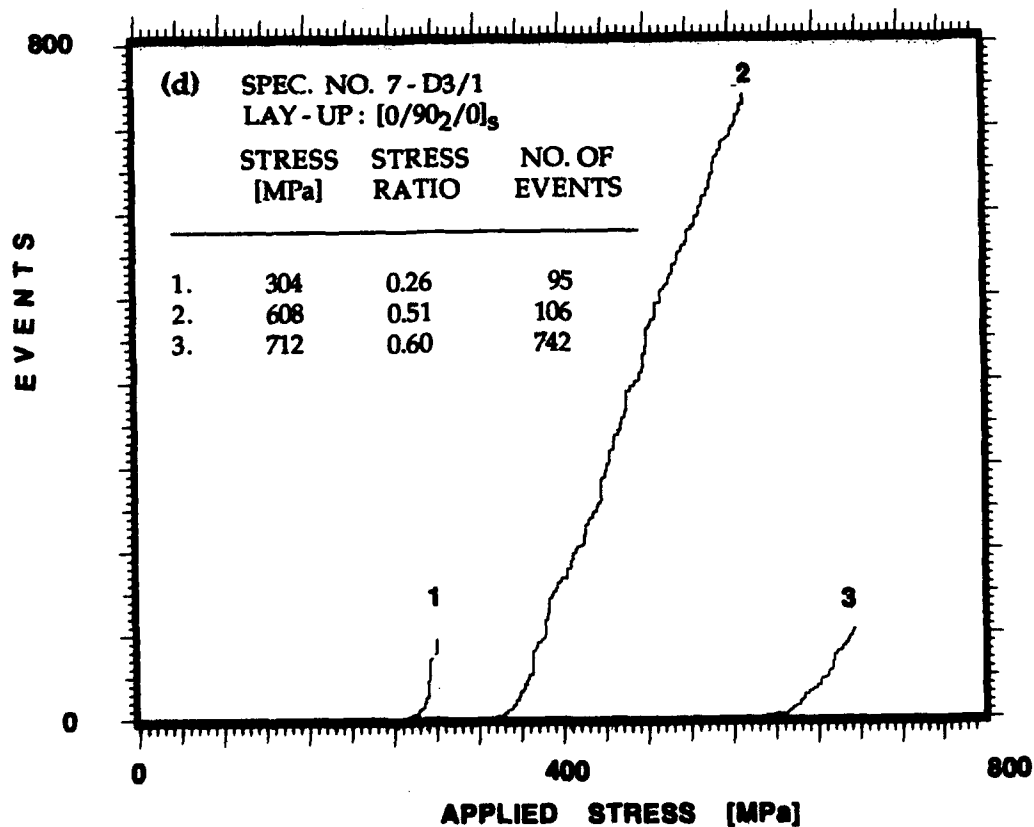
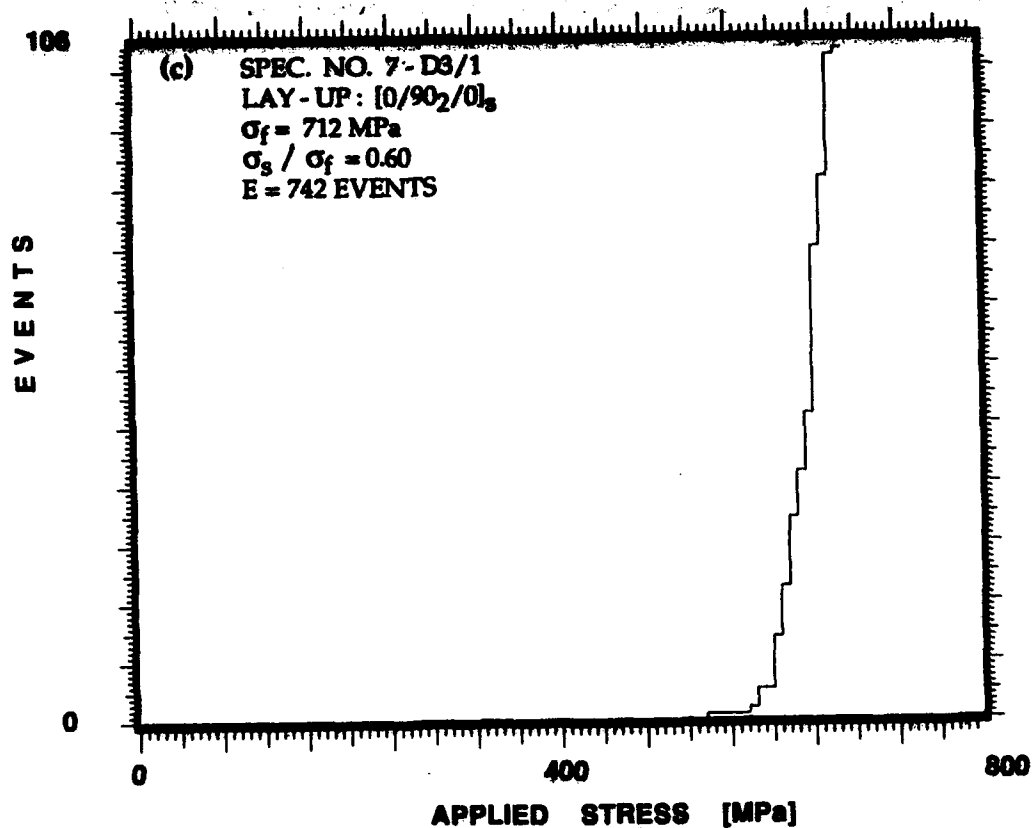


Figure 6.35. Concluded.

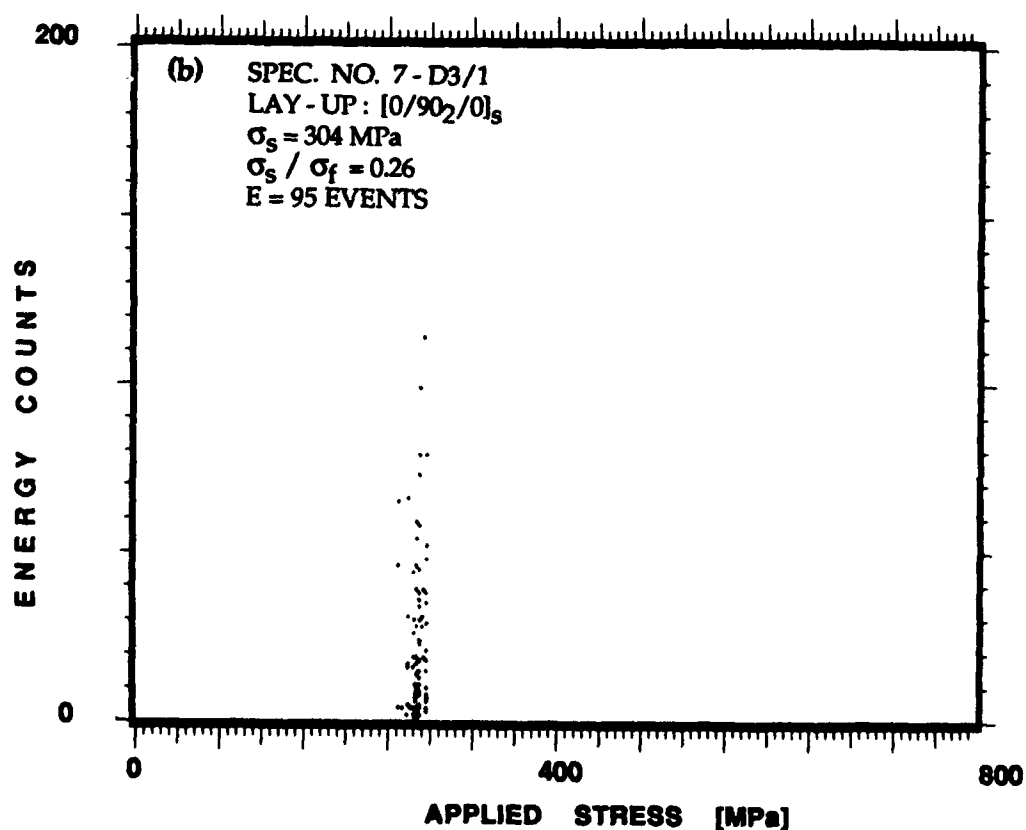
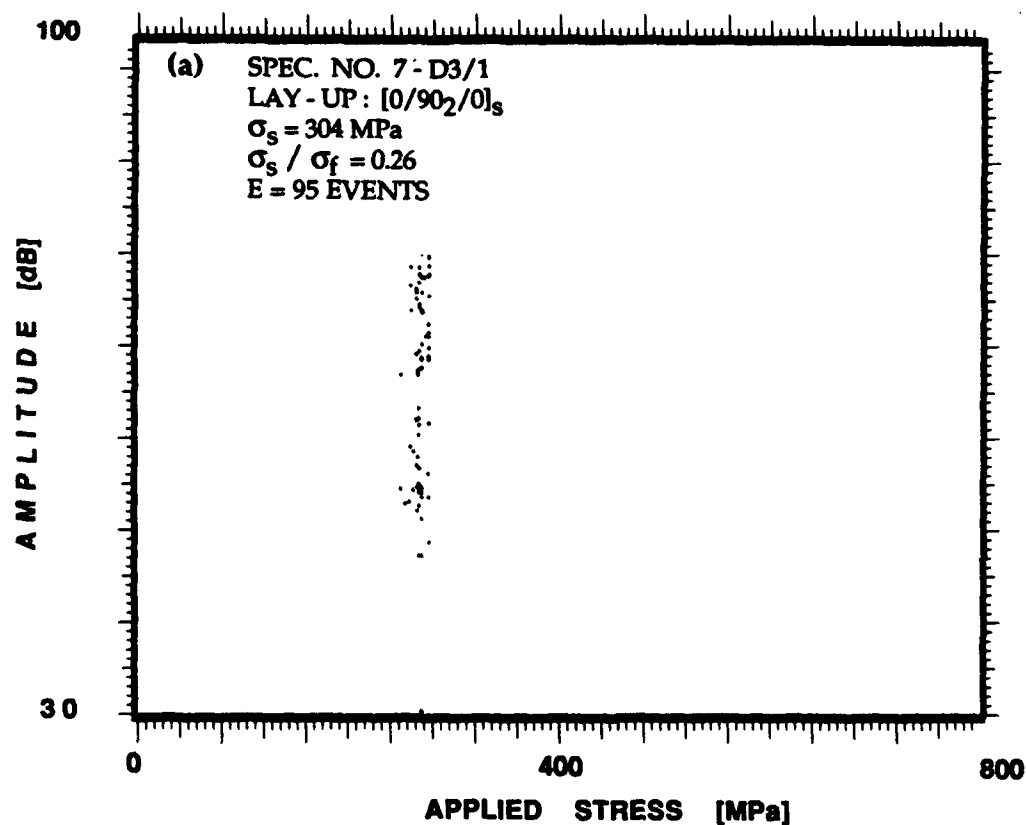


Figure 6.36. Intensities of events as a function of far-field applied stress for all the events accumulated during the three post-fatigue quasi-static loadings shown in Figure 6.35: (a)-(d) first loading; (e)-(h) second loading; and (i)-(l) third loading. Loading sequence is shown in Figure 6.1e. With increasing damage larger is number of low intensity events.

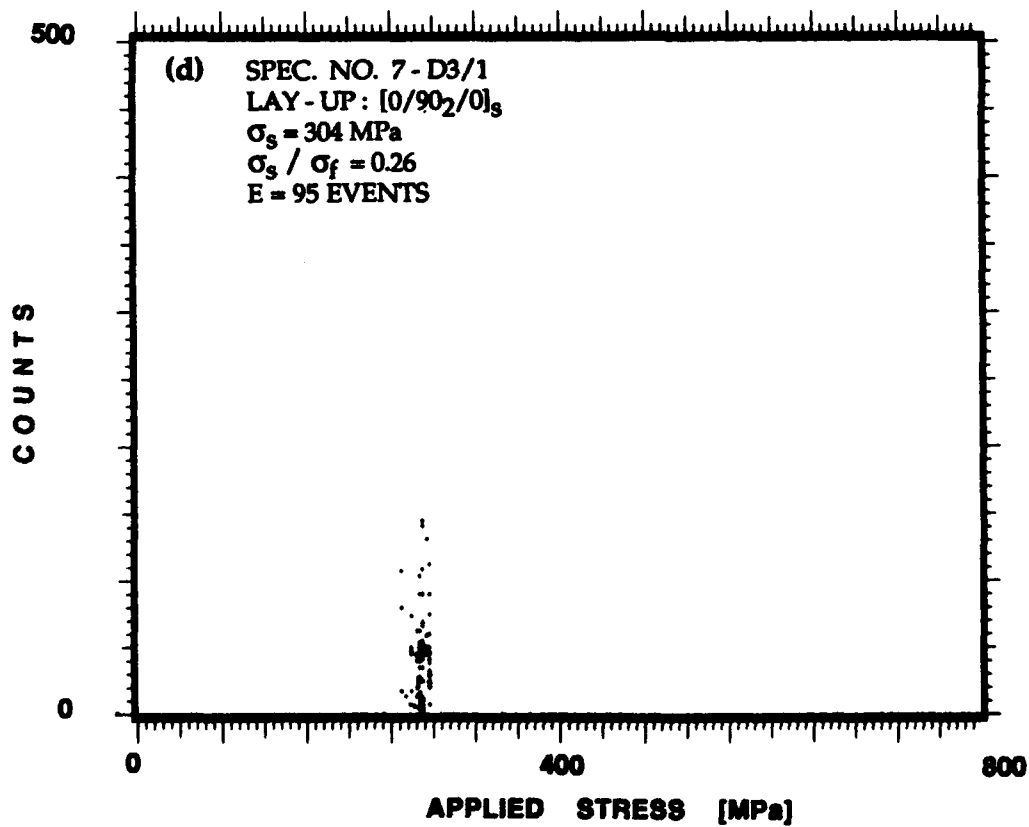
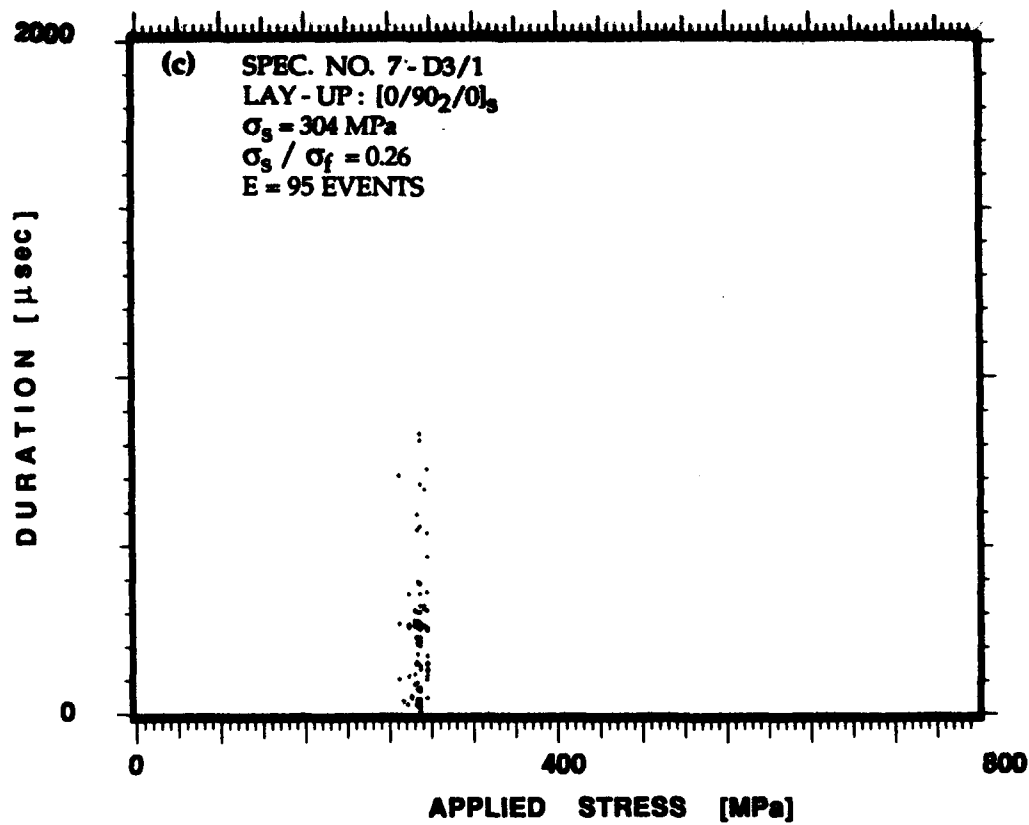


Figure 6.36. Continued.

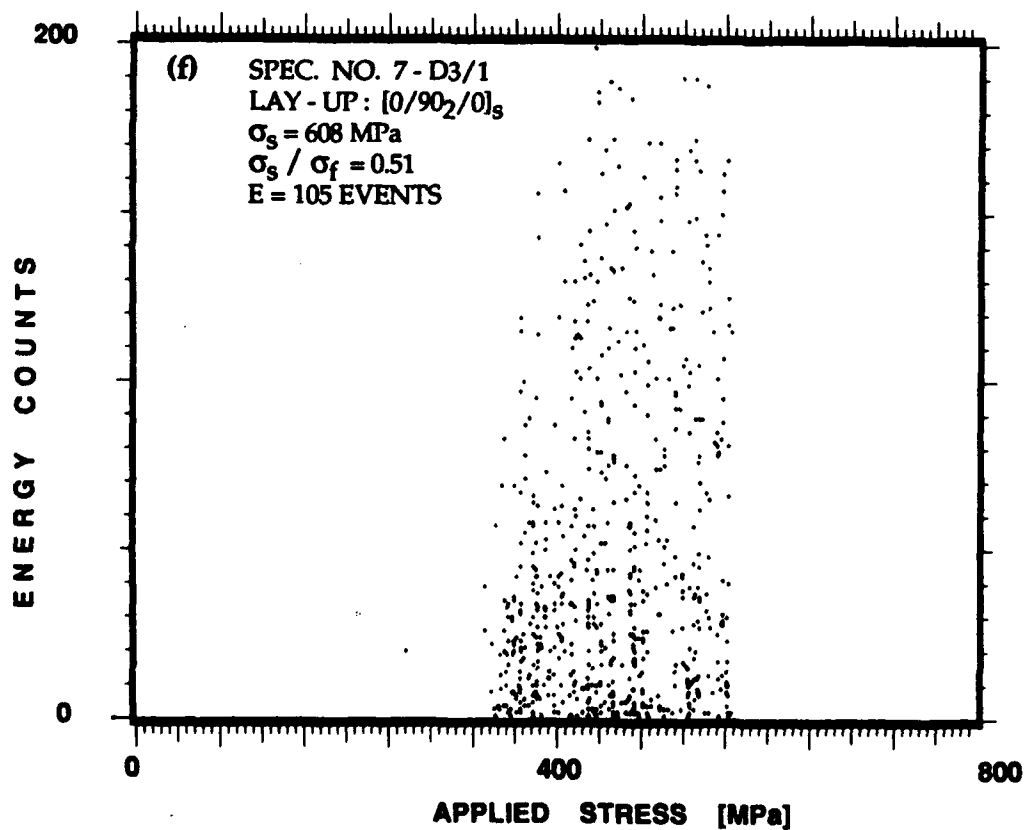
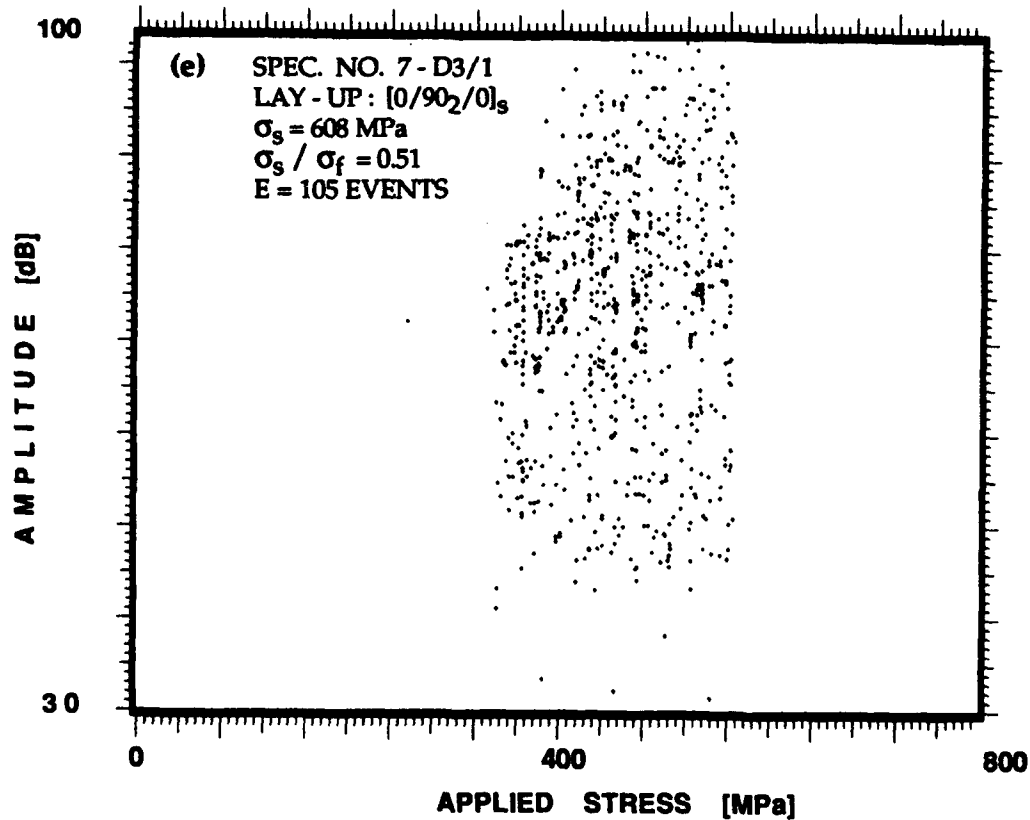


Figure 6.36. Continued.

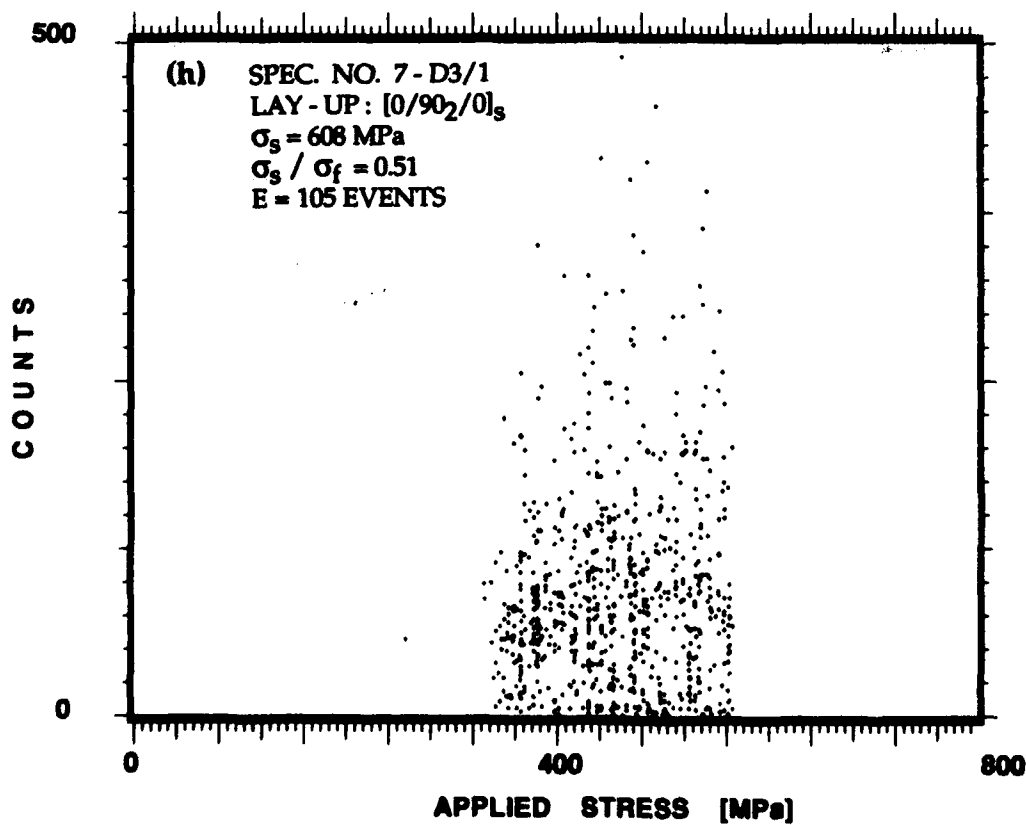
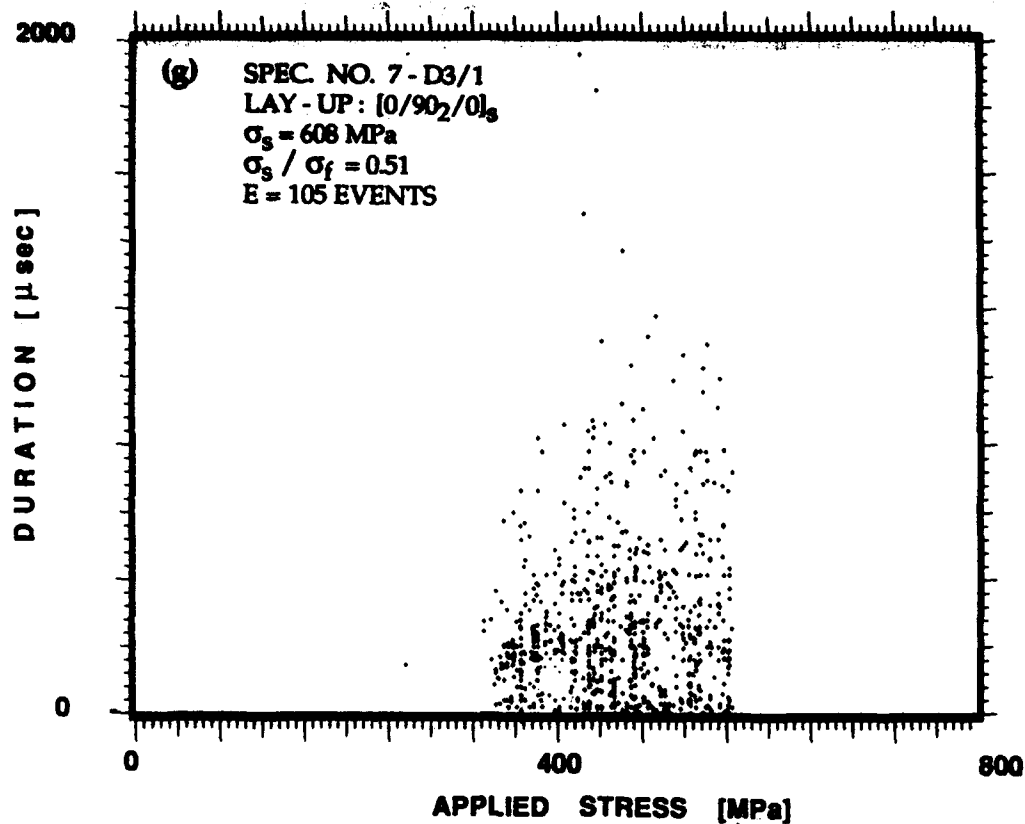


Figure 6.36. Continued.

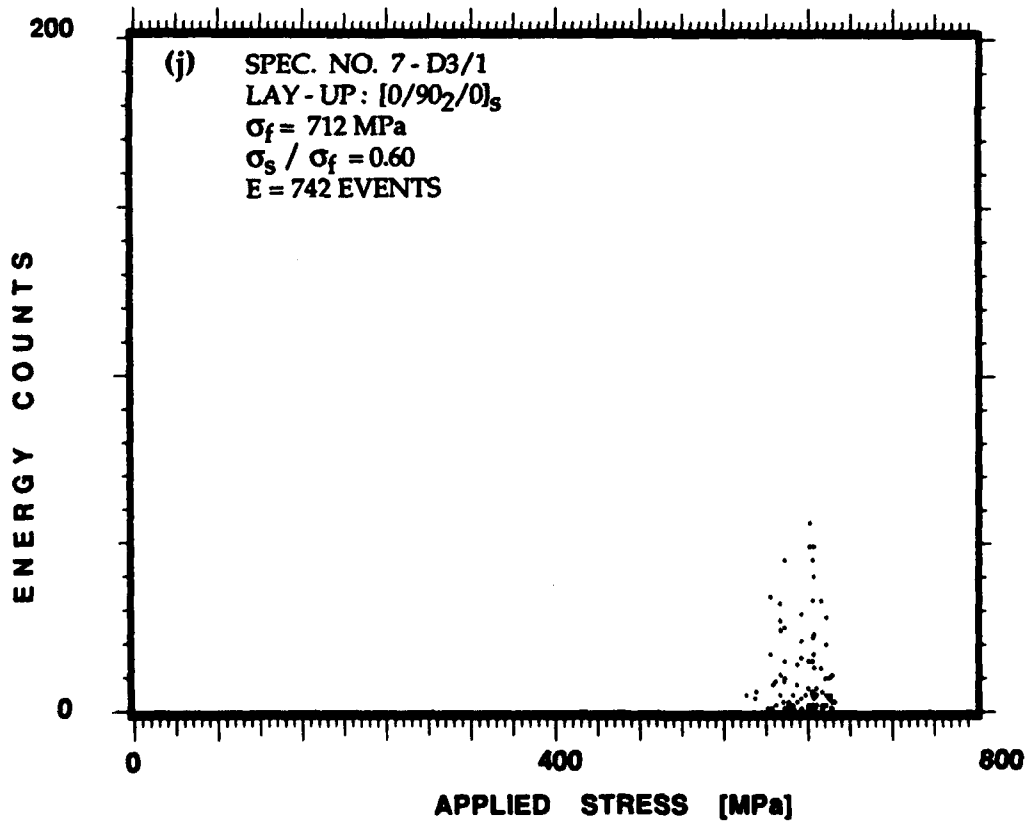
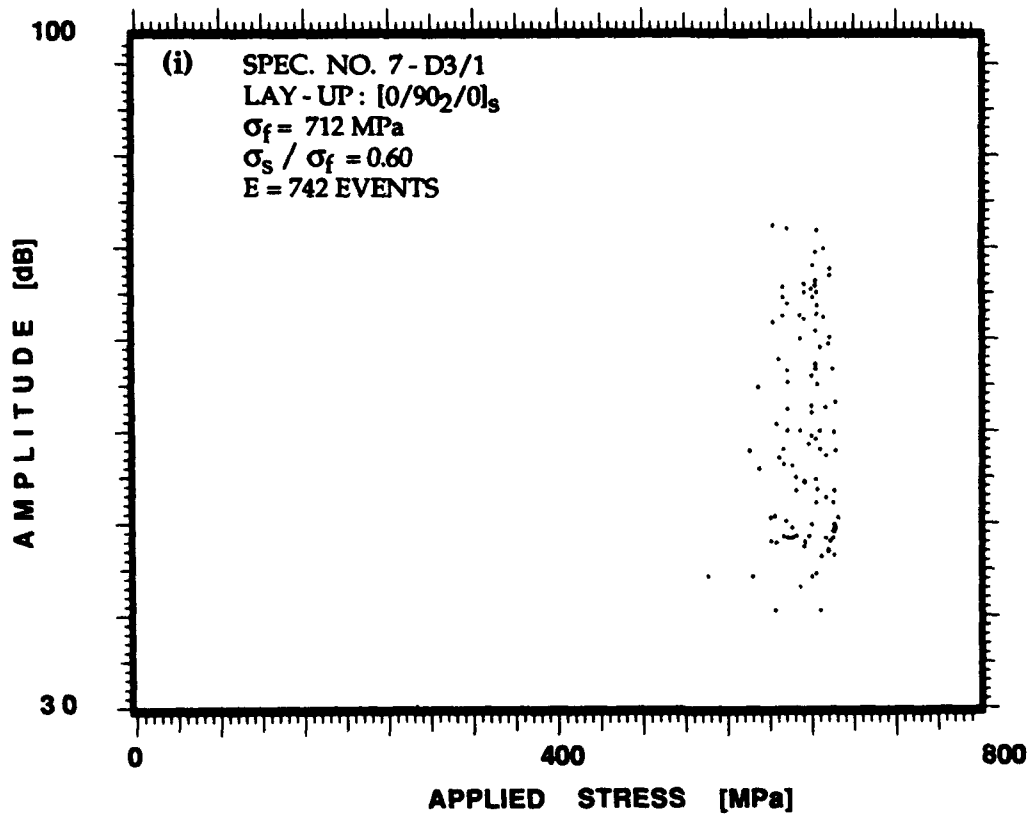


Figure 6.36. Continued.

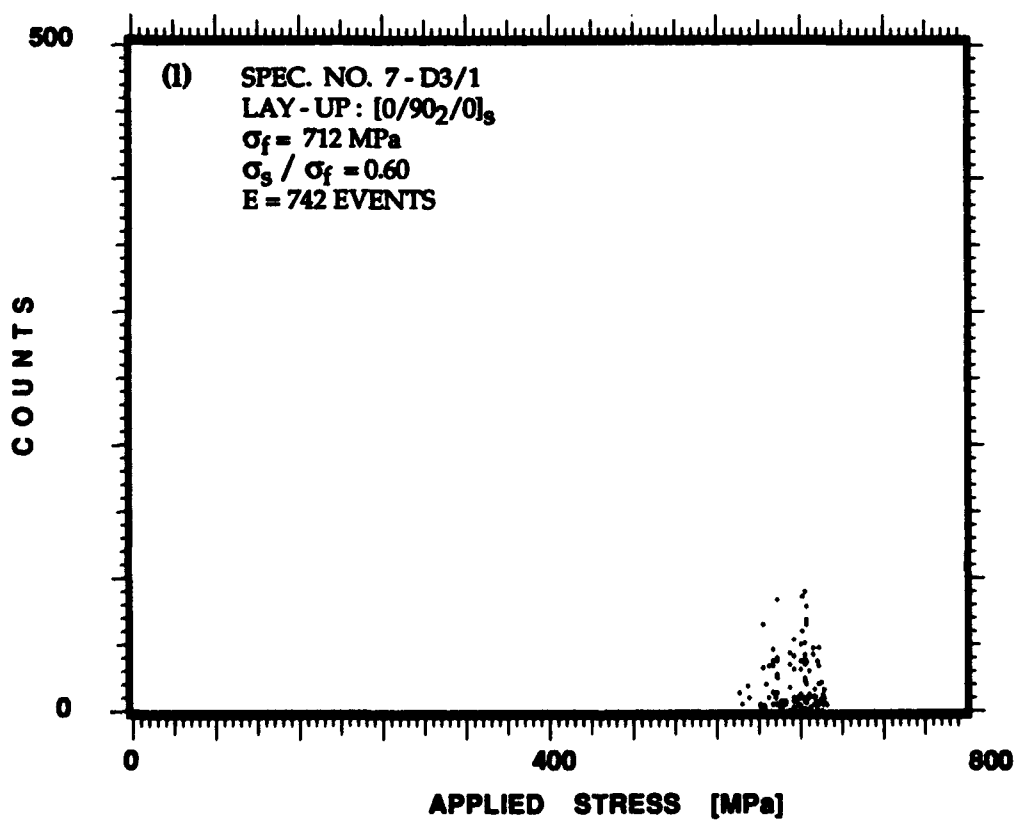
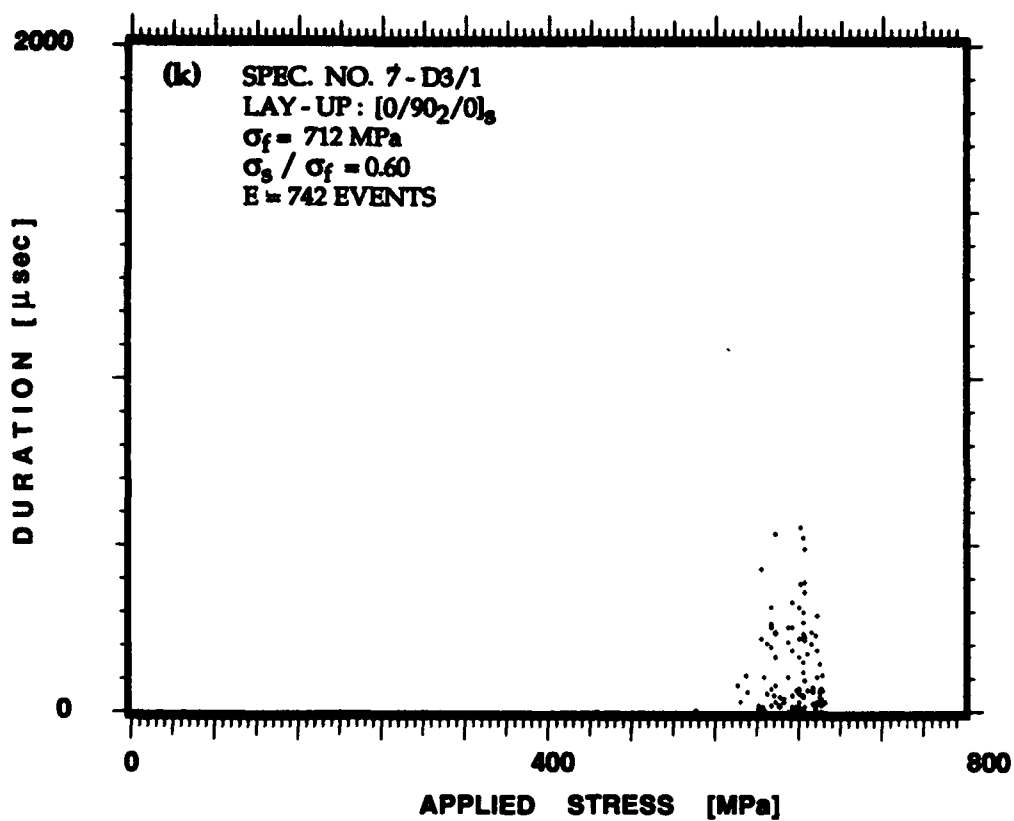


Figure 6.36. Concluded.